Université de Lille
UMR CNRS 8198 – Evo-Eco-Paléo
Ecole Doctorale – 104
Sciences de la Matière, du Rayonnement et de l'Environnement

Biodiversity, biostratigraphy, disparity and macroecology of middle Eocene radiolarians (Rhizaria). Insights into their biotic response to the Middle Eocene Climatic Optimum (MECO).

Biodiversité, biostratigraphie, disparité et macroécologie des radiolaires (Rhizaria) de l'Éocène moyen. Aperçu de leur réponse biotique à l'Optimum Climatique de l'Éocène Moyen (MECO).

Thèse préparée et soutenue publiquement par Mathias Meunier le 13/12/2023, pour obtenir le grade de Docteur en Géosciences, Écologie, Paléontologie et Océanographie.

Membres du jury :

Špela Goričan	ZRC SAZU, Ljubljana, Slovénie	PR	Rapporteuse
Robert Speijer	KU Leuven, Belgique	PR	Rapporteur
Catherine Crônier	Université de Lille, France	PR	Examinatrice, Présidente du jury
Delphine Desmares	Sorbonne Université, Paris, France	MCF	Examinatrice
Jakub Witkowski	Université de Szczecin, Pologne	MCF	Examinateur
Taniel Danelian	Université de Lille, France	PR	Directeur de thèse

Université de Lille
UMR CNRS 8198 Evo-Eco-Paléo
Bâtiment SN5
54 Avenue Paul Langevin
Cité Scientifique
59650 Villeneuve-d’Ascq cedex
France

Ah ! pauvre père ! auras-tu jamais deviné quel amour tu as mis en moi
Et combien à travers toi j'aime toutes les choses de la terre ?

René Guy Cadou – Tout amour, 1951.

Acknowledgments/Remerciements

Ce travail n'aurait pas été possible sans le soutien de l'Université de Lille et de l'Institut de Recherches Pluridisciplinaires en Sciences de l'Environnement (IRePSE), qui m'ont permis, grâce à une allocation de recherches et diverses aides financières, de me consacrer entièrement à l'élaboration de cette thèse.

Qu'il me soit également permis de remercier ici tous ceux qui m'ont servi de guides au cours de ces trois laborieuses années, à commencer par mon directeur de thèse, Taniel Danelian, qui a bien voulu m'accorder sa confiance dans la réalisation de ce projet. Mes remerciements vont aussi aux membres de l'équipe de paléontologie du laboratoire EEP pour leur accueil et leur soutien. Merci en particulier à Claude Monnet et Bert van Bocxlaer pour leurs judicieux conseils en fait d'analyses multivariées, à Sylvie Régnier pour m'avoir gardé de l'empoisonnement au xylène, à Jessie Cuvelier pour m'avoir initié aux arcanes de la gestion des collections de paléontologie, et à Rémi Habert pour son infinie patience lors de l'acquisition des données morphométriques. Je remercie enfin les cinq membres du jury pour avoir accepté de relire et d'évaluer ce travail.

Parmi mes complices doctorants et doctorantes, je voudrais adresser toute mon amitié à Eliott et Valentin pour les séances de psy à l'œil, à Laura pour sa gentillesse naturelle et son aimable société chaque midi, à Veronica pour avoir enduré mon mauvais anglais, et à Marie pour n'avoir jamais éludé une discussion sur quelque point de détail mille fois rebattu concernant les radiolaires du Cénozoïque.

Je suis bien entendu redevable envers mes parents, pour leurs encouragements passionnés et pour m'avoir transmis leur curiosité pour la biodiversité sous toutes ses formes. Merci aussi à la costarmoricaine, rencontrée au bord de l'Atlantique et auprès de laquelle j'ai attisé mon amour pour l'Océan.

Enfin, puisque *les derniers seront les premiers*, je dois te remercier Camille d'être apparue dans ma vie et d'avoir rendu cette fin de thèse un peu plus douce.

Table of contents

Chapter I – Introduction

I.1. Rationale

Radiolarians are marine zooplankton, known to be major contributors to oceanic ecosystems and geochemical cycles. They left an abundant and detailed fossil record through the Cenozoic, which is conducive to biostratigraphic and paleoceanographic studies. These extensive geological archives also give a unique opportunity to understand the long-term evolution of plankton and to decipher the impact of past environmental changes on the biosphere. In a world threatened by global changes induced by human activities, it is indeed of paramount importance to characterize how biological systems respond to environmental perturbations in order to better anticipate future upheavals. In this respect, the middle Eocene (ca. 48–38 Ma) is of particular interest, as it represents a critical period in the evolution of the Cenozoic climate system. The general long-term cooling trend that characterized this geological interval was interrupted by several episodes of global warming, the most important of which being the Middle Eocene Climatic Optimum (MECO). This hyperthermal event occurred around 40 Ma and was related to perturbations of the carbon cycle similar to the present-day anthropogenic global warming, making it one of the best deep-time analogs for near-future climates (Burke et al., 2018).

Despite this promising research framework, Eocene radiolarian climate sensitivity is still poorly understood. Indeed, a substantial part of the middle Eocene radiolarian diversity preserved in the fossil record is still not formally described, hindering any accurate depiction of the biotic changes induced by the MECO warming. The first step of this study was therefore to improve the taxonomic resolution of middle Eocene radiolarians by reexamining and documenting at the species level two remarkable radiolarian assemblages preserved in oceanic sediments from ODP Site 1260 (western equatorial Atlantic) and ODP Site 1051 (western subtropical Atlantic). Based on this robust taxonomical framework, radiolarian paleodiversity dynamics and morphological disparity were then examined across the MECO interval, and compared with the established paleoclimatic proxies, to grasp the long-term macroecological impact of climate change on radiolarians.

I.2. Polycystine radiolarians: a biological proxy to deep time

Radiolarians are planktic single-celled eukaryotes, measuring from tens to hundreds of micrometers, although some species are known to form gelatinous colonies up to over 1 m in length (Boltovskoy et al., 2017). These protists are widely distributed in the world's oceans, from the subsurface down to the bathypelagic zone (Suzuki and Not, 2015; Boltovskoy and Correa, 2016). Radiolarian biogeography and abundance are controlled by ocean productivity and nutrient availability, as well as by the physical properties of the water masses, such as temperature and salinity (Boltovskoy, 2017a, 2017b; Boltovskoy et al., 2017). They feed on a large variety of prey, including phytoplankton, bacteria, and crustacean larvae (Anderson, 1978; Matsuoka, 2007), but numerous species are mixotrophs through symbiosis with intracellular eukaryotic microalgae or bacteria (Matsuoka and Anderson, 1992).

From a phylogenetic point of view, radiolarians are classified amongst the infrakingdom Rhizaria, a large group of amoeboid, mostly heterotrophic protists (Cavalier-Smith et al., 2018). With the foraminifera, they form a monophyletic taxon named Retaria, characterized by a peculiar feeding apparatus composed of reticulose (net-like) pseudopodia (Cavalier-Smith et al., 2018). With the exception of acantharians, whose internal skeleton is made of strontium sulfate mineral (Suzuki and Aita, 2011; Decelle and Not, 2015), most of the radiolarian species bear a morphologically complex skeleton of amorphous opaline silica (Anderson, 1983). They are thus deeply involved in the biogeochemical cycles of silica (De Wever et al., 2001; Llopis Monferrer et al., 2020), and their skeletons are commonly preserved in marine sediments. This vast fossil record, stretching back to the early Cambrian (Obut and Iwata, 2000; Pouille et al., 2011; Aitchison et al., 2017), offers advantages for paleoceanographic studies and for dating and correlating siliceous-bearing strata (De Wever et al., 2001).

After the description by Ehrenberg (1839) of the first fossil radiolarian species, Eocene radiolarians were amongst the first to receive sustained attention from micropaleontologists. A total of ~500 Eocene radiolarian species have been described during the nineteenth century from siliceous-rich chalk beds cropping on Barbados Island (Ehrenberg, 1846; 1847; 1874, 1876; Bury, 1862; Bütschli, 1882a, 1882b; Haeckel, 1887; Carter, 1893, 1895, 1896a, 1896b, 1896c, 1896d, 1896e; Sutton, 1896a, 1896b, 1896c, 1896d). However, many of these species have never been observed since their original description, and there are still uncertainties about their stratigraphic range and the precise extent of their intraspecific morphological disparity (Ogane et al., 2009). These taxa strongly deserve to be re-described and re-illustrated to be included in modern radiolarian studies.

In his classic monograph, Haeckel (1887) also introduced the first comprehensive supraspecific classification of Cenozoic radiolarians. However, this first attempt to classify radiolarians was mainly based on external characteristics and geometry rather than biological concepts. This artificial classification led to profound misconceptions about radiolarian evolution, the consequence of which was to consider radiolarians as displaying a high level of evolutionary conservatism, depriving them of any biostratigraphic value. (Danelian et al., 2017). This partly explains the relative paucity of taxonomic work published on Eocene radiolarians during the first half of the 20th century (e.g., Brandt, 1935; Clark and Campbell, 1942, 1945) and the general lack of interest in fossil radiolarian studies during this time interval (Danelian et al., 2017).

The subsequent development of scientific ocean drilling campaigns during the 1960s and 1970s has led to a renewal of interest in Cenozoic radiolarians. The increased recovery of sediments from deep marine environments allowed extensive studies of radiolarian assemblages from all oceanic basins and resulted in the establishment of the first tropical radiolarian biozonation for the Cenozoic (Riedel and Sanfilippo, 1970; Sanfilippo et al., 1985). The accumulation of fossil material has also favored the description of new species and the redescription, according to modern taxonomic standards, of numerous taxa published in early radiolarian studies (e.g., Riedel and Sanfilippo, 1970, 1971, 1978; Petrushevskaya and Kozlova, 1972; Foreman, 1973; Sanfilippo and Riedel, 1973). A few emblematic nassellarian families have also been the subject of detailed taxonomic investigations, leading to the establishment of several evolutionary lineages (e.g., Nigrini, 1977; Sanfilippo and Riedel, 1982, 1992; Sanfilippo and Caulet, 1998). However, the main goal of most of these studies was biostratigraphy, and little attention was paid to rare morphotypes of no biostratigraphic value, or those belonging to taxonomically challenging families. Finally, in spite of their undeniable importance in fossil plankton assemblages, a substantial part of the radiolarian diversity preserved in the fossil record is still not formally described and documented, hindering the expression of their full biostratigraphic and paleoceanographic potential.

I.3. Paleoclimatic context of the study

The Eocene (56–34 Ma) is a pivotal time for the understanding of global changes in Cenozoic climate system (Figure I.1). After the Early Eocene Climatic Optimum (ca. 56–47 Ma; Lourens et al., 2005; Stap et al., 2010; Sexton et al., 2011), during which global temperatures were more than 10°C higher than they are today, the Earth underwent a long-term gradual cooling that culminated in a shift to coolhouse conditions around the Eocene-Oligocene boundary (ca. 34 Ma; Zachos et al., 2008; Westerhold et al., 2020; Hutchinson et al., 2021). This transitional interval was characterized by significant polar glaciation by the early Oligocene, with the formation of nascent ice-sheet in eastern Antarctica (Miller et al., 1987; Zachos et al., 1996; Coxall et al., 2005; Scher et al., 2014).

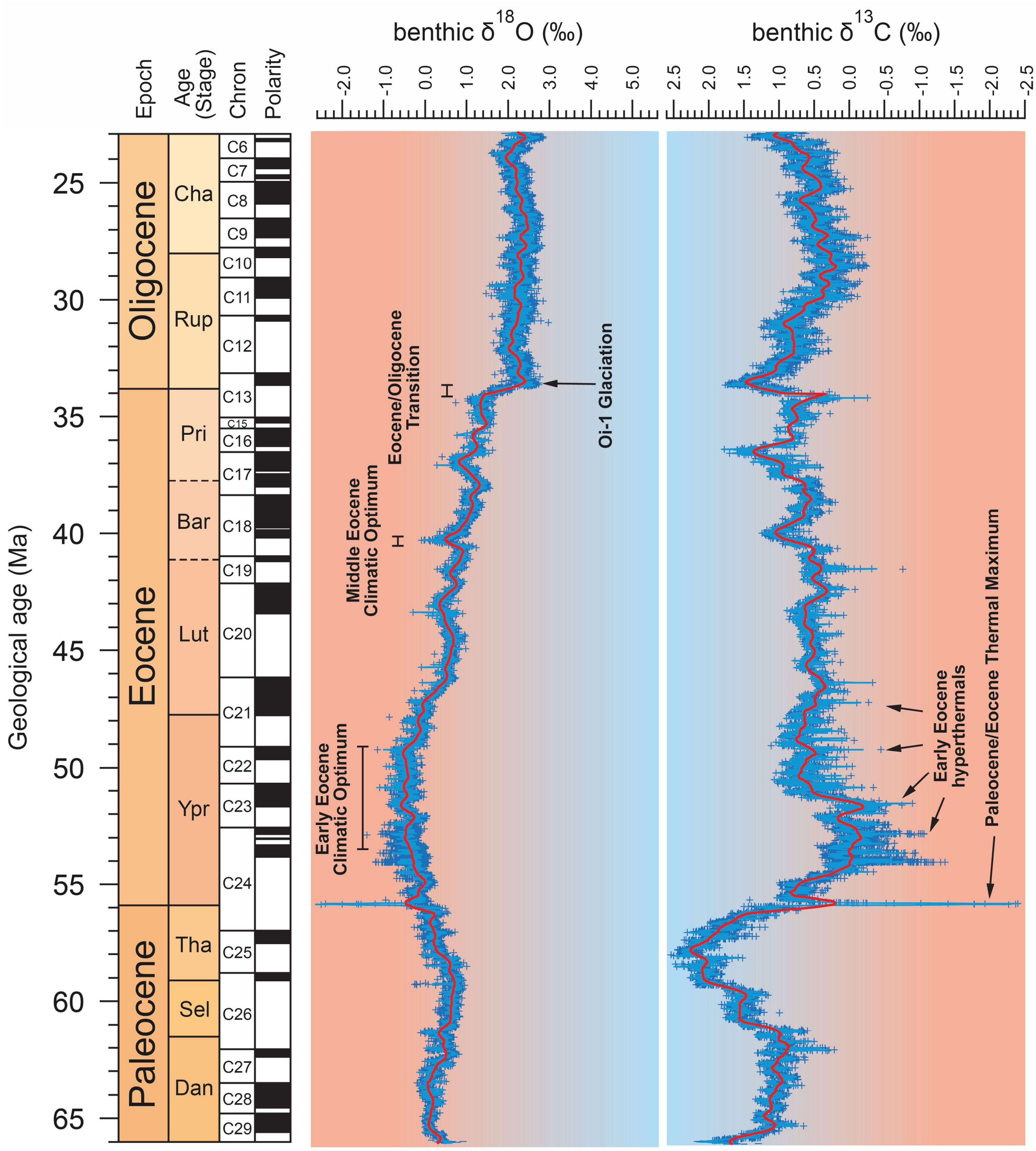

Figure I.1. Variation of geochemical proxies across the Paleogene (66–23 Ma). Stable isotope data and magnetostratigraphy are from Westerhold et al. (2020). Absolute ages for epochs and stages follow Gradstein et al. (2012). Abbreviations: Bar, Bartonian; Cha, Chattian; Dan, Danian; Lut, Lutetian; Oi-1, the first major glacial period in the Oligocene; Pri, Priabonian; Rup, Rupelian; Sel, Selandian; Tha, Thanetian; Ypr, Ypresian.

The middle–late Eocene cooling trend was interrupted by a global warming event and carbon cycle perturbation known as the Middle Eocene Climatic Optimum (MECO; Bohaty and Zachos, 2003; Bohaty et al., 2009; Westerhold and Röhl, 2013). The MECO occurred during the early Bartonian, between 40.45 and 40.05 Ma, and lasted ~400 kyr (Westerhold and Röhl, 2013). It has been recognized in the isotopic record of many marine and continental sections (Figure I.2) as a steady decline of ~1.0–1.5‰ in the oxygen isotope ($\delta^{18}O$) values of both benthic foraminifer and bulk sediments, interpreted as a rise of ~4–6°C in seawater temperature (Bohaty and Zachos, 2003; Bohaty et al., 2009; Bijl et al., 2010).

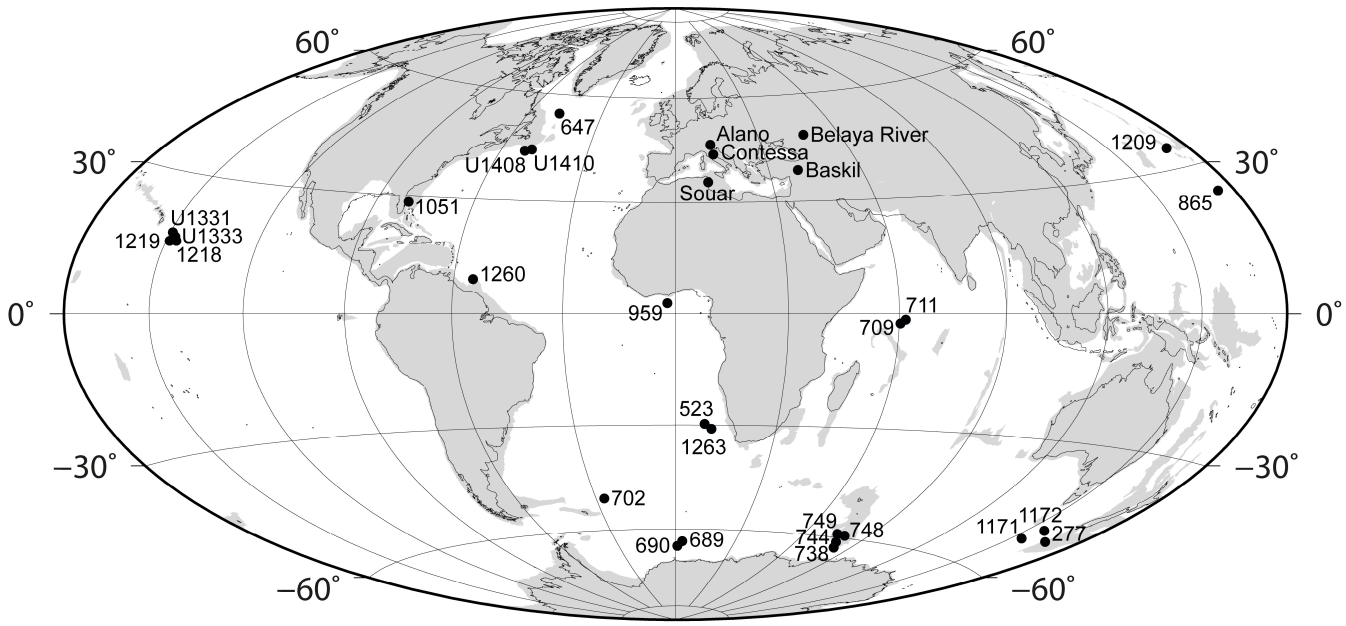

Figure I.2. Actual position of drill sites and sections on land where the Middle Eocene Climatic Optimum (MECO) has been described.

The warmest interval of the MECO is marked by a sharp decrease in $\delta^{18}O$ values at ca. 40 Ma (Westerhold and Röhl, 2013) and is accompanied at some sites by a weak negative excursion (~0.05‰) in carbon isotope ($\delta^{13}C$) values (Giorgioni et al., 2019). The peak warming phase of the MECO lasted less than 100 kyr and was followed by a rapid return to pre-event baseline temperatures (Bohaty et al., 2009; Edgar et al., 2010; Westerhold and Röhl, 2013). The MECO differs from other Paleogene hyperthermal events, such as the Paleocene-Eocene Thermal Maximum (PETM; Kennett and Stott, 1991), by its relatively long duration, the abruptness of its return to pre-event conditions, and the spatial inconsistency of its carbon isotope signature (Giorgioni et al., 2019; Henehan et al., 2020). All these peculiar features make the MECO difficult to interpret, and thus, the actual triggering mechanism of this event still remains poorly understood. Modeling of the carbon cycle suggests an imbalance in long-term carbon fluxes, resulting in an increase of carbon dioxide emissions in the ocean-atmosphere system, which in turn induced ocean acidification through the entire water column and a shoaling of the carbonate saturation profile (Edgar et al., 2007; Bohaty et al., 2009; Sluijs et al., 2013; Cornaggia et al., 2020; Henehan et al., 2020). A favorable orbital configuration, due to a very long eccentricity cycle minimum, has also been put forward to explain the rise of the MECO (Henehan et al., 2020).

The impact of the MECO on oceanic plankton and benthic foraminifera has been extensively studied over the past decade. Significant assemblage changes across the MECO have been shown to occur in the fossil record of several microfossil groups, including planktic and benthic foraminifera (Boscolo Galazzo et al., 2013, 2015; D’Onofrio et al., 2021; Edgar et al., 2013; Luciani et al., 2010; Moebius et al., 2014, 2015), calcareous nannoplankton (Villa et al., 2008; Toffanin et al., 2011), dinocysts (Bijl et al., 2010; Cramwinckel et al., 2019), diatoms (Renaudie et al., 2010; Witkowski et al., 2014) and ebridians (Witkowski et al., 2012). These changes mainly affect the relative abundance and the geographical distribution of species (Lowery et al., 2020). No prominent faunal turnover was observed in any group, suggesting that the magnitude of perturbation of planktic communities reached during the MECO warming did not exceed the threshold to drive extinction. There is also evidence for symbiont ‘bleaching’ in planktic foraminifera induced by the MECO warming, associated with a reduction in average test size (Edgar et al., 2013). However, it is not yet possible to give a general picture of the impact of this warming event on planktic organisms because the available data have a sporadic geographical and bathymetric distribution, and because of irreconcilable discrepancies in paleoproductivity reconstitutions depending on location and studied taxonomic groups (Cramwinckel et al., 2019; Moebius et al., 2015).

Although radiolarians are amongst the major groups of marine plankton, relatively few studies have been conducted on their climate sensitivity and diversity changes in response to the MECO. The MECO warming is known to be associated with an increase in accumulation rates of siliceous plankton (including radiolarians) in the Southern Ocean (Witkowski et al., 2012) and North Atlantic (Witkowski et al., 2014). However, in these two studies, radiolarians were not considered at the species level, hindering any precise interpretation of assemblage changes. Only two species-level radiolarian studies have been conducted previously in relation to the MECO. The first investigated early to middle Eocene radiolarian assemblages from the equatorial Pacific Ocean (IODP Site U1331) and showed a transient decrease in cool-water radiolarian species across the MECO interval (Kamikuri et al., 2013). The second study was carried out on radiolarian-rich sequences from the southwest Pacific Ocean (DSDP Site 277, Campbell Plateau) and highlighted the poleward migration of several tropical radiolarian species to the high latitudes during the MECO (Pascher et al., 2015). However, very few stratigraphic levels were investigated in these studies, and the biodiversity survey was limited to abundant or biostratigraphically important species, which represent only a minute fraction of the total radiolarian fauna.

I.4. Provenance of the studied material

This study is based on chalk samples obtained from archived ocean sediment cores from the low- to mid-latitude North Atlantic Ocean. Two sites were investigated: ODP Site 1260 (western equatorial Atlantic) and ODP Site 1051 (western North Atlantic; Figure I.3).

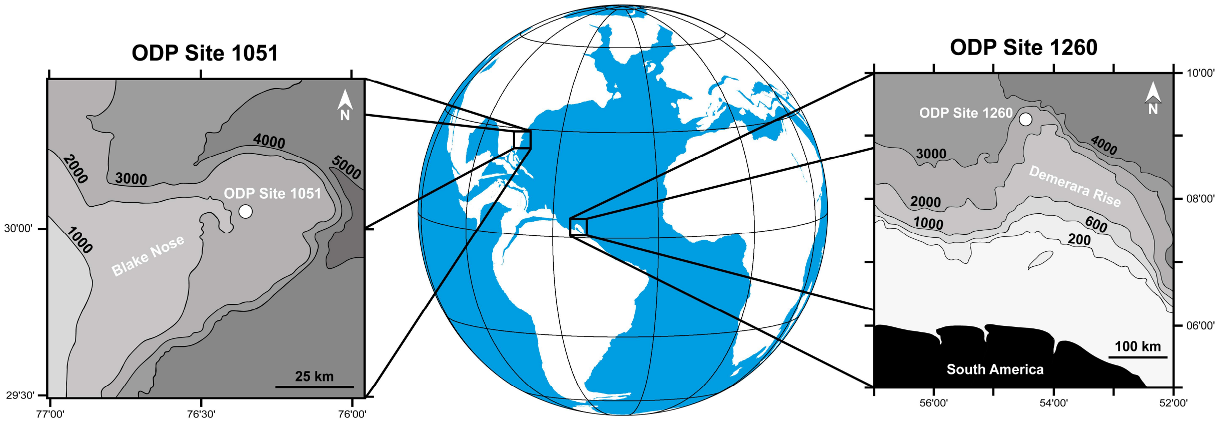

Figure I.3. Middle Eocene (ca. 40 Ma) paleogeographic map showing the location of ODP Site 1051 (Blake Nose, Leg 171B) and ODP Site 1260 (Demerara Rise, Leg 207). Paleogeographic reconstruction drawn after ODSN Plate Tectonic Reconstruction Service (http://www.odsn.de/odsn/services/paleomap/paleomap.html, last access: 31 July 2023).

I.4.1. ODP Site 1260 (western equatorial Atlantic)

ODP Site 1260 (9°16′N, 54°32′W) lies on the north-western margin of Demerara Rise, a submarine plateau stretching along the coast of Surinam and French Guiana (Figure I.3). This site is inferred to have been closer to the equator during the middle Eocene than today, with a paleolatitude of ~1°N (Suganuma and Ogg, 2006). Two holes (1260A and 1260B) were drilled at a modern water depth of 2,549 m below sea level, allowing the recovery of an expanded and nearly continuous Albian–Oligocene sequence (Shipboard Party, 2004). The middle Eocene interval of the site is characterized by nannofossil chalk enriched in biogenic silica, with abundant and diverse radiolarian assemblages (Danelian et al., 2005, 2007), and several other siliceous microfossil groups, including diatoms (Renaudie et al., 2010), ebridians, silicoflagellates and sponge spicules (Figure I.4.A).

Age control for ODP Site 1260 was formerly provided by biostratigraphy (Shipboard Party, 2004) and magnetostratigraphy (Suganuma and Ogg, 2006). However, a high-resolution astronomical framework based on iron (Fe) intensity data was subsequently developed for this site (Westerhold and Röhl, 2013). The orbitally tuned interval corresponds to a 97.26 m thick sequence accumulated between 39.81 and 44 Ma, during the late Lutetian/early Bartonian (sedimentation rate evaluated at ~2.5 cm/kyr). Astrochronological calibration is available every 2 cm of sediment and allows each stratigraphic level to be dated with a high accuracy. For older parts of the radiolarian-rich interval (from 44 Ma to ~44.8 Ma), age-depth models based on magneto-biostratigraphy were used to estimate the age of the samples (Shipboard Party, 2004).

The geochemical framework of ODP Site 1260 is also well-established for the late middle Eocene interval. Notable shifts correlated with the MECO event were recorded in both stable oxygen ($\delta^{18}O$) and carbon ($\delta^{13}C$) isotope records (Bohaty et al., 2009; Edgar et al., 2007). At this site, the onset of the MECO is located around 52 rmcd, in the upper part of magnetochron C18r (Edgar et al., 2007), the benthic foraminiferal $\delta^{18}O$ values subsequently decreased (~1.0 ‰) to reach a minimum during the peak warming interval around 44 rmcd (Edgar et al., 2007; Westerhold and Röhl, 2013). It is noteworthy that the warmest interval of the MECO is also marked at this site by a negative excursion (~0.5‰) in foraminiferal benthic $\delta^{13}C$ values (Edgar et al., 2007). As is usual for this event, the peak warming was followed by a rapid return to pre-event baseline conditions (Bohaty et al., 2009; Edgar et al., 2010; Westerhold and Röhl, 2013). Orbital calibration places the onset of the MECO at 40.50 ± 0.02 Ma, the peak-warming at 40.07 ± 0.02 Ma, and the end of the MECO at 40.05 ± 0.02 Ma (Westerhold and Röhl, 2013).

At ODP Site 1260 we focused on the richest radiolarian interval; a ~147 m-thick sequence ranging from the base of core 20R (~185 rmcd) to the top of core 6R (38.2 rmcd). The base of this sequence lies in the uppermost part of the *Dictyoprora mongolfieri* Zone (RP11; Shipboard Party, 2004), just before the first occurrence of the theoperid species *Eusyringium lagena* (Ehrenberg), which is dated 44.8 Ma in the equatorial Pacific (Kamikuri et al., 2012a). The top of the studied sequence corresponds to the lower part of the *Podocyrtis* (*L.*) *goetheana* Zone (RP16; Shipboard party, 2004), orbitally calibrated at 39.41 Ma (Westerhold and Röhl, 2013).

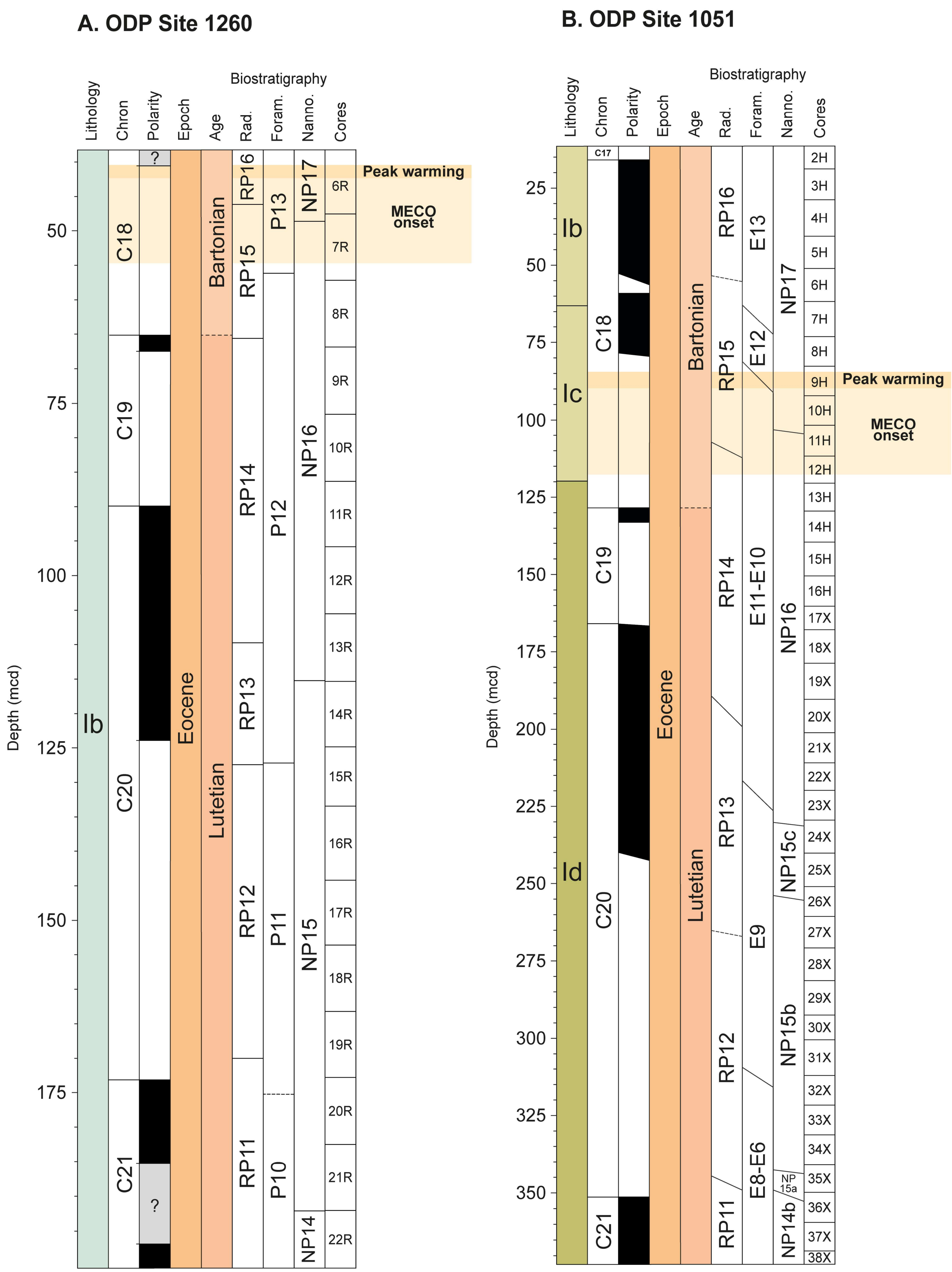
A. ODP Site 1260
B. ODP Site 1051
Biostratigraphy
Lithology
Chron
Polarity
Epoch
Age
Rad.
Foram.
Nanno.
Cores
Depth (mcd)
Peak warming
MECO onset
Eocene
Bartonian
Lutetian
Ib
Ic
Id
C17
C18
C19
C20
C21
RP11
RP12
RP13
RP14
RP15
RP16
P10
P11
P12
P13
E8-E6
E9
E11-E10
E12
E13
NP14
NP14b
NP15
NP15a
NP15b
NP15c
NP16
NP17

Figure I.4. Summary of lithology, magnetostratigraphy, and biostratigraphy of the middle Eocene interval from **A.** ODP Site 1260 (Demerara Rise, Leg 207) and **B.** ODP Site 1051 (Blake Nose, Leg 171B). The lithologic column of ODP Site 1260 is based on data from the Shipboard Party (2004), magnetostratigraphy follows Suganuma and Ogg (2006), and biozonations are after the Shipboard Party (2004), except for radiolarian biozones, which were refined by Meunier and Danelian (2022). Lithologic column of ODP Site 1051 is based on data from Norris et al. (1998), magnetostratigraphy follows Ogg and Bardot (2001), radiolarian biostratigraphy is after Sanfilippo and Blome (2001), calcareous nannofossil biostratigraphy is from Mita (2001) and planktic foraminifera biostratigraphy follows Norris et al. (1998) and Edgar et al. (2010). Abbreviations: mcd, meters composite depth; Nanno., calcareous nannofossils; Foram., planktic foraminifera; Rad., radiolarians.

I.4.2. ODP Site 1051 (western North Atlantic)

ODP Leg 171B drilled five sites on a depth transect across the Blake Nose, a submerged promontory extending on the edge of the Blake Plateau, in the western North Atlantic Ocean (Norris et al., 1998; Figure I.3). ODP Site 1051 (30°03′N, 76°21′W) is located midway along the Blake Nose transect, at an intermediate point in the bathymetric slope profile. Two adjacent holes (1051A and 1051B) were drilled at this site at a modern water depth of ca. 1983 m below sea floor (mbsf; Norris et al., 1998). Hole 1051A was drilled to a depth of 644.6 mbsf, and Hole 1051B was drilled to 526.6 mbsf, providing an expanded and nearly continuous 630 m-thick Paleogene sequence.

The middle Eocene interval of ODP Site 1051 (~370 m-thick) contains mainly oozes and chalks rich in siliceous microfossils, including abundant radiolarians, diatoms and sponge spicules, and a few rare ebridians, silicoflagellates and endoskeletal dinoflagellates (Norris et al., 1998; Sanfilippo and Blome, 2001; Witkowski et al., 2014). The estimated sedimentation rate is ~4 cm/kyr for the middle Eocene sequence of the site (Norris et al., 1998; Edgar et al., 2010), at a paleo-water depth of 1000−2000 m below sea level (lower bathyal; Norris et al., 1998) and at a palaeolatitude of ~25°N (Ogg and Bardot, 2001).

Age control for the middle Eocene interval of ODP Site 1051 is provided by biostratigraphy (Norris et al., 1998; Mita, 2001; Sanfilippo and Blome, 2001; Edgar et al., 2010) and magnetostratigraphy (Ogg and Bardot, 2001). The age-depth models of all Leg 171B sites have recently been updated by Witkowski et al. (2020).

At ODP Site 1051, the MECO is well-defined in stable $\delta^{13}C$ and $\delta^{18}O$ isotope records (Bohaty et al., 2009; Edgar et al., 2010). The onset of the MECO occurs in the upper part of magnetochron C18r, around 118 mcd (Edgar et al., 2010). Then, the benthic foraminiferal $\delta^{18}O$ record gradually decreased, reaching a transient minimum ca. 86 mcd, which also coincides with an abrupt decrease in $\delta^{13}C$ values (Bohaty et al., 2009; Edgar et al., 2010). This minimum is interpreted as the peak warming conditions of the MECO.

The studied sequence at ODP Site 1051 corresponds to the richest and most diverse radiolarian interval, which spans cores 2H to 18X (12.73–174.28 mcd) and was accumulated between 42.7 and 38.53 Ma (Witkowski et al., 2020). The base of the studied sequence lies in the lower part of the *Podocyrtis* (*L.*) *mitra* Zone (RP14), and the upper part of the sequence corresponds to the upper part of the *Podocyrtis* (*L.*) *goetheana* Zone (RP16) (Sanfilippo and Blome, 2001; Figure I.4.B)

I.5. Objectives and thesis structure

The main objectives of this thesis are to quantify the evolution of the taxonomic diversity and morphological disparity of middle Eocene radiolarians across the MECO interval. Diversity and biometric data will be compared with established paleoclimatic proxies to disentangle the long-term macroecological impact of climate change on radiolarian communities.

Chapter II presents the catalog of radiolarian species encountered in the middle Eocene interval from ODP Site 1260 (western equatorial Atlantic) and ODP Site 1051 (western North Atlantic). Unknown morphotypes are not illustrated, only the species already described by previous workers are presented. This biodiversity survey is a necessary prerequisite for the subsequent studies that are presented in Chapters III and IV. Chapter II also contains a contribution to the description of Paleogene radiolarian diversity in the form of two taxonomic articles. This clarification of the middle Eocene radiolarian taxonomic framework also provided an opportunity to conduct a detailed biostratigraphic analysis at ODP Site 1260, which is presented in Chapter III. Our objective was to provide precise calibrations of radiolarian bioevents based on the exceptional cyclostratigraphic framework developed at this site and to assess the reliability of the late middle Eocene radiolarian biozonation by comparing our results with the equatorial Pacific record.

Chapter IV is at the heart of this research project. It is divided into two parts: the first part presents the whole fauna quantitative analysis carried out at ODP Site 1051, which answers these questions: **1** – What are the radiolarian diversity patterns during the MECO? Has global warming led to species turnover/extinction? **2** – Are radiolarian assemblages becoming unstable (e.g., dominance of one or a few species) during the MECO? How do the relative abundances of species vary? **3** – How did climatic and oceanographic changes affect the distribution of fossil radiolarian species? Are cool-water species disappearing during the warmest interval of the MECO? Are tropical species extending their range to higher latitudes? The second part of Chapter IV concerns the impact of the MECO on the morphological disparity of radiolarian shells. This time, the study was focused on a single nassellarian species (*Podocyrtis papalis* Ehrenberg). These questions drive this part of the thesis: **1** – How did the MECO affect the morphological disparity of *Podocyrtis papalis*? **2** – Are periods of increased morphological disparity correlated with periods of rapid environmental change?

Chapter II – Progress on middle Eocene tropical and subtropical radiolarian biodiversity

II.1. Introduction

This taxonomic chapter is divided into two subchapters. First, subchapter **II.2 Systematic paleontology** presents the complete list of all middle Eocene radiolarian species observed during our investigations at ODP Sites 1260 and 1051. A total of 245 taxa are documented from the early Lutetian to the middle Bartonian. This list concerns only the morphospecies that have already been described by previous workers, and for each of them, we provide an image and an exhaustive list of references.

The biodiversity survey conducted at these two sites resulted in the identification of numerous unknown morphotypes that may represent new radiolarian morphospecies. In an effort to improve the taxonomic resolution of the middle Eocene radiolarians, 36 of these unknown morphotypes have been formally described in two papers, which are reproduced as subchapter **II.3. New radiolarian species from ODP Site 1260 (western equatorial Atlantic) and ODP Site 1051 (western North Atlantic)**. We report the discovery of 15 new nassellarian species from ODP Site 1260 (Demerara Rise, western equatorial Atlantic) and 17 nassellarian and four spumellarian species from ODP Site 1051 (Blake Nose, western subtropical Atlantic).

II.2. Systematic paleontology

The supra-generic classification used here is adapted from Riedel (1967a, 1967b), De Wever et al. (2001), and Suzuki et al. (2021).

Infrakingdom Rhizaria Cavalier-Smith, 2002 emend. Cavalier-Smith, 2003
Phylum Retaria Cavalier-Smith, 1999
Class Polycystinea Ehrenberg, 1839
Order Spumellaria Ehrenberg, 1876
Superfamily Hexacromyoidea Haeckel, 1882
Family Hexacaryidae Haeckel, 1882
Genus *Hexancistra* Haeckel, 1879

Type species.— *Hexancistra quadricuspis* Haeckel, 1879, p. 705, pl. 16, fig. 2.

? *Hexancistra tricuspis* Haeckel, 1887
Plate II.1, Figure 1

1887 *Hexancistra* (*Hexancora*) *tricuspis* Haeckel, p. 188, pl. 22, fig. 9.
? 1973 *Astrosphaerin* sp. E Sanfilippo and Riedel, pl. 6, figs. 3, 4 (part).
Occurrence. ODP Site 1260 (Demerara Rise; western equatorial Atlantic).

Superfamily Lithocyclioidea Ehrenberg, 1846
Family Lithocycliidae Ehrenberg, 1846
Genus *Lithocyclia* Ehrenberg, 1846

Type species.— *Lithocyclia ocellus* Ehrenberg, 1854a, pl. 36, fig. 30.

Lithocyclia aristotelis (Ehrenberg, 1847) group
Plate II.1, Figures 4, 5

1847 *Astromma Aristotelis* [sic] Ehrenberg, p. 55, fig. 10.
1854a *Hymeniastrum Pythagorae* [sic] Ehrenberg, pl. 36, fig. 31.
1862 *Hymeniastrum Pythagorae* [sic] Ehrenberg – Haeckel, p. 490.
1862 *Astromma Aristoteles* [sic] Ehrenberg – Bury, pl. 4, fig. 2, pl. 14, figs. 2, 3 (part).
1862 *Astromma* ? Bury, pl. 15, figs. 5, 6 (part).
1873a *Astromma Pythagorae* [sic] Ehrenberg, p. 301.
1873b *Astromma Pythagorae* [sic] Ehrenberg – Ehrenberg, p. 284.
1874 *Astromma Aristotelis* [sic] Ehrenberg – Ehrenberg, p. 217.
1874 *Astromma Pytagorae* [sic] Ehrenberg – Ehrenberg, p. 217.
1876 *Astromma Pythagorae* [sic] Ehrenberg – Ehrenberg, p. 66, pl. 30, fig. 2.
1876 *Astromma Aristotelis* [sic] Ehrenberg – Ehrenberg, p. 66, pl. 30, figs. 3, 4.
1876 *Hymeniastrum Pythagorae* [sic] Ehrenberg – Ehrenberg, p. 76, pl. 30, fig. 5.
1882b *Actinomma Aristotelis* [sic] (Ehrenberg) – Bütschli, pl. 23, fig. 10.
1882b *Hymeniastrum Pythagorae* [sic] Ehrenberg – Bütschli, pl. 23, fig. 11.

1887 *Trigonactura* (*Trigonacturium*) *pythagoræ* [sic] (Ehrenberg) – Haeckel, p. 471.
1887 *Hymenactura* (*Hymenacturium*) *pythagoræ* [sic] (Ehrenberg) – Haeckel, p. 474.
1887 *Hymeniastrum* (*Hymenastrella*) *pythagoræ* [sic] Ehrenberg – Haeckel, p. 531.
1957a *Trigonactura* sp. Riedel, p. 258, pl. 63, fig. 1.
1970 *Lithocyclia aristotelis* (Ehrenberg) group – Riedel and Sanfilippo, p. 522.
1971 *Lithocyclia aristotelis* (Ehrenberg) group – Riedel and Sanfilippo, p. 1588, pl. 3A, figs. 4, 5.
1971 *Lithocyclia aristotelis* (Ehrenberg) group – Moore, p. 737, pl. 4, figs. 4, 5.
1972 *Astractinium aristotelis* (Ehrenberg) group – Petrushevskaya and Kozlova, p. 524, pl. 16, figs. 1–5.
1972 *Trigonactinium pythagorae* (Ehrenberg) – Petrushevskaya and Kozlova, p. 524, pl. 17, fig. 1.
1974 *Lithocyclia aristotelis* (Ehrenberg) group – Nigrini, p. 1065, pl. 2A, fig. 7.
1974 *Lithocyclia aristotelis* (Ehrenberg) group – Johnson, p. 545, pl. 5, figs. 13, 14.
1975 *Lithocyclia aristotelis* (Ehrenberg) group – Ling, p. 725, pl. 3, figs. 7, 8.
1977 *Lithocyclia aristotelis* (Ehrenberg) group – Riedel and Sanfilippo, pl. 10, figs. 2, 3.
1978 *Lithocyclia aristotelis* (Ehrenberg) group – Riedel and Sanfilippo, p. 70, pl. 6, fig. 6.
1986 *Lithocyclia aristotelis* (Ehrenberg) group – Riedel and Sanfilippo, pl. 2, figs. 23, 24.
2006 *Lithocyclia aristotelis* (Ehrenberg) group – Funakawa et al., p. 41, pl. P14, figs. 3a–4b.
2009 *Hymeniastrum pythagorae* Ehrenberg – Ogane et al., pl. 34, figs. 1a–1d.
2009 *Astromma aristotelis* Ehrenberg – Ogane et al., pl. 70, figs. 4a–4c, pl. 71, figs. 1a–2b, 4a–4c, pl. 72, figs. 1a–2c, pl. 73, figs. 1a–1d.
2012 *Lithocyclia aristotelis* (Ehrenberg) group – Moore and Kamikuri, p. 8, pl. P5, figs. 6, 9.
2012a *Lithocyclia aristotelis* (Ehrenberg) group – Kamikuri et al., p. 102, pl. 1, fig. 10.
2015 *Lithocyclia aristotelis* (Ehrenberg) group – Kamikuri, pl. 16, figs. 8–11.
2020 *Lithocyclia aristotelis* (Ehrenberg) – Hollis et al., pl. 2, fig. 9.

Occurrence. ODP Site 1260 (Demerara Rise; western equatorial Atlantic) and ODP Site 1051 (Blake Nose; western north Atlantic).

Lithocyclia ocellus Ehrenberg, 1854a group
Plate II.1, Figures 2, 3

1854a *Lithocyclia Ocellus* [sic] Ehrenberg, pl. 36, fig. 30.
1874 *Lithocyclia Ocellus* [sic] Ehrenberg – Ehrenberg, p. 240.
1874 *Stylocyclia dimidiata* Ehrenberg, p. 257.
1876 *Lithocyclia Ocellus* [sic] Ehrenberg – Ehrenberg, pl. 29, fig. 3.
1876 *Stylocyclia dimidiata* Ehrenberg – Ehrenberg, p. 84, pl. 29, fig. 4.
1882b *Lithocyclia Ocellus* [sic] Ehrenberg – Bütschli, pl. 23, fig. 6.
1887 *Lithocyclia ocellus* Ehrenberg – Haeckel, p. 460.
1887 *Stylocyclia dimidiata* Ehrenberg – Haeckel, p. 462.
1970 *Lithocyclia ocellus* Ehrenberg group – Cita et al., p. 401, pl. 1, fig. C.
1970 *Lithocyclia ocellus* Ehrenberg group – Riedel and Sanfilippo, p. 522, pl. 5, figs. 1, 2.
1971 *Lithocyclia ocellus* Ehrenberg group – Riedel and Sanfilippo, p. 1588, pl. 3A, fig. 6.
1972 *Lithocyclia ocellus* Ehrenberg – Petrushevskaya and Kozlova, p. 523, pl. 15, figs. 1–2.

1973 *Lithocyclia ocellus* Ehrenberg group – Sanfilippo and Riedel, p. 523, pl. 10, figs. 1, 2.
1973 *Lithocyclia ocellus* Ehrenberg group – Riedel and Sanfilippo, p. 739, pl. 2, figs. 7, 8.
1974 *Lithocyclia ocellus* Ehrenberg group – Nigrini, p. 1065, pl. 1D, figs. 3–6.
1975 *Lithocyclia ocellus* Ehrenberg group – Ling, p. 725, pl. 3, fig. 10.
1977 *Lithocyclia ocellus* Ehrenberg group – Riedel and Sanfilippo, pl. 6, fig. 12.
1978 *Lithocyclia ocellus* Ehrenberg group – Weaver and Dinkelman, p. 869, pl. 11, fig. 1.
1978 *Lithocyclia ocellus* Ehrenberg group – Riedel and Sanfilippo, p. 70, pl. 6, fig. 8.
1986 *Lithocyclia ocellus* Ehrenberg group – Riedel and Sanfilippo, pl. 3, figs. 4, 5.
2000 *Lithocyclia ocellus* Ehrenberg group – Nigrini and Sanfilippo, p. 73, pl. 2, figs. 14–17.
2009 *Lithocyclia ocellus* Ehrenberg – Ogane et al., pl. 15, figs. 3a–3c, pl. 32, figs. 2a–3.
2009 *Stylodictya dimidiata* Ehrenberg – Ogane et al., pl. 16, figs. 1a–2c, pl. 17, figs. 1a–3b, pl. 32, figs. 1a–1c.
2012 *Lithocyclia ocellus* Ehrenberg group – Moore and Kamikuri, p. 8, pl. P6, fig. 2.
2012b *Lithocyclia ocellus* Ehrenberg group – Kamikuri et al., p. 4, pl. P2, fig. 6.
2013 *Lithocyclia ocellus* Ehrenberg – Kamikuri et al., pl. 1, fig. 11.
2017 *Lithocyclia ocellus* Ehrenberg – de Souza et al., pl. 1, fig. 3.
2020 *Lithocyclia ocellus* Ehrenberg – Hollis et al., pl. 2, fig. 10.

Occurrence. ODP Site 1260 (Demerara Rise; western equatorial Atlantic) and ODP Site 1051 (Blake Nose; western north Atlantic).

Genus *Heliostylus* Haeckel, 1882

Type species.— *Sethostylus* (*Heliostylus*) *dentatus* Haeckel, 1887, p. 429, pl. 34, fig. 1.

Heliostylus ? *helianthus* (Ehrenberg, 1874)

Plate II.1, Figure 6

1874 *Haliomma Helianthus* [sic] Ehrenberg, p. 235.
1876 *Haliomma Helianthus* [sic] Ehrenberg – Ehrenberg, p. 74, pl. 27, fig. 1.
1887 *Heliodiscus* (*Heliodiscetta*) *helianthus* (Ehrenberg) – Haeckel, p. 446.
2009 *Haliomma helianthus* Ehrenberg – Ogane et al., pl. 15, figs. 1a–2d.

Remarks. This species is tentatively assigned to the genus *Heliostylus* based on its large, lenticular, hollow cortical shell with two polar primary beams and a serrated equatorial girdle.

Occurrence. ODP Site 1260 (Demerara Rise; western equatorial Atlantic).

Family Phacodiscidae Haeckel, 1882

Genus *Periphaena* Ehrenberg, 1874

Type species.— *Periphaena decora* Ehrenberg, 1874, p. 246 (unfigured); Ehrenberg, 1876, p. 80, pl. 28, fig. 6.

Periphaena decora Ehrenberg, 1874

Plate II.1, Figure 7

1874 *Periphaena decora* Ehrenberg, p. 246.
1876 *Periphaena decora* Ehrenberg – Ehrenberg, p. 80, pl. 28, fig. 6.
1882b *Periphaena decora* Ehrenberg – Bütschli, pl. 22, figs. 6a, 6b.
1887 *Periphæna decora* [sic] Ehrenberg – Haeckel, p. 426.

1887 *Periphæna cincta* [sic] Haeckel, p. 426, pl. 33, fig. 4.
1957a *Periphaena decora* Ehrenberg – Riedel, p. 258, pl. 62, fig. 1.
1972 *Periphaena decora* Ehrenberg – Petrushevskaya and Kozlova, p. 523, pl. 14, figs. 1, 2.
1973 *Periphaena decora* Ehrenberg – Sanfilippo and Riedel, p. 523, pl. 8, figs. 8–10, pl. 27, figs. 2–4 (part).
1974 *Periphaena decora* Ehrenberg – Nigrini, p. 1065, pl. 1C, figs. 1, 2, 4, 6 (part).
1975 *Periphaena decora* Ehrenberg – Ling, p. 725, pl. 3, fig. 1 (part).
1977 *Periphaena decora* Ehrenberg – Riedel and Sanfilippo, pl. 6, fig. 9 (part).
1978 *Periphaena decora* Ehrenberg – Weaver and Dinkelman, p. 873, pl. 11, fig. 5.
1992 *Periphaena decora* Ehrenberg – Takemura, p. 743, pl. 6, fig. 8.
1995 *Periphaena decora* Ehrenberg – Strong et al., p. 209, fig. 10J.
1999 *Periphaena heliasteriscus* (Clark and Campbell) – Kozlova, p. 87, pl. 34, fig. 2 (part).
1999 *Periphaena picta* (Kozlova) – Kozlova, p. 174, pl. 16, fig. 4, pl. 19, fig. 12, pl. 40, figs. 10, 12.
2001 *Periphaena cincta* Haeckel – De Wever et al., p. 122, fig. 67.7.
2003 *Periphaena decora* Ehrenberg – Sanfilippo and Fourtanier, p. 12, pl. P2, fig. 26.
2005 *Periphaena decora* Ehrenberg – Funakawa and Nishi, p. 233, pl. 2, fig. 13.
not 2020 *Periphaena decora* Ehrenberg – Hollis et al., pl. 2, fig. 3.
2021 *Periphaena decora* Ehrenberg – de Souza et al., p. 15, pl. 1, fig. 5.

Remarks. This name is used only for specimens with a marginal girdle that is not spinous.

Occurrence. ODP Site 1260 (Demerara Rise; western equatorial Atlantic) and ODP Site 1051 (Blake Nose; western north Atlantic).

Periphaena delta Sanfilippo and Riedel, 1973
Plate II.1, Figure 8

1973 *Periphaena delta* Sanfilippo and Riedel, p. 523, pl. 8, figs. 11, 12, pl. 27, figs. 6, 7.
1974 *Periphaena delta* Sanfilippo and Riedel – Nigrini, p. 1065, pl. 1C, fig. 7.
1977 *Periphaena delta* Sanfilippo and Riedel – Riedel and Sanfilippo, pl. 5, fig. 12.
1978 *Periphaena delta* Sanfilippo and Riedel – Riedel and Sanfilippo, p. 71, pl. 7, fig. 9.
1986 *Periphaena delta* Sanfilippo and Riedel – Riedel and Sanfilippo, pl. 3, fig. 3.

Occurrence. ODP Site 1260 (Demerara Rise; western equatorial Atlantic).

Periphaena heliasteriscus (Clark and Campbell, 1942)
Plate II.1, Figure 9

1942 *Heliodiscus* (*Heliodiscetta*) *heliasteriscus* Clark and Campbell, p. 39, pl. 3, figs. 10, 11.
1958 *Heliosestrum craspedotum* Haeckel – Göke, pl. 2, fig. 1.
1973 *Periphaena heliasteriscus* (Clark and Campbell) – Riedel and Sanfilippo, p. 523, pl. 9, figs. 1–6, pl. 27, figs. 8, 9.
1975 *Periphaena decora* Ehrenberg – Ling, p. 725, pl. 3, fig. 2 (part).
1976 *Heliodiscus heliasteriscus* Clark and Campbell – Dzinoridze et al., pl. 24, fig. 9.
1976 *Heliodiscus perplexus* Clark and Campbell – Dzinoridze et al., pl. 24, fig. 8.
not 1993 *Heliodiscus heliasteriscus* Clark and Campbell – Vitukhin, pl. 7, fig. 1.
1995 *Periphaena heliasteriscus* (Clark and Campbell) – Strong et al., p. 209, figs. 10H, 10I.

1999a *Periphaena heliasteriscus* (Clark and Campbell) – O'Connor, p. 34, pl. 10, fig. 17.
1999 *Periphaena heliasteriscus* (Clark and Campbell) – Kozlova, p. 87, pl. 34, figs. 11, 12, pl. 40, fig. 4 (part).
2008 *Periphaena heliasteriscus* (Clark and Campbell) – Jackett et al., p. 57, pl. 4, fig. 14.
2009b *Heliodiscus perplexus* Clark and Campbell – Suzuki et al., p. 247, pl. 3, fig. 11.
2015 *Heliodiscus heliasteriscus* Clark and Campbell – Kamikuri, pl. 16, fig. 2.
2020 *Periphaena heliasteriscus* (Clark and Campbell) – Hollis et al., pl. 2, fig. 4.
Occurrence. ODP Site 1260 (Demerara Rise; western equatorial Atlantic).

Periphaena humboldtii (Ehrenberg, 1847)
Plate II.1, Figure 10

1847 *Haliomma Humboldtii* [sic] Ehrenberg, p. 55, fig. 8.
1854a *Haliomma Humboldtii* [sic] Ehrenberg – Ehrenberg, pl. 36, fig. 27.
1862 *Heliodiscus humboldti* [sic] (Ehrenberg) – Haeckel, p. 438.
1876 *Haliomma Humboldtii* [sic] Ehrenberg – Ehrenberg, p. 74, pl. 27, fig. 3.
1887 *Heliodiscus* (*Heliodiscomma*) *cingillum* Haeckel, p. 448, pl. 33, fig. 7.
1887 *Heliodiscus* (*Heliodiscomma*) *humboldti* [sic] (Ehrenberg) – Haeckel, p. 449.
1957a *Heliodiscus humboldtii* (Ehrenberg) – Riedel, p. 258, pl. 62, fig. 2.
1973 *Periphaena decora* Ehrenberg – Sanfilippo and Riedel, p. 523, pl. 27, fig. 5 (part).
1974 *Periphaena decora* Ehrenberg – Nigrini, p. 1065, pl. 1C, figs. 3, 5, pl. 2A, fig. 3 (part).
1977 *Periphaena decora* Ehrenberg – Riedel and Sanfilippo, pl. 5, fig. 13 (part).
1986 *Periphaena* sp. Riedel and Sanfilippo, pl. 3, fig. 14.
1986 *Heliodiscus humboldti* [sic] (Ehrenberg) – Göke, fig. 3.5.
2003 *Periphaena heliasteriscus* (Clark and Campbell) – Sanfilippo and Fourtanier, p. 12, pl. P2, fig. 27.
2009 *Haliomma humboldtii* Ehrenberg – Ogane et al., pl. 30, figs. 5a–5d, pl. 31, figs. 3a, 3b, 5a, 5b, pl. 68, figs. 2a–2f, pl. 69, figs. 3a–3d.
2021 *Periphaena heliasteriscus* (Clark and Campbell) – de Souza et al., p. 15, pl. 1, fig. 6.
Occurrence. ODP Site 1260 (Demerara Rise; western equatorial Atlantic) and ODP Site 1051 (Blake Nose; western north Atlantic).

Periphaena pentasteriscus (Clark and Campbell, 1942)
Plate II.1, Figure 11

1942 *Heliodiscus* (*Heliodiscetta*) *pentasteriscus* Clark and Campbell, p. 39, pl. 3, fig. 8.
1972 *Heliodiscus pentasteriscus* Clark and Campbell – Petrushevskaya and Kozlova, p. 523, pl. 13, figs. 6, 7.
Remarks. Cortical shell lenticular, smooth, with very small and dense pores.
Occurrence. ODP Site 1260 (Demerara Rise; western equatorial Atlantic).

Periphaena tripyramis triangula (Sutton, 1896a)
Plate II.1, Figure 12

1896a *Phacotriactis triangula* Sutton, p. 61.

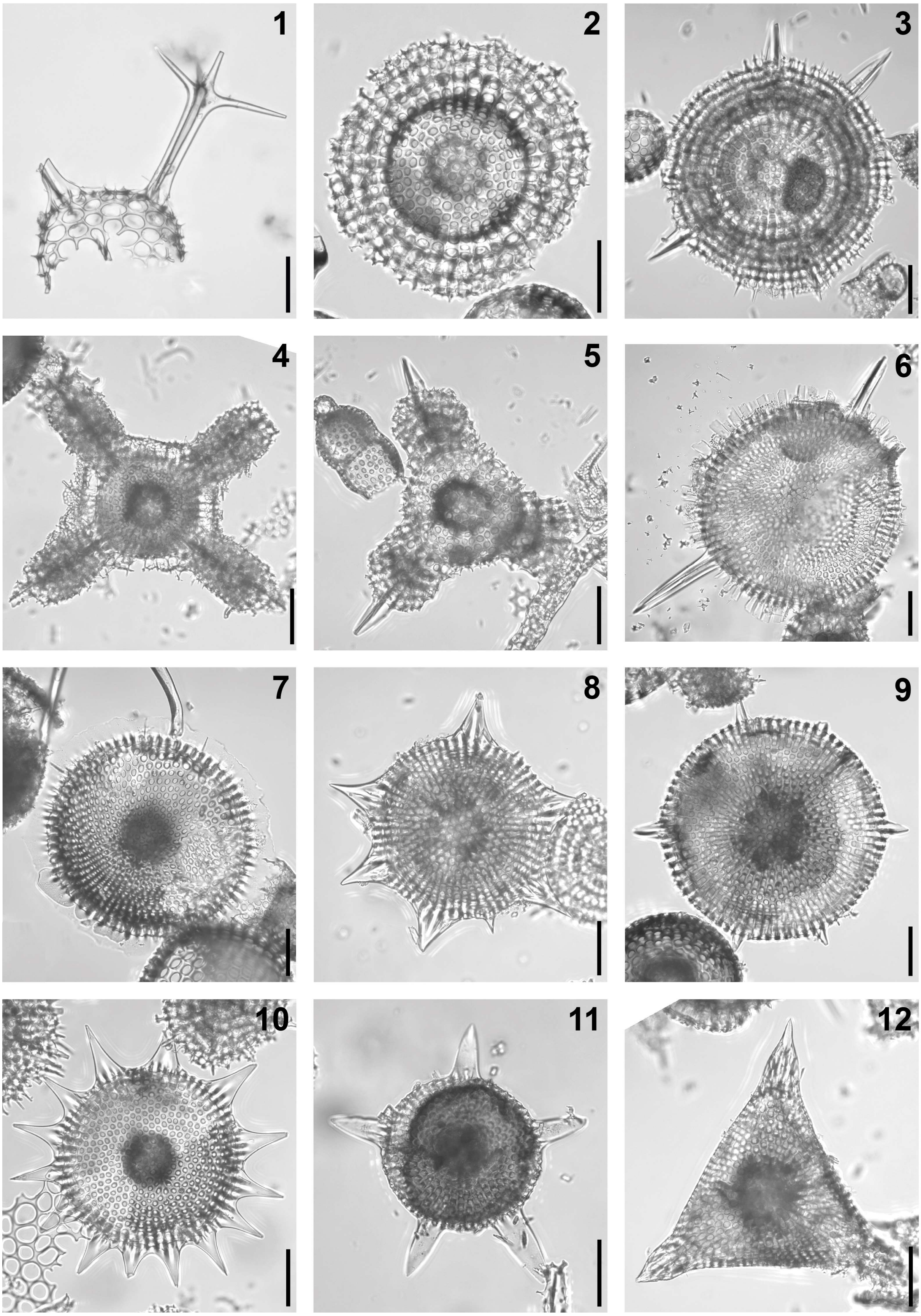
1
2
3
4
5
6
7
8
9
10
11
12

Plate II.1. Composite light micrographs of new radiolarian species from ODP Site 1260 (Demerara Rise, western equatorial Atlantic) and ODP Site 1051 (Blake Nose, western North Atlantic). (**1**) ? *Hexancistra tricuspis* Haeckel, 1887: ODP 1260A-6R-2W, 55–57 cm. (**2, 3**) *Lithocyclia ocellus* Ehrenberg, 1854a group: (**2**) ODP 1260A-9R-5W, 55–57 cm; (**3**) ODP 1260A-10R-1W, 55–57 cm. (**4, 5**) *Lithocyclia aristotelis* (Ehrenberg, 1847) group: (**4**) ODP 1260A-6R-1W, 55–57 cm; (**5**) ODP 1260A-6H-1W, 55–57 cm. (**6**) *Heliostylus* ? *helianthus* (Ehrenberg, 1874): ODP 1260A-13H-1W, 54–56 cm. (**7**) *Periphaena decora* Ehrenberg, 1874: ODP 1260A-17R-CC, 63–177 cm. (**8**) *Periphaena delta* Sanfilippo and Riedel, 1973: ODP 1260A-15R-1W, 55–57 cm. (**9**) *Periphaena heliasteriscus* (Clark and Campbell, 1942): ODP 1260A-6H-CC, 63–177 cm. (**10**) *Periphaena humboldtii* (Ehrenberg, 1847): ODP 1260A-13H-5W, 54–56 cm. (**11**) *Periphaena pentasteriscus* (Clark and Campbell, 1942): ODP 1260A-6H-2W, 55–57 cm. (**12**) *Periphaena tripyramis triangula* (Sutton, 1896a): ODP 1260A-20R-5W, 55–57 cm. All scale bars equal 50 µm.

1970 *Triactis tripyramis triangula* (Sutton) – Riedel and Sanfilippo, p. 521, pl. 4, figs. 9, 10.
1971 *Triactis tripyramis triangula* (Sutton) – Moore, p. 737, pl. 1, fig. 9.
1973 *Periphaena tripyramis triangula* (Sutton) – Riedel and Sanfilippo, p. 523, pl. 9, figs. 10, 11.
1974 *Periphaena tripyramis triangula* (Sutton) – Nigrini, p. 1065, pl. 1D, figs. 1, 2.
1975 *Periphaena tripyramis triangula* (Sutton) – Ling, p. 725, pl. 3, fig. 3.
1977 *Periphaena tripyramis triangula* (Sutton) – Riedel and Sanfilippo, pl. 6, fig. 10.
1986 *Phacotriactis triangula* Sutton – Göke, fig. 5.
2008 *Periphaena tripyramis triangula* (Sutton) – Jackett et al., p. 57, pl. 4, fig. 15.
2012b *Periphaena tripyramis triangula* (Sutton) – Kamikuri et al., p. 4, pl. P2, fig. 5.
Occurrence. ODP Site 1260 (Demerara Rise; western equatorial Atlantic).

Genus *Phacodiscus* Haeckel, 1882

Type species.— *Phacodiscus* (*Phacodiscinus*) *rotula* Haeckel, 1887, p. 424, pl. 35, fig. 7.

Phacodiscus echinatus (Ehrenberg, 1874)

Plate II.2, Figures 1a, 1b

1874 *Haliomma echinatum* Ehrenberg, p. 234.
1876 *Haliomma echinatum* Ehrenberg – Ehrenberg, p. 74, pl. 27, fig. 2.
1887 *Sethodiscus* (*Sethodisculus*) *echinatus* (Ehrenberg) – Haeckel, p. 424.
2009 *Haliomma echinatum* Ehrenberg – Ogane et al., pl. 30, figs. 1a–3b.
2019 *Thecosphaerella tochilinae* Vasilenko, p. 329, pl. 1, figs. 7a–8b.
Remarks. The combination used here is derived from O'Dogherty et al. (2021).
Occurrence. ODP Site 1051 (Blake Nose; western north Atlantic).

Superfamily Spongodiscoidea Haeckel, 1862

Family Spongodiscidae Haeckel, 1862

Genus *Spongodiscus* Ehrenberg, 1854b

Type species.— *Spongodiscus resurgens* Ehrenberg, 1854b, p. 246 (unfigured); Ehrenberg, 1854a, pl. 35B, fig. 16.

Spongodiscus communis Clark and Campbell, 1942

Plate II.2, Figure 2

1942 *Spongodiscus* (*Spongocyclia*) *communis* Clark and Campbell, p. 47, pl. 2, figs. 1, 11, 13, 14, pl. 3, figs. 1, 4.

? 1974 *Spongaster* aff. *communis* Clark and Campbell – Nigrini, p. 1066, pl. 6, fig. 5.

1988 *Spongodiscus communis* Clark and Campbell – Blueford, p. 252, pl. 7, figs. 4, 5.

1976 *Stylospongia communis* (Clark and Campbell) – Dzinoridze et al., pl. 25, figs. 6, 8, 9.

1999 *Spongotrochus* ? *pulcher* (Clark and Campbell) – Kozlova, p. 95, pl. 9, fig. 7.

1999 *Spongotrochus paciferus* (Lipman) – Kozlova, pl. 13, fig. 10.

not 2009b *Spongodiscus communis* Clark and Campbell – Suzuki et al., p. 252, pl. 13, figs. 9a–12b.

2009b *Flustrella* sp. B Suzuki et al., p. 252, pl. 15, figs. 1a, 1b, 3a–6b (part).

not 2015 *Spongodiscus communis* Clark and Campbell – Kamikuri, pl. 16, fig. 14.

Occurrence. ODP Site 1260 (Demerara Rise; western equatorial Atlantic) and ODP Site 1051 (Blake Nose; western north Atlantic).

Spongodiscus rhabdostylus (Ehrenberg, 1874)

Plate II.2, Figure 3

1874 *Spongosphaera rhabdostyla* Ehrenberg, p. 256.

1876 *Spongosphaera rhabdostyla* Ehrenberg – Ehrenberg, p. 82, pl. 26, figs. 1, 2.

1887 *Stylotrochus* (*Stylotrochiscus*) *rhabdostylus* (Ehrenberg) – Haeckel, p. 584.

1973 *Spongodiscus rhabdostylus* (Ehrenberg) – Sanfilippo and Riedel, p. 525, pl. 13, figs. 1–3, pl. 30, figs. 1, 2.

1974 *Spongodiscus rhabdostylus* (Ehrenberg) – Nigrini, p. 1066, pl. 1E, figs. 1–3.

1977 *Spongodiscus rhabdostylus* (Ehrenberg) – Riedel and Sanfilippo, pl. 6, fig. 11, pl. 9, fig. 2.

not 1978 *Spongodiscus rhabdostylus* (Ehrenberg) – Weaver and Dinkelman, p. 873, pl. 11, fig. 3.

1999a *Spongodiscus rhabdostylus* (Ehrenberg) – O’Connor, p. 38, pl. 8, fig. 14.

1999a *Spongodiscus* aff. *rhabdostylus* (Ehrenberg) – O’Connor, p. 38, pl. 10, fig. 21.

2008 *Spongodiscus rhabdostylus* (Ehrenberg) group – Jackett et al., p. 58, pl. 4, fig. 19 (part).

2009 *Spongosphaera rhabdostyla* Ehrenberg – Ogane et al., pl. 33, figs. 1a–1c, pl. 68, figs. 1a–1c.

2009b *Spongodiscus rhabdostyla* (Ehrenberg) – Suzuki et al., p. 251, pl. 13, figs. 1a–3c.

2015 *Spongodiscus rhabdostylus* (Ehrenberg) – Kamikuri, pl. 17, figs. 11–13.

2020 *Spongodiscus rhabdostylus* (Ehrenberg) – Hollis et al., pl. 2, fig. 17.

2021 *Spongodiscus rhabdostylus* (Ehrenberg) – de Souza et al., p. 15, pl. 1, fig. 8.

Occurrence. ODP Site 1260 (Demerara Rise; western equatorial Atlantic) and ODP Site 1051 (Blake Nose; western north Atlantic).

Superfamily Trematodiscoidea Haeckel, 1862
Family Trematodiscidae Haeckel, 1862
Genus *Flustrella* Ehrenberg, 1839

Type species.— *Flustrella concentrica* Ehrenberg, 1839, p. 132 (unfigured); Ehrenberg, 1854a, pl. 20, fig. 42.

Flustrella concentrica Ehrenberg, 1839
Plate II.2, Figure 4

1839 *Flustrella concentrica* Ehrenberg, p. 132.
1854a *Flustrella concentrica* Ehrenberg – Ehrenberg, pl. 20, fig. 42.
1876 *Flustrella concentrica* Ehrenberg – Ehrenberg, p. 72, pl. 22, fig. 13.
1976 *Porodiscus* ? *parvus* Clark and Campbell group – Dzinoridze et al., pl. 36, figs. 8–14, pl. 39, figs. 4, 5 (part).
2009 *Flustrella concentrica* Ehrenberg – Ogane et al., pl. 66, figs. 3a–3c.
2009b *Flustrella parva* (Clark and Campbell) – Suzuki et al., p. 252, pl. 12, figs. 1–5.

Occurrence. ODP Site 1260 (Demerara Rise; western equatorial Atlantic) and ODP Site 1051 (Blake Nose; western north Atlantic).

Flustrella ? *spirale* (Ehrenberg, 1874)
Plate II.2, Figure 5

1874 *Perichlamydium* ? *spirale* Ehrenberg, p. 245.
1876 *Perichlamydium* ? *spirale* Ehrenberg – Ehrenberg, p. 80, pl. 22, fig. 12.
1887 *Perichlamydium spirale* Ehrenberg – Haeckel, p. 499.
? 1977 Litheliid ? gen. and sp. indet. Riedel and Sanfilippo, pl. 11, fig. 15.
2009 *Perichlamydium* ? *spirale* Ehrenberg – Ogane et al., pl. 14, figs. 1a–1d.

Occurrence. ODP Site 1051 (Blake Nose; western north Atlantic).

Genus *Stylodictya* Ehrenberg, 1846

Type species.— *Stylodictya gracilis* Ehrenberg, 1854a, pl. 36, fig. 28; see Haeckel, 1862, p. 499 for the description.

Stylodictya inaequalispina Clark and Campbell, 1942
Plate II.2, Figure 6

1942 *Stylodictya* (*Stylodictyon*) *inaequalispina* Clark and Campbell, p. 45, pl. 3, fig. 5.
1972 *Stylodictya inaequalispina* Clark and Campbell – Petrushevskaya and Kozlova, p. 526, pl. 18, fig. 8.
2015 *Stylodictya inaequalispina* Clark and Campbell – Kamikuri, pl. 17, fig. 15.

Occurrence. ODP Site 1260 (Demerara Rise; western equatorial Atlantic) and ODP Site 1051 (Blake Nose; western north Atlantic).

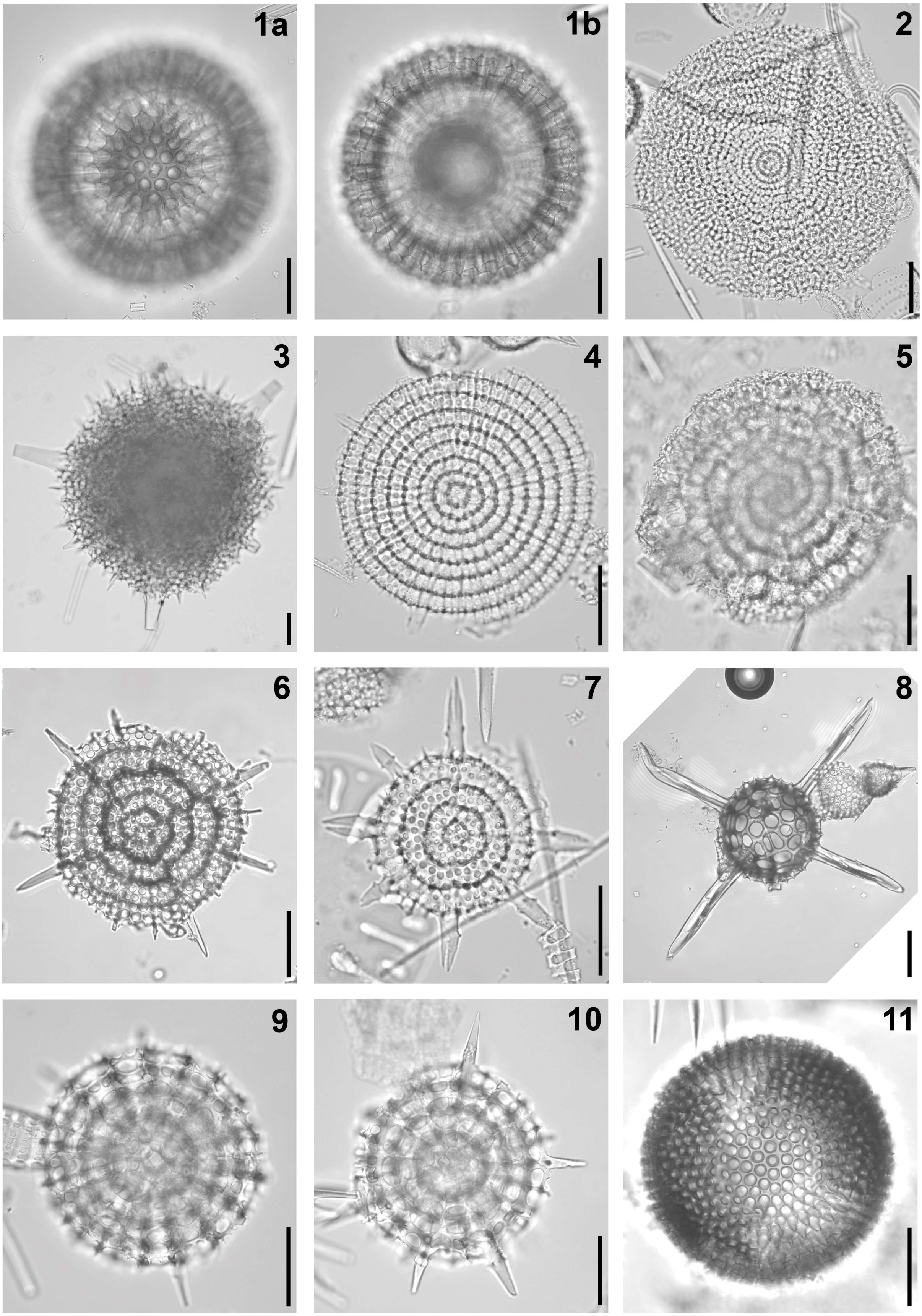
1a
1b
2
3
4
5
6
7
8
9
10
11

Plate II.2. Composite light micrographs of new radiolarian species from ODP Site 1260 (Demerara Rise, western equatorial Atlantic) and ODP Site 1051 (Blake Nose, western North Atlantic). (**1a, 1b**) *Phacodiscus echinatus* (Ehrenberg, 1874): ODP 1051A-16H-5W, 55–57 cm. (**2**) *Spongodiscus communis* Clark and Campbell, 1942: ODP 1051A-9H-2W, 53–55 cm. (**3**) *Spongodiscus rhabdostylus* (Ehrenberg, 1874): ODP 1051A-2H-5W, 55–57 cm. (**4**) *Flustrella concentrica* Ehrenberg, 1839: ODP 1051A-9H-2W, 53–55 cm. (**5**) *Flustrella* ? *spirale* (Ehrenberg, 1874): ODP 1051A-8H-5W, 53–55 cm. (**6**) *Stylodictya inaequalispina* Clark and Campbell, 1942: ODP 1260A-6R-2W, 55–57 cm. (**7**) *Stylodictya hastata* Ehrenberg, 1874: ODP 1051A-9H-2W, 53–55 cm. (**8**) *Actinomma* ? *megaxyphos tetraxyphos* (Clark and Campbell, 1942): ODP 1260A-10R-5W, 55–57 cm. (**9, 10**) *Cromyosphaera* ? *fulgurans* Tetard et al., 2023: (**9**) ODP 1051A-9H-5W, 53–55 cm; (**10**) ODP 1051A-9H-5W, 53–55 cm. (**11**) *Haliomma eocenica* Clark and Campbell, 1945: ODP 1260A-9R-3W, 55–57 cm. All scale bars equal 50 µm.

Stylodictya hastata Ehrenberg, 1874

Plate II.2, Figure 7

1862 *Stylodictya gracilis* Ehrenberg – Bury, pl. 2, fig. 1.
1874 *Stylodictya hastata* Ehrenberg, p. 257.
1876 *Stylodictya hastata* Ehrenberg – Ehrenberg, p. 84, pl. 23, fig. 5.
1887 *Stylodictya* (*Stylodictyon*) *hastata* Ehrenberg – Haeckel, p. 510.
1976 *Stylodictya hastata* Ehrenberg – Dzinoridze et al., pl. 25, fig. 2.
2009 *Stylodictya hastata* Ehrenberg – Ogane et al., pl. 5, figs. 1a–1c.

Occurrence. ODP Site 1051 (Blake Nose; western north Atlantic).

Superfamily Haliommoidea Ehrenberg, 1846

Family Actinommidae Haeckel, 1862

Genus *Actinomma* Haeckel, 1861

Type species.— *Actinomma trinacrium* Haeckel, 1861, p. 815 (unfigured); Haeckel, 1862, p. 441, pl. 24, fig. 6.

Actinomma ? *megaxyphos tetraxyphos* (Clark and Campbell, 1942)

Plate II.2, Figure 8

1942 *Stylosphaera* (*Stylosphaerantha*) *megaxyphos tetraxyphos* Clark and Campbell, p. 26, pl. 6, figs. 1, 8.
? 1977 Actinommid gen. et sp. indet. Riedel and Sanfilippo, pl. 1, fig. 6.

Remarks. The combination used here is derived from O'Dogherty et al. (2021).

Occurrence. ODP Site 1260 (Demerara Rise; western equatorial Atlantic).

Family Haliommidae Ehrenberg, 1846

Genus *Cromyosphaera* Haeckel, 1882

Type species.— *Cromyosphaera quadruplex* Haeckel, 1887, p. 84, pl. 30, figs. 9, 9a.

Cromyosphaera ? *fulgurans* Tetard et al., 2023
Plate II.2, Figures 9, 10

2023 *Cromyosphaera fulgurans* Tetard et al., p. 9, figs. 4r–4u, 6a–6f.

Occurrence. ODP Site 1260 (Demerara Rise; western equatorial Atlantic) and ODP Site 1051 (Blake Nose; western north Atlantic).

Genus *Haliomma* Ehrenberg, 1839

Type species.— *Haliomma medusa* Ehrenberg, 1839, p. 130 (unfigured); Ehrenberg, 1854a, pl. 22, figs. A34, B34.

Haliomma eocenica Clark and Campbell, 1945
Plate II.2, Figure 11

1945 *Cenosphaera* (*Circosphaera*) *eocenica* Clark and Campbell, p. 7, pl. 1, figs. 4 (part).
1988 *Cenosphaera eocenica* Clark and Campbell – Blueford, p. 247, pl. 3, figs. 4, 5.
1999 *Thecosphaerella eocenica* (Clark and Campbell) – Kozlova, p. 78, pl. 6, fig. 4, pl. 7, fig. 5, pl. 19, fig. 8, pl. 32, fig. 6.
2015 *Cenosphaera eocenica* Clark and Campbell – Kamikuri, pl. 15, figs. 7a, 7b.

Remarks. The genus *Cenosphaera* has been synonymized with the genus *Haliomma* by Suzuki et al. (2021, p. 438).

Occurrence. ODP Site 1260 (Demerara Rise; western equatorial Atlantic) and ODP Site 1051 (Blake Nose; western north Atlantic).

Haliomma rotunda (Borisenko, 1960)
Plate II.3, Figures 1a, 1b

1960 *Thecosphaera rotunda* Borisenko, p. 222, pl. 1, figs. 3a, 3b, v, pl. 3, figs. 2a–3b.
1973 *Thecosphaerella rotunda* (Borisenko) – Sanfilippo and Riedel, p. 522, pl. 3, figs. 7–11, pl. 26, fig. 3.
1999 *Thecosphaerella rotunda* (Borisenko) – Kozlova, p. 80, pl. 7, figs. 1, 2, pl. 11, figs. 1, 2, pl. 27, figs. 1, 4.
2015 *Thecosphaerella rotunda* (Borisenko) – Kamikuri, pl. 14, figs. 9a–11b.

Remarks. The genus *Thecosphaera* has been synonymized with the genus *Haliomma* by Petrushevskaya (1975, p. 568).

Occurrence. ODP Site 1260 (Demerara Rise; western equatorial Atlantic) and ODP Site 1051 (Blake Nose; western north Atlantic).

Family Heliodiscidae Haeckel, 1882 sensu De Wever et al., 2001
Genus *Excentrodiscus* Hollande and Enjumet, 1960

Type species.— *Excentrodiscus echinatus* Hollande and Enjumet, 1960, p. 125, pl. 62, fig. 3.

Excentrodiscus ? *entactinia* (Ehrenberg, 1874)
Plate II.3, Figures 2a, 2b

1874 *Haliomma Entactinia* [sic] Ehrenberg, p. 235.
1876 *Haliomma Entactinia* [sic] Ehrenberg – Ehrenberg, p. 74, pl. 26, fig. 4.

1887 *Carposphæra* (*Cerasosphæra*) *entactinia* [sic] Ehrenberg – Haeckel, p. 74.
? 1993 *Haliomma* ? aff. *extima* Petrushevskaya – Vitukhin, pl. 13, figs. 3a, 3b.
2009 *Haliomma entactinia* Ehrenberg – Ogane et al., pl. 1, figs. 5a–5d (part).
Remarks. This species is tentatively assigned to the genus *Excentrodiscus* based on its double medullary shell with an eccentric microsphere (Plate II.3, Figure 2b).
Occurrence. ODP Site 1260 (Demerara Rise; western equatorial Atlantic) and ODP Site 1051 (Blake Nose; western north Atlantic).

Excentrodiscus kamikurii Dumitrică, 2019
Plate II.3, Figure 4

2019 *Excentrodiscus kamikurii* Dumitrică, p. 53, figs. 9f, 9g.
Occurrence. ODP Site 1051 (Blake Nose; western north Atlantic).

Genus *Heliodiscus* Haeckel, 1862

Type species.— *Haliomma phacodiscus* Haeckel, 1861, p. 815 (unfigured); Haeckel, 1862, p. 437, pl. 17, fig. 5.

Heliodiscus contiguus (Ehrenberg, 1874)
Plate II.1, Figure 3

1874 *Haliomma contiguum* Ehrenberg, p. 234.
1876 *Haliomma contiguum* Ehrenberg – Ehrenberg, p. 74, pl. 27, fig. 5.
1882b *Heliodiscus contiguus* (Ehrenberg) – Bütschli, pl. 22, figs. 5a, 5b.
1887 *Heliosestrum* (*Heliosestantha*) *contiguum* (Ehrenberg) – Haeckel, p. 439.
2003 *Heliodiscus inca* Clark and Campbell – Sanfilippo and Fourtanier, p. 12, pl. P1, fig. 6.
2009 *Haliomma contiguum* Ehrenberg – Ogane et al., pl. 31, figs. 1a–2b.
Occurrence. ODP Site 1260 (Demerara Rise; western equatorial Atlantic) and ODP Site 1051 (Blake Nose; western north Atlantic).

Heliodiscus umbonatus (Ehrenberg, 1874)
Plate II.2, Figure 5

1874 *Haliomma umbonatum* Ehrenberg, p. 236.
1876 *Haliomma umbonatum* Ehrenberg – Ehrenberg, p. 74, pl. 27, fig. 4.
1887 *Heliodiscus* (*Heliodiscomma*) *umbonatus* (Ehrenberg) – Haeckel, p. 449.
2009 *Haliomma umbonatum* Ehrenberg – Ogane et al., pl. 14, figs. 5a–5d.
Occurrence. ODP Site 1260 (Demerara Rise; western equatorial Atlantic) and ODP Site 1051 (Blake Nose; western north Atlantic).

Superfamily Lithelioidea Haeckel, 1862 sensu Matsuzaki et al., 2015
Family Litheliidae Haeckel, 1862 emend. Suzuki et al., 2021
Genus *Lithelius* Haeckel, 1861

Type species.— *Lithelius haeckelspiralis* Haeckel, 1861, p. 843 (unfigured); Haeckel, 1862, p. 519, pl. 27, figs. 6, 7.

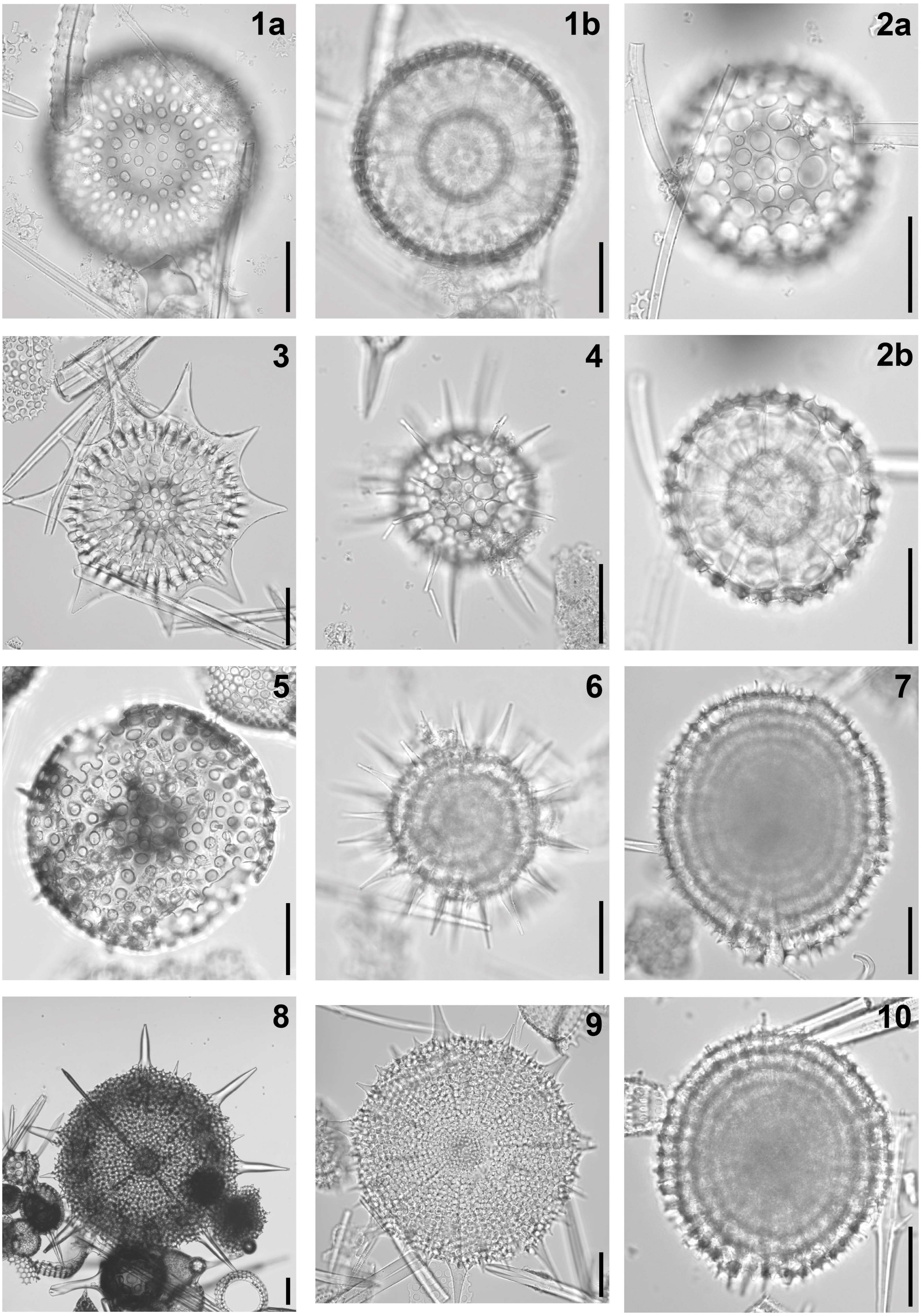
1a
1b
2a
3
4
2b
5
6
7
8
9
10

Plate II.3. Composite light micrographs of new radiolarian species from ODP Site 1260 (Demerara Rise, western equatorial Atlantic) and ODP Site 1051 (Blake Nose, western North Atlantic). (**1a, 1b**) *Haliomma rotunda* (Borisenko, 1960): ODP 1051A-6H-5W, 53–55 cm. (**2a, 2b**) *Excentrodiscus* ? *entactinia* (Ehrenberg, 1874): ODP 1051A-13H-5W, 58–60 cm. (**3**) *Heliodiscus contiguus* (Ehrenberg, 1874): ODP 1051A-12H-2W, 55–57 cm. (**4**) *Excentrodiscus kamikurii* Dumitrică, 2019: ODP 1051A-4H-5W, 56–X58 cm. (**5**) *Heliodiscus umbonatus* (Ehrenberg, 1874): ODP 1260A-10R-1W, 55–57 cm. (**6**) *Lithelius* ? *echinastrum* Ehrenberg, 1874: ODP 1051A-6H-5W, 53–55 cm. (**7, 10**) *Larcopyle hayesi hayesi* (Chen, 1974): (**7**) ODP 1051A-10H-2W, 53–55 cm; (**10**) ODP 1051A-9H-2W, 53–55 cm (**8**) *Annulatospira odoghertyi* Dumitrică, 2020: ODP 1260A-13R-3W, 54–56 cm. (**9**) *Annulatospira serratolabrum* Dumitrică, 2020: ODP 1051A-10H-2W, 53–55 cm. All scale bars equal 50 μm.

Lithelius ? *echinastrum* Ehrenberg, 1874
Plate II.3, Figure 6

1874 *Stylodictya Echinastrum* [sic] Ehrenberg, p. 257.
1876 *Stylodictya Echinastrum* [sic] Ehrenberg – Ehrenberg, p. 84, pl. 23, fig. 1.
1882b *Lithelius Echinastrum* [sic] (Ehrenberg) – Bütschli, pl. 25, fig. 8a, 8b.
1887 *Stylodictya* (*Stylospira*) *echinastrum* Ehrenberg – Haeckel, p. 513.
2009 *Stylodictya echinastrum* Ehrenberg – Ogane et al., pl. 28, figs. 4a–4c, pl. 64, figs. 1a–3b.
2015 *Stylodictya* ? *echinastrum* Ehrenberg – Kamikuri, pl. 17, figs. 5, 8.
Occurrence. ODP Site 1051 (Blake Nose; western north Atlantic).

Family Pyloniidae Haeckel, 1881 emend. Dumitrică, 1989
Genus *Larcopyle* Dreyer, 1889
Type species.— *Larcopyle buetschlii* Dreyer, 1889, p. 48, pl. 5, fig. 70.

Larcopyle hayesi hayesi (Chen, 1974)
Plate II.3, Figures 7, 10

1974 *Prunopyle hayesi* Chen, p. 482, pl. 1, figs. 7, 8, pl. 2, figs. 1, 2.
1975 *Prunopyle hayesi* Chen – Chen, p. 454, pl. 9, figs. 4, 5 (part).
1992 *Prunopyle hayesi* Chen – Takemura, p. 742, pl. 1, figs. 13, 14.
1997 *Prunopyle hayesi* Chen – Hollis et al., p. 48, pl. 2, figs. 12–14.
2003 *Prunopyle hayesi* Chen – Sanfilippo and Fourtanier, p. 12, pl. P1, fig. 5.
2005 *Larcopyle hayesi* variety '*hayesi'* (Chen) – Lazarus et al., p. 119, pl. 11, figs. 1–8, 18–20.
2009b *Larcopyle hayesi hayesi* (Chen) – Suzuki et al., p. 250, pl. 10, figs. 8–18b.
2015 *Larcopyle hayesi hayesi* (Chen) – Kamikuri, pl. 17, fig. 4.
2020 *Larcopyle hayesi* (Chen) – Hollis et al., pl. 4, fig. 4.
2021 *Larcopyle hayesi* (Chen) – de Souza et al., p. 15, pl. 1, fig. 10.
Occurrence. ODP Site 1051 (Blake Nose; western north Atlantic).

Superfamily Phorticioidea Haeckel, 1882
Family Circodiscidae Dumitrică, 1989
Genus *Annulatospira* Clark and Campbell, 1945

Type species.— *Spongodiscus* (*Annulatospira*) *pulcher* Clark and Campbell, 1945, p. 26, pl. 4, fig. 5.

Annulatospira odoghertyi Dumitrică, 2020
Plate II.3, Figure 8

2020 *Annulatospira odoghertyi* Dumitrică, p. 38, pl. 21, figs. 1–7, pl. 22, figs. 1–3

Occurrence. ODP Site 1051 (Blake Nose; western north Atlantic).

Annulatospira serratolabrum Dumitrică, 2020
Plate II.3, Figure 9

1973 *Spongodiscus pulcher* Clark and Campbell – Sanfilippo and Riedel, p. 525, pl. 29, fig. 3 (part).

2020 *Annulatospira serratolabrum* Dumitrică, p. 34, pl. 19, figs. 7, 8, pl. 20, figs. 1–3.

Occurrence. ODP Site 1051 (Blake Nose; western north Atlantic).

Genus *Circodiscus* Kozlova *in* Petrushevskaya and Kozlova, 1972

Type species.— *Trematodiscus microporus* Stöhr, 1880, p. 108, pl. 4, fig. 17.

Circodiscus circularis (Clark and Campbell, 1942)
Plate II.4, Figure 1

1942 *Porodiscus* (*Trematodiscus*) *circularis* Clark and Campbell, p. 42, pl. 2, figs. 2, 6, 10.

1942 *Xiphodictya* (*Xiphodictyon*) *amphixiphos* Clark and Campbell, p. 43, pl. 2, fig. 4.

1972 *Plectodiscus circularis* (Clark and Campbell) – Petrushevskaya and Kozlova, p. 526, pl. 19, figs. 9–12.

1972 *Plectodiscus bergontianus* (Carnevale) – Petrushevskaya and Kozlova, p. 526, pl. 19, fig. 13.

1973 *Xiphospira circularis* (Clark and Campbell) – Sanfilippo and Riedel, p. 526, pl. 14, figs. 8–10, 12, pl. 31, fig. 7 (part).

1976 *Plectodiscus circularis* (Clark and Campbell) – Dzinoridze et al., pl. 24, fig. 11.

1977 *Xiphospira circularis* (Clark and Campbell) – Riedel and Sanfilippo, pl. 1, fig. 10.

1988 *Plectodiscus circularis* (Clark and Campbell) – Blueford, p. 250, pl. 5, figs. 7, 8.

1992 *Xiphospira circularis* (Clark and Campbell) – Nishimura, p. 329, pl. 2, fig. 13, pl. 12, fig. 9.

not 1999 *Circodiscus circularis* (Clark and Campbell) – Kozlova, p. 173, pl. 9, fig. 2.

2002 *Plectodiscus circularis* (Clark and Campbell) – Hollis, p. 288, pl. 2, figs. 20–22.

2008 *Circodiscus circularis* (Clark and Campbell) – Jackett et al., p. 50, pl. 4, fig. 12 (part).

2009b *Circodiscus circularis* (Clark and Campbell) – Suzuki et al., p. 254, pl. 16, figs. 12–13b.

? 2009b *Circodiscus* sp. C Suzuki et al., p. 254, pl. 17, figs. 4a–9.

2015 *Plectodiscus* aff. *runanganus* O'Connor – Kamikuri, pl. 17, figs. 6, 7, 9, 10.

2020 *Circodiscus circularis* (Clark and Campbell) – Dumitrică, p. 23, pl. 12, figs. 1–10.

? 2020 *Xiphospira circularis* (Clark and Campbell) – Hollis et al., pl. 2, fig. 12.

Occurrence. ODP Site 1260 (Demerara Rise; western equatorial Atlantic) and ODP Site 1051 (Blake Nose; western north Atlantic).

Family Cryptolarnaciidae Dumitrică, 1989

Genus *Coccolarnacium* Dumitrică, 1989

Type species.— *Coccolarnacium periphaenoides* Dumitrică, 1989, p. 242, pl. 10, fig. 1.

Coccolarnacium periphaenoides Dumitrică, 1989

Plate II.4, Figure 2

1973 Coccodiscid gen. et sp. indet. Riedel and Sanfilippo, pl. 3, fig. 2.

1989 *Coccolarnacium periphaenoides* Dumitrică, p. 242, pl. 10, figs. 1–4, pl. 14, figs. 2–4, 9.

2001 *Coccolarnacium periphaenoides* Dumitrică – De Wever et al., p. 155, fig. 92.2.

2020 *Coccolarnacium periphaenoides* Dumitrică – Dumitrică, p. 7, pl. 1, figs. 1, 2, 5, 6, 10, pl. 2, figs. 1–9, pl. 7, figs. 1, 2.

Occurrence. ODP Site 1260 (Demerara Rise; western equatorial Atlantic).

Family Histiastridae Dumitrică, 1989

Genus *Amphicraspedula* Haeckel, 1887

Type species.— *Amphicraspedum* (*Amphicraspedula*) *murrayanum* Haeckel, 1887, p. 523, pl. 44, fig. 10.

Amphicraspedula crucifera (Clark and Campbell, 1942)

Plate II.4, Figure 3

1942 *Spongasteriscus* (*Spongasteriscinus*) *cruciferus* Clark and Campbell, p. 50, pl. 1, figs. 1–6, 8, 10, 11, 16–18.

1945 *Spongasteriscus* (*Spongasteriscinus*) *cruciferus* Clark and Campbell – Clark and Campbell, p. 57, pl. 4, figs. 4, 6, 7.

1973 *Spongodiscus cruciferus* (Clark and Campbell) – Sanfilippo and Riedel, p. 524, pl. 11, figs. 14–17, pl. 28, figs. 10, 11.

1977 *Spongodiscus cruciferus* (Clark and Campbell) – Riedel and Sanfilippo, pl. 4, fig. 3.

1992 *Spongodiscus cruciferus* (Clark and Campbell) – Nishimura, p. 329, pl. 2, fig. 14.

1993 *Stylotrochus quadribrachiatus quadribrachiatus* Sanfilippo and Riedel – Hull, p. 12, pl. 7, fig. 11, pl. 8, fig. 9.

1993 *Amphicraspedum murrayanum* Haeckel – Blueford and Amon, p. 80, pl. 2, figs. 5, 7, pl. 3, figs. 1, 5, 6, pl. 6, figs. 4, 9 (part).

1993 *Spongasteriscus cruciferus* Clark and Campbell – Blueford and Amon, p. 78, pl. 2, figs. 1, 4, pl. 3, figs. 2, 4 (part).

1993 *Spongasteriscus cruciferus* Clark and Campbell – Vitukhin, pl. 1, fig. 5, pl. 9, fig. 1, pl. 22, fig. 2, pl. 31, fig. 4 (part).

1998a *Spongodiscus cruciferus* (Clark and Campbell) – Sanfilippo and Nigrini, p. 273, pl. 13.2, fig. 8.

1999a *Spongodiscus cruciferus* (Clark and Campbell) – O'Connor, p. 36, pl. 10, fig. 20.

1999a *Spongodiscus* cf. *cruciferus* (Clark and Campbell) – O'Connor, p. 36, pl. 10, fig. 23.

1999 *Spongasteriscus cruciferus* Clark and Campbell – Kozlova, p. 175, pl. 12, fig. 3, pl. 16, fig. 12, pl. 20, fig. 1, pl. 32, fig. 10, pl. 42, fig. 11.
1999 *Spongasteriscus* sp. cf. *S. cruciferus* Clark and Campbell – Kozlova, pl. 6, fig. 9.
2005 *Spongasteriscus cruciferus* Clark and Campbell – Funakawa and Nishi, p. 233, pl. 3, fig. 1.
2008 *Spongodiscus cruciferus* (Clark and Campbell) – Jackett et al., p. 58, pl. 4, fig. 8.
2009b *Spongodiscus cruciferus* (Clark and Campbell) – Suzuki et al., p. 252, pl. 14, figs. 1a–5b.
2020 *Spongodiscus cruciferus* (Clark and Campbell) – Hollis et al., pl. 2, pl. 15.

Remarks. The combination used here is derived from O'Dogherty et al. (2021).

Occurrence. ODP Site 1260 (Demerara Rise; western equatorial Atlantic) and ODP Site 1051 (Blake Nose; western north Atlantic).

Amphicraspedula murrayana (Haeckel, 1887) group

Plate II.4, Figures 4, 5

1887 *Amphicraspedum* (*Amphicraspedula*) *murrayanum* Haeckel, p. 523, pl. 44, fig. 10.
1973 *Amphicraspedum murrayanum* Haeckel – Sanfilippo and Riedel, p. 524, pl. 10, figs. 3–6, pl. 28, fig. 1.
1974 *Amphicraspedum murrayanum* Haeckel – Nigrini, p. 1065, pl. 3, fig. 2.
1977 *Amphicraspedum murrayanum* Haeckel – Riedel and Sanfilippo, pl. 4, fig. 4.
1978 *Amphicraspedum murrayanum* Haeckel – Johnson, p. 784, pl. 1, fig. 5.
1978 *Amphicraspedum murrayanum* Haeckel – Weaver and Dinkelman, p. 867, pl. 11, fig. 2.
1978 *Amphicraspedum murrayanum* Haeckel – Foreman, p. 784, pl. 1, fig. 5.
1987 *Amphicraspedum murrayanum* Haeckel – Nishimura, p. 719, pl. 1, figs. 14, 18.
1993 *Amphicraspedum murrayanum* Haeckel – Blueford and Amon, p. 80, pl. 1, figs. 9, 10, pl. 2, figs. 2, 3, 8 (part).
1998a *Amphicraspedum murrayanum* Haeckel – Sanfilippo and Nigrini, p. 272, pl. 13.1, fig. 1.
1999a *Amphicraspedum murrayanum* Haeckel – O'Connor, p. 31, pl. 10, fig. 7.
2000 *Amphicraspedum murrayanum* Haeckel – Nigrini and Sanfilippo, p. 72, pl. 3, figs. 11–13.
2001 *Amphicraspedum murrayanum* Haeckel var. A – Sanfilippo and Blome, p. 208, fig. 8a.
2008 *Amphicraspedum murrayanum* Haeckel group – Jackett et al., p. 47, pl. 4, figs. 1, 2.
2020 *Amphicraspedum murrayanum* Haeckel – Hollis et al., pl. 3, fig. 1.

Remarks. The combination used here is derived from O'Dogherty et al. (2021).

Occurrence. ODP Site 1260 (Demerara Rise; western equatorial Atlantic) and ODP Site 1051 (Blake Nose; western north Atlantic).

Genus *Amphymenium* Haeckel, 1882

Type species.— *Amphymenium* (*Ommatogramma*) *zygartus* Haeckel, 1887, p. 515, pl. 44, fig. 7.

Amphymenium connicinum Kim, 1992
Plate II.4, Figures 6, 9

1992 *Amphymenium connicinum* Kim, p. 38, pl. 1, figs. 5, 6.

Occurrence. ODP Site 1260 (Demerara Rise; western equatorial Atlantic) and ODP Site 1051 (Blake Nose; western north Atlantic).

Amphymenium splendiarmatum Clark and Campbell, 1942
Plate II.4, Figures 7, 8

1942 *Amphymenium* (*Ommathymenium*) *splendiarmatum* Clark and Campbell, p. 46, pl. 1, fig. 12, 14

1973 *Amphymenium splendiarmatum* Clark and Campbell – Sanfilippo and Riedel, p. 524, pl. 11, fig. 6–8; pl. 28, fig. 6–8.

1975 *Amphymenium* ? *splendiarmatum* Clark and Campbell – Petrushevskaya, p. 577, pl. 7, fig. 1, pl. 37, fig. 1–3.

1984 *Amphymenium splendiarmatum* Clark and Campbell – Westberg-Smith and Riedel, p. 488, pl. 6, fig. 17.

1987 *Amphymenium splendiarmatum* Clark and Campbell – Nishimura, p. 719, pl. 1, fig. 20.

1992 *Amphymenium splendiarmatum* Clark and Campbell – Blome, p. 643, pl. 2, fig. 10.

1996 *Spongocore* sp. Hull, p. 136, pl. 3, fig. 14.

1997 *Amphymenium* cf. *splendiarmatum* Clark and Campbell – Hollis et al., p. 49, pl. 3, fig. 9.

2003 *Amphymenium splendiarmatum* Clark and Campbell – Sanfilippo and Fourtanier, p. 11, pl. P2, fig. 18.

2009b *Amphymenium splendiarmatum* Clark and Campbell – Suzuki et al., p. 253, pl. 6, fig. 9–12.

2015 *Amphymenium amphistylium* Haeckel – Kamikuri, pl. 16, fig. 3.

2020 *Amphymenium splendiarmatum* Clark and Campbell – Hollis et al., pl. 3, figs. 8, 9.

Occurrence. ODP Site 1260 (Demerara Rise; western equatorial Atlantic) and ODP Site 1051 (Blake Nose; western north Atlantic).

Genus *Histiastrum* Ehrenberg, 1846

Type species.— *Histiastrum quaternarium* Ehrenberg, 1874, p. 237 (unfigured); Ehrenberg, 1876, p. 74, pl. 24, fig. 3.

Histiastrum coronatum Haeckel, 1887
Plate II.4, Figure 10

1862 *Stephanastrum* ? Bury, pl. 4, fig. 1.

1887 *Histiastrum* (*Histiastromma*) *coronatum* Haeckel, p. 546.

2020 *Histiastrum quadribrachiatus quadribrachiatus* (Sanfilippo and Riedel) – Hollis et al., pl. 3, figs. 10, 11.

Occurrence. ODP Site 1260 (Demerara Rise; western equatorial Atlantic).

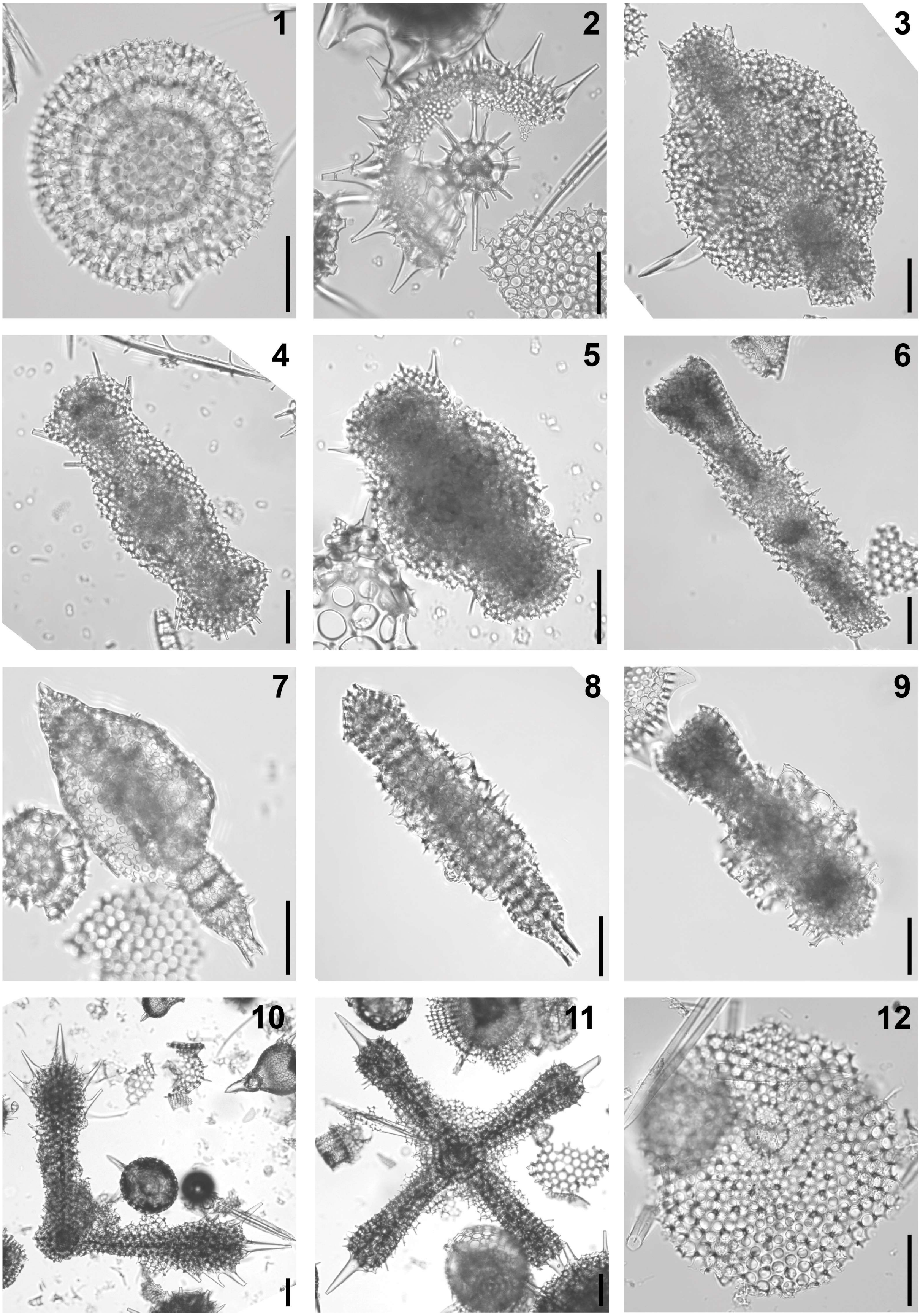
1
2
3
4
5
6
7
8
9
10
11
12

Plate II.4. Composite light micrographs of new radiolarian species from ODP Site 1260 (Demerara Rise, western equatorial Atlantic) and ODP Site 1051 (Blake Nose, western North Atlantic). (**1**) *Circodiscus circularis* (Clark and Campbell, 1942): ODP 1051A-13H-5W, 58–60 cm. (**2**) *Coccolarnacium periphaenoides* Dumitrică, 1989: ODP 1260A-13R-5W, 54–56 cm. (**3**) *Amphicraspedula crucifera* (Clark and Campbell, 1942): ODP 1260A-10R-1W, 55–57 cm. (**4, 5**) *Amphicraspedula murrayana* (Haeckel, 1887) group: (**4**) ODP 1260A-13R-5W, 55–56 cm; (**5**) ODP 1260A-9R-3W, 55–57 cm. (**6, 9**) *Amphymenium connicinum* Kim, 1992: (**6**) ODP 1260A-8R-3W, 54–56 cm; (**9**) ODP 1260A-8R-3W, 54–56 cm. (**7, 8**) *Amphymenium splendiarmatum* Clark and Campbell, 1942: (**7**) ODP 1260A-11R-1W, 55–57 cm; (**8**) ODP 1260A-6R-2W, 55–57 cm. (**10**) *Histiastrum quaternarium* Ehrenberg, 1874: ODP 1260A-13R-5W, 54–56 cm. (**11**) *Histiastrum coronatum* Haeckel, 1887: ODP 1260A-6R-1W, 55–57 cm. (**12**) *Homunculodiscus tainemplekta* (Caulet, 1991): ODP 1051A-10H-5W, 52–54 cm. All scale bars equal 50 μm.

Histiastrum quaternarium Ehrenberg, 1874
Plate II.4, Figure 11

1862 *Astromma* ? Bury, pl. 5, fig. 1.
1874 *Histiastrum quaternarium* Ehrenberg, p. 237.
1876 *Histiastrum quaternarium* Ehrenberg – Ehrenberg, p. 74, pl. 24, fig. 3.
not 1882b *Histiastrum quaternarium* Ehrenberg – Bütschli, pl. 25, fig. 5.
1887 *Histiastrum* (*Histiastromma*) *quaternarium* Ehrenberg – Haeckel, p. 545.
1887 *Histiastrum* (*Histiastromma*) *gladiatum* Haeckel, p. 545.
not 1987 *Histiastrum quaternarium* Ehrenberg – Nishimura, p. 726, pl. 1, fig. 16.
Occurrence. ODP Site 1260 (Demerara Rise; western equatorial Atlantic).

Superfamily Pseudoaulophacoidea Riedel, 1967a sensu De Wever et al., 2001
Family Suttoniidae Schaaf, 1976 sensu Dumitrică, 2019
Genus *Homunculodiscus* Dumitrică, 2019

Type species.— *Stylodictya tainemplekta* Caulet, 1991, p. 533, pl. 1, fig. 8.

Homunculodiscus tainemplekta (Caulet, 1991)
Plate II.4, Figure 12

1991 *Stylodictya tainemplekta* Caulet, p. 533, pl. 1, figs. 8, 9.
2015 *Stylodictya tainemplekta* Caulet – Kamikuri, p. 148, pl. 18, fig. 6.
2019 *Homunculodiscus tainemplecta* [sic] (Caulet) – Dumitrică, p. 42, figs. 3e, 3g, 4a–4d.
2021 *Stylodictya tainemplekta* Caulet – de Souza et al., p. 15, pl. 1, fig. 9.
Occurrence. ODP Site 1051 (Blake Nose; western north Atlantic).

Genus *Suttonium* Schaaf, 1976

Type species.— *Suttonium praedicator* Schaaf, 1976, p. 790, pl. 1, fig. 1.

Suttonium anomalum (Sutton, 1896b)
Plate II.5, Figure 1

1896b *Rhopalastrum* ? *anomalum* Sutton, p. 59, fig. 1.
1983 *Suttonium anomalum* (Sutton) – Dumitrică, p. 42, pl. 2, figs. 1–4, pl. 3, figs. 3, 4, 6–8, 11.
1986 *Suttonium anomalum* (Sutton) – Göke, fig. 5.
2015 *Suttonium anomalum* (Sutton) – Kamikuri, pl. 18, fig. 9.
2019 *Suttonium anomalum* (Sutton) – Dumitrică, p. 46, fig. 6c.
Occurrence. ODP Site 1051 (Blake Nose; western north Atlantic).

Superfamily Stylosphaeroidea Haeckel, 1887
Family Entapiidae Dumitrică *in* De Wever et al., 2001
Genus *Entapium* Sanfilippo and Riedel, 1973

Type species.— *Entapium regulare* Sanfilippo and Riedel, 1973, p. 492, pl. 24, figs. 1, 2.

Entapium regulare Sanfilippo and Riedel, 1973
Plate II.5, Figure 2

1973 *Entapium regulare* Sanfilippo and Riedel, p. 492, pl. 1, figs. 10–19, pl. 24, figs. 1–3.
1992 *Entapium regulare* Sanfilippo and Riedel – Blome, p. 644, pl. 3, fig. 20.
1999 *Entapium regulare* Sanfilippo and Riedel – Kozlova, p. 73, pl. 8, figs. 8, 9.
Occurrence. ODP Site 1260 (Demerara Rise; western equatorial Atlantic).

Genus *Zealithapium* O'Connor, 1999a

Type species.— *Zealithapium oamaru* O'Connor, 1999a, p. 5, pl. 5, figs 29a, 29b.

Zealithapium anoectum (Riedel and Sanfilippo, 1970)
Plate II.5, Figures 4, 5

1970 *Lithapium* ? *anoectum* Riedel and Sanfilippo, p. 520, pl. 4, figs. 4, 5.
1973 *Lithapium anoectum* Riedel and Sanfilippo – Sanfilippo and Riedel, p. 516, pl. 24, figs. 6, 7.
1974 *Lithapium anoectum* Riedel and Sanfilippo – Nigrini, p. 1064, pl. 1A, figs. 1, 2.
1977 *Lithapium anoectum* Riedel and Sanfilippo – Riedel and Sanfilippo, pl. 8, fig. 10.
1978 *Lithapium anoectum* Riedel and Sanfilippo – Riedel and Sanfilippo, p. 69, pl. 5, fig. 17.
1992 *Lithapium anoectum* Riedel and Sanfilippo – Takemura, p. 742, pl. 7, fig. 1.
? 1999 *Lithapium anoectum* Riedel and Sanfilippo – Kozlova, p. 125, pl. 32, fig. 19.
1999a *Zealithapium anoectum* (Riedel and Sanfilippo) – O'Connor, p. 5.
2001 *Zealithapium anoectum* (Riedel and Sanfilippo) – De Wever et al., p. 119, fig. 65.3.
2012 *Zealithapium* cf. *Z. anoectum* (Riedel and Sanfilippo) – Moore and Kamikuri, p. 13, pl. P10, figs. 6, 7.
2012b *Zealithapium anoectum* (Riedel and Sanfilippo) – Kamikuri et al., p. 5, pl. P1, figs. 6a, 6b.
2020 *Zealithapium anoectum* (Riedel and Sanfilippo) – Hollis et al., pl. 1, fig. 9.
Occurrence. ODP Site 1260 (Demerara Rise; western equatorial Atlantic).

Zealithapium mitra (Ehrenberg, 1874)
Plate II.5, Figure 6

1862 *Podocyrtis* ? Bury, pl. 9, fig. 4 (part).
1874 *Cornutella Mitra* [sic] Ehrenberg, p. 221.
1876 *Cornutella Mitra* [sic] Ehrenberg – Ehrenberg, p. 68, pl. 2, figs. 8.
1882a *Ceratocyrtis mitra* (Ehrenberg) – Bütschli, p. 536.
1887 *Cornutella* (*Cornutissa*) *mitra* Ehrenberg – Haeckel, p. 1181.
1887 *Sethoconus* (*Conarachnium*) *mitra* (Ehrenberg) – Haeckel, p. 1291.
1970 *Lithapium* ? *mitra* (Ehrenberg) – Riedel and Sanfilippo, p. 520, pl. 4, figs. 6, 7.
1971 *Lithapium* ? *mitra* (Ehrenberg) – Moore, p. 736, pl. 3, fig. 1.
1977 *Lithapium mitra* (Ehrenberg) – Riedel and Sanfilippo, pl. 8, fig. 15.
1978 *Lithapium mitra* (Ehrenberg) – Riedel and Sanfilippo, p. 69, pl. 6, fig. 1 (part).
1992 *Lithapium* cf. *mitra* (Ehrenberg) – Takemura, p. 742, pl. 7, fig. 2.
1997 *Lithapium mitra* (Ehrenberg) – Hollis et al., p. 45, pl. 1, fig. 20.
1999a *Zealithapium mitra* (Ehrenberg) – O'Connor, p. 5, pl. 9, fig. 47.
2012 *Zealithapium mitra* (Ehrenberg) – Moore and Kamikuri, p. 13, pl. P10, fig. 5.
2020 *Zealithapium mitra* (Ehrenberg) – Hollis et al., pl. 1, fig. 10.

Occurrence. ODP Site 1260 (Demerara Rise; western equatorial Atlantic) and ODP Site 1051 (Blake Nose; western north Atlantic).

Zealithapium plegmacantha Riedel and Sanfilippo, 1970
Plate II.5, Figure 3

1970 *Lithapium* ? *plegmacantha* Riedel and Sanfilippo, p. 520, pl. 4, figs. 2, 3.
1971 *Lithapium* ? *plegmacantha* Riedel and Sanfilippo – Moore, p. 736, pl. 1, fig. 1.
1973 *Lithapium plegmacantha* Riedel and Sanfilippo – Sanfilippo and Riedel, p. 516, pl. 3, figs. 1, 2, pl. 24, figs. 8, 9.
1974 *Lithapium plegmacantha* Riedel and Sanfilippo – Nigrini, p. 1064, pl. 1A, figs. 3–5.
1977 *Lithapium plegmacantha* Riedel and Sanfilippo – Riedel and Sanfilippo, pl. 6, fig. 8.
1986 *Lithapium plegmacantha* Riedel and Sanfilippo – Riedel and Sanfilippo, pl. 2, figs. 4, 5.
1999a *Zealithapium plegmacantha* (Riedel and Sanfilippo) – O'Connor, p. 5.
2012b *Zealithapium plegmacantha* (Riedel and Sanfilippo) – Kamikuri et al., p. 5, pl. P1, figs. 7a, 7b.

Occurrence. ODP Site 1260 (Demerara Rise; western equatorial Atlantic) and ODP Site 1051 (Blake Nose; western north Atlantic).

Family Stylosphaeridae Haeckel, 1887 sensu Dumitrică, 1985
Genus *Lithomespilus* Haeckel, 1882

Type species.— *Lithomespilus phloginus* Haeckel, 1887, p. 302, pl. 14, fig. 16.

Lithomespilus coronatus Squinabol, 1904
Plate II.5, Figures 7, 8

1904 *Lithomespilus coronatus* Squinabol, p. 198, pl. 4, fig. 7.

1973 *Druppatractus* cf. *coronatus* (Squinabol) – Dumitrică, p. 787, pl. 6, figs. 4, 6, pl. 12, fig. 1.
2002 *Lithomespilus coronatus* Squinabol – Hollis, pl. 1, fig. 12.
1960 *Ellipsidium* ? *mendosum* Krasheninnikov, p. 281, pl. 1, fig. 14a, 14b.
1973 *Lithomespilus mendosa* (Krasheninnikov) – Sanfilippo and Riedel, p. 517, pl. 4, figs. 6, 7, pl. 24, figs. 10, 11.
1977 *Lithomespilus mendosa* (Krasheninnikov) – Riedel and Sanfilippo, pl. 1, fig. 4.
1992 *Lithomespilus mendosa* (Krasheninnikov) – Blome, pl. 2, figs. 16.
Occurrence. ODP Site 1260 (Demerara Rise; western equatorial Atlantic) and ODP Site 1051 (Blake Nose; western north Atlantic).

Genus *Stauroxiphos* Haeckel, 1887

Type species.— *Stauroxiphos gladius* Haeckel, 1887, p. 163, pl. 15, fig. 7.

Stauroxiphos ? *gladius* Haeckel, 1887
Plate II.5, Figure 10

1887 *Stauroxiphos gladius* Haeckel, p. 163, pl. 15, fig. 7.
Occurrence. ODP Site 1260 (Demerara Rise; western equatorial Atlantic).

Genus *Stylosphaera* Ehrenberg, 1846

Type species.— *Stylosphaera hispida* Ehrenberg, 1854c, p. 246 (unfigured); Ehrenberg, 1854a, pl. 36, fig. 26.

Stylosphaera ? *agdaraensis* (Mamedov, 1969a)
Plate II.5, Figure 9

? 1969a *Sphaerostylus agdaraensis* Mamedov, p. 96, pl. 2, figs. 1, 2.
1973 *Thecosphaerella* sp. cf. *T. agdaraensis* (Mamedov) – Sanfilippo and Riedel, p. 521, pl. 2, figs. 7–9, pl. 25, fig. 15.
Remarks. This species is tentatively assigned to the genus *Stylosphaera* based on its overall morphology.
Occurrence. ODP Site 1260 (Demerara Rise; western equatorial Atlantic).

Stylosphaera carduus Ehrenberg, 1874
Plate II.5, Figures 11, 12

1874 *Stylosphaera Carduus* [sic] Ehrenberg, p. 258.
1876 *Stylosphaera Carduus* [sic] Ehrenberg – Ehrenberg, p. 84, pl. 25, fig. 7.
1887 *Stylatractus* (*Stylatractylis*) *carduus* (Ehrenberg) – Haeckel, p. 330.
not 1972 *Axoprunum carduum* (Ehrenberg) – Petrushevskaya and Kozlova, p. 521, pl. 10, fig. 1.
1977 *Stylatractus* sp. Riedel and Sanfilippo, pl. 13, fig. 1.
1995 *Stylatractus ostracion* (Haeckel) – Shilov, p. 124, pl. 3, figs. 3a, 3b.
2009 *Stylosphaera carduus* Ehrenberg – Ogane et al., pl. 12, figs. 5a–5d, pl. 29, figs. 1a–1d.
Occurrence. ODP Site 1260 (Demerara Rise; western equatorial Atlantic).

Stylosphaera coronata Ehrenberg, 1874
Plate II.6, Figure 1

1874 *Stylosphaera coronata* Ehrenberg, p. 258.
1876 *Stylosphaera* (*Xiphostylantha*) *coronata* Ehrenberg – Ehrenberg, p. 84, pl. 25, fig. 4.
1887 *Xiphostylus phasianus* Haeckel, p. 127, pl. 13, fig. 9.
1887 *Druppatractus* (*Druppatractylis*) *coronatus* (Ehrenberg) – Haeckel, p. 326.
1942 *Lithatractus* (*Lithatractaria*) *hederae* Clark and Campbell, p. 33, pl. 5, fig. 3.
1942 *Druppatractus* (*Druppatractaria*) *trichopterus* Clark and Campbell, p. 34, pl. 5, fig. 4.
1942 *Ellipsostylus* (*Ellipsostyletta*) *anisoxyphos* Clark and Campbell, p. 32, pl. 5, figs. 7, 11.
1972 *Stylatractus coronatus* (Ehrenberg) – Petrushevskaya and Kozlova, p. 520, pl. 11, fig. 9.
1973 *Stylosphaera coronata coronata* Ehrenberg – Sanfilippo and Riedel, p. 520, pl. 1, figs. 13–17, pl. 25, fig. 4.
1973 *Druppatractus* sp. Dumitrică, p. 787, pl. 12, fig. 3.
1974 *Stylosphaera coronata coronata* Ehrenberg – Nigrini, p. 1064, pl. 1B, figs. 1–3.
1986 *Stylosphaera coronata coronata* Ehrenberg – Riedel and Sanfilippo, pl. 5, fig. 7.
1987 *Stylosphaera coronata coronata* Ehrenberg – Nishimura, p. 729, pl. 1, figs. 1, 2.
1992 *Stylosphaera coronata coronata* Ehrenberg – Nishimura, p. 325, pl. 1, fig. 2, pl. 11, fig. 9.
1994 *Stylosphaera coronata sabaca* Sanfilippo and Riedel – Weinheimer et al., p. 312, pl. 1, fig. 6.
1995 *Stylosphaera coronata* Ehrenberg – Shilov, p. 124, pl. 2, figs. 2a–2c.
1999 *Amphisphaera* sp. ef gr. *A. coronata* (Ehrenberg) – Kozlova, pl. 22, figs. 7, 9, pl. 33, fig. 11 (part).
2008 *Stylosphaera coronata coronata* Ehrenberg – Jackett et al., p. 58, pl. 3, fig. 10.
2009 *Stylosphaera coronata* Ehrenberg – Ogane et al., pl. 12, figs. 1a–1d.
2009b *Stylosphaera* ex. gr. *radiosa* Ehrenberg – Suzuki et al., p. 244, pl. 1, figs. 8a, 8b.
2009b *Stylosphaera gigantea* (Haeckel) – Suzuki et al., p. 244, pl. 1, figs. 9a, 9b.
2013 *Stylosphaera coronata coronata* Ehrenberg – Kamikuri et al., pl. 1, figs. 6a, 6b.

Occurrence. ODP Site 1260 (Demerara Rise; western equatorial Atlantic) and ODP Site 1051 (Blake Nose; western north Atlantic).

Stylosphaera laevis Ehrenberg, 1874
Plate II.6, Figures 2, 3

1874 *Stylosphaera laevis* Ehrenberg, p. 259.
1876 *Stylosphaera laevis* Ehrenberg – Ehrenberg, p. 84, pl. 25, fig. 6.
1887 *Ellipsostylus* (*Ellipsostyletta*) *psittacus* Haeckel, p. 300, pl. 13, fig. 6.
1887 *Druppatractus* (*Druppatractona*) *lævis* [sic] (Ehrenberg) – Haeckel, p. 327.
? 1942 *Ellipsostylus* (*Ellipsostyletta*) *parvus* Clark and Campbell, p. 32, pl. 5, fig. 16.
1958 *Druppatractus* sp. Göke, pl. 3, fig. 3.
1972 *Stylosphaera* ? *laevis* Ehrenberg – Petrushevskaya and Kozlova, p. 520, pl. 11, fig. 8.
1973 *Stylosphaera coronata laevis* Ehrenberg – Sanfilippo and Riedel, p. 520, pl. 1, fig. 19, pl. 25, figs. 5, 6.

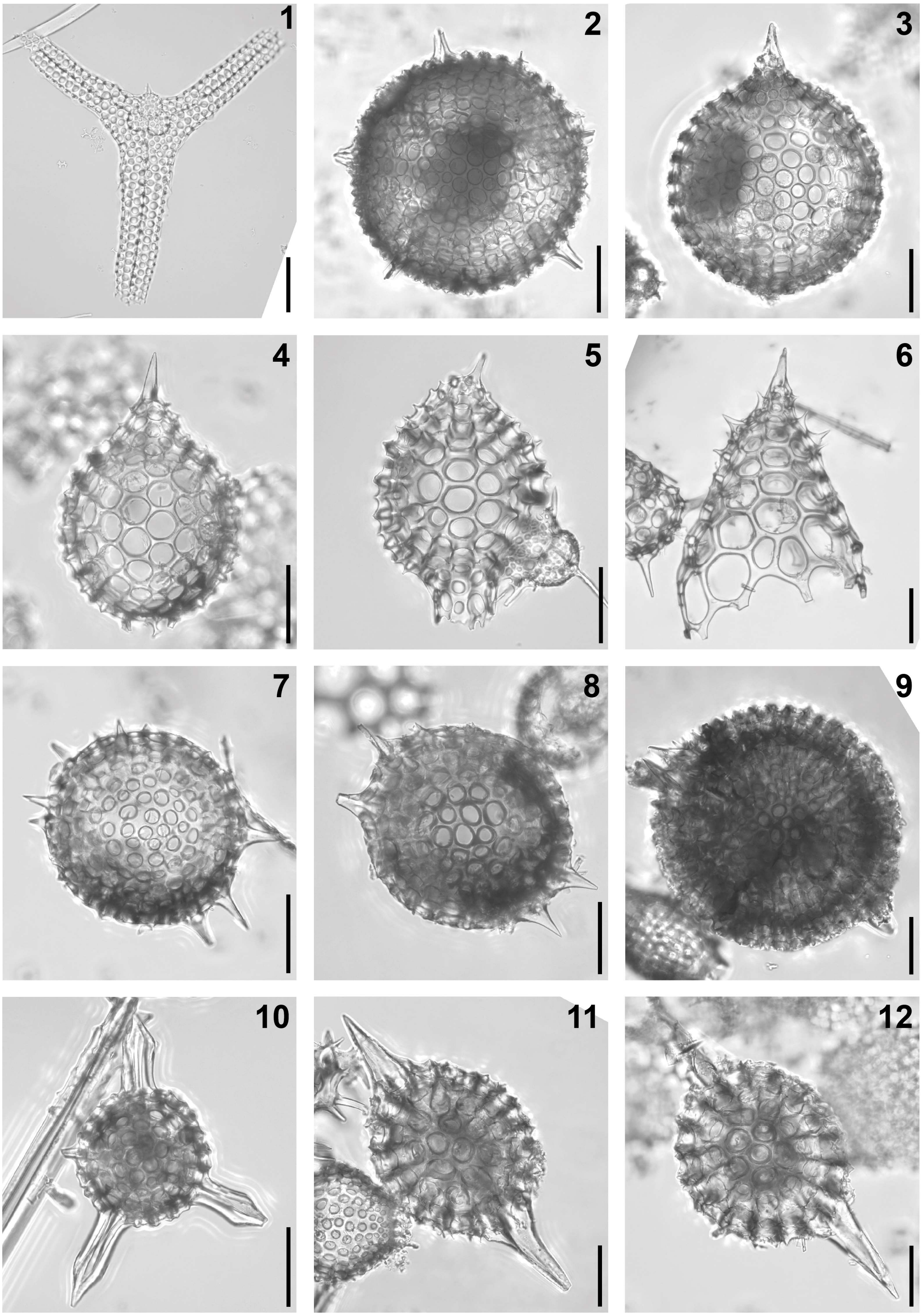
1
2
3
4
5
6
7
8
9
10
11
12

Plate II.5. Composite light micrographs of new radiolarian species from ODP Site 1260 (Demerara Rise, western equatorial Atlantic) and ODP Site 1051 (Blake Nose, western North Atlantic). (**1**) *Suttonium anomalum* (Sutton, 1896b): ODP 1051A-14H-5W, 52–54 cm. (**2**) *Entapium regulare* Sanfilippo and Riedel, 1973: ODP 1260A-8R-5W, 54–56 cm. (**3**) *Zealithapium plegmacantha* Riedel and Sanfilippo, 1970: ODP 1260A-17R-3W, 55–57 cm. (**4, 5**) *Zealithapium anoectum* (Riedel and Sanfilippo, 1970): (**4**) closed specimen, ODP 1260A-11R-4W, 55–57 cm; (**5**) specimen with a pylome, ODP 1260A-11R-4W, 55–57 cm. (**6**) *Zealithapium mitra* (Ehrenberg, 1874): ODP 1260A-8R-6W, 54–56 cm. (**7, 8**) *Lithomespilus coronatus* Squinabol, 1904: (**7**) ODP 1260A-9R-3W, 55–57 cm; (**8**) ODP 1260A-11R-1W, 55–57 cm. (**9**) *Stylosphaera* ? *agdaraensis* (Mamedov, 1969a): ODP 1260A-15R-1W, 55–57 cm. (**10**) *Stauroxiphos* ? *gladius* Haeckel, 1887: ODP 1260A-17R-CC, 63–177 cm. (**11, 12**) *Stylosphaera carduus* Ehrenberg, 1874: (**11**) ODP 1260A-11R-7W, 55–57 cm; (**12**) ODP 1260A-6R-4W, 55–57 cm. All scale bars equal 50 µm.

not 2005 *Stylosphaera coronata laevis* Ehrenberg – Funakawa and Nishi, p. 238, pl. 1, figs. 10a, 10b.
2009 *Stylosphaera laevis* Ehrenberg – Ogane et al., pl. 29, figs. 3a–4b, 6a, 6b, pl. 61, figs. 2a–2c, pl. 63, figs. 2a, 2b.
2012 *Stylosphaera laevis* Ehrenberg form A – Kamikuri and Wade, pl. 1, figs. 10a, 10b.
2012 *Stylosphaera laevis* Ehrenberg form B – Kamikuri and Wade, pl. 1, figs. 9a, 9b.
2015 *Stylosphaera laevis* Ehrenberg form A – Kamikuri, pl. 14, figs. 5a, 5b, pl. 19, figs. 3a, 3b.
2015 *Stylosphaera laevis* Ehrenberg form B – Kamikuri, pl. 14, figs. 1a-3b, pl. 19, figs. 5a, 5b.
Occurrence. ODP Site 1260 (Demerara Rise; western equatorial Atlantic) and ODP Site 1051 (Blake Nose; western north Atlantic).

Stylosphaera radiosa Ehrenberg, 1874
Plate II.6, Figure 4

1874 *Stylosphaera radiosa* Ehrenberg, p. 259.
1876 *Stylosphaera radiosa* Ehrenberg – Ehrenberg, p. 84, pl. 24, fig. 5.
1887 *Xiphatractus* (*Xiphatractium*) *radiosus* (Ehrenberg) – Haeckel, p. 334.
1975 *Amphisphaera radiosa* (Ehrenberg) group – Petrushevskaya, p. 570, pl. 2, figs. 18–20.
1990 *Stylosphaera radiosa* Ehrenberg – Abelmann, p. 692, pl. 2, fig. 4A-4C.
1997 *Amphisphaera radiosa* (Ehrenberg) – Hollis et al., p. 43, pl. 1, figs. 5, 6.
1997 *Ellipsoxiphus* ? sp. Hollis et al., pl. 1, figs. 3, 4.
? 1999 *Amphisphaera radiosa* (Ehrenberg) – Kozlova, p. 173, pl. 17, fig. 2.
2008 *Stylosphaera goruna* Sanfilippo and Riedel – Jackett et al., p. 58, pl. 10, fig. 12.
2009 *Stylosphaera radiosa* Ehrenberg – Ogane et al., pl. 12, figs. 2a–3d, pl. 61, figs. 1a–1d.
2015 *Stylosphaera goruna* Sanfilippo and Riedel – Kamikuri, pl. 19, fig. 4.
2020 *Amphisphaera radiosa* (Ehrenberg) – Hollis et al., pl. 1, figs. 5a, 5b.
2020 *Amphisphaera* aff. *radiosa* (Ehrenberg) – Hollis et al., pl. 1, figs. 6a, 6b.
Occurrence. ODP Site 1260 (Demerara Rise; western equatorial Atlantic) and ODP Site 1051 (Blake Nose; western north Atlantic).

Stylosphaera spinulosa Ehrenberg, 1874
Plate II.6, Figure 5

1874 *Stylosphaera spinulosa* Ehrenberg 1874, p. 259.
1876 *Stylosphaera spinulosa* Ehrenberg – Ehrenberg, pl. 25, fig. 8.
1887 *Xiphatractus* (*Xiphatractylis*) *spinulosus* Ehrenberg – Haeckel, p. 332.
1972 *Stylatractus spinulosus* (Ehrenberg) group – Petrushevskaya and Kozlova, p. 519, pl. 11, figs. 2–4.
1973 *Stylosphaera goruna* Sanfilippo and Riedel, p. 521, pl. 1, fig. 20–22, pl. 25, fig. 9–10.
1973 *Druppatractus* cf. *coronatus* (Squinabol) – Dumitrică, p. 787, pl. 6, figs. 4, 6, pl. 12, fig. 1.
1977 *Stylosphaera goruna* Sanfilippo and Riedel – Riedel and Sanfilippo, pl. 1, fig. 5.
1980 *Stylosphaera goruna* Sanfilippo and Riedel – Westberg et al., p. 432, pl. 1, fig. 1.
1984 *Stylosphaera goruna* Sanfilippo and Riedel – Westberg-Smith and Riedel, p. 487, pl. 6, fig. 11.
1987 *Stylosphaera goruna* Sanfilippo and Riedel – Nishimura, p. 729, pl. 1, fig. 3.
1992 *Stylosphaera goruna* Sanfilippo and Riedel – Nishimura, p. 326, pl. 1, fig. 1, pl. 11, fig. 8.
1992 *Stylosphaera goruna* Sanfilippo and Riedel – Blome, p. 646, pl. 1, figs. 17–20.
1992 *Stylosphaera goruna* Sanfilippo and Riedel – Kim, p. 38, pl. 1, figs. 3, 4.
1995 *Amphisphaera spinulosa* (Ehrenberg) – Strong et al., p. 208, figs. 9A, 10A, 10B.
2002 *Amphisphaera goruna* (Sanfilippo and Riedel) – Hollis, pl. 1, fig. 5.
2006 *Stylosphaera goruna* Sanfilippo and Riedel – Funakawa et al., p. 40, pl. P3, figs. 3–4.
2009 *Stylosphaera liostylus* Ehrenberg – Ogane et al., pl. 12, figs. 6a–6f (part).
2020 *Amphisphaera spinulosa* (Ehrenberg) – Hollis et al., pl. 1, fig. 2.

Occurrence. ODP Site 1260 (Demerara Rise; western equatorial Atlantic).

Genus *Spongatractus* Haeckel, 1887

Type species.— *Spongosphaera pachystyla* Ehrenberg, 1874, p. 256 (unfigured); Ehrenberg, 1876, p. 82, pl. 26, fig. 3.

Spongatractus balbis Sanfilippo and Riedel, 1973
Plate II.6, Figure 6

1973 *Spongatractus balbis* Sanfilippo and Riedel, p. 518, pl. 2, figs. 1–3, pl. 25, figs. 1, 2.
1974 *Spongatractus balbis* Sanfilippo and Riedel – Nigrini, p. 1064, pl. 1A, figs. 6, 7.
1977 *Spongatractus balbis* Sanfilippo and Riedel – Riedel and Sanfilippo, pl. 5, fig. 6.
1986 *Spongatractus balbis* Sanfilippo and Riedel – Riedel and Sanfilippo, pl. 3, fig. 6.
2017 *Spongatractus balbis* Sanfilippo and Riedel – de Souza et al., pl. 1, figs. 1a, 1b.

Occurrence. ODP Site 1260 (Demerara Rise; western equatorial Atlantic).

Spongatractus pachystylus (Ehrenberg, 1874)
Plate II.6, Figure 7

1862 *Spongosphæra* var. Bury, pl. 4, fig. 6.
1874 *Spongosphaera pachystyla* Ehrenberg, p. 256.

1876 *Spongosphaera pachystyla* Ehrenberg – Ehrenberg, p. 82, pl. 26, fig. 3.
1882b *Spongosphaera pachystyla* Ehrenberg – Bütschli, pl. 24, fig. 1.
1887 *Spongatractus pachystylus* (Ehrenberg) – Haeckel, p. 350.
1887 *Spongoxiphus prunococcus* Haeckel, p. 354, pl. 17, figs. 12, 13.
1958 *Spongatractus pachystylus* (Ehrenberg) – Göke, pl. 2, fig. 3.
1970 *Spongatractus pachystylus* (Ehrenberg) – Cita et al., p. 401, pl. 1, fig. B.
1970 *Spongatractus pachystylus* (Ehrenberg) – Riedel and Sanfilippo, pl. 4, fig. 1.
1972 *Spongosphaera pachystyla* Ehrenberg – Petrushevskaya and Kozlova, p. 521, pl. 10, fig. 5.
1973 *Spongatractus pachystylus* (Ehrenberg) – Sanfilippo and Riedel, p. 519, pl. 2, figs. 4–6, pl. 25, fig. 3.
1974 *Spongatractus pachystylus* (Ehrenberg) – Nigrini, p. 1064, pl. 1A, figs. 8–11.
1977 *Spongatractus pachystylus* (Ehrenberg) – Riedel and Sanfilippo, pl. 6, fig. 7.
1986 *Spongatractus pachystylus* (Ehrenberg) – Riedel and Sanfilippo, pl. 3, figs. 7, 8.
2008 *Spongatractus pachystylus* (Ehrenberg) – Jackett et al., p. 58, pl. 3, fig. 9.
2009 *Spongosphaera pachystyla* Ehrenberg – Ogane et al., pl. 13, figs. 1a–1d, 3a, 3b, pl. 27, figs. 2a–2d.
2012 *Spongatractus pachystylus* (Ehrenberg) – Moore and Kamikuri, p. 10, pl. P7, fig. 10.
2017 *Spongatractus pachystylus* (Ehrenberg) – de Souza et al., pl. 1, figs. 2a, 2b.
2020 *Spongatractus pachystylus* (Ehrenberg) – Hollis et al., pl. 1, fig. 18.

Occurrence. ODP Site 1260 (Demerara Rise; western equatorial Atlantic) and ODP Site 1051 (Blake Nose; western north Atlantic).

Spongatractus ? *klausi* Sanfilippo and Blome, 2001
Plate II.6, Figure 8

2001 *Spongatractus klausi* Sanfilippo and Blome, p. 202, figs. 6a–6c.
2020 *Lithocyclia* sp. Hollis et al., pl. 2, fig. 8.

Occurrence. ODP Site 1260 (Demerara Rise; western equatorial Atlantic) and ODP Site 1051 (Blake Nose; western north Atlantic).

Order Entactinaria Kozur and Mostler, 1982
Superfamily Heliosaturnaloidea Kozur and Mostler, 1972
Family Axoprunidae Dumitrică, 1985
Genus *Axoprunum* Haeckel, 1887

Type species.— *Axoprunum stauraxonium* Haeckel, 1887, p. 239, pl. 48, fig. 4.

Axoprunum pierinae (Clark and Campbell, 1942) group
Plate II.6, Figures 10, 11

1942 *Lithatractus* (*Lithatractona*) *pierinae* Clark and Campbell, p. 34, pl. 5, fig. 25.
1969a *Stylatractus pictus* Mamedov, p. 99, pl. 2, fig. 4–4a.
1972 *Axoprunum liostylum* (Ehrenberg) group – Petrushevskaya and Kozlova, p. 521, pl. 10, fig. 3.

1973 *Axoprunum pierinae* (Clark and Campbell) group – Sanfilippo and Riedel, p. 488, pl. 1, figs. 6–12, pl. 23, fig. 3.
1975 *Axoprunum liostylum* (Ehrenberg) group – Petrushevskaya, p. 571, pl. 2, fig. 22.
1976 *Axoprunum pierinae* (Clark and Campbell) – Dzinoridze et al., pl. 22, fig. 19.
1977 *Axoprunum pierinae* (Clark and Campbell) group – Riedel and Sanfilippo, pl. 4, fig. 16.
1987 *Axoprunum pierinae* (Clark and Campbell) – Nishimura, p. 720, pl. 1, fig. 6.
1989 *Sphaerostylus nicholasi* Blueford – Lazarus and Pallant, p. 364, pl. 6, figs. 19, 20, 23.
1992 *Axoprunum pierinae* (Clark and Campbell) – Takemura, p. 742, pl. 6, figs. 3–6.
1992 *Axoprunum magnum* Kim, p. 37, pl. 1, figs. 1, 2.
1993 *Stylosphaera minor brevichastata* Clark and Campbell – Vitukhin, pl. 6, fig. 7.
1993 *Axoprunum liostylum* (Ehrenberg) group – Vitukhin, pl. 15, figs. 1–4.
1995 *Axoprunum losbanosensis* (Clark and Campbell) – Shilov, p. 124, pl. 3, figs. 1a, 1b.
1995 *Axoprunum pierinae* (Clark and Campbell) – Strong et al., p. 208, fig. 10C.
1997 *Axoprunum pierinae* (Clark and Campbell) – Hollis et al., p. 44, pl. 1, figs. 7–13.
1997 *Axoprunum pierinae* (Clark and Campbell) – Takemura and Ling, p. 111, pl. 1, fig. 1.
1999a *Axoprunum pierinae* (Clark and Campbell) – O'Connor, p. 31, pl. 10, fig. 12.
1999 *Axoprunum chabakovi* (Lipman) – Kozlova, p. 68, pl. 27, fig. 7, pl. 28, fig. 3, pl. 29, fig. 3, pl. 38, fig. 1.
2003 *Axoprunum pierinae* (Clark and Campbell) group – Sanfilippo and Fourtanier, p. 11, pl. P2, fig. 7.
2005 *Axoprunum pierinae* (Clark and Campbell) – Funakawa and Nishi, p. 231, pl. 1, figs. 5a, 5b.
2006 *Axoprunum pierinae* (Clark and Campbell) – Funakawa et al., p. 39, pl. P13, figs. 15a, 15b.
2008 *Axoprunum pierinae* (Clark and Campbell) – Jackett et al., p. 47, pl. 3, fig. 14.
2009b *Axoprunum venustum* (Borisenko) – Suzuki et al., p. 241, pl. 1, figs. 1a, 1b.
2009b *Axoprunum* aff. *venustum* (Borisenko) – Suzuki et al., p. 241, pl. 1, figs. 2a, 2b.
2009b *Axoprunum bispiculum* (Popofsky) – Suzuki et al., p. 241, pl. 1, figs. 3a, 3b (part).
? 2009 *Stylosphaera liostylus* Ehrenberg – Ogane et al., pl. 26, figs. 2a–2c, pl. 63, figs. 1a–1e (part).
2019 *Amphistylus gladiusiacus* Vasilenko, p. 327, pl. 1, figs. 1–6.
2020 *Axoprunum pierinei* [sic] (Clark and Campbell) group – Holli et al., pl. 1, figs. 14, 15.
2021 *Axoprunum pierinae* (Clark and Campbell) – de Souza et al., p. 15, pl. 1, figs. 4a, 4b.

Occurrence. ODP Site 1260 (Demerara Rise; western equatorial Atlantic) and ODP Site 1051 (Blake Nose; western north Atlantic).

Axoprunum minor (Clark and Campbell, 1942)

Plate II.6, Figure 9

1942 *Stylosphaera* (*Stylosphaerantha*) *minor* Clark and Campbell, p. 27, pl. 5, figs. 1, 2, 2a, 12.
1945 *Stylosphaera* (*Stylosphaerantha*) *minor* Clark and Campbell – Clark and Campbell, p. 11, pl. 1, figs. 13–19.

1972 *Stylosphaera minor* Clark and Campbell – Petrushevskaya and Kozlova, p. 520, pl. 10, fig. 9.
1973 *Amphisphaera minor* (Clark and Campbell) – Sanfilippo and Riedel, p. 486, pl. 1, figs. 1–5, pl. 22, fig. 4.
1975 *Amphisphaera minor* (Clark and Campbell) – Chen, p. 452, pl. 3, fig. 1.
not 1976 *Stylosphaera minor* Clark and Campbell – Dzinoridze et al., pl. 22, figs. 12, 13.
1987 *Amphisphaera minor* (Clark and Campbell) – Nishimura, p. 719, pl. 1, fig. 5.
1988 *Stylosphaera minor* Clark and Campbell – Blueford, p. 247, pl. 4, figs. 4, 5 (part).
1992 *Amphisphaera minor* (Clark and Campbell) – Blome, p. 643, pl. 3, fig. 23.
1992 *Amphistylus* ? sp. Takemura, p. 741, pl. 5, figs. 9, 10.
1993 *Stylosphaera minor leptoxyphos* Clark and Campbell – Vitukhin, pl. 6, fig. 6.
1993 *Stylosphaera minor minor* Clark and Campbell – Vitukhin, pl. 22, fig. 5.
1993 *Stylosphaera minor* Clark and Campbell – Vitukhin, pl. 32, fig. 2.
1995 *Stylosphaera minor* Clark and Campbell – Shilov, p. 124, pl. 3, fig. 2.
? 1999a *Stylosphaera minor* Clark and Campbell – O'Connor, p. 38, pl. 8, fig. 23, pl. 10, fig. 28.
1999 *Stylosphaera minor* Clark and Campbell – Kozlova, p. 175, pl. 8, fig. 7, pl. 38, fig. 3.
2002 *Stylosphaera minor* Clark and Campbell – Hollis, pl. 1, fig. 13.
2003 *Amphisphaera minor* (Clark and Campbell) – Sanfilippo and Fourtanier, p. 11, pl. P2, fig. 6.
2008 *Amphisphaera minor* (Clark and Campbell) – Jackett et al., p. 47, pl. 3, fig. 13.
2009b *Axoprunum minor* (Clark and Campbell) – Suzuki et al., p. 241, pl. 1, figs. 5a–6c.
2009b *Xiphosphaerantha pallas* Haeckel – Suzuki et al., p. 241, pl. 1, figs. 7a–7b.
2020 *Axoprunum minor* (Clark and Campbell) – Hollis et al., pl. 1, fig. 12.

Occurrence. ODP Site 1260 (Demerara Rise; western equatorial Atlantic) and ODP Site 1051 (Blake Nose; western north Atlantic).

Family Saturnulidae Suzuki *in* Suzuki et al., 2021

Genus *Saturnalis* Haeckel, 1882

Type species.— *Saturnalis* (*Saturnalina*) *circularis* Haeckel, 1887, p. 131 (unfigured).

Saturnalis kennetti Dumitrică, 1985

Plate II.6, Figure 12

1973 ? *Saturnulus* sp. cf. *planetes* Haeckel – Dumitrică, p. 787, pl. 1, figs. 7, 8, pl. 5, fig. 7.
1976 *Saturnulus planetes* Haeckel – Johnson, p. 784, pl. 1, fig. 8.
1978 *Saturnulus planetes* Haeckel – Foreman, p. 784, pl. 1, fig. 8.
1985 *Saturnalis kennetti* Dumitrică, p. 189, pl. 2, figs. 1, 2, pl. 3, fig. 15.
1992 *Saturnalis* sp. A Blome, p. 645, pl. 4, fig. 9.
2002 *Saturnalis kennetti* Dumitrică – Hollis, pl. 1, fig. 17.
2008 *Saturnalis circularis* Haeckel – Jackett et al., p. 57, pl. 3, fig. 15.
2017 *Saturnalis kennetti* Dumitrică – Dumitrică and Hungerbühler, p. 122, pl. 6, figs. 1–2a.
2020 *Saturnalis circularis* Haeckel – Hollis et al., pl. 1, fig. 17.

Occurrence. ODP Site 1260 (Demerara Rise; western equatorial Atlantic).

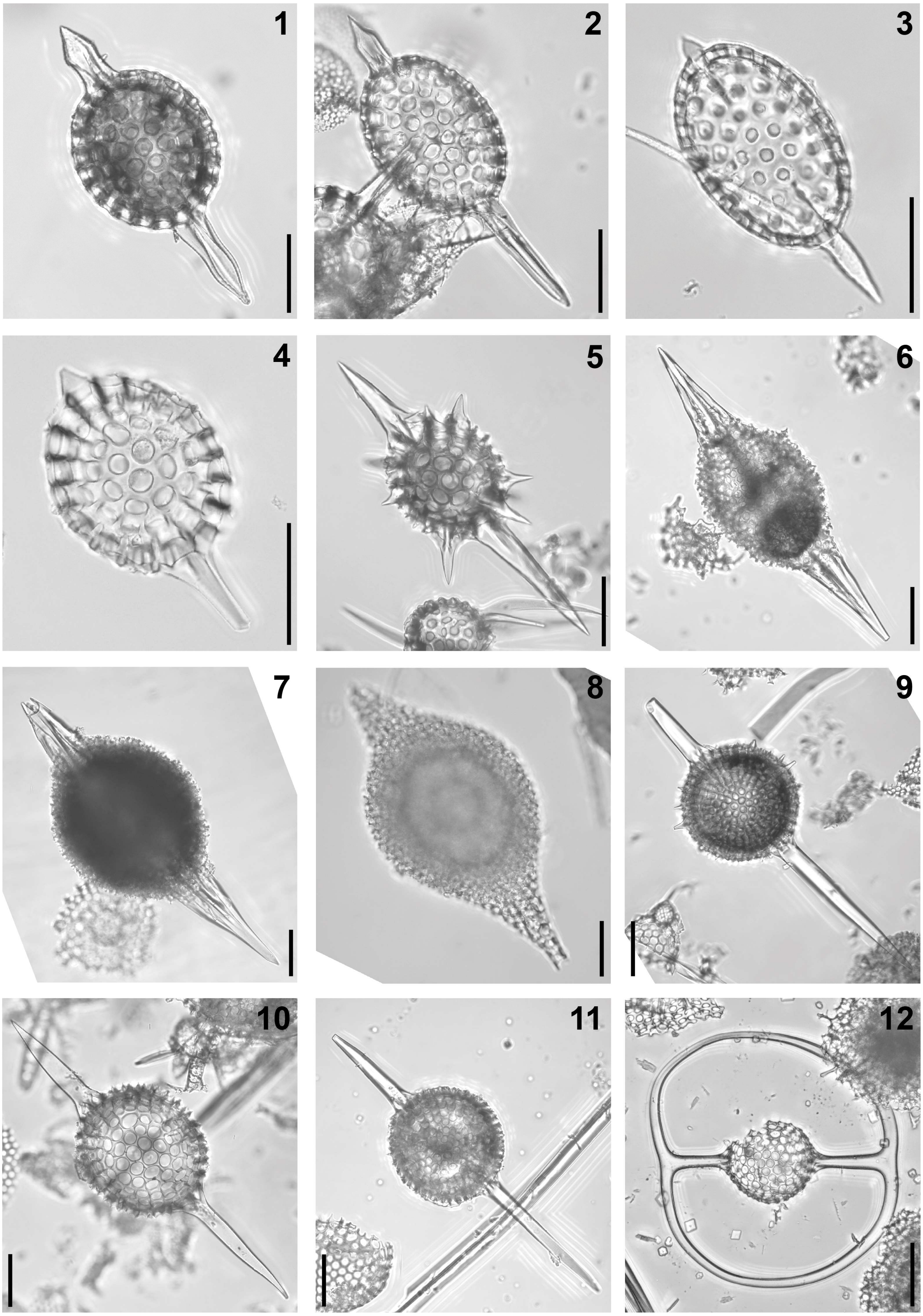
1
2
3
4
5
6
7
8
9
10
11
12

Plate II.6. Composite light micrographs of new radiolarian species from ODP Site 1260 (Demerara Rise, western equatorial Atlantic) and ODP Site 1051 (Blake Nose, western North Atlantic). (**1**) *Stylosphaera coronata* Ehrenberg, 1874: ODP 1260A-6R-CC, 66–177 cm. (**2, 3**) *Stylosphaera laevis* Ehrenberg, 1874: (**2**) ODP 1260A-13R-5W, 55–57 cm; (**3**) ODP 1051A-18X-5W, 54–56 cm. (**4**) *Stylosphaera radiosa* Ehrenberg, 1874: ODP 1051A-18X-5W, 54–56 cm. (**5**) *Stylosphaera spinulosa* Ehrenberg, 1874: ODP 1260A-8R-3W, 54–56 cm. (**6**) *Spongatractus balbis* Sanfilippo and Riedel, 1973: ODP 1260A-17R-3W, 55–57 cm. (**7**) *Spongatractus pachystylus* (Ehrenberg, 1874): ODP 1260A-10R-6W, 55–57 cm. (**8**) *Spongatractus* ? *klausi* Sanfilippo and Blome, 2001: ODP 1051A-9R-5W, 53–55 cm. (**9**) *Axoprunum minor* (Clark and Campbell, 1942): ODP 1260A-6R-4W, 55–57 cm. (**10, 11**) *Axoprunum pierinae* (Clark and Campbell, 1942) group: (**10**) ODP 1260A-13R-5W, 55–57 cm; (**11**) ODP 1260A-15R-1W, 55–57 cm.(**12**) *Saturnalis kennetti* Dumitrică, 1985: ODP 1260A-9R-3W, 55–57 cm. All scale bars equal 50 μm.

Order Nassellaria Ehrenberg, 1876
Superfamily Amphipyndacoidea Riedel, 1967a
Family Amphipyndacidae Riedel, 1967a
Genus *Amphipternis* Foreman, 1973

Type species.— *Lithocampe* ? *clava* Ehrenberg, 1874, p. 238 (unfigured); Ehrenberg, 1876, p. 76, pl. 4, fig. 2.

? *Amphipternis articulatum* (Ehrenberg, 1874)
Plate II.7, Figure 2

1874 *Eucyrtidium articulatum* Ehrenberg, p. 226.
1876 *Eucyrtidium articulatum* Ehrenberg – Ehrenberg, p. 70, pl. 11, figs. 2, 3.
1882a *Lithostrobus articulatus* (Ehrenberg) – Bütschli, p. 529.
1887 *Dictyomitra* (*Dictyomitrella*) *articulata* (Ehrenberg) – Haeckel, p. 1476.
? 1887 *Stichocapsa compacta* Haeckel, p. 1517, pl. 76, fig. 3.
1973 *Amphipternis clava* (Ehrenberg) – Foreman, p. 430, pl. 7, figs. 16, 17, pl. 9, figs. 2.
1976 *Amphipternis clava* (Ehrenberg) – Dzinoridze et al., pl. 29, fig. 11.
1977 *Amphipternis clava* (Ehrenberg) – Riedel and Sanfilippo, pl. 6, fig. 6.
1978 *Amphipternis clava* (Ehrenberg) – Johnson, p. 784, pl. 1, fig. 12.
1978 *Amphipternis clava* (Ehrenberg) – Foreman, p. 784, pl. 1, fig. 12.
1999 *Amphipternis clava* (Ehrenberg) – Kozlova, pl. 3, fig. 11.
2008 *Amphipternis clava* (Ehrenberg) – Jackett et al., p. 47, pl. 3, figs. 20, 21.
2009 *Eucyrtidium articulatum* Ehrenberg – Ogane et al., pl. 22, figs. 1a–1f.

Remarks. The combination used here is derived from O'Dogherty et al. (2021).
Occurrence. ODP Site 1260 (Demerara Rise; western equatorial Atlantic).

Amphipternis clava (Ehrenberg, 1874)
Plate II.7, Figure 1

1874 *Lithocampe* ? *Clava* [sic] Ehrenberg, p. 238.

1876 *Lithocampe* ? *Clava* [sic] Ehrenberg – Ehrenberg, p. 76, pl. 4, fig. 2.
1882a *Eucyrtidium Clava* [sic] (Ehrenberg) – Bütschli, p. 529.
1882b *Eucyrtidium clava* (Ehrenberg) – Bütschli, pl. 30, fig. 22.
1887 *Lithocampe* (*Lithocampium*) *clava* Ehrenberg – Haeckel, p. 1507.
2009 *Lithocampe clava* Ehrenberg – Ogane et al., pl. 25, figs. 2a–2c.
Remarks. The combination used here is derived from O'Dogherty et al. (2021).
Occurrence. ODP Site 1260 (Demerara Rise; western equatorial Atlantic).

Superfamily Archaeodictyomitroidea Pessagno, 1976
Family Archaeodictyomitridae Pessagno, 1976
Genus *Dictyomitra* Zittel, 1876

Type species.— *Dictyomitra multicostata* Zittel, 1876, p. 81, pl. 2, fig. 2.

Dictyomitra parva (Kim, 1992)
Plate II.7, Figure 3

1974 Theoperid gen. et sp. indet. Johnson, 1974, pl. 3, fig. 12 (part).
1974 sp. cf. *Lithomitra elizabethae* Clark and Campbell – Nigrini, p. 1070, pl. 1M, figs. 14–17, pl. 4, figs. 6, 7.
1977 *Siphocampe elizabethae* (Clark and Campbell) – Nigrini, p. 256, pl. 3, fig. 6.
1992 *Archaeodictyomitra* ? sp. Takemura, p. 744, pl. 3, figs. 1, 2.
1992 *Eucyrtidium parva* Kim, p. 43, pl. 2, figs. 7, 8.
1995 *Dictyomitra amygdala* Shilov, p. 126, pl. 1, fig. 4–6b.
1997 *Siphocampe* ? *"elizabethae"* (Clark and Campbell) – Hollis et al., p. 55, pl. 4, figs. 21–26.
1999 *Siphocampe minuta* (Clark and Campbell) – Kozlova, p. 141, pl. 18, fig. 9, pl. 24, fig. 9.
1999 *Siphocampe* ? *pusilla* Kozlova, p. 141, pl. 18, fig. 10 (part).
2002 *Siphocampe* ? *elizabethae* (Clark and Campbell) – Apel et al., p. 21, pl. P9, fig. 18.
2009b *Dictyoprora* ? *amygdala* (Shilov) – Suzuki et al., p. 263, pl. 18, fig. 3.
2020 *Siphocampe* ? *amygdala* (Shilov) – Hollis et al., pl. 8, figs. 11, 12.
Remarks. The combination used here is derived from O'Dogherty et al. (2021).
Occurrence. ODP Site 1260 (Demerara Rise; western equatorial Atlantic) and ODP Site 1051 (Blake Nose; western north Atlantic).

Superfamily Eucyrtidioidea Ehrenberg, 1846 emend. Suzuki et al., 2021
Family Eucyrtidiidae Ehrenberg, 1846 emend. Suzuki et al., 2021
Genus *Eucyrtidium* Ehrenberg, 1846

Type species.— *Lithocampe acuminata* Ehrenberg, 1844, p. 84, (unfigured); Ehrenberg, 1854a, pl. 22, fig. 27.

Eucyrtidium montiparum Ehrenberg, 1874
Plate II.7, Figure 4

1874 *Eucyrtidium montiparum* Ehrenberg, p. 230.

1876 *Eucyrtidium montiparum* Ehrenberg – Ehrenberg, p. 72, pl. 9, fig. 11.
1882a *Eucyrtidium montiparum* Ehrenberg – Bütschli, p. 529.
1887 *Eucyrtidium* (*Artocyrtis*) *montiparum* Ehrenberg – Haeckel, p. 1493.
1974 Theoperid gen. et sp. indet. Johnson, pl. 4, figs. 13, 14 (part).
1997 *Eucyrtidium montiparum* Ehrenberg – Hollis et al., p. 61, pl. 5, figs. 25–27.
1999a *Eucyrtidium ventriosum* O'Connor, p. 21, pl. 3, fig. 17–21b, pl. 6, fig. 28a–31.
not 2006 *Eucyrtidium montiparum* Ehrenberg – Funakawa et al., p. 23, pl. P5, figs. 10a–10b.
2006 *Eucyrtidium* sp. F Funakawa et al., p. 23, pl. P6, figs. 1a–2b (part).
2009 *Eucyrtidium montiparum* Ehrenberg – Ogane et al., pl. 1, figs. 6a–6e (part).
2020 *Eucyrtidium montiparum* Ehrenberg – Hollis et al., pl. 10, fig. 4.
2021 *Eucyrtidium montiparum* Ehrenberg – de Souza et al., p. 15, pl. 3, figs. 1a, 1b.
Occurrence. ODP Site 1260 (Demerara Rise; western equatorial Atlantic) and ODP Site 1051 (Blake Nose; western north Atlantic).

Eucyrtidium ? *microporum* Ehrenberg, 1874
Plate II.7, Figure 5

1874 *Eucyrtidium microporum* Ehrenberg, p. 230.
1876 *Eucyrtidium microporum* Ehrenberg – Ehrenberg, p. 72, pl. 11, fig. 20.
1882a *Lithostrobus microporus* (Ehrenberg) – Bütschli, p. 529.
1887 *Lithostrobus* (*Cyrtostrobus*) *microporus* (Ehrenberg) – Haeckel, p. 1474.
1972 *Stichopodium* ? *microporum* (Ehrenberg) – Petrushevskaya and Kozlova, p. 548, pl. 25, figs. 4–6.
2006 *Stichopodium* ? *microporum* (Ehrenberg) – Funakawa et al., p. 37, pl. P13, figs. 3a–4b.
2009 *Eucyrtidium microporum* Ehrenberg – Ogane et al., pl. 6, figs. 5a-5c, pl. 85, figs. 5a-5f.
2020 *Eucyrtidium microporum* Ehrenberg – Hollis et al., pl. 10, fig. 3.
Occurrence. ODP Site 1260 (Demerara Rise; western equatorial Atlantic) and ODP Site 1051 (Blake Nose; western north Atlantic).

Family Lithostrobidae Petrushevskaya, 1975
Genus *Lithostrobus* Bütschli, 1882a

Type species.— *Eucyrtidium argus* Ehrenberg, 1874, p. 225 (unfigured); Ehrenberg, 1876, p. 70, pl. 9, fig. 1.

Lithostrobus argus (Ehrenberg, 1874)
Plate II.7, Figure 6

1874 *Eucyrtidium Argus* [sic] Ehrenberg, p. 225.
1876 *Eucyrtidium Argus* [sic] Ehrenberg – Ehrenberg, p. 70, pl. 9, fig. 1.
1882a *Lithostrobus Argus* [sic] (Ehrenberg) – Bütschli, p. 529.
2009 *Eucyrtidium argus* Ehrenberg – Ogane et al., pl. 48, figs. 8a–8f.
Occurrence. ODP Site 1260 (Demerara Rise; western equatorial Atlantic).

Lithostrobus picus Ehrenberg, 1874

Plate II.7, Figures 7, 8

1874 *Eucyrtidium Picus* [sic] Ehrenberg, p. 232.

1876 *Eucyrtidium Picus* [sic] Ehrenberg – Ehrenberg, p. 72, pl. 11, fig. 1.

1882a *Lithostrobus Picus* [sic] (Ehrenberg) – Bütschli, p. 529.

not 1976 *Eucyrtidium* ? *picus* Ehrenberg – Dzinoridze et al., pl. 29, fig. 9.

1977 Artostrobiid gen. et sp. indet. Riedel and Sanfilippo, pl. 9, fig. 16.

2009 *Eucyrtidium picus* Ehrenberg – Ogane et al., pl. 86, figs. 6a–6g

Occurrence. ODP Site 1260 (Demerara Rise; western equatorial Atlantic) and ODP Site 1051 (Blake Nose; western north Atlantic).

Superfamily Plectopyramidoidea Haecker, 1908

Family Plectopyramididae Haecker, 1908

Genus *Bathropyramis* Haeckel, 1882

Type species.— *Bathropyramis* (*Acropyramis*) *acephala* Haeckel, 1887, p. 1159 (unfigured).

Bathropyramis scalaris (Ehrenberg, 1874)

Plate II.7, Figure 9

1874 *Cornutella scalaris* Ehrenberg, p. 221.

1876 *Cornutella scalaris* Ehrenberg – Ehrenberg, p. 68, pl. 2, fig. 1.

1887 *Sethopyramis* (*Sestropyramis*) *scalaris* (Ehrenberg) – Haeckel, p. 1253.

? 1887 *Sethopyramis* (*Cephalopyramis*) *enneactis* Haeckel, p. 1254, pl. 56, fig. 7.

1887 *Plectopyramis* (*Hexapleuris*) *magnifica* Haeckel, p. 1257.

1945 *Sethopyramis* (*Sestropyramis*) *pulcherrima* Clark and Campbell, p. 39, pl. 10, fig. 3.

1972 *Bathropyramis scalaris* (Ehrenberg) – Petrushevskaya and Kozlova, p. 551, pl. 31, fig. 6.

2009 *Cornutella scalaris* Ehrenberg – Ogane et al., pl. 21, 6a-6d.

2020 *Cinclopyramis scalaris* (Ehrenberg) – Hollis et al., pl. 8, figs. 28, 29.

Occurrence. ODP Site 1260 (Demerara Rise; western equatorial Atlantic) and ODP Site 1051 (Blake Nose; western north Atlantic).

Genus *Cornutella* Ehrenberg, 1839

Type species.— *Cornutella clathrata* Ehrenberg, 1839, p. 129; Ehrenberg, 1854a, pl. 22, fig. 39a.

Cornutella californica Campbell and Clark, 1944

Plate II.7, Figure 10

1944 *Cornutella* (*Cornutissa*) *californica* Campbell and Clark, p. 22, pl. 7, fig. 42.

1944 *Cornutella* (*Cornutissa*) *californica* var. brevis Campbell and Clark, p. 23, pl. 7, figs. 33, 34, 43.

1973 *Cornutella californica* Clark and Campbell – Dumitrică, p. 788, pl. 10, fig. 1.

1976 *Cornutella* sp. aff. *C. californica* Clark and Campbell – Bjørklund, p. 1124, pl. 23, figs. 23, 24.

1976 *Cornutella* sp. aff. *C. californica* Clark and Campbell – Dzinoridze et al., pl. 32, fig. 30.

1992 *Cornutella californica* Clark and Campbell – Blome, p. 644, pl. 3, figs. 13, 24.
1996 *Cornutella* sp. aff. *C. californica* Clark and Campbell – Hull, p. 138, pl. 5, fig. 6.
1996 *Cornutella profunda* Ehrenberg group – Hull, p. 138, pl. 5, fig. 17.
1996 *Cornutella* sp. Hull, p. 138, pl. 5, fig. 7.
1999a *Cornutella californica* Clark and Campbell – O'Connor, p. 31, pl. 9, fig. 12.
1999 *Cornutella californica* Clark and Campbell – Kozlova, p. 173, pl. 3, fig. 9.
2002 *Cornutella californica* Clark and Campbell – Hollis, pl. 6, fig. 5 (part).
2002 *Cornutella profunda* Ehrenberg group – Apel et al., p. 17, pl. P6, fig. 15 (part).
2013 *Cornutella profunda* Ehrenberg – Kochhann et al., p. 541, pl. 3, fig. A.
2021 *Cornutella profunda* Ehrenberg – de Souza et al., p. 15, pl. 2, fig. 15.
Occurrence. ODP Site 1260 (Demerara Rise; western equatorial Atlantic) and ODP Site 1051 (Blake Nose; western north Atlantic).

Cornutella circularis Ehrenberg, 1874
Plate II.7, Figure 12

1874 *Cornutella circularis* Ehrenberg, p. 221.
1876 *Cornutella circularis* Ehrenberg – Ehrenberg, p.68, pl. 2, fig. 4.
1882a *Ceratocyrtis circularis* (Ehrenberg) – Bütschli, p. 536.
1887 *Cornutella* (*Cornutissa*) *circularis* Ehrenberg – Haeckel, p. 1181.
1978 *Lithapium mitra* (Ehrenberg) – Riedel and Sanfilippo, p. 69, pl. 6, fig. 2 (part).
2015 *Cornutella* sp. A Kamikuri, pl. 13, figs. 28a, 28b.
Occurrence. ODP Site 1051 (Blake Nose; western north Atlantic).

Cornutella clava Petrushevskaya *in* Petrushevskaya and Kozlova, 1972
Plate II.7, Figure 11

1972 *Cornutella clava* Petrushevskaya *in* Petrushevskaya and Kozlova, p. 551, pl. 30, figs. 11, 16.
1977 *Cornutella* sp. Riedel and Sanfilippo, pl. 15, fig. 4 (part).
Occurrence. ODP Site 1051 (Blake Nose; western north Atlantic).

Cornutella stiligera Ehrenberg, 1854a
Plate II.7, Figure 13

1854a *Cornutella stiligera* Ehrenberg, pl. 36, fig. 4.
1876 *Cornutella stiligera* Ehrenberg – Ehrenberg, p. 68, pl. 2, fig. 3.
1882a *Cornutella stiligera* Ehrenberg – Bütschli, p. 537.
1887 *Cornutella* (*Cornutellium*) *stiligera* Ehrenberg – Haeckel, p. 1181.
1972 *Cornutella stiligera* Ehrenberg group – Petrushevskaya and Kozlova, p. 551, pl. 30, figs. 14, 15.
1975 *Cornutella profunda* Ehrenberg – Ling, p. 728, pl. 9, figs. 5–8.
1976 *Cornutella longisetta* [sic] Ehrenberg – Dzinoridze et al., pl. 32, fig. 31.
1977 *Cornutella* sp. Riedel and Sanfilippo, pl. 7, fig. 14, pl. 15, fig. 3 (part).
2002 *Cornutella profunda* Ehrenberg group – Apel et al., p. 17, pl. P6, figs. 13, 14 (part).
2009 *Cornutella stiligera* Ehrenberg – Ogane et al., pl. 7, figs. 6a, 6b, pl. 21, figs. 8a–9c.

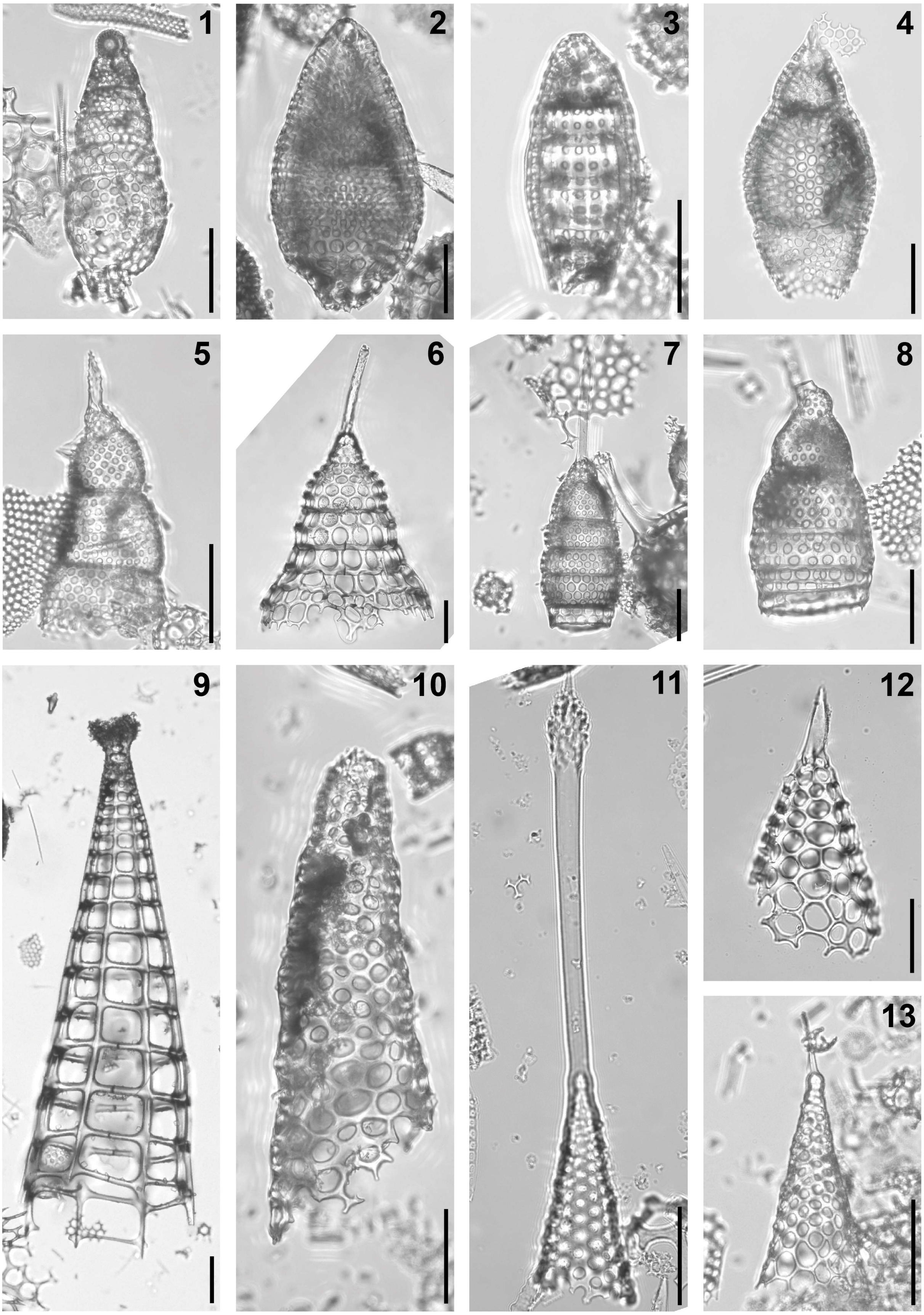
1
2
3
4
5
6
7
8
9
10
11
12
13

Plate II.7. Composite light micrographs of new radiolarian species from ODP Site 1260 (Demerara Rise, western equatorial Atlantic) and ODP Site 1051 (Blake Nose, western North Atlantic). (**1**) *Amphipternis clava* (Ehrenberg, 1874): ODP 1260A-20R-1W, 55–57 cm. (**2**) ? *Amphipternis articulatum* (Ehrenberg, 1874): ODP 1260A-9R-2W, 55–57 cm. (**3**) *Dictyomitra parva* (Kim, 1992): ODP 1260A-18R-2W, 55–57 cm. (**4**) *Eucyrtidium montiparum* Ehrenberg, 1874: ODP 1260A-6R-1W, 55–57 cm. (**5**) *Eucyrtidium* ? *microporum* Ehrenberg, 1874: ODP 1260A-18R-2W, 55–57 cm. (**6**) *Lithostrobus argus* (Ehrenberg, 1874): ODP 1260A-11R-7W, 55–57 cm. (**7, 8**) *Lithostrobus picus* Ehrenberg, 1874: (**7**) ODP 1260A-17R-2W, 55–57 cm; (**8**) ODP 1260A-13R-4W, 55–57 cm. (**9**) *Bathropyramis scalaris* (Ehrenberg, 1874): ODP 1260A-13R-4W, 55–57 cm. (**10**) *Cornutella californica* Campbell and Clark, 1944: ODP 1260A-13R-6W, 54–56 cm. (**11**) *Cornutella clava* Petrushevskaya *in* Petrushevskaya and Kozlova, 1972: ODP 1051A-11H-5W, 59–61 cm. (**12**) *Cornutella circularis* Ehrenberg, 1874: ODP 1051A-14H-5W, 54–56 cm. (**13**) *Cornutella stiligera* Ehrenberg, 1854a: ODP 1260A-12R-1W, 55–57 cm. All scale bars equal 50 µm.

2009b *Cornutella profunda* Ehrenberg – Suzuki et al., p. 263, pl. 22, figs. 12a, 12b.

Occurrence. ODP Site 1260 (Demerara Rise; western equatorial Atlantic) and ODP Site 1051 (Blake Nose; western north Atlantic).

Superfamily Carpocanioidea Haeckel, 1882

Family Carpocaniidae Haeckel, 1882 sensu Sugiyama, 1998

Genus *Carpocanium* Ehrenberg, 1846

Type species.— *Lithocampe solitaria* Ehrenberg, 1839, p. 130 (unfigured); Ehrenberg, 1854a, pl. 22, fig. 28.

Carpocanium azyx (Sanfilippo and Riedel, 1973)

Plate II.8, Figure 1

1973 *Carpocanistrum* ? *azyx* Sanfilippo and Riedel, p. 530, pl. 35, fig. 9.
1984 *Carpocanistrum* ? *azyx* Sanfilippo and Riedel – Saunders et al., p. 412, pl. 5, figs. 2, 3.
1984 *Cryptoprora ornata* Ehrenberg – Saunders et al., p. 412, pl. 5, fig. 4.
1992 *Carpocanistrum azyx* Sanfilippo and Riedel – Riedel and Sanfilippo, pl. 11, fig. 5.
1978 *Carpocanistrum azyx* Sanfilippo and Riedel – Riedel and Sanfilippo, p. 67, pl. 4, fig. 5.
1992 *Cryptocarpium azyx* (Sanfilippo and Riedel) – Sanfilippo and Riedel, p. 6, pl. 2, fig. 21
2000 *Cryptocarpium azyx* (Sanfilippo and Riedel) – Nigrini and Sanfilippo, p. 72, pl. 2, figs. 4–6.
2006 *Cryptocarpium azyx* (Sanfilippo and Riedel) – Funakawa et al., p. 28, pl. P9, figs. 5a, 5b.
2012 *Cryptocarpium azyx* (Sanfilippo and Riedel) – Moore and Kamikuri, p. 5, pl. P2, fig. 1.
2012 *Cryptocarpium azyx* (Sanfilippo and Riedel) – Kamikuri and Wade, pl. 1, fig. 14.
2012a *Cryptocarpium azyx* (Sanfilippo and Riedel) – Kamikuri et al., p. 96, pl. 3, figs. 9a, 9b.
2015 *Cryptocarpium azyx* (Sanfilippo and Riedel) – Kamikuri, pl. 12, figs. 17a–18.
not 2020 *Cryptocarpium azyx* (Sanfilippo and Riedel) – Hollis et al., pl. 17, figs. 6a, 6b.

Remarks. The combination used here is derived from O'Dogherty et al. (2021).
Occurrence. ODP Site 1051 (Blake Nose; western north Atlantic).

Genus *Carpocanopsis* Riedel and Sanfilippo, 1971

Type species.— *Carpocanopsis cingulatum* Riedel and Sanfilippo, 1971, p. 1597, pl. 8, fig. 8.

Carpocanopsis ballisticum O'Connor, 1999a

Plate II.8, Figure 2

1999a *Carpocanopsis ballisticum* O'Connor, p. 11, pl. 2, figs. 1–5, pl. 5, figs. 25a–28.
Occurrence. ODP Site 1051 (Blake Nose; western north Atlantic).

Carpocanopsis ornata (Ehrenberg, 1874)

Plate II.8, Figure 3

1874 *Cryptoprora ornata* Ehrenberg, p. 222.
1876 *Cryptoprora ornata* Ehrenberg – Ehrenberg, p. 68, pl. 5, fig. 8.
1882a *Cryptoprora ornata* Ehrenberg – Bütschli, p. 535.
1882b *Cryptoprora ornata* Ehrenberg – Bütschli, pl. 31, fig. 8.
1887 *Alacorys ornata* Ehrenberg – Haeckel, p. 1375.
1974 *Cryptoprora ornata* Ehrenberg – Johnson, p. 550, pl. 5, fig. 9.
1992 *Cryptocarpium ornata* (Ehrenberg) – Sanfilippo and Riedel, p. 6, 36, pl. 2, figs. 18–20.
1997 *Cryptocarpium ornatum* (Ehrenberg) – Hollis et al., p. 66, pl. 6, figs. 24, 25 (part).
? 2006 *Cryptocarpium ornatum* (Ehrenberg) – Funakawa et al., p. 28, pl. P9, figs. 8a, 8b (part).
2009 *Cryptoprora ornata* Ehrenberg – Ogane et al., pl. 6, figs. 2a–2c, pl. 83, figs. 5a–6d.
not 2012 *Cryptocarpium ornatum* (Ehrenberg) – Moore and Kamikuri, p. 6, pl. P2, figs. 2–4.
? 2012 *Cryptocarpium ornatum* (Ehrenberg) – Kamikuri and Wade, pl. 1, figs. 4a, 4b.
? 2015 *Cryptocarpium ornatum* (Ehrenberg) – Kamikuri, pl. 12, figs. 21a, 21b.
2017 *Cryptocarpium ornatum* (Ehrenberg) – de Souza et al., pl. 1, fig. 5.
2020 *Cryptocarpium ornatum* (Ehrenberg) – Hollis et al., pl. 17, figs. 9a, 9b.
2021 *Cryptocarpium ornatum* (Ehrenberg) – de Souza et al., p. 15, pl. 3, fig. 17a, 17b.
Remarks. The combination used here is derived from O'Dogherty et al. (2021).
Occurrence. ODP Site 1260 (Demerara Rise; western equatorial Atlantic) and ODP Site 1051 (Blake Nose; western north Atlantic).

Superfamily Artostrobioidea Riedel, 1967a

Family Artostrobiidae Riedel, 1967a sensu Sugiyama, 1998

Genus *Botryostrobus* Haeckel, 1887 emend. Nigrini, 1977

Type species.— *Lithostrobus* (*Botryostrobus*) *botryocyrtis* Haeckel, 1887, p. 1475, pl. 79, figs. 18, 19.

Botryostrobus joides Petrushevskaya, 1975

Plate II.8, Figure 4

1972 *Botryostrobus* sp. P Petrushevskaya and Kozlova, p. 539, pl. 24, figs. 8–11

1975 *Botryostrobus joides* Petrushevskaya, p. 585, pl. 10, fig. 37.
1976 *Botryostrobus joides* Petrushevskaya – Bjørklund, pl. 23, figs. 7–14.
not 1976 *Botryostrobus joides* Petrushevskaya – Dzinoridze et al., pl. 29, fig. 8.
1979 *Botryostrobus joides narratus* Petrushevskaya and Kozlova, p. 148, fig. 361.
1989 *Botryostrobus joides* Petrushevskaya group – Lazarus and Pallant, p. 361, pl. 4, fig. 13 (part).
1989 Nassellarian gen. et sp. indet. Lazarus and Pallant, pl. 4, figs. 17, 18.
1996 *Botryostrobus joides* Petrushevskaya – Hull, p. 137, pl. 4, figs. 5, 6, 20.
1997 *Spirocyrtis* sp. A Hollis et al., p. 56, pl. 4, figs. 33–35.
2002 *Spirocyrtis greeni* O'Connor – Apel et al., p. 21, pl. P9, fig. 1.
2003 *Botryostrobus joides* Petrushevskaya – Sanfilippo and Fourtanier, p. 11, pl. P1, figs.3, 12.
2009b *Lithostrobus cyrtoceras* Haeckel – Suzuki et al., p. 259, pl. 21, fig. 16.
2020 *Spirocyrtis greeni* O'Connor – Hollis et al., pl. 8, figs. 13a, 13b.
not 2020 *Spirocyrtis joides* (Petrushevskaya) – Hollis et al., pl. 8, figs. 14a, 14b.
2021 *Botryostrobus joides* Petrushevskaya – de Souza et al., p. 15, pl. 2, fig. 12.

Occurrence. ODP Site 1260 (Demerara Rise; western equatorial Atlantic) and ODP Site 1051 (Blake Nose; western north Atlantic).

Botryostrobus kerguelensis Caulet, 1991
Plate II.8, Figure 5

1985 *Botryostrobus* sp. Caulet, pl. 6, fig. 2.
1991 *Botryostrobus kerguelensis* Caulet, p. 535, pl. 3, figs. 6–8.
2002 *Botryostrobus kerguelensis* Caulet – Apel et al., p. 17, pl. P9, fig. 2.

Occurrence. ODP Site 1260 (Demerara Rise; western equatorial Atlantic) and ODP Site 1051 (Blake Nose; western north Atlantic).

Genus *Buryella* Foreman, 1973

Type species.— *Buryella tetradica* Foreman, 1973, p. 433, pl. 9, fig. 14.

Buryella ? *apiculata* Tetard et al., 2023
Plate II.8, Figure 8

2023 *Buryella apiculata* Tetard et al., p. 8, figs. 4k, 4l, 5k–5o.

Occurrence. ODP Site 1260 (Demerara Rise; western equatorial Atlantic)

Buryella clinata Foreman, 1973
Plate II.8, Figure 6

1970 *Lithocampe* sp. Cita et al., p. 404, pl. 2, fig. M.
1970 *Lithocampium* sp. Riedel and Sanfilippo, p. 533, pl. 10, fig. 8.
1973 *Buryella clinata* Foreman, p. 433, pl. 8, figs. 1–3, pl. 9, fig. 19.
1974 *Buryella clinata* Foreman – Nigrini, p. 1067, pl. 4, fig. 1.
1975 *Buryella clinata* Foreman – Foreman, p. 620, pl. 9, figs. 35, 36.
1977 *Buryella clinata* Foreman – Riedel and Sanfilippo, pl. 7, fig. 16.

1978 *Buryella clinata* Foreman – Weaver and Dinkelman, p. 867, pl. 8, figs. 6, 7.
1978 *Buryella clinata* Foreman – Riedel and Sanfilippo, p. 65, pl. 3, fig. 4.
1985 *Buryella clinata* Foreman – Sanfilippo et al., p. 668, figs. 14.1a–14.1f.
1987 *Buryella clinata* Foreman – Nishimura, p. 720, pl. 2, figs. 5, 6.
1998a *Buryella clinata* Foreman – Sanfilippo and Nigrini, p. 272, pl. 13.1, figs. 5, 6.
1999 *Buryella clinata* Foreman – Kozlova, p. 135, pl. 24, fig. 11, pl. 44, fig. 20.
2008 *Buryella clinata* Foreman – Jackett et al., p. 48, pl. 2, fig. 17.
2015 *Buryella clinata* Foreman – Kamikuri, pl. 12, fig. 9.
2017 *Buryella clinata* Foreman – de Souza et al., pl. 2, figs. 3a, 3b.
Occurrence. ODP Site 1051 (Blake Nose; western north Atlantic).

Buryella tetradica Foreman, 1973
Plate II.8, Figure 7

1971 *Lithocampium* sp. A Riedel and Sanfilippo, p. 1594, pl. 7, fig. 12.
1972 *Lithocampium* sp. A Benson, p. 1093, pl. 2, figs. 8, 9.
1973 *Buryella tetradica* Foreman, p. 433, pl. 8, figs. 4, 5, pl. 9, figs. 13, 14.
1975 *Buryella tetradica* Foreman – Petrushevskaya, pl. 8, fig. 23.
1978 *Buryella tetradica* Foreman – Johnson, p. 784, pl. 1, fig. 11.
1978 *Buryella tetradica* Foreman – Riedel and Sanfilippo, p. 65, pl. 3, fig. 5.
1978 *Buryella tetradica* Foreman – Foreman, p. 784, pl. 1, fig. 11.
1980 *Buryella tetradica* Foreman – Westberg et al., p. 431, pl. 1, fig. 9.
1985 *Buryella tetradica* Foreman – Sanfilippo et al., p. 668, figs. 14.3a, 14.3b.
1985 *Buryella tetradica* Foreman – Riedel and Sanfilippo, pl. 5, fig. 14.
1987 *Buryella tetradica* Foreman – Nishimura, p. 721, pl. 2, fig. 8.
1992 *Buryella tetradica* Foreman – Nishimura, p. 329, pl. 10, fig. 12.
1992 *Buryella tetradica* Foreman – Kim, p. 42, pl. 1, figs. 12, 13.
1993 *Buryella tetradica* Foreman – Hull, p. 12, pl. 7, fig. 2.
not 1993 *Buryella tetradica* Foreman – Vitukhin, p. 84, pl. 1, fig. 4.
1995 *Buryella tetradica* Foreman – Strong et al., p. 208, figs. 8N, 9Q, 9R.
1997 *Buryella tetradica* Foreman – Hollis et al., p. 81, pl. 21, figs. 16–19.
1998a *Buryella tetradica* Foreman – Sanfilippo and Nigrini, p. 272, pl. 13.1, figs. 8, 9.
1999 *Buryella tetradica* Foreman – Kozlova, p. 136, pl. 7, fig. 8, pl. 8, fig. 16, pl. 14, fig. 11, pl. 44, fig. 25.
2000 ? *Buryella tetradica* Foreman – Nigrini and Sanfilippo, p. 72, pl. 3, fig. 3.
2001 *Buryella tetradica* Foreman – Sanfilippo and Blome, p. 210.
2001 *Buryella tetradica* Foreman var. A – Sanfilippo and Blome, p. 210, figs. 8d, 8e.
2002 *Buryella tetradica tetradica* Foreman – Hollis, p. 300, pl. 4, figs. 13, 14.
2008 *Buryella tetradica* Foreman s.s. – Jackett et al., p. 48, pl. 2, fig. 20.
2008 *Buryella tetradica* Foreman var. A – Jackett et al., p. 48, pl. 2, fig. 21.
2015 *Buryella tetradica* Foreman – Kamikuri, pl. 12, fig. 12.
2017 *Buryella tetradica* Foreman – de Souza et al., pl. 2, figs. 4a, 4b.
2020 *Buryella tetradica* Foreman – Hollis et al., pl. 8, fig. 3.
Occurrence. ODP Site 1051 (Blake Nose; western north Atlantic).

Genus *Dictyoprora* Haeckel, 1887

Type species.— *Dictyocephalus* (*Dictyoprora*) *amphora* Haeckel, 1887, p. 1305, pl. 62, fig. 4.

Dictyoprora armadillo (Ehrenberg, 1874) group

Plate II.8, Figure 9

1874 *Eucyrtidium Armadillo* [sic] Ehrenberg, p. 225.
1876 *Eucyrtidium Armadillo* [sic] Ehrenberg – Ehrenberg, p. 70, pl. 9, fig. 10.
1882a *Eucyrtidium Armadillo* [sic] Ehrenberg – Bütschli, p. 528.
1887 *Sethocorys armadillo* (Ehrenberg) – Haeckel, p. 1302.
1971 *Theocampe armadillo* (Ehrenberg) group – Riedel and Sanfilippo, p. 1601, pl. 3E, figs. 3, 5 (part).
1974 *Theocampe armadillo* (Ehrenberg) group – Nigrini, p. 1070, pl. 1M, fig. 6 (part).
1977 *Theocampe armadillo* (Ehrenberg) group – Riedel and Sanfilippo, pl. 11, fig. 8 (part).
1977 *Dictyoprora armadillo* (Ehrenberg) – Nigrini, p. 250, pl. 4, fig. 4.
1981 *Dictyoprora armadillo* (Ehrenberg) – De Wever, p. 511, pl. 4, fig. 5.
2005 *Dictyoprora armadillo* (Ehrenberg) group – Nigrini et al., p. 31, pl. 6, fig. 9
2006 *Dictyoprora armadillo* (Ehrenberg) – Funakawa et al., p. 17, pl. P2, figs. 3a–4b.
2009 *Eucyrtidium armadillo* Ehrenberg – Ogane et al., pl. 83, figs. 1a–2b.
2012 *Dictyoprora armadillo* (Ehrenberg) group – Moore and Kamikuri, p. 6, pl. P2, fig. 5.
2015 *Dictyoprora armadillo* (Ehrenberg) – Kamikuri, pl. 12, figs. 7 (part).

Occurrence. ODP Site 1260 (Demerara Rise; western equatorial Atlantic) and ODP Site 1051 (Blake Nose; western north Atlantic).

Dictyoprora crassiceps (Ehrenberg, 1874) group

Plate II.8, Figure 14

1874 *Eucyrtidium crassiceps* Ehrenberg, p. 227.
1876 *Eucyrtidium crassiceps* Ehrenberg – Ehrenberg, p. 70, pl. 11, fig. 4.
1887 *Dictyocephalus* (*Dictyoprora*) *urceolus* Haeckel, p. 1305, pl. 62, fig. 4.
1887 *Dictyocephalus* (*Dictyoprora*) *crassiceps* (Ehrenberg) – Haeckel, p. 1306.
1971 *Lithomitra* sp. aff. *L. lineata* (Ehrenberg) group – Riedel and Sanfilippo, pl. 3E, figs. 17, 18 (part).
1973 *Theocampe urceolus* (Haeckel) – Foreman, p. 432, pl. 8, figs. 14–17, pl. 9, figs. 6, 7.
1977 *Dictyoprora urceolus* (Haeckel) – Nigrini, p. 251, pl. 4, figs. 9, 10.
1981 *Dictyoprora urceolus* (Haeckel) – De Wever, p. 511, pl. 4, fig. 14.
1987 *Dictyoprora urceolus* (Haeckel) – Nishimura, p. 725, pl. 2, fig. 2 (part).
1992 *Dictyoprora pirum* (Ehrenberg) – Takemura, p. 743, pl. 5, fig. 11.
1995 *Theocampe urceolus* (Haeckel) – Strong et al., p. 209, fig. 10Q.
1997 *Theocampe urceolus* (Haeckel) – Hollis et al., p. 56, pl. 4, figs. 36, 37.
2003 *Dictyoprora urceolus* (Haeckel) – Sanfilippo and Fourtanier, p. 12, pl. P2, fig. 10 (part).
2008 *Dictyoprora urceolus* (Haeckel) – Jackett et al., p. 52, pl. 3, fig. 17.
2020 *Theocampe urceolus* (Haeckel) – Hollis et al., pl. 8, fig. 22.
2021 *Dictyoprora urceolus* (Haeckel) – de Souza et al., p. 15, pl. 2, fig. 13.

Remarks. The combination used here is derived from O'Dogherty et al. (2021).

Occurrence. ODP Site 1260 (Demerara Rise; western equatorial Atlantic) and ODP Site 1051 (Blake Nose; western north Atlantic).

Dictyoprora excellens (Ehrenberg, 1874) group
Plate II.8, Figures 11, 12

1874 *Eucyrtidium excellens* Ehrenberg, p. 228.
1876 *Eucyrtidium excellens* Ehrenberg – Ehrenberg, p. 70, pl. 10, fig. 2.
1882a *Eucyrtidium excellens* Ehrenberg – Bütschli, pl. 33, figs. 31a, 31b.
1882b *Eucyrtidium excellens* Ehrenberg – Bütschli, pl. 30, fig. 18.
1887 *Dictyocephalus* (*Dictyoprora*) *amphora* Haeckel, p. 1305, pl. 62, fig. 4.
1887 *Dictyocephalus* (*Dictyoprora*) *excellens* (Ehrenberg) – Haeckel, p. 1306.
1973 *Theocampe amphora* (Haeckel) group – Foreman, p. 431, pl. 8, figs. 7, 9–13.
1974 *Theocampe amphora* (Haeckel) group – Nigrini, p. 1070, pl. 1M, figs. 2–5 (part).
1977 *Theocampe amphora* (Haeckel) group – Riedel and Sanfilippo, pl. 9, fig. 13 (part).
1977 *Dictyoprora amphora* (Haeckel) group – Nigrini, p. 250, pl. 4, figs. 1, 2
1986 *Dictyoprora amphora* (Haeckel) group – Riedel and Sanfilippo, pl. 4, fig. 8.
? 1987 *Dictyoprora amphora* (Haeckel) – Nishimura, p. 725, pl. 2, fig. 3.
not 1989 ? *Dictyoprora amphora* (Haeckel) – Lazarus and Pallant, p. 363, pl. 6, figs. 8, 9.
? 1999 *Buryella longa* Kozlova – Kozlova, p. 136, pl. 23, fig. 13.
not 2006 *Dictyoprora amphora* (Haeckel) group – Funakawa et al., p. 16, pl. P2, figs. 1a–2b.
2008 *Dictyoprora amphora* (Haeckel) – Jackett et al., p. 52, pl. 3, fig. 18.
2009 *Eucyrtidium gemmatum* Ehrenberg – Ogane et al., pl. 48, figs. 1a–1c (part).
2009 *Eucyrtidium excellens* Ehrenberg – Ogane et al., pl. 48, figs. 2a–4d (part).
2020 *Theocampe amphora* (Haeckel) – Hollis et al., pl. 8, figs. 20a, 20b.

Remarks. The combination used here is derived from O'Dogherty et al. (2021).
Occurrence. ODP Site 1260 (Demerara Rise; western equatorial Atlantic).

Dictyoprora gibsoni O'Connor, 1994
Plate II.8, Figure 16

1971 *Lithomitra* sp. aff. *L. lineata* (Ehrenberg) group – Riedel and Sanfilippo, pl. 3E, fig. 15 (part).
1981 *Dictyoprora pirum* (Ehrenberg) – De Wever, p. 511, pl. 4, fig. 7.
1994 *Dictyoprora gibsoni* O'Connor, p. 338, pl. 1, figs. 5, 6, 8, pl. 3, figs. 4–7.
1997 *Theocampe urceolus* (Haeckel) – Hollis et al., p. 56, pl. 4, fig. 36 (part).
? 2003 *Dictyoprora urceolus* (Haeckel) – Sanfilippo and Fourtanier, p. 12, pl. P2, figs. 11, 12 (part).
2015 *Dictyoprora gibsoni* O'Connor – Kamikuri, pl. 12, fig. 13.

Occurrence. ODP Site 1260 (Demerara Rise; western equatorial Atlantic) and ODP Site 1051 (Blake Nose; western north Atlantic).

Dictyoprora mongolfieri (Ehrenberg, 1854a)
Plate II.8, Figure 13

1854a *Eucyrtidium Mongolfieri* [sic] Ehrenberg, pl. 36, fig. 18.

1862 *Eucyrtidium Mongolfieri* [sic] Ehrenberg – Bury, p. 5, fig. 2.
? 1874 *Eucyrtidium gemmatum* Ehrenberg, p. 229.
1874 *Eucyrtidium Mongolfieri* [sic] Ehrenberg – Ehrenberg, p. 230.
? 1876 *Eucyrtidium gemmatum* Ehrenberg – Ehrenberg, p. 70, pl. 10, fig. 6.
1876 *Eucyrtidium Mongolfieri* [sic] Ehrenberg – Ehrenberg, p. 72, pl. 10, fig. 3.
? 1882a *Eucyrtidium gemmatum* Ehrenberg – Bütschli, p. 528.
1882a *Eucyrtidium Mongolfieri* [sic] Ehrenberg – Bütschli, p. 528.
1887 *Sethamphora* (*Dictyoprona*) *mongolfieri* (Ehrenberg) – Haeckel, p. 1251.
1887 *Sethamphora* (*Dictyoprona*) *costata* Haeckel, p. 1251, pl. 62, fig. 3.
? 1887 *Theocampe* (*Theocamptra*) *gemmata* (Ehrenberg) – Haeckel, p. 1425.
1887 *Theocampe* (*Theocamptra*) *costata* Haeckel, p. 1426, pl. 66, fig. 24.
1944 *Dictyocephalus* (*Dictyoprora*) sp. Campbell and Clark, p. 28, pl. 7, fig. 20.
1957a *Sethamphora mongolfieri* (Ehrenberg) – Riedel, p. 260, pl. 63, fig. 6.
1957b *Sethamphora mongolfieri* (Ehrenberg) – Riedel, p. 81, pl. 1, fig. 7.
1970 *Sethamphora mongolfieri* (Ehrenberg) – Cita et al., p. 401, pl. 1, fig. F.
1970 *Theocampe mongolfieri* (Ehrenberg) – Riedel and Sanfilippo, p. 536, pl. 12, fig. 9.
1971 *Theocampe mongolfieri* (Ehrenberg) – Riedel and Sanfilippo, p. 1601, pl. 3E, fig. 13.
1971 *Theocampe mongolfieri* (Ehrenberg) – Moore, p. 744, pl. 2, fig. 3.
1973 *Theocampe mongolfieri* (Ehrenberg) – Foreman, p. 432, pl. 8, fig. 6, pl. 9, fig. 17.
1974 *Theocampe mongolfieri* (Ehrenberg) – Nigrini, p. 1070, pl. 1M, figs. 7–10, pl. 2E, fig. 9.
1974 *Theocampe mongolfieri* (Ehrenberg) – Johnson, p. 552, pl. 2, figs. 3, 5, pl. 5, fig. 1.
1975 *Theocampe amphora* (Haeckel) group – Ling, p. 732, pl. 13, figs. 14.
1975 *Theocampe mongolfieri* (Ehrenberg) – Ling, p. 732, pl. 13, figs. 16, 17.
1977 *Theocampe mongolfieri* (Ehrenberg) – Riedel and Sanfilippo, pl. 8, fig. 7.
1977 *Theocampe amphora* (Haeckel) group – Riedel and Sanfilippo, pl. 9, fig. 14 (part).
1977 *Dictyoprora mongolfieri* (Ehrenberg) – Nigrini, p. 250, pl. 4, fig. 7
1978 *Theocampe mongolfieri* (Ehrenberg) – Riedel and Sanfilippo, p. 76, pl. 9, fig. 13.
1981 *Dictyoprora mongolfieri* (Ehrenberg) – De Wever, p. 511, pl. 4, figs. 8–10.
1986 *Dictyoprora mongolfieri* (Ehrenberg) – Riedel and Sanfilippo, pl. 4, fig. 9.
1992 *Dictyoprora mongolfieri* (Ehrenberg) – Takemura, p. 743, pl. 7, fig. 12.
1995 *Dictyoprora mongolfieri* (Ehrenberg) – Shilov, p. 126, pl. 2, fig. 6.
1995 *Theocampe mongolfieri* (Ehrenberg) – Strong et al., p. 209, fig. 10P.
2000 *Dictyoprora mongolfieri* (Ehrenberg) – Nigrini and Sanfilippo, p. 72, pl. 1, fig. 10, pl. 2, fig. 9.
2006 *Dictyoprora mongolfieri* (Ehrenberg) – Funakawa et al., p. 17, pl. P2, figs. 5a–6b.
2009b *Dictyoprora mongolfieri* (Ehrenberg) – Suzuki et al., p. 263, pl. 18, figs. 2a, 2b.
? 2009 *Eucyrtidium gemmatum* Ehrenberg – Ogane et al., pl. 18, figs. 9a–9e (part).
2012 *Dictyoprora mongolfieri* (Ehrenberg) – Moore and Kamikuri, p. 6, pl. P2, fig. 6.
2012 *Dictyoprora mongolfieri* (Ehrenberg) – Kamikuri and Wade, pl. 1, fig. 15.
2012a *Dictyoprora mongolfieri* (Ehrenberg) – Kamikuri et al., p. 98, pl. 3, figs. 6a, 6b.
2012b *Dictyoprora mongolfieri* (Ehrenberg) – Kamikuri et al., p. 3, pl. P1, fig. 9.
2015 *Dictyoprora mongolfieri* (Ehrenberg) – Kamikuri, pl. 12, figs. 15, 16.
2017 *Dictyoprora mongolfieri* (Ehrenberg) – de Souza et al., pl. 1, figs. 4a, 4b.

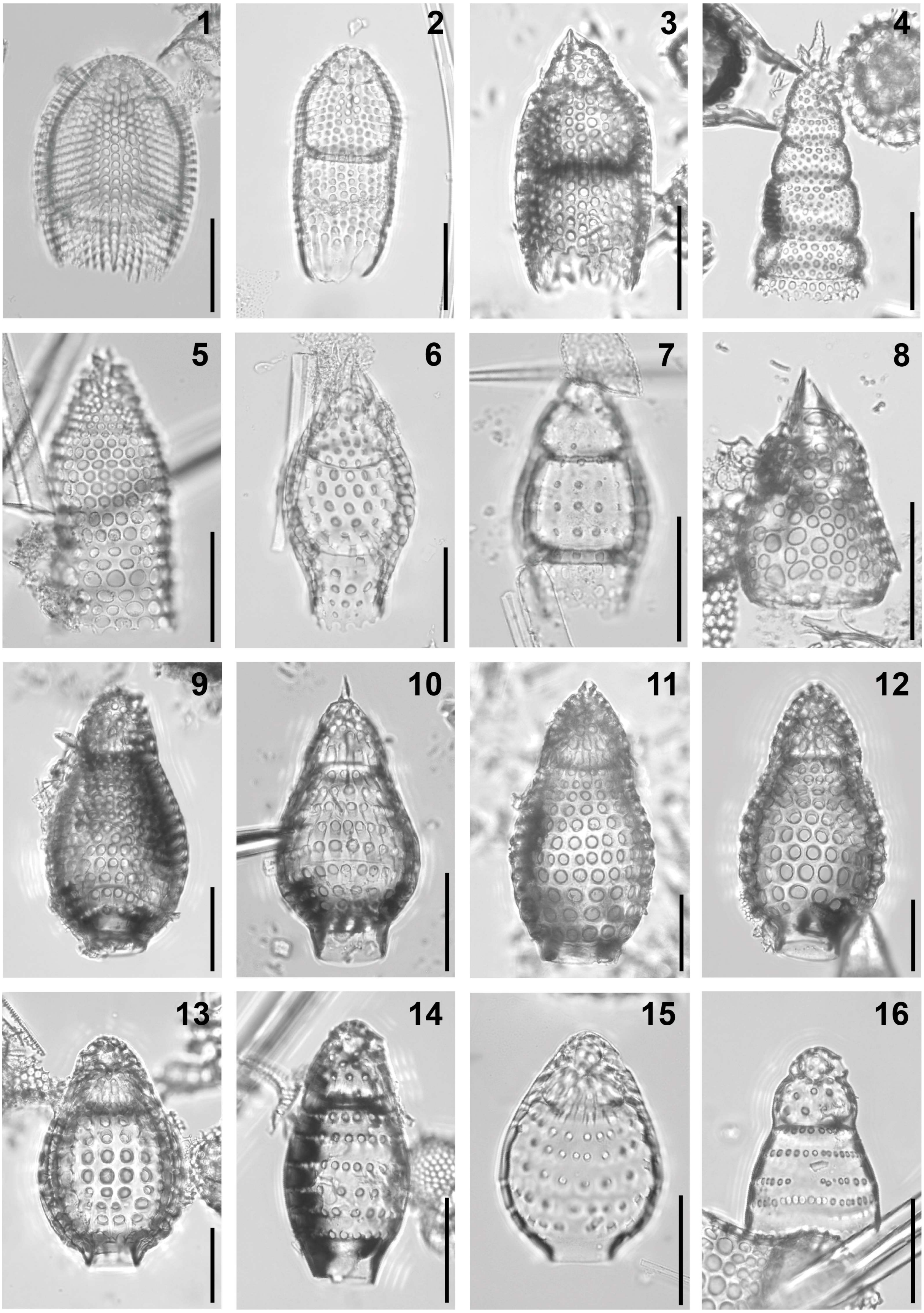
1
2
3
4
5
6
7
8
9
10
11
12
13
14
15
16

Plate II.8. Composite light micrographs of new radiolarian species from ODP Site 1260 (Demerara Rise, western equatorial Atlantic) and ODP Site 1051 (Blake Nose, western North Atlantic). (**1**) *Carpocanium azyx* (Sanfilippo and Riedel, 1973): ODP 1051A-4H-5W, 56–58 cm. (**2**) *Carpocanopsis ballisticum* O'Connor, 1999a: ODP 1051A-18X-5W, 54–56 cm. (**3**) *Carpocanopsis ornata* (Ehrenberg, 1874): ODP 1260A-17R-2W, 55–57 cm. (**4**) *Botryostrobus joides* Petrushevskaya, 1975: ODP 1260A-9R-2W, 55–57 cm. (**5**) *Botryostrobus kerguelensis* Caulet, 1991: ODP 1051A-4H-5W, 56–58 cm. (**6**) *Buryella clinata* Foreman, 1973: ODP 1051A-38X-5W, 55–57 cm. (**7**) *Buryella tetradica* Foreman, 1973: ODP 1051A-6H-5W, 53–55 cm. (**8**) *Buryella* ? *apiculata* Tetard et al., 2023: ODP 1260A-8R-5W, 54–56 cm. (**9**) *Dictyoprora armadillo* (Ehrenberg, 1874) group: ODP 1260A-6R-3W, 55–57 cm. (**10**) *Dictyoprora ovata* (Haeckel, 1887) group: ODP 1260A-9R-3W, 55–57 cm. (**11, 12**) *Dictyoprora excellens* (Ehrenberg, 1874) group: (**11**) ODP 1260A-12R-4W, 55–57 cm; (**12**) ODP 1260A-11R-7W, 55–57 cm. (**13**) *Dictyoprora mongolfieri* (Ehrenberg, 1854a): ODP 1260A-13R-5W, 55–57 cm. (**14**) *Dictyoprora crassiceps* (Ehrenberg, 1874) group: ODP 1260A-6R-3W, 55–57 cm. (**15**) *Dictyoprora pirum* (Ehrenberg, 1874): ODP 1051A-9H-5W, 53–55 cm. (**16**) *Dictyoprora gibsoni* O'Connor, 1994: ODP 1260A-11R-7W, 55–57 cm. All scale bars equal 50 µm.

2020 *Theocampe mongolfieri* (Ehrenberg) – Hollis et al., pl. 8, figs. 18a, 18b.
2020 *Theocampe* cf. *mongolfieri* (Ehrenberg) – Hollis et al., pl. 8, figs. 19a, 19b.
Occurrence. ODP Site 1260 (Demerara Rise; western equatorial Atlantic) and ODP Site 1051 (Blake Nose; western north Atlantic).

Dictyoprora ovata (Haeckel, 1887) group
Plate II.8, Figure 10

1887 *Theocorys* (*Theocoronium*) *ovata* Haeckel, p. 1416, pl. 69, fig. 16.
1958 *Theocorys* sp. Göke, pl. 4, fig. 2.
1971 *Theocampe armadillo* (Ehrenberg) group – Riedel and Sanfilippo, p. 1601, pl. 3E, figs. 4, 6 (part).
1974 *Theocampe amphora* (Haeckel) group – Nigrini, p. 1070, pl. 2E, fig. 7 (part).
1974 *Theocampe armadillo* (Ehrenberg) group – Nigrini, p. 1070, pl. 2E, fig. 8 (part).
1974 *Theocampe amphora* (Haeckel) group – Johnson, p. 552, pl. 4, fig. 2 (part).
1975 *Theocampe armadillo* (Ehrenberg) – Ling, p. 732, pl. 13, fig. 15.
1977 *Theocampe armadillo* (Ehrenberg) group – Riedel and Sanfilippo, pl. 11, fig. 9 (part).
2005 *Dictyoprora* cf. *D. ovata* (Haeckel) – Nigrini et al., pl. P6, fig. 8.
2006 *Dictyoprora ovata* (Haeckel) – Funakawa et al., p. 17, pl. P2, figs. 7a, 7b
2015 *Dictyoprora armadillo* (Ehrenberg) – Kamikuri, pl. 12, figs. 4a, 4b (part).
Occurrence. ODP Site 1260 (Demerara Rise; western equatorial Atlantic) and ODP Site 1051 (Blake Nose; western north Atlantic).

Dictyoprora pirum (Ehrenberg, 1874)
Plate II.8, Figure 15

1874 *Eucyrtidium Pirum* [sic] Ehrenberg, p. 232.

1876 *Eucyrtidium Pirum* [sic] Ehrenberg – Ehrenberg, p. 72, pl. 10, fig. 14.
1882a *Eucyrtidium Pirum* [sic] Ehrenberg – Bütschli, p. 528.
1887 *Theocampe* (*Theocampana*) *pirum* (Ehrenberg) – Haeckel, p. 1423.
1971 *Theocampe pirum* (Ehrenberg) – Riedel and Sanfilippo, p. 1601, pl. 3E, figs. 10, 11.
1974 *Theocampe pirum* (Ehrenberg) – Nigrini, p. 1070, pl. 2E, fig. 10.
1974 *Theocampe pirum* (Ehrenberg) – Johnson, p. 552, pl. 6, fig. 14.
1974 *Theocampe vanderhoofi* Campbell and Clark – Johnson, pl. 1, fig. 9.
1975 *Theocampe pirum* (Ehrenberg) – Ling, p. 732, pl. 13, fig. 18.
1977 *Theocampe pirum* (Ehrenberg) – Riedel and Sanfilippo, pl. 11, fig. 7.
1977 *Dictyoprora pirum* (Ehrenberg) – Nigrini, p. 251, pl. 4, fig. 8.
1978 *Theocampe pirum* (Ehrenberg) – Riedel and Sanfilippo, p. 76, pl. 9, fig. 14.
1989 *Siphocampe* spp. group B Lazarus and Pallant, p. 363, pl. 6, fig. 4 (part).
1998a *Dictyoprora urceolus* (Haeckel) – Sanfilippo and Nigrini, p. 272, pl. 13.1, fig. 11.
1999a *Dictyoprora urceolus* (Haeckel) – O'Connor, p. 32, pl. 9, fig. 44.
1999 *Dictyoprora urceolus* (Haeckel) – Kozlova, p. 137, pl. 18, fig. 8, pl. 44, figs. 22, 23.
2001 *Dictyoprora pirum* (Ehrenberg) s.s. – Sanfilippo and Blome, p. 211, fig. 8b.
2005 *Dictyoprora pirum* (Ehrenberg) – Nigrini et al., p. 31, pl. P6, figs. 10, 11.
2006 *Dictyoprora pirum* (Ehrenberg) – Funakawa et al., p. 18, pl. P2, figs. 8–9b
2015 *Dictyoprora pirum* (Ehrenberg) – Kamikuri, pl. 12, fig. 14.
2020 *Theocampe pirum* (Ehrenberg) – Hollis et al., pl. 8, figs. 21a, 21b.
Occurrence. ODP Site 1260 (Demerara Rise; western equatorial Atlantic) and ODP Site 1051 (Blake Nose; western north Atlantic).

Genus *Plannapus* O'Connor, 1997a
Type species.— *Dicolocapsa microcephala* Haeckel, 1887, p. 1312, pl. 57, fig. 1.

Plannapus hornibrooki O'Connor, 1999a
Plate II.9, Figure 1
1999a *Plannapus hornibrooki* O'Connor, p. 7, pl. 1, figs. 7a–10, pl. 5, figs. 8a–11.
Occurrence. ODP Site 1260 (Demerara Rise; western equatorial Atlantic) and ODP Site 1051 (Blake Nose; western north Atlantic).

Plannapus microcephalus (Haeckel, 1887)
Plate II.9, Figure 2
1887 *Dicolocapsa microcephala* Haeckel, p. 1312, pl. 57, fig. 1.
1970 *Dicolocapsa microcephala* Haeckel – Sanfilippo and Riedel, pl. 1, fig. 7.
1975 *Dicolocapsa microcephala* Haeckel – Ling, p. 731, pl. 13, fig. 9.
1977 *Dicolocapsa microcephala* Haeckel – Riedel and Sanfilippo, pl. 15, fig. 18.
1983 *Dicolocapsa microcephala* Haeckel – Johnson, p. 788, pl. 1, fig. 10.
1989 ? *Dicolocapsa microcephala* Haeckel – Lazarus and Pallant, p. 362, pl. 5, figs. 2, 3.
1992 *Dicolocapsa microcephala* Haeckel – Takemura, p. 746, pl. 4, figs. 14, 15.
1992 *Plannapus microcephalus* (Haeckel) – Sanfilippo and Fourtanier, p. 12, pl. P2, fig. 5.

1997a *Plannapus microcephalus* (Haeckel) – O'Connor, p. 70, pl. 1, figs. 10–14, pl. 5, figs. 10–12, pl. 6, figs. 1–5.
2005 *Dicolocapsa microcephala* Haeckel – Funakawa and Nishi, p. 231, pl. 3, figs. 10a, 10b.
2021 *Dicolocapsa microcephala* Haeckel – de Souza et al., p. 15, pl. 2, figs. 9a, 9b.
Occurrence. ODP Site 1051 (Blake Nose; western north Atlantic).

Genus *Siphocampe* Haeckel, 1882
Type species.— *Siphocampe* (*Siphocampula*) *annulosa* Haeckel, 1887, p. 1500, pl. 79, fig. 10.

Siphocampe acephala (Ehrenberg, 1874)
Plate II.9, Figure 3

1874 *Eucyrtidium acephalum* Ehrenberg, p. 224.
1874 *Eucyrtidium* ? *obstipum* Ehrenberg, p. 231.
1876 *Eucyrtidium acephalum* Ehrenberg – Ehrenberg, p. 70, pl. 11, fig. 5.
1876 *Eucyrtidium* ? *obstipum* Ehrenberg – Ehrenberg, p. 72, pl. 11, fig. 17.
1882a *Lithomitra acephala* (Ehrenberg) – Bütschli, p. 529.
1882a *Lithomitra obstipa* (Ehrenberg) – Bütschli, p. 529.
? 1887 *Tricolocampe* (*Tricolocampium*) *amphizona* Haeckel, p. 1413, pl. 66, fig. 17.
1887 *Lithomitra* (*Lithomitrella*) *acephala* (Ehrenberg) – Haeckel, p. 1484.
1942 *Lithocampe* (*Lithocampula*) *urnula* Clark and Campbell, p. 91, pl. 9, fig. 19.
1942 *Lithocampe* (*Lithocampula*) *elizabethae* Clark and Campbell, p. 92, pl. 9, fig. 18.
1942 *Lithocampe* (*Lithocampula*) *minuta* Clark and Campbell, p. 93, pl. 9, fig. 17.
1975 *Lithomitra* sp. cf. *L. elizabethae* Clark and Campbell – Ling, p. 731, pl. 13, fig. 12.
1975 *Theocampe minuta* (Clark and Campbell) – Petrushevskaya, p. 578, pl. 10, fig. 7, pl. 26, figs. 5, 6.
1976 *Lithomitra* sp. Bjørklund, p. 1124, pl. 23, figs. 1–3.
1976 *Lithomitra* ? *elegans* Ehrenberg group – Dzinoridze et al., pl. 32, fig. 20 (part).
1976 *Lithomitra* ? *minuta* (Clark and Campbell) – Dzinoridze et al., pl. 32, fig. 22–24.
1976 *Lithomitra* ? sp. aff. *Eucyrtidium elegans* Ehrenberg – Dzinoridze et al., pl. 32, fig. 21.
1976 *Lithomitra* ? sp. P. Dzinoridze et al., pl. 29, fig. 4, pl. 32, figs. 2–7, pl. 33, figs. 2–4 (part).
1976 *Lithomitra* ? sp. T. Dzinoridze et al., pl. 33, fig. 5 (part).
1977 *Siphocampe acephala* (Ehrenberg) – Nigrini, p. 254, pl. 3, fig. 5.
1979 *Lithomitrella acephala* (Ehrenberg) – Petrushevskaya and Kozlova, p. 150, figs. 380, 409.
1981 *Siphocampe acephala* (Ehrenberg) – De Wever, p. 511, pl. 4, fig. 11.
1981 *Siphocampe elizabethae* (Clark and Campbell) – De Wever, p. 511, pl. 4, fig. 12.
1989 *Siphocampe acephala* (Ehrenberg) – Lazarus and Pallant, p. 363, pl. 6, figs. 10, 11.
1992 *Siphocampe acephala* (Ehrenberg) – Takemura, p. 743, pl. 6, fig. 9.
? 1995 *Lithomitra micropore* Shilov, p. 126, pl. 1, figs. 9, 10.
1993 *Lithomitrella* sp. Vitukhin, pl. 1, fig. 3 (part).
? 1993 *Lithomitrella elegans* (Ehrenberg) – Vitukhin, pl. 5, fig. 8.
1995 *Lithomitrella minuta* Clark and Campbell – Shilov, p. 127, pl. 2, fig. 5.
1996 *Siphocampe minuta* (Clark and Campbell) – Hull, p. 141, pl. 8, figs. 7–9.

1997 *Siphocampe acephala* (Ehrenberg) group – Hollis et al., p. 54, pl. 4, figs. 9, 10, 12, 14, 19, 20 (part).
1999a *Siphocampe* cf. *acephala* (Ehrenberg) – O'Connor, p. 36, pl. 9, fig. 41.
2009 *Eucyrtidium* ? *obstipum* Ehrenberg – Ogane et al., pl. 6, figs. 4a–4e.
2009 *Eucyrtidium acephalum* Ehrenberg – Ogane et al., pl. 83, figs. 7a–7e.
2009b *Siphocampe minuta* (Clark and Campbell) – Suzuki et al., p. 264, pl. 18, figs. 6a, 6b (part).
2020 *Siphocampe* ? *acephala* (Ehrenberg) group – Hollis et al., pl. 8, fig. 9 (part).
2021 *Siphocampe* ? *acephala* (Ehrenberg) group – de Souza et al., p. 15, pl. 2, figs. 10a, 10b.
Occurrence. ODP Site 1260 (Demerara Rise; western equatorial Atlantic) and ODP Site 1051 (Blake Nose; western north Atlantic).

Siphocampe ? *elegans* (Ehrenberg, 1854a)
Plate II.9, Figure 4
1854a *Eucyrtidium elegans* Ehrenberg, pl. 36, fig. 17.
1876 *Eucyrtidium elegans* Ehrenberg – Ehrenberg, p. 70, pl. 11, fig. 12.
1882a *Eucyrtidium elegans* Ehrenberg – Bütschli, p. 528.
1887 *Theocorys* (*Theocorypha*) *elegans* (Ehrenberg) – Haeckel, p. 1406.
1976 *Lithomitra* ? *elegans* Ehrenberg group – Dzinoridze et al., pl. 32, figs. 18, 19 (part).
1993 *Lithomitrella* sp. Vitukhin, pl. 19, fig. 14 (part).
1997 *Siphocampe acephala* (Ehrenberg) group – Hollis et al., p. 54, pl. 4, figs. 11, 13, 15–18 (part).
1999 *Lithomitrella insensis* Kozlova – Kozlova, p. 139, pl. 3, fig. 19.
2009 *Eucyrtidium elegans* Ehrenberg – Ogane et al., pl. 6, figs. 11a, 11b.
2009b *Dictyoprora* sp. A Suzuki et al., p. 263, pl. 18, figs. 4a, 4b.
2020 *Siphocampe* ? *acephala* (Ehrenberg) group – Hollis et al., pl. 8, fig. 10 (part).
Remarks. This species is assigned to the genus *Siphocampe* based on its overall morphology.
Occurrence. ODP Site 1260 (Demerara Rise; western equatorial Atlantic).

Siphocampe ewingensis Kochhann *in* Kochhann et al., 2013
Plate II.9, Figure 5
? 1996 *Siphocampe acephala* (Ehrenberg) – Hull, p. 140, pl. 7, figs. 1–3.
? 1996 *Siphocampe septata* Petrushevskaya – Hull, p. 141, pl. 7, figs. 5, 6.
1997 *Siphocampe acephala* (Ehrenberg) group – Hollis et al., p. 54, pl. 4, figs. 15–18 (part).
2002 *Siphocampe acephala* (Ehrenberg) group – Apel et al., p. 20, pl. P9, figs. 14–17.
2013 *Siphocampe ewingensis* Kochhann *in* Kochhann et al., p. 541, pl. 3, figs. F–P.
2020 *Siphocampe* ? *acephala* (Ehrenberg) group – Hollis et al., pl. 8, fig. 8 (part).
Occurrence. ODP Site 1051 (Blake Nose; western north Atlantic).

Siphocampe imbricata (Ehrenberg, 1874)
Plate II.9, Figure 6
1874 *Eucyrtidium imbricatum* Ehrenberg, p. 229
1876 *Eucyrtidium imbricatum* Ehrenberg – Ehrenberg, p. 72, pl. 11, fig. 22.

1882a *Lithomitra imbricata* (Ehrenberg) – Bütschli, p. 529.
1887 *Lithomitra* (*Lithomitrella*) *nodosaria* Haeckel, p. 1484, pl. 79, fig. 1.
1967 *Lithomitra nodosaria* Haeckel – Petrushevskaya, pl. 83, figs. 8, 9.
? 1969 *Lithomitra nodosaria* Haeckel group – Kruglikova, pl. 4, fig. 3.
1972 *Lithomitra nodosaria* Haeckel group – Petrushevskaya and Kozlova, p. 539, pl. 24, figs. 29, 30.
? 1972 *Lithomitra eruca* Haeckel – Petrushevskaya and Kozlova, p. 539, pl. 24, figs. 32, 33.
1973 cf. *Lithomitra lineata* (Ehrenberg) group – Foreman, pl. 8, fig. 18.
1973 *Lithomitra lineata* (Ehrenberg) group – Foreman, p. 431, pl. 8, fig. 19.
1975 *Lithomitra nodosaria* Haeckel group – Petrushevskaya, p. 586, pl. 10, fig. 18.
1977 *Siphocampe nodosaria* (Haeckel) – Nigrini, p. 256, pl. 3, fig. 11.
1989 *Siphocampe* spp. group A Lazarus and Pallant, p. 363, pl. 6, figs. 1, 2.
1991 *Siphocampe imbricata* (Ehrenberg) – Caulet, p. 539, pl. 3, fig. 13.
1992 *Siphocampe* sp. aff. *S. arachnea* (Ehrenberg) group – Blome, p. 645, pl. 1, figs. 5, 6.
1992 *Siphocampe nodosaria* (Haeckel) – Takemura, p. 743, pl. 3, fig. 15.
1993 *Siphocampe eruca* (Haeckel) – Vitukhin, pl. 5, fig. 7, pl. 11, fig. 4.
1996 *Siphocampe imbricata* (Ehrenberg) – Hull, p. 141, pl. 8, fig. 13.
1997 *Siphocampe nodosaria* (Haeckel) – Hollis et al., p. 55, pl. 4, figs. 28–32.
1999a *Siphocampe nodosaria* (Haeckel) – O'Connor, p. 36, pl. 9, fig. 42.
1999 *Siphocampe* sp. aff. *S. nodosaria* (Haeckel) – Kozlova, p. 142, pl. 3, fig. 17.
2002 *Siphocampe nodosaria* (Haeckel) – Hollis, p. 300, pl. 5, figs. 4a, 4b.
2002 *Siphocampe nodosaria* (Haeckel) – Apel et al., p. 21, pl. P9, fig. 11.
2003 *Siphocampe nodosaria* (Haeckel) – Sanfilippo and Fourtanier, p. 12, pl. P2, figs. 14, 15.
2008 *Siphocampe altamontensis* (Campbell and Clark) – Jackett et al., p. 58, pl. 3, fig. 19.
2009 *Eucyrtidium imbricatum* Ehrenberg – Ogane et al., pl. 6, figs. 7a–7c.
2009b *Siphocampe elegans* (Ehrenberg) – Suzuki et al., p. 263, pl. 18, fig. 10.
2009b *Siphocampe imbricata* (Ehrenberg) – Suzuki et al., p. 264, pl. 18, figs. 12a, 12b.
2013 *Siphocampe nodosaria* (Haeckel) – Kochhann et al., p. 542, pl. 3, fig. Q.
2020 *Siphocampe nodosaria* (Haeckel) – Hollis et al., pl. 8, fig. 7.

Occurrence. ODP Site 1260 (Demerara Rise; western equatorial Atlantic) and ODP Site 1051 (Blake Nose; western north Atlantic).

Siphocampe missilis O'Connor, 1994

Plate II.9, Figure 7

1994 *Siphocampe missilis* O'Connor, p. 340, pl. 1, figs. 7, 9–12, pl. 3, figs. 8–12.

Occurrence. ODP Site 1051 (Blake Nose; western north Atlantic).

Siphocampe ? *paupera* (Ehrenberg, 1874)

Plate II.9, Figure 8

1874 *Eucyrtidium pauperum* Ehrenberg, p. 231.
1876 *Eucyrtidium pauperum* Ehrenberg – Ehrenberg, p. 72, pl. 11, fig. 13
1882a *Lithomitra paupera* (Ehrenberg) – Bütschli, p. 529.
1882b *Lithomitra paupera* (Ehrenberg) – Bütschli, pl. 30, fig. 25.

1887 *Theocyrtis* (*Theocorypha*) *paupera* (Ehrenberg) – Haeckel, p. 1407.
2009 *Eucyrtidium pauperum* Ehrenberg – Ogane et al., pl. 82, figs. 7a-7c.
Remarks. This species is assigned to the genus *Siphocampe* based on its overall morphology.
Occurrence. ODP Site 1051 (Blake Nose; western north Atlantic).

Siphocampe pupa (Ehrenberg, 1861a)
Plate II.9, Figure 9

1861a *Eucyrtidium Pupa* [sic] Ehrenberg, p. 768.
1861b *Eucyrtidium Pupa* [sic] Ehrenberg – Ehrenberg, p. 823.
1873a *Eucyrtidium Pupa* [sic] Ehrenberg – Ehrenberg, p. 292, pl. 7, fig. 16.
1873b *Eucyrtidium Pupa* [sic] Ehrenberg – Ehrenberg, p. 311.
1882a *Eucyrtidium Pupa* [sic] Ehrenberg – Bütschli, p. 528.
1887 *Tricolocampe* (*Tricolocampium*) *pupa* (Ehrenberg) – Haeckel, p. 1412.
? 1972 *Lithamphora* ? sp. Petrushevskaya and Kozlova, pl. 24, fig. 7 (part).
1993 *Siphocampe kylindrica* Vitukhin, p. 84, pl. 5, figs. 5, 6.
2009a *Eucyrtidium pupa* Ehrenberg – Suzuki et al., pl. 55, figs. 8a–8c.
Occurrence. ODP Site 1260 (Demerara Rise; western equatorial Atlantic) and ODP Site 1051 (Blake Nose; western north Atlantic).

Siphocampe ? *quadrata* (Petrushevskaya *in* Petrushevskaya and Kozlova, 1972)
Plate II.9, Figures 10, 11

1972 *Lithamphora sacculifera quadrata* Petrushevskaya *in* Petrushevskaya and Kozlova, p. 539, pl. 30, figs. 4–6.
1972 *Lithamphora* sp. Petrushevskaya and Kozlova, p. 539, pl. 30, fig. 2.
1972 *Lithamphora* ? sp. Petrushevskaya and Kozlova, pl. 30, fig. 1 (part).
1973 *Lithomitra docilis* Foreman, p. 431, pl. 8, figs. 20–22, pl. 9, figs. 3–5.
1974 *Lithomitra docilis* Foreman – Johnson, p. 552, pl. 3, fig. 16.
1975 *Lithamphora quadrata* Petrushevskaya and Kozlova – Petrushevskaya, p. 585, pl. 10, figs. 19, 20.
1976 *Lithamphora* sp. aff. *L. quadrata* Petrushevskaya and Kozlova – Dzinoridze et al., pl. 29, fig. 1.
1977 *Siphocampe* ? *quadrata* (Petrushevskaya and Kozlova) – Nigrini, p. 257, pl. 3, fig. 12.
1974 *Lithomitra docilis* Foreman – Riedel and Sanfilippo, pl. 3, fig. 13.
1992 *Lithomitra docilis* Foreman – Blome, p. 645, pl. 1, fig. 4.
1992 *Lithomitra docilis* Foreman – Nishimura, p. 329, pl. 10, fig. 11, pl. 13, fig. 19.
1992 *Siphocampe* ? *quadrata* (Petrushevskaya and Kozlova) – Takemura, p. 743, pl. 7, fig. 7.
1995 *Siphocampe quadrata* (Petrushevskaya and Kozlova) – Strong et al., p. 209, fig. 10R.
1997 *Siphocampe quadrata* (Petrushevskaya and Kozlova) – Hollis et al., p. 55, pl. 4, fig. 27.
2002 *Siphocampe quadrata* (Petrushevskaya and Kozlova) – Hollis, p. 301, pl. 5, figs. 5, 6.
2003 *Siphocampe* ? *quadrata* (Petrushevskaya and Kozlova) – Sanfilippo and Fourtanier, p. 12, pl. P2, fig. 24.
2006 *Siphocampe quadrata* (Petrushevskaya and Kozlova) – Funakawa et al., p. 19, pl. 2, figs. 14a–15b.

2009b *Siphocampe quadrata* (Petrushevskaya and Kozlova) – Suzuki et al., p. 264, pl. 18, fig. 9.
2009b *Siphocampe sacculifera* (Clark and Campbell) – Suzuki et al., p. 264, pl. 18, figs. 11a, 11b.
2015 *Lithomitra docilis* Foreman – Kamikuri, pl. 12, fig. 5.
2020 *Siphocampe quadrata* (Petrushevskaya and Kozlova) – Hollis et al., pl. 8, fig. 6.
2021 *Siphocampe quadrata* (Petrushevskaya and Kozlova) – de Souza et al., p. 15, pl. 2, fig. 11.
Occurrence. ODP Site 1260 (Demerara Rise; western equatorial Atlantic) and ODP Site 1051 (Blake Nose; western north Atlantic).

Genus *Spirocyrtis* Haeckel, 1882 emend. Nigrini, 1977

Type species.— *Spirocyrtis* (*Spirocyrtidium*) *scalaris* Haeckel, 1887, p. 1509, pl. 76, fig. 14.

Spirocyrtis proboscis O'Connor, 1994
Plate II.9, Figure 12

1994 *Spirocyrtis proboscis* O'Connor, p. 341, pl. 2, fig. 1–4, pl. 3, fig. 13–16.
Occurrence. ODP Site 1051 (Blake Nose; western north Atlantic).

Family Rhopalosyringiidae Empson-Morin, 1981
? Genus *Artostrobus* Haeckel, 1887

Type species.— *Cornutella* ? *annulata* Bailey, 1856, p. 3, pl. 1, fig. 5b.

Artostrobus quadriporus Bjørklund, 1976
Plate II.9, Figure 13

1976 *Artostrobus quadriporus* Bjørklund, p. 1125, pl. 23, figs. 15–21.
1976 *Lithamphora* sp. aff. *Corocalyptra kruegeri* Popofsky – Dzinoridze et al., pl. 32, figs. 13–15 (part), pl. 33, fig. 1.
1979 *Lithamphora quadripora* Bjørklund – Petrushevskaya and Kozlova, p. 149, figs. 358, 479–481, 536.
1989 *Botryostrobus joides* Petrushevskaya group – Lazarus and Pallant, p. 361, pl. 4, figs. 15, 16 (part).
1996 *Artostrobus quadriporus* Bjørklund – Hull, p. 137, pl. 4, fig. 12.
2013 *Artostrobus quadriporus* Bjørklund – Kochhann, p. 540, pl. 2, fig. AA.
Occurrence. ODP Site 1260 (Demerara Rise; western equatorial Atlantic).

Genus *Pterocyrtidium* Bütschli, 1882a

Type species.— *Pterocanium barbadense* Ehrenberg, 1874, p. 254 (unfigured); Ehrenberg, 1876, p. 82, pl. 17, fig. 6.

Pterocyrtidium ? *austellum* (Sanfilippo and Blome, 2001)
Plate II.9, Figure 14

2001 *Sethochytris austellus* Sanfilippo and Blome, p. 206, figs. 6h, 6i.

Occurrence. ODP Site 1051 (Blake Nose; western north Atlantic).

Pterocyrtidium barbadense (Ehrenberg, 1874)
Plate II.9, Figures 15, 16

1874 *Pterocanium barbadense* Ehrenberg, p. 254.
1876 *Pterocanium barbadense* Ehrenberg – Ehrenberg, p. 82, pl. 17, fig. 6.
1882a *Pterocyrtidium barbadense* (Ehrenberg) – Bütschli, p. 531.
1887 *Pterocorys* (*Pterocyrtidium*) *barbadensis* (Ehrenberg) – Haeckel, p. 1318.
1972 *Pterocyrtidium barbadense* (Ehrenberg) group – Petrushevskaya and Kozlova, p. 552, pl. 27, fig. 19 (part).
not 1975 *Pterocyrtidium barbadense* (Ehrenberg) – Ling, p. 729, pl. 10, fig. 17.
1975 *Pterocyrtidium* sp. Ling, p. 729, pl. 10, figs. 18, 19.
1977 *Lipmanella* ? sp. Riedel and Sanfilippo, pl. 7, fig. 11.
1998 *Lophocyrtis* (*Lophocyrtis* ?) *barbadense* (Ehrenberg) – Sanfilippo and Caulet, p. 8, pl. 4, figs. 9, 10a, 10b.
2006 *Lophocyrtis* (*Lophocyrtis* ?) *barbadense* (Ehrenberg) – Funakawa et al., p. 26, pl. P8, figs. 4a–5b.

Occurrence. ODP Site 1260 (Demerara Rise; western equatorial Atlantic).

Genus *Rhopalosyringium* Campbell and Clark, 1944

Type species.— *Rhopalosyringium magnificum* Campbell and Clark, 1944, p. 30, pl. 7, fig. 16.

Rhopalosyringium ? *auriculaleporis* (Clark and Campbell, 1942)
Plate II.10, Figure 2

1942 *Lophophaena* (*Lophophaenula*) *auriculaleporis* Clark and Campbell, p. 76, pl. 8, figs. 20, 27–29.
1970 *Lophocyrtis biaurita* (Ehrenberg) – Cita et al., p. 404, pl. 2, fig. K (part).
1973 *Lophocyrtis biaurita* (Ehrenberg) – Foreman, p. 442, pl. 8, fig. 23 (part).
1974 *Lophocyrtis biaurita* (Ehrenberg) – Johnson, p. 552, pl. 2, fig. 2 (part).
1976 *Eucyrtidium* ? *biauritum* Ehrenberg – Dzinoridze et al., pl. 32, fig. 8.
1976 *Lophocyrtis* sp. Dzinoridze et al., pl. 28, fig. 13 (part).
1976 *Lophocyrtis* ? sp. aff. *Lophocorys auriculaleporis* (Clark and Campbell) – Dzinoridze et al., pl. 28, fig. 16.
1977 *Lophocyrtis biaurita* (Ehrenberg) – Riedel and Sanfilippo, pl. 8, fig. 9.
1979 *Artobotrys auriculaleporis* (Clark and Campbell) – Petrushevskaya and Kozlova, p. 137, fig. 515.
1988 *Lophophaena auriculaleporis* Clark and Campbell – Blueford, p. 246, pl. 3, figs. 1–3.
1991 *Artobotrys auriculaleporis* (Clark and Campbell) – Caulet, p. 537.
1995 *Artobotrys auriculaleporis* (Clark and Campbell) – Shilov, p. 127, pl. 4, figs. 4a, 4b.
1995 *Lophocyrtis* ? *auriculaleporis* (Clark and Campbell) – Strong et al., p. 208, figs. 10S, 10T.
1997 *Cycladophora* ? *auriculaleporis* (Clark and Campbell) – Hollis et al., p. 59, pl. 3, fig. 31.

1999 *Artobotrys auriculaleporis* (Clark and Campbell) – Kozlova, p. 133, pl. 27, fig. 14, pl. 31, figs. 2, 3, pl. 46, fig. 1 (part).
2003 *Lophocyrtis biaurita* (Ehrenberg) – Sanfilippo and Fourtanier, p. 12, pl. P2, fig. 23 (part).
2009b *Artobotrys auriculaleporis* (Clark and Campbell) – Suzuki et al., p. 258, pl. 21, figs. 1a, 1b.
2009b *Artobotrys biauritus* (Ehrenberg) – Suzuki et al., p. 258, pl. 21, figs. 2a, 2b.
2009b *Artobotrys norvegiensis* (Bjørklund and Kellogg) – Suzuki et al., p. 258, pl. 21, fig. 3.
2020 *Artobotrys auriculaleporis* (Clark and Campbell) – Hollis et al., pl. 7, figs. 1a–3b.

Remarks. The combination used here is derived from O'Dogherty et al. (2021).

Occurrence. ODP Site 1260 (Demerara Rise; western equatorial Atlantic) and ODP Site 1051 (Blake Nose; western north Atlantic).

Rhopalosyringium ? *biauritum* (Ehrenberg, 1874)
Plate II.10, Figure 1

1874 *Eucyrtidium biauritum* Ehrenberg, p. 226.
1874 *Eucyrtidium bicorne* Ehrenberg, p. 226.
1876 *Eucyrtidium biauritum* Ehrenberg – Ehrenberg, p. 70, pl. 10, figs. 7, 8.
1876 *Eucyrtidium bicorne* Ehrenberg – Ehrenberg, p. 70, pl. 11, fig. 7.
1882a *Eucyrtidium biauritum* Ehrenberg – Bütschli, pl. 33, figs. 38a–38f.
1882b *Eucyrtidium biauritum* Ehrenberg – Bütschli, pl. 31, fig. 1.
1887 *Lophocyrtis biaurita* (Ehrenberg) – Haeckel, p. 1411.
1970 *Lophocyrtis biaurita* (Ehrenberg) – Cita et al., p. 404, pl. 2, figs. I, J (part).
1973 *Lophocyrtis biaurita* (Ehrenberg) – Foreman, p. 442, pl. 8, figs. 24–26 (part).
1974 *Lophocyrtis biaurita* (Ehrenberg) – Nigrini, p. 1070, pl. 1M, fig. 11–13.
1974 *Lophocyrtis biaurita* (Ehrenberg) – Johnson, p. 552, pl. 2, fig. 1 (part).
1975 *Lophocyrtis biaurita* (Ehrenberg) – Chen, p. 461, pl. 3, fig. 2.
1976 *Lophocyrtis biaurita* (Ehrenberg) – Bjørklund, p. 1124, pl. 21, figs. 16, 17.
1976 *Lophocyrtis* ? *bicorne* (Ehrenberg) – Dzinoridze et al., pl. 28, fig. 12, pl. 34, fig. 4.
1978 *Lophocyrtis biaurita* (Ehrenberg) – Riedel and Sanfilippo, p. 70, pl. 6, fig. 13.
1984 *Lophocyrtis biaurita* (Ehrenberg) – Westberg-Smith and Riedel, p. 493, pl. 6, fig. 13.
1992 *Lophocyrtis biaurita* (Ehrenberg) – Takemura, p. 747, pl. 7, fig. 8.
1999 *Artobotrys auriculaleporis* (Clark and Campbell) – Kozlova, p. 133, pl. 31, fig. 1 (part).
2003 *Lophocyrtis biaurita* (Ehrenberg) – Sanfilippo and Fourtanier, p. 12, pl. P2, fig. 22 (part).
2009 *Eucyrtidium biauritum* Ehrenberg – Ogane et al., pl. 18, figs. 8a–8d, pl. 20, figs. 1a–2b, 6.
2009 *Eucyrtidium bicorne* Ehrenberg – Ogane et al., pl. 20, figs. 3a, 3b, 4a–4c, 5a–5c.
2020 *Artobotrys biaurita* (Ehrenberg) – Hollis et al., pl. 7, figs. 4, 5.

Remarks. The combination used here is derived from O'Dogherty et al. (2021).

Occurrence. ODP Site 1260 (Demerara Rise; western equatorial Atlantic) and ODP Site 1051 (Blake Nose; western north Atlantic).

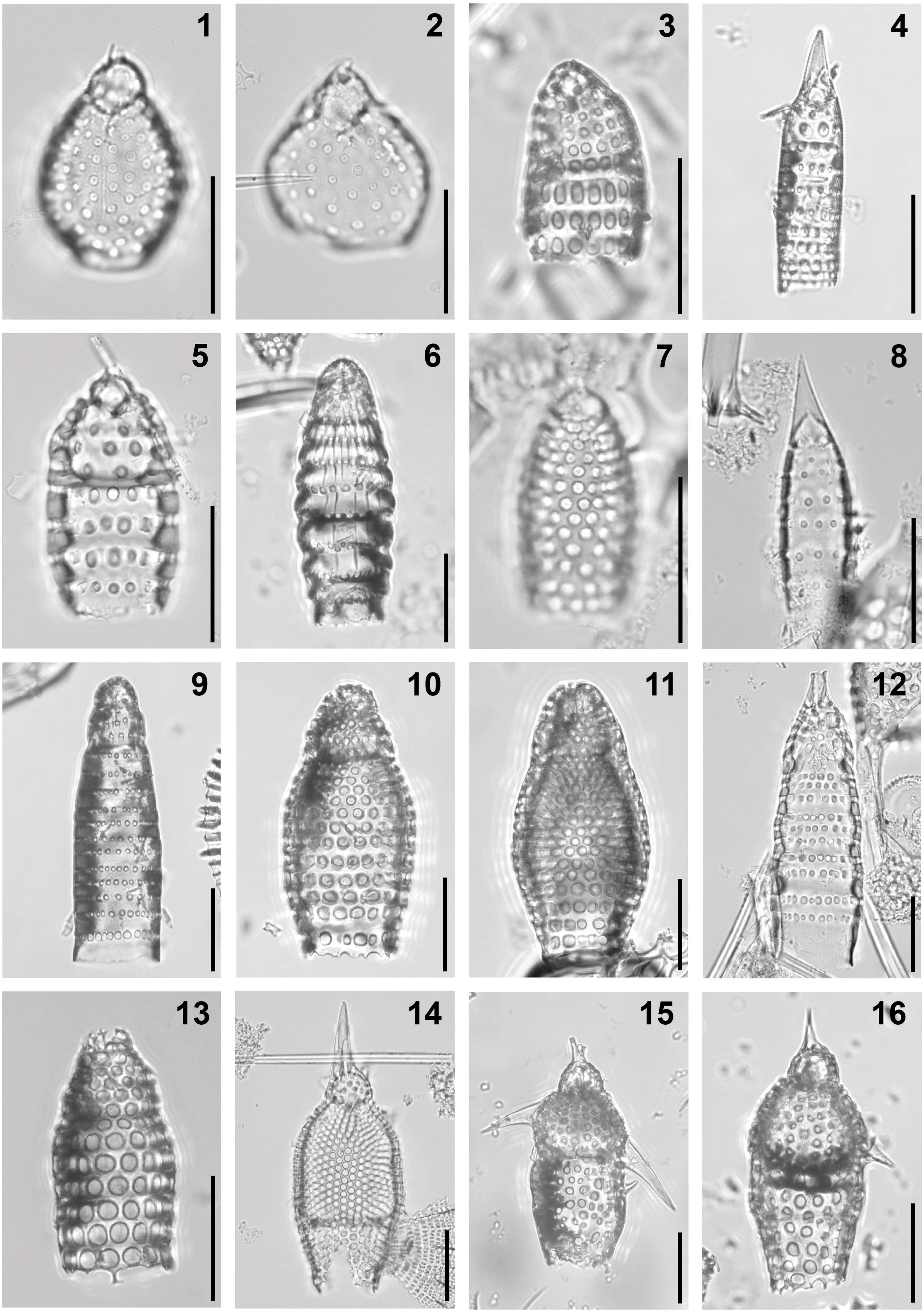
1
2
3
4
5
6
7
8
9
10
11
12
13
14
15
16

Plate II.9. Composite light micrographs of new radiolarian species from ODP Site 1260 (Demerara Rise, western equatorial Atlantic) and ODP Site 1051 (Blake Nose, western North Atlantic). (**1**) *Plannapus hornibrooki* O'Connor, 1999a: ODP 1051A-2H-5W, 55–57 cm. (**2**) *Plannapus microcephalus* (Haeckel, 1887): ODP 1051A-14H-5W, 55–57 cm. (**3**) *Siphocampe acephala* (Ehrenberg, 1874): ODP 1260A-8R-5W, 54–56 cm. (**4**) *Siphocampe* ? *elegans* (Ehrenberg, 1854a): ODP 1260A-6R-2W, 55–57 cm. (**5**) *Siphocampe ewingensis* Kochhann *in* Kochhann et al., 2013: ODP 1051A-12H-2W, 55–57 cm. (**6**) *Siphocampe imbricata* (Ehrenberg, 1874): ODP 1260A-9R-3W, 55–57 cm. (**7**) *Siphocampe missilis* O'Connor, 1994: ODP 1051A-2H-5W, 55–57 cm. (**8**) *Siphocampe* ? *paupera* (Ehrenberg, 1874): ODP 1051A-2H-5W, 55–57 cm. (**9**) *Siphocampe pupa* (Ehrenberg, 1861a): ODP 1260A-10R-4W, 55–57 cm. (**10, 11**) *Siphocampe* ? *quadrata* (Petrushevskaya *in* Petrushevskaya and Kozlova, 1972): (**10**) ODP 1260A-11R-7W, 55–57 cm; (**11**) ODP 1260A-8R-2W, 55–57 cm. (**12**) *Spirocyrtis proboscis* O'Connor, 1994: ODP 1051A-6H-5W, 53–55 cm. (**13**) *Artostrobus quadriporus* Bjørklund, 1976: ODP 1260A-8R-3W, 54–56 cm. (**14**) *Pterocyrtidium* ? *austellum* (Sanfilippo and Blome, 2001): ODP 1051A-12H-2W, 55–57 cm. (**15, 16**) *Pterocyrtidium barbadense* (Ehrenberg, 1874): (**15**) ODP 1260A-13R-5W, 54–56 cm; (**16**) ODP 1260A-11R-6W, 55–57 cm. All scale bars equal 50 µm.

Superfamily Acanthodesmioidea Haeckel, 1862 sensu Dumitrică *in* De Wever et al., 2001

Family Acanthodesmiidae Haeckel, 1862

Genus *Dictyospyris* Ehrenberg, 1846

Type species.— *Dictyospyris triloba* Ehrenberg, 1854a, pl. 36, figs. 24a, 24b; description in Haeckel, 1862, p. 292.

Dictyospyris gigas Ehrenberg, 1874

Plate II.10, Figure 3

1874 *Dictyospyris Gigas* [sic] Ehrenberg, p. 224.
1876 *Dictyospyris Gigas* [sic] Ehrenberg – Ehrenberg, p. 68, pl. 19, fig. 6.
1882a *Dictyospyris Gigas* [sic] Ehrenberg – Bütschli, pl. 32, figs. 14a, 14b.
1882b *Dictyospyris Gigas* [sic] Ehrenberg – Bütschli, pl. 28, fig. 14, pl. 29, fig. 1.
1887 *Circospyris gigas* (Ehrenberg) – Haeckel, p. 1072.
1973 *Dictyospyris gigas* Ehrenberg – Sanfilippo and Riedel, p. 527, pl. 16, figs. 9, 10, pl. 32, figs. 10, 11.
1987 *Dictyospyris gigas* Ehrenberg – Nishimura, p. 725, pl. 3, fig. 20.
2002 *Dendrospyris stabilis* Goll – Apel et al., p. 18, pl. P8, figs. 8a, 8b (part).
not 2009 *Dictyospyris gigas* Ehrenberg – Ogane et al., pl. 18, figs. 1a, 1b.
2015 *Dictyospyris gigas* Ehrenberg – Kamikuri, pl. 19, fig. 11.

Occurrence. ODP Site 1260 (Demerara Rise; western equatorial Atlantic) and ODP Site 1051 (Blake Nose; western north Atlantic).

Dictyospyris melissium Sanfilippo and Riedel, 1973
Plate II.10, Figure 9

1973 *Dictyospyris melissium* Sanfilippo and Riedel, p. 527, pl. 17, figs. 1, 2, pl. 32, fig. 13.
2001 *Dictyospyris melissium* Sanfilippo and Riedel – De Wever et al., p. 231, fig. 146.7.
Occurrence. ODP Site 1260 (Demerara Rise; western equatorial Atlantic) and ODP Site 1051 (Blake Nose; western north Atlantic).

Dictyospyris tetrastoma Ehrenberg, 1874
Plate II.10, Figure 4

1874 *Dictyospyris tetrastoma* Ehrenberg, p. 224.
1876 *Dictyospyris tetrastoma* Ehrenberg – Ehrenberg, p. 70, pl. 19, fig. 12.
1887 *Dictyospyris* (*Dictyospyrissa*) *tetrastoma* Ehrenberg – Haeckel, p. 1075.
1999 *Dicryospyrella asymmetrica* [sic] Kozlova, p. 163, pl. 15, figs. 16, 17, 21, pl. 18, fig. 15, pl. 20, fig. 11 (part).
2002 *Dendrospyris* sp. A Apel et al., pl. P8, figs. 6a, 6b.
2009 *Dictyospyris tetrastoma* Ehrenberg – Ogane et al., pl. 38, figs. 2a, 2b (part).
2009 *Dictyospyris tetrasoma* [sic] Ehrenberg – Ogane et al., pl. 18, figs. 2a–2c.
Occurrence. ODP Site 1260 (Demerara Rise; western equatorial Atlantic).

Dictyospyris tristoma Ehrenberg, 1874
Plate II.10, Figure 5

1874 *Dictyospyris tristoma* Ehrenberg, p. 224.
1876 *Dictyospyris tristoma* Ehrenberg – Ehrenberg, p. 70, pl. 19, fig. 9.
1887 *Dictyospyris* (*Dictyospyrella*) *tristoma* Ehrenberg – Haeckel, p. 1074.
1999 *Dictyospyrella tristoma* (Ehrenberg) – Kozlova, p. 164, pl. 36, figs. 22, 23.
2009 *Dictyospyris tristoma* Ehrenberg – Ogane et al., pl. 75, figs. 3a–3c.
2015 *Dictyospyris tristoma* Ehrenberg – Kamikuri, pl. 11, fig. 22.
Occurrence. ODP Site 1260 (Demerara Rise; western equatorial Atlantic).

Genus *Eucoronis* Haeckel, 1882
Type species.— *Eucoronis* (*Acrocoronis*) *perspicillum* Haeckel, 1887, p. 977, pl. 82, fig. 6.

Eucoronis hertwigii Bütschli, 1882a
Plate II.10, Figures 7, 8

1862 *Acanthodesmia* Bury, pl. 23, fig. 7.
1882a *Acanthodesmia Hertwigii* [sic] Bütschli, p. 499, pl. 32, fig. 9a–9c.
1882b *Acanthodesmia Hertwigii* [sic] Bütschli – Bütschli, pl. 28, fig. 12.
1887 *Tristephanium* (*Triostephus*) *hertwigii* (Bütschli) – Haeckel, p. 983.
1972 *Eucoronis hertwigii* (Bütschli) group – Petrushevskaya and Kozlova, p. 533, pl. 41, figs. 15–17.
1975 *Eucoronis hertwigii* (Bütschli) group – Ling, p. 727, pl. 8, fig. 14.
2015 *Eucoronis hertwigii* (Bütschli) group – Kamikuri, pl. 13, fig. 18.

Occurrence. ODP Site 1260 (Demerara Rise; western equatorial Atlantic) and ODP Site 1051 (Blake Nose; western north Atlantic).

Genus *Tympaniscus* Haeckel, 1887

Type species.— *Tympaniscus corona* Haeckel, 1887, p. 1001 (unfigured).

Tympaniscus fibula Ehrenberg, 1874
Plate II.10, Figures 6, 10

1874 *Ceratospyris Fibula* [sic] Ehrenberg, p. 219.
1876 *Ceratospyris Fibula* [sic] Ehrenberg – Ehrenberg, p. 66, pl. 20, fig. 3.
1882b *Ceratospyris Fibula* [sic] Ehrenberg – Bütschli, pl. 29, fig. 3.
1887 *Tympaniscus fibula* (Ehrenberg) – Haeckel, p. 1002.

Occurrence. ODP Site 1260 (Demerara Rise; western equatorial Atlantic).

Family Cephalospyrididae Haeckel, 1882
Genus *Ceratospyris* Ehrenberg, 1846

Type species.— *Haliomma* ? *radicatum* Ehrenberg, 1844, p. 83 (unfigured); Ehrenberg, 1854a, pl. 22, fig. 37.

Ceratospyris articulata Ehrenberg, 1874
Plate II.10, Figure 11

1874 *Ceratospyris articulata* Ehrenberg, p. 218.
1876 *Ceratospyris articulata* Ehrenberg – Ehrenberg, p. 66, pl. 20, fig. 4.
1887 *Hexaspyris* (*Hexacorethra*) *articulata* (Ehrenberg) – Haeckel, p. 1048.
1973 *Ceratospyris articulata* Ehrenberg – Sanfilippo and Riedel, p. 526, pl. 15, figs. 1–3, pl. 31, figs. 8, 9
1978 *Ceratospyris articulata* Ehrenberg – Riedel and Sanfilippo, p. 67, pl. 4, figs. 9, 10.
1987 *Ceratospyris articulata* Ehrenberg – Nishimura, p. 721, pl. 3, fig. 16.
2009 *Ceratospyris articulata* Ehrenberg – Ogane et al., pl. 18, figs. 3a–3c.

Occurrence. ODP Site 1260 (Demerara Rise; western equatorial Atlantic).

Ceratospyris clavata Bütschli, 1882a
Plate II.10, Figure 12

1882a *Ceratospyris clavata* Bütschli, p. 539, pl. 32, figs. 13a–13c.
not 1975 *Ceratospyris clavata* Bütschli – Ling, p. 726, pl. 4, fig. 11.

Occurrence. ODP Site 1260 (Demerara Rise; western equatorial Atlantic) and ODP Site 1051 (Blake Nose; western north Atlantic).

Ceratospyris echinus Ehrenberg, 1874
Plate II.10, Figure 13

1874 *Ceratospyris Echinus* [sic] Ehrenberg, p. 219.
1876 *Ceratospyris Echinus* [sic] Ehrenberg – Ehrenberg, p. 66, pl. 20, fig. 12.
1887 *Ceratospyris* (*Lophospyris*) *echinus* Ehrenberg – Haeckel, p. 1068.

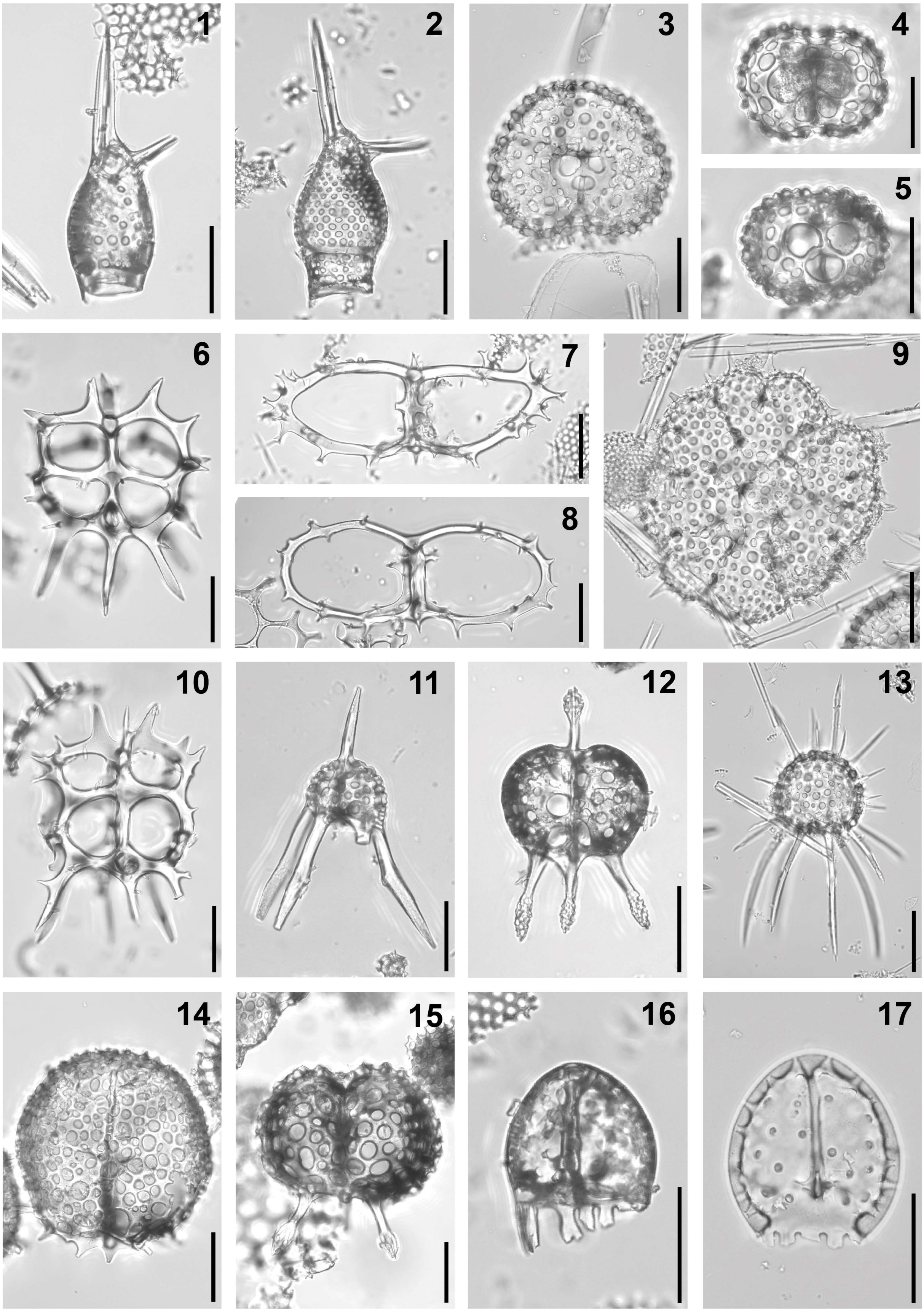
1
2
3
4
5
6
7
8
9
10
11
12
13
14
15
16
17

Plate II.10. Composite light micrographs of new radiolarian species from ODP Site 1260 (Demerara Rise, western equatorial Atlantic) and ODP Site 1051 (Blake Nose, western North Atlantic). (**1**) *Rhopalosyringium* ? *biauritum* (Ehrenberg, 1874): ODP 1260A-10R-4W, 55–57 cm. (**2**) *Rhopalosyringium* ? *auriculaleporis* (Clark and Campbell, 1942): ODP 1260A-9R-3W, 55–57 cm. (**3**) *Dictyospyris gigas* Ehrenberg, 1874: ODP 1051A-38X-5W, 55–57 cm. (**4**) *Dictyospyris tetrastoma* Ehrenberg, 1874: ODP 1260A-20R-4W, 63–177 cm. (**5**) *Dictyospyris tristoma* Ehrenberg, 1874: ODP 1260A-20R-4W, 63–177 cm. (**6, 10**) *Tympaniscus fibula* (Ehrenberg, 1874): (**6**) ODP 1260A-7R-4W, 54–56 cm; (**10**) ODP 1260A-7R-4W, 54–56 cm. (**7, 8**) *Eucoronis hertwigii* Bütschli, 1882a: (**7**) ODP 1260A-8R-6W, 54–56 cm; (**8**) ODP 1260A-9R-4W, 55–57 cm. (**9**) *Dictyospyris melissium* Sanfilippo and Riedel, 197: ODP 1051A-12R-2W, 55–57 cm. (**11**) *Ceratospyris articulata* Ehrenberg, 1874: ODP 1260A-14R-CC, 63–177 cm. (**12**) *Ceratospyris clavata* Bütschli, 1882a: ODP 1260A-8R-3W, 54–56 cm. (**13**) *Ceratospyris echinus* Ehrenberg, 1874: ODP 1051A-4H-5W, 56–58 cm. (**14**) *Ceratospyris* ? *metroid* Tetard et al., 2023: ODP 1260A-6R-1W, 55–57 cm. (**15**) *Ceratospyris* ? *okazakii* Tetard et al., 2023: ODP 1260A-9R-6W, 55–57 cm. (**16, 17**) *Dendrospyris fragoides* Sanfilippo and Riedel, 1973: (**16**) ODP 1260A-9R-3W, 55–57 cm; (**17**) ODP 1051A-38X-5W, 55–57 cm. All scale bars equal 50 µm.

1957a *Ceratospyris* aff. *C. echinus* Ehrenberg – Riedel, p. 259, pl. 63, fig. 4.
1975 *Ceratospyris* sp. cf. *C. echinus* Ehrenberg – Ling, p. 726, pl. 4, figs. 12, 13.
? 1999a *Dendrospyris inferispina* Goll – O'Connor, p. 31, pl. 10, fig. 37.
2009 *Ceratospyris echinus* Ehrenberg – Ogane et al., pl. 9, figs. 5a–5d.
2015 *Dendrospyris echinus* (Ehrenberg) – Kamikuri, pl. 19, fig. 16.
Occurrence. ODP Site 1260 (Demerara Rise; western equatorial Atlantic) and ODP Site 1051 (Blake Nose; western north Atlantic).

Ceratospyris ? *metroid* Tetard et al., 2023
Plate II.10, Figure 14

2023 *Ceratospyris metroid* Tetard et al., p. 5, figs. 4a–4d, 5a–5d.
Occurrence. ODP Site 1260 (Demerara Rise; western equatorial Atlantic) and ODP Site 1051 (Blake Nose; western north Atlantic).

Ceratospyris ? *okazakii* Tetard et al., 2023
Plate II.10, Figure 15

2023 *Ceratospyris okazakii* Tetard et al., p. 5, figs. 4e–4g, 5e, 5f.
Occurrence. ODP Site 1260 (Demerara Rise; western equatorial Atlantic) and ODP Site 1051 (Blake Nose; western north Atlantic).

Genus *Dendrospyris* Haeckel, 1882

Type species.— *Ceratospyris stylophora* Ehrenberg, 1874, 220 (unfigured); Ehrenberg, 1876, p. 66, pl. 20, fig. 10.

Dendrospyris fragoides Sanfilippo and Riedel, 1973
Plate II.10, Figures 16, 17

1973 *Dendrospyris fragoides* Sanfilippo and Riedel, p. 526, pl. 15, figs. 8–13, pl. 31, figs. 13, 14.
2015 *Dendrospyris fragoides* Sanfilippo and Riedel – Kamikuri, pl. 11, fig. 23.
Occurrence. ODP Site 1260 (Demerara Rise; western equatorial Atlantic) and ODP Site 1051 (Blake Nose; western north Atlantic).

Dendrospyris golli Nishimura, 1992
Plate II.11, Figure 1

1992 *Dendrospyris golli* Nishimura, p. 330, pl. 3, figs. 1, 2, pl. 12, fig. 11.
Occurrence. ODP Site 1260 (Demerara Rise; western equatorial Atlantic).

Dendrospyris stylophora (Ehrenberg, 1874)
Plate II.11, Figure 2

1874 *Ceratospyris stylophora* Ehrenberg, p. 220.
1876 *Ceratospyris stylophora* Ehrenberg – Ehrenberg, p. 66, pl. 20, fig. 10.
1887 *Dendrospyris stylophora* (Ehrenberg) – Haeckel, p. 1038.
1968 *Dendrospyris stylophora* (Ehrenberg) – Goll, p. 1423, pl. 173, figs. 21–24, text-fig. 8.
2009 *Ceratospyris stylophora* Ehrenberg – Ogane et al., pl. 38, fig. 6a–6c, pl. 39, figs. 6a, 6b.
2009b *Triceraspyris palmipodiscus* Petrushevskaya in Petrushevskaya and Kozlova – Suzuki et al., p. 258, pl. 19, figs. 14a, 14b.
Occurrence. ODP Site 1260 (Demerara Rise; western equatorial Atlantic) and ODP Site 1051 (Blake Nose; western north Atlantic).

Genus *Desmospyris* Haeckel, 1882

Type species.— *Desmospyris mammillata* Haeckel, 1887, p. 1089, pl. 83, fig. 14.

Desmospyris biloba Tetard et al., 2023
Plate II.11, Figure 7

? 1999 *Desmospyris* ? sp. Kozlova, pl. 31, fig. 18.
2023 *Desmospyris biloba* Tetard et al., p. 8, figs. 4h–4j, 5g–5j.
Occurrence. ODP Site 1260 (Demerara Rise; western equatorial Atlantic) and ODP Site 1051 (Blake Nose; western north Atlantic).

Desmospyris cyrillium (Sanfilippo and Riedel, 1973)
Plate II.11, Figure 3

1973 *Giraffospyris cyrillium* Sanfilippo and Riedel, p. 528, pl. 18, figs. 1–3, pl. 33, fig. 3.
1978 *Giraffospyris cyrillium* Sanfilippo and Riedel – Weaver and Dinkelman, p. 869, pl. 5, fig. 8.
Remarks. The combination used here is derived from O'Dogherty et al. (2021).
Occurrence. ODP Site 1051 (Blake Nose; western north Atlantic).

Desmospyris lata (Goll, 1969)
Plate II.11, Figure 4

1969 *Giraffospyris lata* Goll, p. 334, pl. 58, figs. 22, 24–26, text-fig. 2.
1972 *Desmospyris* sp. aff. *Giraffospyris lata* (Goll) – Petrushevskaya and Kozlova, p. 532, pl. 38, fig. 1.
1975 *Desmospyris* ? *lata* (Goll) – Petrushevskaya, pl. 10, fig. 30.
1973 *Giraffospyris lata* Goll – Sanfilippo and Riedel, p. 529, pl. 18, figs. 3–7, pl. 33, fig. 4.
1978 *Giraffospyris lata* Goll – Weaver and Dinkelman, p. 869, pl. 5, fig. 7.
1981 *Giraffospyris lata* Goll – De Wever, p. 511, pl. 2, fig. 5.
1993 *Giraffospyris lata* Goll – Hull, p. 12, pl. 7, fig. 4, pl. 8, fig. 4.
1998a *Giraffospyris lata* Goll – Sanfilippo and Nigrini, p. 272, pl. 13.1, figs. 12, 13.
2008 *Girafospyris lata* [sic] Goll – Jackett et al., p. 52, pl. 4, fig. 16.
Occurrence. ODP Site 1051 (Blake Nose; western north Atlantic).

Desmospyris obtusus Bütschli, 1882a
Plate II.11, Figure 8

1882a *Dictyocephalus obtusus* Bütschli, p. 535, pl. 36, figs. 20a–20c.
1882b *Dictyocephalus obtusus* Bütschli – Bütschli, pl. 31, figs. 10a, 10b.
1887 *Desmospyris mammillata* Haeckel, p. 1089, pl. 83, fig. 14.
1975 *Dendrospyris stabilis* Goll – Chen, p. 455, pl. 7, fig. 3.
1975 *Desmospyris* sp. cf. *D. anthocyrtoides* (Bütschli) – Ling, p. 726, pl. 7, fig. 1.
1992 *Dendrospyris stabilis* Goll – Takemura, p. 743, pl. 4, fig. 7.
2002 *Dendrospyris stabilis* Goll – Apel et al., p. 18, pl. P8, fig. 7 (part).
Remarks. The combination used here is derived from O'Dogherty et al. (2021).
Occurrence. ODP Site 1260 (Demerara Rise; western equatorial Atlantic) and ODP Site 1051 (Blake Nose; western north Atlantic).

Genus *Dorcadospyris* Haeckel, 1882
Type species.— *Dorcadospyris dentata* Haeckel, 1887, p. 1040, pl. 85, fig. 6.

Dorcadospyris anastasis Sanfilippo *in* Nigrini et al., 2005
Plate II.11, Figure 5

2005 *Dorcadospyris anastasis* Sanfilippo *in* Nigrini et al., p. 33, pl. P1, figs. 11, 12.
2012 *Dorcadospyris anastasis* Sanfilippo *in* Nigrini et al. – Moore and Kamikuri, p. 6, pl. P2, figs. 7, 8.
Occurrence. ODP Site 1260 (Demerara Rise; western equatorial Atlantic).

Dorcadospyris ombros Sanfilippo *in* Nigrini, 2005
Plate II.11, Figure 6

2005 *Dorcadospyris ombros* Sanfilippo *in* Nigrini et al., p. 36, pl. P2, figs. 5, 6.
2012 *Dorcadospyris ombros* Sanfilippo *in* Nigrini et al. – Moore and Kamikuri, p. 7, pl. P3, figs. 3, 4.
Occurrence. ODP Site 1260 (Demerara Rise; western equatorial Atlantic).

Dorcadospyris ? *flexuosa* (Ehrenberg, 1874)
Plate II.11, Figure 9

1862 *Rhabdolithes pipa* [sic] Ehrenberg – Bury, pl. 3, fig. 4 (part).
1874 *Stylosphaera flexuosa* Ehrenberg, p. 258.
1876 *Stylosphaera flexuosa* Ehrenberg – Ehrenberg, p. 84, pl. 25, fig. 5.
1887 *Sphærostylus (Sphærostylantha) flexuosus* [sic] (Ehrenberg) – Haeckel, p. 138.
1986 *Stylosphaera flexuosa* Ehrenberg – Göke, fig. 3.2.
2009 *Stylosphaera flexuosa* Ehrenberg – Ogane et al., pl. 11, fig. 4d (part).

Remarks. The combination used here is derived from O'Dogherty et al. (2021).

Occurrence. ODP Site 1260 (Demerara Rise; western equatorial Atlantic) and ODP Site 1051 (Blake Nose; western north Atlantic).

Genus *Elaphospyris* Haeckel, 1882

Type species.— *Ceratospyris heptaceros* Ehrenberg, 1874, p. 219 (unfigured); Ehrenberg, 1876, p. 66, pl. 20, fig. 2.

Elaphospyris didiceros (Ehrenberg, 1874) group
Plate II.11, Figures 10, 11

1862 *Petalospiris diaboliscus* [sic] Ehrenberg – Bury, pl. 17, fig. 6.
1874 *Ceratospyris didiceros* Ehrenberg, p. 218.
1876 *Ceratospyris didiceros* Ehrenberg – Ehrenberg, p. 66, pl. 21, fig. 6.
1887 *Triceraspyris* (*Triospyris*) *didiceros* (Ehrenberg) – Haeckel, p. 1030.
1887 *Triceraspyris* (*Triospyrium*) *giraffa* Haeckel, p. 1031, pl. 84, fig. 11.
1958 *Aegospyris longibarba* (Ehrenberg) – Göke, pl. 3, fig. 1.
1969 *Giraffospyris didiceros* (Ehrenberg) – Goll, p. 332, pl. 60, figs. 5–7, 9, text-fig. 2.
1970 *Giraffospyris didiceros* (Ehrenberg) group – Riedel and Sanfilippo, pl. 5, figs. 3–5.
1970 *Dendrospyris didiceros* (Ehrenberg) group – Petrushevskaya and Kozlova, p. 532, pl. 40, fig. 12.
1974 *Giraffospyris didiceros* (Ehrenberg) – Johnson, p. 547, pl. 3, fig. 7.
1975 *Giraffospyris didiceros* (Ehrenberg) – Chen, p. 456, pl. 3, fig. 4.
1975 *Dendrospyris didiceros* (Ehrenberg) group – Ling, p. 726, pl. 4, fig. 16.
1977 Spyrid gen. and sp. indet. Riedel and Sanfilippo, pl. 6, fig. 15 (part).
1981 *Giraffospyris didiceros* (Ehrenberg) – De Wever, p. 511, pl. 2, fig. 13.
1992 *Giraffospyris didiceros* (Ehrenberg) – Kim, p. 40, pl. 1, figs. 8, 9.
1995 Spyrida gen. et spp. undet. Strong et al., fig. 10N (part).
2009 *Ceratospyris heptaceros* Ehrenberg – Ogane et al., pl. 18, figs. 4a–4e, pl. 38, figs. 7a–7c, pl. 39, figs. 7a, 7b (part).
2009 *Ceratospyris didiceros* Ehrenberg – Ogane et al., pl. 39, figs. 1a–1c.
2009b *Giraffospyris incertecoronata* (Clark and Campbell) – Suzuki et al., p. 258, pl. 19, figs. 12a, 12b.
2013 *Dendrospyris didiceros* (Ehrenberg) – Kamikuri et al., pl. 1, fig. 7.
2015 *Dorcadospyris* aff. *furcata* (Ehrenberg) – Kamikuri, pl. 13, fig. 15, pl. 19, fig. 15.
2020 *Giraffospyris didiceros* (Ehrenberg) – Hollis et al., pl. 5, fig. 2.

Remarks. The combination used here is derived from O'Dogherty et al. (2021).
Occurrence. ODP Site 1260 (Demerara Rise; western equatorial Atlantic) and ODP Site 1051 (Blake Nose; western north Atlantic).

Genus *Liriospyris* Haeckel, 1882

Type species.— *Liriospyris hexapoda* Haeckel, 1887, p. 1049, pl. 86, fig. 7.

Liriospyris clathrata (Ehrenberg, 1854a)

Plate II.11, Figures 12, 13

1854a *Dictyospyris clathrus* Ehrenberg, pl. 36, fig. 25.
1862 *Petalospyris clathrus* (Ehrenberg) – Haeckel, p. 295.
1874 *Dictyospyris clathrata* Ehrenberg – Ehrenberg, p. 224.
1876 *Dictyospyris clathrata* Ehrenberg – Ehrenberg, p. 68, pl. 19, fig. 7.
1882a *Dictyospyris clathrata* Ehrenberg – Bütschli, p. 506, pl. 32, figs. 10a, 10b.
1887 *Liriospyris clathrata* (Ehrenberg) – Haeckel, p. 1049.
1968 *Liriospyris clathrata* (Ehrenberg) – Goll, p. 175, figs. 12, 13, 16, 17.
1972 *Dictyospyris* ? *clathrata* Ehrenberg – Petrushevskaya and Kozlova, pl. 39, fig. 14.
1972 *Liriospyris* sp. aff. *D. clathrata* Ehrenberg – Petrushevskaya and Kozlova, p. 531, pl. 39, fig. 15.
1975 *Liriospyris clathrata* (Ehrenberg) – Ling, p. 726, pl. 7, figs. 6–9.
not 1999a *Liriospyris clathrata* (Ehrenberg) – O'Connor, p. 32, pl. 10, fig. 39.
2009 *Ceratospyris heptaceros* Ehrenberg – Ogane et al., pl. 1, figs. 2a–2c (part).
2015 *Liriospyris spinulosa* (Ehrenberg) – Kamikuri, pl. 13, figs. 26–27b.

Occurrence. ODP Site 1260 (Demerara Rise; western equatorial Atlantic) and ODP Site 1051 (Blake Nose; western north Atlantic).

Liriospyris ramosa (Ehrenberg, 1847)

Plate II.12, Figures 1, 2

1847 *Cladospyris ramosa* Ehrenberg, p. 54.
1874 *Ceratospyris ramosa* (Ehrenberg) – Ehrenberg, p. 219.
1876 *Ceratospyris ramosa* (Ehrenberg) – Ehrenberg, p. 66, pl. 20, fig. 7.
1887 *Ceratospyris* (*Cladospyris*) *ramosa* (Ehrenberg) – Haeckel, p. 1069.
2009 *Ceratospyris ramosa* (Ehrenberg) – Ogane et al., pl. 76, figs. 4a–4d.
2015 *Liriospyris spinulosa* (Ehrenberg) – Kamikuri, pl. 13, figs. 26–27b.

Remarks. The combination used here is derived from O'Dogherty et al. (2021).
Occurrence. ODP Site 1051 (Blake Nose; western north Atlantic).

Liriospyris turrita (Ehrenberg, 1874)

Plate II.12, Figure 3

1874 *Ceratospyris turrita* Ehrenberg, p. 220.
1876 *Ceratospyris turrita* Ehrenberg – Ehrenberg, p. 66, pl. 20, fig. 1.
1887 *Liriospyris turrita* (Ehrenberg) – Haeckel, p. 1050.
2009 *Ceratospyris turrita* Ehrenberg – Ogane et al., pl. 76, figs. 1a–2c.

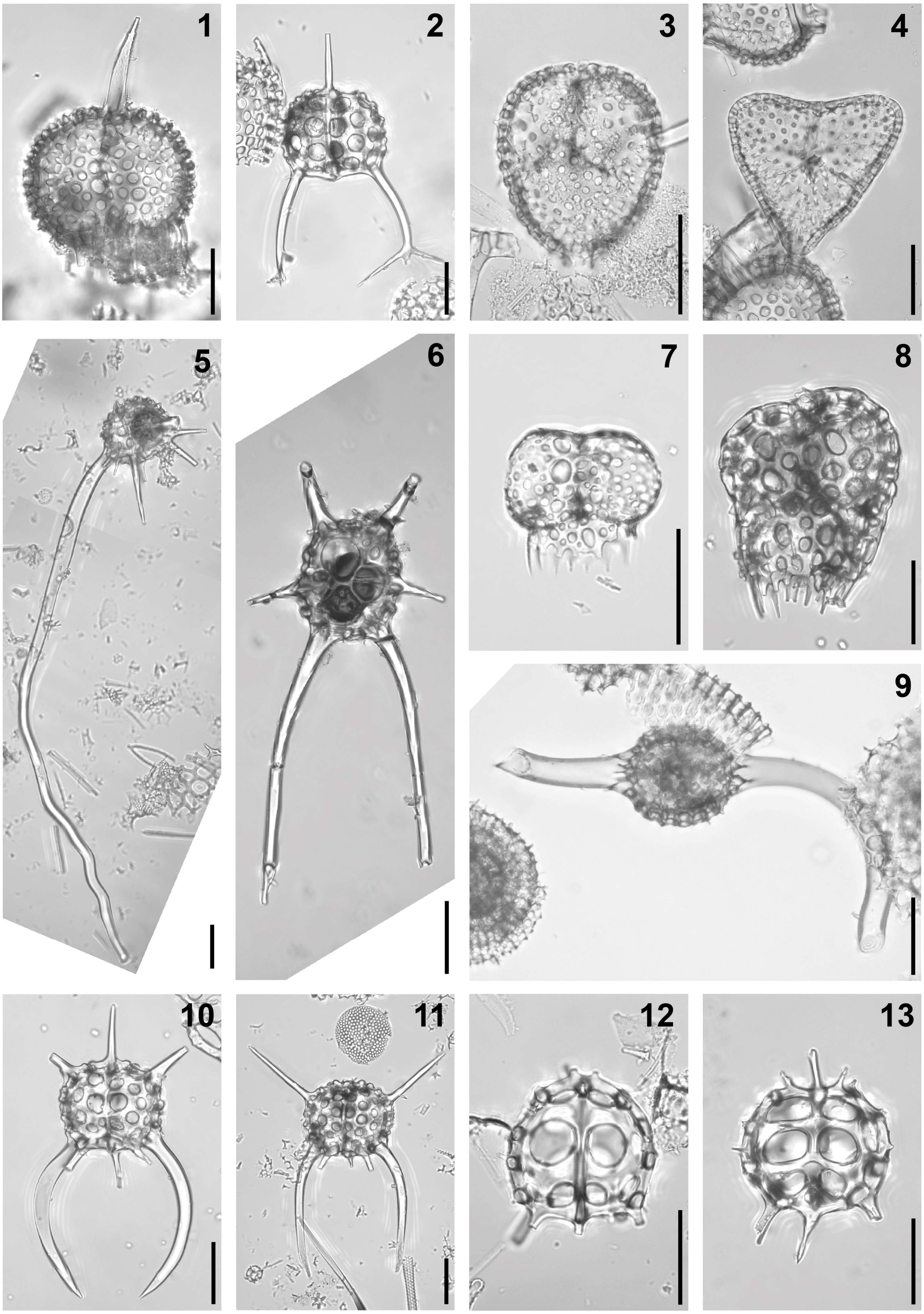
1
2
3
4
5
6
7
8
9
10
11
12
13

Plate II.11. Composite light micrographs of new radiolarian species from ODP Site 1260 (Demerara Rise, western equatorial Atlantic) and ODP Site 1051 (Blake Nose, western North Atlantic). (**1**) *Dendrospyris golli* Nishimura, 1992: ODP 1260A-13R-1W, 54–55 cm. (**2**) *Dendrospyris stylophora* (Ehrenberg, 1874): ODP 1260A-10R-1W, 55–57 cm. (**3**) *Desmospyris cyrillium* (Sanfilippo and Riedel, 1973): ODP 1510A-38X-5W, 55–57 cm. (**4**) *Desmospyris lata* (Goll, 1969): ODP 1051A-38X-5W, 55–57 cm. (**5**) *Dorcadospyris anastasis* Sanfilippo *in* Nigrini et al., 2005: ODP 1260A-6R-2W, 55–57 cm. (**6**) *Dorcadospyris ombros* Sanfilippo in Nigrini, 2005: ODP 1260A-6R-3W, 55–57 cm. (**7**) *Desmospyris* ? *biloba* Tetard et al., 2023: ODP 1260A-6R-2W, 55–57 cm. (**8**) *Desmospyris obtusus* Bütschli, 1882a: ODP 1260A-6R-3W, 55–57 cm. (**9**) *Dorcadospyris* ? *flexuosa* (Ehrenberg, 1874): ODP 1260A-6R-2W, 55–57 cm. (**10, 11**) *Elaphospyris didiceros* (Ehrenberg, 1874) group: (**10**) ODP 1260A-9R-7W, 55–57 cm; (**11**) ODP 1260A-11R-4W, 55–57 cm. (**12, 13**) *Liriospyris clathrata* (Ehrenberg, 1854a): ODP 1051A-9H-2W, 53–55 cm; (**13**) ODP 1260A-9R-4W, 55–57 cm. All scale bars equal 50 µm.

2015 *Dorcadospyris costatescens* Goll – Kamikuri, pl. 13, figs. 5–7.
Occurrence. ODP Site 1051 (Blake Nose; western north Atlantic).

Genus *Petalospyris* Ehrenberg, 1846

Type species.— *Petalospyris diaboliscus* Ehrenberg, 1847, p. 55, fig. 6.

Petalospyris argiscus Ehrenberg, 1874

Plate II.12, Figure 4

1874 *Petalospyris Argiscus* [sic] Ehrenberg, p. 246.
? 1874 *Petalospyris carinata* Ehrenberg, p. 246.
1874 *Petalospyris eupetala* Ehrenberg, p. 247.
1876 *Petalospyris Argiscus* [sic] Ehrenberg – Ehrenberg, p. 80, pl. 22, figs. 1, 2.
? 1876 *Petalospyris carinata* Ehrenberg – Ehrenberg, p. 80, pl. 22, fig. 6.
1876 *Petalospyris eupetala* Ehrenberg – Ehrenberg, p. 80, pl. 22, fig. 4.
1882a *Petalospyris Argiscus* [sic] Ehrenberg – Bütschli, p. 539, pl. 32, figs. 17a, 17b.
1882b *Petalospyris Argiscus* [sic] Ehrenberg – Bütschli, pl. 29, figs. 6a, 6b.
1887 *Petalospyris* (*Petalospyrissa*) *eupetala* Ehrenberg – Haeckel, p. 1061.
1887 *Petalospyris* (*Petalospyromma*) *argiscus* Ehrenberg – Haeckel, p. 1062.
1957a *Petalospyris platyacantha* Ehrenberg – Riedel, p. 259, pl. 63, fig. 3.
1969 *Dorcadospyris argisca* (Ehrenberg) – Goll, p. 336, pl. 56, figs. 9–11.
1975 *Dorcadospyris argisca* (Ehrenberg) – Chen, p. 456, pl. 3, fig. 9.
1975 *Petalospyris foveolata* Ehrenberg – Ling, p. 727, pl. 7, fig. 23.
? 1975 *Petalospyris* sp. cf. *P. foveolata* Ehrenberg – Ling, p. 727, pl. 7, fig. 24.
1981 *Dorcadospyris argisca* (Ehrenberg) – De Wever, p. 511, pl. 2, fig. 12.
? 2008 *Petalospyris platyacantha* Ehrenberg group – Jackett et al., p. 52, pl. 4, fig. 17.
2009 *Petalospyris argiscus* Ehrenberg – Ogane et al., pl. 2, fig. 11, pl. 18, figs. 7a–7e, pl. 39, figs. 8a–8c (part).

? 2009 *Petalospyris carinata* Ehrenberg – Ogane et al., pl. 40, figs. 5a–5d.
2009 *Petalospyris eupetala* Ehrenberg – Ogane et al., pl. 39, figs. 9a–9c.
2009 *Petalospyris flabellum* Ehrenberg – Ogane et al., pl. 2, figs. 14a, 14b (part).
2009b *Petalospyris* cf. *eupetala* Ehrenberg – Suzuki et al., p. 258, pl. 19, figs. 13a, 13b.
2015 *Dorcadospyris argisca* (Ehrenberg) – Kamikuri, pl. 13, figs. 1a, 1b, 22.
2020 *Dorcadospyris argisca* (Ehrenberg) – Hollis et al., pl. 5, fig. 1.
Occurrence. ODP Site 1260 (Demerara Rise; western equatorial Atlantic) and ODP Site 1051 (Blake Nose; western north Atlantic).

Petalospyris confluens Ehrenberg, 1874
Plate II.12, Figures 5, 6

1874 *Petalospyris confluens* Ehrenberg, p. 246.
1876 *Petalospyris confluens* Ehrenberg – Ehrenberg, p. 80, pl. 22, fig. 5.
1887 *Patagospyris confluens* (Ehrenberg) – Haeckel, p. 1088.
1969 *Dorcadospyris confluens* (Ehrenberg) – Goll, p. 337, pl. 58, figs. 9–12, text-fig. 2.
not 1973 *Dorcadospyris confluens* (Ehrenberg) – Sanfilippo and Riedel, p. 528, pl. 17, figs. 6–10, pl. 33, fig. 1.
not 1987 *Dorcadospyris confluens* (Ehrenberg) – Nishimura, p. 725, pl. 3, figs. 18, 19.
not 1999 *Patagospyris confluens* (Ehrenberg) – Kozlova, p. 166, pl. 8, fig. 14.
2009 *Petalospyris confluens* Ehrenberg – Ogane et al., pl. 75, fig. 5a, 5b, pl. 77, fig. 2a–2c (part).
2015 *Dorcadospyris confluens* (Ehrenberg) – Kamikuri, pl. 13, figs. 16, 17.
Occurrence. ODP Site 1260 (Demerara Rise; western equatorial Atlantic) and ODP Site 1051 (Blake Nose; western north Atlantic).

Petalospyris diaboliscus Ehrenberg, 1847
Plate II.12, Figure 7

1847 *Petalospyris Diaboliscus* [sic] Ehrenberg, p. 55, fig. 6.
1874 *Petalospyris Diaboliscus* [sic] Ehrenberg – Ehrenberg, p. 246.
1887 *Anthospyris diaboliscus* (Ehrenberg) – Haeckel, p. 1065.
1975 *Petalospyris diaboliscus* Ehrenberg – Ling, p. 727, pl. 7, fig. 22.
1981 Spyrid De Wever, pl. 2, fig. 11.
2009 *Petalospyris diaboliscus* Ehrenberg – Ogane et al., pl. 5, figs. 6a–6c, pl. 76, 3a–3c.
2015 *Dorcadospyris diaboliscus* Ehrenberg – Kamikuri, pl. 13, fig. 23.
Occurrence. ODP Site 1260 (Demerara Rise; western equatorial Atlantic) and ODP Site 1051 (Blake Nose; western north Atlantic).

Petalospyris flabellum Ehrenberg, 1874
Plate II.12, Figure 8

1874 *Petalospyris Flabellum* [sic] Ehrenberg, p. 247.
1876 *Petalospyris Flabellum* [sic] Ehrenberg – Ehrenberg, p. 80, pl. 22, fig. 7.
1887 *Phænocalpis flabellum* [sic] (Ehrenberg) – Haeckel, p. 1174.

2009 *Petalospyris flabellum* Ehrenberg – Ogane et al., pl. 2, figs. 13a, 13b, pl. 5, figs. 4a, 4b, pl. 18, figs. 5a, 5b (part).

Occurrence. ODP Site 1260 (Demerara Rise; western equatorial Atlantic).

Petalospyris pentas Ehrenberg, 1874

Plate II.12, Figures 9, 10

1874 *Petalospyris Pentas* [sic] Ehrenberg, p. 247.

1876 *Petalospyris Pentas* [sic] Ehrenberg – Ehrenberg, p. 80, pl. 22, fig. 11.

1887 *Gorgospyris* (*Gorgospyrium*) *ehrenbergii* Haeckel, p. 1070.

1972 *Patagospyris pentas* (Ehrenberg) – Petrushevskaya and Kozlova, p. 532, pl. 39, figs. 32, 33.

1987 *Dorcadospyris pentas* (Ehrenberg) – Nishimura, p. 725, pl. 3, fig. 17.

1995 *Gorgospyris hemisphaerica* Clark and Campbell – Shilov, p. 127, pl. 1, figs. 7, 8.

1999 *Petalospyrella pentas* (Ehrenberg) – Kozlova, p. 167, pl. 14, fig. 19.

2005 ? *Pentaspyris paradoxa* Clark and Campbell – Funakawa and Nishi, p. 233, pl. 3, fig. 8.

2009 *Petalospyris pentas* Ehrenberg – Ogane et al., pl. 9, figs. 1a–1e.

Occurrence. ODP Site 1260 (Demerara Rise; western equatorial Atlantic) and ODP Site 1051 (Blake Nose; western north Atlantic).

Petalospyris platyacantha Ehrenberg, 1874 group

Plate II.12, Figure 11

1874 *Petalospyris platyacantha* Ehrenberg, p. 247.

1876 *Petalospyris platyacantha* Ehrenberg – Ehrenberg, p. 80, pl. 22, fig. 8.

1887 *Petalospyris* (*Petalospyrella*) *platyacantha* Ehrenberg – Haeckel, p. 1060.

1973 *Dorcadospyris platyacantha* (Ehrenberg) – Sanfilippo and Riedel, p. 528, pl. 17, figs. 11–15, pl. 33, fig. 2.

1975 *Patagospyris confluens* (Ehrenberg) – Ling, p. 727, pl. 7, fig. 21.

? 1977 Spyrid gen. and sp. indet. Riedel and Sanfilippo, pl. 6, fig. 15 (part).

1992 *Dorcadospyris platyacantha* (Ehrenberg) – Nishimura, p. 329, pl. 3, figs. 3–4b.

1994 *Dorcadospyris platyacantha* (Ehrenberg) – Weinheimer et al., p. 311, pl. 1, fig. 7.

2009 *Petalospyris platyacantha* Ehrenberg – Ogane et al., pl. 77, figs. 3a–3c.

Occurrence. ODP Site 1260 (Demerara Rise; western equatorial Atlantic) and ODP Site 1051 (Blake Nose; western north Atlantic).

Genus *Semantidium* Haeckel, 1887

Type species.— *Semantidium hexastoma* Haeckel, 1887, p. 960, pl. 92, fig. 6.

Semantidium haeckelii (Bütschli, 1882a)

Plate II.12, Figure 12

1882a *Stephanolithis Haeckelii* [sic] Bütschli, p. 538, pl. 32, figs. 6a, 6b.

1882b *Stephanolithis Haeckelii* [sic] – Bütschli, pl. 28, fig. 11.

1969 *Giraffospyris haeckelii* (Bütschli) – Goll, p. 334, pl. 57, figs. 5–7, text-fig. 2.

Remarks. The combination used here is derived from O'Dogherty et al. (2021).

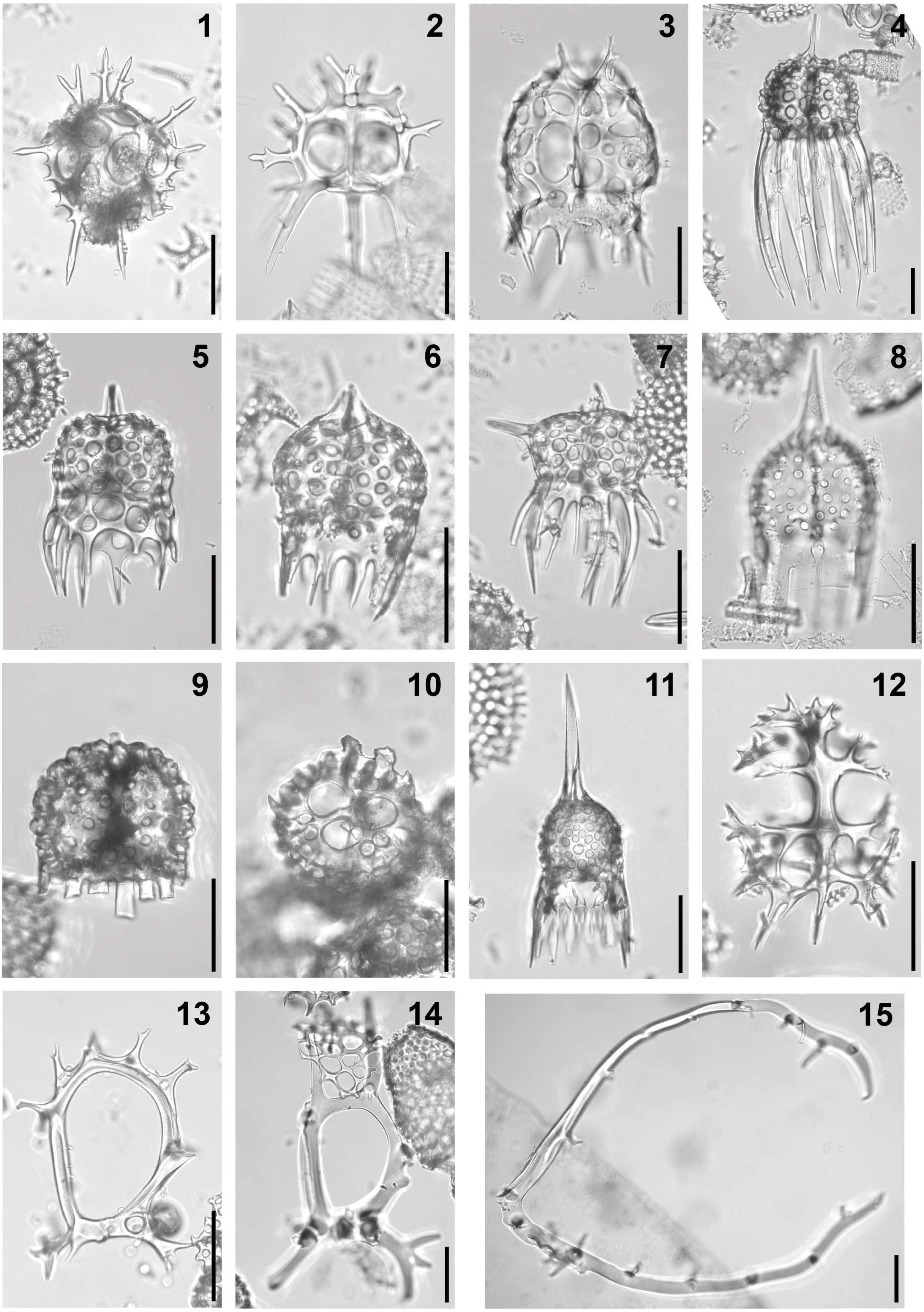
1
2
3
4
5
6
7
8
9
10
11
12
13
14
15

Plate II.12. Composite light micrographs of new radiolarian species from ODP Site 1260 (Demerara Rise, western equatorial Atlantic) and ODP Site 1051 (Blake Nose, western North Atlantic). (**1, 2**) *Liriospyris ramosa* (Ehrenberg, 1847): ODP 1260A-6R-1W, 55–57 cm; (**2**) ODP 1051A-10H-2W, 53–55 cm. (**3**) *Liriospyris turrita* (Ehrenberg, 1874): ODP 1051A-2H-5W, 55–57 cm. (**4**) *Petalospyris argiscus* Ehrenberg, 1874: ODP 1260A-11R-4W, 55–57 cm. (**5, 6**) *Petalospyris confluens* Ehrenberg, 1874: (**5**) ODP 1260A-6R-2W, 55–57 cm; (**6**) ODP 1260A-12R-2W, 55–57 cm. (**7**) *Petalospyris diaboliscus* Ehrenberg, 1847: ODP 1260A-9R-3W, 55–57 cm. (**8**) *Petalospyris flabellum* Ehrenberg, 1874: ODP 1051A-8H-5W, 53–55 cm. (**9, 10**) *Petalospyris pentas* Ehrenberg, 1874: (**9**) ODP 1260A-19R-6W, 55–57 cm; (**10**) ODP 1260A-20R-4W, 63–177 cm. (**11**) *Petalospyris platyacantha* Ehrenberg, 1874 group: ODP 1260A-7R-4W, 54–56 cm. (**12**) *Semantidium haeckelii* (Bütschli, 1882a): ODP 1260A-11R-7W, 55–57 cm. (**13**) *Zygocircus butschlii* Haeckel, 1887: ODP 1260A-9R-4W, 55–57 cm. (**14**) *Zygocircus* ? *spinescens* (Ehrenberg, 1854a): ODP 1260A-6R-2W, 55–57 cm. (**15**) *Zygocircus cimelium* Petrushevskaya *in* Petrushevskaya and Kozlova, 1972: ODP 1260A-13R-1W, 54–56 cm. All scale bars equal 50 µm.

Occurrence. ODP Site 1260 (Demerara Rise; western equatorial Atlantic) and ODP Site 1051 (Blake Nose; western north Atlantic).

Family Stephaniidae Haeckel, 1882

Genus *Zygocircus* Bütschli, 1882a

Type species.— *Lithocircus productus* Hertwig, 1879, p. 197, pl. 7, fig. 4.

Zygocircus butschlii Haeckel, 1887

Plate II.12, Figure 13

1887 *Zygocircus bütschlii* [sic] Haeckel, p. 948.
1972 *Zygocircus bütschlii* [sic] Haeckel – Petrushevskaya and Kozlova, p. 534, pl. 41, figs. 8–11.
1986 *Dendrocircus barbadensis* Haeckel – Göke, fig. 3.6.
1992 *Zygocircus bütschli* [sic] Haeckel – Takemura, 1992, p. 743, pl. 5, fig. 4.
1997 *Zygocircus bütschli* [sic] Haeckel – Hollis et al., p. 51, pl. 3, fig. 11.
1997 *Zygocircus bütschli* [sic] Haeckel – Takemura and Ling, p. 114, pl. 1, fig. 4.
1999a *Zygocircus buetschlii* [sic] Haeckel – O'Connor, p. 40, pl. 10, fig. 43.
2005 *Zygocircus bütschlii* [sic] Haeckel – Funakawa and Nishi, p. 238, pl. 3, fig. 9.
2009b *Zygocircus triangularis* (Clark and Campbell) – Suzuki et al., p. 257, pl. 22, fig. 15.
2020 *Zygocircus bütschli* [sic] Haeckel – Hollis et al., pl. 5, fig. 4.
2021 *Zygocircus bütschli* [sic] Haeckel – de Souza et al., p. 15, pl. 2, fig. 2.

Occurrence. ODP Site 1260 (Demerara Rise; western equatorial Atlantic) and ODP Site 1051 (Blake Nose; western north Atlantic).

Zygocircus cimelium Petrushevskaya in Petrushevskaya and Kozlova, 1972
Plate II.12, Figure 15

1972 *Zygocircus cimelium* Petrushevskaya *in* Petrushevskaya and Kozlova, p. 534, pl. 41, figs. 5, 6.

2005 *Zygocircus cimelium* Petrushevskaya *in* Petrushevskaya and Kozlova – Nigrini et al., p. 56, pl. P3, figs. 9–12.

2012 *Zygocircus cimelium* Petrushevskaya *in* Petrushevskaya and Kozlova – Moore and Kamikuri, p. 13, pl. P10, figs. 8, 9.

Occurrence. ODP Site 1260 (Demerara Rise; western equatorial Atlantic) and ODP Site 1051 (Blake Nose; western north Atlantic).

Zygocircus ? *spinescens* (Ehrenberg, 1854a)
Plate II.12, Figure 14

1854a *Stephanolithis spinescens* Ehrenberg, p. 160, pl. 1, fig. 29.

1876 *Stephanolithis spinescens* Ehrenberg – Ehrenberg, pl. 36, figs. B57, C57.

1882a *Stephanolithis spinescens* Ehrenberg – Bütschli, p. 497, pl. 32, figs. 7a, 7b.

1882b *Stephanolithis spinescens* Ehrenberg – Bütschli, pl. 28, fig. 10.

1887 *Semantis spinescens* (Ehrenberg) – Haeckel, p. 958.

1957a *Semantis spinescens* (Ehrenberg) – Riedel, p. 259, pl. 63, fig. 2.

Remarks. The combination used here is derived from O'Dogherty et al. (2021).

Occurrence. ODP Site 1260 (Demerara Rise; western equatorial Atlantic) and ODP Site 1051 (Blake Nose; western north Atlantic).

Superfamily Archipilioidea Haeckel, 1882 sensu Sandin et al., 2019
Family Theophormididae Haeckel, 1882 emend. Suzuki et al., 2021
Genus *Velicucullus* Riedel and Campbell, 1952

Type species.— *Soreuma* (*Soreumium* ?) *magnificum* Clark and Campbell, 1942, p. 51, pl. 4, fig. 15.

? *Velicucullus discoides* (Ehrenberg, 1874)
Plate II.13, Figures 1, 2

1874 *Cycladophora discoides* Ehrenberg, p. 222.

1876 *Cycladophora* ? *discoides* Ehrenberg – Ehrenberg, p. 68, pl. 18, fig. 4.

1887 *Theocalyptra discoides* (Ehrenberg) – Haeckel, p. 1397.

2009 *Cycladophora discoides* Ehrenberg – Ogane et al., pl. 6, figs. 6a–6c, pl. 80, figs. 1a–1d.

Remarks. The combination used here is derived from O'Dogherty et al. (2021).

Occurrence. ODP Site 1260 (Demerara Rise; western equatorial Atlantic).

Superfamily Theopilioidea Haeckel, 1882 emend. Suzuki et al., 2021
Family Anthocyrtididae Haeckel, 1882 emend. Suzuki et al., 2021
Genus *Anthocyrtis* Ehrenberg, 1846

Type species.— *Anthocyrtis mespilus* Ehrenberg, 1847, p. 55, fig. 9.

Anthocyrtis collaris Ehrenberg, 1874
Plate II.13, Figure 3

1874 *Anthocyrtis collaris* Ehrenberg, p. 215.
1876 *Anthocyrtis collaris* Ehrenberg – Ehrenberg, p. 64, pl. 6, fig. 8.
1887 *Anthocyrtium* (*Anthocyrtarium*) *collare* (Ehrenberg) – Haeckel, p. 1273.
1887 *Clathrocyclas* (*Clathrocyclia*) *collaris* Haeckel, p. 1387, pl. 74, fig. 8.
1975 *Anthocyrtella* sp. Ling, p. 728, pl. 8, fig. 19.
2009 *Anthocyrtis collaris* Ehrenberg – Ogane et al., pl. 50, figs. 3a–3h.
2015 *Anthocyrtis collaris* Ehrenberg – Kamikuri, pl. 10, fig. 2a, 2b.

Occurrence. ODP Site 1260 (Demerara Rise; western equatorial Atlantic) and ODP Site 1051 (Blake Nose; western north Atlantic).

Anthocyrtis mespilus Ehrenberg, 1847
Plate II.13, Figure 4

1847 *Anthocyrtis Mespilus* [sic] Ehrenberg, p. 55, fig. 9.
1854a *Anthocyrtis mespilus* [sic] Ehrenberg – Ehrenberg, pl. 36, fig. 13.
1874 *Anthocyrtis furcata* Ehrenberg, 1847, p. 216.
1876 *Anthocyrtis furcata* Ehrenberg – Ehrenberg, p. 64, pl. 6, fig. 2.
1876 *Anthocyrtis mespilus* Ehrenberg – Ehrenberg, p. 66, pl. 6, figs. 4, 5.
1887 *Anthocyrtis* (*Anthocyrtella*) *mespilus* Ehrenberg – Haeckel, p. 1269.
1887 *Anthocyrtis* (*Anthocyrtella*) *furcata* Ehrenberg – Haeckel, p. 1269.
2006 *Anthocyrtis furcata* Ehrenberg – Funakawa et al., p. 38, pl. P13, figs. 5a, 5b.
2009 *Anthocyrtis mespilus* Ehrenberg – Ogane et al., pl. 50, figs. 2a, 2b, pl. 80, figs. 5a–5e, pl. 81, figs. 1a–2d.
2009 *Anthocyrtis furcata* Ehrenberg – Ogane et al., pl. 80, figs. 4a–4f.
2015 *Anthocyrtis mespilus* Ehrenberg – Kamikuri, pl. 10, figs. 4a–6.

Occurrence. ODP Site 1260 (Demerara Rise; western equatorial Atlantic) and ODP Site 1051 (Blake Nose; western north Atlantic).

Anthocyrtis ? *spatiosa* (Ehrenberg, 1874)
Plate II.13, Figures 5, 6

1874 *Cycladophora spatiosa* Ehrenberg, p. 222.
1876 *Cycladophora spatiosa* Ehrenberg – Ehrenberg, p. 68, pl. 18, figs. 5, 6.
1882a *Cycladophora spatiosa* Ehrenberg – Bütschli, p. 527.
1882b *Cycladophora spatiosa* Ehrenberg – Bütschli, pl. 30, fig. 15.
1887 *Cycladophora* (*Cyclampterium*) *spatiosa* Ehrenberg – Haeckel, p. 1379.
1972 *Anthocyrtella spatiosa* (Ehrenberg) group – Petrushevskaya and Kozlova, p. 541, pl. 33, figs. 1–3.
1977 *Anthocyrtella* sp. – Riedel and Sanfilippo, pl. 10, fig. 7.
2006 *Anthocyrtella spatiosa* (Ehrenberg) group – Funakawa et al., p. 38, pl. P13, figs. 7a–8b.
2009 *Cycladophora spatiosa* Ehrenberg – Ogane et al., pl. 87, figs. 4a, 4b, pl. 9, figs. 6a, 6b.

Remarks. The combination used here is derived from O’Dogherty et al. (2021).

Occurrence. ODP Site 1260 (Demerara Rise; western equatorial Atlantic) and ODP Site 1051 (Blake Nose; western north Atlantic).

Genus *Eurystomoskevos* Caulet, 1991 emend. O'Connor, 1999a

Type species.— *Eurystomoskevos petrushevskayae* Caulet, 1991, p. 536, pl. 3, fig. 14.

Eurystomoskevos petrushevskayae Caulet, 1991

Plate II.13, Figure 7

1972 *Diplocyclas* sp. A group Petrushevskaya and Kozlova, p. 541, pl. 33, fig. 14–16.
1975 *Diplocyclas* sp. A group Petrushevskaya, p. 587, pl. 24, fig. 4.
1975 *Diplocyclas* sp. A group Chen, p. 460, pl. 7, fig. 4, 5.
1991 *Eurystomoskevos petrushevskayae* Caulet, p. 536, pl. 3, fig. 14, 15.
1992 *Diplocyclas* sp. Takemura, p. 746, pl. 3, fig. 16.
1997 *Eurystomoskevos petrushevskayaae* [sic] Caulet – Hollis et al., p. 62, pl. 5, figs. 22, 23.
2002 *Eurystomoskevos petrushevskaae* [sic] Caulet – Hollis, p. 310, pl. 7, figs. 7–10.
2002 *Eurystomoskevos petrushevskaae* [sic] Caulet – Apel et al., p. 18, pl. P7, fig. 13.
2005 *Eurystomoskevos petrushevskaae* [sic] Caulet – Funakawa and Nishi, p. 233, pl. 4, figs. 13a, 13b.
2005 ? *Cycladophora conica* Lombari and Lazarus – Funakawa and Nishi, p. 231, pl. 4, figs. 11a, 11b.
2006 *Eurystomoskevos petrushevskaae* [sic] Caulet – Funakawa et al., p. 38, pl. P13, figs. 9a, 9b.
2009b *Eurystomoskevos petrushevskaae* [sic] Caulet – Suzuki et al., p. 265, pl. 22, figs. 5a–6.
2020 *Eurystomoskevos petrushevskaae* [sic] Caulet – Hollis et al., pl. 10, fig. 8.
2021 *Eurystomoskevos petrushevskaae* [sic] Caulet – de Souza et al., p. 15, pl. 3, fig. 4.

Occurrence. ODP Site 1260 (Demerara Rise; western equatorial Atlantic) and ODP Site 1051 (Blake Nose; western north Atlantic).

Superfamily Stichopilioidea Haeckel, 1882

Family Stichopiliidae Haeckel, 1882

Genus *Lophoconus* Haeckel, 1887

Type species.— *Eucyrtidium antilope* Ehrenberg, 1873a, p. 308 (unfigured); Ehrenberg, 1873b, p. 290, pl. 9, fig. 18.

Lophoconus antilope (Ehrenberg, 1874)

Plate II.13, Figure 8

1873a *Eucyrtidium antilope* Ehrenberg, p. 308.
1873b *Eucyrtidium antilope* Ehrenberg – Ehrenberg, p. 290, pl. 9, fig. 18.
1887 *Lophoconus antilope* (Ehrenberg) – Haeckel, p. 1404.
1977 Theoperid gen. et sp. indet. Riedel and Sanfilippo, pl. 7, fig. 7.
2009a *Eucyrtidium antilope* Ehrenberg – Suzuki et al., pl. 77, figs. 1a–1d.

Occurrence. ODP Site 1260 (Demerara Rise; western equatorial Atlantic).

Superfamily Plagiacanthoidea Hertwig, 1879 emend. Sandin et al., 2019

Family Lophophaenidae Haeckel, 1882 sensu Petrushevskaya, 1971

Genus *Ceratospyris* Haeckel, 1882

Type species.— *Cornutella* ? *cucullaris* Ehrenberg, 1874, p. 221 (unfigured); Ehrenberg, 1876, p. 68, pl. 2, fig. 7.

Ceratospyris ampliata (Ehrenberg, 1874)

Plate II.13, Figure 9

1874 *Cornutella ampliata* Ehrenberg, p. 221.
1876 *Cornutella ampliata* Ehrenberg – Ehrenberg, p. 68, pl. 2, fig. 5.
1882a *Ceratocyrtis ampliata* (Ehrenberg) – Bütschli, p. 536.
1887 *Sethoconus* (*Conarachnium*) *ampliatus* (Ehrenberg) – Haeckel, p. 1291.
1999 *Ceratocyrtis ampliata* (Clark and Campbell) – Kozlova, p. 173, pl. 35, fig. 9.
1999 *Ceratocyrtis rhabdophora* (Clark and Campbell) – Kozlova, p. 115, pl. 47, fig. 14.
2009 *Cornutella ampliata* Ehrenberg – Ogane et al., pl. 35, figs. 1a–1g (part).

Occurrence. ODP Site 1260 (Demerara Rise; western equatorial Atlantic) and ODP Site 1051 (Blake Nose; western north Atlantic).

Ceratocyrtis rhabdophora (Clark and Campbell, 1945)

Plate II.13, Figure 10

1882a *Ceratocyrtis cucullaris* (Ehrenberg) – Bütschli, pl. 33, figs. 36a, 36b.
1945 *Bathrocalpis rhabdophora* Clark and Campbell, p. 34, pl. 7, figs. 36–41.
1976 *Ceratocyrtis cucullaris* (Ehrenberg) – Dzinoridze et al., pl. 26, fig. 12, pl. 37, figs. 4–6.
? 1977 *Lamprotripus* ? sp. Riedel and Sanfilippo, pl. 7, fig. 5.
2009b *Ceratocyrtis rhabdophora* (Clark and Campbell) – Suzuki et al., p. 255, pl. 20, figs. 12a, 12b.

Occurrence. ODP Site 1260 (Demerara Rise; western equatorial Atlantic) and ODP Site 1051 (Blake Nose; western north Atlantic).

Genus *Lophophaena* Ehrenberg, 1847 emend. Petrushevskaya, 1971

Type species.— *Lophophaena galeaorci* Ehrenberg, 1854c, p. 245 (unfigured); Stöhr, 1880, p. 99, pl. 3, fig. 17.

Lophophaena capito Ehrenberg, 1874

Plate II.13, Figures 14, 15

1874 *Lophophaena Capito* [sic] Ehrenberg, p. 242.
1876 *Lophophaena Capito* [sic] Ehrenberg – Ehrenberg, p. 78, pl. 8, fig. 6.
1972 *Lophophaena* ? *capito* Ehrenberg group – Petrushevskaya and Kozlova, p. 535, pl. 33, figs. 20–23.
not 1975 *Lophophaena* ? *capito* Ehrenberg group – Petrushevskaya, pl. 9, fig. 21.
1975 *Lophophaena* sp. G Petrushevskaya, pl. 9, fig. 22
1975 *Lamptonium sanfilippoae* Foreman – Ling, p. 729, pl. 9, fig. 23 (part).
1977 Plagoniid gen. et sp. indet. Riedel and Sanfilippo, pl. 7, fig. 3, pl. 8, fig. 11 (part).

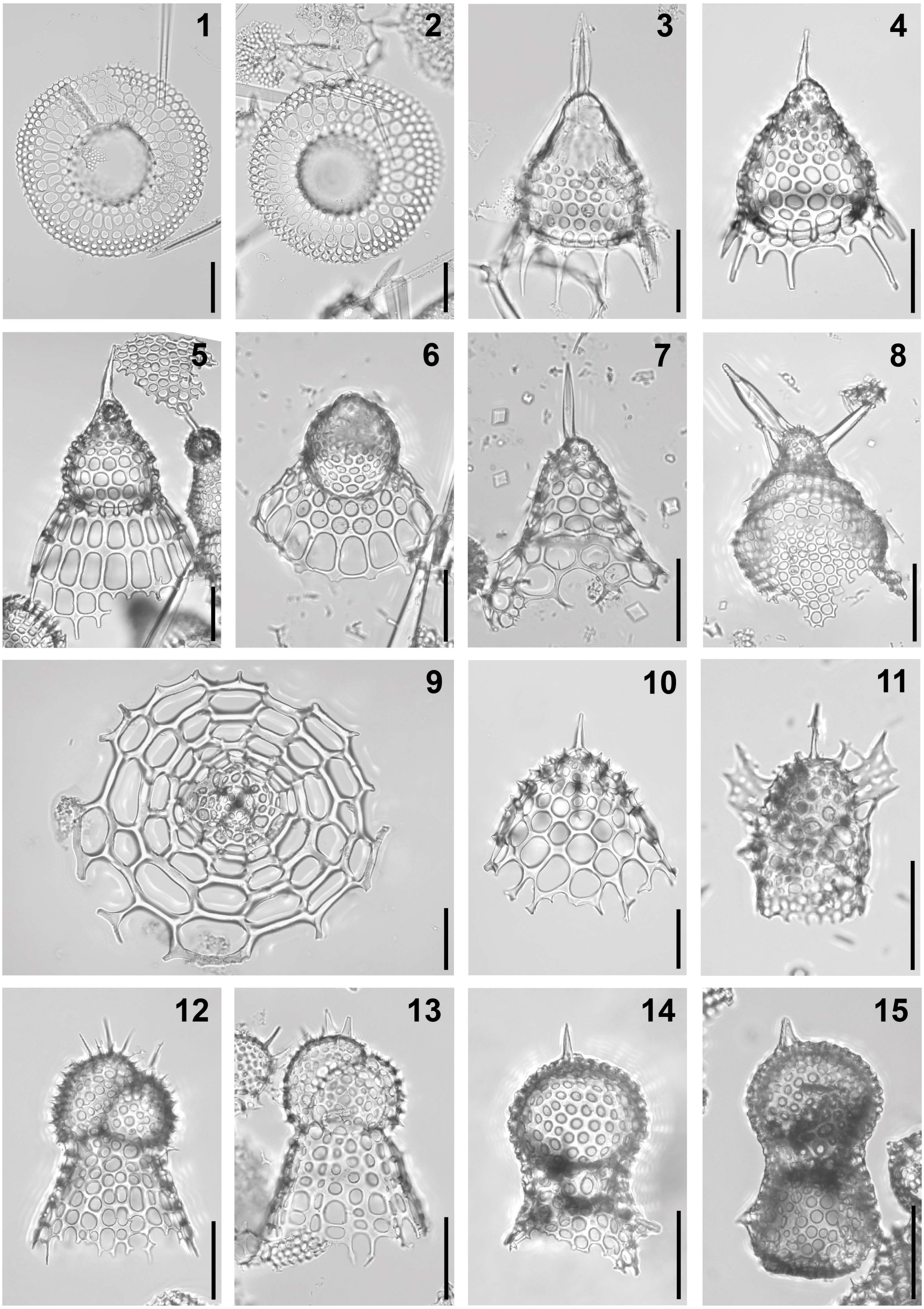
1
2
3
4
5
6
7
8
9
10
11
12
13
14
15

Plate II.13. Composite light micrographs of new radiolarian species from ODP Site 1260 (Demerara Rise, western equatorial Atlantic) and ODP Site 1051 (Blake Nose, western North Atlantic). (**1, 2**) ? *Velicucullus discoides* (Ehrenberg, 1874): (**1**) ODP 1051A-11H-2W, 62–64 cm; (**2**) ODP 1260A-9H-2W, 53–55 cm. (**3**) *Anthocyrtis collaris* Ehrenberg, 1874: ODP 1051A-11H-2W, 62–64 cm. (**4**) *Anthocyrtis mespilus* Ehrenberg, 1847: ODP 1260A-13R-3W, 54–56 cm. (**5, 6**) *Anthocyrtis* ? *spatiosa* (Ehrenberg, 1874) group: (**5**) ODP 1260A-13R-3W, 54–56 cm; (**6**) ODP 1260A-11R-4W, 55–57 cm. (**7**) *Eurystomoskevos petrushevskayae* Caulet, 1991: ODP 1260A-9R-3W, 55–57 cm. (**8**) *Lophoconus antilope* (Ehrenberg, 1874): ODP 1260A-13R-4W, 55–57 cm. (**9**) *Ceratospyris ampliata* (Ehrenberg, 1874): ODP 1260A-8R-3W, 54–56 cm. (**10**) *Ceratocyrtis rhabdophora* (Clark and Campbell, 1945): ODP 1260A-13R-4W, 55–57 cm. (**11**) *Lophophaena radians* Ehrenberg, 1874: ODP 1260A-9R-6W, 55–57 cm. (**12, 13**) *Lophophaena galeaorci* Ehrenberg, 1854c: (**12**) ODP 1260A-11R-7W, 55–57 cm; (**13**) ODP 1051A-9H-5W, 53–55 cm. (**14, 15**) *Lophophaena capito* Ehrenberg, 1874: (**14**) ODP 1260A-11R-7W, 55–57 cm; (**15**) ODP 1260A-9R-5W, 55–57 cm. All scale bars equal 50 μm.

not 2002 *Lophophaena capito* Ehrenberg – Apel et al., p. 18, pl. P6, fig. 6.
2006 *Lophophaena capito* Ehrenberg group – Funakawa et al., p. 20, Pl. P3, figs. 3, 4.
2009 *Lophophaena capito* Ehrenberg – Ogane et al., pl. 19, figs. 8a–8c, pl. 34, figs. 3a–3c, pl. 79, figs. 2a–2c.
2015 *Lithomelissa lautouri* O'Connor – Kamikuri, pl. 11, figs. 10–12.
2020 *Lophophaena capito* Ehrenberg – Hollis et al., pl. 6, fig. 15.

Occurrence. ODP Site 1260 (Demerara Rise; western equatorial Atlantic) and ODP Site 1051 (Blake Nose; western north Atlantic).

Lophophaena galeaorci Ehrenberg, 1854c
Plate II.13, Figures 12, 13

1854c *Lophophaena Galea Orci* [sic] Ehrenberg, p. 245.
1862 *Lophophaena Galea Orci* [sic] Ehrenberg – Haeckel, p. 298.
1874 *Lophophaena apiculata* Ehrenberg, p. 242.
1876 *Lophophaena apiculata* Ehrenberg – Ehrenberg, p. 78, pl. 8, figs. 11.
1880 *Lophophaena Galea Orci* [sic] Ehrenberg – Stöhr, p. 99, pl. 3, fig. 17.
1882a *Dictyocephalus Galea Orci* [sic] (Ehrenberg) – Bütschli, p. 535.
1882a *Dictyocephalus apiculata* (Ehrenberg) – Bütschli, p. 535.
1887 *Lophophæna* (*Lophophænula*) *galea* [sic] Ehrenberg – Haeckel, p. 1303.
1977 Plagoniid gen. et sp. indet. Riedel and Sanfilippo, pl. 7, fig. 1 (part).
1983 Artostrobid, gen. et sp. indet. Johnson, pl. 2, fig. 8.
1999 Plagiacanthidae gen. et sp. indet. Kozlova, pl. 3, fig. 8.
2006 Sethoperid sp. A Funakawa et al., pl. P3, figs. 10a, 10b, 11a–12b.
2006 Sethoperid sp. B Funakawa et al., pl. P3, figs. 13a, 13b, 14a–15b.
2009 *Lophophaena apiculata* Ehrenberg – Ogane et al., pl. 25, figs. 3a–3d.
2015 *Dictyocephalus obtusa* (Ehrenberg) – Kamikuri, pl. 11, figs. 4–6.

Occurrence. ODP Site 1260 (Demerara Rise; western equatorial Atlantic) and ODP Site 1051 (Blake Nose; western north Atlantic).

Lophophaena radians Ehrenberg, 1874
Plate II.13, Figure 11

1874 *Lophophaena radians* Ehrenberg, p. 243.
1876 *Lophophaena radians* Ehrenberg – Ehrenberg, p. 78, pl. 8, figs. 7–9.
1887 *Lophophœna* (*Lophophœnula*) *radians* [sic] Ehrenberg – Haeckel, p. 1303.
2006 *Lophophaena radians* Ehrenberg – Funakawa et al., p. 20, pl. P3, figs. 5a–6b.
2009 *Lophophaena radians* Ehrenberg – Ogane et al., pl. 3, figs. 3a–3e, 5a-5d, pl. 79, figs. 4a–4c.
2015 *Lophophaena radians* Ehrenberg – Kamikuri, pl. 13, figs. 30a, 30b.
not 2020 *Lophophaena radians* Ehrenberg – Hollis et al., pl. 6, fig. 16.

Occurrence. ODP Site 1260 (Demerara Rise; western equatorial Atlantic) and ODP Site 1051 (Blake Nose; western north Atlantic).

Genus *Lithomelissa* Ehrenberg, 1847

Type species.— *Lithomelissa microptera* Ehrenberg, 1854a, pl. 36, fig. 2; description in Haeckel, 1862, p. 303.

Lithomelissa ? *acutispina* Clark and Campbell, 1942
Plate II.14, Figure 1

1942 *Lithomelissa* (*Acromelissa*) *acutispina* Clark and Campbell, p. 69, pl. 9, fig. 21.

Occurrence. ODP Site 1051 (Blake Nose; western north Atlantic).

Lithomelissa dupliphysa Caulet, 1991
Plate II.14, Figure 2

1991 *Lithomelissa dupliphysa* Caulet, p. 534, pl. 2, fig. 4.
2021 *Lithomelissa challengerae* Chen – de Souza et al., p. 15, pl. 2, figs. 3a, 3b.

Occurrence. ODP Site 1260 (Demerara Rise; western equatorial Atlantic).

Lithomelissa macroptera Ehrenberg, 1874
Plate II.14, Figure 3

1874 *Lithomelissa macroptera* Ehrenberg, p. 241.
1876 *Lithomelissa macroptera* Ehrenberg – Ehrenberg, p. 78, pl 3, figs. 9, 10 (part).
1887 *Lithomelissa* (*Acromelissa*) *macroptera* Ehrenberg – Haeckel, p. 1204.
1976 *Lithomelissa macroptera* Ehrenberg – Dzinoridze et al., pl. 29, figs. 14, 15, pl. 37, fig. 9 (part).
2009 *Lithomelissa macroptera* Ehrenberg – Ogane et al., pl. 19, figs. 6a–6d, pl. 79, figs. 6a–6c (part).
1978 *Lithomelissa* sp. cf. *L. macroptera* Ehrenberg – Weaver and Dinkelman, p. 869, pl. 1, fig. 11.

Occurrence. ODP Site 1260 (Demerara Rise; western equatorial Atlantic) and ODP Site 1051 (Blake Nose; western north Atlantic).

Lithomelissa tricornis Chen, 1975
Plate II.14, Figure 4

1975 *Lithomelissa tricornis* Chen, p. 458, pl. 8, figs. 6, 7.
1990 *Lithomelissa tricornis* Chen – Abelmann, p. 695, pl. 5, fig. 3.
1992 *Lithomelissa tricornis* Chen – Takemura, p. 744, pl. 2, figs. 5, 6.
Occurrence. ODP Site 1260 (Demerara Rise; western equatorial Atlantic).

Genus *Pelagomanes* Trubovitz et al., 2022
Type species.— *Lithomelissa* ? *kozoi* Renaudie and Lazarus, 2013a, p. 73, pl. 5, figs. 10a–11, 13a, 13b, 15, pl. 8, fig. 5.

Pelagomanes thaumasia (Caulet, 1991)
Plate II.14, Figure 5

1991 *Lophophaena* ? *thaumasia* Caulet, p. 534, pl. 2, figs. 5, 6.
2022 *Pelagomanes thaumasia* (Caulet) – Trubovitz et al., p. 83, pl. 39, figs. 10a–11.
Occurrence. ODP Site 1051 (Blake Nose; western north Atlantic).

Family Plagiacanthidae Hertwig, 1879 sensu Dumitrică, 2004
Genus *Neosemantis* Popofsky, 1913
Type species.— *Neosemantis distephanus* Popofsky, 1913, p. 229, pl. 29, fig. 2.

Neosemantis mimicus Goll, 1979
Plate II.14, Figure 6

1979 *Neosemantis bjoerklundi mimicus* Goll, p. 383, pl. 3, figs. 1–12.
Occurrence. ODP Site 1260 (Demerara Rise; western equatorial Atlantic).

Family Ximolzidae Dumitrică *in* Suzuki et al., 2021
Genus *Rhabdolithis* Ehrenberg, 1847
Type species.— *Rhabdolithis pipa* Ehrenberg, 1854a, pl. 36, fig. 59; description in Ehrenberg, 1876, p. 159.

Rhabdolithis ellida Sanfilippo and Riedel, 1973
Plate II.14, Figure 7

1973 *Rhabdolithis ellida* Sanfilippo and Riedel, p. 529, pl. 18, figs. 8–11, pl. 33, figs. 5–8.
1977 *Rhabdolithis ellida* Sanfilippo and Riedel – Riedel and Sanfilippo, pl. 4, fig. 5.
Occurrence. ODP Site 1260 (Demerara Rise; western equatorial Atlantic) and ODP Site 1051 (Blake Nose; western north Atlantic).

Rhabdolithis pipa Ehrenberg, 1854a
Plate II.14, Figures 8, 9

1854a *Rhabdolithis Pipa* [sic] Ehrenberg, pl. 36, fig. 59.

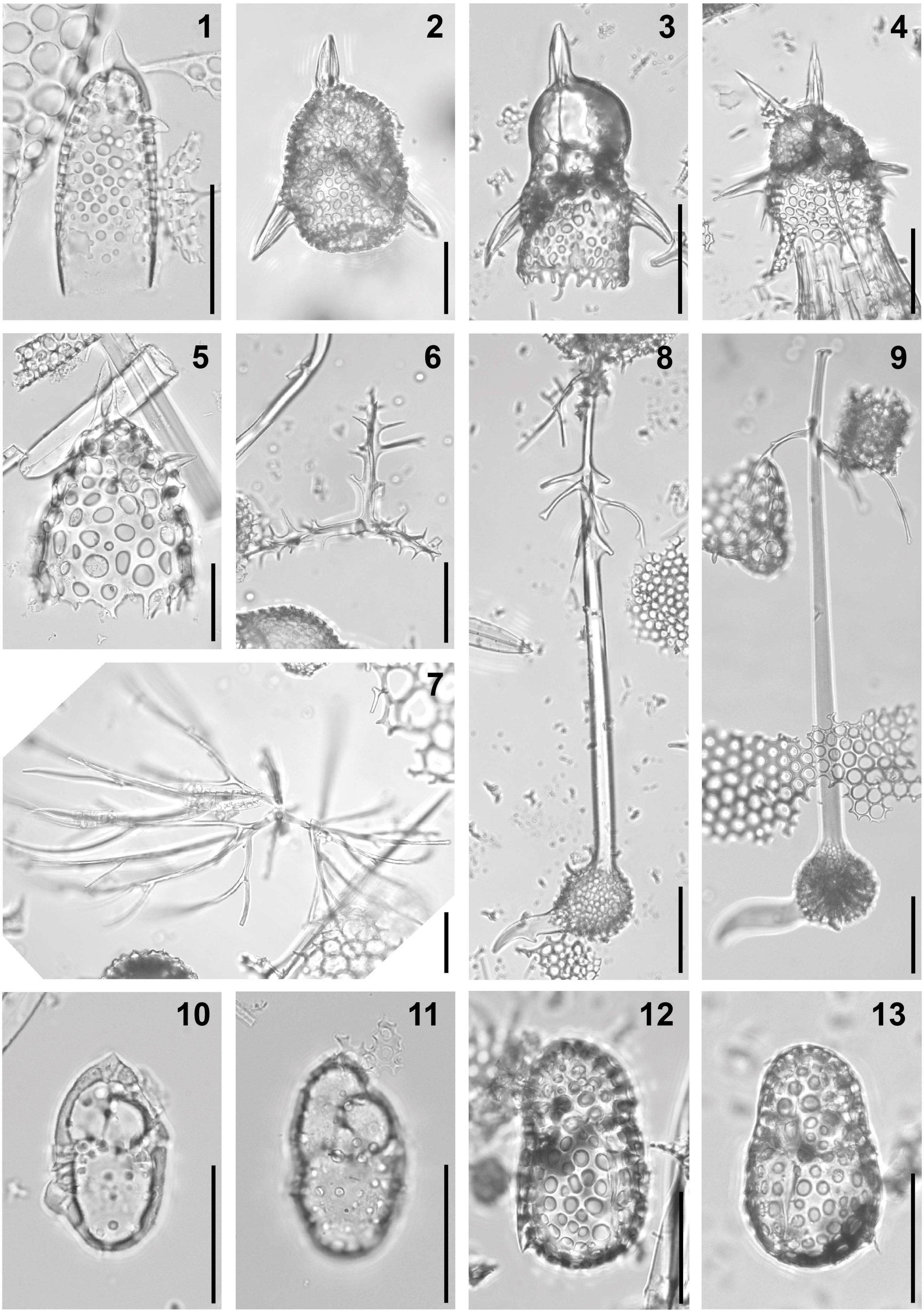
1
2
3
4
5
6
8
9
7
10
11
12
13

Plate II.14. Composite light micrographs of new radiolarian species from ODP Site 1260 (Demerara Rise, western equatorial Atlantic) and ODP Site 1051 (Blake Nose, western North Atlantic).(**1**) *Lithomelissa* ? *acutispina* Clark and Campbell, 1942: ODP 1051A-14H-5W, 52–54 cm. (**2**) *Lithomelissa dupliphysa* Caulet, 1991: ODP 1260A-11R-7W, 55–57 cm. (**3**) *Lithomelissa macroptera* Ehrenberg, 1874: ODP 1260A-6R-2W, 55–57 cm. (**4**) *Lithomelissa tricornis* Chen, 1975: ODP 1260A-9R-6W, 55–57 cm. (**5**) *Pelagomanes thaumasia* (Caulet, 1991): ODP 1051A-6H-5W, 53–55 cm. (**6**) *Neosemantis mimicus* Goll, 1979: ODP 1260A-9R-3W, 55–57 cm. (**7, 8**) *Rhabdolithis pipa* Ehrenberg, 1854a: (**7**) ODP 1260A-11R-6W, 55–57 cm; (**8**) ODP 1260A-10R-4W, 55–57 cm. (**9**) *Rhabdolithis ellida* Sanfilippo and Riedel, 1973: ODP 1260A-13R-5W, 54–56 cm. (**10**) *Botryocella nucula* (Ehrenberg, 1874): ODP 1051A-13H-2W, 52–54 cm. (**11**) *Botryocella adspersa* (Ehrenberg, 1854a): ODP 1051A-9H-2W, 53–55 cm. (**12, 13**) *Lithocorythium* ? *amblyostauros* Ehrenberg, 1874: (**12**) ODP 1260A-13R-5W, 55–57 cm; (**13**) ODP 1260A-12R-1W, 55–57 cm. All scale bars equal 50 μm.

1862 *Rhabdolithes pipa* [sic] Ehrenberg – Bury, pl. 2, fig. 4 (part).
1876 *Rhabdolithis Pipa* [sic] Ehrenberg – Ehrenberg, p. 159, pl. 1, fig. 27.
1882b *Rhabdolithis Pipa* [sic] Ehrenberg – Bütschli, pl. 21, fig. 8.
1887 *Xiphostylus* (*Xiphostylissa*) *falco* Haeckel, p. 130, pl. 13, fig. 14.
1887 *Xiphostylus* (*Xiphostylomma*) *emberiza* Haeckel, p. 131, pl. 13, fig. 11.
1973 *Rhabdolithis pipa* Ehrenberg – Sanfilippo and Riedel, p. 529, pl. 18, figs. 12–16, pl. 33, figs. 9, 10.
1973 *Rhabdolithis pipa* Ehrenberg – Riedel and Sanfilippo, 739, pl. 3, figs. 7, 8.
1977 *Rhabdolithis pipa* Ehrenberg – Riedel and Sanfilippo, pl. 9, fig. 3.
1978 *Rhabdolithis pipa* Ehrenberg – Riedel and Sanfilippo, p. 72, pl. 9, figs. 3, 4.
Occurrence. ODP Site 1260 (Demerara Rise; western equatorial Atlantic) and ODP Site 1051 (Blake Nose; western north Atlantic).

Superfamily Pylobotrydoidea Haeckel, 1882
Family Pylobotrydidae Haeckel, 1882 sensu Sugiyama, 1998
Genus *Botryocella* Haeckel, 1887

Type species.— *Lithobotrys nucula* Ehrenberg, 1874, p. 238 (unfigured); Ehrenberg, 1876, p. 76, pl. 3, fig. 16.

Botryocella adspersa (Ehrenberg, 1854a)
Plate II.14, Figure 11

1854a *Lithobotrys adspersa* Ehrenberg, pl. 36, fig. 5.
1874 *Lithobotrys adspersa* Ehrenberg – Ehrenberg, p. 237.
1876 *Lithobotrys adspersa* Ehrenberg – Ehrenberg, p. 76, pl. 3, fig. 15.
2009 *Lithobotrys adspersa* Ehrenberg – Ogane et al., 2009, pl. 61, figs. 4a–5d.
Remarks. The combination used here is derived from O'Dogherty et al. (2021).
Occurrence. ODP Site 1260 (Demerara Rise; western equatorial Atlantic) and ODP Site 1051 (Blake Nose; western north Atlantic).

Botryocella nucula (Ehrenberg, 1874)
Plate II.14, Figure 10

1874 *Lithobotrys Nucula* [sic] Ehrenberg, p. 238.
1876 *Lithobotrys Nucula* [sic] Ehrenberg – Ehrenberg, p. 76, pl. 3, fig. 16.
1887 *Botryocella nucula* (Ehrenberg) – Haeckel, p. 1116.
2009 *Lithobotrys nucula* Ehrenberg – Ogane et al., 2009, pl. 6, figs. 8a–8d.

Remarks. The combination used here is derived from O'Dogherty et al. (2021).
Occurrence. ODP Site 1260 (Demerara Rise; western equatorial Atlantic) and ODP Site 1051 (Blake Nose; western north Atlantic).

Genus *Lithocorythium* Ehrenberg, 1847

Type species.— *Lithobotrys galea* Ehrenberg, 1844, p. 83 (unfigured); Ehrenberg, 1854a, pl. 22, figs. 29a, 29b.

Lithocorythium ? *amblyostauros* Ehrenberg, 1874
Plate II.14, Figures 12, 13

1874 *Lithopera amblyostauros* Ehrenberg, p. 241.
1876 *Lithopera amblyostauros* Ehrenberg – Ehrenberg, p. 78, pl. 3, fig. 5.

Remarks. The combination used here is derived from O'Dogherty et al. (2021).
Occurrence. ODP Site 1260 (Demerara Rise; western equatorial Atlantic).

Lithocorythium ? *niduspendulus* Ehrenberg, 1874
Plate II.15, Figures 1, 2

1874 *Lithopera Nidus pendulus* [sic] Ehrenberg, p. 241.
1876 *Lithopera Nidus pendulus* [sic] Ehrenberg – Ehrenberg, p. 78, pl. 3, fig. 7.
1882a *Lithomelissa microptera* Ehrenberg – Bütschli, pl. 30, fig. 2.
1882a *Anthocyrtis Nidus pendulus* [sic] Ehrenberg – Bütschli, p. 533.
1887 *Sethocapsa nidus* [sic] (Ehrenberg) – Haeckel, p. 1311.
1970 Gen. et sp. indet. Riedel and Sanfilippo, pl. 12, fig. 10.
1973 Cannobotrythids gen(n). et sp(p). indet. Sanfilippo and Riedel, pl. 21, fig. 6–10, 12, pl. 36, figs. 6–8 (part).
1977 Cannobotrythid gen. et sp. indet. Riedel and Sanfilippo, pl. 8, fig. 8.
1979 *Lithobotrys geminata* (Ehrenberg) – Petrushevskaya and Kozlova, fig. 275 (part).
2009 *Lithopera nidus-pendulus* [sic] Ehrenberg – Ogane et al., pl. 21, figs. 4a–4c.

Remarks. The combination used here is derived from O'Dogherty et al. (2021).
Occurrence. ODP Site 1260 (Demerara Rise; western equatorial Atlantic) and ODP Site 1051 (Blake Nose; western north Atlantic).

Superfamily Sethoperoidea Haeckel, 1882
Family Sethoperidae Haeckel, 1882 emend. Suzuki et al., 2021
Genus *Clathrocorys* Haeckel, 1882

Type species.— *Clathrocorys murrayi* Haeckel, 1887, p. 1219, pl. 64, fig. 8.

Clathrocorys atavia (Goll, 1979)
Plate II.15, Figure 3

1979 *Callimitra atavia* Goll, p. 388, pl. 5, figs. 1, 5–9, 11.
? 1999a *Callimitra atavia* Goll – O'Connor, p. 31, pl. 9, fig. 4.
Remarks. The combination used here is derived from O'Dogherty et al. (2021).
Occurrence. ODP Site 1260 (Demerara Rise; western equatorial Atlantic).

Clathrocorys tribrachiata (Ehrenberg, 1874)
Plate II.15, Figure 4

1874 *Cladospyris tribrachiata* Ehrenberg, p. 220.
1876 *Cladospyris tribrachiata* Ehrenberg – Ehrenberg, p. 68, pl. 21, fig. 8.
1882b *Ceratospyris tribrachiata* Ehrenberg – Bütschli, pl. 29, fig. 5.
1887 *Tripospyris* (*Tripospyromma*) *tribrachiata* (Ehrenberg) – Haeckel, p. 1029.
1942 *Tripilidium* (*Tristylocorys*) *clavipes* Clark and Campbell, p. 64, pl. 9, fig. 29.
1979 *Tripodiscinus clavipes* (Clark and Campbell) – Petrushevskaya and Kozlova, p. 115, fig. 302.
1988 *Tripilidium* (*Tristylocorys*) *clavipes* Clark and Campbell – Blueford, p. 244, pl. 1, figs. 7–9.
1997 *Tripodiscinus clavipes* (Clark and Campbell) – Hollis et al., p. 53, pl. 3, figs. 28, 29.
2002 *Tripodiscinus clavipes* (Clark and Campbell) – Apel et al., p. 21, pl. P6, fig. 9.
not 2005 *Tripilidium clavipes* Clark and Campbell – Funakawa and Nishi, p. 238, pl. 4, figs. 8a, 8b.
2005 *Tripilidium* cf. *clavipes* Clark and Campbell – Funakawa and Nishi, p. 238, pl. 4, figs. 7a, 7b.
2009 *Cladospyris tribrachiata* Ehrenberg – Ogane et al., pl. 35, figs. 2a– 2c, pl. 15, figs. 1a–2d.
2020 *Tripodiscinus clavipes* (Clark and Campbell) – Hollis et al., pl. 6, fig. 27.
Remarks. The combination used here is derived from O'Dogherty et al. (2021).
Occurrence. ODP Site 1260 (Demerara Rise; western equatorial Atlantic) and ODP Site 1051 (Blake Nose; western north Atlantic).

Superfamily Lithochytridoidea Ehrenberg, 1846
Family Lithochytrididae Ehrenberg, 1846 sensu Suzuki *in* Matsuzaki et al., 2015

? Genus *Dictyophimus* Ehrenberg, 1847 sensu Nigrini, 1967
Type species.— *Dictyophimus crisae* Ehrenberg, 1854c, p. 241 (unfigured); Suzuki et al., 2009a, pl. 35, figs. 1a–1d.

Dictyophimus craticula Ehrenberg, 1874
Plate II.15, Figure 5

1862 *Actiniscus* ? Bury, pl. 7, fig. 5.
1874 *Dictyophimus Craticula* [sic] Ehrenberg, p. 223.
1876 *Dictyophimus Craticula* [sic] Ehrenberg – Ehrenberg, p. 68, pl. 5, figs. 4, 5.

1882a *Dictyophimus Craticula* [sic] Ehrenberg – Bütschli, pl. 33, fig. 35.
1882b *Dictyophimus Craticula* [sic] Ehrenberg – Bütschli, pl. 29, fig. 10.
1887 *Dictyophimus* (*Dictyophimium*) *craticula* Ehrenberg – Haeckel, p. 1196.
1970 *Dictyophimus craticula* Ehrenberg – Riedel and Sanfilippo, pl. 10, fig. 6.
1973 *Dictyophimus craticula* Ehrenberg – Sanfilippo and Riedel, p. 529, pl. 19, fig. 1 (part).
1977 *Dictyophimus craticula* Ehrenberg – Riedel and Sanfilippo, pl. 7, fig. 6.
1978 *Dictyophimus craticula* Ehrenberg – Riedel and Sanfilippo, p. 68, pl. 4, fig. 19.
1986 *Dictyophimus craticula* Ehrenberg – Riedel and Sanfilippo, pl. 4, figs. 13, 14.
2009 *Dictyophimus craticula* Ehrenberg – Ogane et al., pl. 21, fig. 5, pl. 36, figs. 1a–1f, pl. 37, figs. 2a–4.
2012b *Dictyophimus craticula* Ehrenberg – Kamikuri et al., p. 3, pl. P2, fig. 7.
2020 *Dictyophimus craticula* Ehrenberg – Hollis et al., pl. 12, figs. 4a, 4b.

Occurrence. ODP Site 1260 (Demerara Rise; western equatorial Atlantic) and ODP Site 1051 (Blake Nose; western north Atlantic).

Genus *Lithochytris* Ehrenberg, 1846

Type species.— *Lithochytris vespertilio* Ehrenberg, 1874, p. 239 (unfigured); Ehrenberg, 1876, p. 76, pl. 4, fig. 10.

Lithochytris pyramidalis Ehrenberg, 1874

Plate II.15, Figures 9, 10

1874 *Lithochytris pyramidalis* Ehrenberg, p. 239.
1874 *Lithochytris Vespertilio* [sic] Ehrenberg, p. 239.
1876 *Lithochytris pyramidalis* Ehrenberg – Ehrenberg, p. 76, pl. 5, fig. 1.
1876 *Lithochytris Vespertilio* [sic] Ehrenberg – Ehrenberg, p. 76, pl. 4, fig. 10.
1882a *Lithochytris pyramidalis* Ehrenberg – Bütschli, p. 532.
1882a *Lithochytris Vespertilio* [sic] Ehrenberg – Bütschli, p. 532.
1882b *Lithochytris Vespertilio* [sic] Ehrenberg – Bütschli, pl. 31, fig. 4.
1887 *Lithochytris* (*Lithochytridium*) *lucerna* Haeckel, p. 1364, pl. 67, fig. 14.
1887 *Lithochytris* (*Lithochytridium*) *pyramidalis* Ehrenberg – Haeckel, p. 1364.
1887 *Lithochytris* (*Lithochytridium*) *pteropus* Haeckel, p. 1364, pl. 67, fig. 15.
1887 *Lithochytris* (*Lithochytridium*) *vespertilio* Ehrenberg – Haeckel, p. 1365.
1942 *Lithochytris* (*Lithochytridium*) *cheopsis* Clark and Campbell, p. 81, pl. 9, fig. 37.
1957a *Lithochytris* aff. *L. cheopsis* Clark and Campbell – Riedel, p. 261, pl. 62, fig. 5.
? 1970 *Lithochytris* sp(p) Cita et al., p. 403, pl. 2, figs. D, E.
1970 *Lithochytris vespertilio* Ehrenberg – Riedel and Sanfilippo, p. 518, pl. 9, figs. 8, 9.
1971 *Lithochytris vespertilio* Ehrenberg – Moore, p. 741, pl. 1, fig.4.
1973 *Lithochytris vespertilio* Ehrenberg – Foreman, p. 436, pl. 2, figs. 2, 3, pl. 11, fig. 3.
1974 *Lithochytris vespertilio* Ehrenberg – Nigrini, p. 1067, pl. 1G, figs. 4–6.
1975 *Lithochytris vespertilio* Ehrenberg – Chen, p. 461, pl. 1, fig. 1.
1975 *Lithochytris vespertilio* Ehrenberg – Ling, p. 729, pl. 10, figs. 1–3.
1977 *Lithochytris vespertilio* Ehrenberg – Riedel and Sanfilippo, pl. 7, fig. 15.
1978 *Lithochytris vespertilio* Ehrenberg – Riedel and Sanfilippo, p. 69, pl. 6, fig. 4.
1986 *Lithochytris pyramidalis* Ehrenberg – Göke, fig. 3.1.

2000 *Lithochytris vespertilio* Ehrenberg – Nigrini and Sanfilippo, p. 73, pl. 1, fig. 15, pl. 2, fig. 10.
2008 *Lithochytris vespertilio* Ehrenberg – Jackett et al., p. 56, pl. 2, fig. 19.
2009 *Lithochytris vespertilio* Ehrenberg – Ogane et al., pl. 45, figs. 1a–3e.
2009 *Lithochytris pyramidalis* Ehrenberg – Ogane et al., pl. 61, figs. 6a–6c.
2012 *Lithochytris vespertilio* Ehrenberg – Moore and Kamikuri, p. 8, pl. P5, fig. 4.
2020 *Lithochytris vespertilio* Ehrenberg – Hollis et al., pl. 12, fig. 18.
Occurrence. ODP Site 1260 (Demerara Rise; western equatorial Atlantic).

Genus *Lychnocanium* Ehrenberg, 1846

Type species.— *Lychnocanium lucerna* Ehrenberg, 1847, p. 55, Figure 5.

Lychnocanium alma O'Connor, 1999a

Plate II.15, Figure 13

1999a *Lychnocanium alma* O'Connor, p. 24, pl. 4, figs. 1–5, pl. 7, figs. 8a–11.
2020 *Lychnocanium alma* O'Connor – Hollis et al., pl. 12, figs. 24a, 24b.
Occurrence. ODP Site 1051 (Blake Nose; western north Atlantic).

Lychnocanium bellum Clark and Campbell, 1942

Plate II.16, Figure 5

1942 *Lychnocanium* (*Lychnocanissa*) *bellum* Clark and Campbell, p. 72, pl. 9, figs. 35, 39.
1957a *Lychnocanium* sp. Riedel, p. 259, pl. 63, fig. 5.
1970 *Lychnocanium bellum* Clark and Campbell – Cita et al., p. 401, pl. 1, fig. E.
1970 *Lychnocanium bellum* Clark and Campbell – Riedel and Sanfilippo, p. 529, pl. 10, fig. 5.
1973 *Lychnocanoma bellum* (Clark and Campbell) – Foreman, p. 437, pl. 11, fig. 9 (part).
1974 *Lychnocanoma bellum* (Clark and Campbell) – Nigrini, p. 1068, pl. 1H, figs. 1–3, pl. 2D, fig. 1.
1977 *Lychnocanoma bellum* (Clark and Campbell) – Riedel and Sanfilippo, pl. 10, fig. 10.
1978 *Lychnocanoma bellum* (Clark and Campbell) – Weaver and Dinkelman, p. 873, pl. 5, figs. 9, 10.
1986 *Lychnocanoma bellum* (Clark and Campbell) – Riedel and Sanfilippo, pl. 1, fig. 12.
1986 *Lychnocanium* sp. Göke, fig. 3.4.
1987 *Lychnocanoma bellum* (Clark and Campbell) – Nishimura, p. 727, pl. 3, fig. 8.
1995 *Lychnocanoma bellum* (Clark and Campbell) – Strong et al., 209, figs. 11I, 11J.
1997 *Lychnocanium bellum* Clark and Campbell – Hollis et al., p. 63, pl. 6, figs. 5, 6.
1999 *Lychnocanium bellum* Clark and Campbell – Kozlova, p. 128, pl. 23, figs. 16, 17, pl. 31, figs. 6, 7, pl. 45, fig. 2.
2001 *Lychnocanoma bellum* (Clark and Campbell) – Sanfilippo and Blome, p. 214, fig. 9n.
2008 *Lychnocanoma bellum* (Clark and Campbell) – Jackett et al., p. 56, pl. 2, fig. 18.
2009b *Lychnocanoma bellum* (Clark and Campbell) – Suzuki et al., p. 261, pl. 19, figs. 1a, 1b.
2015 *Lychnocanoma* aff. *bellum* (Clark and Campbell) – Kamikuri, pl. 1, figs. 7a, 7b.
2017 *Lychnocanoma bellum* (Clark and Campbell) – de Souza et al., pl. 3, figs. 14a, 14b.

2020 *Lychnocanium bellum* Clark and Campbell – Hollis et al., pl. 13, fig. 6.
Occurrence. ODP Site 1051 (Blake Nose; western north Atlantic).

Lychnocanium carinatum Ehrenberg, 1874
Plate II.15, Figure 15

1874 *Lychnocanium carinatum* Ehrenberg, p. 243.
1876 *Lychnocanium carinatum* Ehrenberg – Ehrenberg, p. 78, pl. 8, fig. 5.
1887 *Lychnocanium* (*Lychnocanella*) *carinatum* Ehrenberg – Haeckel, p. 1226.
not 1987 *Lychnocanium* ? *carinatum* Ehrenberg – Nishimura, p. 727, pl. 3, figs. 6, 11.
not 2008 *Lychnocanium carinatum* Ehrenberg – Jackett et al., p. 56, pl. 1, fig. 25.
2009 *Lychnocanium carinatum* Ehrenberg – Ogane et al., pl. 44, figs. 3a–3f.
Occurrence. ODP Site 1260 (Demerara Rise; western equatorial Atlantic) and ODP Site 1051 (Blake Nose; western north Atlantic).

Lychnocanium continuum Ehrenberg, 1874
Plate II.15, Figure 16

1874 *Lychnocanium continuum* Ehrenberg, p. 243.
1876 *Lychnocanium continuum* Ehrenberg – Ehrenberg, p.78, pl. 7, fig. 11.
1887 *Lychnocanium* (*Lychnocanella*) *continuum* Ehrenberg – Haeckel, p. 1225.
2006 *Lychnocanium continuum* Ehrenberg – Funakawa et al., p. 37, pl. P12, figs. 7a, 7b.
2009 *Lychnocanium continuum* Ehrenberg – Ogane et al., pl. 98, figs. 5a–5d.
2015 *Lychnocanium continuum* Ehrenberg – Kamikuri, pl. 2, figs. 3a, 3b.
2020 *Lychnocanium continuum* Ehrenberg – Hollis et al., pl. 13, figs. 12a, 12b.
Occurrence. ODP Site 1051 (Blake Nose; western north Atlantic).

Lychnocanium falciferum Ehrenberg, 1854a
Plate II.16, Figure 2

1854a *Lychnocanium falciferum* Ehrenberg, pl. 36, fig. 7.
1862 *Lithomelissa falcifera* (Ehrenberg) – Haeckel, p. 303.
1876 *Lychnocanium falciferum* Ehrenberg – Ehrenberg, p.78, pl. 8, fig. 4.
1887 *Lychnocanium* (*Lychnocanissa*) *falciferum* Ehrenberg – Haeckel, p. 1227.
not 1999 *Lychnocanium falciferum* Ehrenberg – Kozlova, p. 174, pl. 45, fig. 8.
2009 *Lychnocanium falciferum* Ehrenberg – Ogane et al., p. 43, figs. 1a–1c.
Occurrence. ODP Site 1051 (Blake Nose; western north Atlantic).

Lychnocanium lucerna Ehrenberg, 1847
Plate II.15, Figure 8

1847 *Lychnocanium Lucerna* [sic] Ehrenberg, p. 55, fig. 5.
1854a *Lychnocanium Lucerna* [sic] Ehrenberg – Ehrenberg, pl. 36, fig. 6.
1862 *Lychnocanium lucerna* Ehrenberg – Haeckel, p. 311.
1874 *Lychnocanium Lucerna* [sic] Ehrenberg – Ehrenberg, p. 244.
1876 *Lychnocanium Lucerna* [sic] Ehrenberg – Ehrenberg, p. 80, pl. 8, fig. 3.
1887 *Dictyophimus* (*Dictyophimium*) *lucerna* (Ehrenberg) – Haeckel, p. 1199.

2009 *Lychnocanium lucerna* Ehrenberg – Ogane et al., pl. 42, figs. 4a, 4b, pl. 43, figs. 6a, 6b, pl. 44, figs. 1a–1d.
2001 *Lychnocanoma lucerna* (Ehrenberg) – Sanfilippo and Blome, p. 214, figs. 9k–9m.
2015 *Lychnocanoma lucerna* (Ehrenberg) – Kamikuri, pl. 3, figs. 6a, 6b.
Occurrence. ODP Site 1051 (Blake Nose; western north Atlantic).

Lychnocanium pileatum (Ehrenberg, 1874)
Plate II.15, Figure 11

1874 *Lithochytris pileata* Ehrenberg, p. 239.
1874 *Lithochytris Tripodium* [sic] Ehrenberg, p. 239.
1876 *Lithochytris pileata* Ehrenberg – Ehrenberg, p. 76, pl. 5, fig. 3.
1876 *Lithochytris Tripodium* [sic] Ehrenberg – Ehrenberg, p. 76, pl. 4, fig. 11.
1882a *Lithochytris pileata* Ehrenberg – Bütschli, p. 532.
1887 *Lychnocanium* (*Lychnocanoma*) *tripodium* Ehrenberg – Haeckel, p. 1229.
1887 *Lithochytris* (*Lithochytridium*) *pileata* Ehrenberg – Haeckel, p. 1363.
1970 Gen. et sp. indet. Riedel and Sanfilippo, p. 528, pl. 9, fig. 4.
2009 *Lithochytris pileata* Ehrenberg – Ogane et al., pl. 22, figs. 9a–9c.
2009 *Lithochytris tripodium* Ehrenberg – Ogane et al., pl. 22, figs. 9a–9c.
Occurrence. ODP Site 1260 (Demerara Rise; western equatorial Atlantic).

Lychnocanium tribulus (Ehrenberg, 1874) group
Plate II.15, Figure 12

1874 *Lychnocanium Tribulus* [sic] Ehrenberg, p. 245.
1876 *Lychnocanium Tribulus* [sic] Ehrenberg – Ehrenberg, p. 80, pl. 7, fig. 5.
1887 *Lychnocanium* (*Lychnocanella*) *tribulus* Ehrenberg – Haeckel, p. 1226.
1942 *Dictyophimus* (*Dictyophimium*) *babylonis* Clark and Campbell, p. 67, pl. 9, figs. 32, 36.
1944 *Dictyophimus* (*Dictyophimium*) *hindsi* Campbell and Clark, p. 24, pl. 7, fig. 29.
1957b *Dictyophimus babylonis* Clark and Campbell – Riedel, p. 81, pl. 1, fig. 6.
1958 *Lychnocanium ventricosum* Ehrenberg – Göke, pl. 3, fig. 2.
1970 *Dictyophimus babylonis* Clark and Campbell – Cita et al., p. 401, pl. 1, fig. D.
1970 *Sethochytris babylonis* (Clark and Campbell) group – Riedel and Sanfilippo, p. 528, pl. 9, figs. 1–3.
1970 *Sethochytris babylonis* (Clark and Campbell) group – Riedel and Sanfilippo, p. 1595, pl. 3B, fig. 13.
1971 *Sethochytris babylonis* (Clark and Campbell) group – Moore, p. 741, pl. 3, figs. 9, 10.
1973 *Lychnocanoma babylonis* (Clark and Campbell) group – Foreman, p. 437, pl. 2, fig. 1.
1974 *Lychnocanoma babylonis* (Clark and Campbell) group – Nigrini, p. 1068, pl. 1G, figs. 9–14, pl. 2D, fig. 4.
1974 *Lychnocanoma babylonis* (Clark and Campbell) group – Johnson, p. 548, pl. 2, fig. 13.
1975 *Lychnocanoma babylonis* (Clark and Campbell) – Chen, p. 462, pl. 2, fig. 8.
1975 *Lychnocanoma babylonis-turgidulum* [sic] group – Ling, p. 729, pl. 10, figs. 8, 9.
1977 *Lychnocanoma babylonis* (Clark and Campbell) group – Riedel and Sanfilippo, pl. 7, fig. 17.

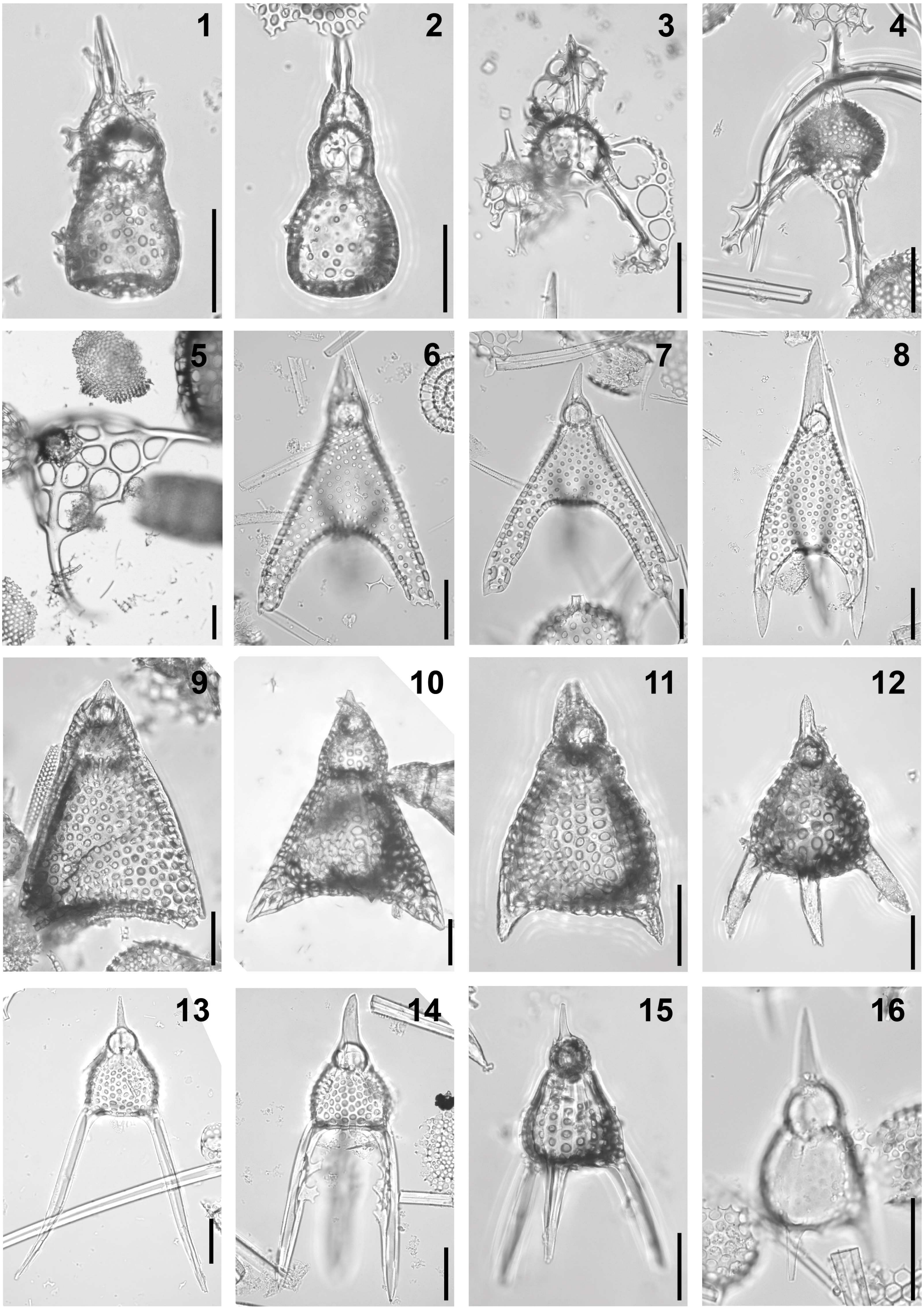
1
2
3
4
5
6
7
8
9
10
11
12
13
14
15
16

Plate II.15. Composite light micrographs of new radiolarian species from ODP Site 1260 (Demerara Rise, western equatorial Atlantic) and ODP Site 1051 (Blake Nose, western North Atlantic). (**1, 2**) *Lithocorythium* ? *niduspendulus* Ehrenberg, 1874: (**1**) ODP 1260A-11R-1W, 55–57 cm; (**2**) ODP 1260A-11R-7W, 55–57 cm. (**3**) *Clathrocorys atavia* (Goll, 1979): ODP 1260A-6R-4W, 55–57 cm. (**4**) *Clathrocorys tribrachiata* (Ehrenberg, 1874): ODP 1260A-10R-4W, 55–57 cm. (**5**) *Dictyophimus craticula* Ehrenberg, 1874: ODP 1260A-11R-4W, 55–57 cm. (**6, 7**) *Sethochytris triconiscus* Haeckel, 1887: (**6**) 1051A-11H-5W, 59–61 cm; (**7**) ODP 1051A-14H-5W, 52–54 cm. (**8**) *Lychnocanium lucerna* Ehrenberg, 1847: ODP 1051A-4H-5W, 56–58 cm. (**9, 10**) *Lithochytris pyramidalis* Ehrenberg, 1874: (**9**) ODP 1260A-13R-5W, 54–56 cm; (**10**) ODP 1260A-17R-CC, 63–177 cm. (**11**) *Lychnocanium pileatum* (Ehrenberg, 1874): ODP 1260A-11R-7W, 55–57 cm. (**12**) *Lychnocanium tribulus* (Ehrenberg, 1874) group: ODP 1260A-10R-6W, 55–57 cm. (**13**) *Lychnocanium alma* O'Connor, 1999a: ODP 1051A-9H-2W, 53–55 cm. (**14**) *Lychnocanium waiareka* O'Connor, 1999a: ODP 1051A-2H-5W, 55–57 cm. (**15**) *Lychnocanium carinatum* Ehrenberg, 1874: ODP 1260A-9R-5W, 55–57 cm. (**16**) *Lychnocanium continuum* Ehrenberg, 1874: ODP 1051A-11H-2W, 62–64 cm. All scale bars equal 50 µm.

1986 *Lychnocanoma babylonis* (Clark and Campbell) – Riedel and Sanfilippo, pl. 2, fig. 17.
not 1992 *Lychnocanoma* cf. *babylonis* (Clark and Campbell) – Takemura, p. 747, pl. 7, fig. 13.
? 1995 *Lychnocanoma babylonis* (Clark and Campbell) – Strong et al., p. 208, figs. 11A, 11B.
1997 *Sethochytris babylonis* (Clark and Campbell) – Hollis et al., p. 65, pl. 5, fig. 32.
1999a *Sethochytris babylonis* (Clark and Campbell) group – O'Connor, p. 36, pl. 9, fig. 40.
not 1999 *Lychnocanoma babylonis* (Clark and Campbell) – Kozlova, pl. 12, fig. 10.
2006 *Lychnocanoma babylonis* (Clark and Campbell) group – Funakawa et al., p. 35, pl. P13, figs. 1a, 1b.
2009 *Lychnocanium tribulus* Ehrenberg – Ogane et al., pl. 43, figs. 3a–4c, pl. 44, figs. 4a–4c, pl. 61, figs. 3a–3c.
2012 *Lychnocanoma babylonis* (Clark and Campbell) group – Moore and Kamikuri, p. 9, pl. P7, fig. 3.
2012 *Lychnocanoma babylonis* (Clark and Campbell) – Kamikuri and Wade, pl. 1, fig. 11.
2015 *Lychnocanoma babylonis* (Clark and Campbell) group – Kamikuri, pl. 2, figs. 4, 10a, 10b.
2020 *Lychnocanium babylonis* (Clark and Campbell) – Hollis et al., pl. 13, figs. 4a–5.

Occurrence. ODP Site 1260 (Demerara Rise; western equatorial Atlantic) and ODP Site 1051 (Blake Nose; western north Atlantic).

Lychnocanium trichopus Ehrenberg, 1874
Plate II.16, Figure 1

1874 *Lychnocanium Trichopus* [sic] Ehrenberg, p. 244.
1876 *Lychnocanium Trichopus* [sic] Ehrenberg – Ehrenberg, p. 80, pl. 7, fig. 5.

1887 *Lychnocanium* (*Lychnocanissa*) *trichopus* Ehrenberg – Haeckel, p. 1228.
2009 *Lychnocanium trichopus* Ehrenberg – Ogane et al., pl. 42, figs. 2a–2d (part).
2020 *Lychnocanium trichopus* Ehrenberg – Hollis et al., pl. 14, figs. 1–3b.
Occurrence. ODP Site 1260 (Demerara Rise; western equatorial Atlantic).

Lychnocanium turgidum Ehrenberg, 1874
Plate II.16, Figure 3

1874 *Lychnocanium turgidum* Ehrenberg, p. 245.
1876 *Lychnocanium turgidum* Ehrenberg – Ehrenberg, p. 80, pl. 7, fig. 6.
1887 *Pterocorys* (*Pterocyrtidium*) *turgida* (Ehrenberg) – Haeckel, p. 1319.
1970 Gen. et sp. indet. Riedel and Sanfilippo, pl. 8, fig. 10.
1972 *Lithochytris* (*Lithochytrodes*) *turgidum* (Ehrenberg) – Petrushevskaya and Kozlova, p. 552, pl. 27, figs. 8, 9.
1975 *Lychnocanoma babylonis-turgidulum* [sic] group – Ling, p. 729, pl. 10, fig. 10.
2005 *Lychnocanium turgidum* Ehrenberg – Nigrini et al., p. 44, pl. P4, fig. 6.
2015 *Lychnocanoma turgidum* Ehrenberg – Kamikuri, pl. 8, figs. 4a, 4b.
2020 *Lychnocanium turgidum* Ehrenberg – Hollis et al., pl. 14, figs. 5a, 5b.
Occurrence. ODP Site 1260 (Demerara Rise; western equatorial Atlantic) and ODP Site 1051 (Blake Nose; western north Atlantic).

Lychnocanium waiareka O'Connor, 1999a
Plate II.15, Figure 14

? 1974 *Lychnocanoma* sp. Johnson, pl. 2, fig. 10.
1999a *Lychnocanium waiareka* O'Connor, p. 25, pl. 4, figs. 6–11, pl. 7, figs. 12a–15.
2015 *Lychnocanium waiareka* O'Connor – Kamikuri, pl. 1, figs. 1a, 1b.
? 2020 *Lychnocanium waiareka* O'Connor – Hollis et al., pl. 14, figs. 6a, 6b.
Occurrence. ODP Site 1051 (Blake Nose; western north Atlantic).

Genus *Lychnocanoma* Haeckel, 1887

Type species.— *Lychnocanium* (*Lychnocanoma*) *clavigerum* Haeckel, 1887, p. 1230, pl. 61, fig. 4.

Lychnocanoma amphitrite Foreman, 1973
Plate II.16, Figure 6

1971 *Lychnocanium* sp. aff. *L. bellum* Clark and Campbell Riedel and Sanfilippo, pl. 3C, figs. 1, 2.
1973 *Lychnocanoma amphitrite* Foreman, p. 437, pl. 11, fig. 10.
? 1973 *Lychnocanoma bellum* (Clark and Campbell) – Foreman, p. 437, pl. 1, fig. 17 (part).
1974 *Lychnocanoma amphitrite* Foreman – Nigrini, p. 1067, pl. 2D, figs. 2, 3.
1975 *Lychnocanoma amphitrite* Foreman – Chen, p. 462, pl. 2, fig. 7.
1975 *Lychnocanoma* sp. A Ling, p. 729, pl. 10, fig. 13.
1977 *Lychnocanoma amphitrite* Foreman – Riedel and Sanfilippo, pl. 10, fig. 9.
1978 *Lychnocanoma amphitrite* Foreman – Riedel and Sanfilippo, p. 70, pl. 7, figs. 2, 3.
1978 *Lychnocanoma amphitrite* Foreman – Sanfilippo and Riedel, p. 504, pl 1, figs. 5, 6.

1984 *Lychnocanoma amphitrite* Foreman – Westberg-Smith and Riedel, p. 493, pl. 6, fig. 14.
1986 *Lychnocanoma amphitrite* Foreman – Riedel and Sanfilippo, pl. 1, fig. 13.
1992 *Lychnocanoma amphitrite* Foreman – Kim, p. 46, pl. 2, figs. 12, 13.
1992 *Lychnocanoma amphitrite* Foreman – Takemura, p. 747, pl. 7, figs. 9, 10.
1995 *Lychnocanoma amphitrite* Foreman – Strong et al., p. 208, figs. 11K, 11L.
1997 *Lychnocanoma amphitrite* Foreman – Takemura and Ling, p. 114, pl. 1, fig. 21.
1997 *Lychnocanium amphitrite* (Foreman) – Hollis et al., p. 63, pl. 6, figs. 1–4.
1999a *Lychnocanium amphitrite* (Foreman) – O'Connor, p. 34, pl. 9, fig. 33.
2001 *Lychnocanoma amphitrite* Foreman – Sanfilippo and Blome, p. 214, figs. 9g–9j.
2005 *Lychnocanoma amphitrite* Foreman – Funakawa and Nishi, p. 233, pl. 4, figs. 14a, 14b.
2006 *Lychnocanoma amphitrite* Foreman – Funakawa et al., p. 35, pl. P12, figs, 8a, 8b.
2009b *Lychnocanoma amphitrite* Foreman – Suzuki et al., p. 261, pl. 19, figs. 5a–6b.
2012 *Lychnocanoma amphitrite* Foreman – Moore and Kamikuri, p. 9, pl. P7, figs. 1, 2.
2015 *Lychnocanoma amphitrite* Foreman – Kamikuri, pl. 8, figs. 3a, 3b, 7.
2020 *Lychnocanium amphitrite* (Foreman) – Hollis et al., pl. 12, figs. 25–28.
2021 *Lychnocanoma amphitrite* Foreman – de Souza et al., p. 15, pl. 3, fig. 6.

Occurrence. ODP Site 1051 (Blake Nose; western north Atlantic).

Lychnocanoma bajunensis Renz, 1984

Plate II.16, Figure 4

1975 *Lychnocanoma* sp. B Ling, p. 729, pl. 10, fig. 14.
1977 *Lychnocanoma* sp. Riedel and Sanfilippo, pl. 7, fig. 12.
1984 *Lychnocanoma bajunensis* Renz, p. 459, pl. 1, figs. 4–6.

Occurrence. ODP Site 1260 (Demerara Rise; western equatorial Atlantic) and ODP Site 1051 (Blake Nose; western north Atlantic).

Genus *Sethochytris* Haeckel, 1882

Type species.— *Sethochytris triconiscus* Haeckel, 1887, p. 1239, pl. 57, fig. 13.

Sethochytris triconiscus Haeckel, 1887

Plate II.15, Figures 6, 7

1862 *Rhopalocanium* Bury, pl. 5, fig. 4.
1887 *Sethochytris triconiscus* Haeckel, p. 1239, pl. 57, fig. 13.
? 1970 Gen. et sp. indet. Riedel and Sanfilippo, pl. 9, fig. 5.
1970 ? *Sethochytris triconiscus* Haeckel – Riedel and Sanfilippo, p. 528, pl. 9, fig. 6.
1971 ? *Sethochytris triconiscus* Haeckel – Moore, p. 741, pl. 3, fig. 11.
1975 *Sethochytris triconiscus* Haeckel – Ling, p. 727, pl. 11, figs. 4–6.
1977 *Sethochytris triconiscus* Haeckel – Riedel and Sanfilippo, pl. 9, fig. 7.
1978 *Sethochytris triconiscus* Haeckel – Riedel and Sanfilippo, p. 73, pl. 9, fig. 6.
1991 *Sethochytris triconiscus* Haeckel – Scherer, p. 352, pl. 4, fig. 5 (part).
2000 *Sethochytris triconiscus* Haeckel – Nigrini and Sanfilippo, p. 74, pl. 1, fig. 8.
2001 *Sethochytris triconiscus* Haeckel – Sanfilippo and Blome, p. 217, fig. 11a.
2012 *Sethochytris triconiscus* Haeckel – Moore and Kamikuri, p. 10, pl. P7, fig. 14.

2017 *Sethochytris triconiscus* Haeckel – de Souza et al., pl. 3, fig. 13.
2020 *Sethochytris triconiscus* Haeckel – Hollis et al., pl. 14, figs. 27a, 27b.
Occurrence. ODP Site 1260 (Demerara Rise; western equatorial Atlantic) and ODP Site 1051 (Blake Nose; western north Atlantic).

Genus *Verutotholus* O'Connor, 1999a

Type species.— *Verutotholus doigi* O'Connor, 1999a, p. 14, pl. 6, figs. 1a, 1b.

Verutotholus doigi O'Connor, 1999a

Plate II.16, Figure 7

1999a *Verutotholus doigi* O'Connor, p. 14, pl. 2, figs. 12a–16, pl. 6, figs. 1a–4.
2015 *Cycladophora spatiosa* Ehrenberg – Kamikuri, pl. 10, figs. 7a, 7b.
Occurrence. ODP Site 1051 (Blake Nose; western north Atlantic).

Superfamily Pterocorythoidea Haeckel, 1882 emend. Suzuki et al., 2021

Family Lophocyrtiidae Sanfilippo and Caulet *in* De Wever et al., 2001

Genus *Apoplanius* Sanfilippo and Caulet, 1998

Type species.— *Lophocyrtis* (*Apoplanius*) *klydus* Sanfilippo and Caulet, 1998, p. 12, pl. 5, Figure 5a.

Apoplanius asperus (Ehrenberg, 1874)

Plate II.16, Figure 8

1874 *Eucyrtidium asperum* Ehrenberg, p. 226.
1876 *Eucyrtidium asperum* Ehrenberg – Ehrenberg, p. 70, pl. 8, fig. 15.
1882a *Thyrsocyrtis aspera* (Ehrenberg) – Bütschli, p. 527.
1887 *Theocyrtis* (*Theocorusca*) *aspera* (Ehrenberg) – Haeckel, p. 1408.
1972 *Calocyclas asperum* (Ehrenberg) – Petrushevskaya and Kozlova, p. 548, pl. 28, figs. 16–18.
1992 *Calocyclas* sp. B Takemura, p. 745, pl. 5, fig. 13.
? 1995 *Calocyclas asperum* (Ehrenberg) – Strong et al., p. 208, fig. 9E.
1997 *Calocyclas* sp. B Hollis et al., p. 58, pl. 5, figs. 7–10.
1997 *Calocyclas* sp. B Takemura and Ling, p. 111, pl. 1, fig. 15.
1998 *Theocorys minuta* Takemura and Ling, p. 162, figs. 3.16–3.21, 5.5, 5.6.
1998 *Lophocyrtis* (*Apoplanius*) *aspera* (Ehrenberg) – Sanfilippo and Caulet, p. 14, pl. 3A, figs. 5–10, pl. 3B, figs. 1, 2, 5–9, pl. 6, figs. 6–8.
1999a *Lophocyrtis* (*Apoplanius*) *aspera* (Ehrenberg) – O'Connor, p. 32, pl. 9, fig. 5.
1999 *Calocyclas asperum* (Ehrenberg) – Kozlova, p. 153, pl. 35, fig. 6, pl. 46, fig. 10.
2006 *Lophocyrtis* (*Apoplanius*) *aspera* (Ehrenberg) – Funakawa et al., p. 25, pl. P7, figs. 4a–7b.
2009 *Eucyrtidium asperum* Ehrenberg – Ogane et al., pl. 89, figs. 3a–3g.
2013 *Lophocyrtis* (*Apoplanius*) *aspera* (Ehrenberg) – Kamikuri et al., pl. 1, figs. 3a, 3b.
2015 *Lophocyrtis* (*Apoplanius*) *aspera* (Ehrenberg) – Kamikuri, pl. 6, figs. 3a, 3b.

2020 *Lophocyrtis* (*Apoplanius*) *aspera* (Ehrenberg) form B – Hollis et al., pl. 15, figs. 17a–19b.
2021 *Lophocyrtis* (*Apoplanius*) *aspera* (Ehrenberg) – de Souza et al., p. 15, pl. 3, fig. 12.
Remarks. The combination used here is derived from O'Dogherty et al. (2021).
Occurrence. ODP Site 1260 (Demerara Rise; western equatorial Atlantic) and ODP Site 1051 (Blake Nose; western north Atlantic).

Apoplanius kerasperus (Sanfilippo and Caulet, 1998)
Plate II.16, Figure 10

1998 *Lophocyrtis* (*Apoplanius*) *keraspera* Sanfilippo and Caulet, p.14, pl. 3A, figs. 13–15, pl. 3B, figs. 12–14, pl. 6, figs. 9–12.
2020 *Lophocyrtis* (*Apoplanius*) *keraspera* Sanfilippo and Caulet – Hollis et al., pl. 15, figs. 20–24.
2021 *Lophocyrtis* (*Apoplanius*) *keraspera* Sanfilippo and Caulet – de Souza et al., p. 15, pl. 3, figs. 13a, 13b.
Remarks. The combination used here is derived from O'Dogherty et al. (2021).
Occurrence. ODP Site 1260 (Demerara Rise; western equatorial Atlantic) and ODP Site 1051 (Blake Nose; western north Atlantic).

Apoplanius klydus (Sanfilippo and Caulet, 1998)
Plate II.16, Figure 11

1998 *Lophocyrtis* (*Apoplanius*) *klydus* Sanfilippo and Caulet, p. 12, pl. 3A, figs. 11, 12, pl. 3B, figs. 10, 11, pl. 5, figs. 4a–5b, 8, 10, 11.
Remarks. The combination used here is derived from O'Dogherty et al. (2021).
Occurrence. ODP Site 1260 (Demerara Rise; western equatorial Atlantic).

Genus *Lophocyrtis* Haeckel, 1887

Type species.— *Eucyrtidium stephanophorum* Ehrenberg, 1874, p. 233 (unfigured); Ehrenberg, 1876, p. 72, pl. 8, fig. 14.

Lophocyrtis alauda (Ehrenberg, 1874)
Plate II.16, Figures 12–15

1874 *Eucyrtidium Alauda* [sic] Ehrenberg, p. 225.
1874 *Eucyrtidium versipellis* Ehrenberg, p. 233.
1876 *Eucyrtidium Alauda* [sic] Ehrenberg – Ehrenberg, p. 70, pl. 9, fig. 4.
1876 *Eucyrtidium versipellis* Ehrenberg – Ehrenberg, p. 72, pl. 11, fig. 14.
1882a *Eucyrtidium Alauda* [sic] Ehrenberg – Bütschli, p. 528.
1882a *Eucyrtidium versipellis* Ehrenberg – Bütschli, p. 528.
1882b *Eucyrtidium Alauda* [sic] Ehrenberg – Bütschli, pl. 30, fig. 17.
1887 *Theocorys* (*Theocorythium*) *alauda* (Ehrenberg) – Haeckel, p. 1418.
1887 *Theocampe* (*Theocamptra*) *versipellis* (Ehrenberg) – Haeckel, p. 1425.
1942 *Calocyclas* (*Calocycletta*) *semipolita semipolita* Clark and Campbell, p. 83, pl. 8, figs. 12, 14, 17–19, 22, 23.

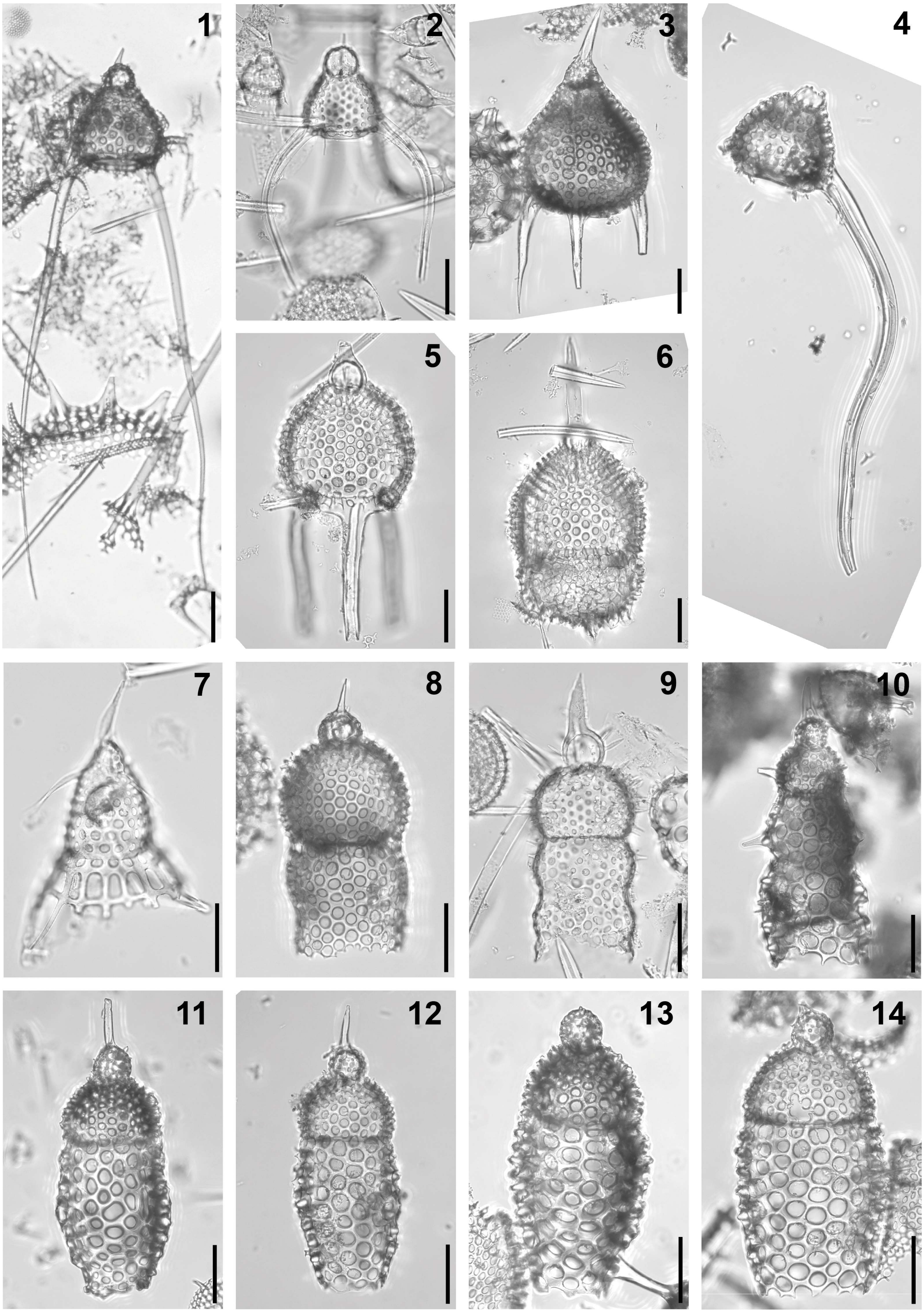
1
2
3
4
5
6
7
8
9
10
11
12
13
14

Plate II.16. Composite light micrographs of new radiolarian species from ODP Site 1260 (Demerara Rise, western equatorial Atlantic) and ODP Site 1051 (Blake Nose, western North Atlantic). (**1**) *Lychnocanium trichopus* Ehrenberg, 1874: ODP 1260A-13R-5W, 54–56 cm. (**2**) *Lychnocanium falciferum* Ehrenberg, 1854a: ODP 1051A-9H-2W, 53–55 cm. (**3**) *Lychnocanium turgidum* Ehrenberg, 1874: ODP 1260A-10R-5W, 55–57 cm. (**4**) *Lychnocanoma bajunensis* Renz, 1984: ODP 1260A-10R-1W, 55–57 cm. (**5**) *Lychnocanium bellum* Clark and Campbell, 1942: ODP 1051A-18X-5W, 54–56 cm. (**6**) *Lychnocanoma amphitrite* Foreman, 1973: ODP 1051A-4H-5W, 56–58 cm. (**7**) *Verutotholus doigi* O'Connor, 1999a: ODP 1051A-13H-2W, 52–54 cm. (**8**) *Apoplanius aspera* (Ehrenberg, 1874): ODP 1260A-11R-1W, 55–57 cm. (**9**) *Apoplanius keraspera* (Sanfilippo and Caulet, 1998): ODP 1051A-9H-2W, 53–5 cm. (**10**) *Apoplanius klydus* (Sanfilippo and Caulet, 1998): ODP 1260A-6R-CC, 63–177 cm. (**11–14**) *Lophocyrtis alauda* (Ehrenberg, 1874): (**11**) ODP 1260A-13R-4W, 55–57 cm; (**12**) ODP 1260A-13R-1W, 54–56 cm; (**13**) ODP 1260A-17R-3W, 55–57 cm; (**14**) ODP 1260A-11R-7W, 55–57 cm. All scale bars equal 50 µm.

1945 *Calocyclas* (*Calocycletta*) *semipolita semipolita* Clark and Campbell, p.44, pl. 6, fig. 12 (part).
1975 ? *Calocyclas semipolita* Clark and Campbell – Chen, p. 459, pl. 6, figs. 3, 6 (part).
not 1988 *Calocyclas semipolita* Clark and Campbell – Blueford, p. 246, pl. 2, figs. 4, 5.
1998 *Lophocyrtis* (*Lophocyrtis* ?) cf. *semipolita* (Clark and Campbell) – Sanfilippo and Caulet, p. 10, pl. 4, fig. 7.
2009 *Eucyrtidium alauda* Ehrenberg – Ogane et al., pl. 49, figs. 1a–1e.
2009 *Eucyrtidium versipellis* Ehrenberg – Ogane et al., pl. 2, figs. 1a–1d, pl. 22, fig. 5, pl. 49, fig. 3, pl. 89, fig. 4a–4c.
Remarks. The combination used here is derived from O'Dogherty et al. (2021).
Occurrence. ODP Site 1260 (Demerara Rise; western equatorial Atlantic).

Lophocyrtis attenuata (Ehrenberg, 1874)
Plate II.17, Figures 1, 2

1874 *Eucyrtidium attenuatum* Ehrenberg, p. 226.
? 1874 *Eucyrtidium Hillaby* [sic] Ehrenberg, p. 229.
1876 *Eucyrtidium attenuatum* Ehrenberg – Ehrenberg, p. 70, pl. 11, fig. 16.
? 1876 *Eucyrtidium Hillaby* [sic] Ehrenberg – Ehrenberg, p. 72, pl. 11, fig. 8.
1882a *Eucyrtidium attenuatum* Ehrenberg – Bütschli, p. 528.
1887 *Theocorys* (*Theocorythium*) *attenuata* (Ehrenberg) – Haeckel, p. 1417.
? 1975 *Theocyrtis* (*Theocorypha*) *diabloensis* Clark and Campbell – Chen, p. 459, pl. 5, figs. 4, 5, 6 (part).
2009 *Eucyrtidium attenuatum* Ehrenberg – Ogane et al., pl. 23, figs. 3a–4c, pl. 48, figs. 5a, 5b.
Remarks. The combination used here is derived from O'Dogherty et al. (2021).
Occurrence. ODP Site 1260 (Demerara Rise; western equatorial Atlantic) and ODP Site 1051 (Blake Nose; western north Atlantic).

Lophocyrtis ? *coronata* (Ehrenberg, 1874)
Plate II.17, Figure 7

1874 *Eucyrtidium coronatum* Ehrenberg, p. 227.
1876 *Eucyrtidium coronatum* Ehrenberg – Ehrenberg, p. 70, pl. 10, fig. 9.
1887 *Lophocyrtis coronata* (Ehrenberg) – Haeckel, p. 1411.
2009 *Eucyrtidium coronatum* Ehrenberg – Ogane et al., pl. 19, figs. 4a–4e.

Remarks. The combination used here is derived from O'Dogherty et al. (2021).
Occurrence. ODP Site 1260 (Demerara Rise; western equatorial Atlantic).

Lophocyrtis cortesei Tetard et al., 2023
Plate II.17, Figure 6

2023 *Lophocyrtis cortesei* Tetard et al., p. 8, figs. 4o–4q, 5r, 5s.

Occurrence. ODP Site 1260 (Demerara Rise; western equatorial Atlantic).

Lophocyrtis microtheca (Ehrenberg, 1874)
Plate II.17, Figures 3, 4

1874 *Eucyrtidium microtheca* Ehrenberg, p. 230.
1876 *Eucyrtidium microtheca* Ehrenberg – Ehrenberg, p. 72, pl. 11, fig. 10.
1882a *Thyrsocyrtis microtheca* (Ehrenberg) – Bütschli, p. 528.
1887 *Theocyrtis* (*Theocorypha*) *microtheca* (Ehrenberg) – Haeckel, p. 1407.
1974 Theoperid gen. et sp. indet. Johnson, pl. 2, figs. 14, 15, 17 (part).
2006 *Eucyrtidium* ? *hillaby* Ehrenberg – Funakawa et al., p. 22, pl. P5, figs. 6a–8b.
2009 *Eucyrtidium microtheca* Ehrenberg – Ogane et al., pl. 84, fig. 2a–2c.

Remarks. The combination used here is derived from O'Dogherty et al. (2021).
Occurrence. ODP Site 1260 (Demerara Rise; western equatorial Atlantic) and ODP Site 1051 (Blake Nose; western north Atlantic).

Lophocyrtis panthera (Ehrenberg, 1874)
Plate II.17, Figure 5

1874 *Eucyrtidium Panthera* [sic] Ehrenberg, p. 231.
1876 *Eucyrtidium Panthera* [sic] Ehrenberg – Ehrenberg, p. 72, pl. 11, fig. 18.
1882a *Thyrsocyrtis Panthera* [sic] (Ehrenberg) – Bütschli, p. 528.
1887 *Tricolocampe* (*Tricolocampium*) *panthera* (Ehrenberg) – Haeckel, p. 1413.
1975 *Theocyrtis* (*Theocorypha*) *diabloensis* Clark and Campbell – Chen, p. 459, pl. 5, fig. 7 (part).
1975 *Eucyrtidium* sp. cf. *E. panthera* Ehrenberg – Ling, p. 731, pl. 12, fig. 18.
2006 *Eucyrtidium* ? *panthera* Ehrenberg – Funakawa et al., p. 23, pl. P5, figs. 9a, 9b.
2009 *Eucyrtidium panthera* Ehrenberg – Ogane et al., pl. 6, figs. 10a, 10b, pl. 84, figs. 1a–1d.

Remarks. The combination used here is derived from O'Dogherty et al. (2021).
Occurrence. ODP Site 1260 (Demerara Rise; western equatorial Atlantic) and ODP Site 1051 (Blake Nose; western north Atlantic).

Genus *Paralampterium* Sanfilippo, 1990

Type species.— *Lophocyrtis* (*Paralampterium*) *dumitricai* Sanfilippo, 1990, p. 308, pl. 3, fig. 8.

Paralampterium ? *eurylophus* (Ehrenberg, 1874)

Plate II.17, Figure 8

1887 *Dictyopodium eurylophus* Ehrenberg – Haeckel, p. 1352.
1978 Theoperid gen. et sp. indet. Weaver and Dinkelman, pl. 8, fig. 10 (part).
2006 *Dictyopodium eurylophus* Ehrenberg – Funakawa et al., pl. P6, figs. 8a–10.
2015 *Dictyopodium eurylophus* Ehrenberg – Kamikuri, pl. 19, figs. 7a, 7b.

Remarks. The combination used here is derived from O'Dogherty et al. (2021).

Occurrence. ODP Site 1260 (Demerara Rise; western equatorial Atlantic) and ODP Site 1051 (Blake Nose; western north Atlantic).

Family Pterocorythidae Haeckel, 1882 emend. Riedel, 1967b emend. Moore, 1972

Genus *Lamprocyclas* Haeckel, 1882

Type species.— *Lamprocyclas* (*Lamprocyclia*) *nuptialis* Haeckel, 1887, p. 1390, pl. 74, fig. 15.

? *Lamprocyclas inexpectata* Caulet, 1991

Plate II.17, Figures 9, 10

1991 *Lamprocyclas inexpectata* Caulet, p. 534, pl. 3, figs. 2, 3.

Occurrence. ODP Site 1051 (Blake Nose; western north Atlantic).

Genus *Phormocyrtis* Haeckel, 1887

Type species.— *Phormocyrtis longicornis* Haeckel, 1887, p. 1370, pl. 69, fig. 15.

Phormocyrtis embolum (Ehrenberg, 1874)

Plate II.17, Figure 11

1874 *Eucyrtidium Embolum* [sic] Ehrenberg, p. 228.
1876 *Eucyrtidium Embolum* [sic] Ehrenberg – Ehrenberg, p. 70, pl. 10, fig. 5.
1882a *Eucyrtidium Embolum* [sic] Ehrenberg – Bütschli, p. 528.
1887 *Phormocyrtis embolum* (Ehrenberg) – Haeckel, p. 1369.
1957b *Phormocyrtis embolum* (Ehrenberg) – Riedel, p. 88, pl. 3, fig. 6 (part).
1942 *Phormocyrtis ligulata* Clark and Campbell, p. 81, pl. 7, figs. 22, 23, 27, 28.
1945 *Phormocyrtis ligulata* Clark and Campbell – Clark and Campbell, p. 43, pl. 6, figs. 10, 11.
1957b *Phormocyrtis embolum* (Ehrenberg) – Riedel, p. 88, pl. 3, fig. 6 (part).
1970 *Phormocyrtis embolum* (Ehrenberg) – Cita et al., p. 403, pl. 2, fig. E.
1974 *Phormocyrtis embolum* (Ehrenberg) – Nigrini, p. 1068, pl. 1H, figs. 4, 5.
1974 *Phormocyrtis embolum* (Ehrenberg) – Johnson, p. 548, pl. 2, fig. 11, pl. 4, fig. 5 (part).
1975 *Phormocyrtis embolum* (Ehrenberg) group – Ling, p. 729, pl. 10, fig. 15.
1986 *Phormocyrtis embolum* (Ehrenberg) – Riedel and Sanfilippo, pl. 7, fig. 2.
1988 *Phormocyrtis ligulata* Clark and Campbell – Blueford, p. 246, pl. 2, figs. 7–9.

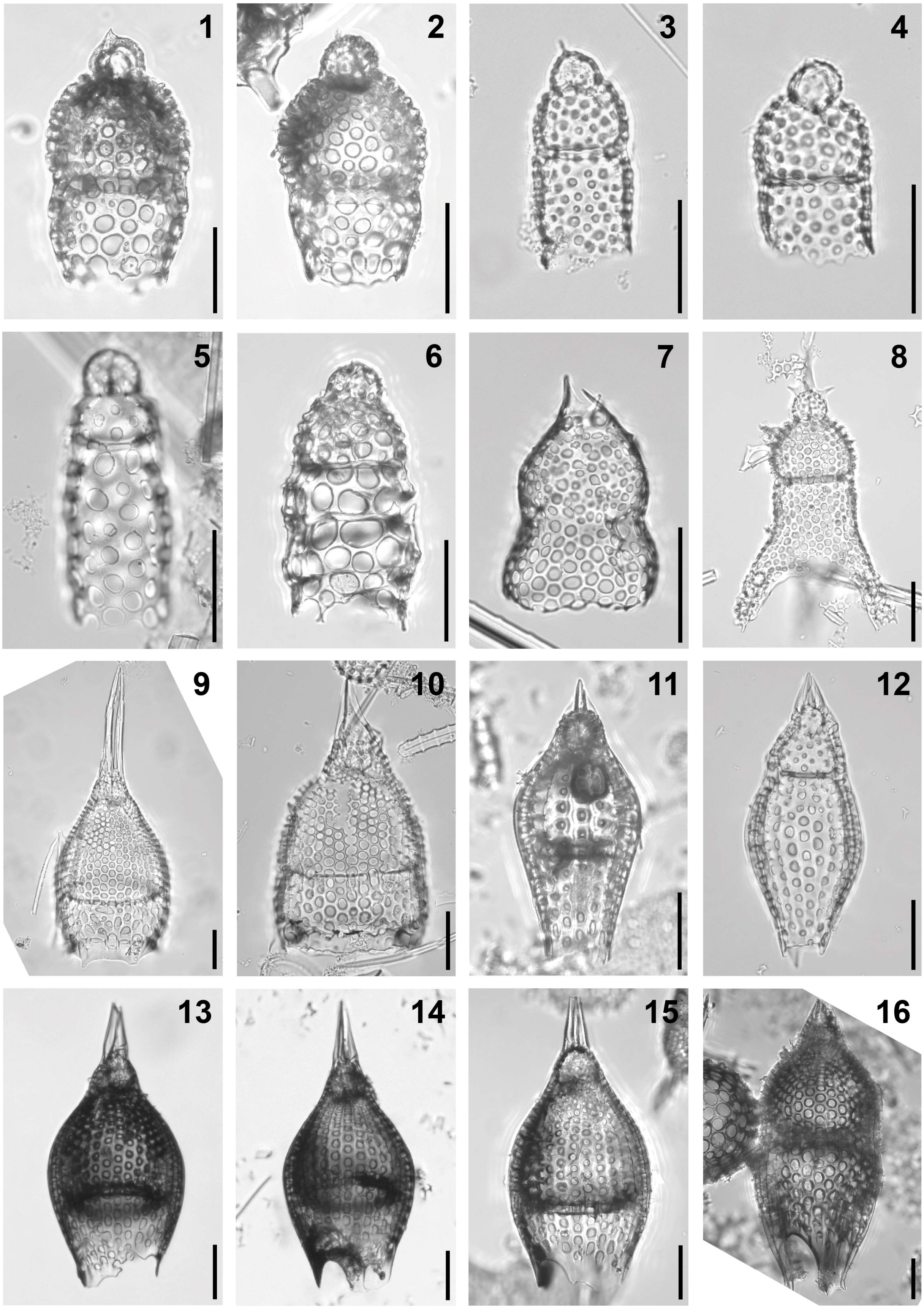
1
2
3
4
5
6
7
8
9
10
11
12
13
14
15
16

Plate II.17. Composite light micrographs of new radiolarian species from ODP Site 1260 (Demerara Rise, western equatorial Atlantic) and ODP Site 1051 (Blake Nose, western North Atlantic). (**1, 2**) *Lophocyrtis attenuata* (Ehrenberg, 1874): (**1**) ODP 1260A-11R-3W, 55–57 cm; (**2**) ODP 1260A-17R-3W, 55–57 cm. (**3, 4**) *Lophocyrtis microtheca* (Ehrenberg, 1874): (**3**) ODP 1051A-9H-2W, 53–55 cm; (**4**) ODP 1051A-14H-5W, 52–54 cm. (**5**) *Lophocyrtis panthera* (Ehrenberg, 1874): ODP 1051A-2H-5W, 55–57 cm. (**6**) *Lophocyrtis cortesei* Tetard et al., 2023: ODP 1260A-6R-4W, 55–57 cm. (**7**) *Lophocyrtis* ? *coronata* (Ehrenberg, 1874): ODP 1260A-13R-3W, 54–56 cm. (**8**) *Paralampterium* ? *eurylophus* (Ehrenberg, 1874): ODP 1051A-12H-2W, 55–57 cm. (**9, 10**) ? *Lamprocyclas inexpectata* Caulet, 1991: (**9**) ODP 1051A-9H-2W, 53–55 cm; (**10**) ODP 1051A-9H-2W, 53–55 cm. (**11**) *Phormocyrtis embolum* (Ehrenberg, 1874): ODP 1260A-14R-1W, 55–57 cm. (**12**) *Phormocyrtis striata striata* Brandt *in* Wetzel, 1935: ODP 1051A-38X-5W, 55–57 cm. (**13–15**) *Podocyrtis* (*Podocyrtis*) *papalis* Ehrenberg, 1847: (**13**) ODP 1260A-10R-6W, 55–57 cm; (**14**) ODP 1260A-8R-6W, 54–56 cm; (**15**) ODP 1260A-9R-3W, 55–57 cm. (**16**) ? *Podocyrtis* (*Lampterium*) *acalles* Sanfilippo and Riedel, 1992: ODP 1260A-20R-4W, 55–57 cm. All scale bars equal 50 µm.

1993 *Cryptocarpium* sp. Hull, p. 13, pl. 7, fig. 3.
1995 *Phormocyrtis ligulata* Clark and Campbell – Strong et al., p. 209, figs. 11U, 11V.
1999 *Phormocyrtis embolum* (Ehrenberg) – Kozlova, p. 148, pl. 31, fig. 14.
2009 *Eucyrtidium embolum* Ehrenberg – Ogane et al., pl. 22, figs. 6a–6c.
2013 *Phormocyrtis embolum* (Ehrenberg) – Kamikuri et al., pl. 1, fig. 1a, 1b.
? 2015 *Phormocyrtis embolum* (Ehrenberg) – Kamikuri, pl. 19, fig. 12
2020 *Phormocyrtis ligulata* Clark and Campbell – Hollis et al., pl. 10, figs. 17a, 17b.
Occurrence. ODP Site 1260 (Demerara Rise; western equatorial Atlantic) and ODP Site 1051 (Blake Nose; western north Atlantic).

Phormocyrtis striata striata Brandt *in* Wetzel, 1935
Plate II.17, Figure 12

1935 *Phormocyrtis striata* Brandt *in* Wetzel, p. 55, pl. 9, fig. 12.
1969b *Theocorys costata* Mamedov, p. 37, pl. 1, fig. 5.
1970 *Phormocyrtis striata* Brandt – Cita et al., p. 404, pl. 2, fig. F.
1970 *Phormocyrtis striata* Brandt – Riedel and Sanfilippo, p. 532, pl. 10, fig. 7.
1971 *Phormocyrtis striata* Brandt – Moore, p. 742, pl. 1, fig. 2.
1972 *Phormocyrtis striata* Brandt – Benson, p. 1093, pl. 2, fig. 5.
1972 *Eusyringium striata* (Brandt) – Petrushevskaya and Kozlova, p. 549, pl. 32, figs. 1, 2.
1973 *Phormocyrtis striata striata* Brandt – Foreman, p. 438, pl. 7, figs. 5, 6, 9.
1973 *Phormocyrtis striata striata* Brandt – Nigrini, p. 1068, pl. 1F, figs. 15–18.
1974 *Phormocyrtis striata striata* Brandt – Johnson, p. 548, pl. 2, figs. 6, 7.
1975 *Phormocyrtis striata striata* Brandt – Chen, p. 456, pl. 3, fig. 8.
1977 *Phormocyrtis striata striata* Brandt – Riedel and Sanfilippo, pl. 3, fig. 11.
1978 *Phormocyrtis striata striata* Brandt – Weaver and Dinkelman, p. 873, pl. 8, fig. 5.
1978 *Phormocyrtis striata striata* Brandt – Riedel and Sanfilippo, p. 71, pl. 7, fig. 11.

1984 *Phormocyrtis striata striata* Brandt – Westberg-Smith and Riedel, p. 493, pl. 6, fig. 12.
1985 *Phormocyrtis striata striata* Brandt – Sanfilippo et al., p. 679, figs. 20.1a, 20.1b.
1987 *Phormocyrtis striata striata* Brandt – Nishimura, p. 727, pl. 2, figs. 10, 11.
1993 *Phormocyrtis striata striata* Brandt – Hull, p. 12, pl. 7, fig. 5.
1994 *Phormocyrtis striata striata* Brandt – Weinheimer et al., p. 311, pl. 1, figs. 10a, 10b.
1995 *Eusyringium striata* (Brandt) – Shilov, p. 126, pl. 2, figs. 3a, 3b.
1995 *Phormocyrtis striata striata* Brandt – Strong et al., p. 209, figs. 9O, 9P.
1998a *Phormocyrtis striata striata* Brandt – Sanfilippo and Nigrini, p. 273, pl. 13.2, fig. 2.
1999 *Phormocyrtis striata striata* Brandt – Kozlova, p. 156, pl. 15, fig. 10, pl. 18, fig. 6.
2008 *Phormocyrtis striata striata* Brandt – Jackett et al., p. 57, pl. 1, fig. 19.
2015 *Phormocyrtis striata striata* Brandt – Hollis, pl. 12, fig. 8.
2017 *Phormocyrtis striata striata* Brandt – de Souza et al., pl. 2, figs. 8a, 8b.
2020 *Phormocyrtis striata striata* Brandt – Hollis et al., pl. 10, figs. 19a, 19b.
Occurrence. ODP Site 1051 (Blake Nose; western north Atlantic).

Genus *Podocyrtis* Ehrenberg, 1846

Type species.— *Podocyrtis papalis* Ehrenberg, 1847, p. 55, fig. 2.

? *Podocyrtis* (*Lampterium*) *acalles* Sanfilippo and Riedel, 1992

Plate II.17, Figure 16

1970 *Podocyrtis* (*Lampterium*) *acalles* Sanfilippo and Riedel, p. 12, pl. 3, figs. 2–5.
1993 *Podocyrtis* (*Lampterium*) *acalles* Sanfilippo and Riedel – Hull, p. 13, pl. 8, fig. 1.
1994 *Podocyrtis* (*Lampterium*) *acalles* Sanfilippo and Riedel – Weinheimer et al., p. 312, pl. 1, fig. 14.
1998a *Podocyrtis* (*Lampterium*) *acalles* Sanfilippo and Riedel – Sanfilippo and Nigrini, p. 273, pl. 13.2, fig. 4.
? 2017 *Podocyrtis* (*Lampterium*) *acalles* Sanfilippo and Riedel – de Souza et al., pl. 1, figs. 6a, 6b.
2020 *Podocyrtis* (*Lampterium*) *acalles* Sanfilippo and Riedel – Hollis et al., pl. 17, figs. 19a, 19b.
Occurrence. ODP Site 1260 (Demerara Rise; western equatorial Atlantic).

Podocyrtis (*Lampterium*) *chalara* Riedel and Sanfilippo, 1970

Plate II.18, Figure 7

1862 *Podocyrtis* ? Bury, pl. 12, fig. 2 (part).
1958 *Podocyrtis eulophos* Ehrenberg – Göke, pl. 1, fig. 5.
1970 *Podocyrtis* (*Lampterium*) *chalara* Riedel and Sanfilippo, p. 535, pl. 12, figs. 2, 3.
1971 *Podocyrtis* (*Lampterium*) *chalara* Riedel and Sanfilippo – Moore, p. 743, pl. 3, figs. 5, 6.
1972 *Lampterium chalara* Riedel and Sanfilippo – Petrushevskaya and Kozlova, p. 543, pl. 32, fig. 12.
1972 *Lampterium* sp. G Petrushevskaya and Kozlova, pl. 32, fig. 10.
1977 *Podocyrtis chalara* Riedel and Sanfilippo – Riedel and Sanfilippo, pl. 10, fig. 1.

1978 *Podocyrtis chalara* Riedel and Sanfilippo – Riedel and Sanfilippo, p. 71, pl. 8, fig. 3.
1985 *Podocyrtis* (*Lampterium*) *chalara* Riedel and Sanfilippo – Sanfilippo et al., p. 697, fig. 30.11.
1986 *Podocyrtis* (*Lampterium*) *chalara* Riedel and Sanfilippo – Riedel and Sanfilippo, pl. 2, fig. 14, pl. 4, figs. 10, 11.
1991 *Podocyrtis chalara* Riedel and Sanfilippo – Scherer, p. 352, pl. 4, fig. 3.
2012 *Podocyrtis* (*Lampterium*) *chalara* Riedel and Sanfilippo – Moore and Kamikuri, p. 9, pl. P7, fig. 8.
2012a *Podocyrtis* (*Lampterium*) *chalara* Riedel and Sanfilippo – Kamikuri et al., p. 103, pl. 3, figs. 2a, 2b.
2012b *Podocyrtis* (*Lampterium*) *chalara* Riedel and Sanfilippo – Kamikuri et al., p. 4, pl. P1, figs. 2a, 2b.
2023 *Podocyrtis* (*Lampterium*) *chalara* Riedel and Sanfilippo – Pínto et al., p. 3, pl. 1, figs. A, B.

Occurrence. ODP Site 1260 (Demerara Rise; western equatorial Atlantic) and ODP Site 1051 (Blake Nose; western north Atlantic).

Podocyrtis (*Lampterium*) *goetheana* (Haeckel, 1887)
Plate II.18, Figure 8

? 1887 *Alacorys* (*Tetralacorys*) *lutheri* Haeckel, p. 1370, pl. 65, fig. 4.
1887 *Cycladophora* (*Lampterium*) *gœtheana* [sic] Haeckel, p. 1376, pl. 65, fig. 5.
1970 *Podocyrtis* (*Lampterium*) *goetheana* (Haeckel) – Riedel and Sanfilippo, p. 535.
1971 *Podocyrtis* (*Lampterium*) *goetheana* (Haeckel) – Riedel and Sanfilippo, p. 1598, pl. 8, fig. 13.
1971 *Podocyrtis* (*Lampterium*) *goetheana* (Haeckel) – Moore, p. 743, pl. 3, figs. 7, 8.
1972 *Lampterium* sp. aff. *L. goetheana* (Haeckel) – Petrushevskaya and Kozlova, pl. 32, fig. 14 (part).
1977 *Podocyrtis goetheana* (Haeckel) – Riedel and Sanfilippo, pl. 11, fig. 6.
1978 *Podocyrtis goetheana* (Haeckel) – Riedel and Sanfilippo, p. 72, pl. 8, fig. 6.
1978 *Podocyrtis goetheana* (Haeckel) – Riedel and Sanfilippo, pl. 4, fig. 12.
2005 *Podocyrtis* (*Lampterium*) *goetheana* (Haeckel) – Nigrini et al., p. 45, pl. P5, figs. 11, 12.
2006 *Podocyrtis* (*Lampterium*) *goetheana* (Haeckel) – Funakawa et al., p. 29, pl. P9, figs. 12a, 12b.
2006 *Podocyrtis* (*Lampterium*) *chalara* Riedel and Sanfilippo – Funakawa et al., p. 29, pl. P9, figs. 11a, 11b (diminutive form).
2012 *Podocyrtis* (*Lampterium*) *goetheana* (Haeckel) – Moore and Kamikuri, p. 9, pl. P7, fig. 9.
2012a *Podocyrtis* (*Lampterium*) *goetheana* (Haeckel) – Kamikuri et al., p. 103, pl. 3, fig. 1.
2012b *Podocyrtis* (*Lampterium*) *goetheana* (Haeckel) – Kamikuri et al., p. 4, pl. P1, figs. 3a, 3b.
2015 *Podocyrtis* (*Lampterium*) *goetheana* (Haeckel) – Kamikuri, pl. 6, fig. 6.
2023 *Podocyrtis* (*Lampterium*) *goetheana* (Haeckel) – Pínto et al., p. 3, pl. 1, figs. M–O.

Occurrence. ODP Site 1260 (Demerara Rise; western equatorial Atlantic).

Podocyrtis (*Lampterium*) *fasciolata* Nigrini, 1974
Plate II.18, Figure 9

1973 *Podocyrtis* sp. A Riedel and Sanfilippo, p. 739, pl. 4, figs.1, 2 (part).
1974 *Podocyrtis* (*Podocyrtis*) *ampla fasciolata* Nigrini, p. 1069, pl. 1K, figs. 1, 2, pl. 4, figs. 2, 3.
1978 *Podocyrtis ampla fasciolata* Nigrini – Riedel and Sanfilippo, p. 71, pl. 8, fig. 2.
1985 *Podocyrtis* (*Lampterium*) *fasciolata* Nigrini – Sanfilippo et al., p. 697, fig. 30.7.
2017 *Podocyrtis* (*Lampterium*) *fasciolata* Nigrini – de Souza et al., pl. 1, fig. 9.
Occurrence. ODP Site 1260 (Demerara Rise; western equatorial Atlantic).

Podocyrtis (*Lampterium*) *helenae* Nigrini, 1974
Plate II.18, Figure 6

1973 *Podocyrtis* sp. B Riedel and Sanfilippo, p. 739, pl. 4, figs. 4–6.
1974 *Podocyrtis* (*Lampterium*) *helenae* Nigrini, p. 1070, pl. 1L, figs. 9–11, pl. 4, figs. 4, 5.
2017 *Podocyrtis* (*Lampterium*) *helenae* Nigrini – de Souza et al., pl. 1, figs. 10a, 10b.
Occurrence. ODP Site 1260 (Demerara Rise; western equatorial Atlantic).

Podocyrtis (*Lampterium*) *mitra* Ehrenberg, 1854a
Plate II.18, Figures 3, 4

1854a *Podocyrtis Mitra* [sic] Ehrenberg, pl. 36, fig. 20.
not 1862 *Podocyrtis mitra* Ehrenberg – Bury, pl. 5, fig. 3.
1874 *Podocyrtis eulophos* Ehrenberg, p. 251.
1874 *Podocyrtis Mitra* [sic] Ehrenberg – Ehrenberg, p. 251.
1876 *Podocyrtis Eulophos* [sic] Ehrenberg – Ehrenberg, p. 82, pl. 14, fig. 6.
1876 *Podocyrtis Mitra* [sic] Ehrenberg – Ehrenberg, p. 82, pl. 15, fig. 4.
1882b *Podocyrtis Eulophus* [sic] Ehrenberg – Bütschli, pl. 30, fig. 12.
1887 *Podocyrtis* (*Podocyrtidium*) *mitra* Ehrenberg – Haeckel, p. 1345.
1887 *Podocyrtis* (*Podocyrtidium*) *eulophos* Ehrenberg – Haeckel, p. 1346.
1887 *Podocyrtis* (*Podocyrtonium*) *pedicellaria* Haeckel, p. 1347, pl. 72, fig. 8.
1887 *Podocyrtis* (*Podocyrtonium*) *lithoconus* Haeckel, p. 1348, pl. 72, fig. 3.
1970 *Podocyrtis* (*Lampterium*) *mitra* Ehrenberg – Riedel and Sanfilippo, p. 534, pl. 11, figs. 5, 6.
1971 *Podocyrtis* (*Lampterium*) *mitra* Ehrenberg – Riedel and Sanfilippo, p. 1598, pl. 3D, fig. 19.
1973 *Podocyrtis mitra* Ehrenberg – Riedel and Sanfilippo, p. 739, pl. 3, fig. 1.
1974 *Podocyrtis* (*Lampterium*) *mitra* Ehrenberg – Nigrini, p. 1070, pl. 1L, figs. 5, 6.
1974 *Podocyrtis* (*Lampterium*) *mitra* Ehrenberg – Johnson, p. 551, pl. 4, fig. 15.
1974 *Podocyrtis* sp. Johnson, pl. 4, fig. 16 (part).
1975 *Podocyrtis* (*Lampterium*) *mitra* Ehrenberg – Ling, p. 731, pl. 13, figs. 3, 4.
1975 *Podocyrtis mitra* Ehrenberg – Riedel and Sanfilippo, pl. 9, fig. 11.
1978 *Podocyrtis mitra* Ehrenberg – Riedel and Sanfilippo, p. 72, pl. 8, fig. 7.

1986 *Podocyrtis* (*Lampterium*) *mitra* Ehrenberg – Riedel and Sanfilippo, pl. 2, fig. 13.
1991 *Podocyrtis* (*Lampterium*) *mitra* Ehrenberg – Scherer, p. 352, pl. 4, fig. 4.
2000 *Podocyrtis* (*Lampterium*) *mitra* Ehrenberg – Nigrini and Sanfilippo, p. 74, pl. 1, fig. 12.
2001 *Podocyrtis* (*Lampterium*) *mitra* Ehrenberg – Sanfilippo and Blome, p. 215, figs. 10a, 10b.
2001 *Podocyrtis pedicellaria* Haeckel – De Wever et al., p. 259, fig. 169.4.
2001 *Podocyrtis goetheana* (Haeckel) – De Wever et al., p. 259, fig. 169.5.
2012a *Podocyrtis* (*Lampterium*) *mitra* Ehrenberg – Kamikuri et al., p. 103, pl. 3, figs. 3a, 3b.
2012b *Podocyrtis* (*Lampterium*) *mitra* Ehrenberg – Kamikuri et al., p. 4, pl. P1, fig. 1.
2017 *Podocyrtis* (*Lampterium*) *mitra* Ehrenberg – de Souza et al., pl. 1, figs. 11a, 11b.
Occurrence. ODP Site 1260 (Demerara Rise; western equatorial Atlantic) and ODP Site 1051 (Blake Nose; western north Atlantic).

Podocyrtis (*Lampterium*) *sinuosa* Ehrenberg, 1874
Plate II.18, Figures 1, 2

1874 *Podocyrtis sinuosa* Ehrenberg, p. 253.
1876 *Podocyrtis sinuosa* Ehrenberg – Ehrenberg, p. 82, pl. 15, fig. 5.
1882a *Podocyrtis sinuosa* Ehrenberg – Bütschli, p. 540, pl. 33, fig. 33.
1887 *Podocyrtis* (*Podocyrtonium*) *sinuosa* Ehrenberg – Haeckel, p. 1347.
1969 *Podocyrtis sinuosa* Ehrenberg – Riedel and Hays, pl. 1, fig. E.
1970 *Podocyrtis* sp. A Cita et al., p. 403, pl. 1, fig. I.
1970 ? *Podocyrtis* (*Lampterium*) *sinuosa* Ehrenberg – Riedel and Sanfilippo, p. 534, pl. 11, figs. 3, 4.
1973 ? *Podocyrtis* (*Lampterium*) *sinuosa* Ehrenberg – Riedel and Sanfilippo, p. 532, pl. 21, figs. 4, 5.
1974 ? *Podocyrtis* (*Lampterium*) *sinuosa* Ehrenberg – Nigrini, p. 1070, pl. 1L, figs. 1–4.
1974 *Podocyrtis* (*Lampterium*) *sinuosa* Ehrenberg – Johnson, p. 551, pl. 4, fig. 18.
1977 *Podocyrtis sinuosa* Ehrenberg – Riedel and Sanfilippo, pl. 8, fig. 4.
1978 ? *Podocyrtis sinuosa* Ehrenberg – Weaver and Dinkelman, p. 873, pl. 5, fig. 4.
1978 *Podocyrtis sinuosa* Ehrenberg – Riedel and Sanfilippo, p. 72, pl. 8, fig. 9.
1987 *Podocyrtis sinuosa* Ehrenberg – Nishimura, p. 728, pl. 2, fig. 18.
1992 *Podocyrtis* (*Lampterium*) *sinuosa* Ehrenberg – Sanfilippo and Riedel, pl. 3, fig. 6.
1993 *Podocyrtis* (*Lampterium*) *sinuosa* Ehrenberg – Hull, p. 13, pl. 7, fig. 9.
2012a *Podocyrtis* (*Lampterium*) *sinuosa* Ehrenberg – Kamikuri et al., p. 103, pl. 1, figs. 11a, 11b.
2017 *Podocyrtis* (*Lampterium*) *sinuosa* Ehrenberg – de Souza et al., pl. 1, figs. 13a, 13b.
Occurrence. ODP Site 1260 (Demerara Rise; western equatorial Atlantic).

Podocyrtis (*Lampterium*) *trachodes* Riedel and Sanfilippo, 1970
Plate II.18, Figure 5

1970 *Podocyrtis* (*Lampterium*) *trachodes* Riedel and Sanfilippo, p. 535, pl. 11, fig. 7; pl. 12, fig. 1.

1974 *Podocyrtis* (Lampterium) *trachodes* Riedel and Sanfilippo – Nigrini, p. 1070, pl. 1L, figs. 7, 8.
1974 *Podocyrtis* (Lampterium) *trachodes* Riedel and Sanfilippo – Johnson, p. 551, pl. 5, figs. 11, 12.
1978 *Podocyrtis trachodes* Riedel and Sanfilippo – Riedel and Sanfilippo, p. 72, pl. 8, fig. 10.
1985 *Podocyrtis* (*Lampterium*) *trachodes* Riedel and Sanfilippo – Sanfilippo et al., p. 699, fig. 30.14.
2000 *Podocyrtis* (*Lampterium*) *trachodes* Riedel and Sanfilippo – Nigrini and Sanfilippo, p. 74, pl. 2, fig. 13.
2001 *Podocyrtis* (*Lampterium*) *trachodes* Riedel and Sanfilippo – Sanfilippo and Blome, p. 215, fig. 10c.
2012 *Podocyrtis* (*Lampterium*) *trachodes* Riedel and Sanfilippo – Moore and Kamikuri, p. 9, pl. P7, fig. 5.
2017 *Podocyrtis* (*Lampterium*) *trachodes* Riedel and Sanfilippo – de Souza et al., pl. 2, figs. 1a, 1b.

Occurrence. ODP Site 1260 (Demerara Rise; western equatorial Atlantic).

Podocyrtis (*Podocyrtoges*) *ampla* Ehrenberg, 1874
Plate II.18, Figure 12

1874 *Podocyrtis* ? *ampla* Ehrenberg, p. 248.
1876 *Podocyrtis* ? *ampla* Ehrenberg – Ehrenberg, p. 80, pl. 16, fig. 7.
1882a *Cycladophora ampla* (Ehrenberg) – Bütschli, p. 527, pl. 32, fig. 16.
1887 *Podocyrtis* (*Podocyrtonium*) *ampla* Ehrenberg – Haeckel, p. 1348.
1970 *Podocyrtis* (*Podocyrtis*) *ampla* Ehrenberg – Riedel and Sanfilippo, p. 533, pl. 12, figs. 7, 8.
1971 *Podocyrtis* (*Podocyrtis*) *ampla* Ehrenberg – Moore, p. 743, pl. 2, fig. 6.
1977 *Podocyrtis ampla* Ehrenberg – Riedel and Sanfilippo, pl. 8, fig. 14.
1978 *Podocyrtis ampla ampla* Ehrenberg – Riedel and Sanfilippo, p. 71, pl. 8, fig. 1.
1986 *Podocyrtis* (*Podocyrtis*) *ampla* Ehrenberg – Riedel and Sanfilippo, pl. 2, fig. 16.
1992 *Podocyrtis* (*Podocyrtoges*) *ampla* Ehrenberg – Sanfilippo and Riedel, p. 14, pl. 5, fig. 4.
2012a *Podocyrtis* (*Podocyrtoges*) *ampla* Ehrenberg – Kamikuri et al., p. 103, pl. 3, figs. 8a, 8b.
2017 *Podocyrtis* (*Podocyrtoges*) *ampla* Ehrenberg – de Souza et al., pl. 1, figs. 7a, 7b.

Occurrence. ODP Site 1260 (Demerara Rise; western equatorial Atlantic).

Podocyrtis (*Podocyrtoges*) *diamesa* Riedel and Sanfilippo, 1970
Plate II.18, Figure 10

1970 *Podocyrtis* (*Podocyrtis*) *diamesa* Riedel and Sanfilippo, p. 533, pl. 12, fig. 4 (part).
1971 *Podocyrtis* (*Podocyrtis*) *diamesa* Riedel and Sanfilippo – Moore, p. 743, pl. 2, fig. 5.
1973 *Podocyrtis* (*Podocyrtis*) *diamesa* Riedel and Sanfilippo – Sanfilippo and Riedel, p. 531, pl. 20, figs. 9, 10, pl. 35, figs. 10, 11.

1974 *Podocyrtis* (*Podocyrtis*) *diamesa* Riedel and Sanfilippo – Nigrini, p. 1069, pl. 1K, figs. 3–5.
1977 *Podocyrtis diamesa* Riedel and Sanfilippo – Riedel and Sanfilippo, pl. 8, fig. 5.
1978 *Podocyrtis diamesa* Riedel and Sanfilippo – Riedel and Sanfilippo, p. 72, pl. 8, fig. 4.
1992 *Podocyrtis* (*Podocyrtoges*) *diamesa* Sanfilippo and Riedel – Sanfilippo and Riedel, p. 14.
2005 *Podocyrtis* (*Podocyrtoges*) *diamesa* Sanfilippo and Riedel – Nigrini et al., p. 46, pl. P5, fig. 10.
2021a *Podocyrtis* (*Podocyrtoges*) *diamesa* Sanfilippo and Riedel – Kamikuri et al., p. 4, pl. P2, figs. 4a, 4b.
2015 *Podocyrtis* (*Podocyrtoges*) *diamesa* Sanfilippo and Riedel – Kamikuri, pl. 9, figs. 3a, 3b, 5a, 5b.
2017 *Podocyrtis* (*Podocyrtis*) *diamesa* Sanfilippo and Riedel – de Souza et al., pl. 1, figs. 8a, 8b.
Occurrence. ODP Site 1260 (Demerara Rise; western equatorial Atlantic).

Podocyrtis (*Podocyrtoges*) *phyxis* Sanfilippo and Riedel, 1973
Plate II.18, Figure 11

1970 *Podocyrtis* (*Podocyrtis*) *diamesa* Riedel and Sanfilippo, p. 533, pl. 12, fig. 6 (part).
1973 *Podocyrtis* (*Podocyrtis*) *phyxis* Sanfilippo and Riedel, p. 531.
1977 *Podocyrtis phyxis* Sanfilippo and Riedel – Riedel and Sanfilippo, pl. 8, fig. 6.
1978 *Podocyrtis phyxis* Sanfilippo and Riedel – Riedel and Sanfilippo, p. 72, pl. 8, fig. 8.
1986 *Podocyrtis* (*Podocyrtis*) *phyxis* Sanfilippo and Riedel – Riedel and Sanfilippo, pl. 2, fig. 15.
1992 *Podocyrtis* (*Podocyrtoges*) *phyxis* Sanfilippo and Riedel – Sanfilippo and Riedel, p. 14.
2012a *Podocyrtis* (*Podocyrtoges*) *phyxis* Sanfilippo and Riedel – Kamikuri et al., p. 103, pl. 1, fig. 13.
2017 *Podocyrtis* (*Podocyrtoges*) *phyxis* Sanfilippo and Riedel – de Souza et al., pl. 1, fig. 12.
Occurrence. ODP Site 1260 (Demerara Rise; western equatorial Atlantic).

Podocyrtis (*Podocyrtis*) *papalis* Ehrenberg, 1847
Plate II.17, Figures 13–15

1847 *Podocyrtis papalis* Ehrenberg, p. 55, fig. 2.
1854a *Podocyrtis papalis* Ehrenberg – Ehrenberg, pl. 36, fig. 23.
1862 *Podocyrtis papalis* Ehrenberg – Bury, pl. 10, fig. 5.
1874 *Podocyrtis Mitrella* [sic] Ehrenberg, p. 251.
1874 *Podocyrtis papalis* Ehrenberg – Ehrenberg, p. 251.
1876 *Podocyrtis Mitrella* [sic] Ehrenberg – Ehrenberg, p. 82, pl. 15, fig. 3.
1887 *Podocyrtis* (*Podocyrtidium*) *papalis* Ehrenberg – Haeckel, p. 1344.
1887 *Podocyrtis* (*Podocyrtidium*) *mitrella* Ehrenberg – Haeckel, p. 1345.
1942 *Podocyrtis* (*Podocyrtidium*) *fasciata* Clark and Campbell, p. 80, pl. 7, figs. 29, 33.
1958 *Podocyrtis papalis* Ehrenberg – Göke, pl. 1, fig. 3.
1969 *Podocyrtis papalis* Ehrenberg – Riedel and Hays, pl. 1, fig. C.

1970 *Podocyrtis* (*Podocyrtis*) *papalis* Ehrenberg – Cita et al., p. 403, pl. 1, fig. H.
1970 *Podocyrtis* (*Podocyrtis*) *papalis* Ehrenberg – Riedel and Sanfilippo, p. 533, pl. 11, fig. 1.
1971 *Podocyrtis* (*Podocyrtis*) *papalis* Ehrenberg – Moore, p. 743, pl. 2, fig. 4.
1971 *Podocyrtis* (*Podocyrtis*) *papalis* Ehrenberg – Riedel and Sanfilippo, p. 1598, pl. 3E, fig. 1.
1972 *Podocyrtis papalis* Ehrenberg – Petrushevskaya and Kozlova, p. 543, pl. 35, fig. 1.
1972 *Podocyrtis* sp. Petrushevskaya and Kozlova, pl. 35, fig. 2.
1973 *Podocyrtis* (*Podocyrtis*) *papalis* Ehrenberg – Sanfilippo and Riedel, p. 531, pl. 20, figs. 11–14, pl. 36, figs. 2, 3.
1974 *Podocyrtis* (*Podocyrtis*) *papalis* Ehrenberg – Nigrini, p. 1069, pl. 1K, figs. 7–10.
1974 *Podocyrtis* (*Podocyrtis*) *papalis* Ehrenberg – Johnson, p. 551, pl. 4, fig. 12.
1975 *Podocyrtis* (*Podocyrtis*) *papalis* Ehrenberg – Ling, p. 731, pl. 13, fig. 5.
1977 *Podocyrtis papalis* Ehrenberg – Riedel and Sanfilippo, pl. 9, fig. 12.
1985 *Podocyrtis papalis* Ehrenberg – Sanfilippo et al., fig. 30.1.
1986 *Podocyrtis papalis* Ehrenberg – Riedel and Sanfilippo, pl. 7, fig. 1.
1987 *Podocyrtis papalis* Ehrenberg – Nishimura, p. 727, pl. 2, fig. 7.
1988 *Podocyrtis fasciata* Clark and Campbell – Blueford, p. 246, pl. 1, figs. 10–12.
1992 *Podocyrtis* (?) sp. aff. *P. papalis* – Nishimura, p. 329, pl. 10, figs. 1–3, pl. 13, fig. 18.
1993 *Podocyrtis* (*Podocyrtis*) *papalis* Ehrenberg – Hull, p. 13, pl. 7, figs. 7, 8, pl. 8, fig. 10.
1995 *Podocyrtis mitrella* Ehrenberg – Shilov, p. 127, pl. 1, fig. 3.
1995 *Podocyrtis papilis* [sic] Ehrenberg – Strong et al., p. 209, fig. 9S.
1998a *Podocyrtis papalis* Ehrenberg – Sanfilippo and Nigrini, p. 273, pl. 13.2, fig. 5.
1999 *Podocyrtis papalis* Ehrenberg – Kozlova, p. 151, pl. 15, fig. 6, pl. 24, figs. 16, 17.
2000 *Podocyrtis* (*Podocyrtis*) *papalis* Ehrenberg – Nigrini and Sanfilippo, p. 74, pl. 2, fig. 11, pl. 3, figs. 6, 7.
2001 *Podocyrtis* (*Podocyrtis*) *papalis* Ehrenberg – Sanfilippo and Blome, p. 215, fig. 1f.
2005 *Podocyrtis* (*Podocyrtis*) *papalis* Ehrenberg – Nigrini et al., p. 46, pl. P5, fig. 13.
2008 *Podocyrtis* (*Podocyrtis*) *papalis* Ehrenberg – Jackett et al., p. 57, pl. 2, fig. 22.
2009 *Podocyrtis mitrella* Ehrenberg – Ogane et al., pl. 24, figs. 4a–4c, pl. 57, figs. 3a–3d.
2009 *Podocyrtis papalis* Ehrenberg – Ogane et al., pl. 58, figs. 1a–1f.
2012 *Podocyrtis* (*Podocyrtis*) *papalis* Ehrenberg – Kamikuri and Wade, pl. 1, figs. 6a, 6b.
2012 *Podocyrtis* (*Podocyrtis*) *papalis* Ehrenberg – Moore and Kamikuri, p. 9, pl. P7, fig. 6.
2015 *Podocyrtis* (*Podocyrtis*) *papalis* Ehrenberg – Kamikuri, pl. 9, figs. 2a, 2b (part).
2020 *Podocyrtis* (*Podocyrtis*) *papalis* Ehrenberg – Hollis et al., pl. 17, figs. 20a, 20b.

Occurrence. ODP Site 1260 (Demerara Rise; western equatorial Atlantic) and ODP Site 1051 (Blake Nose; western north Atlantic).

Podocyrtis (*Podocyrtopsis*) *apeza* Sanfilippo and Riedel, 1992

Plate II.18, Figure 13

1992 *Podocyrtis* (*Podocyrtopsis*) *apeza* Sanfilippo and Riedel, p. 14, pl. 3, figs. 13–15.
2012 *Podocyrtis* (*Podocyrtopsis*) *apeza* Sanfilippo and Riedel – Moore and Kamikuri, p. 10, pl. P7, fig. 7.

Occurrence. ODP Site 1260 (Demerara Rise; western equatorial Atlantic) and ODP Site 1051 (Blake Nose; western north Atlantic).

Genus *Anthocyrtoma* Haeckel, 1887

Type species.— *Anthocyrtoma serrulata* Ehrenberg, 1874, p. 217 (unfigured); Ehrenberg, 1876, p. 64, pl. 6, fig. 7.

Anthocyrtoma leptostyla (Ehrenberg, 1874)

Plate II.19, Figures 1, 2

1874 *Anthocyrtis leptostyla* Ehrenberg, p. 216.
1876 *Anthocyrtis leptostyla* Ehrenberg – Ehrenberg, p. 64, pl. 6, fig. 1.
1887 *Anthocyrtidium* (*Anthocyrtonium*) *leptostylum* (Ehrenberg) – Haeckel, p. 1275.
2009 *Anthocyrtis leptostyla* Ehrenberg – Ogane et al., pl. 52, figs. 3a–3f.

Remarks. The combination used here is derived from O'Dogherty et al. (2021).

Occurrence. ODP Site 1260 (Demerara Rise; western equatorial Atlantic).

Anthocyrtoma serrulata (Ehrenberg, 1874)

Plate II.18, Figure 14

1874 *Anthocyrtis serrulata* Ehrenberg, p. 217.
1874 *Anthocyrtis ventricosa* Ehrenberg, p. 217.
1874 *Cycladophora Erinaceus* [sic] Ehrenberg, p. 222.
1876 *Anthocyrtis serrulata* Ehrenberg – Ehrenberg, p. 66, pl. 6, fig. 7.
1876 *Anthocyrtis ventricosa* Ehrenberg – Ehrenberg, p. 66, pl. 8, fig. 1.
1876 *Cycladophora Erinaceus* [sic] Ehrenberg – Ehrenberg, p. 68, pl. 18, fig. 2.
1882a *Thyrsocyrtis Erinaceus* [sic] (Ehrenberg) – Bütschli, p. 527.
1882a *Anthocyrtis serrulata* Ehrenberg – Bütschli, p. 533.
1882a *Anthocyrtis ventricosa* Ehrenberg – Bütschli, p. 533.
1887 *Anthocyrtoma serrulata* (Ehrenberg) – Haeckel, p. 1268.
1887 *Anthocyrtis* (*Anthocyrtella*) *ventricosa* Ehrenberg – Haeckel, p. 1270.
1887 *Calocyclas* (*Calocyclissa*) *erinaceus* (Ehrenberg) – Haeckel, p. 1383.
1969b *Anthocyrtidium apscheronense* Mamedov, p. 33, pl. 1, fig. 1.
1969b *Anthocyrtium mirandum* Mamedov, p. 34, pl. 1, figs. 2, 3.
1970 *Anthocyrtoma* sp. Riedel and Sanfilippo, p. 524, pl. 6, figs. 2–4
1972 *Anthocyrtoma* sp. Petrushevskaya and Kozlova, pl. 34, figs. 1, 2
1973 *Anthocyrtoma* sp. Riedel and Sanfilippo, p. 737, pl. 3, fig. 5.
1974 *Anthocyrtoma* sp. Nigrini, p. 1066, pl. 1E, figs. 5–9.
1977 *Calocycloma ampulla* (Ehrenberg) – Riedel and Sanfilippo, pl. 8, fig. 1.
1978 *Anthocyrtoma* sp. Weaver and Dinkelman, p. 867, pl. 8, fig. 9.
2005 *Anthocyrtoma* spp. Nigrini et al., 2005, p. 25, pl. P3, figs. 15, 16.
2009 *Anthocyrtis serrulata* Ehrenberg – Ogane et al., pl. 51, figs. 1a–2d.
2009 *Anthocyrtis ventricosa* Ehrenberg – Ogane et al., pl. 51, figs. 3a–3d.
2009 *Cycladophora erinaceus* Ehrenberg – Ogane et al., pl. 52, figs. 1a–1g.
2012 *Anthocyrtoma* spp. Moore and Kamikuri, p. 5, pl. P1, fig. 1.

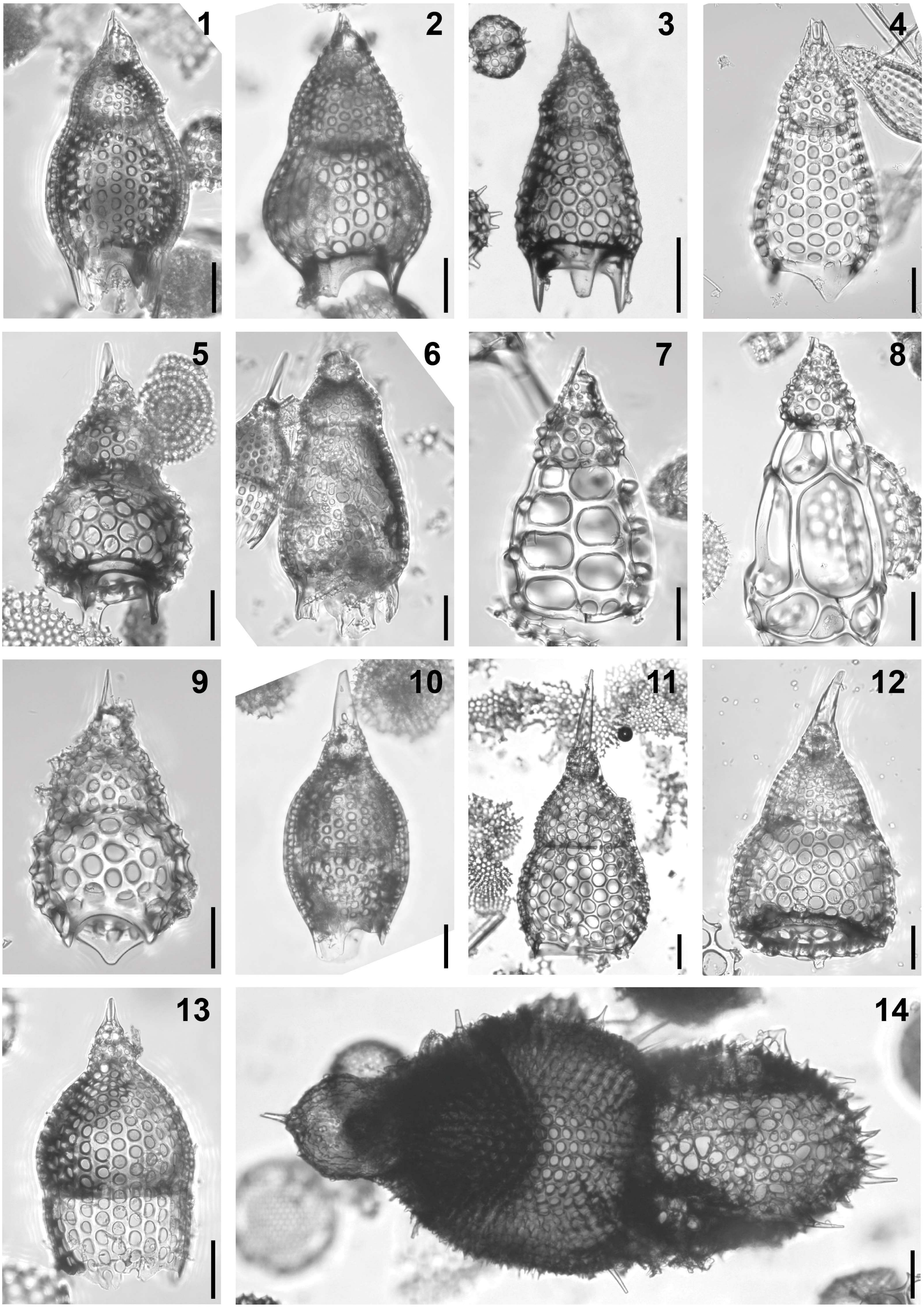

1
2
3
4
5
6
7
8
9
10
11
12
13
14

Plate II.18. Composite light micrographs of new radiolarian species from ODP Site 1260 (Demerara Rise, western equatorial Atlantic) and ODP Site 1051 (Blake Nose, western North Atlantic). (**1, 2**) *Podocyrtis* (*Lampterium*) *sinuosa* Ehrenberg, 1874: (**1**) ODP 1260A-20R-1W, 55–57 cm; (**2**) ODP 1260A-17R-CC, 63–177 cm. (**3, 4**) *Podocyrtis* (*Lampterium*) *mitra* Ehrenberg, 1854a: (**3**) ODP 1260A-9R-5W, 55–57 cm; (**4**) ODP 1051A-16H-5W, 55–57 cm. (**5**) *Podocyrtis* (*Lampterium*) *trachodes* Riedel and Sanfilippo, 1970: ODP 1260A-10R-6W, 55–57 cm. (**6**) *Podocyrtis* (*Lampterium*) *helenae* Nigrini, 1974: ODP 1260A-12R-CC, 63–177 cm. (**7**) *Podocyrtis* (*Lampterium*) *chalara* Riedel and Sanfilippo, 1970: ODP 1260A-6R-4W, 55–57 cm. (**8**) *Podocyrtis* (*Lampterium*) *goetheana* (Haeckel, 1887): ODP 1260A-6R-2W, 55–57 cm. (**9**) *Podocyrtis* (*Lampterium*) *fasciolata* Nigrini, 1974: ODP 1260A-11R-7W, 55–57 cm. (**10**) *Podocyrtis* (*Podocyrtoges*) *diamesa* Riedel and Sanfilippo, 1970: ODP 1260A-17R-CC, 63–177 cm. (**11**) *Podocyrtis* (*Podocyrtoges*) *phyxis* Sanfilippo and Riedel, 1973: ODP 1260A-16R-1W, 55–57 cm. (**12**) *Podocyrtis* (*Podocyrtoges*) *ampla* Ehrenberg, 1874: ODP 1260A-17R-3W, 55–57 cm. (**13**) *Podocyrtis* (*Podocyrtopsis*) *apeza* Sanfilippo and Riedel, 1992: ODP 1260A-10R-6W, 55–57 cm. (**14**) *Anthocyrtoma serrulata* (Ehrenberg, 1874): ODP 1260A-13R-5W, 54–56 cm. All scale bars equal 50 µm.

2015 *Anthocyrtoma serrulata* (Ehrenberg) – Kamikuri, pl. 1, fig. 5.
2015 *Anthocyrtoma ventricosa* (Ehrenberg) – Kamikuri, pl. 10, figs. 8–9b.
Occurrence. ODP Site 1260 (Demerara Rise; western equatorial Atlantic) and ODP Site 1051 (Blake Nose; western north Atlantic).

Family Theocotylidae Petrushevskaya, 1981
Genus *Lamptonium* Haeckel, 1887
Type species.— *Cycladophora* (*Lamptonium*) *enneapleura* Haeckel, 1887, p. 1378 (unfigured).

Lamptonium fabaeforme fabaeforme (Krasheninnikov, 1960)
Plate II.19, Figure 3

1960 *Cyrtocalpis fabaeformis* Krasheninnikov, p. 296, pl. 3, fig. 11.
1969b *Eucyrtidium cybaeum* Mamedov, p. 38, pl. 1, fig. 6.
1970 *Lamptonium* ? *fabaeforme fabaeforme* (Krasheninnikov) – Riedel and Sanfilippo, p. 523, pl. 5, fig. 6.
1971 *Lamptonium* ? *fabaeforme* ? *fabaeforme* (Krasheninnikov) – Moore, p. 740, pl. 1, fig. 6.
1973 *Lamptonium fabaeforme* ? *fabaeforme* (Krasheninnikov) – Foreman, p. 436, pl. 6, figs. 6–9.
1974 *Lamptonium fabaeforme* ? *fabaeforme* (Krasheninnikov) – Nigrini, p. 1067, pl. 1G, fig. 3.
1978 *Lamptonium fabaeforme fabaeforme* (Krasheninnikov) – Johnson, p. 784, pl. 2, fig. 5.
1978 *Lamptonium fabaeforme fabaeforme* (Krasheninnikov) – Weaver and Dinkelman, p. 869, pl. 6, figs. 7–10.
1978 *Lamptonium fabaeforme fabaeforme* (Krasheninnikov) – Riedel and Sanfilippo, p. 69, pl. 5, fig. 13.

1978 *Lamptonium fabaeforme fabaeforme* (Krasheninnikov) – Foreman, p. 784, pl. 2, fig. 5.
1985 *Lamptonium* ? *fabaeforme fabaeforme* (Krasheninnikov) – Sanfilippo et al., p. 674, fig. 18.2.
1987 *Lamptonium* ? *fabaeforme fabaeforme* (Krasheninnikov) – Nishimura, p. 726, pl. 2, fig. 20.
1998a *Lamptonium fabaeforme fabaeforme* (Krasheninnikov) – Sanfilippo and Nigrini, p. 272, pl. 13.1, fig. 17.
1999 *Lamptonium* sp. cf. *L. fabaeforme fabaeforme* (Krasheninnikov) – Kozlova, p. 158, pl. 22, fig. 12, pl. 23, fig. 14, pl. 46, fig. 20.
2008 *Lamptonium fabaeforme fabaeforme* (Krasheninnikov) – Jackett et al., p. 54, pl. 2, fig. 12.
? 2017 *Lamptonium fabaeforme fabaeforme* (Krasheninnikov) – de Souza et al., pl. 3, figs. 1a, 1b.
Occurrence. ODP Site 1260 (Demerara Rise; western equatorial Atlantic).

Lamptonium fabaeforme chaunothorax Riedel and Sanfilippo, 1970
Plate II.19, Figure 4

1970 *Lamptonium fabaeforme chaunothorax* Riedel and Sanfilippo, p. 524, pl. 5, figs. 8, 9.
1971 *Lamptonium* ? *fabaeforme* ? *chaunothorax* Riedel and Sanfilippo – Moore, p. 740, pl. 1, fig. 6.
1973 *Lamptonium* ? *fabaeforme* ? *chaunothorax* Riedel and Sanfilippo – Dinkelman, p. 777, pl. 2, fig. 3.
1973 *Lamptonium fabaeforme* ? *chaunothorax* Riedel and Sanfilippo – Foreman, p. 436, pl. 6, figs. 10–12.
1974 *Lamptonium fabaeforme* ? *chaunothorax* Riedel and Sanfilippo – Nigrini, p. 1067, pl. 1G, fig. 1.
1978 *Lamptonium fabaeforme chaunothorax* Riedel and Sanfilippo – Riedel and Sanfilippo, p. 69, pl. 5, fig. 11.
1978 *Lamptonium fabaeforme chaunothorax* Riedel and Sanfilippo – Foreman, p. 784, pl. 2, fig. 3.
1998a *Lamptonium fabaeforme chaunothorax* Riedel and Sanfilippo – Sanfilippo and Nigrini, p. 272, pl. 13.1, fig. 14.
2008 *Lamptonium fabaeforme chaunothorax* Riedel and Sanfilippo – Jackett et al., p. 54, pl. 2, fig. 13.
Occurrence. ODP Site 1260 (Demerara Rise; western equatorial Atlantic).

Genus *Theocotyle* Sanfilippo and Riedel, 1970
Type species.— *Theocotyle venezuelensis* Riedel and Sanfilippo, p. 525, pl. 6, fig. 10.

Theocotyle conica Foreman, 1973
Plate II.19, Figure 7

? 1969c *Theocampe piriformis* Mamedov, p. 28, pl. 2, figs. 2, 3.

1973 *Theocotyle* (*Theocotyle*) *cryptocephala* (?) *conica* Foreman, p. 440, pl. 4, fig. 11, pl. 12, figs. 19, 20.
1974 *Theocotyle* (*Theocotyle*) *cryptocephala* (?) *conica* Foreman – Nigrini, p. 1068, pl. 1I, fig. 4.
1977 *Theocotyle cryptocephala conica* Foreman – Riedel and Sanfilippo, pl. 6, fig. 4.
1982 *Theocotyle conica* Foreman – Sanfilippo and Riedel, p. 177, pl. 2, fig. 13.
1987 *Theocotyle cryptocephala* (?) *conica* Foreman – Nishimura, p. 729, pl. 2, fig. 22.
2017 *Theocotyle* (*Theocotyle*) *conica* Foreman – de Souza et al., pl. 2, figs. 9a, 9b.
Occurrence. ODP Site 1260 (Demerara Rise; western equatorial Atlantic) and ODP Site 1051 (Blake Nose; western north Atlantic).

Theocotyle cryptocephala (Ehrenberg, 1874)
Plate II.19, Figure 6

1874 *Eucyrtidium cryptocephalum* Ehrenberg, p. 277.
1876 *Eucyrtidium cryptocephalum* Ehrenberg – Ehrenberg, p. 70, pl. 11, fig. 11.
1882a *Eucyrtidium cryptocephalum* Ehrenberg – Bütschli, p. 528.
1887 *Theocampe* (*Theocamptra*) *cryptocephala* (Ehrenberg) – Haeckel, p. 1426.
1970 ? *Theocotyle cryptocephala cryptocephala* (Ehrenberg) – Riedel and Sanfilippo, p. 525, pl. 6, figs. 7, 8.
1973 ? *Theocotyle* (*Theocotyle*) *cryptocephala cryptocephala* (Ehrenberg) – Foreman, p. 440, pl. 4, figs. 6, 7, pl. 12, fig. 18.
1974 ? *Theocotyle* (*Theocotyle*) *cryptocephala cryptocephala* (Ehrenberg) – Nigrini, p. 1068, pl. 1I, figs. 2, 3.
1974 *Theocotyle* (*Theocotyle*) *cryptocephala cryptocephala* (Ehrenberg) – Johnson, p. 549, pl. 2, fig. 8.
1975 *Theocotyle* (*Theocotyle*) *cryptocephala cryptocephala* (Ehrenberg) – Ling, p. 730, pl. 10, fig. 14.
1978 *Theocotyle cryptocephala cryptocephala* (Ehrenberg) – Riedel and Sanfilippo, p. 78, pl. 9, fig. 19.
1982 *Theocotyle cryptocephala* (Ehrenberg) – Sanfilippo and Riedel, p. 178, pl. 2, figs. 4–7.
1994 *Theocotyle cryptocephala* (Ehrenberg) – Weinheimer et al., p. 312, pl. 1, figs. 9a, 9b.
2009 *Eucyrtidium cryptocephalum* Ehrenberg – Ogane et al., pl. 95, figs. 2a–2d.
2012a *Theocotyle cryptocephala* (Ehrenberg) – Kamikuri et al., p. 104, pl. 3, figs. 14a, 14b.
2017 *Theocotyle cryptocephala* (Ehrenberg) – de Souza et al., pl. 2, figs. 10a, 10b.
Occurrence. ODP Site 1260 (Demerara Rise; western equatorial Atlantic).

Theocotyle nigriniae Riedel and Sanfilippo, 1970
Plate II.19, Figure 5

1970 *Theocorys* sp. Cita et al., p. 404, pl. 2, fig. L.
1970 *Theocotyle cryptocephala* (?) *nigriniae* Riedel and Sanfilippo, p. 525, pl. 6, fig. 5 (part).
1971 *Theocotyle cryptocephala* (?) *nigriniae* Riedel and Sanfilippo – Moore, p. 740, pl. 1, fig. 10.

1973 *Theocotyle* (*Theocotyle*) *cryptocephala* (?) *nigriniae* Riedel and Sanfilippo – Foreman, p. 440, pl. 4, figs. 3–5 (part).
1974 *Theocotyle* (*Theocotyle*) *cryptocephala* (?) *nigriniae* Riedel and Sanfilippo – Nigrini, p. 1068, pl. 1I, fig. 1.
1976 *Theocotyle* (*Theocotyle*) *cryptocephala* (?) *nigriniae* Riedel and Sanfilippo – Johnson, p. 784, pl. 2, fig. 15.
1977 *Theocotyle cryptocephala nigriniae* Riedel and Sanfilippo – Riedel and Sanfilippo, pl. 5, fig. 3.
1978 *Theocotyle cryptocephala nigriniae* Riedel and Sanfilippo – Weaver and Dinkelman, p. 873, pl. 9, figs. 9–11.
1978 *Theocotyle cryptocephala nigriniae* Riedel and Sanfilippo – Riedel and Sanfilippo, p. 78, pl. 10, figs. 1, 2.
1978 *Theocotyle* (*Theocotyle*) *cryptocephala nigriniae* Riedel and Sanfilippo – Foreman, p. 784, pl. 2, fig. 15.
1982 *Theocotyle nigriniae* Riedel and Sanfilippo – Riedel and Sanfilippo, p. 178, pl. 2, figs. 1–3.
1986 *Theocotyle nigriniae* Riedel and Sanfilippo – Riedel and Sanfilippo, pl. 1, figs. 17, 18.

1994 *Theocotyle nigriniae* Riedel and Sanfilippo – Weinheimer et al., p. 312, pl. 1, figs. 8a, 8b.
1998a *Theocotyle nigriniae* Riedel and Sanfilippo – Sanfilippo and Nigrini, p. 273, pl. 13.2, figs. 17, 18.
2001 *Theocotyle nigriniae* Riedel and Sanfilippo – Sanfilippo and Blome, p. 219, figs. 11e, 11f.
2008 *Theocotyle nigriniae* Riedel and Sanfilippo – Jackett et al., p. 59, pl. 2, fig. 7.
2012a *Theocotyle nigriniae* Riedel and Sanfilippo – Kamikuri et al., p. 104, pl. 1, fig. 12.
? 2017 *Theocotyle nigriniae* Riedel and Sanfilippo – de Souza et al., pl. 2, fig. 11.
2020 *Theocotyle nigriniae* Riedel and Sanfilippo – Hollis et al., pl. 11, fig. 10.
Occurrence. ODP Site 1260 (Demerara Rise; western equatorial Atlantic) and ODP Site 1051 (Blake Nose; western north Atlantic).

Theocotyle venezuelensis Riedel and Sanfilippo, 1970
Plate II.19, Figure 8

1970 *Theocotyle venezuelensis* Riedel and Sanfilippo, p. 525, pl. 6, figs. 9, 10, pl. 7, figs. 1, 2.
1971 *Theocotyle venezuelensis* Riedel and Sanfilippo – Moore, p. 740, pl. 1, fig. 11.
1973 *Theocotyle* (*Theocotyle*) *venezuelensis* Riedel and Sanfilippo – Foreman, p. 440, pl. 4, fig. 12.
1977 *Theocotyle venezuelensis* Riedel and Sanfilippo – Riedel and Sanfilippo, pl. 7, fig. 18.
1982 *Theocotyle venezuelensis* Riedel and Sanfilippo – Sanfilippo and Riedel, p. 179, pl. 2, figs. 8–12.
2017 *Theocotyle venezuelensis* Riedel and Sanfilippo – de Souza et al., pl. 2, figs. 12a, 12b.
Occurrence. ODP Site 1260 (Demerara Rise; western equatorial Atlantic).

Genus *Theocotylissa* Foreman, 1973

Type species.— *Eucyrtidium ficus* Ehrenberg, 1874, p. 228 (unfigured); Ehrenberg, 1876, p. 70, pl. 11, fig. 19.

Theocotylissa ficus (Ehrenberg, 1874)

Plate II.19, Figure 9

1874 *Eucyrtidium Ficus* [sic] Ehrenberg, p. 228.
1876 *Eucyrtidium Ficus* [sic] Ehrenberg – Ehrenberg, p. 70, pl. 11, fig. 19.
1882a *Anthocyrtis Ficus* [sic] (Ehrenberg) – Bütschli, p. 533.
1882b *Anthocyrtis* ? *Ficus* [sic] (Ehrenberg) – Bütschli, pl. 31, fig. 7.
1887 *Theoconus* (*Theocorbis*) *ficus* (Ehrenberg) – Haeckel, p. 1403.
1969c *Cyrtocalpis originaris* Mamedov, p. 26, pl. 2, figs. 4, 5.
1970 *Theocotyle* ? *ficus* (Ehrenberg) – Riedel and Sanfilippo, p. 525, pl. 7, figs. 3–5.
1971 *Theocotyle* ? *ficus* (Ehrenberg) – Moore, p. 740, pl. 1, fig. 12.
1973 *Theocotyle* (*Theocotylissa*) *ficus* (Ehrenberg) – Foreman, p. 441, pl. 4, figs. 16–20.
1974 *Theocotyle* (*Theocotylissa*) *ficus* (Ehrenberg) – Nigrini, p. 1068, pl. 1I, figs. 5–8.
1974 *Theocotyle* (*Theocotylissa*) *ficus* (Ehrenberg) – Johnson, p. 549, pl. 4, figs. 10, 11.
1977 *Theocotyle ficus* (Ehrenberg) – Riedel and Sanfilippo, pl. 9, fig. 8.
1982 *Theocotylissa ficus* (Ehrenberg) – Sanfilippo and Riedel, p. 180, pl. 2, figs. 19, 20.
1987 *Theocotyle* ? *ficus* (Ehrenberg) – Nishimura, p. 729, pl. 2, fig. 23.
1994 *Theocotylissa ficus* (Ehrenberg) – Weinheimer et al., p. 312, pl. 1, fig. 11.
1998a *Theocotylissa ficus* (Ehrenberg) – Sanfilippo and Nigrini, p. 273, pl. 13.2, fig. 21.
2001 *Theocotylissa ficus* (Ehrenberg) – De Wever et al., p. 280, fig. 185.1.
2005 *Theocotylissa ficus* (Ehrenberg) – Nigrini et al., p. 49, pl. P5, fig. 1.
2008 *Theocotylissa ficus* (Ehrenberg) – Jackett et al., p. 59, pl. 2, fig. 8.
2009 *Eucyrtidium ficus* Ehrenberg – Ogane et al., pl. 59, figs. 2a–2c
2012 *Theocotylissa ficus* (Ehrenberg) – Moore and Kamikuri, p. 10, pl. P7, fig. 16.
2015 *Theocotylissa ficus* (Ehrenberg) – Kamikuri, pl. 8, figs. 1a, 1b.
2017 *Theocotylissa ficus* (Ehrenberg) – de Souza et al., pl. 3, figs. 10a, 10b.
2020 *Theocotylissa ficus* (Ehrenberg) – Hollis et al., pl. 11, fig. 11.

Occurrence. ODP Site 1260 (Demerara Rise; western equatorial Atlantic) and ODP Site 1051 (Blake Nose; western north Atlantic).

Genus *Thyrsocyrtis* Ehrenberg, 1847

Type species.— *Thyrsocyrtis rhizodon* Ehrenberg, 1874, p. 262 (unfigured); Ehrenberg, 1876, p. 84, pl. 12, fig.1.

Thyrsocyrtis (*Thyrsocyrtis*) *argulus* (Ehrenberg, 1874)

Plate II.19, Figure 11

1862 *Podocyrtis* ? *mitra* Ehrenberg – Bury, pl. 10, fig. 4.
1874 *Podocyrtis Argulus* [sic] Ehrenberg, p. 248.
1874 *Podocyrtis Argus* [sic] Ehrenberg, p. 248.
1874 *Podocyrtis attenuata* Ehrenberg, p. 249.
1874 *Thyrsocyrtis Rhizodon* [sic] Ehrenberg, p. 262.
1876 *Podocyrtis Argulus* [sic] Ehrenberg – Ehrenberg, p. 80, pl. 16, fig. 2.

1876 *Podocyrtis Argus* [sic] Ehrenberg – Ehrenberg, p. 80, pl. 16, fig. 9.
1876 *Podocyrtis attenuata* Ehrenberg – Ehrenberg, p. 80, pl. 16, fig. 5.
1876 *Thyrsocyrtis Rhizodon* [sic] Ehrenberg – Ehrenberg, p. 84, pl. 12, fig. 1.
1882b *Podocyrtis Rhizodon* [sic] (Ehrenberg) – Bütschli, pl. 30, fig. 11.
1887 *Podocyrtis* (*Podocyrtarium*) *tripodiscus* Haeckel, p. 1338, pl. 72, fig. 4.
? 1887 *Podocyrtis* (*Podocyrtarium*) *corythæola* Haeckel, p. 1339, pl. 72, fig. 2.
1887 *Podocyrtis* (*Podocyrtarium*) *surena* Haeckel, p. 1340, pl. 72, fig. 10.
1887 *Podocyrtis* (*Podocyrtecium*) *divergens* Haeckel, p. 1340, pl. 72, fig. 6.
1887 *Podocyrtis* (*Podocyrtecium*) *argulus* Ehrenberg – Haeckel, p. 1344.
1887 *Podocyrtis* (*Podocyrtidium*) *argus* Ehrenberg – Haeckel, p. 1346.
1887 *Thyrsocyrtis rhizodon* Ehrenberg – Haeckel, p. 1350.
1957a *Podocyrtis* aff. *P. argus* Ehrenberg – Riedel, p. 260, pl. 62, fig. 4, pl. 63, fig. 8.
1958 *Podocyrtis rhizodon* (Ehrenberg) – Göke, pl. 1, fig. 1.
1969c *Podocyrtis trifidus* Mamedov, p. 29, pl. 2, fig. 1.
1970 *Thyrsocyrtis rhizodon* Ehrenberg – Riedel and Sanfilippo, p. 525, pl. 7, figs. 6, 7.
1971 *Thyrsocyrtis rhizodon* Ehrenberg – Riedel and Sanfilippo, p. 1596, pl. 3C, fig. 6.
1971 *Thyrsocyrtis rhizodon* Ehrenberg – Moore, p. 740, pl. 2, figs. 8, 9.
1973 *Thyrsocyrtis rhizodon* Ehrenberg – Foreman, p. 442, pl. 3, fig. 1, 2.
1974 *Thyrsocyrtis rhizodon* Ehrenberg – Johnson, p. 549, pl. 4, figs. 6–9.
1975 *Thyrsocyrtis rhizodon* Ehrenberg – Holdsworth, p. 531, pl. 1, figs. 15, 22, 23.
1975 *Thyrsocyrtis* ? *rhizodon* Ehrenberg – Holdsworth, pl. 1, fig. 24.
1975 *Thyrsocyrtis rhizodon* Ehrenberg – Ling, p. 730, pl. 11, fig. 18.
1977 *Thyrsocyrtis rhizodon* Ehrenberg – Riedel and Sanfilippo, pl. 9, fig. 9.
1982 *Thyrsocyrtis* (*Thyrsocyrtis*) *rhizodon* Ehrenberg – Sanfilippo and Riedel, p. 173, pl. 1, figs. 14–16, pl. 3, figs. 12–17.
1994 *Thyrsocyrtis* (*Thyrsocyrtis*) *rhizodon* Ehrenberg – Weinheimer et al., p. 312, pl. 1, fig. 12.
2000 *Thyrsocyrtis* (*Thyrsocyrtis*) *rhizodon* Ehrenberg – Nigrini and Sanfilippo, p. 75, pl. 1, fig. 14.
2001 *Thyrsocyrtis rhizodon* Ehrenberg – Sanfilippo and Blome, p. 220, figs. 7k, 7o.
2001 *Thyrsocyrtis* (*Thyrsocyrtis*) *rhizodon* Ehrenberg – De Wever et al., p. 280, fig. 185.5.
2008 *Thyrsocyrtis* (*Thyrsocyrtis*) *rhizodon* Ehrenberg – Jackett et al., p. 59, pl. 2, fig. 11.
2009 *Podocyrtis argulus* Ehrenberg – Ogane et al., pl. 24, figs. 5a–5d.
2009 *Podocyrtis argus* Ehrenberg – Ogane et al., pl. 10, figs. 6a–6c, pl. 95, figs. 3a–3d.
2009 *Podocyrtis attenuata* Ehrenberg – Ogane et al., pl. 56, figs. 2a–2d.
2009 *Thyrsocyrtis rhizodon* Ehrenberg – Ogane et al., pl. 56, figs. 1a–1e.
2012 *Thyrsocyrtis* (*Thyrsocyrtis*) *rhizodon* Ehrenberg – Moore and Kamikuri, p. 12, pl. P10, fig. 1.
2012 *Thyrsocyrtis* (*Thyrsocyrtis*) *rhizodon* Ehrenberg – Kamikuri and Wade, pl. 1, figs. 3a, 3b.
2015 *Thyrsocyrtis* (*Thyrsocyrtis*) *rhizodon* Ehrenberg – Kamikuri, pl. 11, figs. 1a–2b, 7a, 7b, pl. 19, fig. 6a, 6b.
2017 *Thyrsocyrtis* (*Thyrsocyrtis*) *rhizodon* Ehrenberg – de Souza et al., pl. 3, figs. 4a, 4b.

2020 *Thyrsocyrtis* (*Thyrsocyrtis*) *rhizodon* Ehrenberg – Hollis et al., pl. 11, figs. 16a–18b.
Remarks. The combination used here is derived from O'Dogherty et al. (2021).
Occurrence. ODP Site 1260 (Demerara Rise; western equatorial Atlantic) and ODP Site 1051 (Blake Nose; western north Atlantic).

Thyrsocyrtis (*Thyrsocyrtis*) *bromia* Ehrenberg, 1874 group
Plate II.19, Figure 13

1874 *Thyrsocyrtis Bromia* [sic] Ehrenberg, p. 260.
1876 *Thyrsocyrtis Bromia* [sic] Ehrenberg – Ehrenberg, p. 84, pl. 12, fig. 12.
1887 *Podocyrtis* (*Podocyrtonium*) *bromia* (Ehrenberg) – Haeckel, p. 1349.
1971 *Thyrsocyrtis bromia* Ehrenberg – Riedel and Sanfilippo, p. 1596, pl. 8, fig. 6.
1971 *Thyrsocyrtis bromia* Ehrenberg – Moore, p. 740, pl. 5, figs. 1–3.
1973 *Thyrsocyrtis bromia* Ehrenberg – Dinkelman, p. 787, pl. 3, figs. 1–4, 6.
1973 *Thyrsocyrtis* sp. aff. *T. bromia* Ehrenberg – Dinkelman, pl. 3, figs. 5.
1974 *Thyrsocyrtis bromia* Ehrenberg – Nigrini, p. 1068, pl. 2D, fig. 6.
1974 *Thyrsocyrtis bromia* Ehrenberg – Johnson, p. 549, pl. 5, fig. 7.
1975 *Thyrsocyrtis bromia* Ehrenberg – Holdsworth, p. 531, pl. 1, figs. 12–14, 19–21.
1975 *Thyrsocyrtis bromia* Ehrenberg – Ling, p. 730, pl. 11, figs. 15, 16.
1977 *Thyrsocyrtis bromia* Ehrenberg – Riedel and Sanfilippo, pl. 11, fig. 2.
1978 *Thyrsocyrtis bromia* Ehrenberg – Riedel and Sanfilippo, p. 78, pl. 10, figs. 4, 5.
1982 *Thyrsocyrtis* (*Thyrsocyrtis*) *bromia* Ehrenberg – Sanfilippo and Riedel, p. 172, pl. 1, fig. 20 (part).
1986 *Thyrsocyrtis bromia* Ehrenberg – Riedel and Sanfilippo, pl. 6, fig. 1.
2006 *Thyrsocyrtis* (*Thyrsocyrtis*) *bromia* Ehrenberg – Funakawa et al., p. 33, pl. P11, figs. 3a, 3b.
2006 *Thyrsocyrtis* (*Thyrsocyrtis*) *bromia* Ehrenberg form A– Funakawa et al., p. 33, pl. P11, figs. 4a–6b.
2012 *Thyrsocyrtis* (*Thyrsocyrtis*) *bromia* Ehrenberg – Moore and Kamikuri, p. 11, pl. P9, figs. 3–10.
2012 *Thyrsocyrtis* (*Thyrsocyrtis*) *bromia* Ehrenberg – Kamikuri and Wade, pl. 1, figs. 8a, 8b.
2012b *Thyrsocyrtis* (*Thyrsocyrtis*) *bromia* Ehrenberg – Kamikuri et al., p. 5, pl. P2, figs. 8a, 8b.
2015 *Thyrsocyrtis* (*Thyrsocyrtis*) *bromia* Ehrenberg – Kamikuri, pl. 11, figs. 8a, 8b.
Occurrence. ODP Site 1051 (Blake Nose; western north Atlantic).

Thyrsocyrtis (*Thyrsocyrtis*) *norrisi* Sanfilippo and Blome, 2001
Plate II.19, Figure 12

2009 *Thyrsocyrtis* (*Thyrsocyrtis*) *norrisi* Sanfilippo and Blome, p. 207, figs. 7f–7j, 7l, 7m.
2015 *Thyrsocyrtis* (*Thyrsocyrtis*) *norrisi* Sanfilippo and Blome – Kamikuri, pl. 7, figs. 7a–8b.
Occurrence. ODP Site 1260 (Demerara Rise; western equatorial Atlantic) and ODP Site 1051 (Blake Nose; western north Atlantic).

Thyrsocyrtis (*Thyrsocyrtis*) *robusta* Riedel and Sanfilippo, 1970
Plate II.19, Figure 10

1970 *Thyrsocyrtis hirsuta robusta* Riedel and Sanfilippo, p. 526, pl. 8, fig. 1.
1971 *Thyrsocyrtis hirsuta robusta* Riedel and Sanfilippo – Moore, p. 740, pl. 2, fig. 7.
1973 *Thyrsocyrtis hirsuta robusta* Riedel and Sanfilippo – Foreman, p. 442, pl. 3, fig. 17.
1974 *Thyrsocyrtis hirsuta robusta* Riedel and Sanfilippo – Nigrini, p. 1069, pl. 1J, figs. 3, 4.
1977 *Thyrsocyrtis hirsuta robusta* Riedel and Sanfilippo – Riedel and Sanfilippo, pl. 6, fig. 3.
2012b *Thyrsocyrtis* (*Thyrsocyrtis*) *robusta* Riedel and Sanfilippo – Kamikuri et al., p. 5, pl. P2, figs. 1a, 1b.
2017 *Thyrsocyrtis* (*Thyrsocyrtis*) *robusta* Riedel and Sanfilippo – de Souza et al., pl. 3, figs. 5a, 5b.

Occurrence. ODP Site 1260 (Demerara Rise; western equatorial Atlantic).

Thyrsocyrtis (*Pentalacorys*) *parvipes* (Ehrenberg, 1874)
Plate II.20, Figure 1

1874 *Podocyrtis parvipes* Ehrenberg, p. 252.
1876 *Podocyrtis parvipes* Ehrenberg – Ehrenberg, p. 82, pl. 14, fig. 4.
1973 *Thyrsocyrtis tetracantha* (Ehrenberg) – Dinkelman, p. 787, pl. 2, figs. 4, 5.
1973 *Thyrsocyrtis* cf. *T. triacantha* (Ehrenberg) – Dinkelman, pl. 2, fig. 8.
? 1973 *Thyrsocyrtis* sp. aff. *T. bromia* Ehrenberg – Dinkelman, pl. 3, fig. 5.
1974 *Thyrsocyrtis tetracantha* (Ehrenberg) – Johnson, p. 549, pl. 5, fig. 15.
1977 *Thyrsocyrtis tetracantha* (Ehrenberg) – Riedel and Sanfilippo, pl. 11, fig. 3 (part).
1978 *Thyrsocyrtis tetracantha* (Ehrenberg) – Riedel and Sanfilippo, p. 81, pl. 10, fig. 9 (part).
1985 *Thyrsocyrtis* (*Pentalacorys*) *tetracantha* (Ehrenberg) – Sanfilippo et al., p. 690, fig. 26.8b (part).
1982 *Thyrsocyrtis* (*Pentalacorys*) *tetracantha* (Ehrenberg) – Sanfilippo and Riedel, p. 176 pl. 1, fig. 11 (part).
1986 *Thyrsocyrtis* (*Pentalacorys*) *tetracantha* (Ehrenberg) – Riedel and Sanfilippo, pl. 6, fig. 3.
2000 *Thyrsocyrtis* (*Pentalacorys*) *tetracantha* (Ehrenberg) – Nigrini and Sanfilippo, p. 74, pl. 1, fig. 2.
2001 *Thyrsocyrtis* (*Pentalacorys*) *krooni* Sanfilippo and Blome, p. 207, figs. 7a–7e.
2006 *Thyrsocyrtis* (*Pentalacorys*) *tetracantha* (Ehrenberg) – Funakawa et al., p. 31, pl. P11, figs. 9a, 9b.
2009 *Podocyrtis parvipes* Ehrenberg Ogane et al., pl. 87, figs. 5a, 5b, pl. 90, figs. 6a, 6b.
2012 *Thyrsocyrtis* (*Pentalacorys*) *krooni* Sanfilippo and Blome – Moore and Kamikuri, p. 11, pl. P8, figs. 7, 8.
2015 *Thyrsocyrtis* (*Pentalacorys*) *krooni* Sanfilippo and Blome – Kamikuri, pl. 4, figs. 3a, 3b, 6a–7b.

Remarks. The combination used here is derived from O'Dogherty et al. (2021).
Occurrence. ODP Site 1260 (Demerara Rise; western equatorial Atlantic) and ODP Site 1051 (Blake Nose; western north Atlantic).

Thyrsocyrtis (*Pentalacorys*) *schomburgkii* (Ehrenberg, 1847)
Plate II.19, Figures 14, 15

1847 *Podocyrtis Schomburgkii* [sic] Ehrenberg, p. 55, fig. 1.
1854a *Podocyrtis Schomburgkii* [sic] Ehrenberg – Ehrenberg, pl. 36, fig. 22.
1854a *Podocyrtis cothurnata* Ehrenberg, pl. 36, fig. B21.
1862 *Podocyrtis cothurnata* Ehrenberg – Bury, pl. 7, fig. 7.
1862 *Anthocyrtis cothurnata* (Ehrenberg) – Haeckel, p. 310.
1862 *Podocyrtis Schomburgki* [sic] Ehrenberg – Haeckel, p. 339.
1874 *Podocyrtis bicornis* Ehrenberg, p. 249.
1874 *Podocyrtis Centriscus* [sic] Ehrenberg, p. 249.
1874 *Podocyrtis cothurnata* Ehrenberg – Ehrenberg, p. 250.
1874 *Podocyrtis Dipus* [sic] Ehrenberg – Ehrenberg, p. 250.
1874 *Podocyrtis Euceros* [sic] Ehrenberg, p. 250.
1874 *Podocyrtis Princeps* [sic] Ehrenberg, p. 252.
1874 *Podocyrtis radicata* Ehrenberg, p. 253.
1874 *Podocyrtis Schomburgkii* [sic] Ehrenberg – Ehrenberg, p. 253.
1874 *Podocyrtis Triacantha* [sic] Ehrenberg, p. 254.
1874 *Podocyrtis ventricosa* Ehrenberg, p. 254.
1876 *Podocyrtis bicornis* Ehrenberg – Ehrenberg, p. 80, pl. 16, fig. 8.
1876 *Podocyrtis Centriscus* [sic] Ehrenberg – Ehrenberg, p. 80, pl. 14, fig. 2.
1876 *Podocyrtis cothurnata* Ehrenberg – Ehrenberg, p. 82, pl. 14, fig. 1.
1876 *Podocyrtis Dipus* [sic] Ehrenberg – Ehrenberg, p. 82, pl. 12, fig. 11.
1876 *Podocyrtis Euceros* [sic] Ehrenberg – Ehrenberg, p. 82, pl. 15, fig. 1.
1876 *Podocyrtis Princeps* [sic] Ehrenberg – Ehrenberg, p. 82, pl. 13, fig. 1.
1876 *Podocyrtis radicata* Ehrenberg – Ehrenberg, p. 82, pl. 13, fig. 5.
1876 *Podocyrtis schomburgkii* Ehrenberg – Ehrenberg, p. 82, pl. 14, fig. 7.
1876 *Podocyrtis Triacantha* [sic] Ehrenberg – Ehrenberg, p. 82, pl. 13, fig. 4.
1876 *Podocyrtis ventricosa* Ehrenberg – Ehrenberg, p. 82, pl. 16, fig. 3.
1879 *Dictyopodium moseleyi* Haeckel, p. 706, pl. 16, fig. 10.
1882a *Podocyrtis Princeps* [sic] Ehrenberg – Bütschli, p. 540, pl. 33, figs. 32a–32c.
1882b *Podocyrtis cothurnata* Ehrenberg – Bütschli, pl. 30, fig. 13.
1882b *Podocyrtis Princeps* [sic] Ehrenberg – Bütschli, pl. 30, figs. 14a–14b.
1887 *Podocyrtis* (*Podocyrtecium*) *ventricosa* Ehrenberg – Haeckel, p. 1341.
? 1887 *Podocyrtis* (*Podocyrtecium*) *flosculata* Haeckel, p. 1341, pl. 72, fig. 9.
1887 *Podocyrtis* (*Podocyrtecium*) *centriscus* Ehrenberg – Haeckel, p. 1341.
1887 *Podocyrtis* (*Podocyrtecium*) *magnifica* Haeckel, p. 1341.
1887 *Podocyrtis* (*Podocyrtecium*) *princeps* Ehrenberg – Haeckel, p. 1342.
1887 *Podocyrtis* (*Podocyrtecium*) *euceros* Ehrenberg – Haeckel, p. 1342.
1887 *Podocyrtis* (*Podocyrtecium*) *cristata* Haeckel, p. 1342, pl. 72, fig. 7.
1887 *Podocyrtis* (*Podocyrtecium*) *schomburgkii* Ehrenberg – Haeckel, p. 1343.
1887 *Podocyrtis* (*Podocyrtonium*) *tripus* Haeckel, p. 1349.
1887 *Podocyrtis* (*Podocyrtonium*) *triacantha* Ehrenberg – Haeckel, p. 1350.
1887 *Thyrsocyrtis radicata* (Ehrenberg) – Haeckel, p. 1351.

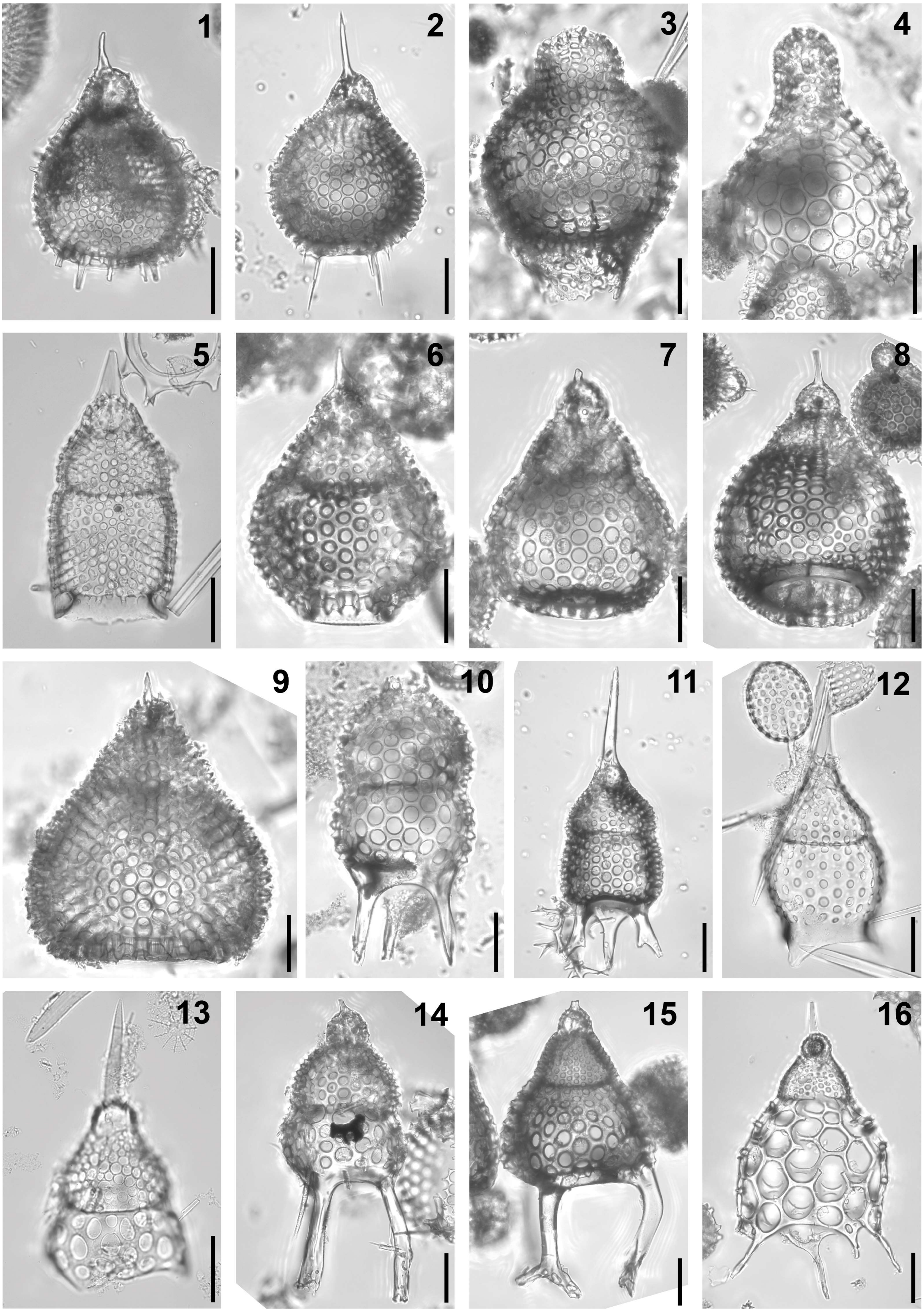
1
2
3
4
5
6
7
8
9
10
11
12
13
14
15
16

Plate II.19. Composite light micrographs of new radiolarian species from ODP Site 1260 (Demerara Rise, western equatorial Atlantic) and ODP Site 1051 (Blake Nose, western North Atlantic). (**1, 2**) *Anthocyrtoma leptostyla* (Ehrenberg, 1874): (**1**) ODP 1260A-13R-CC, 63–177 cm; (**2**) ODP 1260A-16R-1W, 55–57 cm. (**3**) *Lamptonium fabaeforme fabaeforme* (Krasheninnikov, 1960): ODP 1260A-20R-4W, 55–57 cm. (**4**) *Lamptonium fabaeforme chaunothorax* Riedel and Sanfilippo, 1970: ODP 1260A-20R-4W, 55–57 cm. (**5**) *Theocotyle nigriniae* Riedel and Sanfilippo, 1970: ODP 1051A-38X-5W, 55–57 cm. (**6**) *Theocotyle cryptocephala* (Ehrenberg, 1874): ODP 1260A-19R-CC, 63–177 cm. (**7**) *Theocotyle conica* Foreman, 1973: ODP 1260A-17R-CC, 63–177 cm. (**8**) *Theocotyle venezuelensis* Riedel and Sanfilippo, 1970: ODP 1260A-17R-CC, 63–177 cm. (**9**) *Theocotylissa ficus* (Ehrenberg, 1874): ODP 1260A-15R-2W, 55–57 cm. (**10**) *Thyrsocyrtis* (*Thyrsocyrtis*) *robusta* Riedel and Sanfilippo, 1970: ODP 1260A-20R-4W, 55–57 cm. (**11**) *Thyrsocyrtis* (*Thyrsocyrtis*) *argulus* (Ehrenberg, 1874): ODP 1260A-9R-3W, 55–57 cm. (**12**) *Thyrsocyrtis* (*Thyrsocyrtis*) *norrisi* Sanfilippo and Blome, 2001: ODP 1051A-13H-5W, 58–60 cm. (**13**) *Thyrsocyrtis* (*Thyrsocyrtis*) *bromia* Ehrenberg, 1874 group: ODP 1051A-2H-5W, 55–57 cm. (**14, 15**) *Thyrsocyrtis* (*Pentalacorys*) *schomburgkii* (Ehrenberg, 1847): (**14**) early morphotype, ODP 1260A-20R-1W, 55–57 cm; (**15**) ODP 1260A-10R-5W, 55–57 cm. (**16**) *Thyrsocyrtis* (*Pentalacorys*) *tetracantha* (Ehrenberg, 1874): ODP 1260A-6R-2W, 55–57 cm. All scale bars equal 50 µm.

1887 *Dictyopodium scaphopodium* Haeckel, p. 1353, pl. 73, fig. 8.
1887 *Dictyopodium cothurnatum* (Ehrenberg) – Haeckel, p. 1353.
1887 *Dictyopodium thyrsolophus* Haeckel, p. 1354, pl. 73, fig. 7.
1944 *Podocyrtis* (*Podocyrtecium*) *elegantissima* Campbell and Clark, p. 29, pl. 7, fig. 25.
1957a *Podocyrtis triacantha* Ehrenberg – Riedel, p. 260, pl. 63, fig. 9.
1958 *Podocyrtis triacantha* Ehrenberg – Göke, pl. 1, fig. 6.
1970 *Thyrsocyrtis triacantha* (Ehrenberg) – Riedel and Sanfilippo, p. 526, pl. 8, figs. 2, 3.
1971 *Thyrsocyrtis triacantha* (Ehrenberg) – Riedel and Sanfilippo, p. 1596, pl. 3C, fig. 7.
1971 *Thyrsocyrtis triacantha* (Ehrenberg) – Moore, p. 740, pl. 4, fig. 2.
1972 *Thyrsocyrtis triacantha* (Ehrenberg) – Petrushevskaya and Kozlova, p. 542, pl. 32, fig. 9, pl. 34, fig. 6.
1973 *Thyrsocyrtis triacantha* (Ehrenberg) – Dinkelman, p. 787, pl. 2, fig. 7.
1973 *Thyrsocyrtis triacantha* (Ehrenberg) – Foreman, p. 442, pl. 12, figs. 9–11.
1974 *Thyrsocyrtis triacantha* (Ehrenberg) – Nigrini, p. 1069, pl. 1J, figs. 5–7, pl. 2E, fig. 1.
1974 *Thyrsocyrtis triacantha* (Ehrenberg) – Johnson, p. 549, pl. 5, fig. 16.
1975 *Thyrsocyrtis triacantha* (Ehrenberg) – Holdsworth, p. 531, pl. 1, fig. 18.
1975 *Thyrsocyrtis triacantha* (Ehrenberg) – Ling, p. 730, pl. 11, fig. 20.
1977 *Thyrsocyrtis triacantha* (Ehrenberg) – Riedel and Sanfilippo, pl. 8, figs. 2, 3.
1978 *Thyrsocyrtis triacantha* (Ehrenberg) – Riedel and Sanfilippo, p. 82, pl. 10, figs. 10, 11.
1982 *Thyrsocyrtis* (*Pentalacorys*) *triacantha* (Ehrenberg) – Sanfilippo and Riedel, p. 176, pl. 1, figs. 8–10, pl. 3, figs. 3, 4, text-fig. 1.
1985 *Thyrsocyrtis* (*Pentalacorys*) *triacantha* (Ehrenberg) – Sanfilippo et al., p. 690, figs. 26.7a, 26.7b.

1986 *Thyrsocyrtis* (*Pentalacorys*) *triacantha* (Ehrenberg) – Riedel and Sanfilippo, pl. 4, fig. 18, pl. 6, fig. 2.
1993 *Thyrsocyrtis* (*Pentalacorys*) *triacantha* (Ehrenberg) – Hull, p. 13, pl. 7, fig. 12, pl. 8, fig. 2.
2000 *Thyrsocyrtis* (*Pentalacorys*) *triacantha* (Ehrenberg) – Nigrini and Sanfilippo, p. 74, pl. 1, figs. 13, 16, 17.
2006 *Thyrsocyrtis* (*Pentalacorys*) *triacantha* (Ehrenberg) – Funakawa et al., p. 32, pl. P11, figs. 8a, 8b.
2009 *Podocyrtis bicornis* Ehrenberg – Ogane et al., pl. 9, figs. 8a–8d, pl. 55, figs. 2a–2e.
2009 *Podocyrtis euceros* Ehrenberg – Ogane et al., pl. 10, figs. 4a, 4b.
2009 *Podocyrtis schomburgkii* Ehrenberg – Ogane et al., pl. 57, figs. 1a–1f.
2009 *Podocyrtis dipus* Ehrenberg – Ogane et al., pl. 91, figs. 1a–1d.
2009 *Podocyrtis triacantha* Ehrenberg – Ogane et al., pl. 91, figs. 2a–3c.
2009 *Podocyrtis tetracantha* Ehrenberg – Ogane et al., pl. 91, figs. 4a–4c (part).
2012 *Thyrsocyrtis* (*Pentalacorys*) *triacantha* (Ehrenberg) – Moore and Kamikuri, p. 11, pl. P9, figs. 1, 2.
2012 *Thyrsocyrtis* (*Pentalacorys*) *triacantha* (Ehrenberg) – Kamikuri and Wade, pl. 1, figs. 2a, 2b.
2012b *Thyrsocyrtis* (*Pentalacorys*) *triacantha* (Ehrenberg) – Kamikuri et al., p. 5, pl. P2, figs. 2a, 2b.
2013 *Thyrsocyrtis* (*Pentalacorys*) *triacantha* (Ehrenberg) – Kamikuri et al., pl. 1, figs. 10a, 10b.
2015 *Thyrsocyrtis* (*Pentalacorys*) *triacantha* (Ehrenberg) – Kamikuri, pl. 4, figs. 4a–5b, 8.
2017 *Thyrsocyrtis* (*Pentalacorys*) *triacantha* (Ehrenberg) – de Souza et al., pl. 3, fig. 8.

Remarks. The combination used here is derived from O'Dogherty et al. (2021).

Occurrence. ODP Site 1260 (Demerara Rise; western equatorial Atlantic) and ODP Site 1051 (Blake Nose; western north Atlantic).

Thyrsocyrtis (*Pentalacorys*) *tetracantha* (Ehrenberg, 1874)
Plate II.19, Figure 16

1862 *Podocyrtis Schomburgki* [sic] Ehrenberg – Bury, pl. 17, fig. 2.
? 1874 *Podocyrtis aculeata* Ehrenberg, p. 248.
? 1874 *Podocyrtis Pentacantha* [sic] Ehrenberg, p. 252.
1874 *Podocyrtis Tetracantha* [sic] Ehrenberg, p. 254.
? 1876 *Podocyrtis aculeata* Ehrenberg – Ehrenberg, p. 80, pl. 13, fig. 3.
? 1876 *Podocyrtis Pentacantha* [sic] Ehrenberg – Ehrenberg, p. 82, pl. 17, fig. 1.
1876 *Podocyrtis Tetracantha* [sic] Ehrenberg – Ehrenberg, p. 82, pl. 13, fig. 2.
? 1882a *Podocyrtis aculeata* Ehrenberg – Bütschli, pl. 33, figs. 34a, 34b.
1887 *Alacorys* (*Tetralacorys*) *tetracantha* (Ehrenberg) – Haeckel, p. 1371.
1887 *Alacorys* (*Hexalacorys*) *guilelmi* Haeckel, p. 1372, pl. 65, fig. 2.
? 1887 *Alacorys* (*Octalacorys*) *aculeata* (Ehrenberg) – Haeckel, p. 1373.
1971 *Thyrsocyrtis tetracantha* (Ehrenberg) – Moore, p. 741, pl. 4, fig. 3.

1974 *Thyrsocyrtis tetracantha* (Ehrenberg) – Nigrini, p. 1069, pl. 2E, fig. 2.
1975 *Thyrsocyrtis tetracantha* (Ehrenberg) – Ling, p. 730, pl. 11, fig. 19.
1977 *Thyrsocyrtis tetracantha* (Ehrenberg) – Riedel and Sanfilippo, pl. 11, fig. 4 (part).
1978 *Thyrsocyrtis tetracantha* (Ehrenberg) – Riedel and Sanfilippo, p. 81, pl. 10, fig. 8 (part).
1982 *Thyrsocyrtis* (*Pentalacorys*) *tetracantha* (Ehrenberg) – Sanfilippo and Riedel, p. 176, pl. 1, fig. 12, pl. 3, fig. 10, text-fig. 1 (part).
1985 *Thyrsocyrtis* (*Pentalacorys*) *tetracantha* (Ehrenberg) – Sanfilippo et al., p. 690, fig. 26.8a (part).
2009 *Podocyrtis tetracantha* Ehrenberg – Ogane et al., pl. 90, figs. 4a, 4b, pl. 92, figs. 1a–2b (part).
2001 *Thyrsocyrtis* (*Pentalacorys*) *tetracantha* (Ehrenberg) – De Wever et al., p. 280, fig. 185.4.
2009 *Podocyrtis aculeata* Ehrenberg – Ogane et al., pl. 92, figs. 3a–3d.
2009 *Podocyrtis pentacantha* Ehrenberg – Ogane et al., pl. 93, figs. 1a–1d.
2012a *Thyrsocyrtis* (*Pentalacorys*) *tetracantha* (Ehrenberg) – Kamikuri et al., p. 104, pl. 3, figs. 4a, 4b.

Occurrence. ODP Site 1260 (Demerara Rise; western equatorial Atlantic).

Family Theoperidae Haeckel, 1882 emend. Riedel, 1967b

Genus *Artophormis* Haeckel, 1882

Type species.— *Artophormis horrida* Haeckel, 1887, p. 1458, pl. 75, fig. 2.

Artophormis ? *barbadensis* (Ehrenberg, 1874)

Plate II.20, Figure 2

1874 *Calocyclas barbadensis* Ehrenberg, p. 217.
1874 *Thyrsocyrtis anthophora* Ehrenberg, p. 260.
1876 *Calocyclas barbadensis* Ehrenberg – Ehrenberg, p. 66, pl. 18, fig. 8.
1876 *Thyrsocyrtis anthophora* Ehrenberg – Ehrenberg, p. 84, pl. 12, fig. 9.
1887 *Artophormis barbadensis* (Ehrenberg) – Haeckel, p. 1459.
1887 *Eucyrtidium* (*Artocyrtis*) *anthophorum* (Ehrenberg) – Haeckel, p. 1491.
1970 *Artophormis barbadensis* (Ehrenberg) – Riedel and Sanfilippo, p. 532, pl. 13, fig. 5.
1971 *Artophormis barbadensis* (Ehrenberg) – Riedel and Sanfilippo, p. 1592, pl. 3B, figs. 8, 9.
? 1971 *Artophormis barbadensis* (Ehrenberg) – Moore, p. 742, pl. 5, fig. 9.
1974 *Artophormis barbadensis* (Ehrenberg) – Johnson, p. 547, pl. 5, fig. 6.
1975 *Artophormis barbadensis* (Ehrenberg) – Ling, p. 728, pl. 9, figs. 9, 10.
1977 *Artophormis barbadensis* (Ehrenberg) – Riedel and Sanfilippo, pl. 10, fig. 12.
1985 *Artophormis barbadensis* (Ehrenberg) – Sanfilippo et al., p. 666, figs. 12.1a, 12.1b.
2006 *Artophormis barbadensis* (Ehrenberg) – Funakawa et al., p. 21, pl. P4, figs. 1a, 1b.
2009 *Thyrsocyrtis anthophora* Ehrenberg – Ogane et al., pl. 1, figs. 7a–7e.
2009 *Calocyclas barbadensis* Ehrenberg – Ogane et al., pl. 96, fig. 3a–3c.
2012 *Artophormis barbadensis* (Ehrenberg) – Moore and Kamikuri, p. 5, pl. P1, fig. 2.
2015 *Artophormis barbadensis* (Ehrenberg) – Kamikuri, pl. 9, figs. 14a, 14b.
2017 *Artophormis barbadensis* (Ehrenberg) – de Souza et al., pl. 2, figs. 2a, 2b.

Occurrence. ODP Site 1260 (Demerara Rise; western equatorial Atlantic) and ODP Site 1051 (Blake Nose; western north Atlantic).

Genus *Calocyclas* Ehrenberg, 1847

Type species.— *Calocyclas turris* Ehrenberg, 1847b, p. 218 (unfigured); Ehrenberg, 1876, p. 66, pl. 18, fig. 7.

Calocyclas aphradia Sanfilippo and Blome, 2001

Plate II.20, Figure 3

1974 Theoperid gen. et sp. indet. Sanfilippo and Riedel, pl. 3, figs. 5, 6.
1979 Unidentified theoperid Sanfilippo and Riedel, pl. 1, fig. 12.
2001 *Calocyclas aphradia* Sanfilippo and Blome, p. 202, figs. 6d–6f.
2015 *Calocyclas aphradia* Sanfilippo and Blome – Kamikuri, pl. 9, fig. 15.

Occurrence. ODP Site 1051 (Blake Nose; western north Atlantic).

Calocyclas ? *chrysallis* (Sanfilippo and Blome, 2001)

Plate II.20, Figure 6

1975 *Sethocyrtis* sp. Chen, p. 459, pl. 1, fig. 5 (part).
1992 *Sethocyrtis* sp. Takemura, p. 747, pl. 7, figs. 14, 15.
1995 *Sethocyrtis* ? spp. Strong et al., p. 209, fig. 11W.
1997 *Sethocyrtis* sp. Takemura and Ling, p. 114, pl. 1, fig. 11.
1997 *Sethocyrtis* sp. A Hollis et al., p. 65, pl. 6, fig. 7.
2001 *Sethocyrtis chrysallis* Sanfilippo and Blome, p. 206, figs. 6j–6n.
2015 *Sethocyrtis chrysallis* Sanfilippo and Blome – Kamikuri, pl. 11, figs. 14–15b.
2020 *Sethocyrtis chrysallis* Sanfilippo and Blome – Hollis et al., pl. 10, figs. 20a, 20b.

Remarks. The combination used here is derived from O'Dogherty et al. (2021).

Occurrence. ODP Site 1260 (Demerara Rise; western equatorial Atlantic) and ODP Site 1051 (Blake Nose; western north Atlantic).

Calocyclas hispida (Ehrenberg, 1874)

Plate II.20, Figure 4

1874 *Anthocyrtis hispida* Ehrenberg, p. 216.
1876 *Anthocyrtis hispida* Ehrenberg – Ehrenberg, p. 64, pl. 8, fig. 2.
1882a *Anthocyrtis hispida* Ehrenberg – Bütschli, pl. 33, figs. 30a, 30b.
1882b *Anthocyrtis hispida* Ehrenberg – Bütschli, pl. 31, fig. 5.
1887 *Anthocyrtidium* (*Anthocyrtonium*) *hispidum* (Ehrenberg) – Haeckel, p. 1275.
1957a ? *Anthocyrtidium hispidum* (Ehrenberg) – Riedel, p. 260, pl. 63, fig. 7.
1970 *Anthocyrtidium hispidum* (Ehrenberg) – Cita et al., p. 403, pl. 1, fig. G.
1970 *Cycladophora hispida* (Ehrenberg) – Riedel and Sanfilippo, p. 529, pl. 10, fig. 9.
1971 *Cycladophora hispida* (Ehrenberg) – Riedel and Sanfilippo, p. 1593, pl. 3B, figs. 10, 11.
1971 *Cycladophora hispida* (Ehrenberg) – Moore, p. 741, pl. 4, figs. 6, 7.
1973 *Calocyclas hispida* (Ehrenberg) – Foreman, p. 434, pl. 1, figs. 12–15, pl. 9, fig. 18.
1974 *Calocyclas hispida* (Ehrenberg) – Nigrini, p. 1067, pl. 1F, figs. 5–8.

1974 *Calocyclas hispida* (Ehrenberg) – Johnson, p. 547, pl. 4, fig. 1.
1975 *Calocyclas hispida* (Ehrenberg) – Chen, p. 459, pl. 3, fig. 10.
1975 *Calocyclas hispida* (Ehrenberg) – Ling, p. 728, pl. 9, fig. 12.
1977 *Calocyclas hispida* (Ehrenberg) – Riedel and Sanfilippo, pl. 9, fig. 10.
1978 *Calocyclas hispida* (Ehrenberg) – Riedel and Sanfilippo, p. 65, pl. 3, fig. 6.
1986 *Calocyclas hispida* (Ehrenberg) – Riedel and Sanfilippo, pl. 2, fig. 10.
1993 *Calocyclas hispida* (Ehrenberg) – Hull, p. 12, pl. 7, fig. 1.
not 2001 *Calocyclas hispida* (Ehrenberg) s.s. – Sanfilippo and Blome, p. 210, fig. 6g.
2001 *Calocyclas hispida* (Ehrenberg) var. A – Sanfilippo and Blome, p. 211, fig. 8m.
2006 *Calocyclas hispida* (Ehrenberg) – Funakawa et al., p. 22, pl. P5, figs. 4a, 4b.
2008 *Calocyclas hispida* (Ehrenberg) – Jackett et al., p. 48, pl. 2, fig. 1.
2009 *Anthocyrtis hispida* Ehrenberg – Ogane et al., pl. 2, figs. 7a–9c, pl. 50, figs. 4a, 4b.
2012 *Calocyclas hispida* (Ehrenberg) – Moore and Kamikuri, p. 5, pl. P1, figs. 7, 8.
2012 *Calocyclas hispida* (Ehrenberg) – Kamikuri and Wade, pl. 1, figs. 1a, 1b.
2012b *Calocyclas hispida* (Ehrenberg) – Kamikuri et al., p. 3, pl. P1, figs. 8a, 8b.
2015 *Calocyclas hispida* (Ehrenberg) – Kamikuri, pl. 8, figs. 9a–10b.
2017 *Calocyclas hispida* (Ehrenberg) – de Souza et al., pl. 2, figs. 5a, 5b.
2020 *Calocyclas hispida* (Ehrenberg) – Hollis et al., pl. 9, figs. 5a, 5b.

Occurrence. ODP Site 1260 (Demerara Rise; western equatorial Atlantic) and ODP Site 1051 (Blake Nose; western north Atlantic).

Calocyclas turris Ehrenberg, 1874
Plate II.20, Figure 5

1874 *Calocyclas Turris* [sic] Ehrenberg, p. 218.
1874 *Cycladophora stiligera* Ehrenberg, p. 223.
1876 *Calocyclas Turris* [sic] Ehrenberg – Ehrenberg, p. 66, pl. 18, fig. 7.
1876 *Cycladophora stiligera* Ehrenberg – Ehrenberg, p. 68, pl. 18, fig. 3.
1882a *Calocyclas Turris* [sic] Ehrenberg – Bütschli, p. 534.
1882b *Cycladophora stiligera* Ehrenberg – Bütschli, pl. 30, fig. 16.
1882b *Calocyclas Turris* [sic] Ehrenberg – Bütschli, pl. 31, fig. 9.
1887 *Cycladophora* (*Cyclamptidium*) *fenestrata* Haeckel, p. 1380, pl. 68, fig. 2.
1887 *Calocyclas* (*Calocyclissa*) *turris* Ehrenberg – Haeckel, p. 1383.
1957b *Calocyclas turris* Ehrenberg – Riedel, p. 89, pl. 3, fig. 8, pl. 4, figs. 1, 2.
1957a *Calocyclas turris* Ehrenberg – Riedel, p. 261, pl. 62, fig. 6.
1970 *Cycladophora turris* (Ehrenberg) – Riedel and Sanfilippo, p. 529, pl. 13, figs. 3, 4.
1971 *Cycladophora turris* (Ehrenberg) – Moore, p. 741, pl. 4, fig. 8.
1974 *Calocyclas turris* Ehrenberg – Nigrini, p. 1067, pl. 2C, fig. 6.
1974 *Calocyclas turris* Ehrenberg – Johnson, p. 547, pl. 5, fig. 2.
1975 *Calocyclas turris* Ehrenberg – Ling, p. 728, pl. 9, fig. 13.
1977 *Calocyclas turris* Ehrenberg – Riedel and Sanfilippo, pl. 11, fig. 1.
1978 *Calocyclas turris* Ehrenberg – Riedel and Sanfilippo, p. 65, pl. 3, figs. 7, 8.
1984 *Calocyclas turris* Ehrenberg – Saunders et al., p. 412, pl. 5, fig. 12.
1986 *Calocyclas turris* Ehrenberg – Riedel and Sanfilippo, pl. 2, fig. 11, pl. 5, fig. 3.

2001 *Calocyclas turris* Ehrenberg – Sanfilippo and Blome, 2001, p. 211, figs. 8i–8k.
2006 *Calocyclas turris* Ehrenberg – Funakawa et al., p. 22, pl. P5, figs. 5a, 5b.
2009 *Calocyclas turris* Ehrenberg – Ogane et al., pl. 94, figs. 1a–7d.
2009 *Cycladophora stiligera* Ehrenberg – Ogane et al., pl. 10, figs. 2a–2d.
2012 *Calocyclas turris* Ehrenberg – Moore and Kamikuri, p. 5, pl. P1, figs. 9, 10.
2015 *Calocyclas turris* Ehrenberg – Kamikuri, pl. 5, figs. 4, 6a, 6b.
Occurrence. ODP Site 1051 (Blake Nose; western north Atlantic).

Genus *Calocycloma* Haeckel, 1887

Type species.— *Calocyclas* (*Calocycloma*) *casta* Haeckel, 1887, p. 1384, pl. 73, fig. 10.

Calocycloma ampulla (Ehrenberg, 1854a)

Plate II.20, Figure 8

1854a *Eucyrtidium Ampulla* [sic] Ehrenberg, pl. 36, figs. 15a, 15b.
1874 *Eucyrtidium Ampulla* [sic] Ehrenberg – Ehrenberg, p. 225.
1876 *Eucyrtidium Ampulla* [sic] Ehrenberg – Ehrenberg, p. 70, pl. 10, figs. 11, 12.
1887 *Sethamphora* (*Dictyoprona*) *ampulla* (Ehrenberg) – Haeckel, p. 1251.
1958 *Sethamphora ampulla* (Ehrenberg) – Göke, pl. 2, fig. 4.
1970 *Calocycloma* ? *ampulla* (Ehrenberg) – Riedel and Sanfilippo, p. 524, pl. 6, fig. 1.
1971 *Calocycloma* ? *ampulla* (Ehrenberg) – Riedel and Sanfilippo, p. 1593, pl. 3B, fig. 4.
1973 *Calocycloma ampulla* (Ehrenberg) – Foreman, p. 434, pl. 1, figs. 1–5, pl. 9, fig. 20.
1974 *Calocycloma ampulla* (Ehrenberg) – Nigrini, p. 1067, pl. 1F, figs. 1–4.
1974 *Calocycloma ampulla* (Ehrenberg) – Johnson, p. 548, pl. 5, fig. 8.
1975 *Calocycloma ampulla* (Ehrenberg) – Ling, p. 728, pl. 9, fig. 14.
1987 *Calocycloma castum* (Ehrenberg) – Nishimura, p. 721, pl. 3, fig. 2.
1995 *Calocycloma castum* (Ehrenberg) – Strong et al., p. 208, figs. 9V–9X.
2008 *Calocycloma ampulla* (Ehrenberg) – Jackett et al., p. 50, pl. 2, fig. 2.
2009 *Eucyrtidium ampulla* Ehrenberg – Ogane et al., pl. 60, figs. 1a–3d.
2012 *Calocycloma ampulla* (Ehrenberg) – Moore and Kamikuri, p. 5, pl. P1, fig. 12.
2015 *Calocycloma ampulla* (Ehrenberg) – Kamikuri, pl. 10, figs. 10a, 10b.
not 2015 *Calocycloma ampulla* (Ehrenberg) – Hollis et al., pl. 9, figs. 7a, 7b.
Occurrence. ODP Site 1260 (Demerara Rise; western equatorial Atlantic) and ODP Site 1051 (Blake Nose; western north Atlantic).

Calocycloma castum (Haeckel, 1887)

Plate II.20, Figure 7

1887 *Calocyclas* (*Calocycloma*) *casta* Haeckel, p. 1384, pl. 73, fig. 10.
1970 *Calocyclas casta* Haeckel – Cita et al., p. 404, pl. 2, fig. H.
1973 *Calocycloma castum* (Haeckel) – Foreman, p. 434, pl. 1, figs. 7, 9, 10.
1978 *Calocycloma castum* (Haeckel) – Weaver and Dinkelman, p. 868, pl. 5, fig. 11.
1978 *Calocycloma castum* (Haeckel) – Riedel and Sanfilippo, p. 66, pl. 1, fig. 9, pl. 3, fig. 15.
1987 *Calocycloma castum* (Haeckel) – Nishimura, p. 721, pl. 3, fig. 1.
1998a *Calocycloma castum* (Haeckel) – Sanfilippo and Nigrini, p. 272, pl. 13.1, fig. 10.

2008 *Calocycloma castum* (Haeckel) – Jackett et al., p. 50, pl. 2, fig. 3.
2001 *Calocycloma castum* (Haeckel) –Sanfilippo and Blome, p. 211, figs. 8n, 8o.
2017 *Calocycloma ampulla* (Ehrenberg) – de Souza et al., pl. 2, fig. 6.
Occurrence. ODP Site 1260 (Demerara Rise; western equatorial Atlantic).

Genus *Cyrtocapsa* Haeckel, 1881 emend. O'Connor, 1997a

Type species.— *Cyrtocapsa ovalis* Rüst, 1885, p. 320, pl. 42, fig. 11.

Cyrtocapsa osculum O'Connor, 1997a

Plate II.21, Figure 1

1973 *Theocorys* sp. aff. *Theocorys* ? *spongoconus* Kling – Foreman, p. 440, pl. 11, fig. 14.
1997a *Cyrtocapsa osculum* O'Connor, p. 75, pl. 1, figs. 15–17, pl. 2, figs. 1, 2, pl. 8, figs. 3–10.
? 2003 ? *Cyrtocapsa osculum* O'Connor – Sanfilippo and Fourtanier, p. 11, pl. P2, figs. 19, 20.
2020 *Cyrtocapsa osculum* O'Connor – Hollis et al., pl. 9, figs. 17a, 17b.
Occurrence. ODP Site 1051 (Blake Nose; western north Atlantic).

Genus *Eusyringium* Haeckel, 1882

Type species.— *Eusyringium* (*Eusyringartus*) *conosiphon* Haeckel, 1887, p. 1496, pl. 78, fig. 10.

Eusyringium lagena (Ehrenberg, 1874)

Plate II.20, Figure 12

1874 *Lithopera Lagena* [sic] Ehrenberg, p. 241.
1876 *Lithopera Lagena* [sic] Ehrenberg – Ehrenberg, p. 78, pl. 3, fig. 4.
1882a *Anthocyrtis Lagena* [sic] Ehrenberg –, p. 533.
1887 *Sethocapsa lagena* (Ehrenberg) – Haeckel, p. 1310, pl. 57, fig. 2.
1970 ? *Eusyringium lagena* (Ehrenberg) – Riedel and Sanfilippo, p. 527, pl. 8, figs. 5–7.
1971 ? *Eusyringium lagena* (Ehrenberg) – Moore, p. 741, pl. 4, fig. 9.
1973 *Eusyringium lagena* (Ehrenberg) – Foreman, p. 435, pl. 11, figs. 4, 5.
1973 *Eusyringium lagena* (Ehrenberg) – Nigrini, p. 1067, pl. 1F, figs. 13, 14.
1974 ? *Eusyringium lagena* (Ehrenberg) – Johnson, p. 548, pl. 5, fig. 3.
1975 *Eusyringium lagena* (Ehrenberg) – Ling, p. 729, pl. 9, fig. 21.
1977 *Eusyringium lagena* (Ehrenberg) – Riedel and Sanfilippo, pl. 9, fig. 4.
1978 *Eusyringium lagena* (Ehrenberg) – Weaver and Dinkelman, p. 869, pl. 5, figs. 2, 3.
1978 *Eusyringium lagena* (Ehrenberg) – Riedel and Sanfilippo, p. 68, pl. 5, fig. 8.
1986 *Eusyringium lagena* (Ehrenberg) – Riedel and Sanfilippo, pl. 2, fig. 18.
1995 *Eusyringium lagena* (Ehrenberg) – Strong et al., p. 208, fig. 11C.
1997 *Eusyringium lagena* (Ehrenberg) – Hollis et al., p. 62, pl. 5, figs. 15, 16.
1999 *Eusyringium lagena* (Ehrenberg) – Kozlova, p. 155, pl. 27, figs. 17, 18, pl. 32, fig. 16.
2009 *Lithocampe lagena* [sic] Ehrenberg – Ogane et al., pl. 2, figs. 10a, 10b.
2009 *Lithopera lagena* Ehrenberg – Ogane et al., pl. 23, figs. 1a–2c.
2012a *Eusyringium lagena* (Ehrenberg) – Kamikuri et al., p. 102, pl. 3, fig. 13.
2012b *Eusyringium lagena* (Ehrenberg) – Kamikuri et al., p. 3, pl. P1, figs. 5a, 5b.

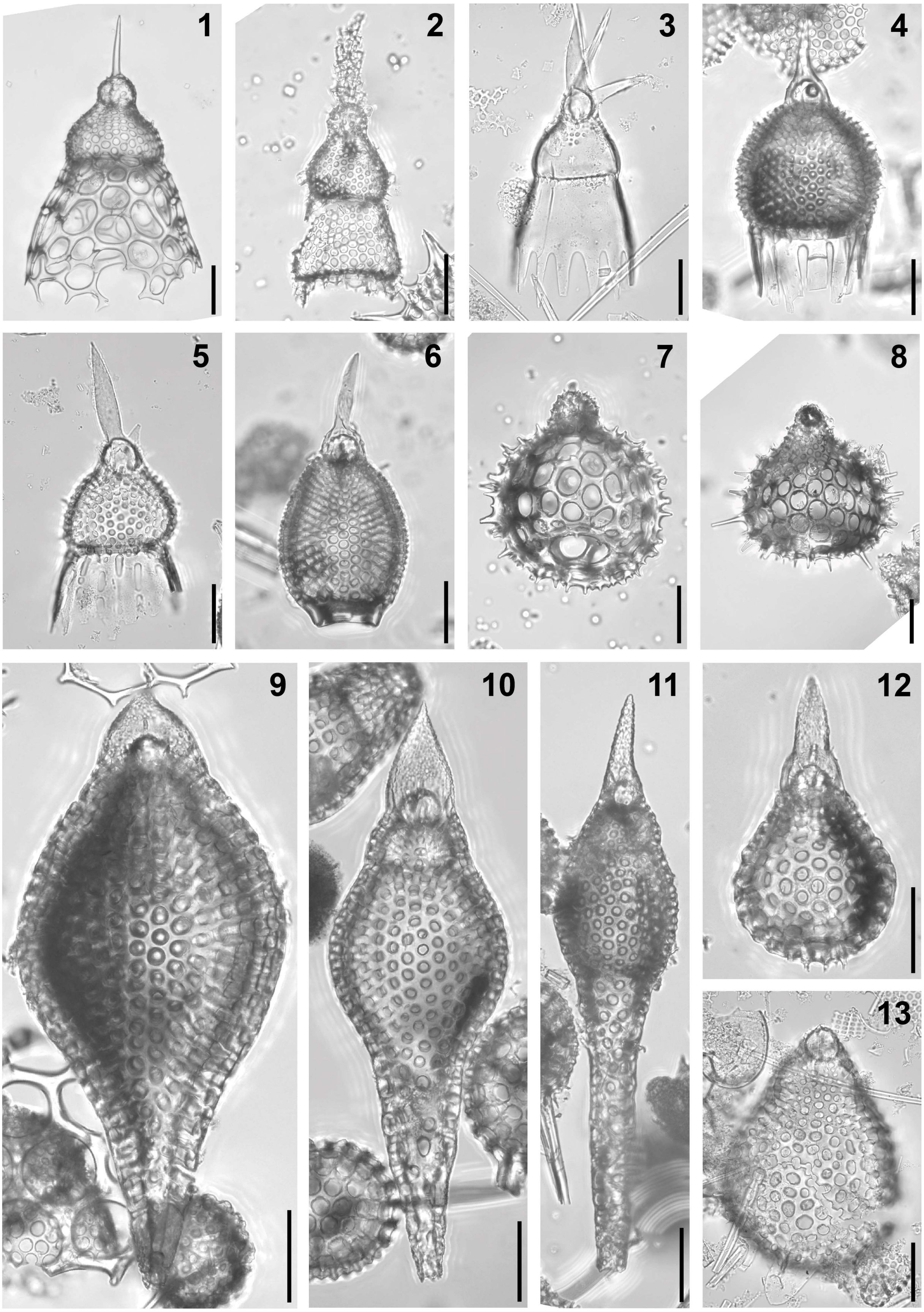
1
2
3
4
5
6
7
8
9
10
11
12
13

Plate II.20. Composite light micrographs of new radiolarian species from ODP Site 1260 (Demerara Rise, western equatorial Atlantic) and ODP Site 1051 (Blake Nose, western North Atlantic). (**1**) *Thyrsocyrtis* (*Pentalacorys*) *parvipes* (Ehrenberg, 1874): ODP 1260A-6R-2W, 55–57 cm. (**2**) *Artophormis* ? *barbadensis* (Ehrenberg, 1874): ODP 1260A-9R-3W, 55–57 cm. (**3**) *Calocyclas aphradia* Sanfilippo and Blome, 2001: ODP 1051A-11H-5W, 59–61 cm. (**4**) *Calocyclas hispida* (Ehrenberg, 1874): ODP 1260A-11R-5W, 55–57 cm. (**5**) *Calocyclas turris* Ehrenberg, 1874: ODP 1051A-4H-5W, 56–58 cm. (**6**) *Calocyclas* ? *chrysallis* (Sanfilippo and Blome, 2001): ODP 1260A-9R-3W, 55–57 cm. (**7**) *Calocycloma castum* (Haeckel, 1887): ODP 1260A-17R-3W, 55–57 cm. (**8**) *Calocycloma ampulla* (Ehrenberg, 1854a): ODP 1260A-8R-2W, 55–57 cm. (**9–11**) *Eusyringium tubulus* (Ehrenberg, 1854a) group: (**9**) ODP 1260A-6R-CC, 63–177 cm; (**10**) ODP 1260A-11R-7W, 55–57 cm; (**11**): ODP 1260A-8R-6W, 54–56 cm. (**12**) *Eusyringium lagena* (Ehrenberg, 1874): ODP 1260A-14R-CC, 63–177 cm. (**13**) *Eusyringium* ? *ventricosum* (Ehrenberg, 1874): ODP 1051A-8H-5W, 53–55 cm. All scale bars equal 50 µm.

2017 *Eusyringium lagena* (Ehrenberg) – de Souza et al., pl. 3, figs. 12a, 12b.
2020 *Eusyringium lagena* (Ehrenberg) – Hollis et al., pl. 10, fig. 14.
Occurrence. ODP Site 1260 (Demerara Rise; western equatorial Atlantic).

Eusyringium tubulus (Ehrenberg, 1854a) group
Plate II.20, Figures 9–11

1854a *Eucyrtidium Tubulus* [sic] Ehrenberg, pl. 36, fig. 19.
1862 *Rhopalocanium ornatum* Ehrenberg – Bury, pl. 6, fig. 3 (part).
1862 *Eucyrtidium tubulous* [sic] Ehrenberg – Bury, pl. 11, fig. 2.
1862 *Eucyrtidium tubulus* Ehrenberg – Bury, pl. 22, fig. 8.
1874 *Eucyrtidium fistuligerum* Ehrenberg, p. 229.
1874 *Eucyrtidium Sipho* [sic] Ehrenberg, p. 233.
1874 *Eucyrtidium Tubulus* [sic] Ehrenberg – Ehrenberg, p. 233.
1876 *Eucyrtidium fistuligerum* Ehrenberg – Ehrenberg, p. 70, pl. 9, fig. 3.
1876 *Eucyrtidium Sipho* [sic] Ehrenberg – Ehrenberg, p. 72, pl. 9, fig. 2.
1876 *Eucyrtidium Tubulus* [sic] Ehrenberg – Ehrenberg, p. 72, pl. 9, fig. 6.
1882a *Lithopera fistuligera* (Ehrenberg) – Bütschli, p. 532.
1882a *Lithopera Sipho* [sic] (Ehrenberg) – Bütschli, p. 532.
1882a *Lithopera Tubulus* [sic] (Ehrenberg) – Bütschli, p. 532.
1882b *Lithopera Sipho* [sic] (Ehrenberg) – Bütschli, pl. 31, fig. 3.
1887 *Theosyringium tibia* Haeckel, p. 1409, pl. 68, fig. 4.
1887 *Pterocorys* (*Pterosyringium*) *tubulosa* Haeckel, p. 1419, pl. 68, fig. 6.
1887 *Eusyringium* (*Eusyringartus*) *conosiphon* Haeckel, p. 1496, pl. 78, fig. 10.
1887 *Eusyringium* (*Eusyringartus*) *pachysiphon* Haeckel, p. 1496, pl. 78, fig. 11.
1887 *Eusyringium* (*Eusyringartus*) *macrosiphon* Haeckel, p. 1497, pl. 78, fig. 12.
1887 *Eusyringium* (*Eusyringartus*) *sipho* (Ehrenberg) – Haeckel, p. 1497.

1887 *Eusyringium* (*Eusyringartus*) *fistuligerum* (Ehrenberg) – Haeckel, p. 1498.
1957a ? *Eusyringium* aff. *E. fistuligerum* (Ehrenberg) – Riedel, p. 261, pl. 62, fig. 8.
1957b *Eusyringium fistuligerum* (Ehrenberg) – Riedel, p. 94, pl. 4, fig. 8.
1970 *Eusyringium fistuligerum* (Ehrenberg) – Riedel and Sanfilippo, p. 527, pl. 8, figs. 8, 9.
1971 *Eusyringium fistuligerum* (Ehrenberg) – Riedel and Sanfilippo, p. 1594, pl. 3B, fig. 14.
1971 *Eusyringium fistuligerum* (Ehrenberg) – Moore, p. 741, pl. 4, figs. 10, 11.
1972 *Eusyringium fistuligerum* (Ehrenberg) – Petrushevskaya and Kozlova, p. 549, pl. 32, fig. 3.
1972 *Eucyrtidium tubulus* Ehrenberg – Petrushevskaya and Kozlova, p. 549, pl. 32, figs. 4, 5.
1973 *Eusyringium fistuligerum* (Ehrenberg) – Foreman, p. 435, pl. 11, fig. 6.
1974 *Eusyringium fistuligerum* (Ehrenberg) – Nigrini, p. 1067, pl. 1F, figs. 9–12, pl. 2C, fig. 9.
1974 *Eusyringium fistuligerum* (Ehrenberg) – Johnson, p. 548, pl. 5, fig. 4.
1975 *Eusyringium fistuligerum* (Ehrenberg) – Chen, p. 461, pl. 3, fig. 3.
1975 *Eusyringium fistuligerum* (Ehrenberg) – Ling, p. 728, pl. 9, figs. 19, 20.
1975 *Eusyringium tubulus* (Ehrenberg) – Ling, p. 729, pl. 9, fig. 22.
1977 *Eusyringium fistuligerum* (Ehrenberg) – Riedel and Sanfilippo, pl. 9, fig. 5.
1977 ? *Eusyringium fistuligerum* (Ehrenberg) – Riedel and Sanfilippo, pl. 9, fig. 6.
1978 *Eusyringium fistuligerum* (Ehrenberg) – Weaver and Dinkelman, p. 869, pl. 5, fig. 1.
1978 *Eusyringium fistuligerum* (Ehrenberg) – Riedel and Sanfilippo, p. 68, pl. 5, figs. 6, 7.
1985 *Eusyringium fistuligerum* (Ehrenberg) – Sanfilippo et al., p. 672, figs. 17.2a-17.2c.
1992 *Eusyringium fistuligerum* (Ehrenberg) – Takemura, p. 746, pl. 7, figs. 5, 6.
1995 *Eusyringium fistuligerum* (Ehrenberg) – Strong et al., p. 208, figs. 11D, 11E.
2000 *Eusyringium fistuligerum* (Ehrenberg) – Nigrini and Sanfilippo, p. 73, pl. 2, figs. 2, 3.
2001 *Eusyringium fistuligerum* (Ehrenberg) – Sanfilippo and Blome, p. 212, fig. 9a–9d.
2001 *Eusyringium conosiphon* Haeckel – De Wever et al., p. 282, fig. 187.1.
2001 *Pterosyringium tubulosum* (Haeckel) – De Wever et al., p. 282, fig. 187.4.
2006 *Eusyringium fistuligerum* (Ehrenberg) – Funakawa et al., p. 35, pl. P12, figs. 1a–3.
2009b *Eusyringium fistuligerum* (Ehrenberg) – Suzuki et al., p. 262, pl. 22, figs. 14a, 14b.
2009 *Eucyrtidium fistuligerum* Ehrenberg – Ogane et al., pl. 47, figs. 3a–3f.
2009 *Eucyrtidium sipho* Ehrenberg – Ogane et al., pl. 23, figs. 7a–7d, pl. 47, figs. 1a–1f, 4a, 4b, 6a, 6b.
2009 *Eucyrtidium tubulus* Ehrenberg – Ogane et al., pl. 47, figs. 2a, 2b, 5a–5d.
2012 *Eusyringium fistuligerum* (Ehrenberg) – Moore and Kamikuri, p. 8, pl. P5, fig. 1.
2012b *Eusyringium fistuligerum* (Ehrenberg) – Kamikuri et al., p. 3, pl. P1, figs. 4a, 4b.
2015 *Eusyringium fistuligerum* (Ehrenberg) group – Kamikuri, pl. 12, figs. 22–24.
2017 *Eusyringium fistuligerum* (Ehrenberg) – de Souza et al., pl. 3, figs. 11a, 11b.
2020 *Eusyringium fistuligerum* (Ehrenberg) – Hollis et al., pl. 10, figs. 11–13.
2021 *Eusyringium fistuligerum* (Ehrenberg) – de Souza et al., p. 15, pl. 3, fig. 5.

Remarks. The great morphological disparity observed in *Eusyringium tubulus* (Ehrenberg) and *E. fistuligerum* (Ehrenberg), with a gradient of specimens displaying an intermediate morphology between these two morphospecies, leads us to consider them as a group of closely related species.

Occurrence. ODP Site 1260 (Demerara Rise; western equatorial Atlantic) and ODP Site 1051 (Blake Nose; western north Atlantic).

Eusyringium ? *ventricosum* (Ehrenberg, 1874)
Plate II.20, Figure 13

1874 *Lithomelissa ventricosa* Ehrenberg, p. 241.
1876 *Lithomelissa ventricosa* Ehrenberg – Ehrenberg, p. 78, pl. 3, fig. 11.
1887 *Micromelissa ventricosa* (Ehrenberg) – Haeckel, p. 1236.
2009 *Lithomelissa ventricosa* Ehrenberg – Ogane et al., pl. 96, figs. 1a–2d.
2012 *Lychnocanoma turgidum* Ehrenberg – Moore and Kamikuri, p. 9, pl. P7, fig. 4.
2015 *Lithomelissa* ? *ventricosa* Ehrenberg – Kamikuri, pl. 11, figs. 9a, 9b.

Remarks. The combination used here is derived from O'Dogherty et al. (2021).
Occurrence. ODP Site 1051 (Blake Nose; western north Atlantic).

Genus *Rhopalocanium* Ehrenberg, 1846
Type species.— *Rhopalocanium ornatum* Ehrenberg, 1847, p. 55, fig. 3.

Rhopalocanium ornatum Ehrenberg, 1847
Plate II.21, Figure 2

1847 *Rhopalocanium ornatum* Ehrenberg, fig. 3.
1854a *Lithornithium Loxia* [sic] Ehrenberg, pl. 36, fig. 8.
1854a *Rhopalocanium ornatum* Ehrenberg – Ehrenberg, pl. 36, fig. 9.
1862 *Rhopalocanium ornatum* Ehrenberg – Bury, pl. 6, figs. 1, 2 (part).
1874 *Lithornithium Loxia* [sic] Ehrenberg – Ehrenberg, p. 242.
1874 *Lithornithium Luscinia* [sic] Ehrenberg, p. 242.
1874 *Rhopalocanium ornatum* Ehrenberg – Ehrenberg, p. 256.
1876 *Lithornithium Loxia* [sic] Ehrenberg – Ehrenberg, p. 78, pl. 4, fig. 8.
1876 *Lithornithium Luscinia* [sic] Ehrenberg – Ehrenberg, p. 78, pl. 4, fig. 9
1876 *Rhopalocanium ornatum* Ehrenberg – Ehrenberg, p. 82, pl. 17, fig. 8.
1882b *Lithornithium Luscinia* [sic] Ehrenberg – Bütschli, pl. 30, fig. 9.
1887 *Theopera luscinia* (Ehrenberg) – Haeckel, p. 1358.
1887 *Theopera cortina* Haeckel, p. 1358, pl. 67, fig. 8.
1887 *Rhopalatractus fenestratus* (Haeckel) – Haeckel, p. 1361, pl. 68, fig. 12.
1887 *Artopera loxia* (Ehrenberg) – Haeckel, 1452.
1970 Gen. et sp. indet. Riedel and Sanfilippo, pl. 10, fig. 1.
1972 *Rhopalocanium ornatum* Ehrenberg – Petrushevskaya and Kozlova, p. 552, pl. 27, figs. 13, 14.
1973 *Rhopalocanium ornatum* Ehrenberg – Foreman, p. 439, pl. 2, figs. 8–10, pl. 12, fig. 3.
1974 *Rhopalocanium ornatum* Ehrenberg – Nigrini, p. 1068, pl. 1H, figs. 6–10.
1974 *Rhopalocanium ornatum* Ehrenberg – Johnson, p. 549, pl. 5, fig. 18.
1975 *Rhopalocanium ornatum* Ehrenberg – Ling, p. 729, pl. 11, figs. 1–3.
1977 *Rhopalocanium ornatum* Ehrenberg – Riedel and Sanfilippo, pl. 9, fig. 15.
1978 Theoperid gen. et sp. indet. Weaver and Dinkelman, pl. 9, fig. 12 (part).

1978 *Rhopalocanium ornatum* Ehrenberg – Riedel and Sanfilippo, p. 72, pl. 9, fig. 5.
2001 *Rhopalocanium ornatum* Ehrenberg – Sanfilippo and Blome, p. 217, figs. 10o, 10p.
2001 *Rhopalocanium ornatum* Ehrenberg – De Wever et al., p. 282, fig. 187.5.
2001 *Lithornithium loxia* Ehrenberg – De Wever et al., p. 282, fig. 187.6.
2009 *Lithocorythium loxia* Ehrenberg – Ogane et al., pl. 24, figs. 1a–1d, 2a, 2b, 3a–3e.
2009 *Lithornithium luscinia* Ehrenberg – Ogane et al., pl. 46, figs. 1a–1e.
2012 *Rhopalocanium ornatum* Ehrenberg – Moore and Kamikuri, p. 10, pl. P7, fig. 13.
2015 *Rhopalocanium ornatum* Ehrenberg – Kamikuri, pl. 1, figs. 2–3b.
2020 *Rhopalocanium ornatum* Ehrenberg – Hollis et al., pl. 14, figs. 19, 20.
Occurrence. ODP Site 1260 (Demerara Rise; western equatorial Atlantic) and ODP Site 1051 (Blake Nose; western north Atlantic).

Rhopalocanium sphinx (Ehrenberg, 1874)
Plate II.21, Figure 3

1874 *Pterocanium* ? *Sphinx* [sic] Ehrenberg, p. 255.
1876 *Pterocanium* ? *Sphinx* [sic] Ehrenberg – Ehrenberg, p. 82, pl. 17, fig. 5.
1882b *Rhopalocanium Bombus* [sic] (Ehrenberg) – Bütschli, pl. 30, fig. 10.
1887 *Pteropilium sphinx* (Ehrenberg) – Haeckel, p. 1443.
1972 *Stichopilidium sphinx* (Ehrenberg) – Petrushevskaya and Kozlova, p. 552, pl. 27, fig. 1.
1977 *Pteropilium sphinx* (Ehrenberg) – Riedel and Sanfilippo, pl. 7, fig. 10.
not 2006 *Stichopilidium sphinx* Ehrenberg – Funakawa et al., p. 31, pl. P11, figs. 1a, 1b.
2009 *Pterocanium sphinx* Ehrenberg – Ogane, pl. 1, fis. 4a–4d, pl. 46, figs. 2a–3c, pl. 97, figs. 4a–4d.
2015 *Stichopilidium sphinx* Ehrenberg – Kamikuri, pl. 5, figs. 5a, 5b.
Remarks. The combination used here is derived from O'Dogherty et al. (2021).
Occurrence. ODP Site 1260 (Demerara Rise; western equatorial Atlantic).

Genus *Pteropilium* Haeckel, 1882
Type species.— *Pteropilium* (*Clathropilium*) *stratiotes* Haeckel, 1887, p. 1326, pl. 70, fig. 9.

Pteropilium aff. *contiguum* (Ehrenberg, 1874)
Plate II.21, Figure 4

1874 *Pterocanium contiguum* Ehrenberg, p. 255.
1876 *Pterocanium contiguum* Ehrenberg – Ehrenberg, p. 82, pl. 17, fig. 7.
1882a *Pterocyrtidium barbadense* Ehrenberg – Bütschli, pl. 33, figs. 28a, 28b.
1882b *Pterocyrtidium barbadense* Ehrenberg – Bütschli, pl. 31, figs. 2a, 2b.
1887 *Pterocanium* (*Pterocanarium*) *contiguum* Ehrenberg – Haeckel, p. 1330.
1887 *Lithornithium ciconia* Haeckel, p. 1354, pl. 67, fig. 3.
1972 *Pteropilium* ? sp. aff. *Pterocanium contiguum* Ehrenberg group – Petrushevskaya and Kozlova, p. 553, pl. 29, figs. 8–10.
1977 *Pterocanium contiguum* Ehrenberg – Riedel and Sanfilippo, pl. 4, fig. 7.
1991 *Pteropilium* sp. aff. *Pterocanium contiguum* (Ehrenberg) – Caulet, p. 539, pl. 2, fig. 11.
1993 *Pterocanium* ? *contiguum* Ehrenberg – Vitukhin, pl. 23, fig. 3.

1999a *Pteropilium* sp. O'Connor, p. 36, pl. 9, fig. 39.
1999 *Pterocanium contiguum* Ehrenberg – Kozlova, p. 175, pl. 24, fig. 7.
2005 *Pteropilium* sp. aff. *Pterocanium contiguum* (Ehrenberg) – Nigrini et al., p. 47, pl. P5, fig. 2.
2009 *Pterocanium contiguum* Ehrenberg – Ogane et al., pl. 47, figs. 8a–8e.
not 2012 *Pterocanium* sp. aff. *Pterocanium contiguum* Ehrenberg – Moore and Kamikuri, p. 10, pl. P7, fig. 15.
2020 *Pteropilium* aff. *contiguum* (Ehrenberg) – Hollis et al., pl. 14, figs. 16, 17 (part).
2021 *Pteropilium* aff. *contiguum* (Ehrenberg) – de Souza et al., p. 15, pl. 3, figs. 7a, 7b.
Occurrence. ODP Site 1260 (Demerara Rise; western equatorial Atlantic) and ODP Site 1051 (Blake Nose; western north Atlantic).

Pteropilium ? *melitta* Haeckel, 1887
Plate II.21, Figure 5

1862 *Rhopalocanium ornatum* Ehrenberg – Bury, pl. 6, fig. 4 (part).
1887 *Pterocorys* (*Pterocyrtidium*) *melitta* Haeckel, p. 1319.
1972 *Pteropilium* ? sp. Petrushevskaya and Kozlova, pl. 29, fig. 4.
1978 Theoperid gen. et sp. indet. Weaver and Dinkelman, pl. 1, fig. 3 (part).
1986 *Pterocorys melitta* Haeckel – Göke, fig. 3.3.
Remarks. The combination used here is derived from O'Dogherty et al. (2021).
Occurrence. ODP Site 1051 (Blake Nose; western north Atlantic).

Genus *Theocorys* Haeckel, 1881
Type species.— *Theocorys morchellula* Rüst, 1885, p. 308, pl. 37, fig. 6.

Theocorys anaclasta Riedel and Sanfilippo, 1970
Plate II.21, Figure 6

1970 *Theocorys anaclasta* Riedel and Sanfilippo, p. 530, pl. 10, figs. 2, 3.
1971 *Theocorys anaclasta* Riedel and Sanfilippo – Moore, p. 742, pl. 2, fig. 1.
1973 *Theocorys anaclasta* Riedel and Sanfilippo – Foreman, p. 440, pl. 5, figs. 14, 15.
1977 *Theocorys anaclasta* Riedel and Sanfilippo – Riedel and Sanfilippo, pl. 6, fig. 1.
1978 *Theocorys* sp. aff. *Theocorys anaclasta* Riedel and Sanfilippo – Johnson, p. 784, pl. 2, figs. 12, 13.
1978 *Theocorys anaclasta* Riedel and Sanfilippo – Weaver and Dinkelman, p. 873, pl. 7, figs. 1–3.
1978 *Theocorys anaclasta* Riedel and Sanfilippo – Riedel and Sanfilippo, p. 76, plate 1, figs 6–8 .
1978 *Theocorys* sp. aff. *Theocorys anaclasta* Riedel and Sanfilippo – Foreman, p. 784, pl. 2, figs. 12, 13.
1985 *Theocorys anaclasta* Riedel and Sanfilippo – Sanfilippo et al., p. 683, fig. 24.1a-24.1d.
2012a *Theocorys anaclasta anaclasta* Riedel and Sanfilippo – Kamikuri et al., p. 94, pl. 1, figs. 7, 8.

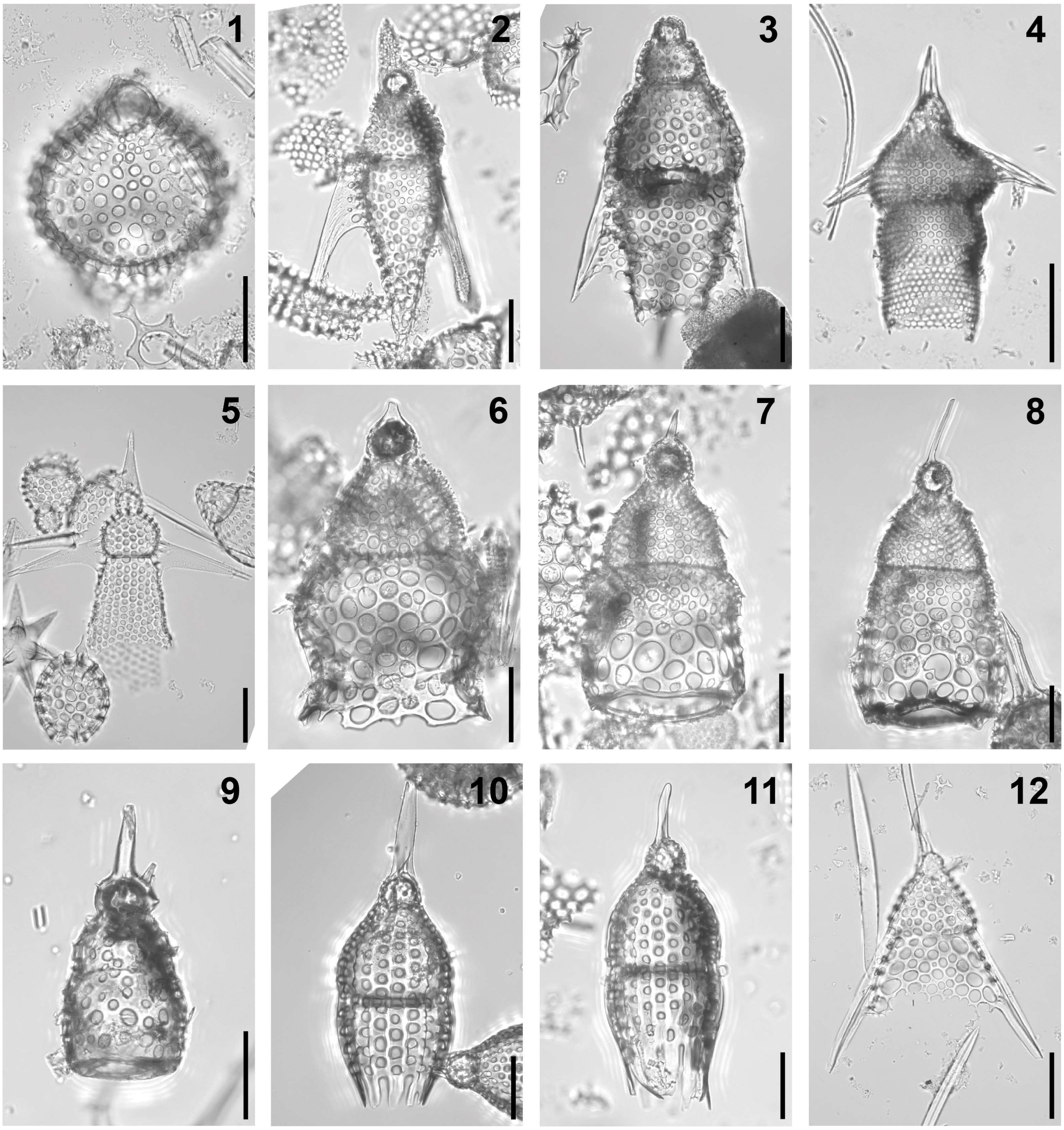

Plate II.21. Composite light micrographs of new radiolarian species from ODP Site 1260 (Demerara Rise, western equatorial Atlantic) and ODP Site 1051 (Blake Nose, western North Atlantic). (**1**) *Cyrtocapsa osculum* O'Connor, 1997a: ODP 1051A-8H-5W, 53–55 cm. (**2**) *Rhopalocanium ornatum* Ehrenberg, 1847: (**1**) ODP 1260A-6R-4W, 55–57 cm. (**3**) *Rhopalocanium sphinx* (Ehrenberg, 1874): ODP 1260A-6R-1W, 55–57 cm. (**4**) *Pteropilium* aff. *contiguum* Ehrenberg, 1874: ODP 1260A-9R-4W, 55–57 cm. (**5**) *Pteropilium* ? *melitta* Haeckel, 1887: ODP 1051A-14H-5W, 52–54 cm. (**6**) *Theocorys anaclasta* Riedel and Sanfilippo, 1970: ODP 1260A-20R-5W, 55–57 cm. (**7, 8**) *Theocorys anapographa* Riedel and Sanfilippo, 1970: (**7**) ODP 1260A-14R-1W, 55–57 cm, (**8**): ODP 1260A-14R-CC, 63–177 cm. (**9**) *Theocorys anapographa* Riedel and Sanfilippo, 1970 var. A: ODP 1260A-6R-2W, 55–57 cm. (**10, 11**) *Theocorys* ? *scolopax* (Ehrenberg, 1874): (**10**) ODP 1260A-13R-4W, 55–57 cm;

(**11**) ODP 1260A-13R-4W, 55–57 cm. (**12**) *Valkyria pukapuka* O'Connor, 1997a: ODP 1051A-13H-2W, 52–54 cm. All scale bars equal 50 µm.

2012a *Theocorys anaclasta clasta* Riedel and Sanfilippo – Kamikuri et al., p. 94, pl. 1, figs. 1a–4b.

Occurrence. ODP Site 1260 (Demerara Rise; western equatorial Atlantic).

Theocorys anapographa Riedel and Sanfilippo, 1970
Plate II.21, Figures 7, 8

? 1887 *Lophoconus rhinoceros* Haeckel, p. 1405, pl. 69, fig. 2.
1970 *Theocorys anapographa* Riedel and Sanfilippo, p. 530, pl. 10, fig. 4.
1971 *Theocorys anapographa* Riedel and Sanfilippo – Moore, p. 742, pl. 2, fig. 1.
1973 *Theocorys anapographa* Riedel and Sanfilippo – Dinkelman, pl. 2, fig. 2.
1973 *Theocorys anapographa* Riedel and Sanfilippo – Foreman, p. 440, pl. 5, figs. 9, 10.
1974 *Theocorys anapographa* Riedel and Sanfilippo – Nigrini, p. 1069, pl. 1I, figs. 9–13, pl. 2D, fig. 7.
1977 *Theocorys anapographa* Riedel and Sanfilippo – Riedel and Sanfilippo, pl. 8, fig. 12.
1978 *Theocorys anapographa* Riedel and Sanfilippo – Weaver and Dinkelman, p. 873, pl. 7, figs. 4, 5.
1978 *Theocorys anapographa* Riedel and Sanfilippo – Riedel and Sanfilippo, p. 76, pl. 9, fig. 15.
1999 *Calocyclura sphaerophilum* (Ehrenberg) – Kozlova, pl. 31, figs. 7, 12, 17.
2012a *Theocorys anapographa* Riedel and Sanfilippo – Kamikuri et al., p. 104, pl. 1, figs. 5a, 5b.
? 2020 *Theocorys anapographa* Riedel and Sanfilippo – Hollis et al., pl. 11, figs. 4, 5.

Occurrence. ODP Site 1260 (Demerara Rise; western equatorial Atlantic) and ODP Site 1051 (Blake Nose; western north Atlantic).

Theocorys anapographa Riedel and Sanfilippo, 1970 var. A
Plate II.21, Figure 9

1973 *Theocorys anapographa* Riedel and Sanfilippo – Riedel and Sanfilippo, p. 740, pl. 3, figs. 10, 11.
1975 *Theocorys anapographa* Riedel and Sanfilippo – Ling, p. 730, pl. 11, figs. 11, 12.
2001 *Theocorys anapographa* Riedel and Sanfilippo var. A – Sanfilippo and Blome, p. 219, figs. 11m, 11n.
2015 *Theocorys* sp. A Kamikuri, pl. 10, figs. 17a, 17b.
? 2015 *Theocorys* sp. B Kamikuri, pl. 10, figs. 18a, 18b.
2020 *Theocorys anapographa* Riedel and Sanfilippo var. A – Hollis et al., pl. 11, figs. 6a, 6b.

Occurrence. ODP Site 1260 (Demerara Rise; western equatorial Atlantic) and ODP Site 1051 (Blake Nose; western north Atlantic).

Theocorys ? *scolopax* (Ehrenberg, 1874)
Plate II.21, Figures 10, 11

1874 *Eucyrtidium Scolopax* [sic] Ehrenberg, p. 232.
1876 *Eucyrtidium Scolopax* [sic] Ehrenberg – Ehrenberg, p. 72, pl. 9, fig. 5.
1882a *Eucyrtidium Scolopax* [sic] Ehrenberg – Bütschli, p. 528.
1887 *Theocorys* (*Theocoronium*) *scolopax* (Ehrenberg) – Haeckel, p. 1416.
? 1977 ? *Phormocyrtis embolum* (Ehrenberg) – Riedel and Sanfilippo, pl. 8, fig. 13.
2002 *Theocyrtis scolopax* (Ehrenberg) – Popova et al., p. 50, fig. 14G.
2009 *Eucyrtidium scolopax* Ehrenberg – Ogane et al., pl. 58, figs. 3a–3f.
Occurrence. ODP Site 1260 (Demerara Rise; western equatorial Atlantic).

? Genus *Valkyria* O'Connor, 1997a

Type species.— *Valkyria pukapuka* O'Connor, 1997a, p. 74, pl. 2, figs. 15, 16.

Valkyria pukapuka O'Connor, 1997a
Plate II.21, Figure 12

1997a *Valkyria pukapuka* O'Connor, p. 74, pl. 2, figs. 15, 16, pl. 3, figs. 1, 2, pl. 7, figs. 11, 12, pl. 8, figs. 1, 2.
2015 *Valkyria pukapuka* O'Connor – Kamikuri, pl. 2, figs. 8a, 8b, pl. 3, figs. 7a, 7b.
Occurrence. ODP Site 1051 (Blake Nose; western north Atlantic).

II.3. New radiolarian species from ODP Site 1260 (western equatorial Atlantic) and ODP Site 1051 (western North Atlantic)

This subchapter consists of two taxonomic papers published in the Journal of Paleontology. The first paper, titled **"Progress in understanding middle Eocene nassellarian (Rhizaria, Polycystinea) diversity; new insights from the western equatorial Atlantic Ocean"**, reports the description of 15 new nassellarian species from ODP Site 1260 (western equatorial Atlantic) and is available online at DOI: https://doi.org/10.1017/jpa.2022.82. The second paper, titled **"New middle Eocene radiolarian species (Rhizaria, Polycystinea) from Blake Nose, subtropical western North Atlantic Ocean",** describes 21 new polycystine radiolarian species from ODP Site 1051 (western North Atlantic) and is currently in the final stages of production.

II.3.1. Progress in understanding middle Eocene nassellarian (Rhizaria, Polycystinea) diversity; new insights from the western equatorial Atlantic Ocean

Mathias Meunier* and Taniel Danelian

Univ. Lille, CNRS, UMR 8198 – Evo-Eco-Paleo, F-59000 Lille, France

<mathias.meunier@univ-lille.fr>

*Corresponding author

Abstract.— Middle Eocene deep-sea sedimentary sequences cored at Ocean Drilling Program Site 1260 (Leg 207; equatorial Atlantic) yielded diverse and abundant radiolarian faunas that are conducive to biostratigraphic and paleoceanographic research, as well as to the study of radiolarian diversity dynamics during this epoch of dramatic climate change. However, many of the species found in these sediments have not been formally described and are therefore neglected in most biodiversity surveys. In an effort to improve the taxonomic resolution of middle Eocene radiolarians, 15 new nassellarian species are described and illustrated. The species are: *Cymaetron* ? *dilatatus* n. sp., *Eucyrtidium levisaltatrix* n. sp. (Eucyrtidiidae), *Siphocampe pollen* n. sp., *Spirocyrtis* ? *renaudiei* n. sp. (Artostrobiidae), *Pterocyrtidium eep* n. sp. (Rhopalosyringiidae), *Petalospyris cometa* n. sp., *Petalospyris castanea* n. sp. (Cephalospyrididae), *Velicucullus armatus* n. sp. (Theophormididae), *Lychnocanium nimrodi* n. sp. (Lithochytrididae), *Aphetocyrtis zamenhofi* n. sp., *Aphetocyrtis* ? *columboi* n. sp., *Aphetocyrtis* ? *spheniscus* n. sp. (Lophocyrtiidae), *Albatrossidium regis* n. sp., *Albatrossidium annikasanfilippoae* n. sp. and *Phormocyrtis lazari* n. sp. (Pterocorythidae). Stratigraphic range data are provided for each new species, as well as the orbitally tuned ages for their first and last occurrences. In addition to these new species, we also illustrated and documented the stratigraphic distribution of four species described in early radiolarian studies, which have rarely been observed since.

UUID: B5993E6B-659B-4220-80C2-C6DDCCC13793

II.3.1.1. Introduction

Reconstructing the paleodiversity dynamics of Eocene tropical radiolarians is hampered primarily by our incomplete taxonomic knowledge of these organisms. Indeed, despite being studied for nearly two centuries (Ehrenberg, 1839), we are still far from having fully documented and described all the species preserved in the Eocene fossil record. The first major contribution to the taxonomy of Eocene radiolarians is attributed to Ehrenberg (1874), who described 265 new species from middle Eocene to lower Oligocene pelagic sequences that crop out today on the Barbados Island (Saunders, 1984; Ogane et al., 2009), 85 of which were subsequently illustrated in Ehrenberg (1876). In his famous monograph, Haeckel (1887) also introduced ~200 middle Eocene radiolarian species from Barbados onshore samples, including illustrations for only half of them. In addition to this body of taxonomic work, several authors punctually published new species and genera throughout the late 19th century (Bury, 1862; Bütschli, 1882a, 1882b; Carter, 1893, 1895, 1896a, 1896b, 1896c, 1896d, 1896e; Sutton, 1896a, 1896b, 1896c, 1896d). However, many species described in these early radiolarian studies have not been observed since, and there are still many uncertainties about their stratigraphic range, biogeographic distribution, and the precise extent of their intraspecific variation (Ogane et al., 2009).

Although little taxonomic progress was achieved on tropical Eocene radiolarians during the first half of the 20th century (e.g., Brandt, 1935), two important publications by Clark and Campbell (1942, 1945) marked this period. They were devoted to the study of middle to late Eocene radiolarian faunas from three Californian shale formations and resulted in the description of 157 new species (Blueford, 1988). The subsequent advent of scientific ocean drilling in the 1960s and 1970s marked a turning point in the history of Cenozoic radiolarian taxonomy. Increased recovery of deep-sea sediments allowed extensive studies of radiolarian assemblages around the world and renewed interest in describing radiolarian diversity (e.g., Riedel and Sanfilippo, 1970, 1971, 1978; Petrushevskaya and Kozlova, 1972; Foreman, 1973; Sanfilippo and Riedel, 1973). The primary goal of these studies was biostratigraphy, and thus they tended to focus on a limited number of stratigraphically useful species that are often abundant in the Eocene fossil record. As a consequence, many rare morphotypes of no biostratigraphic value, or those belonging to morphologically complex taxa, remained undescribed and were neglected in most taxonomic surveys. Concurrently with this biostratigraphic work, some nassellarian families have also been the subject of more detailed taxonomic studies, leading to the establishment of several evolutionary lineages (e.g., Nigrini, 1977; Sanfilippo and Riedel, 1982, 1992; Sanfilippo and Caulet, 1998).

In an effort to improve the taxonomic resolution of tropical Eocene radiolarians, 15 new nassellarian species belonging to 11 genera and seven families are described and illustrated from the upper middle Eocene sequences drilled at Ocean Drilling Program Site 1260 (Leg 207; western Atlantic Ocean). Amongst the undescribed morphotypes encountered in this material, we chose to describe the most abundant and morphologically distinct ones, to best circumscribe the morphological diversity of each new species. As a consequence, a number of potentially new species that are represented by only one or a few isolated specimens have been excluded from this analysis. Information is also provided on the stratigraphic range of each new species, as well as the orbitally tuned ages for the first and last occurrences of most of them. Relationships with previously described species are also suggested. Finally, three species described in early radiolarian studies and rarely observed since are illustrated.

II.3.1.2. Materials and methods

Materials.— All samples examined in this study were collected from Leg 207 ODP Site 1260 (9°15′N, 54°32′W), located on the northwestern slope of Demerara Rise, a continental shelf off Suriname and French Guiana (Figure II.1). Today, the site lies between 9° and 10°N latitude, but according to paleomagnetic data, its position during the middle Eocene is estimated to be paleolatitude ~1°N (Suganuma and Ogg, 2006). Two holes (1260A and 1260B) recovered Paleogene sediments at a water depth of 2549 mbsf, allowing the study of an expanded and nearly continuous sedimentary sequence extending from the lower Albian to the middle Eocene (Shipboard Scientific Party, 2004). The middle Eocene interval at ODP Site 1260 is composed of greenish-white foraminifer-nannofossil chalk that contain abundant and well-preserved radiolarians, and diatoms (Shipboard Scientific Party, 2004; Danelian et al., 2005, 2007; Renaudie et al., 2010). In this study, we focused on the richest radiolarian interval; a 91.72 m thick sequence ranging from 43.77 Ma to 39.83 Ma, corresponding to the late middle Eocene (middle Lutetian to middle Bartonian). A total of 55 samples were selected from 10 cores (15R to 6R) from Hole 1260A, resulting in an average inter-sample spacing of ~1.67 m and an average age resolution of ~71,600 years.

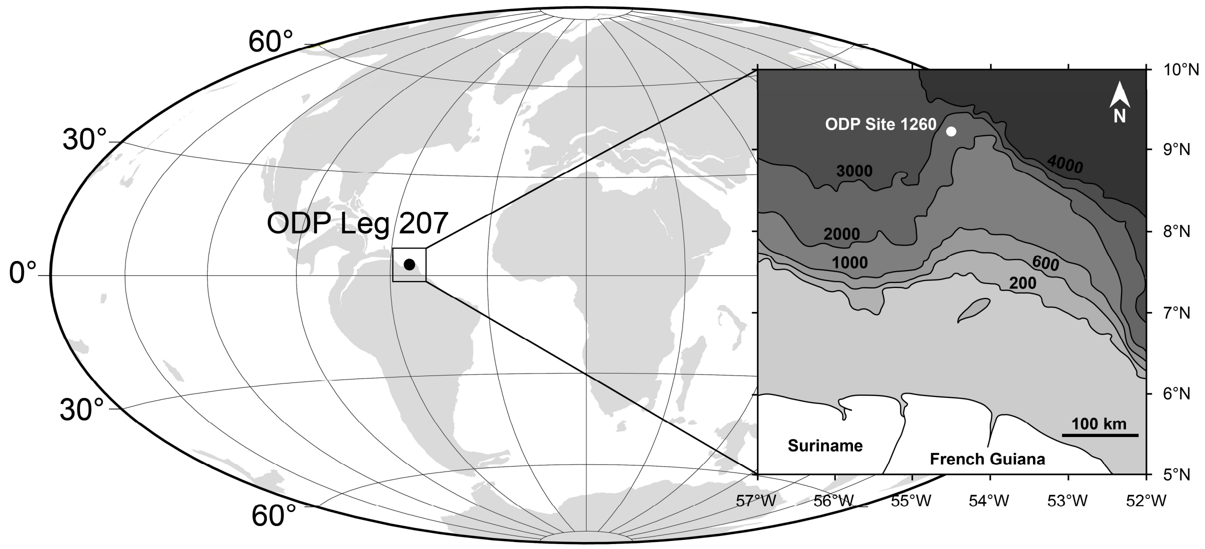

Figure II.1. Middle Eocene (ca. 40 Ma) paleogeographic map showing the location of Demerara Rise (ODP Leg 207) in the western equatorial Atlantic Ocean. The square shows the detailed location of ODP Site 1260 on a modern bathymetric map (modified after Wang et al., 2016). Paleogeographic reconstruction based on the ODSN Plate Tectonic Reconstruction Service (http://www.odsn.de/odsn/services/paleomap/paleomap.html).

A well-defined cyclostratigraphic framework has been developed for ODP Site 1260 using X-ray fluorescence core scanning (Westerhold and Röhl, 2013). Astrochronological calibration is available throughout the sequence at every 2 cm of sediment, allowing each sample to be dated with a high accuracy. Where calibration was not available for portions of Hole 1260A, the absolute ages of the corresponding samples were estimated based on the calibrated ages provided for samples at the same depth in Hole 1260B.

Methods.— Samples were processed according to the protocol described in Sanfilippo et al. (1985). First of all, ~1 cm² of untreated sediment was placed in a beaker and soaked in ~10 % hydrogen peroxide (H_2O_2) and ~30 % hydrochloric acid (HCl) to remove organic matter and carbonate fraction, respectively. The resulting residues were then washed through a 45 µm sieve to remove clay, small diatom frustules, and radiolarian fragments. We chose this relatively fine mesh to improve the recovery of smaller radiolarian species that may be lost when using larger meshes. One to four slides were then prepared for each sample using a few mg of cleaned residue evenly distributed on a coverslip according to the preparation method described by Witkowski et al. (2012). When dry, the coverslips were mounted onto standard glass slides using Norland Optical Adhesive 61 (refractive index 1.56).

All slides were systematically examined for radiolarians by using a Zeiss Axio Imager.A2 as a transmitted light microscope equipped with a Zeiss AxioCam ERc5s digital camera. For each specimen illustrated, a series of five to ten images taken at different focus distances were z-stacked using Helicon Focus v.7.6.6 (HeliconSoft) to produce a fully focused composite image.

In the following section, dimensions are based on a maximum number of specimens observed at different depths in the sedimentary sequence, in order to represent, at best, the intraspecific variation throughout the stratigraphic range of the species. Measurements were made directly on the specimen pictures, using the image processing and analysis software ImageJ (Schneider et al., 2012).

The radiolarian biozonation used here is that introduced by Riedel and Sanfilippo (1970, 1971, 1978) and Sanfilippo et al. (1985), and recently refined by Meunier and Danelian (2022), with the introduction of some subzones. The stratigraphic occurrences of the species are shown in Figure II.2, and the associated bioevents are summarized in Table II.1, along with their tuned ages at ODP Site 1260.

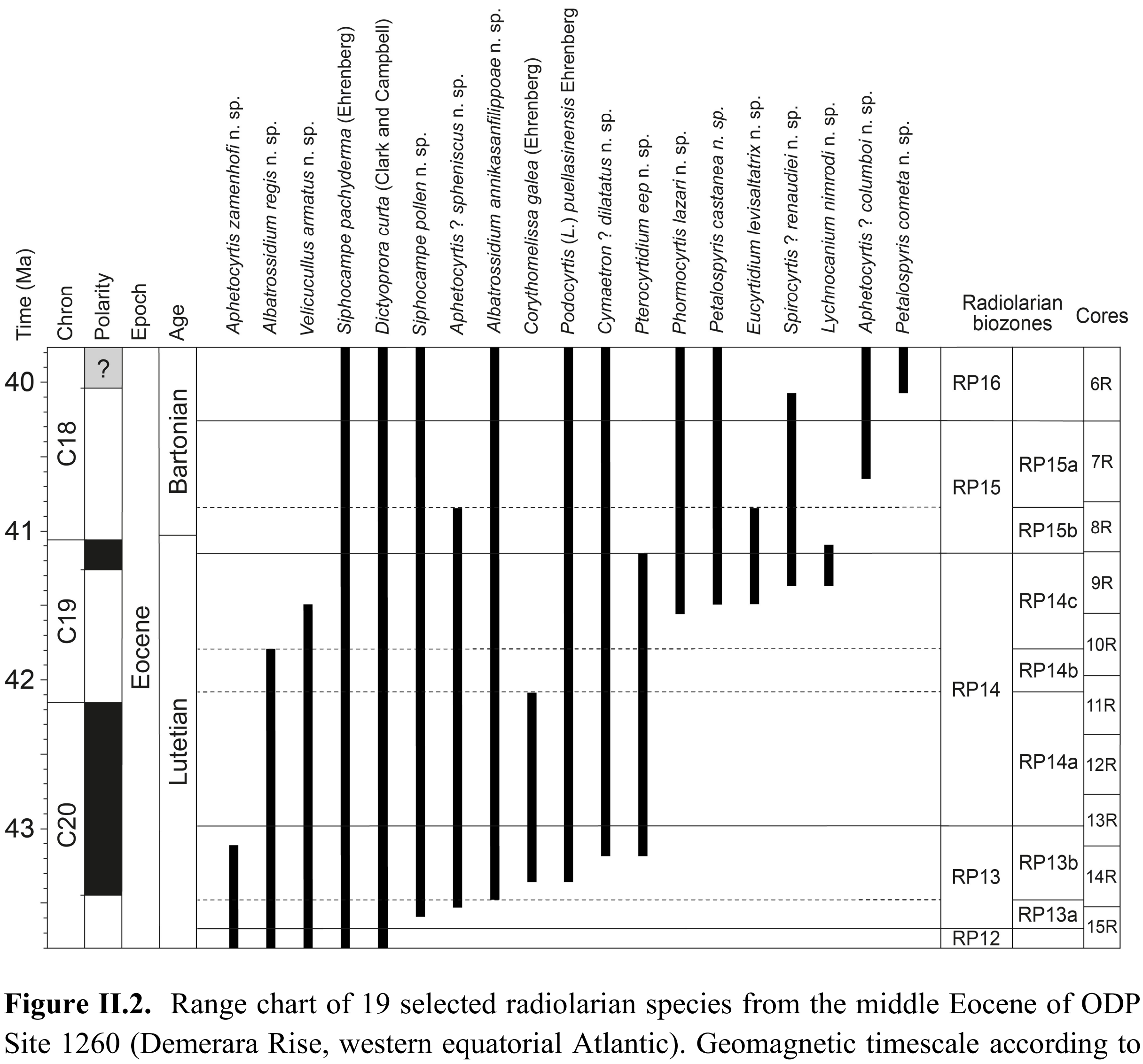

Figure II.2. Range chart of 19 selected radiolarian species from the middle Eocene of ODP Site 1260 (Demerara Rise, western equatorial Atlantic). Geomagnetic timescale according to calibration of Suganuma and Ogg (2006), and radiolarian biozonations according to Meunier and Danelian (2022).

Repositories and institutional abbreviations.— All holotypes and figured specimens (Plates II.22–II.26) are housed in the public paleontological collection of the University of Lille (USTL), France. Specimens are indexed by hole number, core number, section number, interval depth, and England finder coordinates.

Table II.1. Summary of first occurrences (FO) and last occurrences (LO) at ODP Site 1260, drilled on Demerara Rise in the western equatorial Atlantic. Estimated ages and revised meter composite depths (rmcd) are from Westerhold and Röhl (2013).

ODP Site 1260			Tuned age (Ma)	
Radiolarian bioevents	Core, section, interval (cm) Base/top	Depth (rmcd) Base/top	Base/top	Midpoint
FO *Petalospyris cometa* n. sp.	6R-5W, 55–57/6R-4W, 55–57	44.75/43.25	40.11/40.04	40.08
LO *Spirocyrtis* ? *renaudiei* n. sp.	6R-5W, 55–57/6R-4W, 55–57	44.75/43.25	40.11/40.04	40.08
FO *Aphetocyrtis* ? *columboi* n. sp.	7R-6W, 54–56/7R-4W, 54–56	56.04/53.04	40.73/40.57	40.65
LO *Eucyrtidium levisaltatrix* n. sp.	7R-6W, 54–56/7R-4W, 54–56	56.04/53.04	40.73/40.57	40.65
LO *Aphetocyrtis* ? *spheniscus* n. sp.	8R-3W, 54–56/7R-6W, 54–56	61.24/56.04	40.96/40.73	40.85
LO *Lychnocanium nimrodi* n. sp.	8R-6W, 54–56/8R-5W, 54–56	65.74/64.24	41.12/41.07	41.10
LO *Pterocyrtidium eep* n. sp.	9R-1W, 55–57/8R-6W, 54–56	66.85/65.74	41.18/41.12	41.15
FO *Lychnocanium nimrodi* n. sp.	9R-5W, 55–57/9R-4W, 55–57	72.85/71.35	41.40/41.34	41.37
FO *Spirocyrtis* ? *renaudiei* n. sp.	9R-5W, 55–57/9R-4W, 55–57	72.85/71.35	41.40/41.34	41.37
FO *Eucyrtidium levisaltatrix* n. sp.	9R-7W, 55–57/9R-6W, 55–57	75.85/74.35	41.53/41.46	41.50
FO *Petalospyris castanea* n. sp.	9R-7W, 55–57/9R-6W, 55–57	75.85/74.35	41.53/41.46	41.50
LO *Velicucullus armatus* n. sp.	9R-7W, 55–57/9R-6W, 55–57	75.85/74.35	41.53/41.46	41.50
FO *Phormocyrtis lazari* n. sp.	10R-1W, 55–57/9R-7W, 55–57	77.33/75.85	41.59/41.53	41.56
LO *Albatrossidium regis* n. sp.	10R-5W, 55–57/10R-3W, 55–57	83.33/80.33	41.85/41.73	41.79
LO *Corythomelissa galea* (Ehrenberg) n. comb.	11R-3W, 55–57/11R-2W, 55–57	89.55/88.05	42.12/42.05	42.09
LO *Aphetocyrtis zamenhofi* n. sp.	14R-1W, 55–57/13R-6W, 54–56	116.02/112.74	43.16/43.06	43.11
FO *Cymaetron* ? *dilatatus* n. sp.	14R-2W, 55–57/14R-1W, 55–57	117.52/116.02	43.21/43.16	43.19
FO *Pterocyrtidium eep* n. sp.	14R-2W, 55–57/14R-1W, 55–57	117.52/116.02	43.21/43.16	43.19
FO *Corythomelissa galea* (Ehrenberg) n. comb.	14R-5W, 55–57/14R-4W, 55–57	122.02/120.52	43.39/43.33	43.36
FO *Podocyrtis* (*L.*) *puellasinensis* Ehrenberg	14R-5W, 55–57/14R-4W, 55–57	122.02/120.52	43.39/43.33	43.36
FO *Albatrossidium annikasanfilippoae* n. sp.	14R-7W, 55–57/14R-6W, 55–57	125.02/123.52	43.51/43.45	43.48
FO *Aphetocyrtis* ? *spheniscus* n. sp.	15R-1W, 55–57/14R-7W, 55–57	125.97/125.02	43.55/43.51	43.53
FO *Siphocampe pollen* n. sp.	15R-2W, 55–57/15R-1W, 55–57	127.47/125.97	43.63/43.55	43.59

II.3.1.3. Systematic paleontology

The higher-level classification used in this study is based on the most recent and comprehensive radiolarian classification provided by Suzuki et al. (2021). For previously described species, we used combinations derived from O'Dogherty et al. (2021).

The terminology used to designate the different parts of the fundamental nassellarian spicule is based on Petrushevskaya (1984). See also Goll (1968; p. 1413, text-figure 6) for features specific to the family Cephalospyrididae, and Sanfilippo and Caulet (1998; p. 6, text-figure 2) for features specific to the family Lophocyrtiidae.

Infrakingdom Rhizaria Cavalier-Smith, 2002 emend. Cavalier-Smith, 2003

Phylum Retaria Cavalier-Smith, 1999

Class Polycystinea Ehrenberg, 1839

Order Nassellaria Ehrenberg, 1876

Superfamily Eucyrtidioidea Ehrenberg, 1846 emend. Suzuki et al., 2021

Family Eucyrtidiidae Ehrenberg, 1846 emend. Suzuki et al., 2021

Genus *Cymaetron* Caulet, 1991

Type species.— *Cymaetron sinolampas* Caulet, 1991, p. 536, pl. 4, figs. 10–12; by monotypy.

Cymaetron ? *dilatatus* new species

Plate II.22, Figures 1–4

Holotype.— Plate II.22, Figure 1; collection number USTL 3483–1; coordinates V46/2; sample ODP 1260A-9R-4W, 55–57 cm; upper part of the *Podocyrtis* (*L.*) *mitra* Zone, in the *Podocyrtis* (*P.*) *apeza* Subzone (late Lutetian, middle Eocene).

Diagnosis.— Three-segmented eucyrtidiid with an abdomen constricted in two false segments.

Occurrence.— This species occurs sporadically throughout the studied interval, from the upper part of the *Podocyrtis* (*P.*) *ampla* Zone, to the lower part of the *Podocyrtis* (*L.*) *goetheana* Zone.

Description.— Shell three-segmented, smooth and robust, with the collar and lumbar strictures marked externally by a change in the contour of the shell Cephalis proportionally small, globular, poreless or bearing a few small circular pores. Apical spine extending outward as a strong apical tribladed horn longer than the cephalis, and dorsal spine prolonged as thoracic rib on upper thorax. Thorax truncate conical to slightly inflated conical, with subcircular pores, hexagonally framed and quincuncially arranged. Abdomen conspicuously inflated in its proximal part, usually 1.5 to 2 times as wide as thorax, then subcylindrical to truncate conical. The two parts of the abdomen are not subdivided into segments by an inner-ring. Abdominal pores subcircular, hexagonally framed and quincuncially arranged, sometimes less regularly arranged in the most distal part of the segment. Aperture open wide. Abdominal termination invariably ragged along a row of pores.

Etymology.— The specific epithet refers to the expanded proximal part of the abdomen of the new species; *dilatatus* in Latin means ‘dilated, expanded’. The specific epithet is to be treated as an adjective in the nominative singular.

Dimensions.— Based on 10 specimens (mean): total length without the apical horn 145–188 µm (176), length of apical horn: 18–31 µm (24), length of cephalothorax without the apical horn: 45–66 µm (56), length of abdomen: 51–155 µm (117), maximum breadth of abdomen 82–129 µm (95).

Remarks.— *Cymaetron* ? *dilatatus* n. sp. is tentatively assigned to the genus *Cymaetron* based on the characteristic wavy outline of the shell, which is constricted in false segments. However, the generic assignment is doubtful because the genus *Cymaetron* was originally described by Caulet (1991) as a two-segmented eucyrtidiid, while *C*. ? *dilatatus* n. sp. clearly has a three-segmented shell. Furthermore, the new species differs from *C*. *sinolampas* Caulet, 1991, the only other species of the genus, by having only one abdominal constriction. In addition to the characters already mentioned, this new species is distinguished from all other eucyrtidiid species with an open abdomen in not having post-abdominal segments. Finally, *C*. ? *dilatatus* n. sp. superficially resembles *Theocorys anaclasta* Riedel and Sanfilippo, 1970, from which it differs in having a much more elongated shell, a bladed apical horn, and smaller abdominal pores which are regular in size.

Genus *Eucyrtidium* Ehrenberg, 1846

Type species.— *Lithocampe acuminata* Ehrenberg, 1844, p. 84 (unfigured); Ehrenberg, 1854a, pl. 22, fig. 27; subsequent designation by Frizzell and Middour (1951, p. 33).

Eucyrtidium levisaltatrix new species

Plate II.22, Figures 5–8

Holotype.— Plate II.22, Figure 5; collection number USTL 3482–1; coordinates J52/2; sample ODP 1260A-9R-4W, 55–57 cm; upper part of the *Podocyrtis* (*L*.) *mitra* Zone, in the *Podocyrtis* (*P*.) *apeza* Subzone (late Lutetian, middle Eocene).

Diagnosis.— *Eucyrtidium* species with an elongated abdomen, which is the longer segment of the shell.

Occurrence.— This short-lived species is relatively rare from the uppermost part of the *Podocyrtis* (*L.*) *mitra* Zone, to the lower part of the *Podocyrtis* (*L.*) *chalara* Zone.

Description.— Shell multisegmented, conical-elongated and thick-walled. Cephalis relatively small, globular and sparsely pored, bearing a long conical apical horn. Collar stricture marked externally by a change in the contour of the shell. Thorax subspherical to campanulate, with circular pores quincuncially arranged. Dorsal spine of the initial spicule rarely protruding near the thoracic stricture as a reduced, curved thoracic wing (Plate II.22, Figure 8). Abdomen subcylindrical to campanulate, being the longest segment. Abdominal pores circular, slightly larger than thoracic pores, hexagonally framed and longitudinally aligned. First post-abdominal segment with pores of irregular size and shape. Abdomen and first post-abdominal segment separated by a slight external constriction and by a straight (Plate II.22, Figure 7) or wavy (Plate II.22, Figures 5, 6) internal ridge which appears externally as a thick dark band. Distal part of the abdomen invariably ragged along a row of pores.

Etymology.— From the Latin *levis*, meaning ‘light, not heavy’, and *saltatrix*, meaning ‘female dancer, dancing girl’. The specific epithet is to be treated as a noun in the nominative singular standing in apposition to the generic name.

Dimensions.— Based on six specimens (mean): total length without the apical horn: 166–226 µm (194), length of apical horn: 26–38 µm (30), length of cephalothorax: 51–57 µm (55), length of abdomen: 107–134 µm (119), maximum breadth of shell: 101–127 µm (118).

Remarks.— This distinctive species is differentiated from all other middle Eocene *Eucyrtidium* species by its long apical horn, its well-defined abdominal stricture, and by its more conical shape due to the elongation of the abdomen compared to the other segments of the shell. In addition, unlike other large species of the genus *Eucyrtidium*, the shell of *E. levisaltatrix* n. sp. is usually broken at the first post-abdominal segment.

It is likely that the new species originated from a stock of late middle Eocene multisegmented *Eucyrtidium* by elongation of the abdomen. However, further phylogenetic affinities remain unclear due to the sudden appearance of *E. levisaltatrix* n. sp. in the fossil record.

Superfamily Artostrobioidea Riedel, 1967a

Family Artostrobiidae Riedel, 1967a sensu Sugiyama, 1998

Genus *Dictyoprora* Haeckel, 1887

Type species.— *Dictyocephalus amphora* Haeckel, 1887, p. 1305, pl. 62, fig. 4; subsequent designation by Campbell (1953, p. 296).

Dictyoprora curta (Clark and Campbell, 1942)

Plate II.22, Figures 9–12

1942 *Dictyocephalus* (*Dictyoprora*) *pulcherrimus curtus* Clark and Campbell, p. 79, pl. 8, figs. 3, 6, 7.
1973 *Theocampe pirum* (Ehrenberg) – Foreman, p. 432, pl. 9, fig. 11 (part).
1975 *Theocampe urceolus* (Haeckel) – Chen, p. 456, pl. 3, fig. 7.
? 1994 *Dictyoprora amphora* (Haeckel) – Weinheimer et al., p. 311, pl. 1, fig. 13.
1995 *Dictyoprora amphora* (Haeckel) – Shilov, p. 126, pl. 2, figs. 7, 8.
1997 *Theocampe amphora* (Haeckel) – Hollis et al., p. 56, pl. 4, figs. 38, 39.
2005 *Dictyoprora* spp. Nigrini et al., pl. P6, fig. 13 (part).
2006 *Dictyoprora* sp. A Funakawa et al., p. 18, pl. P2, figs. 10a, 10b.

Holotype.— As no type was designated by Clark and Campbell (1942) in their original publication, each of the three illustrated specimens (pl. 8, figs. 3, 6, 7) are candidate lectotypes; they are all housed in the University of California, Museum of Paleontology, San Francisco.

Occurrence.— This species is found throughout the studied interval. It occurs sporadically from the *Thyrsocyrtis* (*P*.) *triacantha*[1] Zone, to the upper part of the *Podocyrtis* (*L*.) *mitra* Zone, and becomes more consistent and abundant from the upper part of the *Podocyrtis* (*L*.) *mitra* Zone to the *Podocyrtis* (*L*.) *goetheana* Zone.

Description.— Ovoid shell consisting of three segments. Shell surface relatively smooth, but with fine surface sculpture on abdomen. Cephalis hemispherical, unarmed, with scattered subcircular pores. Ventral pore large and circular, but no ventral tube developed. Collar stricture externally not defined in most specimens observed. Thorax truncate conical, with irregularly arranged circular pores. Lumbar stricture slightly expressed externally by a change in the shell outline. Globular abdomen perforated by circular downwardly directed pores arranged in five to six transverse rows. Each abdominal pore opens into a furrow dug into the wall thickness and extending almost to the next row of pores. Shell narrows distally and terminates in a cylindrical poreless peristome with a smooth margin.

Dimensions.— Based on 15 specimens (mean): total length: 89–108 µm (97), length of cephalothorax: 29–38 µm (34), length of abdomen: 56–72 µm (63).

1 *Thyrsocyrtis* (*Pentalocorys*) *schomburgkii* (Ehrenberg, 1847) in Chapter II.2.

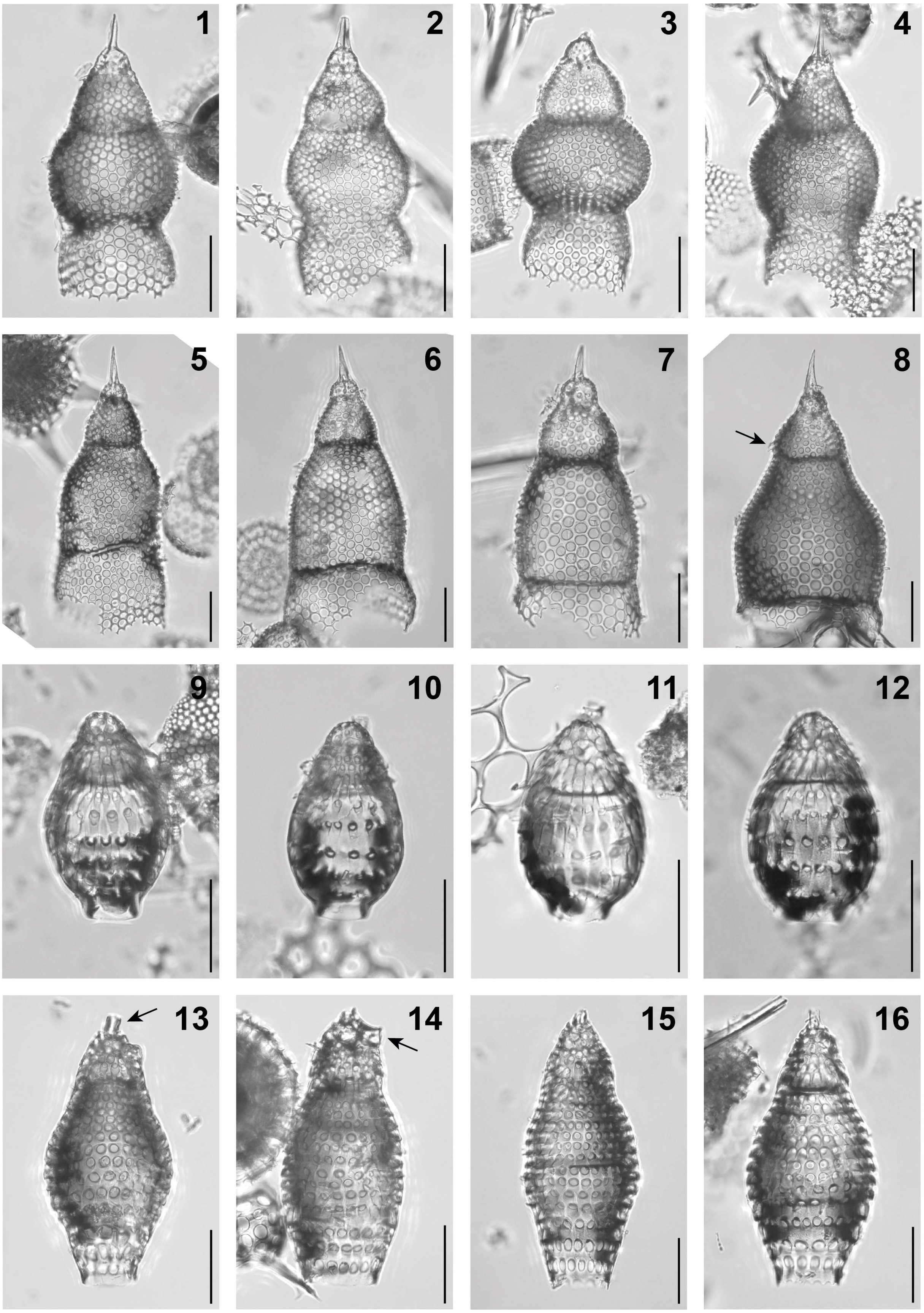
1
2
3
4
5
6
7
8
9
10
11
12
13
14
15
16

Plate II.22. Composite light micrographs of new radiolarian species from ODP Site 1260 (Demerara Rise, western equatorial Atlantic). (**1–4)** *Cymaetron* ? *dilatatus* n. sp.: (**1**) holotype, ODP 1260A-9R-4W, 55–57 cm, USTL 3483–1, V46/2; (**2**) ODP 1260A-9R-4W, 55–57 cm, USTL 3481–1, H41/3; (**3**) ODP 1260A-9R-3W, 55–57 cm, USTL 3479–1, T47/1 (mirrored); (**4**) ODP 1260A-9R-4W, 55–57 cm, USTL 3481–2, J37/2. (**5**–**8**) *Eucyrtidium levisaltatrix* n. sp.: (**5**) holotype, ODP 1260A-9R-4W, 55–57 cm, USTL 3482–1, J52/2; (**6**) ODP 1260A-9R-4W, 55–57 cm, USTL 3484–1, V45/2; (**7**) ODP 1260A-9R-3W, 55–57 cm, USTL 3478–1, E48/4; (**8**) specimen showing thoracic wing (arrow), ODP 1260A-8R-3W, 54–56 cm, USTL 3462–3, Z63/4 (mirrored). (**9**–**12**) *Dictyoprora curta* (Clark and Campbell): **(9)** ODP 1260A-14R-1W, 55–57 cm, USTL 3530–1, J40/1; (**10**) ODP 1260A-6R-3W, 55–57 cm, USTL 3424–1, H60/4; **(11)** ODP 1260A-9R-1W, 55–57 cm, USTL 2848–1, C46/2; (**12**) ODP 1260A-9R-1W, 55–57 cm, USTL 3473–1, L48/1. (**13**–**16**) *Spirocyrtis* ? *renaudiei* n. sp.: **(13)** holotype, showing apical tube (arrow), ODP 1260A-8R-3W, 54–56 cm, USTL 3462–1, Q53/1 (mirrored); (**14**) specimen showing ventral tube (arrow), ODP 1260A-8R-3W, 54–56 cm, USTL 3462–2, L48/1 (mirrored); (**15**) ODP 1260A-7R-6W, 54–56 cm, USTL 3454–1, X45/2; (**16**) ODP 1260A-7R-6W, 54–56 cm, USTL 3454–2, R43/2. All scale bars equal 50 µm.

Remarks.— We have judged it appropriate to re-illustrate this species because it has been rarely observed since its original description by Clark and Campbell (1942) from the upper middle Eocene strata of Mont Diablo, California. *Dictyoprora curta* (Clark and Campbell, 1942) is distinguished from all other dictyoprorids by its small globular abdomen (maximum length of the abdomen <80 µm). This species also differs from *D. pirum* (Ehrenberg, 1874) and *D. gibsoni* O'Connor, 1994 in having more closely spaced rows of pores, a well-developed peristome, and a thick-walled shell rather than a thin hyaline shell; from *D. urceolus* (Haeckel, 1887) by having a globular abdomen and its abdominal pores being downwardly directed; from *D. armadillo* (Ehrenberg, 1874) and *D. ovata* (Haeckel, 1887) in lacking a cephalic horn and in having less than seven rows of abdominal pores. Finally, it differs from *D. mongolfieri* (Ehrenberg, 1854a) in that the abdominal pores are not aligned longitudinally and from *D. amphora* (Haeckel, 1887) in that the abdominal pores are regular in size and shape and aligned in transverse rows.

Genus *Siphocampe* Haeckel, 1882

Type species.— *Siphocampe annulosa* Haeckel, 1887, p. 1500, pl. 79, fig. 10; subsequent designation by Strelkov and Lipman (1959, p. 459).

Siphocampe pachyderma (Ehrenberg, 1874)

Plate II.23, Figures 1–4

1874 *Eucyrtidium pachyderma* Ehrenberg, p. 231.
1876 *Eucyrtidium pachyderma* Ehrenberg – Ehrenberg, p. 72, pl. 11, fig. 21.
1882a *Lithomitra Pachyderma* [sic] (Ehrenberg) – Bütschli, p. 529.
1882b *Lithomitra Pachyderma* [sic] (Ehrenberg) – Bütschli, pl. 30, fig. 26.
1887 *Lithomitra* (*Lithomitrella*) *pachyderma* (Ehrenberg) – Haeckel, p. 1483.
1976 *Lithomitra* ? sp. aff. *Lithocampe minuta* Clark and Campbell – Dzinoridze et al., pl. 32, figs. 16, 17.
1991 *Siphocampe pachyderma* (Ehrenberg) – Caulet, p. 539, pl. 3, fig. 12.
2009 *Eucyrtidium pachyderma* Ehrenberg – Ogane et al., pl 21, figs. 1a–1d.
2013 *Siphocampe* ? sp. Kochhann et al., p. 542, pl. 3 fig. R.

Lectotype.— No holotype was designated by Ehrenberg in the original description of the species. The specimen drawn by Ehrenberg (1876, pl. 11, fig. 21) was re-illustrated by Ogane et al. (2009, pl. 21, figs. 1a-1d) during their re-examination of Ehrenberg's collection held at the Museum für Naturkunde, Humboldt-Universität (Berlin, Germany), and subsequently designated as a lectotype by O'Dogherty et al. (2021; p. 976).

Diagnosis.— Very thick-walled *Siphocampe* species, with an asymmetrically placed cephalis and widely spaced rows of abdominal pores.

Occurrence.— The record of this species is punctuated throughout the studied interval, from the *Thyrsocyrtis* (*P.*) *triacantha*[2] Zone to the *Podocyrtis* (*L.*) *goetheana* Zone.

Description.— Shell three-segmented, small, spindle-shaped, and very thick-walled. Cephalis hemispherical to subspherical, asymmetrically placed, poreless or with a few subcircular pores. Ventral pore present, but ventral tube not developed. Apical horn absent. Collar and lumbar stricture indistinct in most observed specimens. Thorax trapezoidal, with two to four transverse rows of circular pores. Thoracic wall thickened distally. Abdomen elongated, subcylindrical to barrel-shaped and very thick-walled, two to three times longer than the thorax. Abdominal pores small, circular, with tubular projections through the abdominal wall, arranged in three to five transverse rows of pores. Although the abdomen is externally smooth, internal indentations can be distinguished by transparency, the maximum thickness of the abdominal wall being reached between the rows of pores. Shell ends in a smooth, poreless peristome.

Dimensions.— Based on six specimens (mean): total length: 84–119 µm (99), maximum breadth: 43–57 µm (51).

Remarks.— *Siphocampe pachyderma* differs from all other species of the genus *Siphocampe* in having a very thick-walled and almost hyaline shell, and from *Plannapus aitai* O'Connor, 2000 in having a less elongated shell with less than 10 transverse rows of pores.

2 *Thyrsocyrtis* (*Pentalocorys*) *schomburgkii* (Ehrenberg, 1847) in Chapter II.2.

Siphocampe pollen new species

Plate II.23, Figures 5–8

1975 *Theocampe amphora* (Haeckel) group – Chen, p. 456, pl. 2, fig. 2 (part).

1976 *Lithomitra* ? sp. aff. *Lithomitra minuta* Clark and Campbell – Dzinoridze et al., pl. 29, fig. 6.

1997 *Siphocampe acephala* (Ehrenberg) group – Hollis et al., p. 54, pl. 4, fig. 8 (part).

Holotype.— Plate II.23, Figure 5; collection number USTL 2854–1; coordinates L48/1; sample 1260A-13R-4W, 55–56 cm; lowermost part of the *Podocyrtis* (*L.*) *mitra* Zone, in the *Artostrobus quadriporus* Subzone (late Lutetian, middle Eocene).

Diagnosis.— *Siphocampe* species with a symmetrically placed cephalis and a thick-walled abdomen pierced by closely spaced rows of transverse pores.

Occurrence.— This species is found in almost all the studied samples, from the lowermost part of the *Podocyrtis* (*P.*) *ampla* Zone, to the lower part of the *Podocyrtis* (*L.*) *goetheana* Zone.

Description.— Shell of three segments, spindle-shaped and smooth-surfaced. Cephalis hemispherical, asymmetrically placed and partially embedded in the thorax. Apical horn absent. Ventral pore present, but ventral tube not developed. Cephalic pores subcircular, sparse and irregularly arranged. Collar stricture slightly dark on the outside, but not marked by a change in the contour of the shell. Thorax truncate conical with five to six closely spaced transverse rows of small subcircular to circular pores. Lumbar stricture usually dark on the outside. Abdomen elongated, barrel-shaped, and thick-walled, about twice the length of the cephalothorax. Abdominal pores small, circular, cylindrical, arranged in nine to ten transverse rows. Distal part of the abdomen usually ragged (Plate II.23, Figures 6, 7), but in complete specimens the shell terminates in a thin, poreless peristome (Plate II.23, Figure 5).

Etymology.— From the Latin *pollen*, meaning ‘flour flower’, because of its resemblance to a pollen grain (i.e., the male reproductive particles produced by the anther lodges of flower stamens). The specific epithet is to be treated as a noun in the nominative singular standing in apposition to the generic name.

Dimensions.— Based on 24 specimens (mean): total length: 68–129 µm (91), maximum breadth: 30–55 µm (45).

Remarks.— The general shape of the shell of *Siphocampe pollen* n. sp. resembles that of *S. acephala* (Ehrenberg, 1874) and *S. missilis* O’Connor, 1994. It differs from these species in having a thicker abdominal and thoracic wall, and nine to ten transverse rows of pores on the abdomen, instead of four to eight rows in *S. acephala* and eight to seventeen rows in *S. missilis*. The new species also differs from *S. acephala* in having a spindle-shaped rather than subcylindrical abdomen, and from *S. missilis* in having an asymmetrical cephalis. It differs from *S. imbricata* (Ehrenberg, 1874), *S. lineata* (Ehrenberg, 1839) and *S. arachnea* (Ehrenberg, 1862) in the shorter length of the abdomen and the absence of abdominal indentations. The new species differs from the co-occurring species *S. pachyderma* (Ehrenberg, 1874) in having a thinner abdominal wall and closely spaced transverse rows of pores on the abdomen. Finally, *S. pollen* n. sp. differs from the enigmatic *Plannapus* ? *aitai* O’Connor, 2000 in having an asymmetrically placed cephalis that never bears an apical horn, and a three-segmented shell with thinner walls. *S. pollen* n. sp. is probably related to *S. acephala* and *S. pachyderma*, which also have an asymmetrical cephalis. The characteristic thickness of the shell wall also suggests a close relationship between the new species and *S. pachyderma*.

Genus *Spirocyrtis* Haeckel, 1882 emend. Nigrini, 1977

Type species.— *Spirocyrtis scalaris* Haeckel, 1887, p. 1509, pl. 76, fig. 14; subsequent designation by Campbell (1954, p. D142).

Spirocyrtis ? *renaudiei* new species

Plate II.22, Figures 13–16

Holotype.— Plate II.22, Figure 13; collection number USTL 3462–1; coordinates Q53/1; sample ODP 1260A-8R-3W, 54–56 cm; *Podocyrtis* (*L.*) *chalara* Zone, in the *Rhopalosyringium* ? *biauritum* Subzone (late Lutetian, middle Eocene).

Diagnosis.— Artostrobiid with a multisegmented pupoid shell, a short, truncated apical tube, and a flared ventral tube.

Occurrence.— From the uppermost part of the *Podocyrtis* (*L.*) *mitra* Zone, to the lowermost part of the *Podocyrtis* (*L.*) *goetheana* Zone.

Description.— Shell pupoid to spindle-shaped, thick-walled, and multisegmented, with the fourth segment being the widest (rarely the third). Strictures usually indistinct or only slightly dark externally. Cephalis truncate conical, with downwardly directed subcircular pores, bearing a short truncated apical tube (Plate II.22, Figure 13) and a robust, distally flared ventral tube that opens almost perpendicular to the axis of the shell (Plate II.22, Figure 14). Thorax truncate conical, half the length of the cephalis, with two to four transverse rows of subcircular pores.

Abdomen truncate conical or slightly campanulate, longer than thorax, with three to five transverse rows of pores. First post-abdominal segment short, cylindrical, and medially expanded, with its lower margin marked by a narrow hyaline band. Other post-abdominal segments short, truncate conical, broader proximally than distally. All post-abdominal segments with subcircular pores arranged in one to three transerve rows. Pores tend to be larger distally. Last segment terminating in a narrow hyaline peristome (Plate II.22, Figures 13, 14), ragged in most observed specimens (Plate II.22, Figures 15, 16).

Etymology.— This species is named after Dr. Johan Renaudie (Museum für Naturkunde – Humboldt-Universität, Berlin) in honor of his contribution to the study of Cenozoic radiolarians. The specific epithet is to be treated as a noun in the genitive case formed from a modern personal name.

Dimensions.— Based on 20 specimens (mean): total length without the apical tube: 173–216 µm (192), maximum breadth of shell: 66–98 µm (89), length of apical tube: 9–13 µm (10).

Remarks.— *Spirocyrtis* ? *renaudiei* n. sp. differs from all other *Spirocyrtis* species in having a pupoid rather than a conical shell. The new species is also distinguished from *Botryostrobus grantmackiei* (O'Connor, 1997a) and *B*. *hollisi* (O'Connor, 1997a) in having larger pores arranged in more closely spaced transverse rows and in lacking post-abdominal indentations; from *B*. *miralestensis* (Campbell and Clark, 1944) and *B*. *aquilonaris* (Bailey, 1856) in being more elongated and in lacking a hyaline peristome. Finally, it is also more elongated and lacks a hyaline peristome compared to *B*. *miralestensis* (Campbell and Clark, 1944) and *B*. *aquilonaris* (Bailey, 1856).

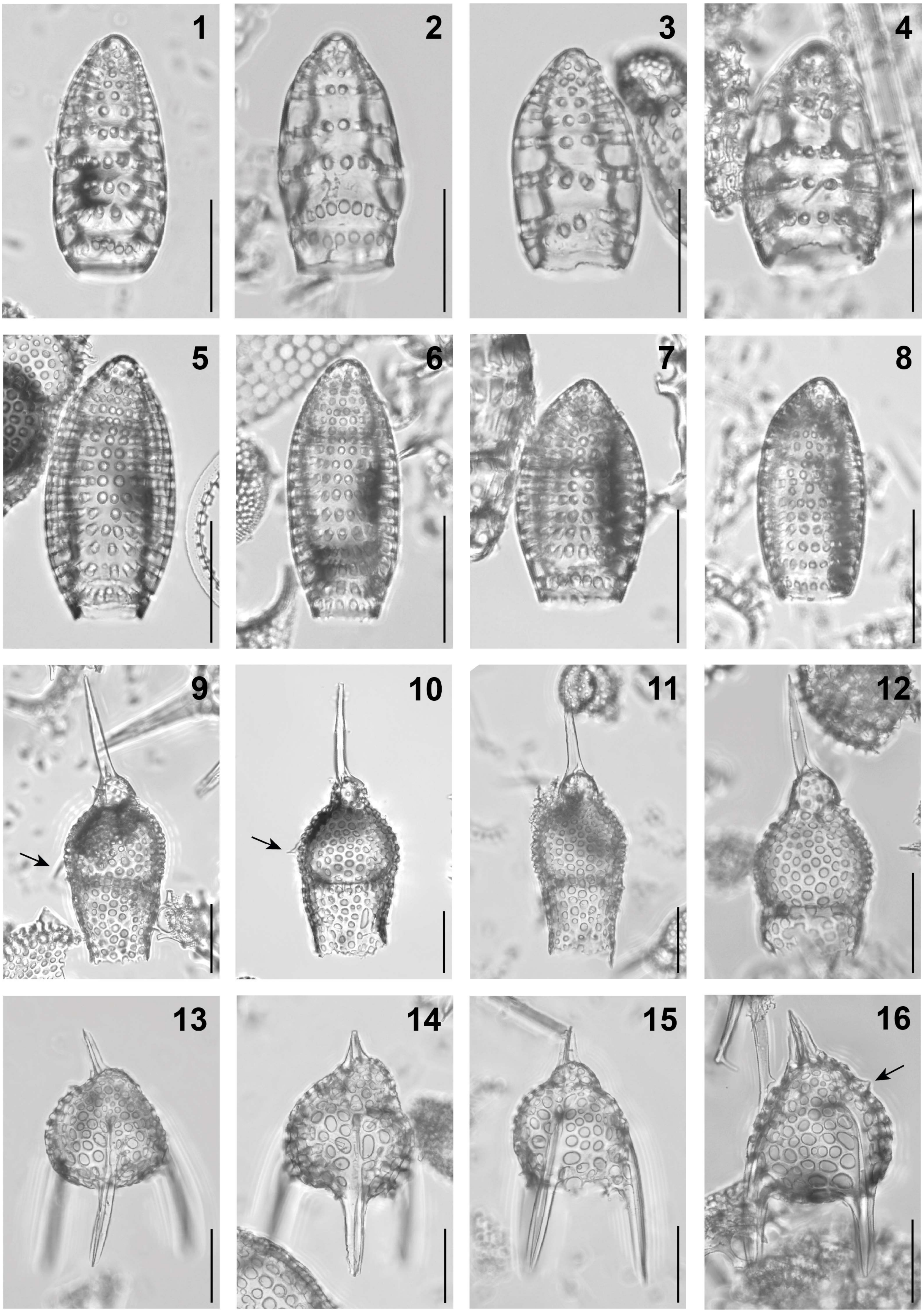
1
2
3
4
5
6
7
8
9
10
11
12
13
14
15
16

Plate II.23. Composite light micrographs of new radiolarian species from ODP Site 1260 (Demerara Rise, western equatorial Atlantic). (**1**–**4**) *Siphocampe pachyderma* (Ehrenberg): (**1**) ODP 1260A-9R-3W, 55–57 cm, USTL 3477–3, V50/3; (**2**) ODP 1260A-12R-6W, 55–57 cm, USTL 3519–1, F39/4; (**3**) ODP 1260A-11R-7W, 55–57 cm, USTL 3506–1, M43/3; (**4**) ODP 1260A-12R-4W, 55–57 cm, USTL 3514–1, S45/4. (**5**–**8**) *Siphocampe pollen* n. sp.: (**5**) holotype, ODP 1260A-13R-4W, 55–56 cm, USTL 2854–1, X67/4; (**6**) ODP 1260A-14R-1W, 55–57 cm, USTL 3530–3, N41/3; (**7**) ODP 1260A-10R-6W, 55–57 cm, USTL 3498–1, L52/2; (**8**) ODP 1260A-14R-1W, 55–57 cm, USTL 3531–1, W56/1. (**9**–**12**) *Pterocyrtidium eep* n. sp.: (**9**) holotype, showing thoracic wing (arrow), ODP 1260A-12R-CC, 63–177 cm, USTL 3521–1, U59/2 (mirrored); (**10**) specimen showing thoracic wing (arrow), ODP 1260A-12R-1W, 55–57 cm, USTL 2851–5, L64/3 (mirrored); (**11**) ODP 1260A-12R-CC, 63–177 cm, USTL 3521–2, U53/3; (**12**) ODP 1260A-12R-CC, 63–177 cm, USTL 3520–1, H36/3 (mirrored). (**13**–**16**) *Corythomelissa galea* (Ehrenberg): (**13**) ODP 1260A-11R-3W, 55–57 cm, USTL 3502–1, W34/4 (mirrored); (**14**) ODP 1260A-11R-4W, 55–57 cm, USTL 3503–1, F36/3 (mirrored); (**15**) ODP 1260A-11R-4W, 55–57 cm, USTL 3503–2, X39/3 (mirrored); (**16**) specimen showing sagittal horn (arrow), ODP 1260A-12R-CC, 63–177 cm, USTL 3520–2, X33/2 (mirrored). All scale bars equal 50 µm.

The generic assignment of *S.* ? *renaudiei* n. sp. is uncertain due to its affinity to both genera *Botryostrobus* and *Spirocyrtis*. The new species shares similarities with the genus *Botryostrobus*, as evidenced by the general pupoid shape of its shell, which tapers distally and widens at or before the fifth segment (O'Connor, 1997a). However, it can be distinguished from all *Botryostrobus* species by the presence of a short apical tube and a distally flared ventral tube, which are two diagnostic characteristics of the genus *Spirocyrtis* (Nigrini, 1977). The oldest known representatives of both genera have been found in upper Paleocene to lower Oligocene sequences: *B. joides* Petrushevskaya, 1975 (upper Eocene–lower Oligocene), *S.* ? *hollisi* Renaudie and Lazarus, 2012 (upper Paleocene, see Hollis, 2002), *S. greeni* O'Connor, 1999a (upper Eocene) and *S. proboscis* O'Connor, 1994 (lower Oligocene). The middle Eocene species *S.* ? *renaudiei* n. sp. is therefore one of the earliest known representatives of the genus *Spirocyrtis,* and its unique combination of features suggests a close relationship to the divergence between the genera *Botryostrobus* and *Spirocyrtis*.

Family Rhopalosyringiidae Empson-Morin, 1981

Genus *Pterocyrtidium* Bütschli, 1882a

Type species.— *Pterocanium barbadense* Ehrenberg, 1874, p. 254 (unfigured); Ehrenberg, 1876, p. 82, pl. 17, fig. 6; subsequent designation by Petrushevskaya and Kozlova (1972, p. 552).

Pterocyrtidium eep new species

Plate II.23, Figures 9–12

Holotype.— Plate II.23, Figure 9; collection number USTL 3521–1; coordinates U59/2; sample ODP 1260A-12R-CC, 63–177 cm; lower part of the *Podocyrtis* (*L.*) *mitra* Zone, in the *Artostrobus quadriporus* Subzone (Lutetian, middle Eocene).

Diagnosis.— *Pterocyrtidium* species with a long apical horn and a roundish thorax that is larger than the abdomen.

Occurrence.— Rare, from the uppermost part of the *Podocyrtis* (*P.*) *ampla* Zone to the upper part of the *Podocyrtis* (*L.*) *mitra* Zone.

Description.— Shell three-segmented, subcylindrical. Cephalis relatively small and globular, penetrated with a few subcircular pores and bearing a remarkably strong apical horn, usually three times as long as the cephalis height. Two dimples are present at the base of the apical horn (Plate II.23, Figure 9). Collar stricture externally expressed as a constriction. Thorax roundish to inflated and penetrated by numerous subcircular pores that are quincuncially arranged and hexagonally framed. In some specimens, primary lateral spines outgrow from the lower thorax as one or two sharply pointed lateral wings (Plate II.23, Figures 9, 10). Lumbar stricture marked by a change in the contour of the shell and a thick internal ridge. Abdominal pores subcircular and roughly aligned in longitudinal rows, and are less numerous in the distal part of the abdomen. Aperture open and bordered by a hyaline band, or ragged along a row of pores.

Etymology.— The specific epithet is to be treated as an arbitrary combination of letters derived from the acronym used to designate the Evolution, Ecology, Paleontology laboratory (EEP) of the University of Lille, as a token of gratitude for the assistance offered to the first author.

Dimensions.— Based on five specimens (mean): total length without the apical horn: 133–153 µm (138), length of apical horn: 61–75 µm (70), length of cephalothorax without the apical horn: 76–84 µm (79), length of abdomen: 54–71 µm (58).

Remarks.— *Pterocyrtidium eep* n. sp. is distinguished from *P. barbadense* (Ehrenberg, 1874) and *P. praebarbadense* Kozlova, 1983 by its long sharpely pointed apical horn, and from *P. borisenkoi* Nishimura, 1992 by possessing a roundish thorax instead of a pyramidal thorax. The new species also differs from *P. genrietta* Nishimura, 1992 by having a longer apical horn and a thorax wider than the abdomen. Finally, *P. eep* n. sp. differs from *P. zitteli* Bütschli, 1882a by having a simple, conical apical horn instead of a dichotomous, bladed apical horn, and by the absence of a ventral horn on the cephalis. Additionally, it differs from similarly shaped upper Paleogene Pterocorythids by having an unilobed cephalis.

Superfamily Acanthodesmioidea Haeckel, 1862

Family Cephalospyrididae Haeckel, 1882

Genus *Petalospyris* Ehrenberg, 1846

Type species.— *Petalospyris diaboliscus* Ehrenberg, 1847, p. 55, fig. 6; by monotypy.

Petalospyris cometa new species

Plate II.24, Figures 1–3

Holotype.— Plate II.24, Figure 1; collection number USTL 3421–1; coordinates W42/3; sample ODP 1260A-6R-2W, 55–57 cm; lower part of the *Podocyrtis* (*L.*) *goetheana* Zone (early Bartonian, middle Eocene).

Diagnosis.— Spyrid with a tuberculate shell, large cephalic pores, and nine conical feet.

Occurrence.— At ODP Site 1260, this species appears in the lowermost part of the *Podocyrtis* (*L.*) *goetheana* Zone.

Description.— Lattice shell tuberculate, thick-walled, with a slight external sagittal stricture, and not extending below the basal ring. Sagittal ring D-shaped. Apical horn robust and triangular, with variable length, generally less than half the height of the lattice shell. Cephalic pores subcircular to quadrate, unequal in size, and arranged symmetrically with respect to the sagittal stricture. Vertical pore present, showing a strong vertical spine. Presence of nine conical feet with pointed ends that emerge directly from the basal ring. Each foot is well-individualized, straight or slightly divergent, with most of the curvature proximally.

Etymology.— From the Latin *cometa*, meaning ‘comet’. The specific epithet is to be treated as a noun in the nominative singular standing in apposition to the generic name.

Dimensions.— Based on 15 specimens (mean): length of cephalis without the apical horn: 74–100 µm (86), maximum breadth of cephalis: 104–132 µm (118), length of apical horn: 33–85 µm (62), length of lamellar feet: 70–180 µm (129).

Remarks.— The new species differs from all *Dorcadospyris* species and from *Dendrospyris stylophora* (Ehrenberg, 1874) in having at least eight lamellar feet emerging from the basal ring, instead of a reduced number of curved or straight feet that are round in cross-section. Representatives of *Petalospyris cometa* n. sp. differ from those of *P. confluens* Ehrenberg, 1874 in having larger cephalic pores, and long and well-individualized lamellar feet (Plate II.24, Figure 8). *P. cometa* n. sp. differs from *P. inferispina* (Goll, 1968), *P. flabellum* Ehrenberg, 1874, *P. platyacantha* Ehrenberg, 1874, and *Dendrospyris* ? *golli* Nishimura, 1992 in having larger pores, a rougher surface, and an apical horn that is shorter than the lattice shell. *P. cometa* n. sp. differs also from *P. diaboliscus* Ehrenberg, 1847 and *P. castanea* n. sp. by the absence of two lateral spines on the cephalis. Additionally, the new species is distinguished from *P. argiscus* (Plate II.24, Figure 4), *P. carinata* Ehrenberg, 1874, and *P. eupetala* Ehrenberg, 1874 by having less than 10 pores on the circumference of the cephalis at its widest part, a robust apical horn shorter than the lattice shell, and a wide vertical pore.

The origin of *P. cometa* n. sp. is to be found within a number of middle Eocene spyrids introduced by Ehrenberg (1874) as distinct species: *P. argiscus*, *P. carinata* and *P. eupetala*. These species exhibit a cephalis with a pebbly surface and numerous teeth surrounding the cephalic aperture. *P. argiscus* is abundant throughout the studied interval and displays high intraspecific variability, as well as in the length and inclination of the lamellar teeth. At ODP Site 1260, we also observed specimens with proximally carinate lamellar teeth, especially in the *Podocyrtis* (*L.*) *mitra* Zone. These different morphotypes do not form homogeneous groups distinct from typical *P. argiscus* (Plate II.24, Figure 4), therefore we chose to include them all under this species. Our enlarged concept of *P. argiscus* encompasses morphotypes previously assigned to *P. eupetala* and *P. carinata*, so the latter are considered as synonyms of *P. argiscus*. In this revised taxonomic framework, *P. cometa* n. sp. is regarded as an offshoot of *P. argiscus* (Figure II.3).

Petalospyris castanea new species

Plate II.24, Figures 5–7

Holotype.— Plate II.24, Figure 5; collection number USTL 3477–1; coordinates H33/3; sample ODP 1260A-9R-3W, 55–57 cm; upper part of the *Podocyrtis* (*L.*) *mitra* Zone, in the *Podocyrtis* (*P.*) *apeza* Subzone (late Lutetian, middle Eocene).

Diagnosis.— Spyrid with two lateral spines on the cephalis and a latticed thorax that terminates in long teeth.

Occurrence.— This species occurs sporadically from the upper part of the *Podocyrtis* (*L.*) *mitra* Zone until the end of the studied interval, which falls in the lowermost part of the *Podocyrtis* (*L.*) *goetheana* Zone.

Description.— Shell dicyrtid, smooth, with a bilobed cephalis and a short latticed thorax. Cephalis globular, separated into two lobes by a weak sagittal constriction, bearing a short needle-like apical horn and two short lateral spines. Lateral spines developed directly from the latticed shell. Cephalic and thoracic pores subcircular, of different sizes, and randomly distributed. Thorax terminating in a ring of teeth that are as long as the thorax or slightly longer (although they are usually broken). These teeth point distally and are slightly curved inward.

Etymology.— From the Latin *castanea*, meaning 'chestnut', for its resemblance to the fruit of the sweet chestnut tree (*Castanea sativa* Mill.). The specific epithet is to be treated as an adjective in the nominative singular.

Dimensions.— Based on five specimens (mean): length of cephalis without the apical horn: 33–45 µm (40), maximum breadth of cephalis: 61–70 µm (65), maximum length of lamellar feet: 26–64 µm (36).

Remarks.— *Petalospyris castanea* n. sp. is characterized by two lateral spines on the cephalis, distinguishing it from most other species in the genus *Petalospyris*. It can be differentiated from *P. diaboliscus* Ehrenberg, 1847 by its latticed thorax and shorter, straight lateral spines on the cephalis. Additionally, *P. castanea* n. sp. has a shorter thorax than the cephalis height, larger pores, and fewer perioral teeth than *P. tricornis* (Haeckel, 1887).

P. castanea n. sp. appears to have evolved from *P. confluens* Ehrenberg, 1874 in the upper part of the *Podocyrtis* (*L.*) *mitra* Zone, with which it co-occurred afterward throughout the analyzed stratigraphic interval (Figure II.3). *P. diaboliscus*, on the other hand, is thought to have evolved from a stock of *P. castanea* n. sp. in the lower part of the *Podocyrtis* (*L.*) *goetheana* Zone. One major trend in this evolutionary lineage is the appearance and lengthening of two lateral horns on the cephalis, which developed directly from the latticed shell. Additionally, there was resorption of the thoracic pores and lengthening of the perioral teeth. The origin of *P. confluens* remains unclear, and there are no known descendants of *P. diaboliscus*.

Superfamily Archipilioidea Haeckel, 1882 sensu Sandin et al., 2019

Family Theophormididae Haeckel, 1882 emend. Suzuki et al., 2021

Genus *Velicucullus* Riedel and Campbell, 1952

Type species.— *Soreuma* (*Soreumium* ?) *magnificum* Clark and Campbell, 1942, p. 51, pl. 4, fig. 15; by monotypy.

Velicucullus armatus new species

Plate II.24, Figures 13–14

1973 *Velicucullus* sp. Sanfilippo and Riedel, p. 530, pl. 20, figs. 2, 3 (part).

Holotype.— Plate II.24, Figure 13; collection number USTL 3277–1; coordinates Q41/1; sample ODP 1260A-14R-5W, 55–57 cm; *Podocyrtis* (*P.*) *ampla* Zone, in the lower part of the *Coccolarnacium periphaenoides* Subzone (late Lutetian, middle Eocene).

Diagnosis.— *Velicucullus* species with four collar pores subequal in size, and a thorax terminating in ~20 well-individualized radial spines.

Occurrence.— This species occurs sporadically from the *Thyrsocyrtis* (*P.*) *triacantha*[3] Zone, to the upper part of the *Podocyrtis* (*L.*) *mitra* Zone.

Description.— Shell two-segmented, consisting of a large cephalis and a flat extended discoidal thorax. We did not find any specimens in our material that display an entirely developed cephalis. Therefore, the anatomical details of the cephalis remain unknown. Basal ring

3 *Thyrsocyrtis* (*Pentalocorys*) *schomburgkii* (Ehrenberg, 1847) in Chapter II.2.

composed of the dorsal spine, the ventral spine, and two primary lateral spines. The four rods intersect orthogonally at angles of 90°, delimiting four collar pores that are subequal in size. Thoracic pores subcircular to quadrangular, roughly aligned longitudinally and increasing in size toward the periphery. Thorax ending in a narrow hyaline band that is armed with ~20–25 radial spines. Each spine spaced by three or four pores and ventrally connected to the velum. Very reduced velum positioned under the most distal row of thoracic pores and not extending on the oral surface of the thorax (Plate II.24, Figure 14).

Etymology.— From the Latin *armatus*, meaning 'armed'. The specific epithet is to be treated as an adjective in the nominative singular.

Dimensions.— Based on the only two complete specimens found: shell diameter: 251–293 µm.

Remarks.— The fossil record of ODP Site 1260 contains highly fragmented remains of this species, including isolated portions of the thorax. However, the distinct shape of the distal margin of its thorax allows for easy identification, even in the form of small fragments. *Velicucullus armatus* n. sp. can be differentiated from *V. discoides* (Ehrenberg, 1874) and *V. fragilis* O'Connor, 1999a by the presence of radial spines on the distal margin of the thorax. The new species also differs from *V. magnificum* (Clark and Campbell, 1942) in having larger and fewer thoracic pores and well-individualized radial spines, and from *V. palaeocenica* Nishimura, 1992 in having collar pores that are equal in size and an almost flat thorax. Finally, *V. armatus* is found alongside a massive unidentified *Velicucullus* species throughout its observed stratigraphic range. However, this species is only is represented only by fragments in our material, and thus cannot be formally described. This species is distinguished by its larger size (>300 µm), the absence of radial spines, and by its smaller and more numerous thoracic pores.

Superfamily Plagiacanthoidea Hertwig, 1879

Family Pseudodictyophimidae Suzuki *in* Suzuki et al., 2021

Genus *Corythomelissa* Campbell, 1951

Type species.— *Lithomelissa corythium* Ehrenberg, 1874, p. 240 (unfigured); Ehrenberg, 1876, p. 78, pl. 3, fig. 12; subsequent designation by Campbell (1951, p. 529).

Corythomelissa galea (Ehrenberg, 1874) new combination

Plate II.23, Figures 13–16

1874 *Halicalyptra Galea* [sic] Ehrenberg, p. 234.
1876 *Halicalyptra Galea* [sic] Ehrenberg – Ehrenberg, p. 74, pl. 2, fig. 10.
1887 *Tripocalpis galea* (Ehrenberg) – Haeckel, p. 1136.
2009 *Halicalyptra galea* Ehrenberg – Ogane et al., pl. 44, figs. 2a–2g.

Holotype.— No holotype was designated by Ehrenberg in the original description of the species. However, the specimen he drew (1876, pl. 2, fig. 10), which was later re-illustrated by Ogane et al. (2009, pl. 44, figs. 2a–2g) during their reexamination of Ehrenberg's collection kept in the Museum für Naturkunde, Humboldt University (Berlin, Germany), is a potential lectotype.

Diagnosis.— *Corythomelissa* species with a proportionally small cephalis bearing a strong apical horn and sometimes an inconspicuous ventral horn, a closed thorax, and three straight, downwardly directed feet.

Occurrence.— This species has a discontinuous range at ODP Site 1260, extending from the upper part of the *Podocyrtis* (*P.*) *ampla* Zone, to the lower part of the *Podocyrtis* (*L.*) *mitra* Zone.

Description.— Shell composed of two segments, globular and thick-walled. Cephalis subspherical to hemispherical, partially embedded in the thorax, and penetrated by randomly distributed subcircular pores. Apical spine free in the cephalic cavity, extending outside as a stout, bladed apical horn. In some specimens, the ventral spine protrudes as a small sagittal horn (Plate II.23, Figure 16). Dorsal and primary lateral spines elongated as strong ribs or ridges on the thorax, and protruding as three straight bladed feet. Thorax globular, asymmetrical in lateral view due to the development of the dorsal spine. Distal end of the thorax either round or closed. Thoracic pores subcircular to elongated around the thoracic ribs, irregular in size, and generally larger than the cephalic ones.

Dimensions.— Based on five specimens (mean): length of cephalothorax without the apical horn: 82–105 µm (90), length of apical horn: 21–35 µm (29), length of feet: 53–86 µm (64).

Remarks.— *Corythomelissa galea* (Ehrenberg, 1874) n. comb. was assigned to the genus *Corythomelissa* on the basis of its closed thorax, its hemispherical cephalis bearing an apical and a ventral spine, and its dorsal and primary lateral spines prolonged as three straight, downwardly directed feet. The combination recently suggested by O'Dogherty et al. (2021): *Phaenocalpis galea* (Ehrenberg, 1874), was not selected because the species belonging to the

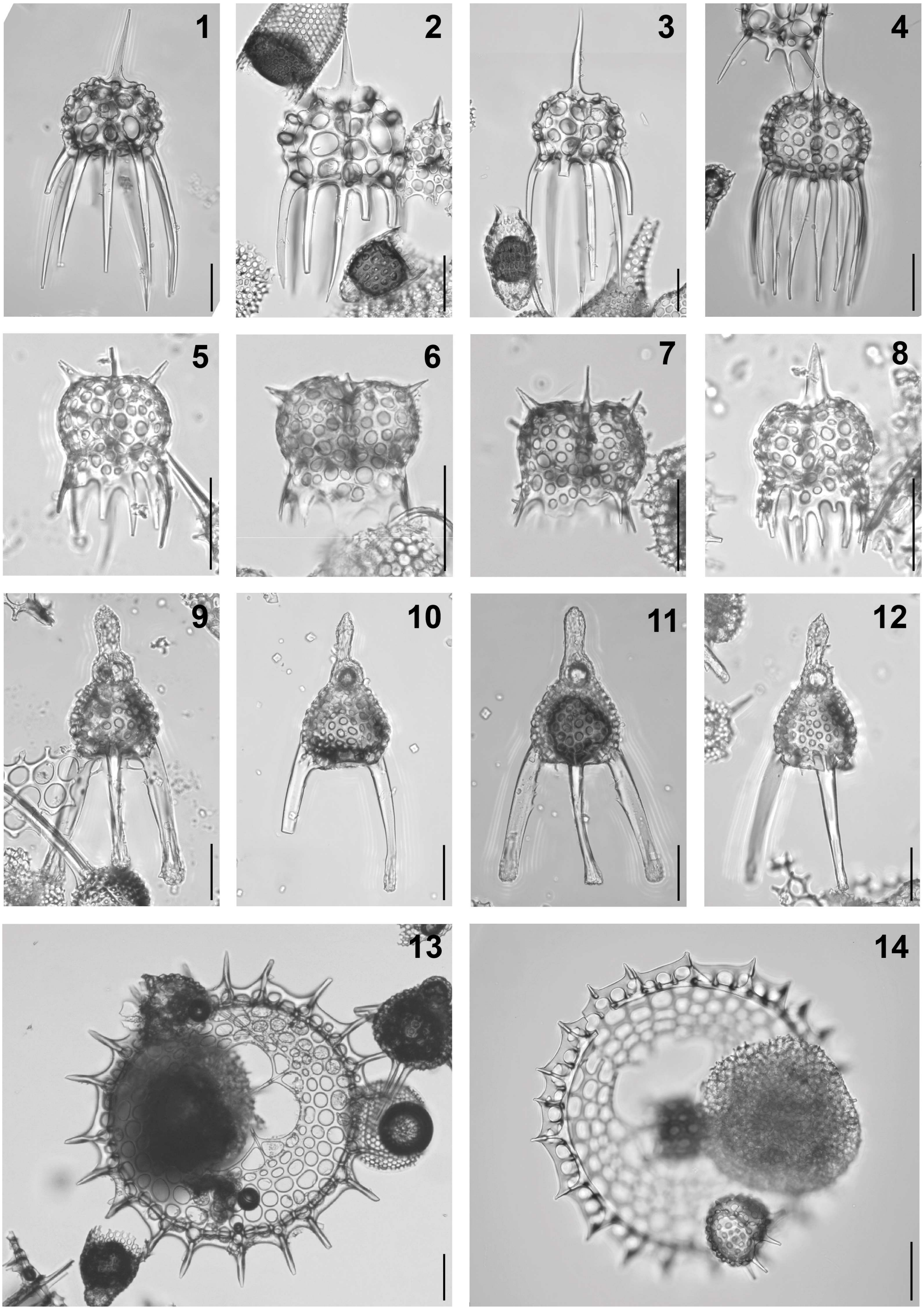
1
2
3
4
5
6
7
8
9
10
11
12
13
14

Plate II.24. Composite light micrographs of new radiolarian species from ODP Site 1260 (Demerara Rise, western equatorial Atlantic). (**1–3**) *Petalospyris cometa* n. sp.: (**1**) holotype, ODP 1260A-6R-2W, 55–57 cm, USTL 3421–1, W42/3; (**2**) ODP 1260A-6R-1W, 55–57 cm, USTL 2847–1, X45/1; (**3**) ODP 1260A-6R-1W, 55–57 cm, USTL 2847–2, D39/2; (**4**) *Petalospyris argiscus* Ehrenberg: ODP 1260A-13R-4W, 55–56 cm, USTL 2854–4, M38/4. (**5-7**) *Petalospyris castanea* n. sp.: (**5**) holotype, ODP 1260A-9R-3W, 55–57 cm, USTL 3477–1, H33/3; (**6**) ODP 1260A-8R-2W, 54–56 cm, USTL 3461–1, R55/3; (**7**) ODP 1260A-9R-3W, 55–57 cm, USTL 3479–2, S42/1**.** (**8**) *Petalospyris confluens* Ehrenberg: ODP 1260A-9R-3W, 55–57 cm, USTL 3478–3, U43/3. (**9–12**) *Lychnocanium nimrodi* n. sp.: (**9**) holotype, ODP 1260A-9R-4W, 55–57 cm, USTL 3483–2, L38/2; (**10**) ODP 1260A-9R-4W, 55–57 cm, USTL 3481–4, U38/3 (mirrored); (**11**) ODP 1260A-9R-4W, 55–57 cm, USTL 3484–2, L36/9; (**12**) ODP 1260A-9R-2W, 55–57 cm, USTL 3474–2, O38/3. (**13, 14**) *Velicucullus armatus* n. sp.: (**13**) holotype, ODP 1260A-14R-5W, 55–57 cm, USTL 3277–1, Q41/1; (**14**) ODP 1260A-13R-4W, 54–56 cm, USTL 2854–3, T61/3. All scale bars equal 50 µm.

genus *Phaenocalpis* are all composed of a single segment. *C. galea* (Ehrenberg, 1874) n. comb differs from *C. horrida* (Petrushevskaya, 1975) group, *C. omoprominentia* Funakawa, 1995a, and *C. spinosa* Funakawa, 1995a in having a smooth-surfaced cephalis bearing shorter apical and ventral horns. It also differs from *C. pachyostraca* Funakawa, 1995a in having a smaller cephalis with shorter apical and ventral horns and a closed thorax. Amongst similar-looking *Pseudodictyophimus* species, *C. galea* (Ehrenberg, 1874) n. comb. differs from *Ps. bicornis* (Ehrenberg, 1874), *Ps. leptoretis* Funakawa, 1995b, *Ps. pyramidalis* Funakawa, 1995b, and *Ps. tanythorax* Funakawa, 1994 in having a shorter ventral horn, three straight, downwardly directed feet, and a closed thorax. It is also distinguished from *Ps.* ? *sphaerothorax* Funakawa, 1995b in having a smaller ventral horn and a proportionally larger thorax, and from *Ps.* ? *charlestonensis* (Clark and Campbell, 1945) in having three straight feet and a cephalis that is conspicuously embedded in the thorax. Finally, *C. galea* (Ehrenberg, 1874) n. comb. differs from *Spongomelissa cucumella* Sanfilippo and Riedel, 1973 in having larger pores, a cephalis that is distinctly smaller than the thorax, and three longer feet.

Superfamily Lithochytridoidea Ehrenberg, 1846

Family Lithochytrididae Ehrenberg, 1846 sensu Suzuki *in* Matsuzaki et al., 2015

Genus *Lychnocanium* Ehrenberg, 1846

Type species.— *Lychnocanium lucerna* Ehrenberg, 1847, p. 55, fig. 5; subsequent monotypy (O'Dogherty et al., 2021).

Lychnocanium nimrodi new species

Plate II.24, Figures 9–12

1985 *Sethochytris babylonis* (Clark and Campbell) group – Sanfilippo et al., fig. 17.8a (part).

Holotype.— Plate II.24, Figure 9; collection number USTL 3483–2; coordinates L38/2; sample ODP 1260A-9R-4W, 55–57 cm; upper part of the *Podocyrtis* (*L.*) *mitra* Zone, in the *Podocyrtis* (*P.*) *apeza* Subzone (late Lutetian, middle Eocene).

Diagnosis.— *Lychnocanium* species with a stout, distally dilated apical horn, and three long subparallel feet that are rectangular in cross-section.

Occurrence.— *Lychnocanium nimrodi* n. sp. ranges from the upper part of the *Podocyrtis* (*L.*) *mitra* Zone to the lowermost part of the *Podocyrtis* (*L.*) *chalara* Zone.

Description.— Cephalis subspherical, thick-walled, and poreless. Apical horn longer than the cephalis, stout, and distally dilated, with a hammered surface. Collar stricture well-defined externally by a change in the contour of the shell. Thorax pyriform, with subcircular pores of different sizes, quincuncially or irregularly arranged. Three long and subparallel feet emerging from the base of the thorax, rectangular in cross section and dilated at the end in heavy silicified specimens (Plate II.24, Figures 9, 11). Feet smooth-surfaced over a large part of their length, then rough when they are dilated.

Etymology.— Named after Nimrod, the ancient king of Babylon who commissioned the construction of the Tower of Babel. The specific epithet is to be treated as a noun in the genitive case formed from a personal name.

Dimensions.— Based on 20 specimens (mean): length of cephalothorax without the apical horn: 81–107 µm (91), length of apical horn: 35–59 µm (46), length of feet: 88–140 µm (117).

Remarks.— *Lychnocanium nimrodi* n. sp. is undoubtedly related to the *L. babylonis* (Clark and Campbell, 1942) group[4]. It is distinguished from all morphotypes grouped under this name in having a rounded thorax rather than a pyramidal thorax with sharp angles, and in having three long subparallel feet, which are rectangular in cross-section and usually distally dilated. A distally dilated apical horn is also a characteristic feature of *L. nimrodi* n. sp. This short-lived species is considered as an offshoot from the *L. babylonis* group[4] (Figure II.3).

Superfamily Pterocorythoidea Haeckel, 1882 emend. Suzuki et al., 2021

Family Lophocyrtiidae Sanfilippo and Caulet *in* De Wever et al., 2001

Genus *Aphetocyrtis* Sanfilippo and Caulet, 1998

Type species.— *Aphetocyrtis gnomabax* Sanfilippo and Caulet, 1998, p. 16, pl. 7, fig. 10.

4 *Lychnocanium tribulus* (Ehrenberg, 1874) group in Chapter II.2.

Aphetocyrtis zamenhofi new species

Plate II.25, Figures 1–4, 8

1977 *Theocorys* sp. Riedel and Sanfilippo, pl. 7, fig. 9.

2006 *Lophocyrtis* (*Apoplanius*) *aspera* (Ehrenberg) – Funakawa et al., p. 25, pl. P7, figs. 5a, 5b (part).

Holotype.— Plate II.25, Figure 1; collection number USTL 3543–1; coordinates Q37/4; sample 1260A-15R-2W, 55–57 cm; lowermost part of the *Podocyrtis* (*P.*) *ampla* Zone, in the *Dictyomitra parva* Subzone (late Lutetian, middle Eocene).

Diagnosis.— *Aphetocyrtis* species with an apical spine that is completely free in the cephalic cavity, an inflated hemispherical thorax and an abdomen divided in two by a constriction.

Occurrence.— From the beginning of the studied interval, which is situated in the *Thyrsocyrtis* (*P.*) *triacantha* Zone, to the upper part of the *Podocyrtis* (*P.*) *ampla* Zone.

Description.— Shell three-segmented, thick-walled and, almost cylindrical. Cephalis proportionally small, spherical and globular, porous. Apical spine fused with the cephalic wall, protruding outside as a small, simple apical horn. Collar constriction expressed externally by a sharp change in the contour of the shell, giving the impression that the cephalis merely rests on the thorax. Thorax inflated hemispherical, perforated by subcircular pores of regular size and shape, that are quincuncially arranged and hexagonally framed by high, sharp ridges, that give the thorax its thorny contour. Lumbar stricture marked by a thick internal ridge that appears externally as a dark band. Abdomen shaped like an hourglass, with an inflated proximal portion followed by a constriction and then an enlargement of the shell. Abdominal pores subcircular to ovoid, unequal in size, randomly distributed or roughly aligned longitudinally. In the proximal part of the abdomen, pores separated by weak ridges, sometimes fused, and arranged longitudinally according to the alignment of the pores. Abdominal termination lacks a peristome or terminal feet.

Etymology.— Named after the Polish ophthalmologist Ludwik Lejzer Zamenhof, who is the creator of Esperanto, one of the most widely used constructed international auxiliary languages. The specific epithet is to be treated as a noun in the genitive case formed from a modern personal name.

Dimensions.— Based on 30 specimens (mean): total length: 120–258 µm (188), length of cephalothorax: 61–107 µm (84), length of abdomen: 59–157 µm (104).

Remarks.— The new species shows strong morphological similarities to early representatives of *Aphetocyrtis gnomabax* Sanfilippo and Caulet, 1998 which can have a constricted abdomen (e.g., Sanfilippo and Caulet, 1998, pl. 2, figs. 14–17). However, *A*. *zamenhofi* n. sp. is distinguished from *A*. *gnomabax* by having an apical spine that is completely free in the cephalic cavity, a more globular cephalis that is well-separated from the thorax, and an inflated hemispherical thorax rather than an inflated campanulate thorax. In addition to the organization of its initial spicule, *A*. *zamenhofi* n. sp. differs from the Southern Ocean species *A*. *rossi* Sanfilippo and Caulet, 1998 and *A*. *catalexis* Sanfilippo and Caulet, 1998, and from the tropical species *A*. ? *columboi* n. sp. in having a constricted abdomen. The new species is separated from *A*. ? *bianulus* (O'Connor, 1997a) by its shorter abdomen with only one constriction. In part of its range, *A*. *zamenhofi* n. sp. co-occurs with *Lophocyrtis alauda* (Ehrenberg, 1874), , which is easily distinguished by its stronger apical horn and its subcylindrical abdomen perforated by pores of regular size and shape. Amongst the Lophocyrtiids, *Apoplanius klydus* (Sanfilippo and Caulet, 1998) also has a wavy abdomen, but this species differs from *A*. *zamenhofi* n. sp. in having a spiny thorax, an apical spine partially included within the cephalis wall, and a stronger apical horn.

Under the original description of the genus *Aphetocyrtis*, Sanfilippo and Caulet (1998) described three species (*A*. *gnomabax*, *A*. *rossi* and *A*. *catalexis*), which were all included in the *A*. *gnomabax* lineage. One of the major trends in this evolutionary lineage during the late Paleogene is the gradual inclusion of the apical spine in the cephalic wall. In *A*. *gnomabax*, the earliest morphospecies of this lineage, known during the earliest middle Eocene, the apical spine is loosely attached to the cephalic wall. Then, the apical spine becomes completely included in the cephalic wall in the youngest Oligocene morphospecies *A*. *rossi* and *A*. *catalexis*. The apical spine of *A*. *zamenhofi* n. sp., which is completely merged in the cephalic wall (Plate II.25, Figure 8), prevents the inclusion of this species in the *A*. *gnomabax* lineage. Therefore, *A*. *zamenhofi* n. sp. is not considered a descendant of *A*. *gnomabax*, in spite of their great morphological proximity; it probably belongs to another evolutionary lineage within the genus *Aphetocyrtis*. In any case, the documentation of this new species allows us to firmly place the origin of the genus *Aphetocyrtis* at the low latitudes since the middle Eocene, before its migration to the high latitudes during the late Eocene (Sanfilippo and Caulet, 1998).

Aphetocyrtis ? *columboi* new species

Plate II.25, Figures 5–7, 9

Holotype.— Plate II.25, Figure 5; collection number USTL 3438–1; coordinates J31/1; sample ODP 1260A-6R-6W, 55–57 cm; lowermost part of the *Podocyrtis* (*L.*) *goetheana* Zone (early Bartonian, middle Eocene).

Diagnosis.— Spindle-shaped shell with a tapered abdomen, ending in a horn-like structure.

Occurrence.— From the upper part of the *Podocyrtis* (*L.*) *chalara* Zone to the *Podocyrtis* (*L.*) *goetheana* Zone.

Description.— Shell three-segmented, spindle-shaped, and thick-walled, with the collar and lumbar strictures expressed externally as a slight change in the contour of the shell. Cephalis spheroidal to flattened ovoid, partially embedded in the thorax, poreless or with a few small and irregularly distributed pores. Apical spine included in the cephalic wall, projecting outward as a reduced apical horn, shorter than the cephalis height. Mitral arches leave the apical spine in the middle of the cephalis, and diverge rapidly at a large angle. Thorax hemispherical to inflated campanulate, as wide as, or wider than the abdomen, with subcircular pores quincuncially arranged. Dorsal and primary lateral spines prolonged in the thoracic wall as externally indistinct ribs, protruding outside the shell as three inconspicuous conical wings usually broken and difficult to see (Plate II.25, Figure 5). Abdomen inverted conical, with subcircular pores roughly arranged in longitudinal rows. Abdomen terminating in a horn-like structure, usually longer than the apical horn (Plate II.25, Figure 5), but ragged along a row of pores in most observed specimens (Plate II.25, Figures 6, 7).

Etymology.— Named after the iconic cigar smoking Lieutenant Columbo of the eponymous American crime drama series Columbo, due to the resemblance of this species to a cigar. The specific epithet is to be treated as a noun in the genitive case formed from a modern personal name.

Dimensions.— Based on 11 specimens (mean): total length: 191–207 µm (193), length of cephalothorax: 71–84 µm (77), length of abdomen: 101–121 µm (116).

Remarks.— This species is tentatively assigned to the genus *Aphetocyrtis* because of the general morphology of its shell and the organization of its initial spicule. Its phylogenetic relationships with other members of the *A*. *gnomabax* lineage are difficult to determine at this time; however, it can be noted that this new species has reached an advanced stage in the inclusion of the apical spine in the cephalic wall early in the history of the genus (Plate II.25, Figure 9). *A*. ? *columboi* n. sp. differs from *A*. *gnomabax* Sanfilippo and Caulet, 1998, *A*. *rossi* Sanfilippo and Caulet, 1998, *A*. *catalexis* Sanfilippo and Caulet, 1998 and *A*. *zamenhofi* n. sp. in having a tapered abdomen terminating in a horn-like structure and a thorax flanked by three small wings. This new species is morphologically close to *Pterosyringium hamata* O'Connor, 1999a, from which it differs in being larger, and in having more regularly arranged abdominal pores. *A*. ? *columboi* n. sp. is also distinguished from *Lophocyrtis versipellis* (Ehrenberg, 1874) in having a flattened ovoid cephalis and smaller abdominal pores. In its general form, *A*. ? *columboi* n. sp. superficially resembles some species of the genus *Glomaria*, especially the middle Miocene species *G*. *thornburgi* (Sanfilippo and Riedel, 1970) and *G*. *baueri* (Sanfilippo and Riedel, 1970). However, the thorax of *A*. *columboi* n. sp. does not consist of a loose spongy network, which allows it to be easily distinguished from all species of the genus *Glomaria*.

The origin of *A*. ? *columboi* n. sp. remains unclair; it is probably closely related to the late Eocene species *P. hamata* (O'Connor, 1999a) described from the Oamaru diatomite.

Aphetocyrtis ? *spheniscus* new species

Plate II.25, Figures 10–13

Holotype.— Plate II.25, Figure 10; collection number USTL 2851–2; coordinates Y49/1; sample ODP 1260A-12R-1W, 55–57 cm; lower part of the *Podocyrtis* (*L.*) *mitra* Zone, in the *Artostrobus quadriporus* Subzone (late Lutetian, middle Eocene).

Diagnosis.— *Aphetocyrtis* species with an elongated shell, a slight abdominal constriction, and an open aperture.

Occurrence.— From the lowermost part of the *Podocyrtis* (*P.*) *ampla* Zone, to the lower part of the *Podocyrtis* (*L.*) *chalara* Zone.

Description.— Shell of three segments, subcylindrical to fusiform and thick-walled. Cephalis subspherical, perforated by a few subcircular pores, and bearing a strong bladed apical horn. Collar stricture expressed as a change in the contour of the shell. Thorax thick-walled, campanulate to truncate conical, with circular pores quincuncially arranged. Thoracic stricture marked externally by a slight constriction of the shell and lined by an internal ridge that appears externally as a dark band. The pores on the thoracic stricture are slightly elongated longitudinally. Abdomen subcylindrical, with circular pores longitudinally aligned, although pore alignment tends to be less regular in the distal part of the abdomen. Short longitudinal ridges may sometimes separate rows of abdominal pores (Plate II.25, Figure 11). Aperture sometimes slightly constricted, and always ragged.

Etymology.— From the Latin *spheniscus*, meaning 'penguin', for its resemblance to the great penguins. The specific epithet is to be treated as a noun in the nominative singular standing in apposition to the generic name.

Dimensions.— Based on 30 specimens (mean): total length: 130–214 µm (159), length of apical horn: 12–23 µm (15), length of cephalothorax: 70–102 µm (80), length of abdomen: 62–144 µm (80).

Remarks.— This species is tentatively assigned to the genus *Aphetocyrtis* because of the absence of a ventral horn, or of any external extensions associated with the dorsal and the primary lateral spines, and because the abdomen terminates in a simple peristome. The new species is morphologically close to the specimen designated as holotype of the species *A. catalexis* Sanfilippo and Caulet, 1998 (pl. 7, figs. 14a, 14b), but it differs in having a truncate conical thorax rather than a hemispherical thorax, and less pronounced abdominal and collar constrictions. *A*. ? *spheniscus* n. sp. differs also from *Theocorys saginata* Takemura and Ling, 1998 in having smaller thoracic and abdominal pores, and a less pronounced constriction between the thorax and the abdomen; from *T. minuta* Takemura and Ling, 1998 and *T. perforalvus* (O'Connor, 1997a) in being more elongated, with a truncate conical thorax instead of a hemispherical to spherical thorax, and in having a stronger apical horn; from *T. spongoconus* (Kling, 1971) in having a latticed abdomen instead of a spongious abdomen; and from *T. kerguelensis* Takemura and Ling, 1998 in having a shorter apical horn, and regular abdominal pores in size and shape. *A.* ? *spheniscus* n. sp. is also distinguished from *Theocyrtis diabloensis* Clark and Campbell, 1942 and *Th. robusta* Clark and Campbell, 1942 in having a less pronounced lumbar stricture, a shorter apical horn and regularly arranged pores. Finally, the new species can be distinguished from *Th.* ? *scolopax* (Ehrenberg, 1874) by its shorter apical horn, its smaller thoracic and abdominal pores, and by the absence of well-defined longitudinal ridges separating the rows of abdominal pores.

Family *Pterocorythidae* Haeckel, 1882

Genus *Albatrossidium* Sanfilippo and Riedel, 1992

Type species.— *Albatrossidium minzok* Sanfilippo and Riedel, 1992, p. 16, pl. 2, fig. 7.

Albatrossidium regis new species

Plate II.25, Figures 14–17

Holotype.— Plate II.25, Figure 14; collection number USTL 2851–1; coordinates Y54/2; sample 1260A-12R-1W, 55–57 cm; lower part of the *Podocyrtis* (*L.*) *mitra* Zone, in the *Artostrobus quadriporus* Subzone (late Lutetian, middle Eocene).

Diagnosis.— *Albatrossidium* species with a cylindrical shell, a large triangular apical horn, and spaced, irregularly arranged pores in the distal part of the abdomen.

Occurrence.— From the beginning of the studied interval, which is situated in the *Thyrsocyrtis* (*P.*) *triacantha*[5] Zone, to the upper part of the *Podocyrtis* (*L.*) *mitra* Zone

5 *Thyrsocyrtis* (*Pentalocorys*) *schomburgkii* (Ehrenberg, 1847) in Chapter II.2.

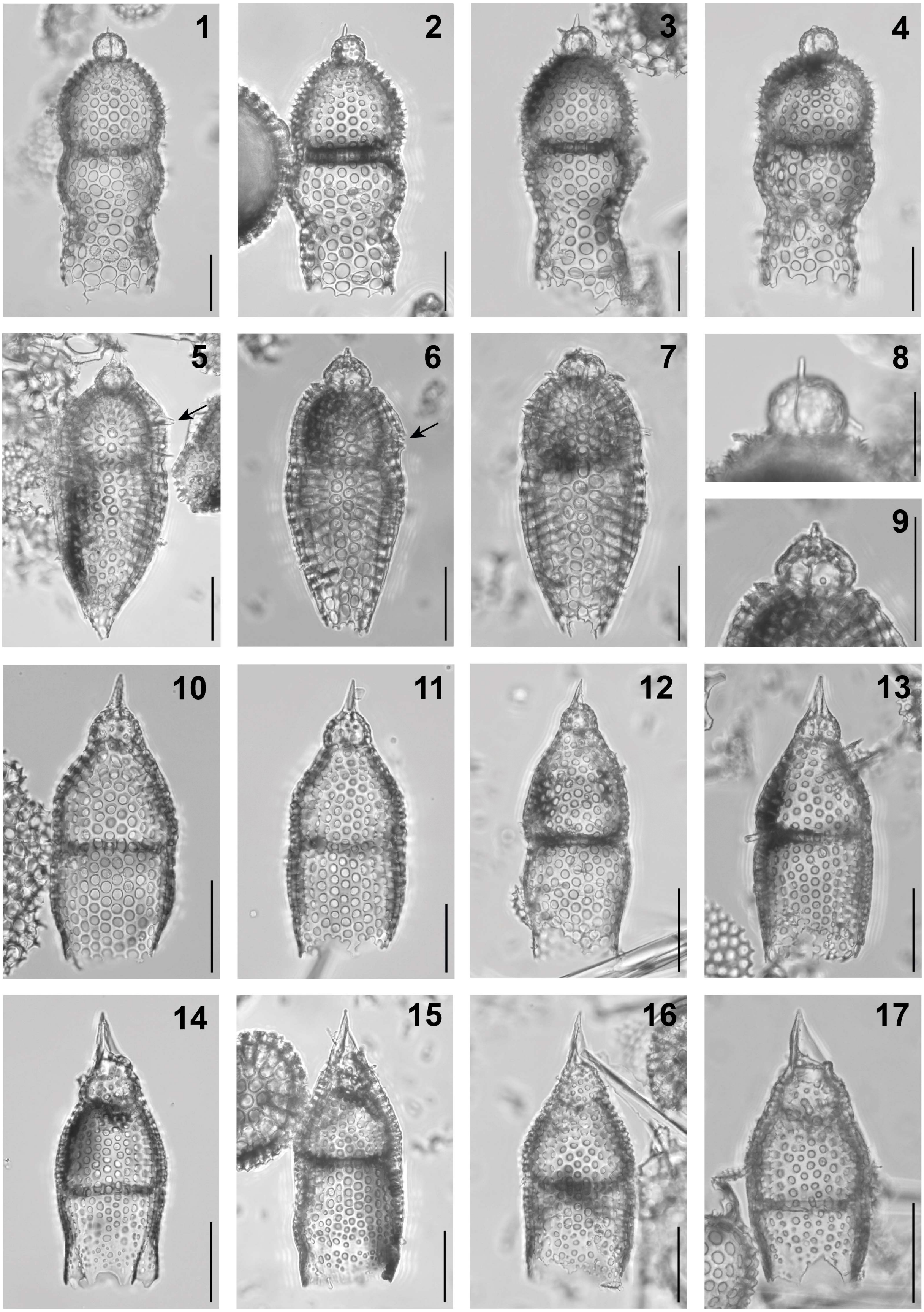
1
2
3
4
5
6
7
8
9
10
11
12
13
14
15
16
17

Plate II.25. Composite light micrographs of new radiolarian species from ODP Site 1260 (Demerara Rise, western equatorial Atlantic). (**1–4**, **8**) *Aphetocyrtis zamenhofi* n. sp.: (**1**) holotype, ODP 1260A-15R-2W, 55–57 cm, USTL 3543–1, Q37/4; (**2**) ODP 1260A-14R-CC, 63–117 cm, USTL 3540–1, P37/1; (**3**) ODP 1260A-15R-1W, 55–57 cm, USTL 3541–1, N47/2; (**4**) ODP 1260A-15R-1W, 55–57 cm, USTL 3541–2, Q54/1; (**8**) focus on the cephalis, ODP 1260A-15R-2W, 55–57 cm, USTL 3543–2. (**5–7**, **9**) *Aphetocyrtis* ? *columboi* n. sp.: (**5**) holotype, showing thoracic wing (arrow), ODP 1260A-6R-6W, 55–57 cm, USTL 3438–1, J31/1; (**6**) specimen showing thoracic wing (arrow), ODP 1260A-6R-6W, 55–57 cm, USTL 3438–2, G46/1; (**7**) ODP 1260A-6R-6W, 55–57 cm, USTL 3438–3, L38/3; (**9**) focus on the cephalis of the specimen illustrated as Figure 10. (**10-13**) *Aphetocyrtis* ? *spheniscus* n. sp.: (**10**) holotype, ODP 1260A-12R-1W, 55–57 cm, USTL 2851–2, Y49/1; (**11)** ODP 1260A-9R-3W, 55–57 cm, USTL 3478–2, S52/4; (**12**) ODP 1260A-12R-1W, 55–57 cm, USTL 2851–3, G45/2 (mirrored); (**13**) ODP 1260A-12R-3W, 55–57 cm, USTL 3512–2, H58/1. (**14–17**) *Albatrossidium regis* n. sp.: (**14**) holotype, ODP 1260A-12R-1W, 55–57 cm, USTL 2851–1, Y54/2 (mirrored); (**15**) ODP 1260A-13R-5W, 54–56 cm, USTL 3525–1, W56/2 (mirrored); (**16**) ODP 1260A-14R-1W, 55–57 cm, USTL 3530–2, M38/1 (mirrored); (**17**) ODP 1260A-12R-5W, 55–57 cm, USTL 3516–1, N49/1 (mirrored). All scale bars equal 50 μm.

Description.— Shell three-segmented, cylindrical and thick-walled. Cephalis hemispherical and trilobate, with a strong pyramidal apical horn and sometimes a few small accessory spines on the margin of the cephalic hole. Cephalic pores subcircular, few in number, and randomly arranged. Inconspicuous collar stricture. Thorax subcylindrical to campanulate, with subcircular pores hexagonally framed and quincuncially arranged. The boundary between the thorax and abdomen is marked by an internal ring, that appears externally as a dark band. Abdomen cylindrical, with subcircular pores longitudinally aligned in the proximal part, then smaller, irregularly arranged, and more widely spaced. Abdomen ending in a simple, almost hyaline peristome, or in three inconspicuous shovel-shaped feet.

Etymology.— This species is named after the late radiolarian specialist Dr. William Rex Riedel, who actively participated in the renewal of radiolarian studies in the second half of the 20th century. The specific epithet is to be treated as a noun in the genitive case formed from a personal name that is Latin.

Dimensions.— Based on 14 specimens (mean): total length without the apical horn: 76–167 µm (121), length of apical horn: 26–38 µm (31), length of cephalothorax without the apical horn: 62–93 µm (70), length of abdomen: 39–85 µm (55).

Remarks.— *Albatrossidium regis* n. sp. is distinguished from the holotype of *A*. *minzok* (Sanfilippo and Riedel, 1992, pl. 2, fig. 7) in having a large triangular apical horn, and three shovel-shaped feet. The new species differs from *A*. *cylindricum* (Ehrenberg, 1874) and *A*. *tenellum* (Foreman, 1973) in having a more elongated apical horn, which is typically accompanied by a few accessory spines near its base, and by the proportion of thoracic length to abdominal length: 1:1 to 1:1.5 in the former, while it is greater than 1:2 for the other two species mentioned. Finally, *A*. *regis* n. sp. differs from *A*. *annikasanfilippoae* n. sp. in being much more cylindrical, with a reduction in the number of pores in the distal part of the abdomen, in having smaller accessory spines, and in not having any perforation in the apical horn.

A. *minzok* is considered to be the ancestral species of the genus (Sanfilippo and Riedel, 1992). Given its stratigraphic position (early Eocene to middle Eocene), this species represents a potential ancestor for the late middle Eocene species *A*. *regis* n. sp. However, due to the absence of *A*. *minzok* at ODP Site 1260, the phylogenetic relationship between these two species could not be determined in this study. A few specimens with a large triangular apical horn and a long cylindrical abdomen perforated by regularly arranged pores were observed in the *Podocyrtis* (*L*.) *goetheana* Zone after the last occurrence of *A*. *regis* n. sp. They correspond well to *A*. *cylindricum* as described by Ehrenberg (1874, p. 227) and illustrated by Ogane et al. (2009, pl. 84, figs. 5a–5d, pl. 85, figs. 1a–1d). These specimens may represent the descendants of *A*. *regis* n. sp. due to their morphological resemblance and stratigraphic position.

Albatrossidium annikasanfilippoae new species

Plate II.26, Figures 1–4

1992 *Albatrossidium minzok* Sanfilippo and Riedel, p. 18, pl. 1, fig. 18 (part).

Holotype.— Plate II.26, Figure 1; collection number USTL 3512–1; coordinates Y39/1; sample ODP 1260A-12R-3W, 55–57 cm; lower part of the *Podocyrtis* (*L.*) *mitra* Zone, in the *Artostrobus quadriporus* Subzone (late Lutetian, middle Eocene).

Diagnosis.— *Albatrossidium* species with a large, triangular, and perforated apical horn, surrounded by several accessory spines.

Occurrence.— From the lower part of the *Podocyrtis* (*P.*) *ampla* Zone, to the end of the studied interval, which is situated in the lower part of the *Podocyrtis* (*L.*) *goetheana* Zone.

Description.— Shell three-segmented, smooth, and thick-walled. Cephalis trilobate, hemispherical, with a strong triangular apical horn and usually two or four accessory spines on the rim of the cephalic hole. Proximal half of the apical horn usually perforated by several subcircular pores. Cephalic pores subcircular and randomly arranged. Collar stricture expressed externally as a slight change in the contour of the shell. Thorax campanulate to inflated campanulate, with subcircular pores with polygonal pore-frames, and quincuncially arranged. Thorax and abdomen separated by an internal septum that is marked externally by a slight change in the contour of the shell. Abdomen subcylindrical, with subcircular pores arranged roughly in longitudinal rows. Abdominal termination undifferentiate, invariably ragged along a row of pores.

Etymology.— The species is named after Dr. Annika Sanfilippo, in recognition of her pioneering work on Paleogene radiolarians. The specific epithet is to be treated as a noun in the genitive case formed from a modern personal name.

Dimensions.— Based on 26 specimens (mean): total length without the apical horn: 110–174 µm (126), length of apical horn: 30–47 µm (39), length of cephalothorax without the apical horn: 61–100 µm (77), length of abdomen: 29–87 µm (49).

Remarks.— *Albatrossidium annikasanfilippoae* n. sp. is distinguished from the holotype of *A. minzok* (Sanfilippo and Riedel, 1992, pl. 2, fig. 7), *A. cylindricum* (Ehrenberg, 1874), and *A. tenellum* (Foreman, 1973) by its perforated apical horn surrounded by several accessory spines, and an abdomen shorter than the thorax. *A. annikasanfilippoae* n. sp. differs from *A. regis* n. sp. as described under this species.

Since *A. minzok* is the earliest member of the genus *Albatrossidium*, known from the early Eocene to the middle Eocene (Sanfilippo and Riedel, 1992), it seems to be a possible ancestor of the late middle Eocene species *A. annikasanfilippoae* n. sp. However, *A. minzok* was not found at ODP Site 1260, and therefore, it is currently impossible to confirm this phylogenetic hypothesis. The cephalic hole observed in *A. annikasanfilippoae* n. sp. resembles the open cephalis of Neogene and Quaternary species of the genus *Lamprocyrtis* (see for example Sanfilippo and Riedel, 1992, pl. 4, figs. 7–9). However, the rest of the cephalis of *Lamprocyrtis* species differs in being longitudinally elongated and indistinctly trilobed. Although the two genera are related (Sanfilippo and Riedel, 1992), it is likely that this remarkable cephalic structure appeared twice independently.

Genus *Phormocyrtis* Haeckel, 1887

Type species.— *Phormocyrtis longicornis* Haeckel, 1887, p. 1370, pl. 69, fig. 15; subsequent designation by Campbell (1954, p. D134).

Phormocyrtis lazari new species

Plate II.26, Figures 5–8

1957b *Phormocyrtis embolum* (Ehrenberg) – Riedel, p. 88, pl. 2, fig. 7 (part).
1972 *Phormocyrtis embolum* (Ehrenberg) group – Petrushevskaya and Kozlova, p. 537, pl. 22, figs. 8, 9.
1974 *Phormocyrtis embolum* (Ehrenberg) – Kruglikova, fig. 3.10.
1975 ? *Phormocyrtis proxima* Clark and Campbell – Chen, p. 456, pl. 2, fig. 6.
? 1999 *Phormocyrtis embolum* (Ehrenberg) – Kozlova, p. 148, pl. 31, fig. 14.
? 1999 *Phormocyrtis* sp. cf. *P. embolum* (Ehrenberg) – Kozlova, pl. 35, fig. 16.

Holotype.— Plate II.26, Figure 5; collection number USTL 3474–1; coordinates T40/4; sample 1260A-9R-2W, 55–57 cm; uppermost part of the *Podocyrtis* (*L.*) *mitra* Zone, in the *Podocyrtis* (*P.*) *apeza* Subzone (late Lutetian, Middle Eocene).

Diagnosis.— *Phormocyrtis* species with a subcylindrical hyaline abdomen that is terminated by lamellar feet.

Occurrence.— From the upper part of the *Podocyrtis* (*L.*) *mitra* Zone, to the end of the studied interval, which is situated in the lower part of the *Podocyrtis* (*L.*) *goetheana* Zone.

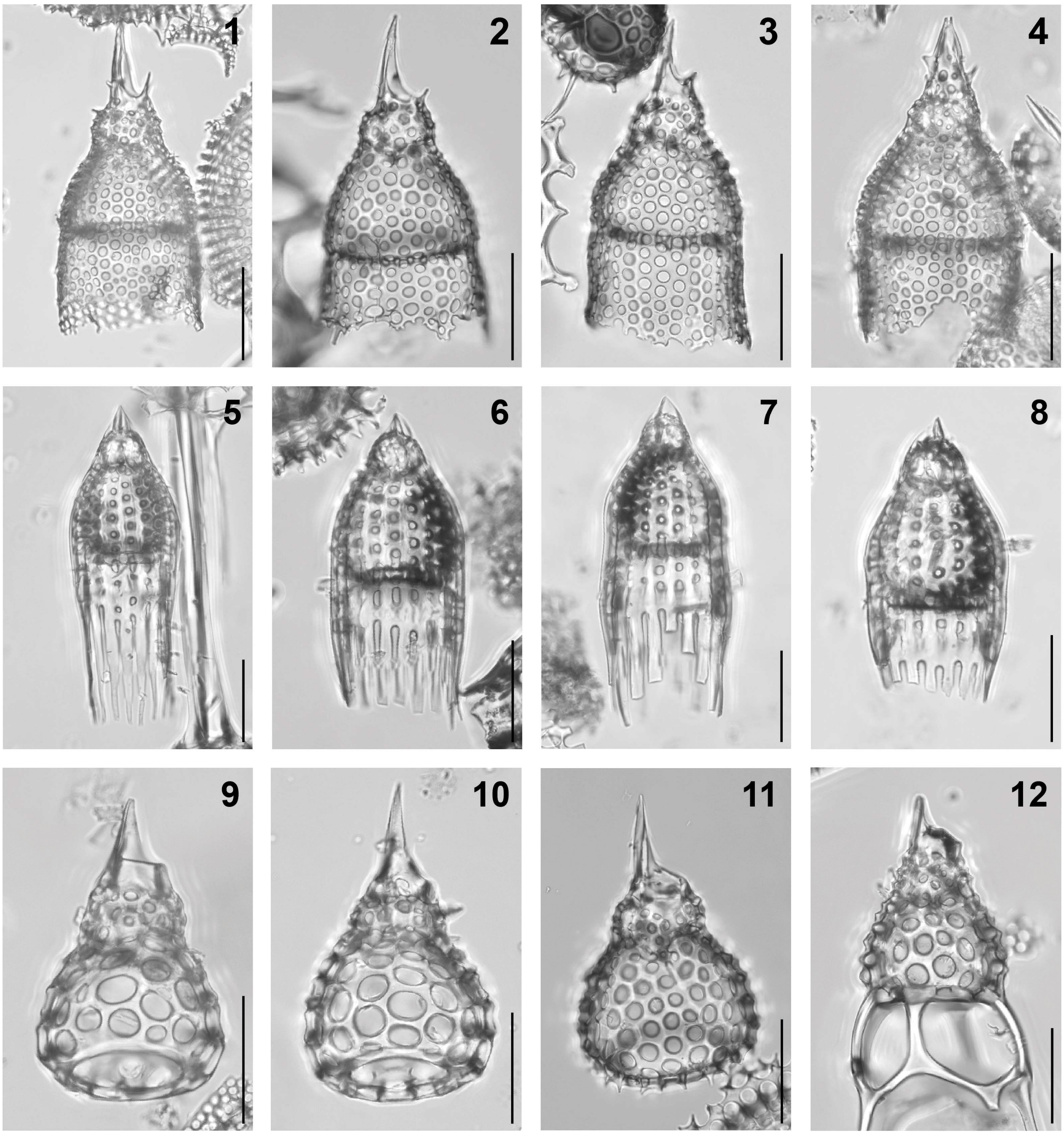

Plate II.26. Composite light micrographs of new radiolarian species from ODP Site 1260 (Demerara Rise, western equatorial Atlantic). (**1**–**4**) *Albatrossidium annikasanfilippoae* n. sp.: (**1**) holotype, ODP 1260A-12R-3W, 55–57 cm, USTL 3512–1, Y39/1; (**2**) ODP 1260A-13R-4W, 55–57 cm, USTL 2854–5, X67/4; (**3**) ODP 1260A-13R-4W, 55–57 cm, USTL 2854–2, O66/1; (**4**) ODP 1260A-9R-3W, 55–57 cm, USTL 3477–2, L56/3. (**5**–**8**) *Phormocyrtis lazari* n. sp.: (**5**) holotype, ODP 1260A-9R-2W, 55–57 cm, USTL 3474–1, T40/4; (**6**) ODP 1260A-9R-3W, 55–57 cm, USTL 3480–1, M35/1; (**7**) ODP 1260A-9R-4W, 55–57 cm, USTL 3482–2, W36/3; (**8**) ODP 1260A-9R-4W, 55–57 cm, USTL 3481–3, E38/3. (**9**–**12**) *Podocyrtis* (*Lampterium*) *puellasinensis* (Ehrenberg): (**9**) ODP 1260A-6R-2W, 55–57 cm, USTL 3420–1, U56/1; (**10**) ODP 1260A-9R-4W, 55–57 cm, USTL 3484–3, D47/3; (**11**) ODP 1260A-12R-1W, 55–57 cm, USTL 2851–4, C47/4 (mirrored). (**12**) *Podocyrtis* (*Lampterium*) *goetheana*

(Haeckel), focus on the cephalothorax, ODP 1260A-8R-2W, 54–56 cm, USTL 3461–2, S49/1 (mirrored). All scale bars equal 50 µm.

Description.— Shell three-segmented, smooth, and thick-walled, with slight collar and lumbar constrictions. Cephalis hemispherical, poreles,s or with a few small subcircular pores, bearing a short conical horn that is weakly bladed, at least in the proximal part. Thorax truncate conical to subcylindrical, with pores in longitudinal rows (six to seven in a row), separated by strong longitudinal ribs. Lower margin of the thorax marked by a well-defined internal septal band. Abdomen subcylindrical to truncate conical, either hyaline or sparsely pored in its upper portion, thence surrounded by ~20 lamellar feet that point distally and vary in length (about 1/2 to 2 length of the hyaline part). If present, abdominal pores are either subcircular or longitudinally elongated, and can be up to three times as long as the thoracic ones.

Etymology.— This species is named in honor of Dr. David Lazarus (Museum für Naturkunde – Humboldt-Universität, Berlin) in recognition of his contribution to the study of Cenozoic radiolarians. The specific epithet is to be treated as a noun in the genitive case formed from a personal name that is Latin.

Dimensions.— Based on 30 specimens (mean): total length without the apical horn: 69–180 µm (129), length of apical horn (when present): 7–15 µm (12), length of cephalothorax without the apical horn: 51–84 µm (72), length of the hyaline proximal part of the abdomen: 18–40 µm (27), length of lamellar feet: 6–68 µm (33).

Remarks.— This species differs from *Phormocyrtis embolum* (Ehrenberg, 1874), *P. ligulata* Clark and Campbell, 1942 and *P. striata* Brandt, 1935 by having a subcylindrical sparsely pored abdomen that terminates in lamellar feet, instead of an inverted truncate conical abdomen with numerous pores and a simple peristome. Additionally, *P. lazari* n. sp. is unique among all *P. striata* subspecies due to the presence of an internal septal band at the lower margin of the thorax. The new species is finally distinguished from *P. proxima* Clark and Campbell, 1942 by its nearly hyaline abdomen terminated by lamellar feet, and from *Phormocyrtis alexandrae* O'Connor, 1997b, *P.* ? *cubense* Riedel and Sanfilippo, 1971, and *P. turgida* (Krasheninnikov, 1960) in lacking a fourth segment.

According to the stratigraphic data collected at ODP Site 1260, it is suggested that *P. lazari* n. sp. originated from *P. embolum*. The latter species disappeared shortly after the first occurrence of *P. lazari* n. sp. (Figure II.3). The two species share many morphological similarities: towards the end of its age range, *P. embolum* tends to become more cylindrical, with a subcylindrical to slightly tapered abdomen. This late morphotype of *P. embolum* corresponds well to the original description of *P. proxima*, supporting the synonymization of these two species. This suggestion was already made by Riedel (1957b), who also included specimens with an abdomen terminated by lamellar teeth, although the original description of *P. proxima* does not mention the presence of such perioral appendages. A few specimens with an intermediate morphology between *P. embolum* and *P. lazari* n. sp. have also been observed at ODP Site 1260, as well as in the Southern Ocean (Hollis et al., 2020, pl. 10, fig. 18). These specimens have a subcylindrical porous abdomen terminated by short lamellar teeth. *P. ligulata* is also likely related to these taxa. Unfortunately, this species has only been reported from the Pacific Ocean (Clark and Campbell, 1942, 1945; Blueford, 1988) and from the Southern Ocean (O'Connor, 1999b; Hollis et al., 2020), and we were therefore unable to clarify its phylogenetic relationships with *P. embolum* and *P. lazari* n. sp.

Genus *Podocyrtis* Ehrenberg, 1846

Type species.— *Podocyrtis papalis* Ehrenberg, 1847, p. 55, fig. 2; subsequent designation by Campbell (1954, p. D130).

Podocyrtis (*Lampterium*) *puellasinensis* Ehrenberg, 1874

Plate II.26, Figures 9–11

1874 *Podocyrtis Puella sinensis* [sic] Ehrenberg, p. 252.
1876 *Podocyrtis Puella sinensis* [sic] Ehrenberg – Ehrenberg, p. 82, pl. 14, fig. 3.
1882a *Cycladophora Puella sinensis* [sic] Ehrenberg – Bütschli, p. 527.
1887 *Clathrocyclas* (*Clathrocyclia*) *puella* [sic] (Ehrenberg) – Haeckel, p. 1387.
2009 *Podocyrtis puella-sinensis* [sic] Ehrenberg – Ogane et al., pl. 48, figs. 9a–9f.

Holotype.— No holotype was designated by Ehrenberg in the original description of the species. However, the specimen he drew (1876, pl. 14, fig. 3), which was later re-illustrated by Ogane et al. (2009, pl. 48, figs. 9a–9f) during their re-examination of Ehrenberg's collection kept in the Museum für Naturkunde, Humboldt University (Berlin, Germany), is a potential lectotype.

Diagnosis.— *Podocyrtis* species with a two-segmented shell, and a well-defined cephalic hole that is delimited by a thick hyaline rim.

Occurrence.— From the upper part of the *Podocyrtis* (*P.*) *ampla* Zone, to the end of the studied interval, which is situated in the lower part of the *Podocyrtis* (*L.*) *goetheana* Zone.

Description.— Shell two-segmented and robust. Cephalis trilobed, with one large unpaired eucephalic lobe, and two small paired lobes dorsally positioned. Cephalic pores subcircular to quadrate, irregular in size and randomly arranged. Apical horn as long as the cephalis, triangular, with a large cephalic hole circumscribed by a thick hyaline rim. Thorax truncate conical to globular, perforated by subcircular pores of various sizes, usually hexagonally framed, and much larger than the cephalic ones. Thorax ending in a smooth hyaline peristome that is doubled by an internal septum, or more rarely in a crown of very short spines (Plate II.26, Figure 11).

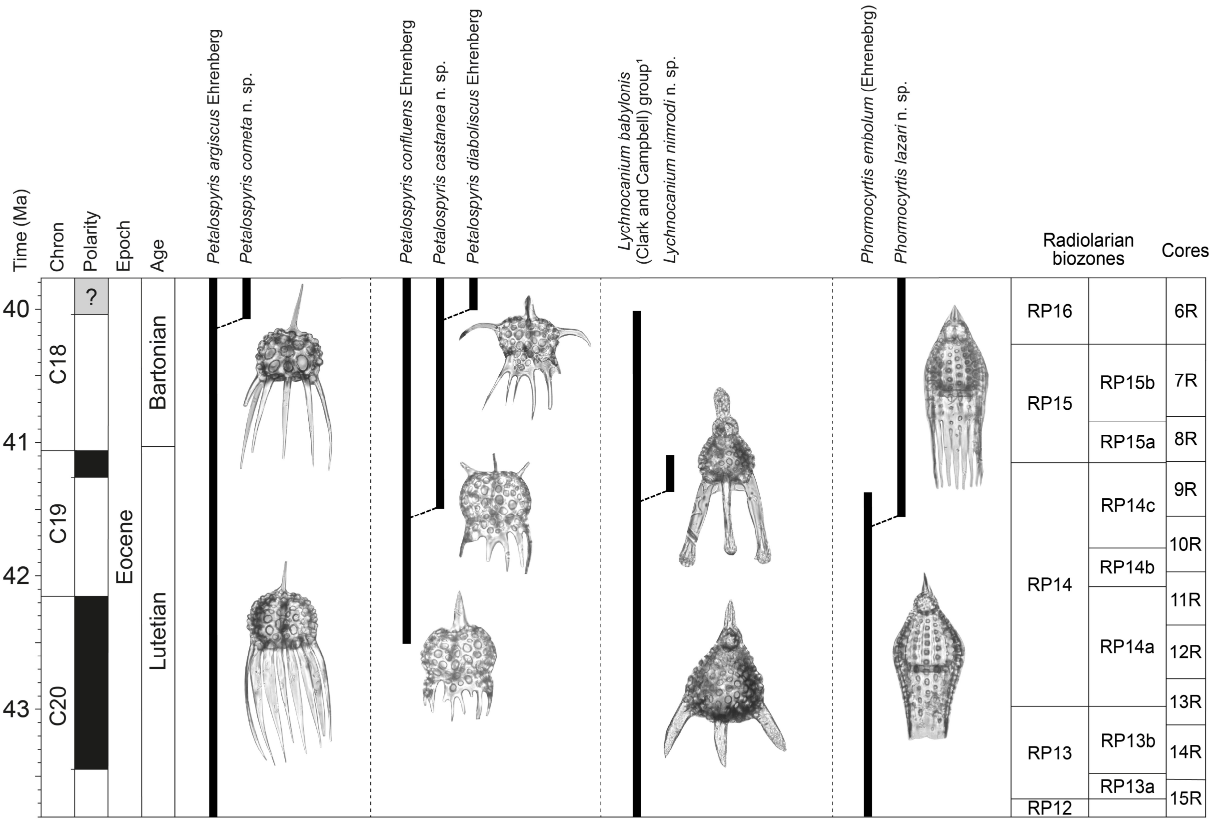

Figure II.3. Stratigraphic ranges and evolutionnary relationships to previously described species of four of the new species described at ODP Site 1260 (Demerara Rise, western equatorial Atlantic). The stratigraphic ranges of *Petalospyris argiscus*, *Petalospyris confluens*, *Petalospyris diaboliscus*, *Lychnocanium babylonis* group[1], and *Phormocyrtis embolum* at ODP Site 1260 are presented according to Meunier and Danelian (2022). Geomagnetic timescale after calibration of Suganuma and Ogg (2006), and radiolarian biozonation after Meunier and Danelian (2022). (1 – *Lychnocanium tribulus* (Ehrenberg, 1874) group in Chapter II.2).

Dimensions.— Based on 18 specimens (mean): length of cephalothorax without the apical horn: 65–90 µm (78), length of apical horn 27–51 µm (41), maximum breadth of shell: 66–92 µm (78).

Remarks.— *Podocyrtis* (*L.*) *puellasinensis* Ehrenberg, 1874 is distinguished from all other *Podocyrtis* species by its two-segmented shell, and its well-developed cephalic hole.

We have decided to retain *P.* (*L.*) *puellasinensis* in the genus *Podocyrtis*, despite the absence of an abdominal segment in this species, which contradicts the diagnosis of the genus (O'Dogherty et al., 2021). This decision was based on the strong morphological similarities between *P.* (*L.*) *puellasinensis* and the cephalothorax of the latter members of the subgenus *Lampterium*, such as *P.* (*L.*) *chalara* Riedel and Sanfilippo, 1970 and *P.* (*L.*) *goetheana* [Haeckel, 1887]). See Plate II.26, Figure 12 for a comparison with a typical *P.* (*Lampterium*) cephalothorax. This unexpected resemblance is noteworthy, especially considering that the first occurrence of *P.* (*L.*) *puellasinensis* dates back to 43.36 Ma at ODP Site 1260, about 2.2 Ma earlier than the first occurrence of *P.* (*L.*) *chalara* (41.15 Ma; Meunier and Danelian, 2022). Therefore, the origin of *P.* (*L.*) *puellasinensis* is difficult to decipher. The most suitable candidate is likely *P.* (*L.*) *sinuosa* Ehrenberg, 1874, despite its thorax being more campanulate and penetrated by smaller pores. In this case, *P.* (*L.*) *puellasinensis* would be an offshoot of the lineage from *P.* (*L.*) *sinuosa* to *P.* (*L.*) *mitra*, and for this reason, it is placed in the subgenus *Lampterium*. In their taxonomic review, O'Dogherty et al. (2021) recognized the subgenus *Lampterium* as a distinct genus and suggested the following combinations: *Lampterium chalara* (Riedel and Sanfilippo, 1970) and *L.* (*L.*) *goetheana* (Haeckel, 1887). We disagree with this view because the *Lampterium* evolutionary lineage that leads from *P.* (*L.*) *acalles* Sanfilippo and Riedel, 1992 to *P.* (*L.*) *goetheana* has been amply demonstrated in previous studies (e.g., Riedel and Sanfilippo, 1970; Sanfilippo and Riedel, 1992), and this taxonomic change would imply that the genus *Podocyrtis* is paraphyletic. An alternative hypothesis to explain the particular morphology of *P.* (*L.*) *puellasinensis* is that this species is the expression of an early stage in the development of the *Podocyrtis* shell, known as neoteny.

II.3.1.4. Conclusions

Examination of middle Eocene sedimentary sequences from the equatorial Atlantic Ocean allowed the description of 15 new radiolarian species and the re-illustration of ffour species that have been rarely seen since their original description in early radiolarian studies. With the exception of a few sporadic species (*Petalospyris castanea* n. sp., *Pterocyrtidium eep* n. sp., *Cymaetron* ? *dilatatus* n. sp. and *Velicucullus armatus* n. sp.), the taxa reported here have a continuous range in the studied interval and can therefore be included in future biostratigraphic studies. Although the studied interval is relatively limited and did not allow the total range of most of these species to be determined, a total of 23 radiolarian bioevents are documented, including 14 first occurrences and nine last occurrences. Orbitally tuned ages are provided for these bioevents through direct calibration to the Astronomical Time Scale, increasing the number of biostratigraphic tiepoints available for the equatorial Atlantic Ocean.

Several new species described here show strong morphological similarities to previously described species, allowing us to suggest phylogenetic hypotheses by integrating stratigraphic data. Despite being fragmentary, these observations are important for establishing new evolutionary lineages, and better understanding the evolutionary dynamics of nassellarians. The documentation of new species has also improved our understanding of the origins of some genera. This is the case of the genus *Aphetocyrtis*, which is now clearly rooted in the tropics, with three new tropical species reported here (*A. zamenhofi* n. sp., *A.* ? *columboi* n. sp. and *A.* ? *spheniscus* n. sp.). Likewise, the documentation of *Spirocyrtis* ? *renaudiei* n. sp., an Artostrobiid species with a mixture of characters borrowed from the genera *Botryostrobus* and *Spirocyrtis*, allows to locate the divergence of these two genera shortly before the late middle Eocene. Finally, this study contributed to the addition of new species to the monotypic genera *Albatrossidium* and *Cymaetron*, which have been poorly known and rarely observed since their original description.

Acknowledgments

We thank the Ocean Drilling Program (ODP) for providing the samples used in this study. Thanks also to Jessie Cuvelier for technical assistance. Constructive comments by the two anonymous reviewers significantly improved the original manuscript.

II.3.2. New middle Eocene radiolarian species (Rhizaria, Polycystinea) from Blake Nose, subtropical western North Atlantic Ocean

Mathias Meunier* and Taniel Danelian

Univ. Lille, CNRS, UMR 8198 – Evo-Eco-Paleo, F-59000 Lille, France

<mathias.meunier@univ-lille.fr>

*Corresponding author

Abstract.— Diverse and well-preserved radiolarian assemblages were recovered from the middle Eocene sedimentary sequences drilled at Ocean Drilling Program Site 1051 (Leg 171B; western subtropical Atlantic). In addition to biostratigraphically important species, several unknown morphotypes were observed in this material, leading to the description of three new spumellarian species and 18 new nassellarian species. Are described herein: *Periphaena petrushevskayae* n. sp. (Phacodiscidae), *Stylodictya oligodonta* n. sp. (Trematodiscidae), *Excentrosphaerella delicata* n. sp. (Heliodiscidae), *Eucyrtidium granatum* n. sp. (Eucyrtidiidae), *Dictyoprora echidna* n. sp., *Spirocyrtis matsuokai* n. sp. (Artostrobiidae), *Elaphospyris cordiformis* n. sp., *Elaphospyris quadricornis* n. sp. (Cephalospyrididae), *Ceratocyrtis oconnori* n. sp. (Lophophaenidae), *Botryocella* ? *alectrida* n. sp., *Pylobotrys* ? *bineti* n. sp. (Pylobotrydidae), *Lychnocanium cheni* n. sp., *Lychnocanium cingulatum* n. sp., *Lychnocanium croizoni* n. sp., *Lychnocanium forficula* n. sp. (Lithochytrididae), *Apoplanius hyalinus* n. sp., *Apoplanius cryptodirus* n. sp. (Lophocyrtiidae), *Albatrossidium messiaeni* n. sp., *Phormocyrtis microtesta* n. sp., *Cryptocarpium* ? *judoka* n. sp. (Pterocorythidae), *Thyrsocyrtis kamikuri* n. sp. (Theocotylidae). Biostratigraphic information is provided for each new species. In addition, we redescribe and illustrate the morphological variability of a remarkable *Pterocyrtidium* species formerly published by Bütschli (1882a).

UUID: A01F7F03-73B0-458A-AF7B-B85DC4666CC2

II.3.2.1. Introduction

Polycystine radiolarians are a large group of marine planktonic protozoans that secrete a morphologically complex skeleton made of opaline silica. Known since the early Cambrian (Obut and Iwata, 2000; Pouille et al., 2011), their extensive fossil record makes them valuable biostratigraphic markers and an ideal taxonomic group for paleoceanography and macroevolutionary studies (De Wever et al., 2001; Lazarus et al., 2021). However, despite their importance in fossil plankton assemblages, a substantial portion of the radiolarian diversity preserved in the fossil record remains undocumented, hindering the expression of their full biostratigraphic and paleoceanographic potential.

Eocene radiolarians were the first to receive sustained attention from micropaleontologists, with the description of several hundred species from siliceous-rich chalk beds cropping on the Barbados Island (Ehrenberg, 1839; 1846; 1847; 1874, 1876; Haeckel, 1887; Bütschli, 1882a, 1882b). This body of early taxonomic work has constituted the core of the Paleogene radiolarian taxonomy for nearly a century, although some contributions were also made in the first half of the 20th century (e.g., Clark and Campbell, 1942, 1945). The launch of scientific ocean drilling programs in the early 1970s marked a pivotal change in the history of Cenozoic radiolarian research, allowing extensive recoveries of radiolarian assemblages around the world and rekindling interest in describing their diversity (e.g., Riedel and Sanfilippo, 1970, 1971, 1978; Petrushevskaya and Kozlova, 1972; Foreman, 1973; Sanfilippo and Riedel, 1973, 1982, 1992; Nigrini, 1977; Sanfilippo and Caulet, 1998). However, most of these studies have focused on biostratigraphically important species, which represent only a minute fraction of the total radiolarian diversity. As a result, many rare morphotypes that are of no interest for biostratigraphic correlations, or those belonging to poorly defined genera and families, were not documented and remain undescribed until recently (i.e., Meunier and Danelian, 2023).

To contribute to our understanding of Paleogene radiolarian diversity, 21 new species distributed amongst 16 genera and 13 families are formally described from the middle Eocene sequences cored at Ocean Drilling Program Site 1051 (Leg 171B; western subtropical Atlantic). Most of these new taxa were previously illustrated by Kamikuri (2015) in an extensive monograph conducted at neighboring ODP Site 1052, but they were left in open nomenclature. Biostratigraphic information is provided for each new species, and stratophenetic relationships to previously described species are suggested.

II.3.2.2. Materials and methods

Materials.— ODP Site 1051 (30°03′N, 76°21′W, modern water depth of ~1983 m below sea level, mbsl) was drilled on the Blake Nose, a promontory at the edge of the Blake Plateau, in the western North Atlantic Ocean (Figure 1). This site provided an expanded and nearly continuous upper Paleocene through lower upper Eocene sedimentary sequence, dominated by silica-bearing nannofossil oozes rich in radiolarians, diatoms, and sponge spicules (Norris et al., 1998). Paleo-water depth estimates based on benthic foraminifera indicate lower bathyal depths (1000−2000 mbsl) at this site during the Eocene (Norris et al., 1998), with a slightly more southerly paleolatitude of ~25°N (Ogg and Bardot, 2001). The estimated sedimentation rate is ~4 cm/kyr (Norris et al., 1998; Edgar et al., 2010).

The species described in this paper are from 16 samples collected from the richest and most diverse radiolarian interval, which spans cores 2H to 18X (12.73– 174.28 meters composite depth, mcd) in Hole 1051A (Sanfilippo and Blome, 2001).

Methods.— Samples were treated according to the procedures described in Sanfilippo et al. (1985) and Tetard et al. (2020). About 2 cm² of untreated sediment were first soaked in a polypropylene beaker containing 30 mL of 30 % hydrochloric acid (HCl) to dissolve calcium carbonate. At the end of this stage, a few mL of HCl were added to ensure the end of the reaction. The resulting residues were then washed with distilled water and soaked in 30 mL of 10 % hydrogen peroxide (H_2O_2) to remove organic material. The siliceous residues were finally sieved through a 45 µm mesh to remove small radiolarian fragments and clay. Three slides were prepared per sample using ~3 mg of dry residues randomly spread on a coverslip (Witkowski et al., 2012). Coverslips were mounted on standard glass slides using Eukitt mounting medium (refractive index = 1.49).

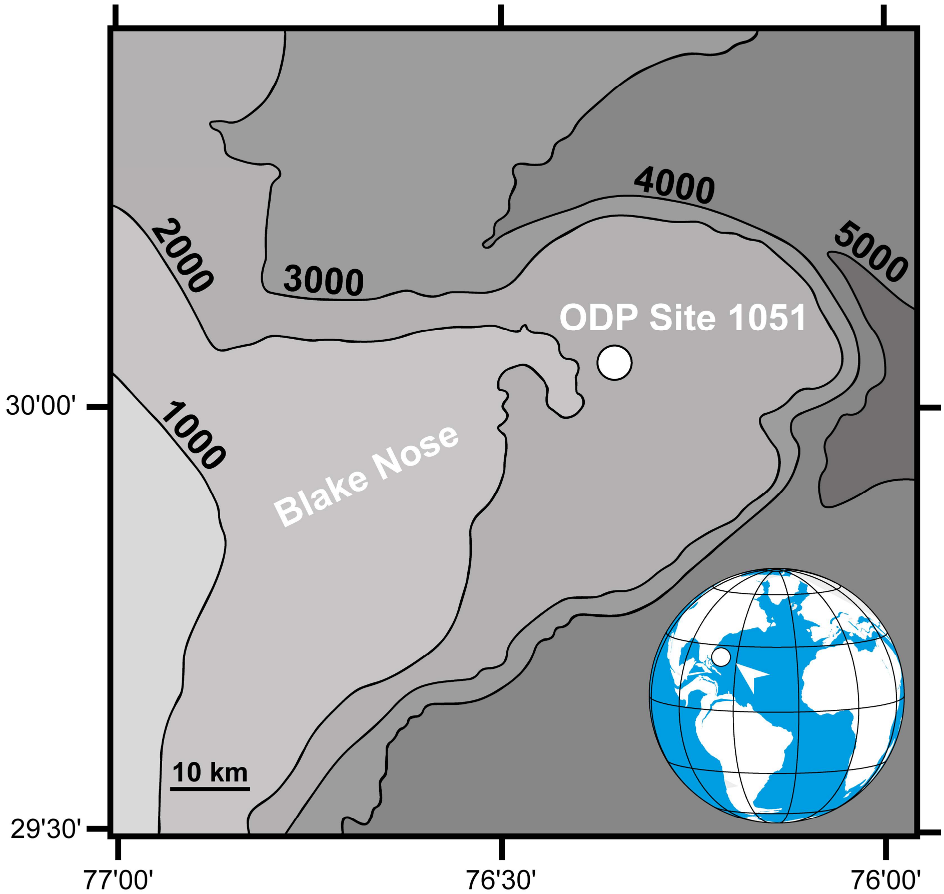

Figure II.4. Location of Blake Nose in the western North Atlantic Ocean (modified from Land et al., 1999). The box shows the detailed location of ODP Site 1051 (Leg 171B) on a bathymetric map (modified from Norris et al., 1998). Bathymetry is in meters.

Observation and identification of radiolarians were performed using a Zeiss Axio Imager.A2 transmitted light microscope at 20x magnification. Images were captured using a

Zeiss AxioCam ERc5s digital camera. To create a fully focused composite image of a single specimen, a set of ~5 images was taken at different f-stops and stacked using Helicon Focus v.7.6.6 (HeliconSoft).

All measurements provided in the systematic paleontology section were performed on specimen images using the image analysis software ImageJ (Schneider et al., 2012). The stratigraphic occurrences of the species are shown in Figure II.5, and the associated bioevents are summarized in Table II.2.

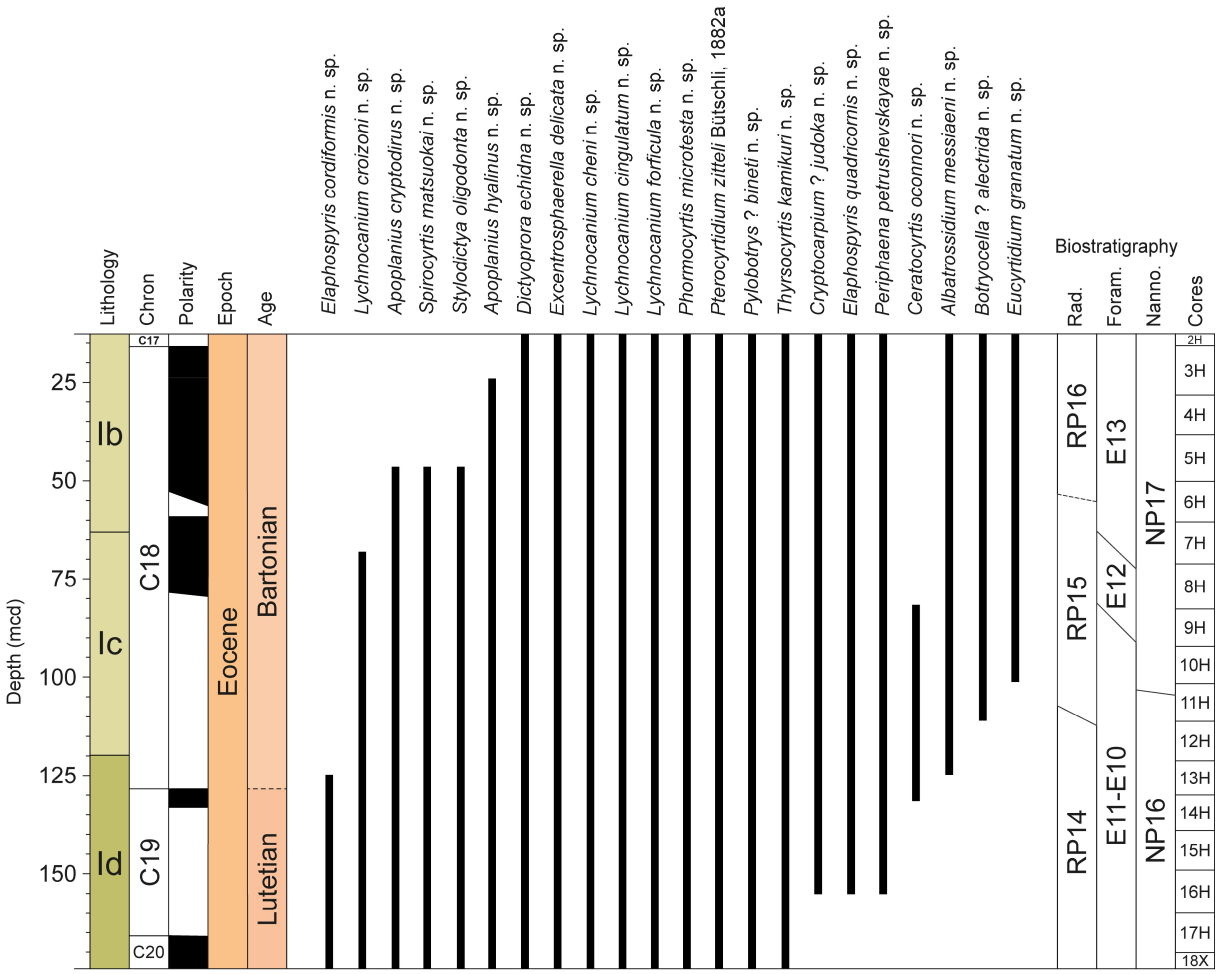

Figure II.5. Range chart of the 21 new radiolarian species from the late middle Eocene of ODP Site 1051 (Blake Nose, western subtropical Atlantic). Lithology column based on data from Norris et al. (1998) and geomagnetic timescale after calibration of Ogg and Bardot (2001). Radiolarian biostratigraphy according to Sanfilippo and Blome (2001), planktonic foraminiferal biostratigraphy according to Norris et al. (1998) and Edgar et al. (2010), and calcareous nannofossil biostratigraphy according to Mita (2001). Abbreviations: mcd, meters composite depth.

Repositories and institutional abbreviations.— All holotypes and figured specimens (Figures 3–8) are deposited in the public paleontological collection of the University of Lille (USTL), France. Specimens are located according to hole number, core number, section number, interval depth, and England Finder coordinates.

Table II.2. Summary of first occurrences (FO) and last occurrences (LO) at ODP Site 1051, drilled on the Blake Plateau (western North Atlantic). Abbreviations: mbsf, meters below seafloor; mcd, meters composite depth.

ODP Site 1051		Depth (m)	
Radiolarian bioevents	Core - section - interval (cm) Base/top	mbsf Base/top	mcd Base/top
LO *Apoplanius hyalinus* n. sp.	4H-5W, 56–58/2R-5W, 55–57	31.36/12.35	35.31/12.73
LO *Apoplanius cryptodirus* n. sp.	6R-5W, 53–55/4R-5W, 56–58	50.33/31.36	57.58/35.31
LO *Spirocyrtis matsuokai* n. sp.	6R-5W, 53–55/4R-5W, 56–58	50.33/31.36	57.58/35.31
LO *Stylodictya oligodonta* n. sp.	6R-5W, 53–55/4R-5W, 56–58	50.33/31.36	57.58/35.31
LO *Lychnocanium croizoni* n. sp.	8H-5W, 61–63/6H-5W, 53–55	68.20/50.33	78.56/57.58
LO *Ceratocyrtis oconnori* n. sp.	9H-2W, 53–55/8H-5W, 61–63	74.33/68.20	84.69/78.56
FO *Eucyrtidium granatum* n. sp.	11H-2W, 62–64/10H-5W, 52–54	93.42/88.32	103.78/98.68
FO *Botryocella* ? *alectrida* n. sp.	12H-2W, 55–57/11H-5W, 59–61	102.85/97.89	113.78/108.25
FO *Albatrossidium messiaeni* n. sp.	13H-5W, 58–60/13H-2W, 52–54	116.88/112.32	127.06/122.50
LO *Elaphospyris cordiformis* n. sp.	13H-5W, 58–60/13H-2W, 52–54	116.88/112.32	127.06/122.50
FO *Ceratocyrtis oconnori* n. sp.	14H-5W, 52–53/13H-5W, 58–60	126.32/116.88	136/127.06
FO *Cryptocarpium* ? *judoka* n. sp.	18X-5W, 54–56/14H-5W, 52–53	164.74/126.32	174.28/136
FO *Elaphospyris quadricornis* n. sp.	18X-5W, 54–56/14H-5W, 52–53	164.74/126.32	174.28/136
FO *Periphaena petrushevskayae* n. sp.	18X-5W, 54–56/14H-5W, 52–53	164.74/126.32	174.28/136

II.3.2.3. Systematic paleontology

The higher-level classification adopted here is based on the most recent and integrative radiolarian classification of Suzuki et al. (2021). Genus assignments of the new species are consistent with the diagnosis provided by O'Dogherty et al. (2021).

The morphological terminology used in the text to designate the different parts of the fundamental nassellarian spicule follows that of Petrushevskaya (1984). See also Goll (1968; p. 1413, text-figure 6) for features specific to the family Cephalospyrididae, and Sanfilippo and Caulet (1998; p. 6, text-figure 2) for the family Lophocyrtiidae.

Infrakingdom Rhizaria Cavalier-Smith, 2002 emend. Cavalier-Smith, 2003

Phylum Retaria Cavalier-Smith, 1999

Class Polycystinea Ehrenberg, 1839

Order Spumellaria Ehrenberg, 1876

Superfamily Lithocyclioidea Ehrenberg, 1846

Family Phacodiscidae Haeckel, 1882

Genre *Periphaena* Ehrenberg, 1874

Type species.— *Periphaena decora* Ehrenberg, 1874, p. 246 (unfigured); Ehrenberg, 1876, p. 80, pl. 28, Figure 6; by monotypy.

Periphaena petrushevskayae new species

Plate II.27, Figures 1–4

1972 *Periphaena* sp. Petrushevskaya and Kozlova, p. 523, pl. 14, figs. 4, 5.

Holotype.— Plate II.27, Figure 1; collection number USTL 4525–1; coordinates K55/2; sample ODP 171B-1051A-9H-2W, 53–55 cm; *Podocyrtis* (*L.*) *chalara* Zone (RP15; Sanfilippo and Blome, 2001); middle Eocene.

Diagnosis.— Phacodiscid species with a thick equatorial hyaline girdle bearing six to 10 triangular spines of variable length.

Occurrence.— This species occurs throughout the studied interval, from the upper part of the *Podocyrtis* (*L.*) *mitra* Zone (RP14) to the lower part of the *Podocyrtis* (*L.*) *goetheana* Zone (RP15).

Description.— Shell lenticular, externally smooth, with a phacodiscid center and a well-developed equatorial hyaline girdle. Six to 10 triangular equatorial spines of variable length arise from the girdle as extensions. Cortical shell about three times the diameter of the medullary shell, perforated by numerous small cylindrical pores that are uniform in size and shape (about 10 pores in a radius). Medullary shell double, globular, attached to the cortical shell by a few thick rods.

Etymology.— The specific epithet honours Dr. Maria G. Petrushevskaya, who was the first to illustrate this radiolarian taxon in the fauna of DSDP Site 144.

Dimensions.— Based on 19 specimens (mean): shell diameter: 133–183 µm (160), length of equatorial spines: 34–156 µm (76).

Remarks.— The new species differs from *Periphaena contiguum* (Ehrenberg, 1874), *P. delta* Sanfilippo and Riedel, 1973, *P. heliasteriscus* (Clark and Campbell, 1942), *P. humboldti* (Ehrenberg 1847) and *P. umbonatum* (Ehrenberg, 1874) in having an equatorial hyaline girdle, and from *P. decora* Ehrenberg, 1874 in having well-developed equatorial spines. Finally, *P. petrushevskayae* n. sp. is distinguished from *P. cingillum* (Haeckel, 1887) in having less than 10 equatorial spines. In many aspects, *P. petrushevskayae* n. sp. resembles *P. decora*, from which it probably evolved by modification of the equatorial girdle.

Superfamily Trematodiscoidea Haeckel, 1862 emend. Suzuki in Suzuki et al., 2021

Family Trematodiscidae Haeckel, 1862 emend. Suzuki in Suzuki et al., 2021

Genre *Stylodictya* Ehrenberg, 1846

Type species.— *Stylodictya gracilis* Ehrenberg, 1854, pl. 36, Figure 28; by monotypy.

Stylodictya oligodonta new species

Plate II.27, Figures 5–8

Holotype.— Plate II.27, Figure 5; collection number USTL 4536–2; coordinates R52/1; sample ODP 171B-1051A-11H-2W, 62–64 cm; lower part of the *Podocyrtis* (*L.*) *chalara* Zone (RP15; Sanfilippo and Blome, 2001); middle Eocene.

Diagnosis.— Small trematodiscid species with less than four annular rings, and a few short equatorial spines.

Occurrence.— This species is found throughout the studied interval, from the upper part of the *Podocyrtis* (*L.*) *mitra* Zone (RP14) to the lower part of the *Podocyrtis* (*L.*) *goetheana* Zone (RP16).

Description.— Shell as a subcircular flat disc, tending to be angular in outline in some specimens. Disc concentrically chambered, with a decussate microsphere surrounded by one (Plate II.27, Figure 8) to three (Plate II.27, Figure 7) annular rings. Margin of the disc bearing many small, triangular to rounded spines of various lengths. Four longer spines are usually present, representing extensions of the cylindrical primary radial rays from the inner disc. Pores subcircular, scattered over the surface, and usually more widely spaced and less numerous on the marginal ring.

Etymology.— The specific epithet means ‘few teeth’ in Greek, alluding to the sparse marginal spines of the new species.

Dimensions.— Based on 11 specimens (mean): shell diameter: 72–119 µm (89), spines length: 4–20 µm (10).

Remarks.— The new species is placed in the genus *Stylodictya* because it has a decussate microsphere surrounded by several narrow concentric rings and from which four primary and many secondary equatorial spines extend. The small size of *Stylodictya oligodonta* n. sp. (shell diameter < 120 µm), as well as its short triangular to rounded spines, allow it to be distinguished from all other middle Eocene flattened spumellarians with a decussate microsphere.

Superfamily Haliommoidea Ehrenberg, 1846

Family Heliodiscidae Haeckel, 1882 emend. Dumitrică, 1984

Genus *Excentrosphaerella* Dumitrică, 1978

Type species.— *Excentrosphaerella sphaeroconcha* Dumitrică, 1978, p. 238, pl. 5, fig. 22; subsequent designation by O'Dogherty et al., 2021.

Excentrosphaerella delicata new species

Plate II.27, Figures 9–12

Holotype.— Plate II.27, Figures 9, 10; collection number USTL 4524–6; coordinates F73/1; sample ODP 171B-1051A-9H-2W, 53–55 cm; *Podocyrtis* (*L.*) *chalara* Zone (RP15; Sanfilippo and Blome, 2001); middle Eocene.

Diagnosis.— Relatively small *Excentrosphaerella* species with a shell ratio of 1:2:3.

Occurrence.— This species occurs sporadically throughout the studied interval, from the upper part of the *Podocyrtis* (*L.*) *mitra* Zone (RP14) to the lower part of the *Podocyrtis* (*L.*) *goetheana* Zone (RP16).

Description.— Delicate four-shelled test with a small eccentric microsphere embedded in a subspherical inner medullary shell. Outer medullary shell surrounded by two concentric spherical shells connected by numerous filamentous radial beams projecting from the cortical shell as long conical spines. Third shell and cortical shell perforated by numerous small, randomly arranged, subcircular pores.

Etymology.— The name is derived from the Latin *delicatus*, meaning ‘soft, delicate’, for the thin-walled cortical shell of the new species.

Dimensions.— Based on five specimens (mean): diameter of microsphere: 12–15 µm (13), of outer medullary shell: 38–44 µm (41), of third shell: 61–73 µm (67), of cortical shell: 102–118 µm (108), length of cortical spines: 15–46 µm (23).

Remarks.— *Excentrosphaerella delicata* n. sp. differs from *E. sphaeroconcha* Dumitrică, 1978 and *Actinomma capillaceum* Haeckel, 1887 in being two times smaller and in having an inner medullary shell to cortical shell ratio of 1:3 instead of a ratio of 1:4 (Dumitrică, 1978; pl. 5, fig. 22), 1:5 (Dumitrică, 2019; figs. 11a, 11b) or 1:7 (Haeckel, 1887; pl. 29, fig. 2). The new species is also distinguished from the middle Miocene specimens illustrated as *E. sphaeroncha* by Sugiyama and Furutani (1992; pl. 12, figs. 1, 2, pl. 16, fig. 3) in having a spherical outer medullary shell.

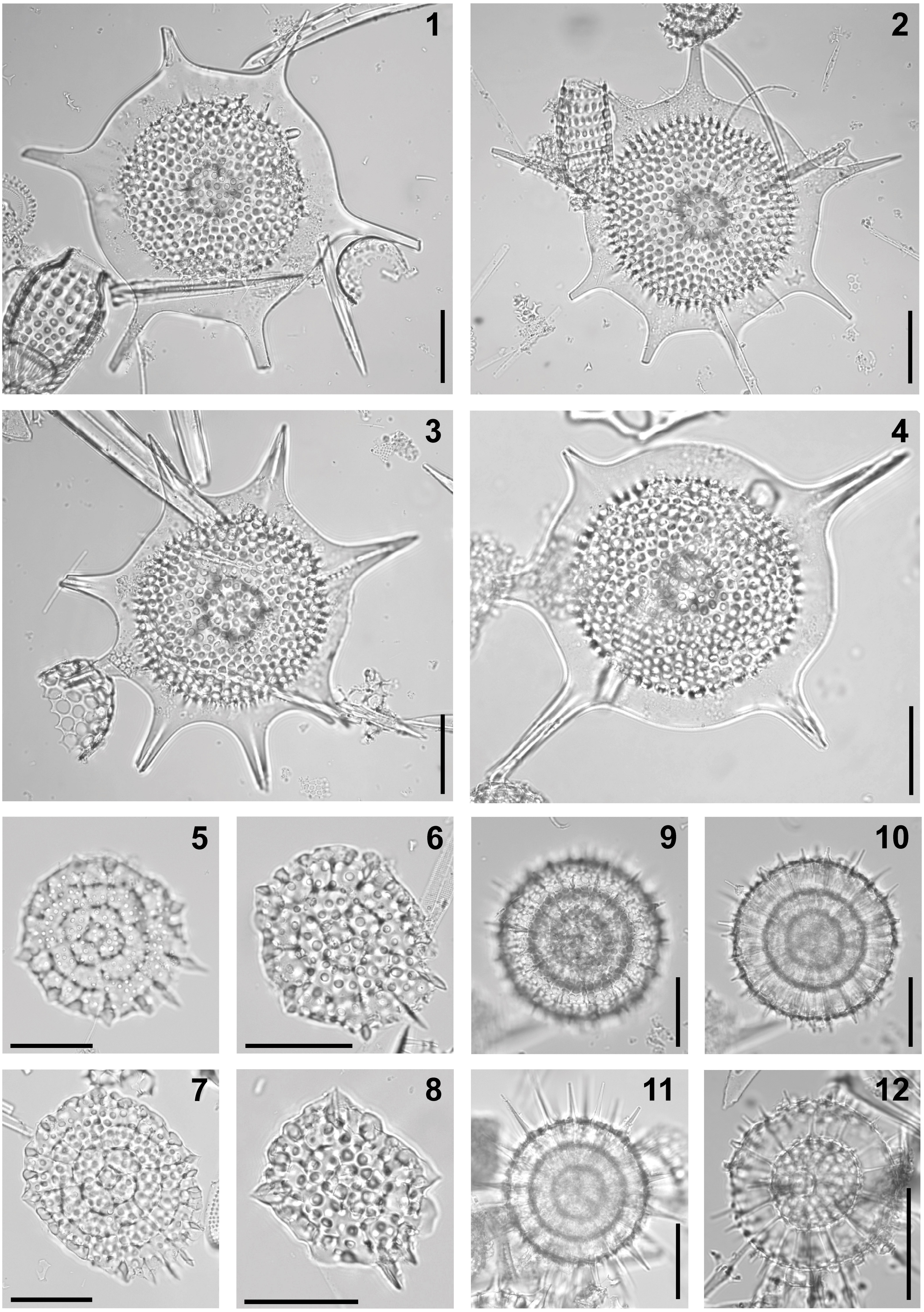
1
2
3
4
5
6
9
10
7
8
11
12

Plate II.27. Composite light micrographs of new radiolarian species from ODP Site 1051 (Blake Nose, western subtropical Atlantic). (**1–4**) *Periphaena petrushevskayae* n. sp.: (**1**) holotype, ODP 171B-1051A-9H-2W, 53–55 cm, USTL 4525–1, K55/2; (**2**) ODP 171B-1051A-9H-2W, 53–55 cm, USTL 4524–2, S55/3; (**3**) ODP 171B-1051A-9H-2W, 53–55 cm, USTL 4524–3, U55/1; (**4**) ODP 171B-1051A-9H-5W, 53–55 cm, USTL 4529–2, K44/2. (**5–8**) *Stylodictya oligodonta* n. sp.: (**5**) holotype, ODP 171B-1051A-11H-2W, 62–64 cm, USTL 4536–2, R52/1; (**6**) ODP 171B-1051A-9H-2W, 53–55 cm, USTL 4526–3, R46/3; (**7**) ODP 171B-1051A-9H-2W, 53–55 cm, USTL 4525–3, T41/3; (**8**) poorly-developed form, ODP 171B-1051A-9H-2W, 53–55 cm, USTL 4525–2, V64/1. (**9–12**) *Excentrosphaerella delicata* n. sp.: (**9**) holotype, cortical shell, ODP 171B-1051A-9H-2W, 53–55 cm, USTL 4524–6, F73/1; (**10**) holotype, inner structure; (**11**) ODP 171B-1051A-9H-2W, 53–55 cm, USTL 4526–2, V49/1; (**12**) inner structure, ODP 171B-1051A-9H-2W, 53–55 cm, USTL 4524–4, O65/3. All scale bars equal 50 µm.

Order Nassellaria Ehrenberg, 1876

Superfamily Eucyrtidioidea Ehrenberg, 1846 emend. Suzuki et al., 2021

Family Eucyrtidiidae Ehrenberg, 1846 emend. Suzuki et al., 2021

Genus *Eucyrtidium* Ehrenberg, 1846

Type species.— *Lithocampe acuminata* Ehrenberg, 1844, p. 84 (unfigured); Ehrenberg, 1854, pl. 22, Figure 27; subsequent designation by Frizzell and Middour, 1951, p. 33.

Eucyrtidium granatum new species

Plate II.28, Figures 1–4

2015 *Eucyrtidium* sp. A Kamikuri, pl. 9, figs. 6a, 6b.

Holotype.— Plate II.28, Figure 1; collection number USTL 4513–1; coordinates M69/3; sample ODP 171B-1051A-2H-5W, 55–57 cm; lower part of the *Podocyrtis* (*L.*) *goetheana* Zone (RP16; Sanfilippo and Blome, 2001); middle Eocene.

Diagnosis.— *Eucyrtidium* species with an abdominal segment that is more than twice as high as the thorax and is perforated by numerous small, closely spaced pores.

Occurrence.— This rare species occurs sporadically from the lower part of the *Podocyrtis* (*P.*) *chalara* Zone (RP15) to the lower part of the *Podocyrtis* (*L.*) *goetheana* Zone (RP16).

Description.— Shell multi-segmented, subcylindrical, and very thick-walled. Cephalis relatively small, hemispherical to subspherical, perforated by a few small subcircular pores, bearing a short apical horn. Collar stricture marked by a slight constriction. Thorax campanulate to truncate conical, thick-walled, with subcircular pores scattered over the surface. Lumbar stricture marked by a moderate constriction, and by a thin internal ridge that appears externally as a dark line. Abdomen subcylindrical, elongated and thick-walled, perforated by numerous, small subcircular pores, which are closely spaced and weakly arranged in longitudinal rows (18–23 in a row). Post-lumbar stricture almost invisible from the outside, marked only by a thin dark line. Fourth segment cylindrical, as broad as the abdomen but always shorter. Abdominal termination open, and invariably ragged along a row of pores.

Etymology.— The name is derived from the Latin *granatus*, meaning ‘having many seeds or grains’, for the shell ornamentation of the new species.

Dimensions.— Based on 5 specimens (mean): total length without the apical horn: 143–179 µm (162), length of apical horn: 12–17 µm (15), length of cephalothorax: 41–48 µm (44), length of abdomen: 86–116 µm (96), length of first post-abdominal segment: 31–45 µm (38).

Remarks.— *Eucyrtidium granatum* n. sp. differs from all other species of the genus *Eucyrtidium* in having a thick-walled shell with a characteristic ornamentation consisting of many small, closely spaced pores.

Superfamily Artostrobioidea Riedel, 1967

Family Artostrobiidae Riedel, 1967 sensu. Sugiyama, 1998

Genus *Dictyoprora* Haeckel, 1887

Type species.— *Dictyocephalus amphora* Haeckel, 1887, p. 1305, pl. 62, fig. 4; subsequent designation by Campbell, 1953, p. 296.

Dictyoprora echidna new species

Plate II.28, Figures 5–8

1973 *Theocampe amphora* (Haeckel) group – Foreman, p. 431, pl. 9, fig. 8 (part).
2015 *Dictyoprora* sp. E Kamikuri, pl. 12, figs. 11a, 11b.

Holotype.— Plate II.28, Figure 5; collection number USTL 4518–1; coordinates M41/3; sample ODP 171B-1051A-6H-5W, 53–55 cm; upper part of the *Podocyrtis* (*L.*) *chalara* Zone (RP15; Sanfilippo and Blome, 2001); middle Eocene.

Diagnosis.— *Dictyoprora* species with a general ovoid shape and an abdominal segment perforated by 8 to ten closely spaced rows of pores.

Occurrence.— This species is abundant from the upper part of the *Podocyrtis* (*L.*) *mitra* Zone (RP14) to the lower part of the *Podocyrtis* (*L.*) *goetheana* Zone (RP16).

Description.— Shell three-segmented, ovoid, and externally smooth. Cephalis subspherical to hemispherical, unarmed, deeply embedded in the thorax. Cephalic pores circular and closely spaced. Ventral pore relatively large, circular to ovoid (Plate II.28, Figures 7, 8). Ventral tube not developed. Collar stricture indistinct. Thorax short, trapezoidal to slightly inflated, with downwardly directed subcircular pores arranged in two or three transverse rows. Lumbar stricture marked by a thin obscure band. Abdomen barrel-shaped, thick-walled, and perforated by 8 to 10 closely spaced rows of downward directed subcircular pores. Shell tapers distally, ending in a hyaline, inverted-truncated conical peristome with a smooth margin.

Etymology.— The specific epithet refers to the Latin name of the spiny anteater (echidna), for the shell ornamentation of the new species, which resembles the texture of the back of these animals covered by spines.

Dimensions.— Based on 26 specimens (mean): total length: 113–159 µm (135), length of cephalothorax: 40–54 µm (47), length of abdomen: 72–107 µm (89), length of hyaline peristome: 13–23 µm (19).

Remarks.— *Dictyoprora echidna* n. sp. differs from other *Dictyoprora* species in having a large cephalis that is deeply embedded in the thoracic segment, and no lumbar constriction, giving the shell an overall ovoid shape. It also differs from *Phormostichoartus ashbyi* Renaudie and Lazarus, 2015 in having a three-segmented shell.

A few specimens exhibiting an intermediate morphology between *D. mongolfieri* (Ehrenberg, 1854) and *D. echidna* n. sp. were observed at ODP Site 1051 (~136 mcd), suggesting that the latter is an offshoot of *D. mongolfieri*. These specimens are characterized by a high number of abdominal pores, which are longitudinally aligned.

Genus *Spirocyrtis* Haeckel, 1882 emend. Nigrini, 1977

Type species.— *Spirocyrtis scalaris* Haeckel, 1887, p. 1509, pl. 76, fig. 14; subsequent designation by Campbell, 1954, p. D142.

Spirocyrtis matsuokai new species

Plate II.28, Figures 9–12

Holotype.— Plate II.28, Figure 9; collection number USTL 4554–1; coordinates S69/2; sample ODP 171B-1051A-14H-5W, 52–54 cm; upper part of the *Podocyrtis* (*L.*) *mitra* Zone (RP14; Sanfilippo and Blome, 2001); middle Eocene.

Diagnosis.— *Spirocyrtis* species with a reduced ventral tube, whose shell is subcylindrical in shape, with slight post-thoracic constrictions.

Occurrence.— This species is found in almost all the studied samples, from the upper part of the *Podocyrtis* (*L.*) *mitra* Zone (RP14) to the lower part of the *Podocyrtis* (*L.*) *goetheana* Zone (RP16).

Description.— Shell multisegmented, smooth, relatively thin-walled, subcylindrical in overall shape. Cephalis hemispherical, poreless, bearing a long straight apical tube and lacking a well-developed ventral tube. Collar stricture almost indistinct. Thorax truncate conical to cylindrical, only slightly longer than the cephalis, and penetrated by downwardly directed subcircular pores. Lumbar stricture marked by a thin dark band. Abdomen and post-abdominal segments barrel-shaped and rounded, the second post-abdominal segment being generally the widest. Each segment is perforated by subcircular pores arranged in three to four transverse rows, except for the third post-abdominal segment, which generally has only two rows of pores. Lumbar and post-lumbar strictures marked by a hyaline band. Last segment ragged along a row of pores in all the observed specimens.

Etymology.— This species is named in honor of Dr. Atsushi Matsuoka (Niigata University, Japan) for his contribution to the study of recent and fossil radiolarians.

Dimensions.— Based on 13 specimens (mean): total length without the apical tube: 143–202 µm (164), length of cephalothorax: 38–43 µm (40), length of apical tube: 8–23 µm (14), length of abdomen: 20–35 µm (27); length of all post-abdominal segments: 77–133 µm (98); maximum breadth of shell: 56–69 µm (63).

Remarks.— The new species differs from *Spirocyrtis cornutella* Haeckel, 1887 in having lumbar and post-lumbar strictures marked by a poreless band; from *S. gyroscalaris* Nigrini, 1977, *S. scalaris* Petrushevskaya and Kozlova, 1972 and *S. subscalaris* Nigrini, 1977 in having a maximum of four transverse rows of pores on the post-abdominal segments, and a less prominent ventral tube; from *S. proboscis* O'Connor, 1994 in having a smaller apical tube and a more cylindrical shell; from *S. scalaris* Haeckel, 1887 in having less than five post-abdominal segments, the constrictions of which are rounded rather than sharply angular; from *S. subtilis* Petrushevskaya and Kozlova, 1972 in having less-developed constrictions between segments, giving the shell a smoother outline; from *S.* ? *hollisi* Renaudie and Lazarus, 2012 and *S.* ? *renaudiei* Meunier and Danelian, 2023 in having a subcylindrical shell rather than a conical or a pupoid shell.

Family Rhopalosyringiidae Empson-Morin, 1981

Genus *Pterocyrtidium* Bütschli, 1882a

Type species.— *Pterocanium barbadense* Ehrenberg, 1874, p. 254 (unfigured); Ehrenberg, 1876, p. 82, pl. 17, fig. 6; subsequent designation by Petrushevskaya and Kozlova, 1972, p. 552.

Pterocyrtidium zitteli Bütschli, 1882a

Plate II.28, Figures 13–16

1882a *Pterocyrtidium Zitteli* [sic] Bütschli, p. 531, pl. 33, figs. 28a, 28b.
2015 *Pterocyrtidium zitteli* Bütschli – Kamikuri, pl. 9, fig. 8.

Diagnosis.— *Pterocyrtidium* species with a dichotomous apical horn, and a sparsely pored thorax and abdomen.

Occurrence.— This species occurs sporadically throughout the studied interval, from the upper part of the *Podocyrtis* (*L.*) *mitra* Zone (RP14) to the lower part of the *Podocyrtis* (*L.*) *goetheana* Zone (RP16).

Description.— Shell composed of three segments, cylindrical, and thick-walled. Cephalis subspherical to globular, poreless, or perforated by a few small circular pores. Apical spine protruding as a stout, dichotomous, bladed apical horn. The main branch of the apical horn lies on the axis of the shell, the second branch extends from the cephalic wall or the proximal part of the main branch at an angle of 45° to 90°. Ventral spine protruding as a pointed vertical spine, which is always shorter than the apical horn. Collar stricture slightly expressed. Thorax thick-walled, subcylindrical to ovoid-elongated. Thoracic pores variabke in number and size,

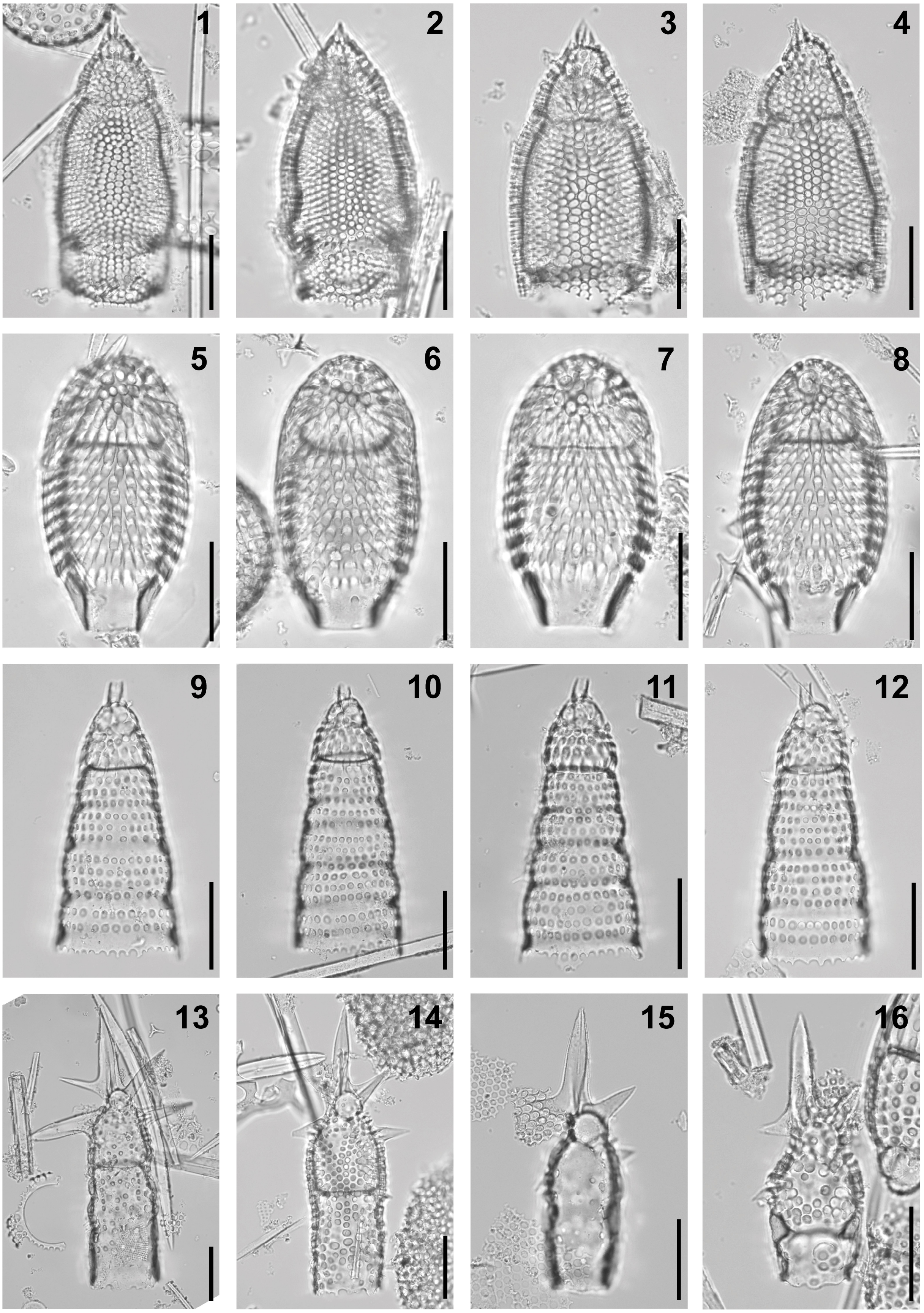
1
2
3
4
5
6
7
8
9
10
11
12
13
14
15
16

Plate II.28. Composite light micrographs of new radiolarian species from ODP Site 1051 (Blake Nose, western subtropical Atlantic). (**1–4**) *Eucyrtidium granatum* n. sp.: (**1**) holotype, ODP 171B-1051A-2H-5W, 55–57 cm, USTL 4513–1, M69/3; (**2**) ODP 171B-1051A-4H-5W, 56–58 cm, USTL 4517–1, V48/3; (**3**) ODP 171B-1051A-4H-5W, 56–58 cm, USTL 4515–4, T70/2; (**4**) ODP 171B-1051A-4H-5W, 56–58 cm, USTL 4515–3, T49/4. (**5–8**) *Dictyoprora echidna* n. sp.: (**5**) holotype, ODP 171B-1051A-6H-5W, 53–55 cm, USTL 4518–1, M41/3; (**6**) ODP 171B-1051A-6H-5W, 53–55 cm, USTL 4519–1, M47/1; (**7**) ventral view, ODP 171B-1051A-2H-5W, 55–57 cm, USTL 4512–1, N63/3; (**8**) ventral view, ODP 171B-1051A-6H-5W, 53–55 cm, USTL 4518–2, H64/2. (**9–12**) *Spirocyrtis matsuokai* n. sp.: (**9**) holotype, ODP 171B-1051A-14H-5W, 52–54 cm, USTL 4554–1, S69/2; (**10**) ODP 171B-1051A-14H-5W, 52–54 cm, USTL 4554–2, H48/3; (**11**) ODP 171B-1051A-9H-2W, 53–55 cm, USTL 4524–1, N41/2; (**12**) ODP 171B-1051A-14H-5W, 52–54 cm, USTL 4554–3, M38/2. (**13–15**) *Pterocyrtidium zitteli* Bütschli, 1882a: (**13**) ODP 171B-1051A-4H-5W, 56–58 cm, USTL 4515–2, K40/4; (**14**) ODP 171B-1051A-9H-2W, 53–55 cm, USTL 4526–1, Q53/1; (**15**) hyaline form, ODP 171B-1051A-18X-5W, 54–56 cm, USTL 4562–2, X63/1; (**16**) poorly-developed form, ODP 171B-1051A-18X-5W, 54–56 cm, USTL 4562–1, P51/2. All scale bars equal 50 µm.

scattered over the surface (Plate II.28, Figure 13) or quincuncially arranged (Plate II.28, Figure 14). In the larger specimens, the primary lateral spines and the dorsal spine usually extend into the upper thorax as long, bladed, pointed wings. Thorax and abdomen separated by an internal ridge that appears externally as a thin dark band. Abdomen subcylindrical, longer than the thorax, pierced by subcircular pores that may be either longitudinally aligned or randomly arranged. Abdomen terminates in an undifferentiated margin, usually ragged along a row of pores.

Dimensions.— Based on 19 specimens (mean): length of main branch of the apical horn: 32–81 µm (64), length of secondary branch of the apical horn (when present): 14–51 µm (32),length of ventral horn (when present): 18–55 µm (33), length of wings (when present): 13–67 µm (36), total length without the apical horn: 87–192 µm (127), length of cephalothorax without the apical horn: 57–88 µm (76), length of abdomen: 31–114 µm (60).

Remarks.— *Pterocyrtidium zitteli* Bütschli, 1882a differs from all other species of the genus *Pterocyrtidium* by its distinctive dichotomous apical horn.

This species shows a great morphological variability in terms of size, number of thoracic wings, and number of thoracic and abdominal pores. Several small, stunted, aberrant morphotypes were found in the material examinated (see Plate II.28, Figures 15, 16), possibly represeting juvenile specimens or aberrant forms.

Superfamily Acanthodesmioidea Haeckel, 1862

Family Cephalospyrididae Hackel, 1882

Genus *Elaphospyris* Haeckel, 1882

Type species.— *Ceratospyris heptaceros* Ehrenberg, 1874, p. 219 (unfigured); Ehrenberg, 1876, p. 66, pl. 20, fig. 2; subsequent designation by Chediya, 1959, p. 180.

Elaphospyris cordiformis new species

Plate II.29, Figures 1–4

Holotype.— Plate II.29, Figure 1; collection number USTL 4562–4; coordinates N51/2; sample ODP 171B-1051A-18X-5W, 54–56 cm; upper part of the *Podocyrtis* (*L.*) *mitra* Zone (RP14; Sanfilippo and Blome, 2001); middle Eocene.

Diagnosis.— Cephalospyridid species with a smooth-surfaced shell pierced by small subcircular pores, and a pair of very short lateral cephalic spines.

Occurrence.— Only the end of the stratigraphic range of the species is documented here. This corresponds to the upper part of the *Podocyrtis* (*L.*) *mitra* Zone (RP14).

Description.— Shell quadrate to cordiform, smooth-surfaced, with a slight sagittal constriction. The sagittal ring appears by transparency as a thick opaque band. Cephalis with a short apical horn and two reduced lateral ones. Ventral side of the cephalis pierced by four elongated unpaired sagittal-lattice pores. Other cephalic pores small, subcircular, and quincuncially arranged. Five conical feet, straight and slightly divergent, arise from the basal ring.

Etymology.— Derived from the Latin *cordi* meaning 'heart' and *forma* meaning 'shape'.

Dimensions.— Based on 21 specimens (mean): length of cephalis: 43–57 µm (50), maximum breadth of cephalis: 65–86 µm (76), length of apical horn (when present): 4–12 µm (8), length of lateral cephalic horns (when present): 3–6 µm (4), length of feet: 27–60 µm (38).

Remarks.— This species is placed in the genus *Elaphospyris* because of its very short apical horn, its pair of lateral cephalic horns, and its five divergent basal feet. *E. cordiformis* n. sp. is distinguished from other species of the genus *Elaphospyris* by its smooth cephalis, which is perforated by relatively small pores and bears three very short spines. The presence of conical feet allows this species to be easily distinguished from cordiform, smooth-surfaced species of the genus *Desmospyris* such as *D. acuta* (Goll, 1968) or *D. lata* (Goll, 1969).

Elaphospyris quadricornis new species

Plate II.29, Figures 5–8

2015 *Dendrospyris* sp. F Kamikuri, pl. 13, figs. 3, 4.

Holotype.— Plate II.29, Figure 5; collection number USTL 4517–2; coordinates T47/2; sample ODP 171B-1051A-4H-5W, 56–58 cm; lower part of the *Podocyrtis* (*L.*) *goetheana* Zone (RP16; Sanfilippo and Blome, 2001); middle Eocene.

Diagnosis.— Cephalospyridid species with a latticed shell and two pairs of lateral cephalic spines.

Occurrence.— This species occurs sporadically throughout the studied interval, from the upper part of the *Podocyrtis* (*L.*) *mitra* Zone (RP14) to the lower part of the *Podocyrtis* (*L.*) *goetheana* Zone (RP16).

Description.— Shell unisegmented, thick-walled, and weakly tuberculate. Sagittal ring D-shaped, dividing the cephalis into two lobes. Cephalis with a needle-shaped apical horn, and two pairs of straight, pointed, lateral horns. First pair of lateral horns of about the same length as the apical horn, forming an angle of ~30° with the sagittal ring; second pair of lateral horns usually longer and stronger, forming an angle of ~90° with the sagittal ring. Ventral side of the cephalis pierced by four large, unpaired sagittal-lattice pores, while the dorsal side has no sagittal-lattice pores. Other cephalic pores subcircular, hexagonally framed, and arranged in symmetry with respect to the sagittal constriction. Five straight, pointed and slightly divergent feet arise from the basal ring.

Etymology.— The specific epithet means 'four-horned' in Latin.

Dimensions.— Based on 12 specimens (mean): length of cephalis: 45–103 µm (74), maximum breadth of cephalis: 58–99 µm (80), length of apical horn: 6–49 µm (25), length of first pair of lateral cephalic horns: 8–50 µm (33), length of second pair of lateral cephalic horns: 19–58 µm (39), length of feet: 27–116 µm (69).

Remarks.— *Elaphospyris quadricornis* n. sp. is placed in the genus *Elaphospyris* because of the general morphology of its shell, which is very similar to that of *E. didiceros* (Ehrenberg, 1874). *E. quadricornis* n. sp. differs from all other species of the genus *Elaphospyris* in having two pairs of well-developed lateral cephalic horns and five long basal feet.

Superfamily Plagiacanthoidea Hertwig, 1879, emend. Sandin et al., 2019

Family Lophophaenidae Haeckel, 1882, sensu Petrushevskaya, 1971

Genus *Ceratocyrtis* Bütschli, 1882a, emend Sugiyama, 1993

Type species.— *Cornutella* ? *cucullaris* Ehrenberg, 1874, p. 221 (unfigured); 1876, p. 68, pl. 2, fig. 7; subsequent designation by Petrushevskaya, 1971, p. 98.

Ceratocyrtis oconnori new species

Plate II.30, Figures 1–4

Holotype.— Plate II.30, Figure 1; collection number USTL 4526–4; coordinates R49/4; sample ODP 171B-1051A-9H-2W, 53–55 cm; *Podocyrtis* (*L.*) *chalara* Zone (RP15; Sanfilippo and Blome, 2001); middle Eocene.

Diagnosis.— *Ceratocyrtis* species with a large, thorny cephalis that is deeply embedded in the thoracic segment.

Occurrence.— This relatively rare species occurs sporadically throughout the studied interval, from the upper part of the *Podocyrtis* (*L.*) *mitra* Zone (RP14) to the *Podocyrtis* (*L.*) *chalara* Zone (RP15).

Description.— Shell composed of two segments, relatively thick-walled and conical to inflated in general shape. Cephalis deeply embedded in the thoracic segment, perforated by subcircular pores and bearing multiple horns. Delineating the cephalis from the thorax is difficult because there is no clear expression of the collar stricture. Thorax conically truncated to inflated ovate, and may have an irregular surface that is roughened by slender spines arising from the intervening pore bars (e.g., Plate II.30, Figure 2). Thoracic pores circular to elongated and randomly arranged. They are noticeably larger towards the oral end, although their size is not consistent. Distal part of the thorax ragged (Plate II.30, Figures 2–4) or flanked by a few long conical spines (Plate II.30, Figure 1). Aperture open wide.

Etymology.— The species is dedicated to Dr. Barry O'Connor (University of Auckland, New Zealand) in honor of his detailed taxonomic study of Cenozoic polycystine radiolarians.

Dimensions.— Based on seven specimens (mean): cephalothorax length without the apical horn: 121–227 µm (159), length of apical horn: 8–41 µm (22), maximum breadth of cephalothorax: 57–163 µm (93).

Remarks.— The newly discovered species bears a close morphological resemblance to the middle Oligocene species *C. mashae* Bjorklund, 1976 and *C. robustus* Bjorklund, 1976, with which it shares a spiny shell and a relatively small cephalis that is partially embedded in the thorax. However, the two latter species are different from *C. oconnori* n. sp. because their cephalis is clearly distinguishable from the thorax, and their thorax is less tapered in its distal half. The new species is also distinguished from similar-looking spumellarian species *Zealithapium mitra* (Ehrenberg, 1874) and *Z. oamaru* O'Connor, 1999 by its rounder overall shape, and its more irregularly arranged thoracic pores.

Superfamily Pylobotrydoidea Haeckel, 1882

Family Pylobotrydidae Haeckel, 1882 sensu. Sugiyama, 1998

Genus *Botryocella* Haeckel, 1887

Type species.— *Lithobotrys nucula* Ehrenberg, 1874, p. 238 (unfigured); Ehrenberg, 1876, p. 76, pl. 3, fig. 16; subsequent designation by Campbell, 1954, p. D144.

Botryocella ? *alectrida* new species

Plate II.29, Figures 9–12

Holotype.— Plate II.29, Figure 9; collection number USTL 4516–1; coordinates Z61/1; sample ODP 171B-1051A-4H-5W, 56–58 cm; lower part of the *Podocyrtis* (*L.*) *goetheana* Zone (RP16; Sanfilippo and Blome, 2001); middle Eocene.

Diagnosis.— Pylobotrydid species with a shell that is densely perforated and has a crest of long, bladed cephalic horns.

Occurrence.— This rare species occurs sporadically from the lower part of the *Podocyrtis* (*L.*) *chalara* Zone (RP15) to the lower part of the *Podocyrtis* (*L.*) *goetheana* Zone (RP16).

Description.— Shell two-segmented, laterally flattened, and relatively thick-walled. Cephalis trilobed, and perforated by numerous small, closely spaced pores, giving it a rough appearance. The anterior part of the eucephalic lobe is covered by a reniform to ovoid ante-cephalis lobe, which has three long-bladed horns (the third/posterior one corresponding to the apical spine). Absence of upper tube. Eucephalic lobe inflated, thick-walled, bearing a long, straight or curved horn. Post-cephalic lobe very reduced, and may have a short protruding horn (Plate II.29, Figure 9), which likely corresponds to the ventral spine. Collar stricture indistinct. Thorax subcylindrical, densely perforated by small, circular pores that are irregularly distributed on its surface. A small thoracic wing may develop from the dorsal spine (Plate II.29, Figure 9). Distal part of the thorax invariably ragged.

Etymology.— The specific epithet means ‘rooster-like’ in Greek, in allusion to the remarkable cephalic horns of the new species.

Dimensions.— Based on 7 specimens (mean): length of cephalothorax without the cephalic spines: 97–78 µm (88), length of eucephalic lobe: 28–33 µm (31), length of ante-cephalic lobe: 36–40 µm (38), length of cephalic spines: 13–39 µm (25), length of thorax: 42–61 µm (51).

Remarks.— The newly discovered species has been tentatively assigned to the genus *Botryocella* due to the fact that its eucephalic lobe is partially embedded into the shell and its collar stricture is not externally well-defined (Petrushevskaya, 1971). However, this classification is only provisional because the new species lacks a galea above the eucephalic lobe. Finally, *B.* ? *alectrida* n. sp. is distinguished from other middle Eocene pylobotrydid species by its remarkable crest of cephalic horns.

Genus *Pylobotrys* Haeckel, 1882

Type species.— *Pylobotrys putealis* Haeckel, 1887, p. 1121, pl. 96, fig. 21; subsequent designation by Campbell, 1954, p. D144.

Pylobotrys ? *bineti* new species

Plate II.29, Figures 13–16

Holotype.— Figure 5.13; collection number USTL 4530–1; coordinates J41/2; sample ODP 171B-1051A-10H-2W, 53–55 cm; *Podocyrtis* (*L.*) *chalara* Zone (RP15; Sanfilippo and Blome, 2001); middle Eocene.

Diagnosis.— Pylobotrydid species with an almost poreless thorax and two cephalic tubes protruding vertically and horizontally.

Occurrence.— This rare species is found throughout the investigated stratigraphic interval, from the upper part of the *Podocyrtis* (*L.*) *mitra* Zone (RP14) to the lower part of the *Podocyrtis* (*L.*) *goetheana* Zone (RP16).

Description.— Shell composed of two segments and almost hyaline. Cephalis poreless and distinctly trilobed, with a small tubular post-cephalic lobe and a large globular eucephalic lobe partially embedded in a reniform ante-cephalic lobe. Ante- and post-cephalic lobes are extended into short, wide tubes that contain the apical and ventral spines. In some specimens, these tubes are open at the distal end. Thorax cylindrical, perforated by a few subcircular pores that are irregular in size and distribution. Aperture closed or undifferentiated.

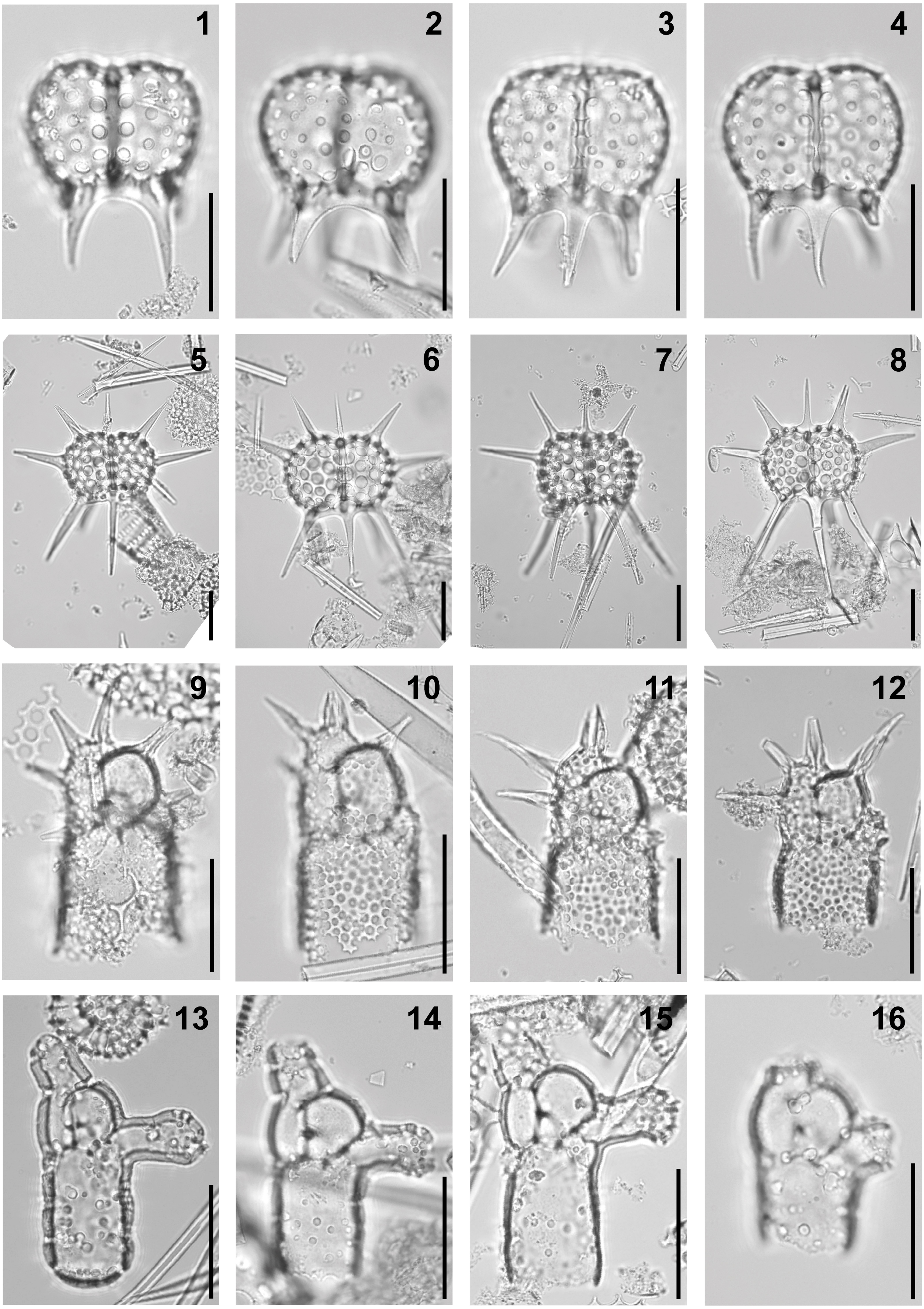
1
2
3
4
5
6
7
8
9
10
11
12
13
14
15
16

Plate II.29. Composite light micrographs of new radiolarian species from ODP Site 1051 (Blake Nose, western subtropical Atlantic). (**1–4**) *Elaphospyris cordiformis* n. sp.: (**1**) holotype, ODP 171B-1051A-18X-5W, 54–56 cm, USTL 4562–4, N51/2; (**2**) ODP 171B-1051A-18X-5W, 54–56 cm, USTL 4561–3, R70/1; (**3**) ODP 171B-1051A-18X-5W, 54–56 cm, USTL 4562–3, U42/3; (**4**) ODP 171B-1051A-18X-5W, 54–56 cm, USTL 4560–3, W52/3. (**5–8**) *Elaphospyris quadricornis* n. sp.: (**5**) holotype, ODP 171B-1051A-4H-5W, 56–58 cm, USTL 4517–2, T47/2; (**6**) ODP 171B-1051A-2H-5W, 55–57 cm, USTL 4513–3, Q66/4; (**7**) ODP 171B-1051A-4H-5W, 56–58 cm, USTL 4516–2, G58/1; (**8**) ODP 171B-1051A-2H-5W, 55–57 cm, USTL 4513–4, D47/3. (**9–12**) *Botryocella* ? *alectrida* n. sp.: (**9**) holotype, ODP 171B-1051A-4H-5W, 56–58 cm, USTL 4516–1, Z61/1; (**10**) ODP 171B-1051A-14H-5W, 52–54 cm, USTL 4554–4, E43/1; (**11**) ODP 171B-1051A-14H-5W, 52–54 cm, USTL 4554–5, G44/4; (**12**) ODP 171B-1051A-9H-2W, 53–55 cm, USTL 4524–4, H60/4. (**13–16**) *Pylobotrys* ? *bineti* n. sp.: (**13**) holotype, ODP 171B-1051A-10H-2W, 53–55 cm, USTL 4530–1, J41/2; (**14**) ODP 171B-1051A-11H-5W, 59–61 cm, USTL 4539–1, L48/3; (**15**) ODP 171B-1051A-10H-5W, 55–57 cm, USTL 4533–2, K46/2; (**16**) ODP 171B-1051A-11H-2W, 62–64 cm, USTL 4536–1, L71/2.All scale bars equal 50 µm.

Etymology.— This species is named after the French *architect and artist* René Binet, who modeled the main entrance of the Paris Exposition Universelle of 1900 after Haeckel's drawing of Cenozoic *radiolarians.*

Dimensions.— Based on eight specimens (mean): height of eucephalic lobe: 23–30 µm (27), height of antecephalic lobe without the apical tube: 20–26 µm (23), length of apical tube: 8–33 µm (22), length of ventral tube: 14–42 µm (29), length of thorax: 33–60 µm (48).

Remarks.— *Pylobotrys* ? *bineti* is tentatively assigned to the genus *Pylobotrys* because of its distally closed, smooth-surfaced shell and its two cephalic tubes, which include the apical and vertical spines. The new species is distinguished from *Acrobotrys disolenia* Haeckel, 1887 by its nearly hyaline shell and its smaller post-cephalic lobe, and from *A*. *tritubus* Riedel, 1957 in having only two cephalic tubes.

Superfamily Lithochytridoidea Ehrenberg, 1846

Family Lithochytrididae Ehrenberg, 1846 sensu Suzuki in Matsuzaki et al., 2015

Genus *Lychnocanium* Ehrenberg, 1846

Type species.— *Lychnocanium lucerna* Ehrenberg, 1847, p. 55, fig. 5; subsequent monotypy (Suzuki et al., 2021).

Lychnocanium cheni new species

Plate II.30, Figures 5–8

1975 *Lychnocanium* sp. Chen, p. 462, pl. 1, figs. 8, 9.
2020 *Lychnocanium tripodium* Ehrenberg – Hollis et al., pl. 14, figs. 8–10b.

Holotype.— Plate II.30, Figure 5; collection number USTL 4562–5; coordinates O41/3; sample ODP 171B-1051A-18X-5W, 54–56 cm; upper part of the *Podocyrtis* (*L.*) *mitra* Zone (RP14; Sanfilippo and Blome, 2001); middle Eocene.

Diagnosis.— Lithochytridid species with a thick-walled, hemispherical thorax and three straight, robust, and subparallel feet, that are ovoid to rectangular in cross-section and longer than twice the length of the thorax.

Occurrence.— This species occurs sporadically from the upper part of the *Podocyrtis* (*P.*) *mitra* Zone (RP14) to the lower part of the *Podocyrtis* (*L.*) *goetheana* Zone (RP16).

Description.— Shell composed of two segments. Cephalis thick-walled, globular, with a short and robust conical apical horn of approximately the same length. Cephalic pores subcircular, few in number, and scattered. Collar stricture expressed externally as a slight change in the shell contour. Thorax hemispherical to truncate-conical, with a thick, rough wall. Thoracic pores subcircular and quincuncially arranged. Distal margin of the thorax constricted and marked by a relatively thick hyaline band. Feet straight, subparallel and ovoid to subrectangular in cross-section. They are more than twice as long as the thorax and extend from the peristome.

Etymology.— This species is named after Dr. Pei-Hsin Chen (Columbia University, New York), who was the first to illustrate it.

Dimensions.— Based on 12 specimens (mean): length of apical horn: 21–46 µm (32), length of cephalis without the apical horn: 21–33 µm (27), length of thorax: 45–72 µm (56), length of feet: 131–256 µm (164).

Remarks.— *Lychnocanium cheni* n. sp. is distinguishable from similar appearing lithochytridid species as follows: from *Lychnocanium babylonis* Clark and Campbell, 1942 group and *L. tribulus* Ehrenberg, 1874 in having longer, subparallel feet, and a hemispherical thorax, rather than a pyramidal or truncate conical thorax; from *L. nimrodi* Meunier and Danelian, 2023 by the absence of distally dilated apical horn and feet; from *L. falciferum* Ehrenberg, 1874 and *L. forficula* n. sp. by its straight feet; from *L. cypselus* Ehrenberg, 1874 in having longer, straighter feet and a hemispherical thorax, rather than an elongated, barrel-shaped thorax; from *L. tripodium* Ehrenberg, 1874 in having larger thoracic pores and conical feet; from *L. trichopus* Ehrenberg, 1874 in having shorter and sturdier feet; from *L. alma* O'Connor, 1999 and *L. waiareka* O'Connor, 1999 in having conical feet, and no vestigial abdomen. Finally, *L. cheni* n. sp. differs from *L. cingulatum* n. sp. in having three straight and robust feet, while those of

L. cingulatum are slenderer and tend to become sinuous in their distal half. Additionally, *L. cheni* n. sp. has a shorter thorax, which is less than twice the height of the cephalis without the apical horn.

Lychnocanium cingulatum new species

Plate II.30, Figures 9–12

1995 *Lychnocanium conicum* Clark and Campbell – Shilov, p. 126, pl. 2, fig. 1.

Holotype.— Plate II.30, Figure 9; collection number USTL 4561–1; coordinates X70/2; sample ODP 171B-1051A-18X-5W, 54–56 cm; upper part of the *Podocyrtis* (*L.*) *mitra* Zone (RP14; Sanfilippo and Blome, 2001); middle Eocene.

Diagnosis.— Lithochytridid species with a subspherical thorax terminating in a hyaline constricted peristome and three slender feet, the distal half of which is sinuous.

Occurrence.— This species is quite abundant throughout the studied interval, from the upper part of the *Podocyrtis* (*L.*) *mitra* Zone (RP14) to the lower part of the *Podocyrtis* (*L.*) *goetheana* Zone (RP16).

Description.— Shell composed of two segments, broadly conical in general shape. Cephalis subspherical, with small subcircular pores, bearing a slender conical apical horn, usually longer than the height of the cephalis. Collar stricture distinct. Thorax subspherical, pierced by small subcircular pores quincuncially arranged. Peristome thick, poreless and constricted, with a smooth margin. Feet slender, downwardly directed, and slightly sinuous in their distal half, originating above the peristome. In some specimens, the feet are reduced to three short claws.

Etymology.— The specific epithet *cingulatum* means ‘with a girdle’ in Latin and refers to the hyaline peristome of the new species.

Dimensions.— Based on 30 specimens (mean): length of apical horn: 16–73 µm (36), length of cephalis without the apical horn: 19–30 µm (24), length of thorax: 46–80 µm (61), thickness of peristome: 5–12 µm (8), length of feet: 44–121 µm (84).

Remarks.— *Lychnocanium cingulatum* n. sp. differs from other middle Eocene lithochytridid species in that its feet originate above the peristome, which is marked by a thick hyaline band.

Lychnocanium croizoni new species

Plate II.31, Figures 1–4

1973 Theoperid gen. et sp. indet. Sanfilippo and Riedel, pl. 35, fig. 6.

Holotype.— Plate II.31, Figure 1; collection number USTL 4528–1; coordinates S67/2; sample ODP 171B-1051A-9H-5W, 53–55 cm; *Podocyrtis* (*L.*) *chalara* Zone (RP15; Sanfilippo and Blome, 2001); middle Eocene.

Diagnosis.— Lithochytridid species whose feet are absent or reduced to three short claws.

Occurrence.— This species occurs throughout the studied interval, from the upper part of the *Podocyrtis* (*L.*) *mitra* Zone (RP14) to the lower part of the *Podocyrtis* (*L.*) *goetheana* Zone (RP16).

Description.— Shell composed of two segments, thick-walled and small. Cephalis globular, poreless, partially embedded in the thorax, with a short conical apical horn. Thorax spindle-shaped to pyriform. Thoracic pores subcircular, and quincuncially arranged, but their arrangement tends to be less regular in the upper part of the thorax. Aperture open and bordered by a thick hyaline peristome with a smooth margin. Three inconspicuous conical feet originating just above the peristome are present in some specimens (Plate II.31, Figure 3).

Etymology.— This species is named after the French athlete Philippe Croizon, the first limbless person to swim across the English Channel.

Dimensions.— Based on 14 specimens (mean): length of cephalothorax without the apical horn: 101–123 µm (112), length of cephalis without the apical horn: 19–26 µm (23), length of apical horn: 7–23 µm (16), length of thorax: 79–98 µm (89), maximum breadth of thorax: 67–78 µm (73), length of feet (when present): 10–12 µm (11).

Remarks.— This remarkable species differs from all other lithochytridid species in being footless, or in having its feet reduced to three short claws. *Lychnocanium croizoni* n. sp. is distinguished from *Dictyophimus ceratium* Clark and Campbell, 1942 in having shorter feet and a more slender shell with no collar constriction. It also differs from *Plannapus hornibrooki* O'Connor, 1999 and *P. mauricei* O'Connor, 1999 in having a thicker cephalic wall, a stronger apical horn, and in lacking a vertical tube.

Lychnocanium forficula new species

Plate II.30, Figures 13–16

Holotype.— Plate II.30, Figure 13; collection number USTL 4561–2; coordinates J55/3; sample ODP 171B-1051A-18X-5W, 54–56 cm; upper part of the *Podocyrtis* (*L.*) *mitra* Zone (RP14; Sanfilippo and Blome, 2001); middle Eocene.

Diagnosis.— Lithochytridid species with a thorax pierced by numerous closely spaced, quincuncially arranged pores and three bladed, inwardly curved feet.

Occurrence.— This species is abundant throughout the investigated interval, from the upper part of the *Podocyrtis* (*L.*) *mitra* Zone (RP14) to the lower part of the *Podocyrtis* (*L.*) *goetheana* Zone (RP16).

Description.— Shell conical, composed of two segments. Cephalis subspherical, perforated by numerous small subcircular pores, bearing a stout conical apical horn. Collar stricture marked by a sharp change in the contour of the shell. Thorax truncate conical to campanulate, with numerous closely spaced subcircular pores that are hexagonally framed and quincuncially arranged. Peristome slightly constricted and marked by a thin internal ridge. Feet three-bladed, longer than the thorax, inwardly curved, and extending from the thoracic margin. In some specimens, an inconspicuous row of reticulations has been observed on the distal margin of the thorax.

Etymology.— The specific epithet refers to the Latin name of the European earwig (*Forficula auricularia* L.), whose male forceps are curved like the feet of the new species.

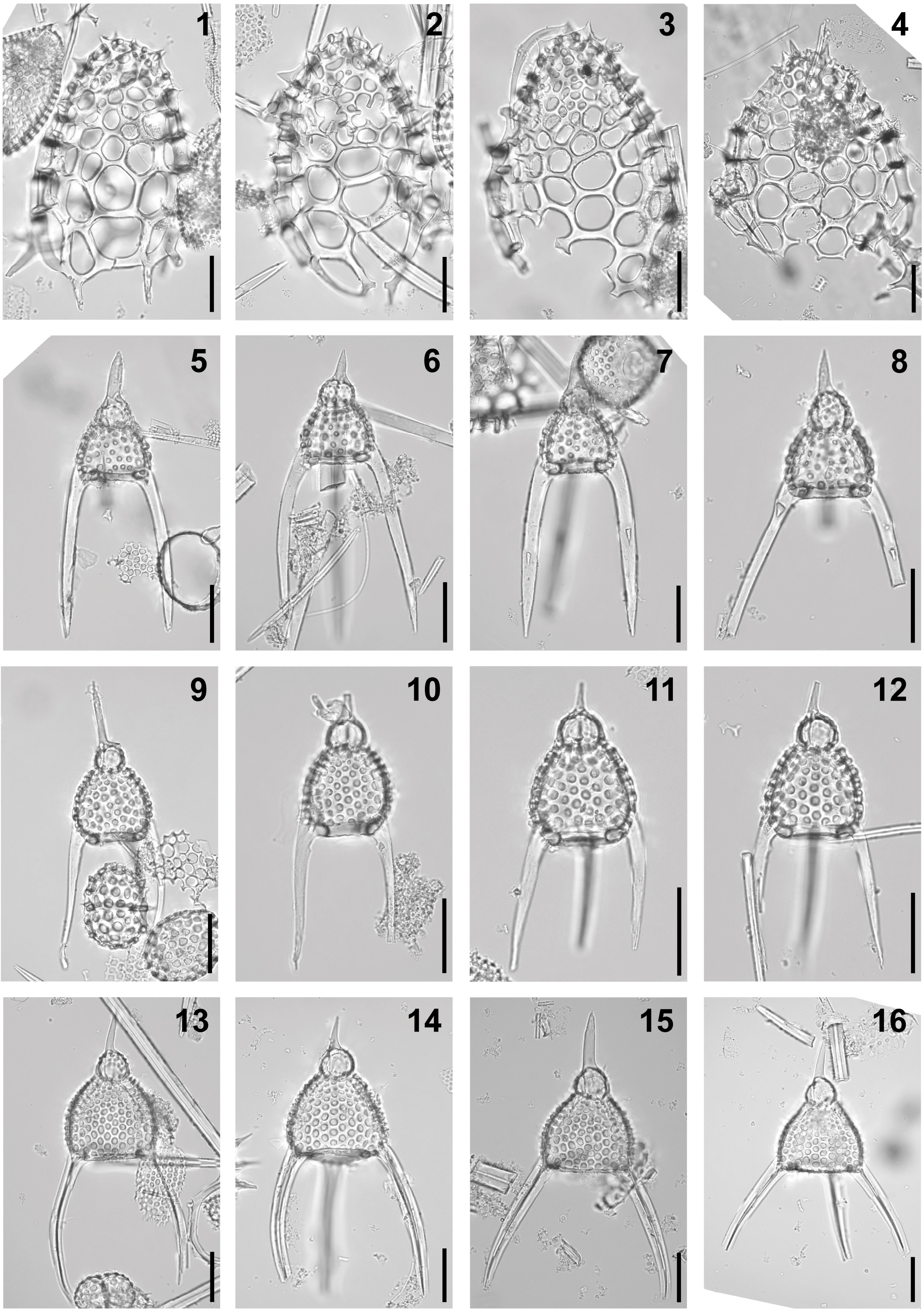
1
2
3
4
5
6
7
8
9
10
11
12
13
14
15
16

Plate II.30. Composite light micrographs of new radiolarian species from ODP Site 1051 (Blake Nose, western subtropical Atlantic). (**1–4**) *Ceratocyrtis oconnori* n. sp.: (**1**) holotype, ODP 171B-1051A-9H-2W, 53–55 cm, USTL 4526–4, R49/4; (**2**) ODP 171B-1051A-9H-2W, 53–55 cm, USTL 4526–5, Q55/2; (**3**) ODP 171B-1051A-9H-5W, 53–55 cm, USTL 4566–1, G57/4; (**4**) ODP 171B-1051A-9H-2W, 53–55 cm, USTL 4525–5, S38/4. (**5–8**) *Lychnocanium cheni* n. sp.: (**5**) holotype, ODP 171B-1051A-18X-5W, 54–56 cm, USTL 4562–5, O41/3; (**6**) ODP 171B-1051A-18X-5W, 54–56 cm, USTL 4561–4, P70/3; (**7**) ODP 171B-1051A-18X-5W, 54–56 cm, USTL 4562–6, D52/3; (**8**) ODP 171B-1051A-18X-5W, 54–56 cm, USTL 4562–7, F60/3. (**9–12**) *Lychnocanium cingulatum* n. sp.: (**9**) holotype, ODP 171B-1051A-18X-5W, 54–56 cm, USTL 4561–1, X70/2; (**10**) ODP 171B-1051A-18X-5W, 55–56 cm, USTL 4560–1, C56/1; (**11**) ODP 171B-1051A-18X-5W, 54–56 cm, USTL 4561–5, O69/4; (**12**) ODP 171B-1051A-18X-5W, 54–56 cm, USTL 4560–2, T55/2. (**13-16**) *Lychnocanium forficula* n. sp.: (**13**) holotype, ODP 171B-1051A-18X-5W, 54–56 cm, USTL 4561–2, J55/3; (**14**) ODP 171B-1051A-11H-2W, 62–64 cm, USTL 4536–3, Q70/4; (**15**) ODP 171B-1051A-2H-5W, 55–57 cm, USTL 4513–2, H48/1; (**16**) ODP 171B-1051A-4H-5W, 56–58 cm, USTL 4515–5, W48/1. All scale bars equal 50 µm.

Dimensions.— Based on 23 specimens (mean): length of cephalis without the apical horn: 22–34 µm (29), length of apical horn: 21–53 µm (40), length of thorax: 66–86 µm (76), length of feet: 117–188 µm (145).

Remarks.— *Lychnocanium forficula* n. sp. differs from the similar-looking species *L. cypselus* Ehrenberg, 1874 in having a truncate conical thorax instead of a barrel-shaped elongated thorax. It is also distinguished from *L. falciferum* Ehrenberg, 1854, *L. bellum* Clark and Campbell, 1942, and *L. trichopus* Ehrenberg, 1874 by its shorter, regularly arcuate feet, which are approximately as long as the cephalothorax (excluding the apical horn). *L. forficula* n. sp. can be distinguished from *L. turgidum* Ehrenberg, 1874 by its longer feet and its longer apical horn; from *L. crassipes* Ehrenberg, 1874 and *L. conicum* Clark and Campbell, 1942 by the presence of bladed feet; from *L. tetrapodium* Ehrenberg, 1874 in having three convergent feet instead of four divergent feet, and from *L. cheni* n. sp., *L. cingulatum* n. sp. and *L. tripodium* Ehrenberg, 1874 in having curved feet instead of straight, subparallel feet. The new species also differs from *L. carinatum* Ehrenberg, 1874, *L. continuum* Ehrenberg, 1874 and *L. tridentatum* Ehrenberg, 1874 and *L. trifolium* Riedel and Sanfilippo, 1971 in having a porous thorax rather than a hyaline or partially hyaline thorax. Finally, the lack of sigmoid feet distinguishes the new species from *Lychnocanoma bajunensis* Renz, 1984.

Superfamily Pterocorythoidea Haeckel, 1882 emend. Suzuki et al., 2021

Family Pterocorythidae Haeckel, 1882

Genus *Albatrossidium* Sanfilippo and Riedel, 1992

Type species.— *Albatrossidium minzok* Sanfilippo and Riedel, 1992, p. 16, pl. 2, fig. 7; original designation.

Albatrossidium messiaeni new species

Plate II.31, Figures 5–8

2015 *Eucyrtidium* ? sp. D Kamikuri, pl. 9, figs. 9a, 9b.

Holotype.— Plate II.31, Figure 5; collection number USTL 4529–1; coordinates X42/4; sample ODP 171B-1051A-9H-5W, 53–55 cm; *Podocyrtis* (*L.*) *chalara* Zone (RP15; Sanfilippo and Blome, 2001); middle Eocene.

Diagnosis.— *Albatrossidium* species with a thick-walled cephalis perforated by ovoid to elongated pores.

Occurrence.— This species is common from the upper part of the *Podocyrtis* (*L.*) *mitra* Zone (RP14) to the lower part of the *Podocyrtis* (*L.*) *goetheana* Zone (RP16).

Description.— Shell three-segmented, cylindrical, and thick-walled. Cephalis hemispherical, very thick-walled, with a prominent, broad-based apical horn. Cephalic pores subcircular, except at the base of the horn where they are longitudinally elongated, and form grooves in the proximal part of the horn. Lateral lobes of the cephalis indistinct. Collar stricture marked by a moderate change in the contour of the shell. Thorax hemispherical, elongated to subcylindrical. Thoracic pores circular and quincuncially arranged. Thorax and abdomen separated by an internal ridge that appears externally as a thick dark band. Abdomen subcylindrical, approximately the same length the thorax, or slightly shorter. Abdominal pores less regular in size and shape compared to the thoracic ones, tending toward longitudinal arrangement. All observed specimens have an abdomen that terminates in an undifferentiated, ragged margin.

Etymology.— Named after Olivier Messiaen, the French composer, organist and ornithologist.

Dimensions.— Based on 30 specimens (mean): total length without the apical horn: 161–207 µm (183), length of apical horn: 18–51 µm (37), length of cephalis without the apical horn: 23–47 µm (32), length of thorax: 73–101 µm (83), length of abdomen: 42–97 µm (70).

Remarks.— *Albatrossidium messiaeni* n. sp. differs from *A. annikasanfilippoae* Meunier and Danelian, 2023 and *A. regis* Meunier and Danelian, 2023 in that it lacks a cephalic hole accessory cephalis spines. The new species is also distinguished from *A. minzok* Sanfilippo and Riedel, 1992 and *A. tenellum* (Foreman, 1973) by its very thick-walled cephalis, which is perforated by ovoid to elongated pores.

Genus *Cryptocarpium* Sanfilippo and Riedel, 1992

Type species.— *Cryptoprora ornata* Ehrenberg, 1874 (unfigured); 1876, p. 222, pl. 5, fig. 8; original designation.

Cryptocarpium ? *judoka* new species

Plate II.31, Figures 9–12

not 1973 *Cryptoprora ornata* Ehrenberg – Sanfilippo and Riedel, pl. 35, figs. 7, 8.
? 1995 *Cryptocarpium* ? *ornatum* (Ehrenberg) – Strong et al., p. 208, pl. 11, figs. S, T.
1997 *Cryptocarpium ornatum* (Ehrenberg) – Hollis et al., p. 66, pl. 6, figs. 24, 25 (part.)
2012 *Cryptocarpium ornatum* (Ehrenberg) – Moore and Kamikuri, p. 6, pl. P2, fig. 4 (part).

Holotype.— Plate II.31, Figure 9; collection number USTL 4551–1; coordinates R40/2; sample ODP 171B-1051A-13H-5W, 58–60 cm; upper part of the *Podocyrtis* (*L.*) *mitra* Zone (RP14; Sanfilippo and Blome, 2001); middle Eocene.

Diagnosis.— Pterocorythid species with a bullet-shaped shell and a short, broad-based apical horn.

Occurrence.— This species is present in all of the analyzed samples, from the upper part of the *Podocyrtis* (*L.*) *mitra* Zone (RP14) to the lower part of the *Podocyrtis* (*L.*) *goetheana* Zone (RP16).

Description.— Shell three-segmented, thick-walled, and bullet-shaped. Cephalis hemispherical and composed of three lobes: a large unpaired eucephalic lobe and two smaller lateral lobes (Plate II.31, Figures 10, 11). The thickness of the shell and the poorly developed external furrows can make the cephalic lobes difficult to distinguish. The cephalis is also slightly embedded in the thorax, giving the species the appearance of a carpocaniid. A short, broad-based apical horn is present in most observed specimens. Thorax campanulate to subcylindrical, thick-walled and pierced by small circular pores quincuncially arranged. Lumbar stricture defined by a thick internal septum that appears externally as a dark band. Abdomen subcylindrical, perforated by subcircular pores that are less regular in size and arrangement than those of the thorax. The end of the abdomen is ragged along a row of pores.

Etymology.— From the Japanese *judoka*, which designates the practitioner of the martial art of judo. The specific epithet refers to the large lumbar septum of the new species, which resembles the black belt of judokas.

Dimensions.— Based on 19 specimens (mean): total length without the apical horn: 109–168 µm (132), length of apical horn: 6–10 µm (7), length of cephalothorax without the apical horn: 20–31 µm (24), length of abdomen: 28–78 µm (41).

Remarks.— *Cryptocarpium* ? *judoka* n. sp. is tentatively assigned to the genus *Cryptocarpium* because of its general "carpocaniid-like" morphology, its very reduced apical horn, and its trilobed cephalic shield, which is partially embedded in the thoracic segment.

The new species differs from the lectotype of *Cr. ornatum* (Ehrenberg, 1874) designated by O'Dogherty et al. (2021) in having a symmetrical cephalis with a short apical horn instead of a hornless asymmetrically placed cephalis, and in having more thoracic pores (~10 in a longitudinal row). *Cr.* ? *judoka* n. sp. is also differs from *Cr.* ? *azyx* (Sanfilippo and Riedel, 1973) by having a subcylindrical, three-segmented shell. In addition to the cephalis structure, the new species differs from the carpocaniid species *Carpocanopsis cingulata* Riedel and

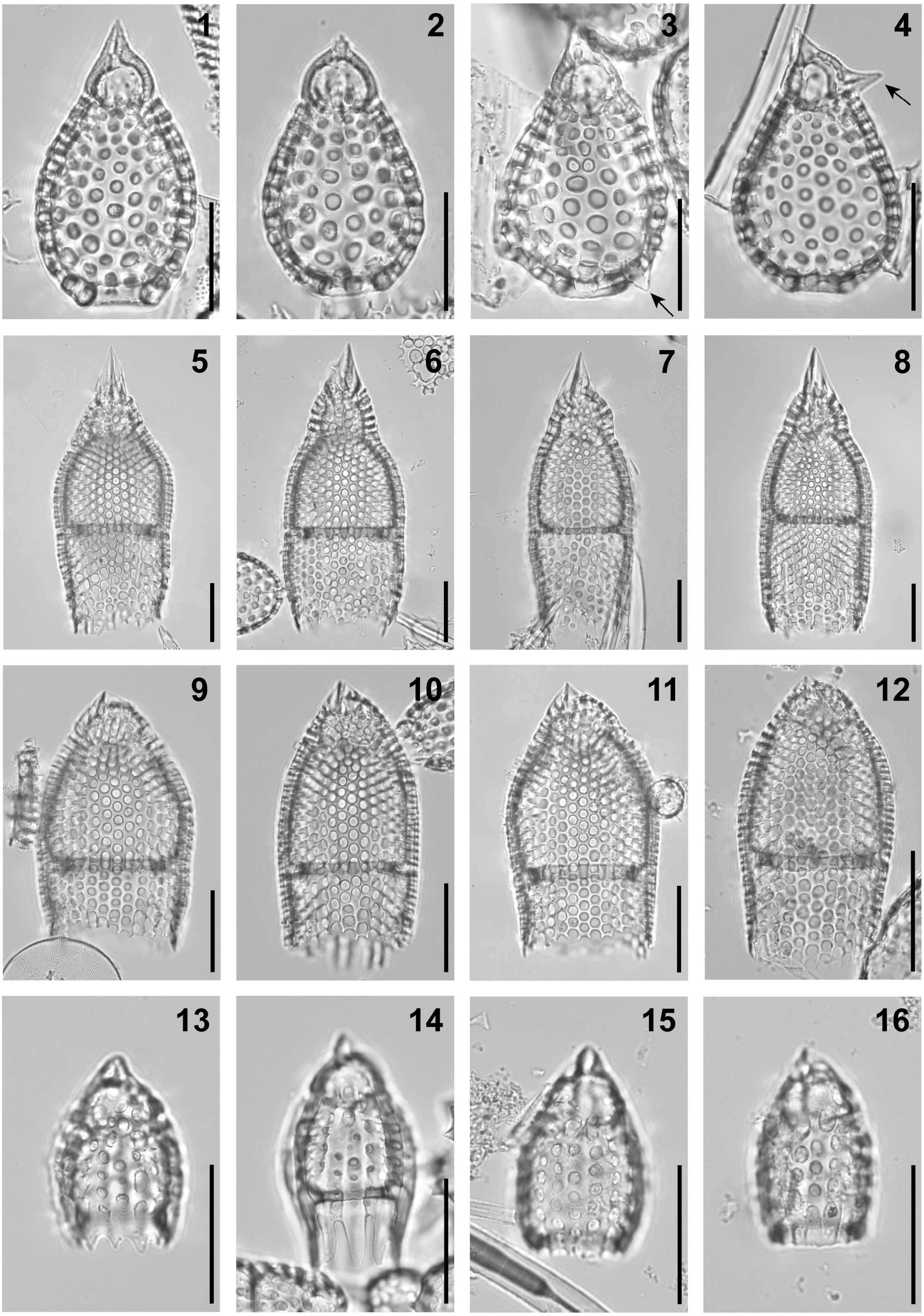
1
2
3
4
5
6
7
8
9
10
11
12
13
14
15
16

Plate II.31. Composite light micrographs of new radiolarian species from ODP Site 1051 (Blake Nose, western subtropical Atlantic). (**1–4**) *Lychnocanium croizoni* n. sp.: (**1**) holotype, ODP 171B-1051A-9H-5W, 53–55 cm, USTL 4528–1, S67/2; (**2**) ODP 171B-1051A-10H-5W, 52–54 cm, USTL 4533–1, F53/3; (**3**) specimen showing short feet (arrow), ODP 171B-1051A-9H-5W, 53–55 cm, USTL 4528–4, V65/2; (**4**) specimen showing ventral horn (arrow), ODP 171B-1051A-10H-2W, 53–55 cm, USTL 4530–4, E60/4. (**5–8**) *Albatrossidium messiaeni* n. sp.: (**5**) holotype, ODP 171B-1051A-9H-5W, 53–55 cm, USTL 4529–1, X42/4; (**6**) ODP 171B-1051A-4H-5W, 56–58 cm, USTL 4515–1, X61/3; (**7**) ODP 171B-1051A-9H-2W, 53–55 cm, USTL 4524–5, F47/3; (**8**) ODP 171B-1051A-9H-5W, 53–55 cm, USTL 4529–3, W09/3. (**9–12**) *Cryptocarpium* ? *judoka* n. sp.: (**9**) holotype, ODP 171B-1051A-13H-5W, 58–60 cm, USTL 4551–1, R40/2; (**10**) ODP 171B-1051A-10H-2W, 53–55 cm, USTL 4530–2, F43/2; (**11**) ODP 171B-1051A-9H-5W, 53–55 cm, USTL 4565–1, S48/4; (**12**) ODP 171B-1051A-9H-2W, 53–55 cm, USTL 4525–6, K69/1. (**13–16**) *Phormocyrtis microtesta* n. sp.: (**13**) holotype, ODP 171B-1051A-9H-5W, 53–55 cm, USTL 4529–4, W46/3; (**14**) ODP 171B-1051A-9H-5W, 53–55 cm, USTL 4528–3, P53/4; (**15**) ODP 171B-1051A-13H-2W, 52–54 cm, USTL 4549–1, W56/2; (**16**) ODP 171B-1051A-13H-2W, 52–54 cm, USTL 4550–1, H60/2. All scale bars equal 50 µm.

Sanfilippo, 1971 by having a subcylindrical thorax and abdomen, instead of an inflated thorax and a tapered abdomen, and from *Ca*. *bramlettei* Riedel and Sanfilippo, 1971 by having a porous abdomen. *Cr*. ? *judoka* n. sp. also differs from the specimens illustrated as 'pterocoryid gen. and sp. indet' by Sanfilippo and Riedel (1973; pl. 35, figs. 7, 8) in having a smaller apical horn and a cephalis that is more deeply embedded in the thoracic segment, and from the specimens illustrated as *Cr*. *ornatum* by Sanfilippo and Riedel (1992; pl. 2, figs. 18–20) in having a subcylindrical shell without a lumbar constriction.

Genus *Phormocyrtis* Haeckel, 1887

Type species.— *Phormocyrtis longicornis* Haeckel, 1887, p. 1370, pl. 69, fig. 15; subsequent designation by Campbell (1954), p. D134.

Phormocyrtis microtesta new species

Plate II.31, Figures 13–16

Holotype.— Plate II.31, Figure 13; collection number USTL 4529–4; coordinates W46/3; sample ODP 171B-1051A-9H-5W, 53–55 cm; *Podocyrtis* (*L.*) *chalara* Zone (RP15; Sanfilippo and Blome, 2001); middle Eocene.

Diagnosis.— *Phormocyrtis* species with a small two-segmented shell.

Occurrence.— This species is very abundant in almost all the studied samples, from the upper part of the *Podocyrtis* (*L.*) *mitra* Zone (RP14) to the lower part of the *Podocyrtis* (*L.*) *goetheana* Zone (RP16).

Description.— Shell small, two-segmented, and thick-walled. Cephalis hemispherical, poreless or pierced by a few subcircular pores, with a short, bladed apical horn. Collar stricture slightly expressed externally. Thorax barrel-shaped to subcylindrical, thick-walled, and twice as long as the cephalis. Thoracic pores subcircular, irregular in size, and weakly arranged in longitudinal rows. These rows contain three to six pores and are sometimes separated by inconspicuous longitudinal ridges. Distal margin of thorax undifferentiated (Plate II.31, Figures 15, 16) or surrounded by a few short, triangular, or rectangular spines (Plate II.31, Figures 13, 14).

Etymology.— The specific epithet means 'small shell' in Greek and refers to the relatively small size of the new species compared to other members of the genus *Phormocyrtis*.

Dimensions.— Based on 18 specimens (mean): length of apical horn: 7–16 µm (10), length of cephalis without the apical horn: 16–29 µm (23), length of thorax: 36–67 µm (51), length of lamellar teeth: 11–30 µm (19).

Remarks.— *Phormocyrtis microtesta* n. sp. is distinguished from other *Phormocyrtis* species by its two-segmented shell, which as an undifferentiated peristome, or a vestigial abdomen reduced to a crown of short spines.

Family Lophocyrtiidae Sanfilippo and Caulet in De Wever et al., 2001

Genus *Apoplanius* Sanfilippo and Caulet, 1998

Type species.— *Lophocyrtis* (*Apoplanius*) *klydus* Sanfilippo and Caulet, 1998, p. 12, pl. 5, fig. 5a; original designation.

Apoplanius cryptodirus new species

Plate II.32, Figures 1–4

Holotype.— Plate II.32, Figure 1; collection number USTL 4533–3; coordinates W52/3; sample ODP 171B-1051A-10H-5W, 52–54 cm; *Podocyrtis* (*L.*) *chalara* Zone (RP15; Sanfilippo and Blome, 2001); middle Eocene.

Diagnosis.— *Apoplanius* species with a short hemispherical to inflated thorax that envelopes the lower part of the cephalis.

Occurrence.— This species is common throughout the studied interval, from the upper part of the *Podocyrtis* (*L.*) *mitra* Zone (RP14) to the lower part of the *Podocyrtis* (*L.*) *goetheana* Zone (RP16).

Description.— Shell three-segmented, robust and broadly cylindrical. Cephalis globular, poreless, very thick-walled, and partially embedded in a loose lattice of spines that originate from the upper margin of the thorax. Apical spine merges with the cephalic wall and is extended outward by a short conical apical horn. A secondary horn may develop on the dorsal side of the cephalis (Plate II.32, Figures 1, 2). Mitral arches depart from the apical spine in the middle of the cephalis and quickly diverge at a great angle (Plate II.32, Figure 4). The collar stricture is indicated by a change in the contour of the shell. Thorax hemispherical to inflated, penetrated by subcircular pores that are irregular in size and shape and arranged in a weak quincuncial pattern. Lumbar stricture marked by an external constriction that is underlined by a thin dark band. Abdomen subcylindrical to inflated campanulate, with subcircular pores smaller than the thoracic ones. Abdominal end ragged along a row of pores or surrounded by a crown of small spines.

Etymology.— The specific epithet means 'hidden neck' in Greek.

Dimensions.— Based on 17 specimens (mean): total length without the apical horn: 77–115 µm (103), length of cephalis without the apical horn: 17–25 µm (14), length of apical horn: 7–18 µm (14), length of ventral horn (when present): 4–10 µm (7), length of thorax: 27–40 µm (32), maximum breadth of thorax: 47–60 µm (56), length of abdomen: 33–60 µm (49), maximum breadth of abdomen: 62–81 µm (68).

Remarks.— *Apoplanius cryptodirus* n. sp. is assigned to the genus *Apoplanius* on the basis of its simple, short apical horn without three proximal openings, and its apical spine, which is partially embedded in the cephalic wall (Sanfilippo and Caulet, 1998; O'Dogherty et al., 2021). The new species differs from *A*. *asperus* (Ehrenberg, 1874) and *A*. *nomas* (Sanfilippo and Caulet, 1998) in having a less swollen thorax, which is always narrower than the abdomen; from *A*. *kerasperus* (Sanfilippo and Caulet, 1998) in having a smaller apical horn and no auxiliary horns on the cephalis; from *A. klydus* (Sanfilippo and Caulet, 1998) in having a subcylindrical abdomen instead of a wavy abdomen, no thoracic wings, and no holes at the base of the apical horn. Finally, *A. cryptodirus* n. sp. is distinguished from *Theocorys minuta* Takemura and Ling, 1998, *T. perforalvus* O'Connor, 1997 and *T. saginata* Takemura and Ling, 1998 in having a horned cephalis that is partially embedded in the thorax.

Apoplanius hyalinus new species

Plate II.32, Figures 5–7

Holotype.— Plate II.32, Figure 5; collection number USTL 4566–2; coordinates N61/4; sample ODP 171B-1051A-9H-5W, 53–55 cm; *Podocyrtis* (*L.*) *chalara* Zone (RP15; Sanfilippo and Blome, 2001); middle Eocene.

Diagnosis.— *Apoplanius* species with a thick-walled hyaline thorax.

Occurrence.— This species occurs sporadically throughout the studied interval, from the upper part of the *Podocyrtis* (*L.*) *mitra* Zone (RP14) to the lower part of the *Podocyrtis* (*L.*) *chalara* Zone (RP15), and it becomes very abundant from the upper part of the *Podocyrtis* (*L.*) *chalara* Zone to the lower part of the *Podocyrtis* (*L.*) *goetheana* Zone (RP16).

Description.— Shell composed of three segments, cylindrical, and almost hyaline. Cephalis globular, thick-walled, and poreless, bearing a stout conical apical horn and sometimes a reduced dorsal horn (Plate II.32, Figure 6). Apical spine incorporated into the cephalic wall before dividing into two mitral arches near the top of the cephalis. Collar stricture well-defined externally by a sharp change in the shell contour. Thorax short, globular flattened to inflated, thick-walled, and hyaline. The maximum thickness of the thoracic wall is reached in the middle part of the thorax, giving the thoracic wall a crescent appearance when viewed under a light microscope. Lumbar stricture marked by a slight constriction. Abdomen subcylindrical, sinuous and twice as long as the thorax. Abdominal pores subcircular, variable in shape and size, scattered over the surface or weakly aligned in longitudinal rows. Abdomen terminating in an undifferentiated margin.

Etymology.— From the Greek *hualinos*, meaning 'hyaline, transparent'.

Dimensions.— Based on 24 specimens (mean): total length without the apical horn: 112–159 µm (133), length of cephalis without the apical horn: 19–26 µm (22), length of apical horn: 32–47 µm (37), length of thorax: 32–47 µm (37), maximum breadth of thorax: 47–72 µm (54), length of abdomen: 55–90 µm (74).

Remarks.— The generic assignment of *Apoplanius hyalinus* n. sp. is based on its short, conical apical horn without three proximal arches, and its apical spine, which partially extends into the cephalic cavity as a columella (Sanfilippo and Caulet, 1998; O'Dogherty et al., 2021). This new species differs from all other documented lophocyrtiid species in having a thick-walled hyaline thorax. *A. hyalinus* n. sp. shares many characteristics with *A. kerasperus* (Sanfilippo and Caulet, 1998) (Plate II.32, Figure 8), especially regarding the initial spicule, suggesting that the two species are closely related.

The occurrence of relatively small and nearly poreless forms is recurrent in several Paleogene naselarian families. These hyaline species appear to be particularly abundant during the middle Eocene. They include the following taxa: *Lychnocanium trifolium* Riedel and Sanfilippo, 1971 and *L. continuum* Ehrenberg, 1874 (Lithochytrididae), *Calocyclas aphradia*

Sanfilippo and Blome, 2001 (Theoperidae), *Theocorys anapographa* Riedel and Sanfilippo, 1970 var. A (Theocotylidae) and *Dendrospyris fragoides* Sanfilippo and Riedel, 1973 (Cephalospyrididae). Some of these species may be juveniles or aberrant forms belonging to species with a perforated skeleton; see, for example, *T. anapographa* var. A, which always occurs with typical *T. anapographa* (e.g., Sanfilippo and Blome, 2001; Meunier and Danelian, 2022).

Family Theocotylidae Petrushevskaya, 1981

Genus *Thyrsocyrtis* Ehrenberg, 1847

Type species.— *Thyrsocyrtis rhizodon* Ehrenberg, 1874, p. 262 (unfigured); Ehrenberg, 1876, p. 84, pl. 12, fig. 1; subsequent designation by Campbell, 1954, p. D130.

Thyrsocyrtis kamikuri new species

Plate II.32, Figures 9–12

2015 *Thyrsocyrtis* sp. D Kamikuri, pl. 5, figs. 1a–2b.
2020 *Thyrsocyrtis* sp. D Hollis et al., pl. 11, figs. 22a–22c.

Holotype.— Plate II.32, Figure 9; collection number USTL 4563–1; coordinates B34/3; sample ODP 171B-1051A-9H-2W, 53–55 cm; *Podocyrtis* (*L.*) *chalara* Zone (RP15; Sanfilippo and Blome, 2001); middle Eocene.

Diagnosis.— *Thyrsocyrtis* species with an inflated abdomen, perforated by pores of the same diameter as those of the thorax, and with three short, perforated feet.

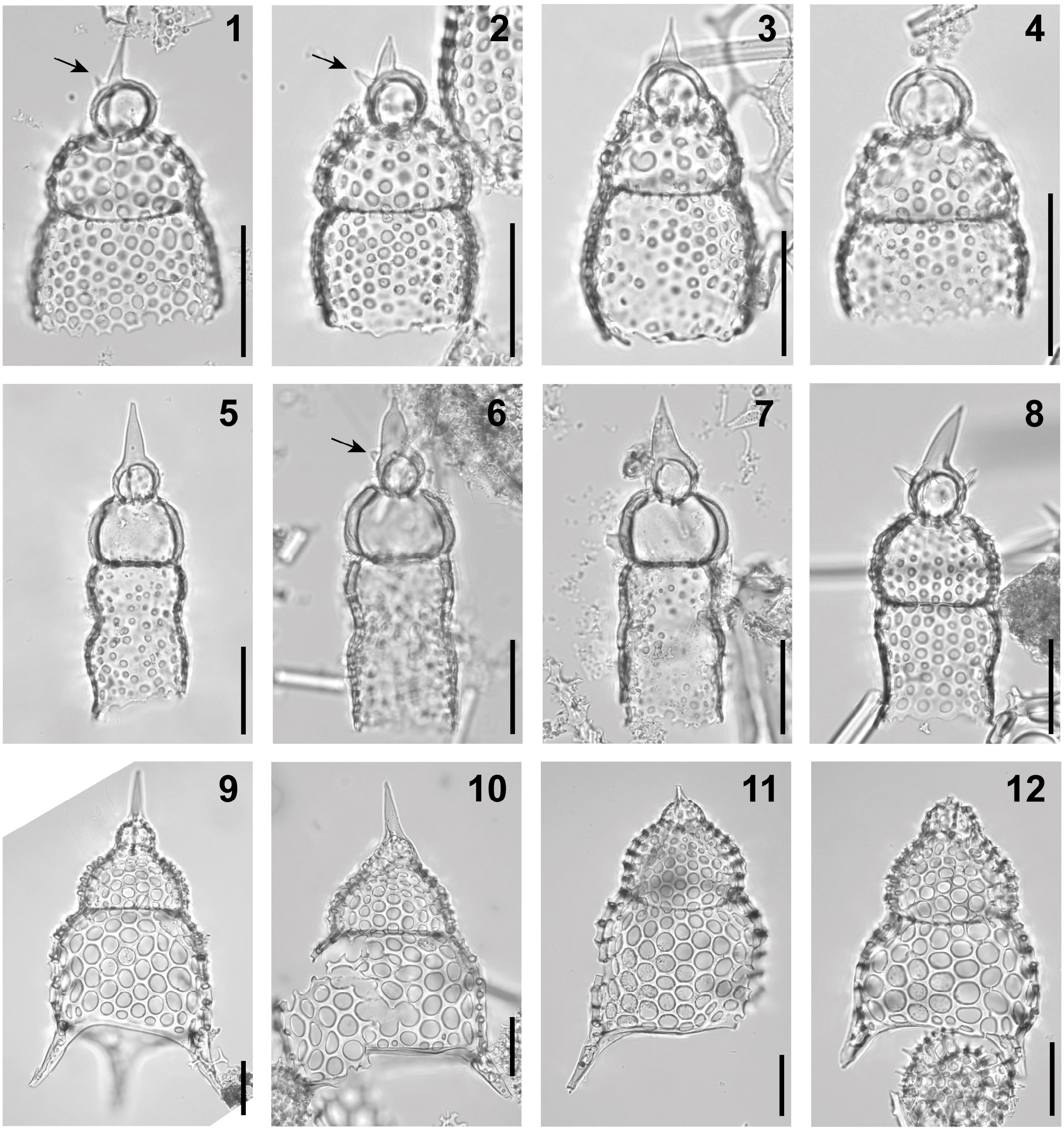

Plate II.32. Composite light micrographs of new radiolarian species from ODP Site 1051 (Blake Nose, western subtropical Atlantic). (**1–4**) *Apoplanius cryptodirus* n. sp.: (**1**) holotype, showing dorsal horn (arrow), ODP 171B-1051A-10H-5W, 52–54 cm, USTL 4533–3, W52/3; (**2**) specimen showing dorsal horn (arrow), ODP 171B-1051A-14H-5W, 52–54 cm, USTL 4554–6, H58/4; (**3**) ODP 171B-1051A-9H-5W, 53–55 cm, USTL 4528–2, D64/1; (**4**) specimen showing mitral arches, ODP 171B-1051A-18X-5W, 54–56 cm, USTL 4562–8, O40/4; (**5–7**) *Apoplanius hyalinus* n. sp.: (**5**) holotype, ODP 171B-1051A-9H-5W, 53–55 cm, USTL 4566–2, S37/2; (**6**) specimen showing dorsal horn (arrow), ODP 171B-1051A-8H-5W, 53–55 cm, USTL 4521–1, S55/3; (**7**) ODP 171B-1051A-8H-5W, 53–55 cm, USTL 4522–1, N61/4; (**8**) *Apoplanius kerasperus* (Sanfilippo and Caulet, 1998): ODP 171B-1051A-10H-2W, 53–55 cm, USTL 4530–3, K60/2; (**9–12**) *Thyrsocyrtis kamikuri* n. sp.: (**9**) holotype, ODP 171B-1051A-

9H-2W, 53–55 cm, USTL 4563–1, B34/3; (**10**) ODP 171B-1051A-9H-5W, 53–55 cm, USTL 4529–5, J44/1; (**11**) ODP 171B-1051A-9H-2W, 53–55 cm, USTL 4563–2, P37/1; (**12**) ODP 171B-1051A-9H-2W, 53–55 cm, USTL 4563–3, D46/3. All scale bars equal 50 µm.

Occurrence.— This species occurs sporadically throughout the studied interval, from the upper part of the *Podocyrtis* (*L.*) *mitra* Zone (RP14) to the lower part of the *Podocyrtis* (*L.*) *goetheana* Zone (RP16).

Description.— Shell composed of three segments, conical to campanulate. Cephalis small, hemispherical, sparsely perforated, bearing a stout, bladed apical horn. Collar stricture moderately expressed. Thorax campanulate, perforated by subcircular pores of variable sizes, the largest being in the middle part of the segment. Thoracic surface sometimes slightly thorny. Lumbar stricture marked by a constriction and a thin internal ridge. Abdomen inflated to truncate conical, wider and longer than the thorax, with 8–10 pores per half-circumference. Abdominal pores subcircular to ovoid, of variable size but usually twice as wide as the thoracic ones. Thoracic and abdominal pores quincuncially arranged, and usually hexagonally framed. Peristome differentiated, widely open. Three short feet arising above the peristome, subparallel to divergent, and perforated by small subcircular pores

Etymology.— This species is named in honor of Dr. Shin-ichi Kamikuri (Ibaraki University, Japan) who first illustrated this species.

Dimensions.— Based on 17 specimens (mean): total length without the apical horn: 161–228 µm (194), length of apical horn: 13–55 µm (45), length of cephalis without the apical horn: 20–29 µm (24), length of thorax: 41–75 µm (63), maximum breadth of thorax: 90–125 µm (102), length of abdomen: 76–138 μm (106), maximum breadth of abdomen: 114–193 μm (153), length of feet: 34–70 μm (56).

Remarks.— *Thyrsocyrtis kamikuri* n. sp. differs from *T. lochites* (Sanfilippo and Riedel, 1982), *T. orthotenes* Nigrini et al., 2005, *T. tetracantha* (Ehrenberg, 1874) and *T. triacantha* (Ehrenberg, 1874) in having abdominal pores less than twice the size of thoracic pores and three short, perforated feet. The new species differs from *T. hirsuta* (Krasheninnikov, 1960), *T. rhizodon* (Ehrenberg, 1874), and *T. tarsipes* Foreman, 1973 in having an abdomen considerably wider than the thorax, and three short, usually divergent feet without distal enlargement. *T. kamikuri* n. sp. also differs from *T. norrisi* Sanfilippo and Blome, 2001 in not having a flared peristome and an unserrated apical horn. Finally, the new species is distinguished from *Dictyopodium oxylophus* Ehrenberg, 1874 in having a campanulate thorax, a relatively larger cephalis that is not partially embedded in the thorax, and no tubular latticed feet.

II.3.2.4. Conclusions

Examination of the middle Eocene radiolarian fauna recovered from ODP Site 1051 resulted in the description of 21 new species, including three spumellarians and 18 nassellarians. We also took advantage of the richness of this material to redescribe and illustrate the morphological variability of the poorly known rhopalosyringiid species *Pterocyrtidium zitteli* Bütschli, 1882a.

Most of the new species described here are abundant throughout the studied interval and can thus be found in almost all the samples. A total of 14 bioevents were recorded: these include the first occurrences of *Albatrossidium messiaeni* n. sp., *Botryocella* ? *alectrida* n. sp., *Ceratocyrtis oconnori* n. sp., *Cryptocarpium*? *judoka* n. sp., *Elaphospyris quadricornis* n. sp., *Eucyrtidium granatum* n. sp. and *Periphaena petrushevskayae* n. sp., and the last occurrences of *Apoplanius cryptodirus* n. sp., *A. hyalinus* n. sp., *Ceratocyrtis oconnori* n. sp., *Elaphospyris* *cordiformis* n. sp., *Lychnocanium croizoni* n. sp., *Spirocyrtis matsuokai* n. sp. and *Stylodictya oligodonta* n. sp. These species might prove to be useful in the future to improve the stratigraphic resolution of the subtropical Atlantic Ocean, where many biostratigraphically relevant species that define the tropical radiolarian biozonation are missing or have different ranges compared to the tropics (Sanfilippo and Blome, 2001).

With the exception of *Periphaena petrushevskayae* n. sp., which was observed at Demerara Rise (DSDP Site 144; Petrushevskaya and Kozlova, 1972), *Dictyoprora echidna* n. sp. and *Lychnocanium cingulatum* n. sp., which were recovered from the Yucatan Shelf (DSDP Site 94; Foreman, 1973; Sanfilippo and Riedel, 1973), *Thyrsocyrtis kamikuri* n. sp. which was found in the Caledonian Basin (DSDP Site 206C; Hollis et al., 2020) and *L. cheni* n. sp. which is known from the Naturaliste Plateau (DSDP Site 264), the new species described here have never been reported before elsewhere. For some species, such as *Botryocella* ? *alectrida* n. sp. or *Pylobotrys* ? *bineti* n. sp., the lack of previous mention may be due to their relative scarcity in the fossil record. On the other hand, the absence in the literature of abundant and easily identifiable species such as *Albatrossidium messiaeni* n. sp. or *Apoplanius hyalinus* n. sp., suggests that the geographic range of these species is relatively limited. These results highlight the potential interest of these species for future paleoceanographic and paleoenvironmental studies.

Acknowledgments

We thank the Ocean Drilling Program (ODP) for providing the samples used in this study, and Holger Kuhlmann and Alex Wülbers from the Bremen Core Repository (Germany). We also thank Sylvie Régnier and Jessie Cuvelier for technical assistance.

Chapter III – Progress on late middle Eocene radiolarian biostratigraphy

This chapter consists of a single article titled **“Astronomical calibration of late middle Eocene radiolarian bioevents from ODP Site 1260 (equatorial Atlantic, Leg 207) and refinement of the global tropical radiolarian biozonation”**, published in the Journal of Micropalaeontology, and available online at DOI: https://doi.org/10.5194/jm-41-1-2022.

Astronomical calibration of late middle Eocene radiolarian bioevents from ODP Site 1260 (equatorial Atlantic, Leg 207) and refinement of the global tropical radiolarian biozonation

Mathias Meunier* and Taniel Danelian

Univ. Lille, CNRS, UMR 8198 – Evo-Eco-Paleo, F-59000 Lille, France

<mathias.meunier@univ-lille.fr>

*Corresponding author

Abstract

The middle Eocene sedimentary sequence drilled at Ocean Drilling Program Site 1260 (Leg 207), Demerara Rise, western equatorial Atlantic, yielded a rich and diverse radiolarian fauna. The expanded and complete sedimentary record of this site, as well as the existence of an orbital chronological framework, allowed us to study a series of radiolarian bioevents with a very fine temporal resolution. We have compiled a well-resolved sequence of 71 radiolarian bioevents and provided calibrations to the geomagnetic polarity timescale and the astronomical timescale. Comparison of the radiolarian successions at ODP Site 1260A with the northwestern Atlantic IODP Site U1403 and the IODP Sites U1331, U1332, and 1333, situated in the eastern equatorial Pacific, allowed the demonstration of the synchroneity of primary radiolarian bioevents that underpin the middle Eocene zonal scheme. Several secondary bioevents were also found to be synchronous between the two oceans and were therefore used to define seven new subzones for the low-latitude middle Eocene sequences: *Dictyomitra parva* interval subzone (RP13a), *Coccolarnacium periphaenoides* interval subzone (RP13b), *Artostrobus quadriporus* interval subzone (RP14a), *Sethochytris triconiscus* interval subzone (RP14b), *Podocyrtis* (*P*.) *apeza* interval subzone (RP14c), *Rhopalosyringium* ? *biauritum* interval subzone (RP15a), and *Thyrsocyrtis* (*P*.) *krooni*[1] interval subzone (RP15b). This refined radiolarian biozonation has significantly improved stratigraphic resolution and age control for the late middle Eocene interval (an average of two subzones per 1.5 million years). A substantial diachronism was also found in 20 secondary radiolarian bioevents between the two oceans. The majority of radiolarian species appear to have evolved first in the equatorial Atlantic Ocean and subsequently in the equatorial Pacific. However, the reasons for this pattern of diachroneity are currently uncertain and would require a greater sampling coverage to be elucidated.

1 *Thyrsocyrtis* (*Pentalocorys*) *parvipes* (Ehrenberg, 1874) in Chapter II.2.

III.1. Introduction

Accurate chronostratigraphic frameworks are essential to decipher past Earth system processes and events, as well as the complex history of life on Earth. Amongst the biostratigraphically important Cenozoic marine microfossils, polycystine radiolaria offer major advantages for dating and correlating marine sediments because they are commonly preserved in the fossil record, they are globally distributed, and have experienced high rates of evolution (De Wever et al., 2001). They are particularly useful in oceanic basins where carbonate fossils are absent or poorly preserved (Lazarus, 2005). Due to old misconceptions about their evolution, radiolarians have long been neglected as they were considered to be long-ranging species of no biostratigraphic value. Riedel (1957b) was the first to emphasize the value of Cenozoic radiolarians for biostratigraphy, based on the study of deep-sea cores collected during the Swedish Deep-Sea Expedition. The subsequent advent of scientific ocean drilling campaigns improved deep-sea sediment recovery and allowed extensive studies of radiolarian assemblages, leading to the establishment of the first tropical radiolarian biozonation for the Cenozoic (Riedel and Sanfilippo, 1970, 1971, 1978; Foreman, 1973; Sanfilippo and Riedel, 1973; Nigrini, 1974; Sanfilippo et al., 1985). Paleocene zones and subzones were later added by Nishimura (1987, 1992) and Hollis (1993) based on material from higher latitudes. Sanfilippo and Nigrini (1998b) revised the tropical biozonation and introduced an alphanumeric code for the Cenozoic (RP1–RP22 for the Paleogene) to facilitate correlation with other microfossil groups.

Radiolarian bioevents defining the Paleogene zones were finally calibrated to the geomagnetic polarity timescale (Kamikuri et al., 2012a; de Souza et al., 2017, 2021; Hollis et al., 2020). Absolute ages were provided by Kamikuri et al. (2012a) for 226 early Eocene to late Oligocene radiolarian bioevents recorded in the equatorial Pacific Ocean by using age–depth models based on magnetostratigraphy. For their part, Hollis et al. (2020) provided absolute ages for 99 middle Paleocene to middle Eocene radiolarian bioevents by using age–depth models based on magnetobiochronology. The recent development of an orbitally calibrated stratigraphy for the Paleogene (Westerhold et al., 2012, 2014, 2015; Westerhold and Röhl, 2013; Boulila et al., 2018) opens new prospects for precise calibration of radiolarian bioevents, especially for the equatorial Atlantic, which remains less well documented and calibrated than the equatorial Pacific.

Here, we present a detailed biostratigraphic analysis of the middle Eocene radiolarian record from Ocean Drilling Program (ODP) Site 1260, drilled on Demerara Rise (western equatorial Atlantic Ocean). This site provided a remarkably complete and continuous middle Eocene sedimentary sequence containing a rich record of both siliceous and carbonate microfossils. A very well-defined framework in terms of both magnetostratigraphy and cyclostratigraphy is now available for this site (Westerhold and Röhl, 2013). Thus, the main objective of this study was to refine the absolute ages of middle Eocene radiolarian bioevents through high-resolution faunal analysis of ODP Site 1260 and direct correlation with the geomagnetic polarity and astronomical timescales. We documented the stratigraphic distribution of radiolarian species at this site, including some species described in very early studies (i.e., Ehrenberg, 1874) and rarely reported since. The absolute ages of radiolarian bioevents derived from ODP Site 1260 were then compared to previous biostratigraphic studies conduced at three low-latitude sites in the Pacific (Kamikuri et al., 2012a) and one mid-latitude site in the Atlantic (Hollis et al., 2020) to assess the degree of synchroneity of radiolarian bioevents between the equatorial Atlantic and Pacific oceans, and between the low and middle latitudes of the Atlantic Ocean.

III.2. Material and methods

All observed samples were collected at ODP Site 1260 (9°16′N, 54°32′W) located on the northwestern margin of Demerara Rise, a submarine plateau off the coast of Suriname and French Guiana (Figure III.1). The site is inferred to have been closer to the equator during the middle Eocene than it is today (paleolatitude of ∼1°N; Suganuma and Ogg, 2006). Two closely spaced holes (1260A and 1260B) were drilled using rotary coring, starting at a modern water depth of 2549 m below sea level. A nearly continuous record of an expanded Albian–Oligocene

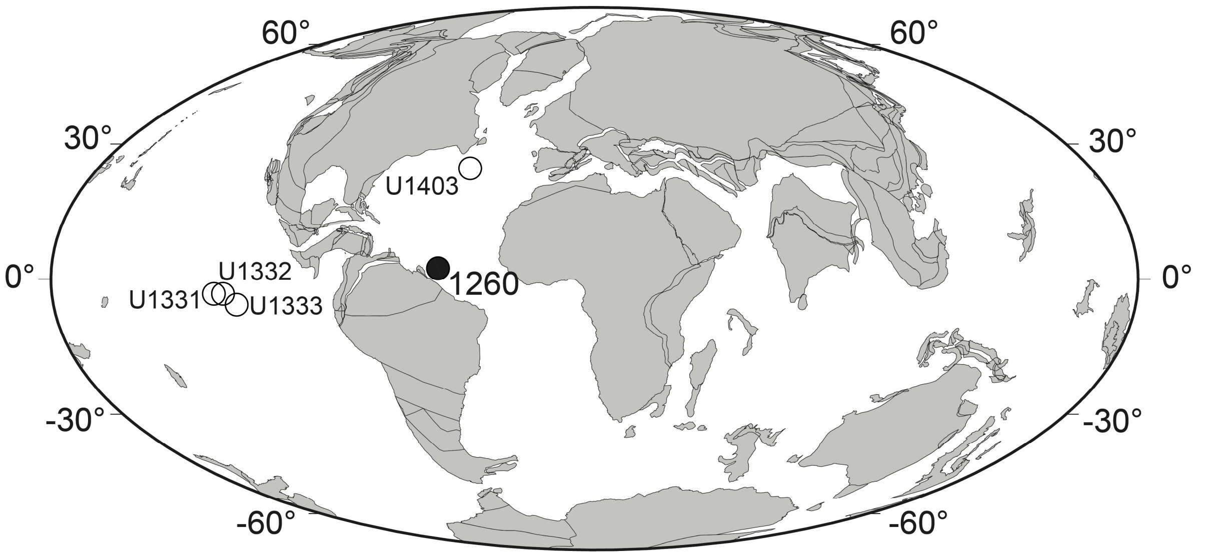

Figure III.1. Middle Eocene (ca. 40 Ma) paleogeographic map showing the location of Demerara Rise (ODP Site 1260, Leg 207) (solid circle) and the four equatorial Pacific and North Atlantic IODP sites used for comparison (open circles). Paleogeographic reconstruction drawn after ODSN Plate Tectonic Reconstruction Service (http://www.odsn.de/odsn/services/paleomap/paleomap.html, last access: 8 January 2021).

sequence was recovered (Shipboard Scientific Party, 2004). The middle Eocene interval of the site is characterized by nannofossil chalk, rich in biogenic silica (i.e., opal), with abundant and well-preserved radiolarian fauna (Danelian et al., 2005, 2007) and some other siliceous microfossil groups, including diatoms (Renaudie et al., 2010), ebridians, silicoflagellates, and sponge spicules. The studied sequence is 91.72 m thick and accumulated in only 3.94 million years, between 43.78 and 39.84 Ma (sedimentation rate estimated at ∼2.3 cm/kyr), during the late middle Eocene (middle Lutetian to early Bartonian). A total of 55 samples were selected from hole 1260A. Sampling was as regular as possible in order to avoid any bias associated with heterogeneous bin durations. The average sample spacing is approximately 1.67 m, and the average age difference between two consecutive samples is ~71 600 years.

An excellent age control for ODP Site 1260 was provided by Westerhold and Röhl (2013), who developed a high-resolution astronomical timescale for this site based on iron (Fe) intensity data obtained by X-ray fluorescence core scanning. Orbitally tuned ages were used to date each sample, and for intervals where no data were available from hole 1260A, the absolute sample ages were estimated from tuned ages provided for samples situated at the same depth in hole 1260B.

Sample preparation followed the protocol described in Sanfilippo et al. (1985). Samples were first soaked in hydrogen peroxide (H_2O_2), and then in hydrochloric acid (HCl) to remove organic matter and carbonate content, respectively. Residues were washed several times through a 45 µm sieve to remove clay, small radiolarian fragments, and diatom frustules, and then dried overnight at ∼40°C. For each sample, one to four slides were prepared by homogeneously spreading ∼5 mg of cleaned residue on a coverslip according to the method described by Witkowski et al. (2012). After drying, the coverslips were mounted on standard glass slides using Norland Optical Adhesive 61 (refractive index 1.56). Species identification was perforemed using a Zeiss Axio Imager.A2 as a light microscope (20× objective lens) equipped with a Zeiss AxioCam ERc5s digital camera. For each specimen illustrated, a series of 5 to 10 images taken at slightly different focal depths were stacked using Helicon Focus v.7.6.6 (HeliconSoft) in order to obtain a composite image of the entire shell. Specimens mounted on a slide were identified to species level where possible. However, as many of the morphotypes encountered have not yet been formally described, most of them were not included in this study.

III.3. Results

III.3.1. Radiolarian bioevents at hole 1260A

Radiolarians are abundant and well-preserved throughout the studied middle Eocene sequence. The assemblages are taxonomically diverse, with at least 29 families recognized according to the latest classification provided by Suzuki et al. (2021). The stratigraphic distribution of 61 species, whose first or last occurrence falls within the studied interval, is shown in Figure III.2, and all species are illustrated in Plates III.1–III.3. A total of 71 bioevents were recognized in hole 1260A (~1.8 events per 100 kyr), including 38 first occurrences (FOs), 29 last occurrences (LOs), and four evolutionary transitions (ETs). These bioevents are summarized in Table III.1, with their calibrated age in hole 1260A.

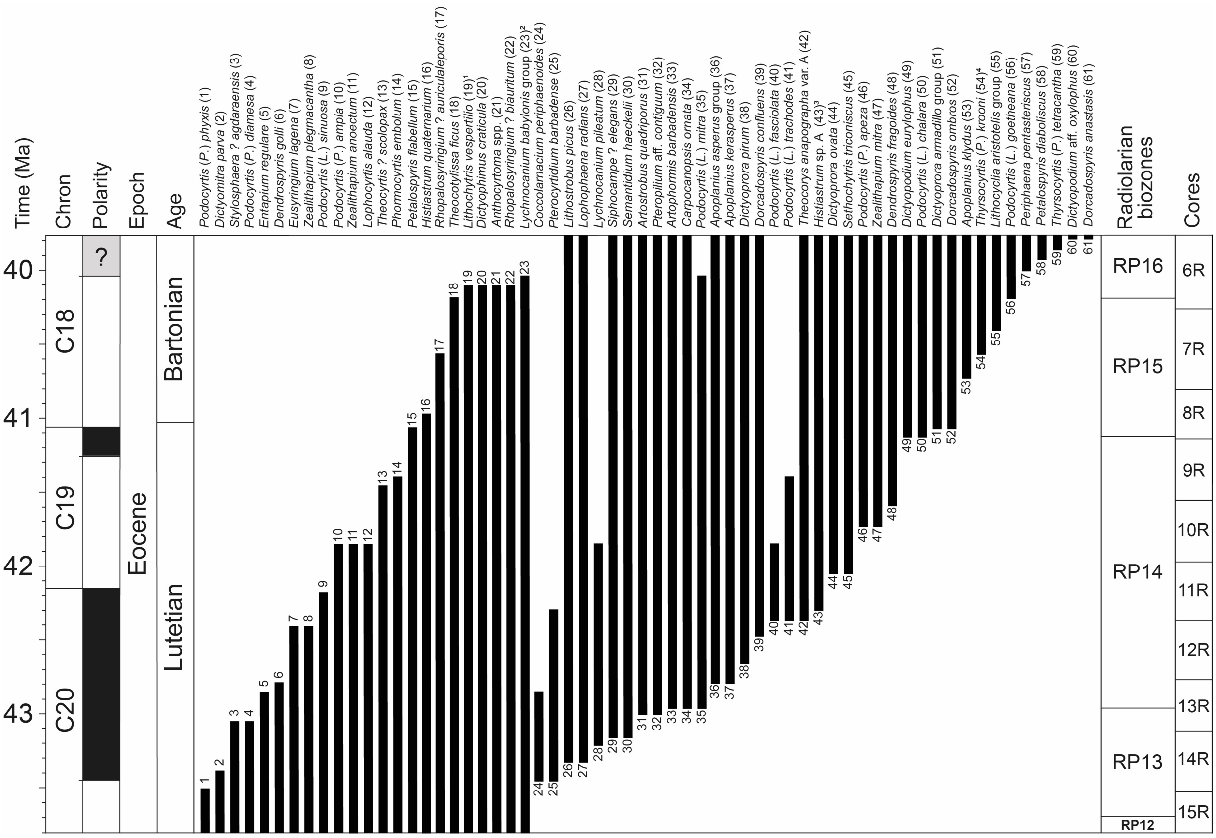

Figure III.2. Range chart of 61 selected radiolarian species from the middle Eocene of ODP hole 1260A. Geomagnetic timescale after calibration of Suganuma and Ogg (2006). (1 – *Lithochytris pyramidalis* Ehrenberg in Chapter II.2; 2 – *Lychnocanium tribulus* (Ehrenberg) group in Chapter II.2; 3 – *Histiastrum coronatum* Haeckel in Chapter II.2; 4 – *Thyrsocyrtis* (*P.*) *parvipes* (Ehrenberg) in Chapter II.2).

Table III.1. Summary of first occurrences (FOs), last occurrences (LOs), and evolutionary transitions (ETs) at ODP Site 1260, drilled on Demerara Rise in the western equatorial Atlantic. Estimated ages and revised meter composite depth (rmcd) are after Westerhold and Röhl (2013). Primary bioevents that define the boundaries of radiolarian zones and subzones, are shown in bold.

Zones	Radiolarian bioevents	This study (ODP Site 1260)				Kamikuri et al., 2012 (IODP Sites U1331-1333)		Hollis et al., 2020 (IODP Site U1403)
		Core - section - interval (cm)	Depth (rmcd)	Tuned age (Ma)		Age (Ma)*	Revised age (Ma)**	Age (Ma)
		Base / Top	Base / Top	Base / Top	Midpoint			
RP16	FO *Dictyopodium* aff. *oxylophus*	6R-2W, 55-57 / 6R-1W, 55-57	40.25 / 38.75	39.91 / 39.84	39.87	-	-	-
	FO *Dorcadospyris anastasis*	6R-2W, 55-57 / 6R-1W, 55-57	40.25 / 38.75	39.91 / 39.84	39.87	39.30	40.20	-
	FO *Thyrsocyrtis* (*P.*) *tetracantha*	6R-3W, 55-57 / 6R-2W, 55-57	41.75 / 40.25	39.97 / 39.91	39.94	38.10	39.10	-
	FO *Petalospyris diaboliscus*	6R-4W, 55-57 / 6R-3W, 55-57	43.25 / 41.75	40.04 / 39.97	40.01	-	-	-
	LO *Podocyrtis* (*L.*) *mitra*	6R-4W, 55-57 / 6R-3W, 55-57	43.25 / 41.75	40.04 / 39.97	40.01	39.20	40.00	-
	LO *Lychnocanium babylonis* group[1]	6R-4W, 55-57 / 6R-3W, 55-57	43.25 / 41.75	40.04 / 39.97	40.01	-	-	-
	LO *Anthocyrtoma* spp.	6R-5W, 55-57 / 6R-4W, 55-57	44.75 / 43.25	40.11 / 40.04	40.08	37.90	38.20	-
	LO *Dictyophimus craticula*	6R-5W, 55-57 / 6R-4W, 55-57	44.75 / 43.25	40.11 / 40.04	40.08	38.30	39.10	-
	LO *Histiastrum quaternarium*	6R-5W, 55-57 / 6R-4W, 55-57	44.75 / 43.25	40.11 / 40.04	40.08	-	-	-
	LO *Lithochytris vespertilio*[2]	6R-5W, 55-57 / 6R-4W, 55-57	44.75 / 43.25	40.11 / 40.04	40.08	39.10	39.80	-
	FO *Periphaena pentasteriscus*	6R-5W, 55-57 / 6R-4W, 55-57	44.75 / 43.25	40.11 / 40.04	40.08	-	-	-
	LO *Theocotylissa ficus*	6R-6W, 55-57 / 6R-5W, 55-57	46.25 / 44.75	40.19 / 40.11	40.15	37.90	38.20	-
	FO *Podocyrtis* (*L.*) *goetheana*	**7R-1W, 54-56 / 6R-6W, 55-57**	**48.54 / 46.25**	**40.32 / 40.19**	**40.26**	**39.30**	**40.10**	-
RP15	FO *Lithocyclia aristotelis* group	7R-3W, 54-56 / 7R-2W, 54-56	51.54 / 50.04	40.48 / 40.40	40.44	38.80	39.60	-
	LO *Rhopalosyringium* ? *auriculaleporis*	7R-4W, 54-56 / 7R-3W, 54-56	53.04 / 51.54	40.57 / 40.48	40.52	-	-	-
	FO *Thyrsocyrtis* (*P.*) *krooni*[3]	7R-6W, 54-56 / 7R-4W, 54-56	56.04 / 53.04	40.73 / 40.57	40.65	38.10	39.10	-
	LO *Rhopalosyringium* ? *biauritum*	**8R-3W, 54-56 / 7R-6W, 54-56**	**61.24 / 56.04**	**40.96 / 40.73**	**40.84**	**40.00**	**40.40**	**40.73**
	FO *Apoplanius klydus*	8R-3W, 54-56 / 7R-6W, 54-56	61.24 / 56.04	40.96 / 40.73	40.84	-	-	-
	LO *Petalospyris flabellum*	8R-5W, 54-56 / 8R-3W, 54-56	64.24 / 61.24	41.07 / 40.96	41.02	-	-	-
	FO *Dictyoprora armadillo* group	8R-6W, 54-56 / 8R-5W, 54-56	65.74 / 64.24	41.12 / 41.07	41.10	-	-	-
	FO *Dorcadospyris ombros*	8R-6W, 54-56 / 8R-5W, 54-56	65.74 / 64.24	41.12 / 41.07	41.10	41.40	42.10	-
	FO *Dictyopodium* aff. *eurylophus*	9R-1W, 55-57 / 8R-6W, 54-56	66.85 / 65.74	41.18 / 41.12	41.15	-	-	-
	FO *Podocyrtis* (*L.*) *chalara*	9R-1W, 55-57 / 8R-6W, 54-56	66.85 / 65.74	41.18 / 41.12	41.15	41.00	41.90	-
	ET *Podocyrtis mitra* → *P. chalara*	**9R-1W, 55-57 / 8R-6W, 54-56**	**66.85 / 65.74**	**41.18 / 41.12**	**41.15**	**40.50**	**41.20**	-
RP14	LO *Phormocyrtis embolum*	9R-5W, 55-57 / 9R-4W, 55-57	72.85 / 71.35	41.40 / 41.34	41.37	-	-	-
	LO *Podocyrtis* (*L.*) *trachodes*	9R-5W, 55-57 / 9R-4W, 55-57	72.85 / 71.35	41.40 / 41.34	41.37	40.60	40.80	41.13
	LO *Theocorys* ? *scolopax*	9R-6W, 55-57 / 9R-5W, 55-57	74.35 / 72.85	41.46 / 41.40	41.43	-	-	-
	FO *Dendrospyris fragoides*	10R-3W, 55-57 / 10R-1W, 55-57	80.33 / 77.33	41.73 / 41.59	41.66	-	-	-
	LO *Lychnocanium pileatum*	10R-5W, 55-57 / 10R-3W, 55-57	83.33 / 80.33	41.85 / 41.73	41.79	-	-	-
	LO *Lophocyrtis alauda*	10R-5W, 55-57 / 10R-3W, 55-57	83.33 / 80.33	41.85 / 41.73	41.79	-	-	-
	LO *Podocyrtis* (*P.*) *ampla*	10R-5W, 55-57 / 10R-3W, 55-57	83.33 / 80.33	41.85 / 41.73	41.79	41.20	41.50	-
	FO *Podocyrtis* (*P.*) *apeza*	**10R-5W, 55-57 / 10R-3W, 55-57**	**83.33 / 80.33**	**41.85 / 41.73**	**41.79**	**41.00**	**41.90**	**41.94**
	LO *Podocyrtis* (*L.*) *fasciolata*	10R-5W, 55-57 / 10R-3W, 55-57	83.33 / 80.33	41.85 / 41.73	41.79	41.20	41.80	42.11
	LO *Zealithapium anoectum*	10R-5W, 55-57 / 10R-3W, 55-57	83.33 / 80.33	41.85 / 41.73	41.79	41.20	41.50	42.11
	FO *Zealithapium mitra*	10R-5W, 55-57 / 10R-3W, 55-57	83.33 / 80.33	41.85 / 41.73	41.79	41.00	41.60	-
	FO *Dictyoprora ovata* group	11R-3W, 55-57 / 11R-2W, 55-57	89.55 / 88.05	42.12 / 42.05	42.08	-	-	-

(Table III.1. continued)

Zones	Radiolarian bioevents	This study (ODP Site 1260) Core - section - interval (cm) Base / Top	Depth (rmcd) Base / Top	Tuned age (Ma) Base / Top	Midpoint	Kamikuri et al., 2012 (IODP Sites U1331-1333) Age (Ma)*	Revised age (Ma)**	Hollis et al., 2020 (IODP Site U1403) Age (Ma)
RP14	**FO *Sethochytris triconiscus***	**11R-3W, 55-57 / 11R-2W, 55-57**	**89.55 / 88.05**	**42.12 / 42.05**	**42.08**	**41.30**	**42.10**	-
	LO *Podocyrtis* (*L.*) *sinuosa*	11R-4W, 55-57 / 11R-3W, 55-57	91.05 / 89.55	42.18 / 42.12	42.15	42.40	41.90	43.06
	LO *Pterocyrtidium barbadense*	11R-6W, 55-57 / 11R-5W, 55-57	94.05 / 92.55	42.30 / 42.24	42.27	-	-	-
	FO *Histiastrum* sp. A[4]	11R-7W, 55-57 / 11R-6W, 55-57	95.55 / 94.05	42.37 / 42.30	42.33	-	-	-
	FO *Podocyrtis* (*L.*) *fasciolata*	12R-1W, 55-57 / 11R-7W, 55-57	96.15 / 95.55	42.41 / 42.37	42.39	42.90	43.60	43.80
	FO *Podocyrtis* (*L.*) *trachodes*	12R-1W, 55-57 / 11R-7W, 55-57	96.15 / 95.55	42.41 / 42.37	42.39	41.90	43.00	42.65
	FO *Theocorys anapographa* var. A	12R-1W, 55-57 / 11R-7W, 55-57	96.15 / 95.55	42.41 / 42.37	42.39	-	-	-
	LO *Eusyringium lagena*	12R-1W, 55-57 / 11R-7W, 55-57	96.15 / 95.55	42.41 / 42.37	42.39	41.40	41.80	42.32
	LO *Zealithapium plegmacantha*	12R-1W, 55-57 / 11R-7W, 55-57	96.15 / 95.55	42.41 / 42.37	42.39	41.20	41.80	42.11
	FO *Dorcadospyris confluens*	12R-3W, 55-57 / 12R-2W, 55-57	99.15 / 97.65	42.54 / 42.48	42.51	-	-	-
	FO *Dictyoprora pirum*	12R-6W-55-57 / 12R-5W-55-57	103.65 / 102.15	42.73 / 42.66	42.69	-	-	-
	LO *Dendrospyris golli*	13R-1W, 54-55 / 12R-6W-55-57	105.24 / 103.65	42.79 / 42.73	42.76	-	-	-
	LO *Coccolarnacium periphaenoides*	13R-2W, 54-55 / 13R-1W, 54-55	106.74 / 105.24	42.86 / 42.79	42.82	-	-	-
	LO *Entapium regulare*	13R-2W, 54-55 / 13R-1W, 54-55	106.74 / 105.24	42.86 / 42.79	42.82	-	-	-
	FO *Apoplanius asperus* group	13R-2W, 54-55 / 13R-1W, 54-55	106.74 / 105.24	42.86 / 42.79	42.82	-	-	-
	FO *Apoplanius kerasperus*	13R-2W, 54-55 / 13R-1W, 54-55	106.74 / 105.24	42.86 / 42.79	42.82	-	-	-
	FO *Artophormis* ? *barbadensis*	13R-5W, 54-56 / 13R-4W, 55-56	111.24 / 109.75	43.01 / 42.96	42.98	-	-	-
	FO *Carpocanopsis ornata*	13R-5W, 54-56 / 13R-4W, 55-56	111.24 / 109.75	43.01 / 42.96	42.98	40.90	41.60	41.86
	FO *Podocyrtis* (*L.*) *mitra*	13R-5W, 54-56 / 13R-4W, 55-56	111.24 / 109.75	43.01 / 42.96	42.98	43.20	43.90	44.29
	ET *Podocyrtis sinuosa* → *P. mitra*	**13R-5W, 54-56 / 13R-4W, 55-56**	**111.24 / 109.75**	**43.01 / 42.96**	**42.98**	**42.50**	**43.20**	-
RP13	FO *Artostrobus quadriporus*	13R-6W, 54-56 / 13R-5W, 54-56	112.74 / 111.24	43.05 / 43.01	43.03	-	-	-
	LO *Podocyrtis* (*P.*) *diamesa*	13R-6W, 54-56 / 13R-5W, 54-56	112.74 / 111.24	43.05 / 43.01	43.03	-	-	-
	FO *Pteropilium* ? *contiguum*	13R-6W, 54-56 / 13R-5W, 54-56	112.74 / 111.24	43.05 / 43.01	43.03	-	-	-
	LO *Stylosphaera* ? *agdaraensis*	13R-6W, 54-56 / 13R-5W, 54-56	112.74 / 111.24	43.05 / 43.01	43.03	-	-	-
	FO *Semantidium haeckelii*	14R-2W, 55-57 / 14R-1W, 55-57	117.52 / 116.02	43.21 / 43.16	43.18	-	-	-
	FO *Siphocampe* ? *elegans*	14R-2W, 55-57 / 14R-1W, 55-57	117.52 / 116.02	43.21 / 43.16	43.18	-	-	-
	FO *Lychnocanium pileatum*	14R-3W, 55-57 / 14R-2W, 55-57	119.02 / 117.52	43.26 / 43.21	43.24	-	-	-
	FO *Lithostrobus picus*	14R-5W, 55-57 / 14R-4W, 55-57	122.02 / 120.52	43.39 / 43.33	43.36	-	-	-
	FO *Lophophaena radians*	14R-5W, 55-57 / 14R-4W, 55-57	122.02 / 120.52	43.39 / 43.33	43.36	-	-	-
	LO *Dictyomitra parva*	14R-5W, 55-57 / 14R-4W, 55-57	122.02 / 120.52	43.39 / 43.33	43.36	-	-	-
	FO *Coccolarnacium periphaenoides*	14R-7W, 55-57 / 14R-6W, 55-57	125.02 / 123.52	43.51 / 43.45	43.48	-	-	-
	FO *Pterocyrtidium barbadense*	14R-7W, 55-57 / 14R-6W, 55-57	125.02 / 123.52	43.51 / 43.45	43.48	-	-	-
	LO *Podocyrtis* (*P.*) *phyxis*	**14R-7W, 55-57 / 14R-6W, 55-57**	**125.02 / 123.52**	**43.51 / 43.45**	**43.48**	**42.90**	**43.60**	-
	ET *Podocyrtis phyxis* → *P. ampla*	**15R-3W, 55-57 / 15R-2W, 55-57**	**128.97 / 127.47**	**43.70 / 43.63**	**43.67**	**43.20**	**43.90**	-

* Absolute ages provided by Kamikuri et al. (2012) based on age-depth models that integrate the geomagnetic time scale of Lourens et al. (2004).
** Revised ages based on age-depth models which integrate the geomagnetic time scale of Speijer et al. (2020).

(1 – *Lychnocanium tribulus* (Ehrenberg, 1874) group in Chapter II.2; 2 – *Lithochytris pyramidalis* Ehrenberg, 1874 in Chapter II.2; *Thyrsocyrtis* (*Pentalocorys*) *parvipes* (Ehrenberg, 1874) in Chapter II.2; *Histiastrum coronatum* Haeckel, 1887 in Chapter II.2).

III.3.2. Correlation between the equatorial Atlantic and Pacific Oceans

Middle Eocene radiolarian bioevents were correlated between ODP Site 1260 and three low-latitude sites located in the eastern equatorial Pacific: IODP Sites U1331, U1332, and 1333 (Kamikuri et al., 2012a), which were considered by these authors as a single site, due to their geographical proximity (<300 km). Of the aforementioned 71 radiolarian bioevents mentioned above, documented between zones RP12 and RP16, 31 are common to the equatorial Pacific record and were therefore used for correlation (Figure III.3). The absolute ages for these radiolarian bioevents provided by Kamikuri et al. (2012a) were obtained after correlation with the geomagnetic polarity timescale (GPTS) provided by Lourens et al. (2004). However, because the calibration of the GPTS has since changed, we have revised the age–depth models for these Pacific sites by using new models generated here (Supplementary Figure III.1) based on the most recent geomagnetic polarity reversal ages provided by Speijer et al. (2020).

Amongst the primary bioevents, the FO of *Podocyrtis* (*L.*) *goetheana* and the ET of *Podocyrtis* (*L.*) *mitra* to *Podocyrtis* (*L.*) *chalara* are nearly isochronous (less than 160 kyr difference) between the equatorial Atlantic and Pacific oceans, whereas the ET of *Podocyrtis* (*L.*) *sinuosa* to *Podocyrtis* (*L.*) *mitra* and the ET of *Podocyrtis* (*P.*) *phyxis* to *Podocyrtis* (*P.*) *ampla* are slightly diachronous (~220 and ~230 kyr difference, respectively). Seven secondary bioevents are also shown to be nearly synchronous (less than 250 kyr difference) and thus reliable for interoceanic correlations. Moreover, since the order of these bioevents is coherent between the Atlantic and the Pacific Oceans they are used to define new subzones (see Section III.3.4). These bioevents concern the FOs of *Podocyrtis* (*P.*) *apeza*, *Sethochytris triconiscus*, and *Zealithapium mitra* and the LOs of *Podocyrtis* (*L.*) *fasciolata*, *Podocyrtis* (*L.*) *mitra*, *Podocyrtis* (*L.*) *sinuosa*, and *Podocyrtis* (*P.*) *phyxis*.

On the other hand, 20 secondary bioevents are shown to be moderately diachronous (between 250 kyr and 1 Ma difference) to highly diachronous (more than 1 Myr difference) between the Atlantic and the Pacific Oceans. Moderately diachronous bioevents include the FOs of *Dorcadospyris anastasis*, *Lithocyclia aristotelis* group, *Podocyrtis* (*L.*) *chalara*, *Podocyrtis* (*L.*) *mitra*, *Podocyrtis* (*L.*) *trachodes*, and *Thyrsocyrtis* (*P.*) *tetracantha* and the LOs of *Rhopalosyringium* ? *biauritum*, *Dictyophimus craticula*, *Eusyringium lagena*, *Lithochytris vespertilio*[2], *Podocyrtis* (*L.*) *trachodes*, *Podocyrtis* (*P.*) *ampla*, *Zealithapium anoectum*, and *Zealithapium plegmacantha*. Highly diachronous bioevents include the FOs of *Cryptocarpium ornatum*, *Dorcadospyris ombros*, *Podocyrtis* (*L.*) *fasciolata*, and *Thyrsocyrtis* (*P.*) *krooni*[3] and the LOs of *Anthocyrtoma* spp. and *Theocotylissa ficus*. Except for the FOs of *Dorcadospyris anastasis*, *Dorcadospyris ombros*, *Podocyrtis* (*L.*) *chalara*, *Podocyrtis* (*L.*) *fasciolata*, *Podocyrtis* (*L.*) *mitra*, and *Podocyrtis* (*L.*) *trachodes*, all these diachronous bioevents occurred earlier in the Atlantic Ocean.

III.3.3. Correlation between low- and middle-latitude sequences in the North Atlantic Ocean

Radiolarian bioevents recorded at ODP Site 1260 were also correlated with the northwestern Atlantic IODP Site U1403 (Hollis et al., 2020). A total of 298 radiolarian bioevents were documented at this site, 29 of which are common to the record in the equatorial Atlantic sequence and were therefore used for correlation (Figure III.4). The absolute ages provided by Hollis et al. (2020) for these radiolarian bioevents were obtained by calibration to the latest version of the GTS Paleogene timescale (Speijer et al., 2020) using calcareous nannofossil biostratigraphy and magnetostratigraphy.

Three secondary bioevents are found to be nearly isochronous (less than 160 kyr difference) between low and mid–latitudes in the North Atlantic Ocean, including the FO of

2 *Lithochytris pyramidalis* Ehrenberg, 1874 in Chapter II.2.
3 *Thyrsocyrtis* (*Pentalocorys*) *parvipes* (Ehrenberg, 1874) in Chapter II.2.

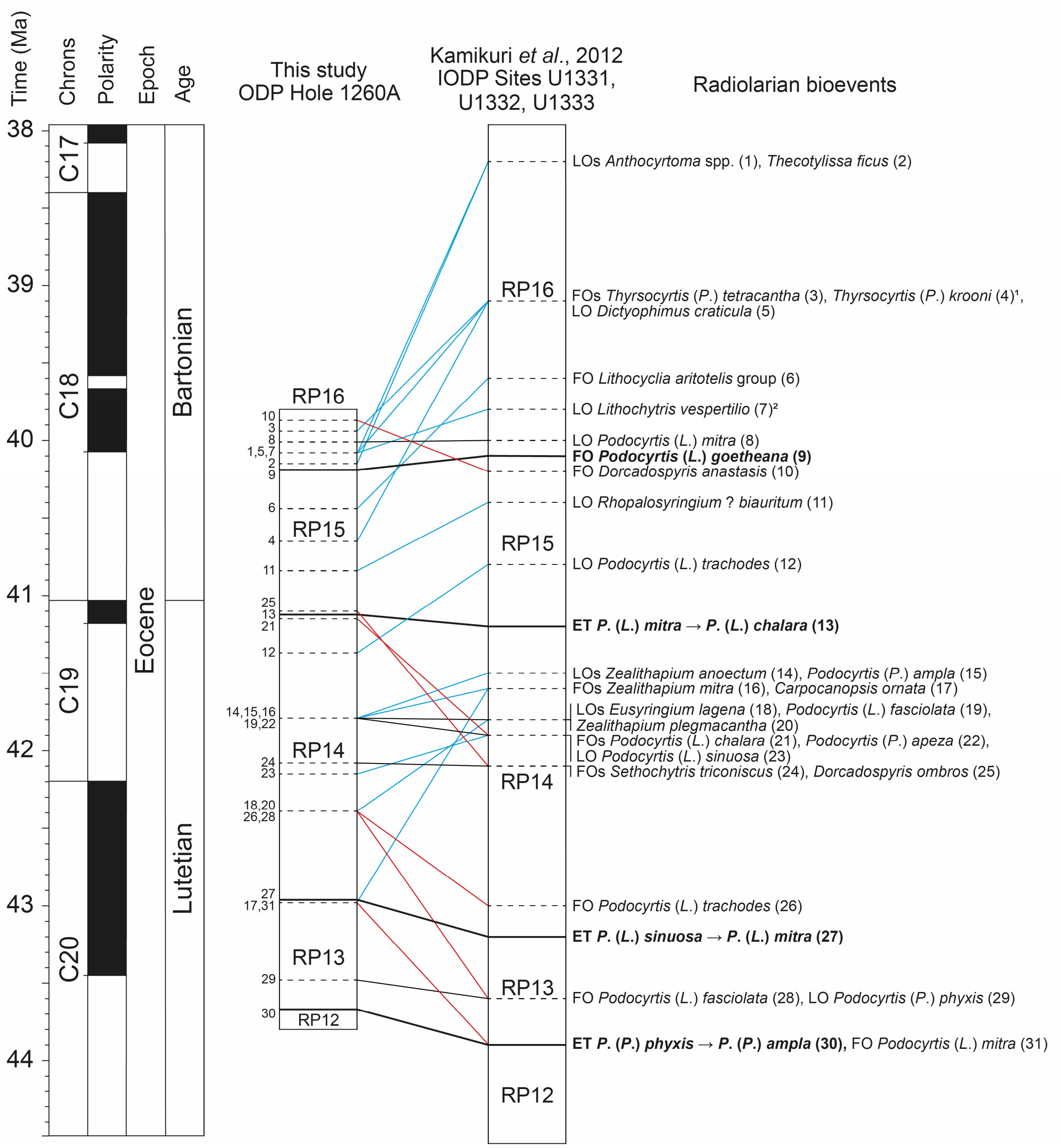

Figure III.3. Correlation of radiolarian bioevents between ODP hole 1260A (this study) and IODP Sites U1331, U1332, and U1333 (Kamikuri et al., 2012a). Black lines represent nearly synchronous bioevents, blue lines represent diachronous bioevents first occurring in the Atlantic Ocean, and red lines represent diachronous bioevents first occurring in the Pacific Ocean. The geomagnetic timescale is after Speijer et al. (2020). (1 – *Thyrsocyrtis* (*P.*) *parvipes* (Ehrenberg) in Chapter II.2; 2 – *Lithochytris pyramidalis* Ehrenberg in Chapter II.2).

Podocyrtis (*P.*) *apeza* and the LOs of *Rhopalosyringium* ? *biauritum* and *Eusyringium lagena*.

On the other hand, nine secondary bioevents are shown to be moderately (250 kyr to 1 Myr difference) to highly diachronous (more than 1 Myr difference) between low and mid– latitudes. Moderately diachronous bioevents include the FO of *Podocyrtis* (*L.*) *trachodes* and the LOs of *Podocyrtis* (*L.*) *fasciolata*, *Podocyrtis* (*L.*) *trachodes*, *Zealithapium mitra*, and *Zealithapium plegmacantha*. Highly diachronous bioevents include the FOs of *Carpocanopsis ornata*, *Podocyrtis* (L.) *fasciolata*, and *Podocyrtis* (*L.*) *mitra,* and the LO of *Podocyrtis* (*L.*) *sinuosa*.

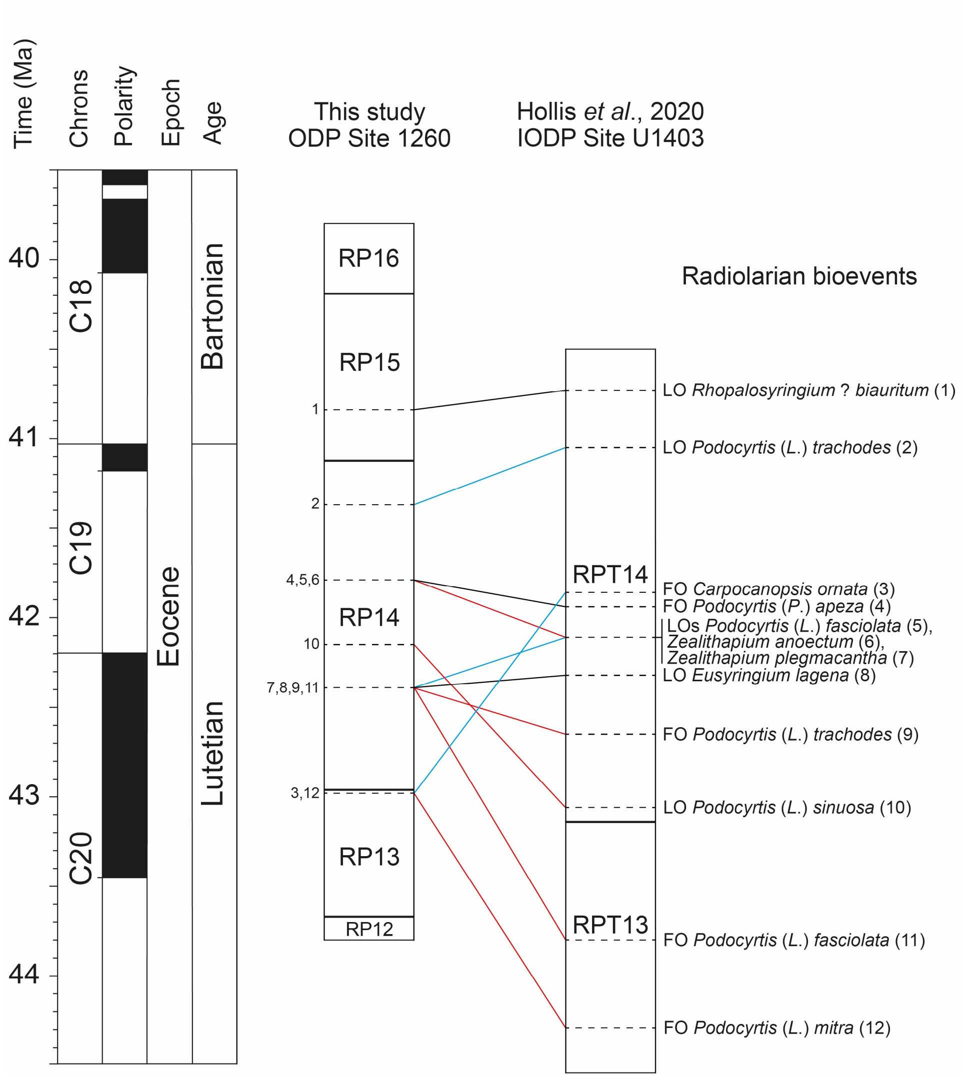

Figure III.4. Correlation of radiolarian bioevents between ODP Site 1260 (this study) and IODP Site U1403 (Hollis et al., 2020). Black lines represent nearly synchronous bioevents, blue lines represent diachronous bioevents that first occur at ODP Site 1260, and red lines represent diachronous bioevents that first occur at IODP Site U1403. The geomagnetic timescale is from Speijer et al. (2020).

III.3.4 Established radiolarian biozones and new subzones

Five biozones of the tropical radiolarian biozonation of Sanfilippo and Nigrini (1998b) were recognized for our studied sequence; they correspond to the upper part of Zone RP12, the entire Zones RP13, RP14 and RP15, and the lower part of Zone RP16. As mentioned above, the correlation of a number of common bioevents between the Atlantic (ODP Site 1260 and IODP Site U1403, see Figure III.4) and the Pacific (IODP Sites U1331, U1332 and U1333, see Figure III.3) allows us to subdivide the RP13 zone into two subzones: *Dictyomitra parva* Subzone (RP13a) and *Coccolarnacium periphaenoides* Subzone (RP13b), and the RP14 zone into three subzones: *Artostrobus quadriporus* Subzone (RP14a), *Sethochytris triconiscus* Subzone (RP14b), and *Podocyrtis* (*Podocyrtopsis*) *apeza* Subzone (RP14c), and the RP15 zone into two subzones: *Rhopalosyringium* ? *biauritum* Subzone (RP15a) and *Thyrsocyrtis* (*Pentalocorys*) *krooni*[4] Subzone (RP15b) (Figure III.5). The pre-established radiolarian zones and the newly defined subzones are given below in stratigraphic order, with their formal definitions, their magnetostratigraphic calibrations, and their absolute age obtained by the orbital time framework provided for ODP Site 1260 (Westerhold and Röhl, 2013). The first occurrences are shown as FO, the last occurrences as LO, and the evolutionary transitions as ET.

RP16 – *Podocyrtis* (*Lampterium*) *goetheana* Interval Zone

(Moore, 1971 emend. Riedel and Sanfilippo, 1978)

Definition: Biostratigraphic interval between the FO of *Podocyrtis* (*Lampterium*) *goetheana* (Haeckel, 1887) (base) and the FO of *Cryptocarpium azyx* (Sanfilippo and Riedel, 1973) (top).

4 *Thyrsocyrtis* (*Pentalocorys*) *parvipes* (Ehrenberg, 1874) in Chapter II.2.

Occurrence at Hole 1260A: The base of this zone is located between samples ODP 1260A-7R-1W, 54–56 cm (48.54 rmcd) and ODP 1260A-6R-6W, 55–57 cm (46.25 rmcd).

Estimated age: The base of the zone is dated to 40.26 Ma in the equatorial Atlantic (Westerhold and Röhl, 2013) and 40.1 Ma in the equatorial Pacific (Kamikuri et al., 2012a; revised age in this study); middle Eocene (early Bartonian).

Magnetostratigraphic calibration: The base of this zone is placed within the uppermost part of Chron C18r at both the Atlantic (this study, in combination with Suganuma and Ogg, 2006) and Pacific sites (Kamikuri et al., 2012a; revised calibration in this study).

Secondary bioevents: Five FOs (*Dictyopodium* aff. *oxylophus*, *Dorcadospyris anastasis*, *Thyrsocyrtis* (*P.*) *tetracantha*, *Petalospyris diaboliscus,* and *Periphaena pentasteriscus*), and seven LOs (*Podocyrtis* (*L.*) *mitra*, *Lychnocanium babylonis* group[5], *Anthocyrtoma* spp., *Dictyophimus craticula*, *Histiastrum quaternarium*, *Lithochytris vespertilio,*[6] and *Theocotylissa ficus*).

Remarks: The record of Zone RP16 is truncated at Hole 1260A. It corresponds to the entire core 6R, above which (>38.2 rmcd) samples contain only rare and/or non-diagnostic radiolarian fragments. Thus, most of the Zone RP16 and associated bioevents are missing, including the FOs of *Cryptocarpium azyx* and *Thyrsocyrtis* (*T.*) *bromia*, some short-lived *Dorcadospyris* species found in the equatorial Pacific (e.g., *Dorcadospyris copelata*; Nigrini et al., 2005), and the acme of *Podocyrtis* (*L.*) *goetheana*. At ODP Hole 1260A, the base of Zone RP16 correlates with the upper part of the planktic foraminiferal Zone P13, and the basal datum is approximately synchronous with the LO of the nannofossil species *Chiasmolithus solitus*, which defines the base of the *Discoaster saipanensis* Zone (NP17).

5 *Lychnocanium tribulus* (Ehrenberg, 1874) group in Chapter II.2.
6 *Lithochytris pyramidalis* Ehrenberg, 1874 in Chapter II.2.

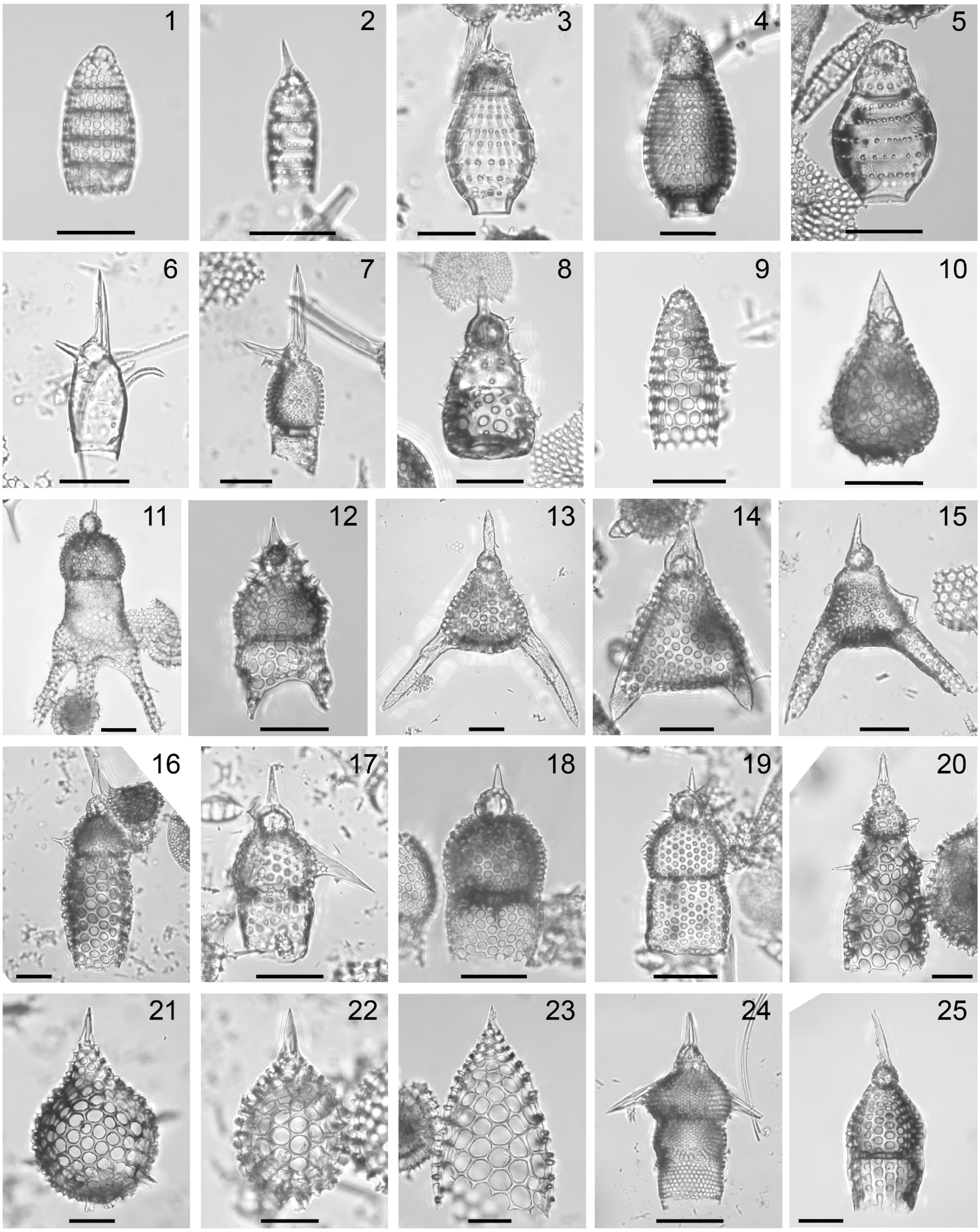

Plate III.1. Composite light micrographs of selected radiolarians from ODP Site 1260. **(1)** *Dictyomitra parva* (Kim), ODP 1260A-15R-4W, 55–57 cm, USTL 3549; **(2)** *Siphocampe* ? *elegans* (Ehrenberg), ODP 1260A-6R-3W, 55–57 cm, USTL 3424; **(3)** *Dictyoprora ovata* (Haeckel) group, ODP 1260A-9R-3W, 55–57 cm, USTL 3477; **(4)** *Dictyoprora armadillo* (Ehrenberg) group, ODP 1260A-6R-3W, 55–57 cm, USTL 3426; **(5)** *Dictyoprora pirum* (Ehrenberg), ODP 1260A-6R-2W, 55–57 cm, USTL 3421; **(6)** *Rhopalosyringium* ? *biauritum*

(Ehrenberg), ODP 1260A-9R-3W, 55–57 cm, USTL 3477; **(7)** *Rhopalosyringium* ? *auriculaleporis* (Clark and Campbell), ODP 1260A-9R-4W, 55–57 cm, USTL 3481; **(8)** *Theocorys anapographa* Riedel and Sanfilippo var. A, ODP 1260A-6R-3W, 55–57cm, USTL 3424; **(9)** *Artostrobus quadriporus* Bjørklund, ODP 1260A-6R-3W, 55–57 cm, USTL 3424; **(10)** *Eusyringium lagena* (Ehrenberg), ODP 1260A-15R-4W, 55–57 cm, USTL 3550; **(11)** *Dictyopodium eurylophus* Ehrenberg, ODP 1260A-6R-2W, 55–57 cm, USTL 3423; **(12)** *Dictyopodium* aff. *oxylophus* Ehrenberg, ODP 1260A-6R-1W, 55–57 cm, USTL 3419; **(13)** *Lychnocanium babylonis* (Clark and Campbell) group (= *Lychnocanium tribulus* (Ehrenberg) group in Chapter II.2), ODP 1260A-11R-1W, 55–57 cm, USTL 3500; **(14)** *Lychnocanium pileatum* (Ehrenberg), ODP 1260A-11R-7W, 55–57 cm, USTL 3506; **(15)** *Sethochytris triconiscus* Haeckel, ODP 1260A-9R-6W, 55–57 cm, USTL 3489; **(16)** *Lophocyrtis alauda* (Ehrenberg), ODP 1260A-13R-6W, 54–56 cm, USTL 3527; **(17)** *Pterocyrtidium barbadense* (Ehrenberg), ODP 1260A-13R-5W, 55–56 cm, USTL 3524; **(18)** *Apoplanius asperus* (Ehrenberg), ODP 1260A-10R-4W, 55–57 cm, USTL 3496; **(19)** *Apoplanius kerasperus* (Sanfilippo and Caulet), ODP 1260A-13R-5W, 55–56 cm, USTL 3524; **(20)** *Apoplanius klydus* (Sanfilippo and Caulet), ODP 1260A-6R-6W, 55–57 cm, USTL 3436; **(21)** *Zealithapium plegmacantha* (Riedel and Sanfilippo), ODP 1260A-14R-1W, 55–57 cm, USTL 3530; **(22)** *Zealithapium anoectum* (Riedel and Sanfilippo), ODP 1260A-12R-3W, 55–57 cm, USTL 3512; **(23)** *Zealithapium mitra* (Ehrenberg), ODP 1260A-7R-4W, 54–56 cm, USTL 3451; **(24)** *Pteropilium* aff. *contiguum* (Ehrenberg), ODP 1260A-9R-4W, 55–57 cm, USTL 3481; **(25)** *Theocyrtis* ? *scolopax* (Ehrenberg), ODP 1260A-10R-6W, 55–57 cm, USTL 3498. All scale bars equal 50 µm.

RP15 – *Podocyrtis* (*Lampterium*) *chalara* Lineage Zone

(Riedel and Sanfilippo, 1970, 1978)

Definition: Biostratigraphic interval between the ET of *Podocyrtis* (*Lampterium*) *mitra* Ehrenberg, 1854 to *Podocyrtis* (*Lampterium*) *chalara* Riedel and Sanfilippo, 1970 (base) and the FO of *Podocyrtis* (*Lampterium*) *goetheana* (Haeckel, 1887) (top).

Occurrence at Hole 1260A: Base: from sample ODP 1260A-8R-6W, 54–56 cm (66.85 rmcd) to sample ODP 1260A-9R-1W, 55–57 cm (65.74 rmcd). Top: from sample ODP 1260A-7R-1W, 54–56 cm (48.54 rmcd) to sample ODP 1260A-6R-6W, 55–57 cm (46.25 rmcd).

Estimated age: From 41.15 Ma to 40.26 Ma in the equatorial Atlantic (Westerhold and Röhl, 2013), and from 41.2 Ma to 40.1 Ma in the equatorial Pacific (Kamikuri et al., 2012a; revised ages); middle Eocene (late Lutetian to early Bartonian).

Magnetostratigraphic calibration: The basal datum is placed within Chron C19n in the equatorial Atlantic (this study in combination with Suganuma and Ogg, 2006), while it falls within the uppermost part of Chron C19r in the equatorial Pacific (Kamikuri et al., 2012a; revised calibration in this study). The top of the zone is placed within the uppermost part of Chron C18r at both the Atlantic (this study in combination with Suganuma and Ogg, 2006) and Pacific sites (Kamikuri et al., 2012a; revised calibration in this study).

Secondary bioevents: Seven FOs (*Lithocyclia aristotelis* group, *Thyrsocyrtis* (*P.*) *krooni*[7], *Apoplanius klydus*, *Dictyoprora armadillo* group, *Dorcadospyris ombros*, *Dictyopodium* aff. *eurylophus* and *Podocyrtis* (*L.*) *chalara*), and three LOs (*Rhopalosyringium* ? *auriculaleporis*, *Rhopalosyringium* ? *biauritum* and *Petalospyris flabellum*).

Remarks: At ODP Hole 1260A, this zone is correlated with the uppermost part of the planktic foraminiferal Zone P12 to the lower part of Zone P13, and to the upper part of the nannofossil Zone NP16. The Lutetian/Bartonian boundary is placed within this zone at ~63.17 rmcd (41.03 Ma), between samples ODP 1260A-8R-6W, 54–56 cm (65.74 rmcd) and ODP 1260A-8R-5W, 54–56 cm (64.24 rmcd). This zone is subdivided into lower (a) and upper (b) subzones.

RP15b – *Thyrsocyrtis* (*Pentalocorys*) *krooni*[7] Interval Subzone

new subzone

Definition: Biostratigraphic interval between the LO of *Rhopalosyringium* ? *biauritum* (Ehrenberg, 1874) (base) and the FO of *Podocyrtis* (*Lampterium*) *goetheana* (Haeckel, 1887) (top).

Occurrence at Hole 1260A: Base: from sample ODP 1260A-8R-3W, 54–56 cm (61.24 rmcd) to sample ODP 1260A-7R-6W, 54–56 cm (56.04 rmcd). Top: from sample ODP

7 *Thyrsocyrtis* (*Pentalocorys*) *parvipes* (Ehrenberg, 1874) in Chapter II.2.

1260A-7R-1W, 54–56 cm (48.54 rmcd) to sample ODP 1260A-6R-6W, 55–57 cm (46.25 rmcd).

Estimated age: From 40.84 Ma to 40.26 Ma in the equatorial Atlantic (Westerhold and Röhl, 2013), and from 40.4 Ma to 40.1 Ma in the equatorial Pacific (Kamikuri et al., 2012a; revised ages in this study); middle Eocene (early Bartonian).

Magnetostratigraphic calibration: The new subzone falls entirely within Chron C18r at both the Atlantic (this study in combination with Suganuma and Ogg, 2006) and Pacific sites (Kamikuri et al., 2012a; revised calibration in this study).

Remarks: The basal datum is nearly isochronous between ODP Hole 1260A (40.84 Ma) and IODP Site U1403 (40.73 Ma), while it is moderately diachronous between ODP Hole 1260A (40.84 Ma) and IODP Sites U1331, U1332 and U1333 (40.40 Ma). However, at each equatorial site, the FO of *Rhopalosyringium* ? *biauritum* is close to the FO of *Orbulinoides beckmanni*, which defines the base of the planktic foraminiferal Zone P13. Futhermore, the FO of *Rhopalosyringium* ? *biauritum* appears to be synchronous on the scale of the eastern equatorial Pacific (Nigrini et al., 2005). As mentioned above, this subzone is correlated in ODP Hole 1260A with the uppermost part of the planktic foraminiferal Zone P12 to the lower part of Zone P13, and the upper part of the nannofossil Zone NP16.

RP15a – *Rhopalosyringium* ? *biauritum* Interval Subzone

new subzone

Definition: Biostratigraphic interval between the ET from *Podocyrtis* (*Lampterium*) *mitra* Ehrenberg, 1854 to *Podocyrtis* (*Lampterium*) *chalara* Riedel and Sanfilippo, 1970 (base) and the LO of *Rhopalosyringium* ? *biauritum* (Ehrenberg, 1874) (top).

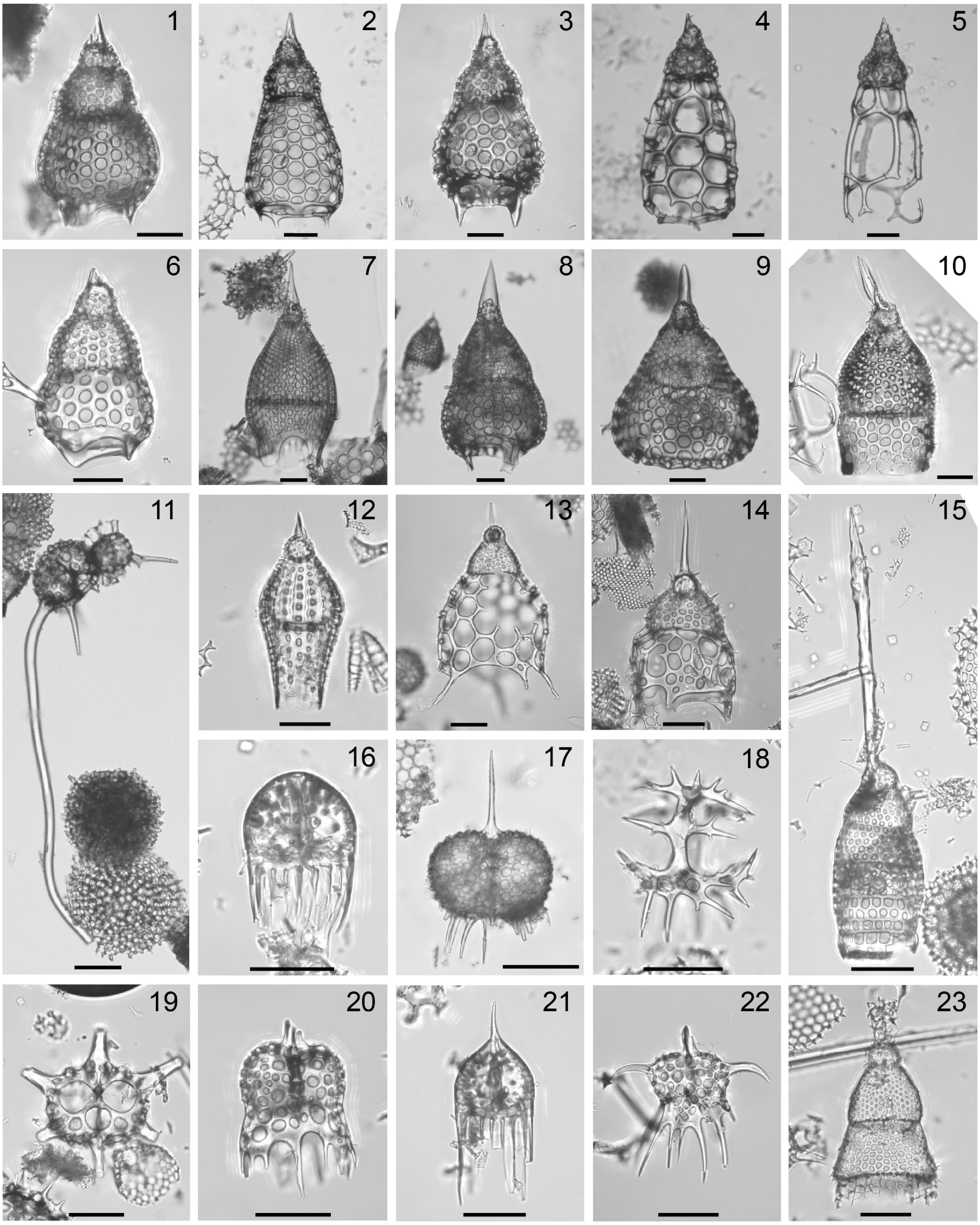

Plate III.2. Composite light micrographs of selected radiolarians from ODP Site 1260. **(1)** *Podocyrtis* (*Lampterium*) *sinuosa* Ehrenberg, ODP 1260A-15R-4W, 55–57 cm, USTL 3552; **(2)** *Podocyrtis* (*Lampterium*) *mitra* Ehrenberg, ODP 1260A-9R-3W, 55–57 cm, USTL 3477; **(3)** *Podocyrtis* (*Lampterium*) *trachodes* Riedel and Sanfilippo, ODP 1260A-10R-6W, 55–57 cm, USTL 3498; **(4)** *Podocyrtis* (*Lampterium*) *chalara* Riedel and Sanfilippo, ODP 1260A-6R-6W, 55–57 cm, USTL 3436; **(5)** *Podocyrtis* (*Lampterium*) *goetheana* (Haeckel), ODP 1260A-

6R-2W, 55–57 cm, USTL 3420; **(6)** *Podocyrtis* (*Lampterium*) *fasciolata* Nigrini, ODP 1260A-11R-7W, 55–57 cm, USTL 3506; **(7)** *Podocyrtis* (*Podocyrtoges*) *diamesa* Riedel and Sanfilippo, ODP 1260A-15R-2W, 55–57 cm, USTL 3543; **(8)** *Podocyrtis* (*Podocyrtoges*) *phyxis* Sanfilippo and Riedel, ODP 1260A-15R-2W, 55–57 cm, USTL 3543; **(9)** *Podocyrtis* (*Podocyrtoges*) *ampla* Ehrenberg, ODP 1260A-10R-6W, 55–57 cm, USTL 3498; **(10)** *Podocyrtis* (*Podocyrtopsis*) *apeza* Sanfilippo and Riedel, ODP 1260A-6R-2W, 55–57 cm, USTL 3421; **(11)** *Dorcadospyris anastasis* Sanfilippo *in* Nigrini et al., ODP 1260A-6R-1W, 55–57 cm, USTL 3419; **(12)** *Phormocyrtis embolum* (Ehrenberg), ODP 1260A-13R-1W, 54–55 cm, USTL 3522; **(13)** *Thyrsocyrtis* (*Pentalocorys*) *tetracantha* (Ehrenberg), ODP 1260A-6R-2W, 55–57 cm, USTL 3420; **(14)** *Thyrsocyrtis* (*Pentalocorys*) *krooni* Sanfilippo and Blome (= *Thyrsocyrtis* (*P.*) *parvipes* (Ehrenberg) in Chapter II.2), ODP 1260A-6R-2W, 55–57 cm, USTL 3421; **(15)** *Lithostrobus picus* (Ehrenberg), ODP 1260A-13R-4W, 55–57 cm, USTL 2854; **(16)** *Dendrospyris fragoides* Sanfilippo and Riedel, ODP 1260A-9R-3W, 55–57 cm, USTL 3478; **(17)** *Dendrospyris golli* Nishimura, ODP 1260A-15R-4W, 55–57 cm, USTL 3550; **(18)** *Semantidium haeckelii* (Bütschli), ODP 1260A-9R-3W, 55–57 cm, USTL 3477; **(19)** *Dorcadospyris ombros* Sanfilippo *in* Nigrini et al., ODP 1260A-7R-6W, 54–56 cm, USTL 3454; **(20)** *Dorcadospyris confluens* (Ehrenberg), ODP 1260A-6R-1W, 55–57 cm, USTL 3419; **(21)** *Petalospyris flabellum* Ehrenberg, ODP 1260A-10R-6W, 55–57 cm, USTL 3498; **(22)** *Petalospyris diaboliscus* Ehrenberg, ODP 1260A-6R-1W, 55–57 cm, USTL 3419; **(23)** *Artophormis barbadensis* (Ehrenberg), ODP 1260A-6R-2W, 55–57 cm, USTL 3420. All scale bars equal 50 µm.

Occurrence at Hole 1260A: Base: from sample ODP 1260A-8R-6W, 54–56 cm (66.85 rmcd) to sample ODP 1260A-9R-1W, 55–57 cm (65.74 rmcd). Top: from sample ODP 1260A-8R-3W, 54–56 cm (61.24 rmcd) to sample ODP 1260A-7R-6W, 54–56 cm (56.04 rmcd).

Estimated age: From 41.15 Ma to 40.84 Ma in the equatorial Atlantic (Westerhold and Röhl, 2013), and from 41.2 Ma to 40.4 Ma in the equatorial Pacific (Kamikuri et al., 2012a; revised ages in this study); middle Eocene (late Lutetian to early Bartonian).

Magnetostratigraphic calibration: The base of the zone falls within Chron C19n, and the top within Chron C18r at both the Atlantic (this study in combination with Suganuma and Ogg, 2006) and Pacific sites (Kamikuri et al., 2012a; revised calibration in this study).

Remarks: The basal datum is synchronous with the FOs of *Dictyopodium* aff. *eurylophus* in ODP Hole 1260A. This subzone corresponds to the uppermost part of the planktic foraminiferal

Zone P12, and the nannofossil Zone NP16. The Lutetian–Bartonian boundary is found in this subzone.

RP14 – *Podocyrtis* (*Lampterium*) *mitra* Lineage Zone

(Riedel and Sanfilippo, 1970, 1978)

Definition: Biostratigraphic interval between the ET from *Podocyrtis* (*Lampterium*) *sinuosa* Ehrenberg, 1874 to *Podocyrtis* (*Lampterium*) *mitra* Ehrenberg, 1854 (base) and the ET from *Podocyrtis* (*Lampterium*) *mitra* Ehrenberg, 1854 to *Podocyrtis* (*Lampterium*) *chalara* Riedel and Sanfilippo, 1970 (top).

Occurrence at Hole 1260A: Base: from sample ODP 1260A-13R-5W, 54–56 cm (111.24 rmcd) to sample ODP 1260A-13R-4W, 55–56 cm (109.75 rmcd). Top: from sample ODP 1260A-9R-1W, 55–57 cm (66.85 rmcd) to sample ODP 1260A-8R-6W, 54–56 cm (65.74 rmcd).

Estimated age: From 42.98 Ma to 41.15 Ma in the equatorial Atlantic (Westerhold and Röhl, 2013), and from 43.2 Ma to 41.2 Ma in the equatorial Pacific (Kamikuri et al., 2012a; revised ages in this study); middle Eocene (late Lutetian).

Magnetostratigraphic calibration: The base of the zone is placed within Chron C20n, and the top within Chron C19n at both the Atlantic (this study in combination with Suganuma and Ogg, 2006) and Pacific sites (Kamikuri et al., 2012a; revised calibration in this study).

Secondary bioevents. Sixteen FOs (*Dendrospyris fragoides*, *Podocyrtis* (*P.*) *apeza*, *Zealithapium mitra*, *Dictyoprora ovata* group, *Sethochytris triconiscus*, *Histiastrum* sp. A[8], *Podocyrtis* (*L.*) *fasciolata*, *Podocyrtis* (*L.*) *trachodes*, *Theocorys anapographa* var. A, *Dorcadospyris confluens*, *Dictyoprora pirum*, *Apoplanius asperus*, *Apoplanius kerasperus*,

8 *Histiastrum coronatum* Haeckel, 1887 in Chapter II.2.

Artophormis barbadensis, *Carpocanopsis ornatum* and *Podocyrtis* (*L.*) *mitra*), fifteen LOs (*Phormocyrtis embolum*, *Podocyrtis* (*L.*) *trachodes*, *Theocorys* ? *scolopax*, *Lophocyrtis alauda*, *Lychnocanium pileatum*, *Podocyrtis* (*P.*) *ampla*, *Podocyrtis* (*L.*) *fasciolata*, *Zealithapium anoectum*, *Podocyrtis* (*L.*) *sinuosa*, *Pterocyrtidium barbadense*, *Eusyringium lagena*, *Zealithapium plegmacantha*, *Dendrospyris golli*, *Coccolarnacium periphaenoides*, *Entapium regulare*).

Remarks: This zone is the longest in ODP Hole 1260A, covering 46% of the studied interval and containing nearly half of the recognized bioevents. The radiolarian Zone RP14 correlates with the planktic foraminiferal Zone P12 and the nannofossil Zone NP16. This zone is subdivided into three subzones.

RP14c – *Podocyrtis* (*Podocyrtopsis*) *apeza* Interval Subzone

new subzone

Definition: Biostratigraphic interval between the FO of *Podocyrtis* (*Podocyrtopsis*) apeza Sanfilippo and Riedel, 1992 (base) and the ET from *Podocyrtis* (*Lampterium*) *mitra* Ehrenberg, 1854 to *Podocyrtis* (*Lampterium*) *chalara* Riedel and Sanfilippo, 1970 (top).

Occurrence at Hole 1260A: Base: from sample ODP 1260A-10R-5W, 55–57 cm (83.33 rmcd) to sample ODP 1260A-10R-3W, 55–57 cm (80.33 rmcd). Top: from sample ODP 1260A-9R-1W, 55–57 cm (66.85 rmcd) to sample ODP 1260A-8R-6W, 54–56 cm (65.74 rmcd).

Estimated age: From 41.79 Ma to 41.15 Ma in the equatorial Atlantic (Westerhold and Röhl, 2013), and from 41.6 Ma to 41.2 Ma in the equatorial Pacific (Kamikuri et al., 2012a; revised ages in this study); middle Eocene (late Lutetian).

Magnetostratigraphic calibration: The base of the zone is within Chron C19r, and the top is within Chron C19n at both the Atlantic (this study in combination with Suganuma and Ogg, 2006) and Pacific sites (Kamikuri et al., 2012a; revised calibration in this study).

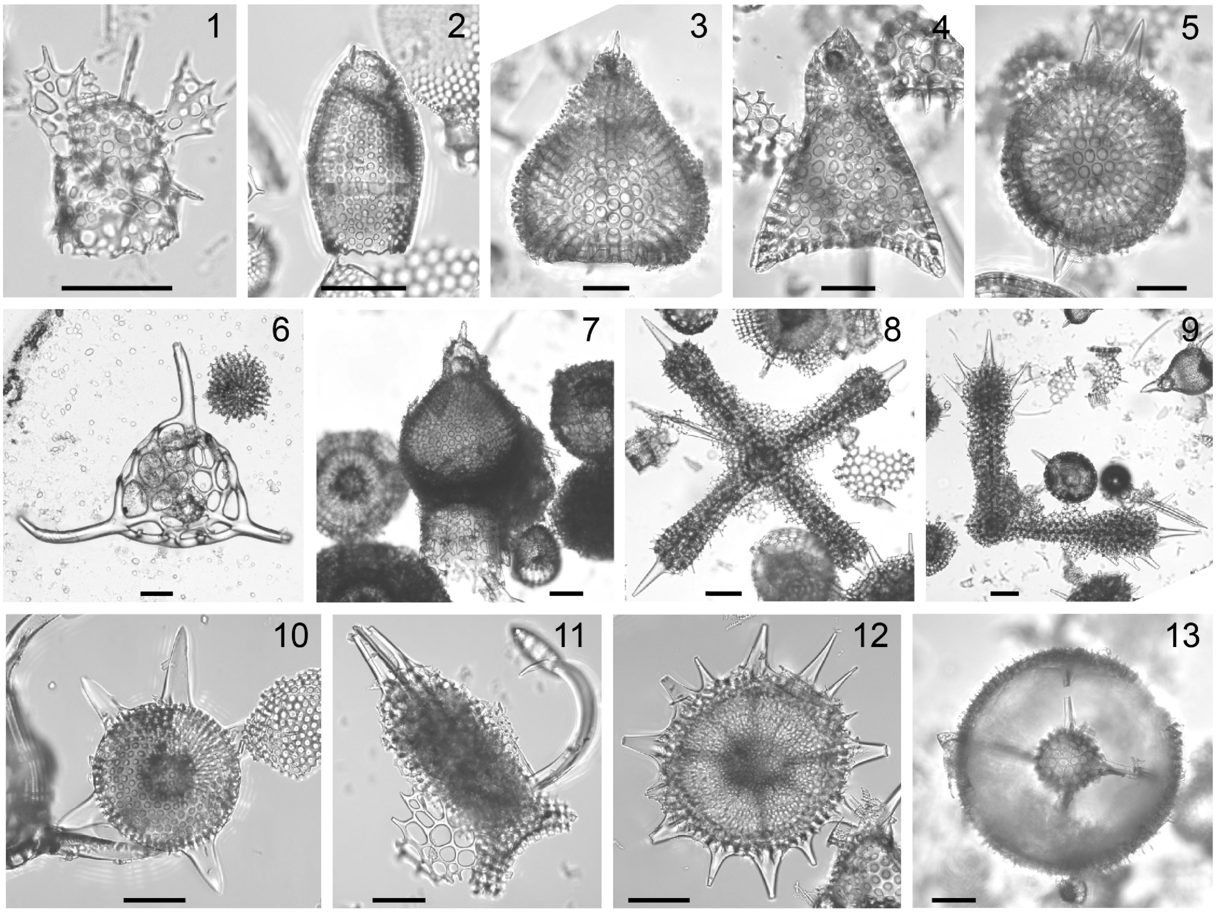

Plate III.3. Composite light micrographs of selected radiolarians from ODP hole 1260A. **(1)** *Lophophaena radians* Ehrenberg, ODP 1260A-9R-3W, 55–57 cm, USTL 3477; **(2)** *Carpocanopsis ornata* (Ehrenberg), ODP 1260A-6R-2W, 55–57 cm, USTL 3420; **(3)** *Theocotylissa ficus* (Ehrenberg), ODP 1260A-15R-2W, 55–57 cm, USTL 3543; **(4)** *Lithochytris vespertilio* Ehrenberg (= *Lithochytris pyramidalis* Ehrenberg in Chapter II.2), ODP 1260A-16R-1W, 55–57 cm, USTL 3558; **(5)** *Stylosphaera* ? *agdaraensis* (Mamedov), ODP 1260A-15R-2W, 55–57 cm, USTL 3543; **(6)** *Dictyophimus craticula* Ehrenberg, ODP 1260A-15R-4W, 55–57 cm, USTL 3551; **(7)** *Anthocyrtoma* spp., ODP 1260A-13R-4W, 55–57 cm, USTL 2854; **(8)** *Histiastrum quaternarium* Ehrenberg, ODP 1260A-13R-5W, 54–56 cm, USTL 3525; **(9)** *Histiastrum* sp. A (= *Histiastrum coronatum* Haeckel in Chapter II.2), ODP 1260A-6R-1W, 55–57 cm, USTL 3419; **(10)** *Periphaena pentasteriscus* (Clark and Campbell), ODP 1260A-6R-2W, 55–57 cm, USTL 3422; **(11)** *Lithocyclia aristotelis* (Ehrenberg) group, ODP 1260A-6R-3W, 55–57 cm, USTL 3425; **(12)** *Coccolarnacium periphaenoides* Dumitrică, ODP 1260A-13R-2W, 54–55 cm, USTL 2852; **(13)** *Entapium regulare* Sanfilippo and Riedel, ODP 1260A-14R-6W, 55–57 cm, USTL 3537. All scale bars equal 50 μm.

Remarks: The base of the subzone is characterized by the FO of *Podocyrtis* (*P.*) *apeza*, which is isochronous between ODP Hole 1260A (41.79 Ma), IODP Sites U1331, U1332, and U1333

(41.6 Ma), and IODP Site U1403 (41.94 Ma). The basal datum is approximately synchronous with a significant faunal turnover involving the FOs of *Podocyrtis* (*P.*) *apeza* and *Zealithapium mitra*, and the LOs of *Lophocyrtis alauda*, *Lychnocanium pileatum*, *Podocyrtis* (*P.*) *ampla*, *Podocyrtis* (*L.*) *fasciolata* and *Zealithapium anoectum*. This subzone correlates with the upper part of planktic foraminiferal Zone P12 and the nannofossil Zone NP16 in ODP Hole 1260A.

RP14b – *Sethochytris triconiscus* Interval Subzone

new subzone

Definition: Biostratigraphic interval between the FO of *Sethochytris triconiscus* Haeckel, 1887 (base) and the FO of *Podocyrtis* (*Podocyrtopsis*) *apeza* Sanfilippo and Riedel, 1992 (top).

Occurrence at Hole 1260A: Base: from sample ODP 1260A-11R-3W, 55–57 cm (89.55 rmcd) to sample ODP 1260A-11R-2W, 55–57 cm (88.05 rmcd). Top: from sample ODP 1260A-10R-5W, 55–57 cm (83.33 rmcd) to sample ODP 1260A-10R-3W, 55–57 cm (80.33 rmcd).

Estimated age: 42.08 Ma to 41.79 Ma in the equatorial Atlantic (Westerhold and Röhl, 2013), and 42.1 Ma to 41.9 Ma in the equatorial Pacific (Kamikuri et al., 2012a; revised ages in this study); middle Eocene (Lutetian).

Magnetostratigraphic calibration: The new subzone falls completely whithin Chron C19r at both the Atlantic (this study in combination with Suganuma and Ogg, 2006) and Pacific sites (Kamikuri et al., 2012a; revised calibration in this study).

Remarks: The base of the subzone is characterized by the FO of *Sethochytris triconiscus*, which is isochronous between ODP Hole 1260A (42.08 Ma) and IODP Sites U1331, U1332 and U1333 (42.1 Ma). The basal datum is synchronous with the FO of *Dictyoprora ovata* group in ODP Hole 1260A. The *Sethochytris triconiscus* Subzone is correlated with the planktic foraminiferal Zone P12 and the nannofossil Zone NP16.

RP14a – *Artostrobus quadriporus* Interval Subzone

new subzone

Definition: Biostratigraphic interval between the ET from *Podocyrtis* (*Lampterium*) *sinuosa* Ehrenberg, 1874 to *Podocyrtis* (*Lampterium*) *mitra* Ehrenberg, 1854 (base) and the FO of *Sethochytris triconiscus* Haeckel, 1887 (top).

Occurrence at Hole 1260A: Base: from sample ODP 1260A-13R-5W, 54–56 cm (111.24 rmcd) to sample ODP 1260A-13R-4W, 55–56 cm (109.75 rmcd). Top: from sample ODP 1260A-11R-3W, 55–57 cm (89.55 rmcd) to sample ODP 1260A-11R-2W, 55–57 cm (88.05 rmcd).

Estimated age: From 42.98 Ma to 42.08 Ma in the equatorial Atlantic (Westerhold and Röhl, 2013), and from 43.2 Ma to 42.1 Ma in the equatorial Pacific (Kamikuri et al., 2012a; revised ages in this study); middle Eocene (Lutetian).

Magnetostratigraphic calibration: The base of the zone is located within Chron C20n, and the top is whithin Chron C19r at both the Atlantic (this study in combination with Suganuma and Ogg, 2006) and Pacific sites (Kamikuri et al., 2012a; revised calibration in this study).

Remarks: The basal datum is nearly synchronous with the FO of *Artostrobus quadriporus* in ODP Hole 1260A. This subzone correlates with the planktic foraminiferal Zone P12 and the lower part of the nannofossil Zone NP16.

RP13 – *Podocyrtis* (*Podocyrtoges*) *ampla* Lineage Zone

(Riedel and Sanfilippo, 1970, 1978)

Definition: Biostratigraphic interval between the ET from *Podocyrtis* (*Podocyrtoges*) *phyxis* Sanfilippo and Riedel, 1973 to *Podocyrtis* (*Podocyrtoges*) *ampla* Ehrenberg, 1874 (base) and the ET from *Podocyrtis* (*Lampterium*) *sinuosa* Ehrenberg, 1874 to *Podocyrtis* (*Lampterium*) *mitra* Ehrenberg, 1854 (top).

Occurrence at Hole 1260A: Base: from sample ODP 1260A-15R-3W, 55–57 cm (128.97 rmcd) to sample ODP 1260A-15R-2W, 55–57 cm (127.47 rmcd). Top: from sample ODP 1260A-13R-5W, 54–56 cm (111.24 rmcd) to sample ODP 1260A-13R-4W, 54–56 cm (109.75 rmcd).

Estimated age: From 43.67 Ma to 42.98 Ma in the equatorial Atlantic (Westerhold and Röhl, 2013), and from 43.9 Ma to 43.2 Ma in the equatorial Pacific (Kamikuri et al., 2012a; revised ages in this study); middle Eocene (middle Lutetian).

Magnetostratigraphic calibration: The base of this zone lies within the upper part of Chron C20r, and the top within the lower part of Chron C20n at both the Atlantic (this study in combination with Suganuma and Ogg, 2006) and Pacific sites (Kamikuri et al., 2012a; revised calibration in this study).

Secondary bioevents: Nine FOs (*Artostrobus quadriporus*, *Coccolarnacium periphaenoides*, *Lithostrobus picus*, *Lophophaena radians*, *Lychnocanium pileatum*, *Pterocyrtidium barbadense*, *Pteropilium* ? *contiguum*, *Semantidium haeckelii* and *Siphocampe* ? *elegans*) and four LOs (*Dictyomitra parva*, *Podocyrtis* (*P.*) *diamesa*, *Podocyrtis* (*P.*) *phyxis* and *Stylosphaera* ? *agdaraensis*).

Remarks: The basal datum is approximately synchronous with the LO of the planktic foraminiferal species *Morozovella aragonensis*, which defines the base of Zone P12. The *Podocyrtis* (*P.*) *ampla* Zone corresponds to the lowermost part of the planktic foraminiferal Zone P12, and to the uppermost part of the nannofossil Zone NP15 to the lowermost part of Zone NP16. This zone is divided into a lower (a) and a upper (b) subzones.

RP13b - *Coccolarnacium periphaenoides* Interval Subzone

new subzone

Definition: Biostratigraphic interval between the LO of *Podocyrtis* (*Podocyrtoges*) *phyxis* Sanfilippo and Riedel, 1973 (base) and the ET from *Podocyrtis* (*Lampterium*) *sinuosa* Ehrenberg, 1874 to *Podocyrtis* (*Lampterium*) *mitra* Ehrenberg, 1854 (top).

Occurrence at Hole 1260A: Base: from sample ODP 1260A-14R-7W, 55–57 cm (125.02 rmcd) to sample ODP 1260A-14R-6W, 55–57 cm (123.52 rmcd). Top: from sample ODP 1260A-13R-5W, 54–56 cm (111.24 rmcd) to sample ODP 1260A-13R-4W, 55–56 cm (109.75 rmcd).

Estimated age: From 43.48 Ma to 42.98 Ma in the equatorial Atlantic (Westerhold and Röhl, 2013), and from 43.6 Ma to 43.2 Ma in the equatorial Pacific (Kamikuri et al., 2012a; revised ages in this study); middle Eocene (middle Lutetian).

Magnetostratigraphic calibration: The subzone falls completely within Chron C20n at both the Atlantic (this study in combination with Suganuma and Ogg, 2006) and Pacific sites (Kamikuri et al., 2012a; revised calibration in this study).

Remarks: This subzone roughly corresponds to the stratigraphic extension of *Coccolarnacium periphaenoides* in ODP Hole 1260A. The FO of the nannofossil species *Nannotetrina fulgens*, which defines the base of Zone NP16 is recorded in this subzone. This subzone correlates with the lowermost part of planktic foraminiferal Zone P12, and the uppermost part of the nannofossil Zone NP15 correlates with the lowermost part of Zone NP16.

RP13a – *Dictyomitra parva* Interval Subzone

new subzone

Definition: Biostratigraphic interval between the ET from *Podocyrtis* (*Podocyrtoges*) *phyxis* Sanfilippo and Riedel, 1973 to *Podocyrtis* (*Podocyrtoges*) *ampla* Ehrenberg, 1874 (base) and the LO of *Podocyrtis* (*Podocyrtoges*) *phyxis* Sanfilippo and Riedel, 1973 (top).

Occurrence at Hole 1260A: Base: from sample ODP 1260A-15R-3W, 55–57 cm (128.97 rmcd) to sample ODP 1260A-15R-2W, 55–57 cm (127.47 rmcd). Top: from sample ODP 1260A-14R-7W, 55–57 cm (125.02 rmcd) to sample ODP 1260A-14R-6W, 55–57 cm (123.52 rmcd).

Estimated age: From 43.67 Ma to 43.48 Ma in the equatorial Atlantic (Westerhold and Röhl, 2013), and from 43.9 Ma to 43.6 Ma in the equatorial Pacific (Kamikuri et al., 2012a; revised ages in this study); middle Eocene (middle Lutetian).

Magnetostratigraphic calibration: The subzone falls completely within Chron C20r at both the Atlantic (this study in combination with Suganuma and Ogg, 2006) and Pacific sites (Kamikuri et al., 2012a; revised calibration in this study).

Remarks: This subzone corresponds to the interval where *Podocyrtis* (*P.*) *phyxis* and its descendant *Podocyrtis* (*P.*) *ampla* occur together. The artostrobiid *Dictyomitra parva* was abundant throughout this subzone, before its sudden extinction in the lower part of the *Coccolarnacium periphaenoides* Subzone. This subzone correlates with the uppermost part of the planktic foraminiferal Zone P11 to the lowermost part of Zone P12, and to the nannofossil Zone NP15.

RP12 – *Thyrsocyrtis* (*Pentalocorys*) *triacantha*[9] Lineage Zone

(Riedel and Sanfilippo, 1970 emend. Riedel and Sanfilippo, 1978)

Definition: Biostratigraphic interval between the FO of *Eusyringium lagena* (Ehrenberg, 1874) (base) and the ET from *Podocyrtis* (*Podocyrtoges*) *phyxis* Sanfilippo and Riedel, 1973 to *Podocyrtis* (*Podocyrtoges*) *ampla* Ehrenberg, 1874 (top).

Occurrence at Hole 1260A: The top of this zone is located between samples ODP 1260A-15R-3W, 55–57 cm (128.97 rmcd) and ODP 1260A-15R-2W, 55–57 cm (127.47 rmcd).

Estimated age: The top of the zone is dated 43.67 Ma in the equatorial Atlantic (Westerhold and Röhl, 2013) and 43.9 Ma in the equatorial Pacific (Kamikuri et al., 2012a; revised age in this study); middle Eocene (Lutetian).

Magnetostratigraphic calibration: The top of this zone is placed within the upper part of Chron C20r at both the Atlantic (this study in combination with Suganuma and Ogg, 2006) and Pacific sites (Kamikuri et al., 2012a; revised calibration in this study).

Remarks: Only the very end of Zone RP12 was found in the studied interval, and it contains no secondary bioevents. Due to the poor recovery of cores 16R and 17R (10.2% and 50.5%, respectively), we decided to stop the sampling at 130.47 rmcd (ODP sample 1260A-15R-4W, 55–57 cm). The end of the radiolarian Zone RP12 correlates with the upper part of the planktic foraminiferal Zone P11 and the nannofossil Zone NP15.

III.4. Discussion

A total of 71 radiolarian bioevents have been identified in the middle Eocene of the equatorial Atlantic Ocean, and calibrated to the Geomagnetic Polarity and Astronomical Time Scales. Our study represents the first attempt to directly calibrate radiolarian bioevents to the Astronomical

9 *Thyrsocyrtis* (*Pentalacorys*) *schomburgkii* (Ehrenberg, 1847) in Chapter II.2.

Time Scale and to assign absolute ages to middle Eocene radiolarian bioevents with an unprecedented resolution. Some species described in very early studies (e.g., Ehrenberg, 1874) are calibrated for the first time in this study. We chose to include them in our analysis in order to increase the number of well-constrained calibration points available to produce age-depth models for the equatorial Atlantic. However, given the limited information available on these species, the assessment of their usefulness for correlations could not be evaluated here; this task requires additional biostratigraphic studies over a broad geographic area.

Comparison of our results with the equatorial Pacific radiolarian record demonstrates the synchronicity of primary radiolarian bioevents that underpin the middle Eocene tropical zonal scheme by means of independent correlational techniques (i.e., paleomagnetic stratigraphy and cyclostratigraphy). These observations reinforce the robustness of the previously established low-latitude radiolarian biozonation and demonstrate its reliability over a large oceanic area. Seven secondary bioevents are also found to be synchronous between the equatorial regions of the Atlantic and Pacific Oceans, and three secondary bioevents between the low and mid–latitudes of the North Atlantic Ocean, making them valuable for correlations. Four of these synchronous bioevents were used for the subdivision of zones RP13, RP14, and RP15 into seven new subzones. The selection of the bioevents used to define these new subzones was motivated by the abundance of associated marker species, their ease of identification, and the overall consistency of their stratigraphic range accros different low-latitude sections (Riedel and Sanfilippo, 1970; Moore, 1971; Dinkelman, 1973; Nigrini et al., 2005). Although the FO of *Podocyrtis* (*P.*) *apeza*, which defines the base of Subzone RP14c, and the LO of *Rhopalosyringium* ? *biauritum*, which defines the base of Subzone RP15b, are synchronous between low et mid–latitudes in the North Atlantic Ocean, the new biostratigraphic scheme is restricted to the low latitudes. As a consequence of biogeographically controlled variations in the stratigraphic range of the species, no primary bioevents for the late Middle Eocene were observed at IODP Site U1403, and the degree of synchroneity of these bioevents with the low latitudes of the Atlantic Ocean could not be tested. In addition, *Podocyrtis* (*P.*) *phyxis*, the first occurrence of which serves as the basal datum for Subzone RP13b, is also a species with tropical affinities. To date, it has only been reported from a few low-latitude sites (e.g., Riedel and Sanfilippo, 1973; Sanfilippo and Riedel, 1973; Johnson, 1974; Renz, 1984; Nigrini et al., 2005) and a single mid-latitude site located in the South Atlantic Ocean (de Souza et al., 2017).

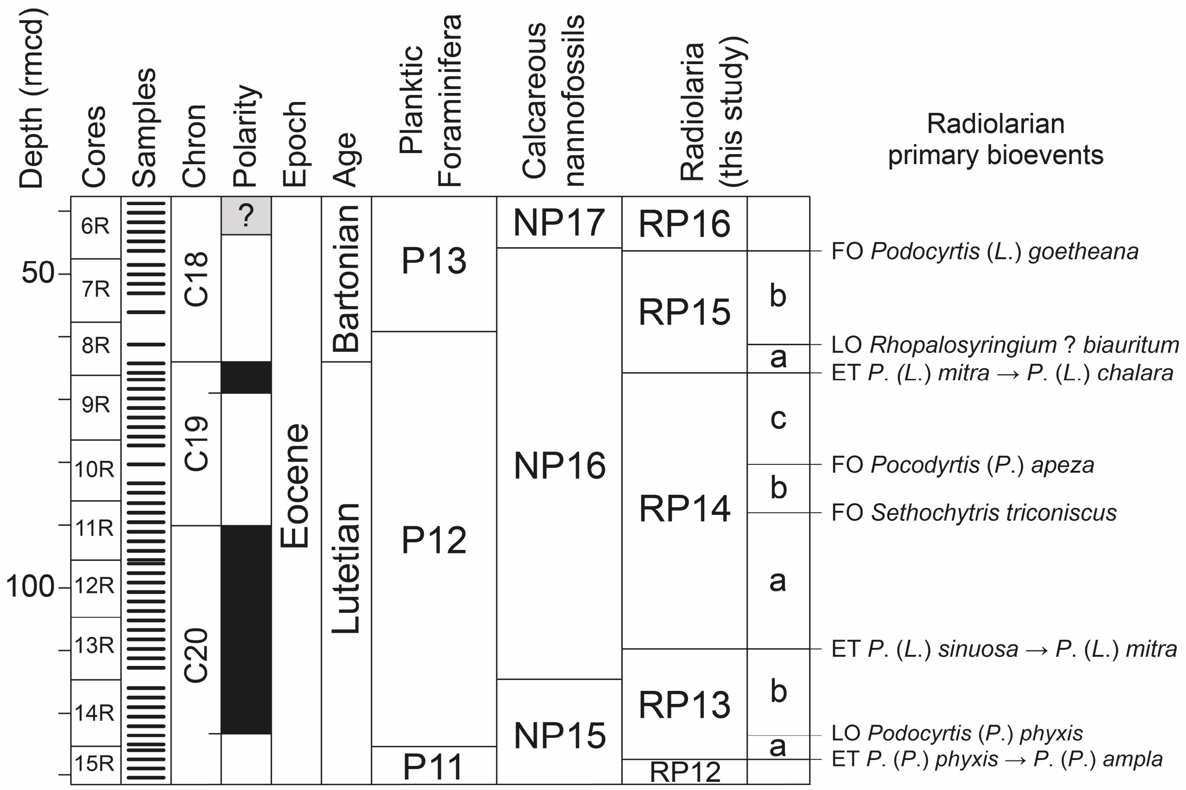

Figure III.5. Biostratigraphic summary of calcareous and siliceous microfossils at ODP Site 1260 after the biostratigraphic results of the Shipboard Scientific Party (2004) and of this study, including the newly defined radiolarian subzones. The geomagnetic timescale used is from Suganuma and Ogg (2006). FO: first occurrence, LO: last occurrence, ET: evolutionary transition.

The new biostratigraphic scheme proposed here allows a substantial increase in the stratigraphic resolution that can be offered in the low latitudes for the middle Eocene. The mean duration of a biostratigraphic unit is about 525 kyr for a middle Eocene biozonation based on radiolarian bioevents, while it is about 1.28 Ma for biozonations based on planktic foraminifera (Wade et al., 2011) and 1.27 Ma for biozonations based on nannofossils (Agnini et al., 2014). Radiolarians are therefore amongst the most accurate biostratigraphic microfossils for the period of interest. Future advances in astronomical dating will allow the extension of the astronomical calibration of radiolarian bioevents to the entire Cenozoic era to obtain a global and consistent biochronological framework, as it has already been achieved for planktic foraminifera (Wade et al., 2011). The development of such a high-resolution temporal framework for Cenozoic radiolarians will benefit a wide range of macroevolutionary studies, including the search for changes in radiolarian diversity or disparity, as well as the study of their ecological response to past climatic events.

On the other hand, two-thirds of the studied radiolarian bioevents were found to be moderately to highly diachronous between the equatorial regions of the Atlantic and Pacific Oceans, as well as three-quarters of the studied bioevents between the low and mid–latitudes of the North Atlantic Ocean. In contrast to previous biostratigraphic analyses carried out in the Indo-Pacific, we found no asymetric distribution of diachronous events between first occurrences and last occurrences (Johnson and Nigrini, 1985a; Nigrini and Caulet, 1992). Hence, among radiolarian datums, first occurrences do not seem to be less reliable for correlations than last occurrences.

The diachroneity of bioevents between sedimentary sections is a common phenomenon in biostratigraphy. In addition to reasons related to the biogeographic dynamics, diachroneity may be the result of a number of different other factors, including differences in sampling intensity, in quality of stratigraphic and age controls, as well as biases in preservation, bioturbation, or errors in species identification. These factors are largely independent of radiolarian biogeography and could lead to an apparent diachronism that is not due to differences in the stratigraphic range of species between different geographic areas. Diachronous bioevents may also be subject to ecological control as it has been amply demonstrated at different scales in radiolarians (e.g., Johnson and Nigrini, 1985a, b; Spencer-Cervato et al., 1993, 1994). In some well-constrained cases, diachronism has been explained by particular environmental conditions, such as in upwelling zones (Nigrini and Caulet, 1992), by large-scale changes in the boundaries of oceanic currents (Moore et al., 1993), or by the discontinuous nature of the stratigraphic range of some species due to local shifts in environmental conditions (Nigrini et al., 2005). The observed patterns of diachroneity between ODP Site 1260, IODP Site U1403, and IODP Sites U1331, 1332, and 1333 are difficult to explain in terms of ecological or paleoceanographic processes, due to the complexity of disentangling radiolarian migration pathways from such a limited spatial coverage. Although a number of radiolarian species first appear in the equatorial Atlantic Ocean and then in the equatorial Pacific, there is no convincing evidence for diachroneity due to interoceanic migration.

III.5. Conclusions

This study examined the stratigraphic range of 61 middle Eocene radiolarian species from the equatorial ODP Site 1260, which preserves an expanded and well-preserved siliceous record. Taking advantage of the unique time framework provided by previous magnetostratigraphic and cyclostratigraphic work conduced on the studied site, our results are placed in a very precise astronomical time frame. The absolute ages of 71 radiolarian bioevents were refined, improving the age control of equatorial Atlantic sections of middle Eocene age and providing new calibration points for the application of age-depth models in future studies. Future macroevolutionary studies of Eocene radiolarians may also benefit from this well-constrained temporal framework.

Subsequently, by comparison with the equatorial Pacific record, we demonstrated the synchronicity of primary radiolarian bioevents that underpin the middle Eocene zonal scheme, thereby reinforcing the robustness of the tropical radiolarian biozonation. Several secondary bioevents were also found to be synchronous between the equatorial regions of the Atlantic and Pacific Oceans and between low and mid–latitudes of the Atlantic Ocean. These bioevents were used to subdivide zones RP13, RP14 and RP15 into seven new subzones: *Dictyomitra parva* Interval Subzone (RP13a), *Coccolarnacium periphaenoides* Interval Subzone (RP13b), *Artostrobus quadriporus* Interval Subzone (RP14a), *Sethochytris triconiscus* Interval Subzone (RP14b), *Podocyrtis* (*Podocyrtopsis*) *apeza* Interval Subzone (RP14c), *Rhopalosyringium* ? *biauritum* Interval Subzone (RP15a) and *Thyrsocyrtis* (*Pentalocorys*) *krooni*[10] Interval Subzone (RP15b). On the other hand, numerous bioevents are shown to be highly diachronous between the two oceans, with generally older appearance and disappearance dates in the Atlantic. Although it is difficult to fully explain the observed patterns of diachroneity, recognition of age-transgressive bioevents in radiolarians could have implications for our understanding of plankton migration pathways between the Atlantic and Pacific Oceans.

Data availability.

Illustrated specimens are housed in the paleontological collection of the University of Lille, Villeneuve-d'Ascq, France.

10 *Thyrsocyrtis* (*Pentalocorys*) *parvipes* (Ehrenberg, 1874) in Chapter II.2.

Author contribution.

T.D. designed and directed the project. **M.M.** was responsible for the data acquisition, analysis, and drawing of figures. The interpretation of data and discussion of results were conducted by both authors. **M.M**. wrote the manuscript, in consultation with **T.D.**

Competing interests.

The authors declare that they have no conflict of interest.

Acknowledgments.

We thank Christopher J. Hollis and an anonymous reviewer for their constructive remarks. The authors are also indebted to the Ocean Drilling Program (ODP) for supplying the samples used in this study.

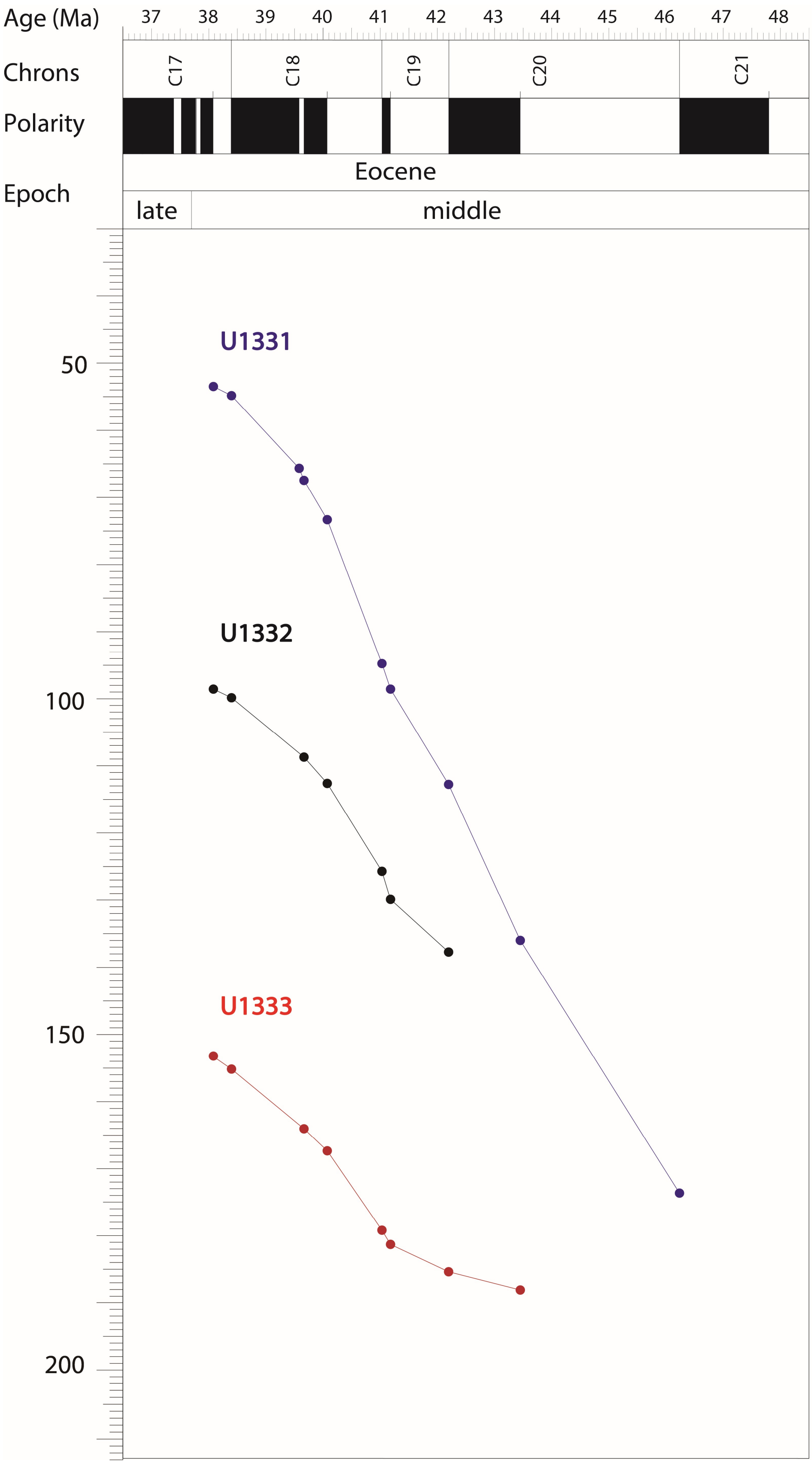

Supplementary Figure III.1. Revised age–depth models for the IODP Sites U1331, U1332, and U1333 (eastern equatorial Pacific, expedition 320, "Pacific Equatorial Age Transect I").

Chapter IV – Biotic impacts of the Middle Eocene Climate Optimum (MECO)

This chapter includes two distinct articles. The first article, titled **“No dramatic changes observed in subtropical radiolarian plankton assemblages during the Middle Eocene Climatic Optimum (MECO); evidence from the North Atlantic ODP Site 1051”** was published in the journal Marine Micropaleontology, and is available online at DOI: https://doi.org/10.1016/j.marmicro.2023.102272. The second article, submitted to the journal Palaeogeography, Palaeoclimatology, Palaeoecology, is an original manuscript titled **“Morphological responses of the plankton to the Middle Eocene Climatic Optimum (MECO): The case of the radiolarian species *Podocyrtis papalis* from the western equatorial Atlantic (ODP Site 1260)”**.

IV.1. No dramatic changes observed in subtropical radiolarian plankton assemblages during the Middle Eocene Climatic Optimum (MECO); Evidence from the North Atlantic ODP Site 1051

Mathias Meunier* and Taniel Danelian

Univ. Lille, CNRS, UMR 8198 – Evo-Eco-Paleo, F-59000 Lille, France

<mathias.meunier@univ-lille.fr>

*Corresponding author

Abstract

The Middle Eocene Climatic Optimum (MECO; ca. 40 Ma) was a prominent global warming event that lasted 400 kyr and was characterized by a 4–6 ◦C increase in high-latitude surface and deep-water temperatures. Since the radiolarian plankton response to this warming event is largely unknown, whole-assemblage quantitative analyses were performed on well-preserved radiolarian assemblages from ODP Site 1051 (western North Atlantic). Although radiolarians at site site apparently benefited from an increase in oceanic fertility induced by the MECO, this event does not appear to have had a severe impact on subtropical radiolarian fauna. No significant faunal turnover was found in the studied interval, suggesting that subtropical radiolarians are relatively resilient to transient warming events. Similarly, variations in radiolarian assemblage composition indicate weak ecological responses to ocean warming. One of the most striking faunal changes associated with the MECO is the clear increase in radiolarian diversity (taxic richness), as a result of the northward migration of warm tropical radiolarian species. Likewise, several typical middle Eocene tropical species are found to be more abundant in the warmest interval. In addition to these poleward migrations, we identified three radiolarian clusters composed of warm-water or cool-water species, as well as two abundant artostrobiid species that may represent nutrient opportunists.

IV.1.1. Introduction

The Eocene epoch (ca. 56–34 million years ago; Ma) is a key period for the understanding of the Cenozoic climate dynamics and the transition from a "warmhouse" to a "coolhouse" climate state. After the early Eocene warmhouse (ca. 56–47 Ma), during which global temperatures were more than 5°C higher than they are today, the Earth underwent a long-term gradual cooling that culminated in a shift to coolhouse conditions around the Eocene-Oligocene boundary (ca. 34 Ma; Zachos et al., 2008; Westerhold et al., 2020; Hutchinson et al., 2021). This middle–late Eocene transitional interval was characterized by the formation of nascent ice sheets in eastern Antarctica and several short-lived warming events (Edgar et al., 2007; Westerhold and Röhl, 2013).

One of them, the Middle Eocene Climatic Optimum (MECO; Bohaty and Zachos, 2003; Bohaty et al., 2009) was a global warming event that occurred during the late middle Eocene (around 40 Ma); it lasted ~400 kyr and resulted to a significant perturbation of the carbon cycle (Edgar et al., 2010; Westerhold and Röhl, 2013). The MECO signature has been identified in the isotopic record of many oceanic sites as a negative shift of ~1.0–1.5‰ in the oxygen isotope ($\delta^{18}O$) values of both benthic foraminiferal and bulk carbonate sediments, which is interpreted as a ~4–6°C rise in high latitude surface and deep water temperatures (Bohaty and Zachos, 2003; Bohaty et al., 2009; Bijl et al., 2010). The warmer interval is marked by a sharp decrease in $\delta^{18}O$ values at ca. 40 Ma (Edgar et al., 2010; Westerhold and Röhl, 2013), and is accompanied at some sites by a weak negative excursion (~0.05‰) in carbon isotope (δ13C) values (Giorgioni et al., 2019). The peak warming phase of the MECO lasted <100 kyr and it was followed by a rapid return to pre-event temperatures (Bohaty et al., 2009; Edgar et al., 2010; Westerhold and Röhl, 2013). The MECO differs from other Paleogene global warming events, such as the Paleocene-Eocene Thermal Maximum (Kennett and Stott, 1991) or the early Eocene hyperthermal events (Lourens et al., 2005; Stap et al., 2010; Sexton et al., 2011) by its relatively long duration, the abruptness of its return to pre-event conditions and the spatial inconsistency of its carbon isotope signature (Giorgioni et al., 2019; Henehan et al., 2020). All these peculiar features make the MECO difficult to interpret, as a result, its triggering mechanism is poorly understood. It is possible that the conjunction of different factors, including volcanic outgassing and a favorable orbital configuration due to a very long eccentricity minimum, played an important role in the rise of the MECO (Henehan et al., 2020). Moreover, the latter occurred between two major carbonate accumulation events (CAE3 and CAE4, Lyle et al., 2005, 2008; Pälike et al., 2012), and is marked by worldwide carbonate dissolution in the deep-sea record, considered to be the result of increased levels of pCO2, which then induced seawater acidification through the entire water column and a deepening of the carbonate compensation depth (Bohaty et al., 2009; Cornaggia et al., 2020).

Significant assemblage changes across the MECO are recorded in several microfossil groups, including planktic and benthic foraminifera (Edgar et al., 2013; Luciani et al., 2010; Boscolo Galazzo et al., 2013, 2015; Moebius et al., 2014, 2015; D'Onofrio et al., 2021), coccolithophorids (Villa et al., 2008; Toffanin et al., 2011), dinocysts (Bijl et al., 2010; Cramwinckel et al., 2019) and diatoms (Renaudie et al., 2010; Witkowski et al., 2014). In contrast, the radiolarian biotic response to the MECO is still very poorly known. Witkowski et al. (2012) documented a high-latitude siliceous plankton assemblage dominated by ebridians and radiolarians (ODP Sites 748 and 749, Kerguelen Plateau) that showed an increase in biosiliceous sedimentation across the MECO interval. Witkowski et al. (2014) have also reported at the mid-latitude ODP Site 1051 (western Atlantic) an increase in the relative abundance of radiolarian skeletons associated with the warmest phase of the MECO event. However, in none of these studies, radiolarians were identified at the species level, hindering any understanding of faunal changes. Only two species-level radiolarian studies have been conducted previously in relation to the MECO, but none of them concerned the mid-latitudes and especially the Blake Nose sediments, which are particularly rich in well-preserved siliceous microfossils. Kamikuri et al. (2013) investigated early to middle Eocene radiolarian assemblages from the eastern equatorial Pacific Ocean (ODP Site U1331), highlighting a decrease in cool-water radiolarian species across the MECO. In addition, Pascher et al. (2015) studied radiolarians from the southwest Pacific Ocean (DSDP Site 277, Campbell Plateau), where they recognized the migration of several tropical radiolarian species to the high latitudes during the MECO. However, only very few stratigraphic levels were investigated in this study and counting was only limited to abundant or biostratigraphically relevant taxa.

Based on a whole assemblage quantitative study of radiolarians from ODP Site 1051 (subtropical Atlantic), this study aims to describe in detail changes in the abundance and assemblage structure of radiolarians across the MECO. The observed changes will be interpreted within the stable isotope paleoclimatic framework established previously for this site and discussed in conjunction with the known record of other microfossil groups.

IV.1.2. Stratigraphic and paleoclimatic framework

ODP Site 1051 (30°03′N, 76°21′W) was drilled on Blake Nose, a submerged peninsula extending from the eastern margin of the Blake Plateau, in the subtropical western North Atlantic Ocean (Figure IV.1.1). A 630 m-thick Paleogene sequence was recovered at this site from two adjacent holes (1051A and 1051B) drilled at a current water depth of ~1983 m below sea level (mbsl) (Norris et al., 1998). During the middle Eocene, the paleodepth of this site was lower bathyal (~1000–2000 mbsl; Norris et al., 1998), with a palaeolatitude of ~25°N (Ogg and Bardot, 2001). The middle Eocene interval of ODP Site 1051 (~370 m-thick) is dominated by nannofossil ooze rich in siliceous microfossils, including abundant and well-preserved radiolarians, diatoms and sponge spicules, and a few rare ebridians, silicoflagellates and endoskeletal dinoflagellates (Norris et al., 1998; Witkowski et al., 2014). Age control for the middle Eocene interval of ODP Site 1051 is provided by biostratigraphy (Norris et al., 1998; Mita, 2001; Sanfilippo and Blome, 2001; Edgar et al., 2010; Witkowski et al., 2020) and magnetostratigraphy (Ogg and Bardot, 2001).

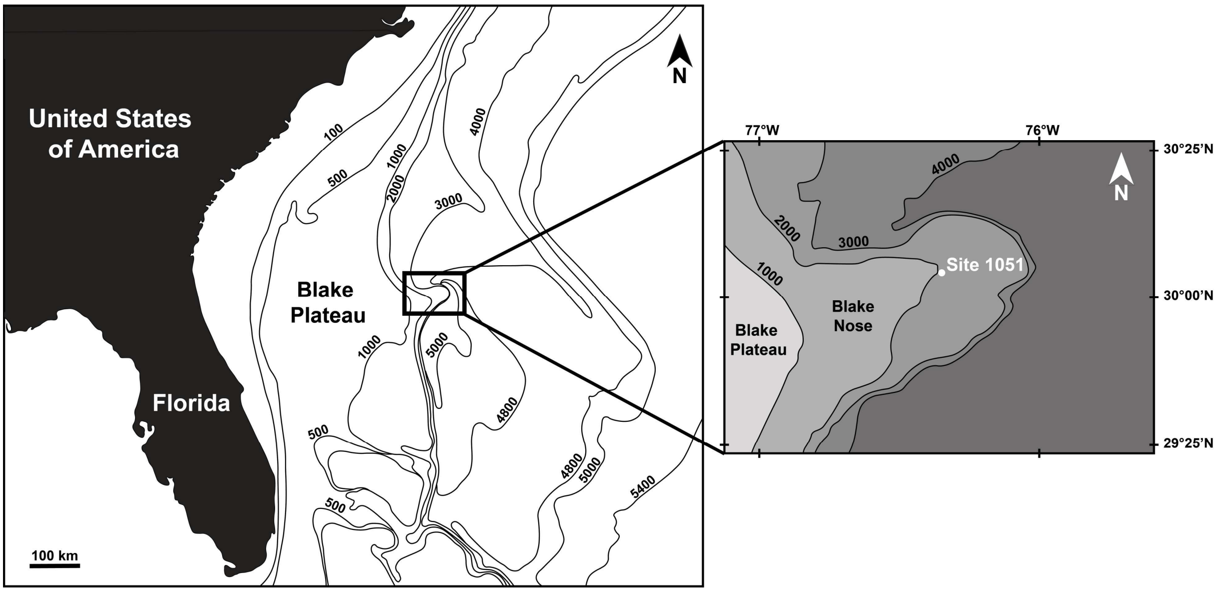

Figure IV.1.1. Location of Blake Nose in the western North Atlantic Ocean (modified from Land et al., 1999). The box shows the detailed location of ODP Site 1051 (Leg 171B) on a bathymetric map (modified from Norris et al., 1998). Bathymetry is in meters.

The middle Eocene sedimentary sequence at ODP Site 1051 is characterized by an overall high sedimentation rate, estimated to be ~4 cm/kyr (Norris et al., 1998; Edgar et al., 2010). A total of 11 samples were selected from hole 1051A, with an average sample spacing of approximately 4.8 m in the MECO interval and an average age difference between two consecutive samples of ~120 kyr. Each sample was approximately 1 cm wide, respresenting an interval of ~250 years. Sampling was as regular as possible to avoid any bias associated with time bins of unequal duration.

At ODP Site 1051, noticeable shifts in both the $\delta^{13}C$ and $\delta^{18}O$ stable isotope records occur within the studied interval and are correlated with the two major phases of the MECO event (Figure IV.1.2; Bohaty et al., 2009; Edgar et al., 2010). The onset of the MECO occurs in the lower part of magnetochron C18r, around 118 mcd (Edgar et al., 2010). Subsequently, the benthic foraminiferal $\delta^{18}O$ record gradually decreased, reaching a brief minimum in the upper part of the magnetochron C18r (ca. 86 mcd), which coincides with an abrupt decrease in $\delta^{13}C$ values (Bohaty et al., 2009; Edgar et al., 2010). This minimum is interpreted as the peak warming condition of the MECO (Figure IV.1.2).

IV.1.3. Material and methods

IV.1.3.1. Sampling interval and sample preparation

Samples were processed according to the method described by Sanfilippo et al. (1985) and Tetard et al. (2020). A small amount (~2 cm2) of unprocessed sediment was collected from each sample and dried overnight at 50 ◦C to remove any residual water. After weighing, sediment samples were soaked for two hours in a 500 mL polypropylene beaker containing 30 mL of 30% hydrochloric acid (HCl) to dissolve their carbonate content and concentrate siliceous microfossils. A few mL of HCl was added at the end of this stage to ensure the end of the reaction. The residues resulting from acidification were then washed by adding ~200 mL of distilled water. After decanting for two hours, the excess water was carefully removed with a pipette. The residues were then soaked for two hours in 30 mL of 10% hydrogen peroxide (H2O2) to remove organic matter. The resulting residues were finally washed through a 45 µm sieve with distilled water and transferred to a storage vial using ethanol. After evaporation, the vial was weighed and the mass of the residues was calculated by subtracting the mass of the empty vial. One slide per sample was prepared from ~3 mg of dry residues randomly settled on a coverslip, following the method described by Witkowski et al. (2012). After drying, the coverslips were mounted on standard glass slides using Eukitt mounting medium (refractive index = 1.49). The weight of the residue used to prepare each slide was then calculated by subtracting the weight of the storage vial before and after sampling.

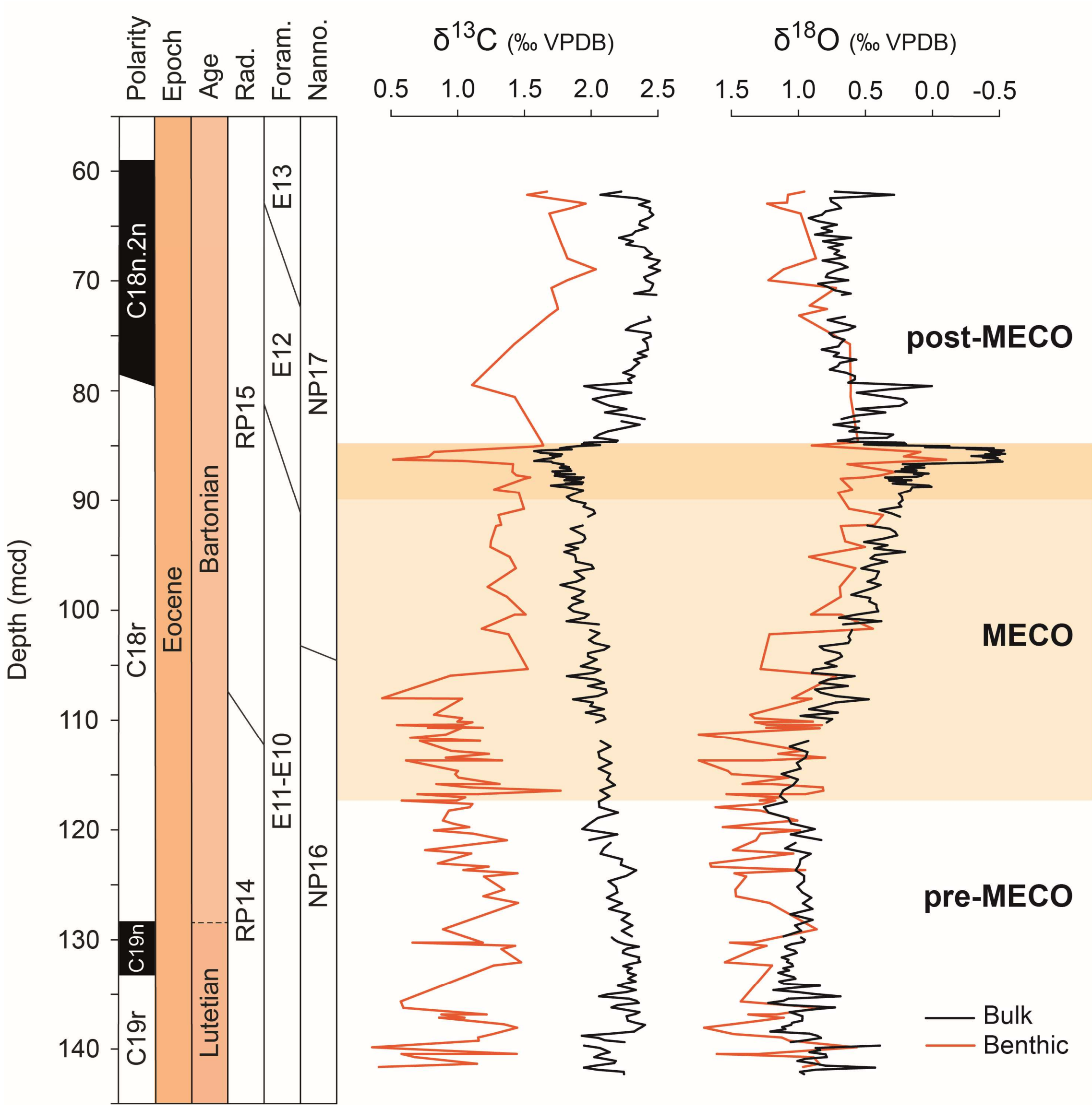

Figure IV.1.2. Variation of geochemical proxies across the MECO interval of ODP Site 1051 (Blake Nose, western North Atlantic). The darker orange zone highlights the peak-MECO interval. Stable isotope data are from Bohaty et al. (2009) for the fine carbonate fraction and from Edgar et al. (2010) for the benthic foraminiferal carbonate record. Magnetostratigraphy follows Ogg and Bardot (2001), the radiolarian biozonation is from Sanfilippo and Blome (2001), the planktic foraminiferal zonation is from Norris et al. (1998) and Edgar et al. (2010), and the calcareous nannofossil biostratigraphy is from Mita (2001). Abbreviations: Foram., planktic foraminifera; mcd, meters composite depth; Nanno., calcareous nannofossils; Rad., radiolarians; VPBD, Vienna Pee Dee Belemnite.

IV.1.3.2. Biodiversity survey

In order to examine variations in radiolarian assemblages across the MECO interval, we documented the entire radiolarian fauna preserved at ODP Site 1051. Rare taxa were thus taken into account, including numerous unknown morphospecies, that were left in open nomenclature (see online appendix: https://doi.org/10.1016/j.marmicro.2023.102272). Most of the enumerated classes were resolved to the species level, but occasionally higher taxonomic levels were used to record broken or unidentifiable specimens. The latter were not included in our diversity analyses. Species identification was performed using a Zeiss Axio Imager.A2 as a light microscope equipped with a Zeiss AxioCam ERc5s digital camera.

Approximately 6,000 specimens were recorded for each sample (see Supplementary Table 1) using a stratified procedure inspired by Renaudie and Lazarus (2013b) and Trubovitz et al. (2020). All specimens were first counted along vertical traverses until ~500 specimens were reached. All specimens mounted on a slide were then counted, excluding species representing >5% of the assemblage in the first sampling step. At the end of the count, the abundance of these common species was extrapolated by using the number of specimens observed in the first sampling step. To assess the robustness of our taxonomic sampling, sample completeness based on Good's U estimator (Good, 1953; Chao et al., 2020) was calculated using the scientific environment R (version 4.1.3; R Core Team, 2022), using the iNext package (version 3.0.0; Hsieh et al., 2016).

IV.1.3.3. Quantitative analyses

To describe the radiolarian response to the paleoenvironmental changes that occurred during the MECO, we calculated several indices of taxonomic richness based on species-level count data. Because many taxonomic inconsistencies remain in Cenozoic radiolarians, we have avoided using genus-level data. First, we determined the sampled-in-bin diversity (SIB), which is the raw count of taxa actually observed in each sample. Since the number of species encountered is expected to increase with the number of individuals sampled, the SIB may be biased by heterogeneous sampling effort between samples (Simpson, 1949; Raup, 1972; Bunge and Fitzpatrick, 1993; Gotelli and Colwell, 2001; Chao et al., 2014). We therefore computed the shareholder quorum subsampling (SQS) diversity (Alroy, 2010a, 2010b, 2010c) to correct for any possible bias introduced by unequal sampling. This coverage-based rarefaction approach draws randomly selected taxa from a sample until the sum of the relative frequencies of these taxa reaches a pre-specified coverage level (the 'quorum'). In this study, SQS diversity was estimated using a quorum level of 0.9, and by including dominant and single-interval taxa.

Several biodiversity indices commonly used in paleoenvironmental reconstructions were also calculated, including the Shannon–Wiever index, which was used as a measure of radiolarian diversity that integrates the relationship between the number of species and the number of individuals in an assemblage (Shannon and Weaver, 1949): $H' = \Sigma pi\ lnpi$, where pi is the relative frequency of species i. This index varies between 0 and 1, with 0 representing minimum diversity and 1 representing maximum diversity. In addition to metrics of species diversity, we also included the Pielou equitability index (Pielou, 1966), which is a measure of species distribution within a sample derived from the Shannon–Wiener index: $J = H'/\log(SIB)$. Low equitability scores indicate an imbalance where only one or a few species dominate the community, while high scores indicate almost evenly distributed species.

In order to group species with similar distributions, a hierarchical cluster analysis (HCA) was performed on the most abundant taxa representing >1% of the total assemblage in at least three samples. We used the UPGMA linkage method (Sokal and Michener, 1958) and the Morisita similarity index (Morisita, 1959), which has the major advantage of being independent of sample size and diversity.

Finally, a one-way Analysis of similarity (ANOSIM) was used to test for significant differences in radiolarian assemblages between the MECO event, and the pre- and post-MECO cooling intervals. ANOSIM was run on a dissimilarity matrix (Bray–Curtis dissimilarity index) computed from raw counts of radiolarian species, using 9999 random permutations of group membership (Clarke, 1993). This type of analysis produces an R statistic ranging from 0 to 1, which indicates the degree of separation between groups. A large positive R indicates dissimilarity in assemblages between groups. Differences between each pair of groups were then assessed using ANOSIM post-hoc tests with p-value adjustments for multiple comparisons. When ANOSIM revealed significant differences between groups, we used the SIMPER (for 'Similarity Percentage') analysis to determine the relative contribution of each species to the overall average dissimilarity observed between groups (Clarke, 1993).

ANOSIM and SIMPER analyses were computed using the R package vegan (version 2.6–4; Oksanen et al., 2013), while all the other biodiversity indices and clustering analysis were calculated using the Paleontological Statistics Software Package (PAST; version 4.12; Hammer et al., 2001).

IV.1.4. Results

At ODP Site 1051, radiolarian assemblages are diverse and remarkably well-preserved across the ~80 m-thick interval investigated. Skeleton fragmentation is moderate and signs of corrosion are rare, with the more delicate skeletal elements being generally preserved (e.g., thin external processes, spumellarian spongy meshwork). The absolute abundance of radiolarian skeletons is characterized by low to moderate values in the pre-MECO interval and during the long-term MECO warming phase (average of 9.3×10^5 radiolarian skeletons per gram of sediment). An exceptionally high abundance (28.5×10^5 g^{-1}) is observed in one sample located in the warmest interval (peak-MECO), around 86.3 mcd (Figure IV.1.3). The post-MECO cooling interval shows decreased radiolarian abundance values (average of 7.1 x 10^5 g^{-1}) that are close to those observed before the MECO.

A total of 326 radiolarian species were identified at ODP Site 1051 (average of 216 species per sample), including most of the typical middle Eocene species found in tropical to warm-subtropical latitudes. A few potentially reworked specimens of the early Eocene species *Buryella tetradica* Foreman and *Phormocyrtis striata striata* Brandt were found. However, they represent a very small fraction of the assemblage and were usually broken in our material, allowing them to be easily distinguished from the in situ fauna. In the considered interval, nassellarians are both very diverse and abundant, accounting for ~80% of the total radiolarian diversity and 70% to 80% of the total counted specimens. A relatively high proportion of species (~27%) are present in all samples. Analysis of sample completeness indicates that all samples have excellent coverage, ranging between 98% and 99%.

IV.1.4.1. Diversity changes across the MECO

Radiolarian paleobiodiversity curves constructed using sampled-in-bin values (SIB; measure of raw taxonomic diversity) and diversity corrected for sampling bias are shown in Figure IV.1.3. The SIB diversity is ~30% higher during the MECO interval, with the highest values recorded in the warmest interval (peak-MECO). The diversity values are lower during the post-MECO cooling phase, although they are slightly higher than those observed during the pre-MECO phase. Rarefied diversity shows similar broad trends to the SIB diversity, suggesting that the observed diversity is not heavily distorted by sampling biases. The most striking difference is a more pronounced decrease in rarefied diversity in the middle part of the MECO interval (98.68 mcd) and a shift of the diversity peak towards the post-MECO interval.

At ODP Site 1051, the species diversity (H′) was calculated from the Shannon-Wiener index ranged from 3.92 to 4.31 (average 4.20) throughout the study interval (Figure IV.1.3).

The lowest value is recorded in the lower part of the MECO event, around 98.68 mcd. The evenness is also stable and high throughout the studied interval, with values ranging between 0.75 and 0.8, and with only two samples (located at 113.78 and 98.68 mcd) characterized by an evenness value lower than the average lower of 0.78 (Figure IV.1.3). These samples are dominated by two small artostrobiids: *Siphocampe acephala* (Ehrenberg) and *S.* ? *paupera* (Ehrenberg), together representing between 16% and 24% of the total assemblage.

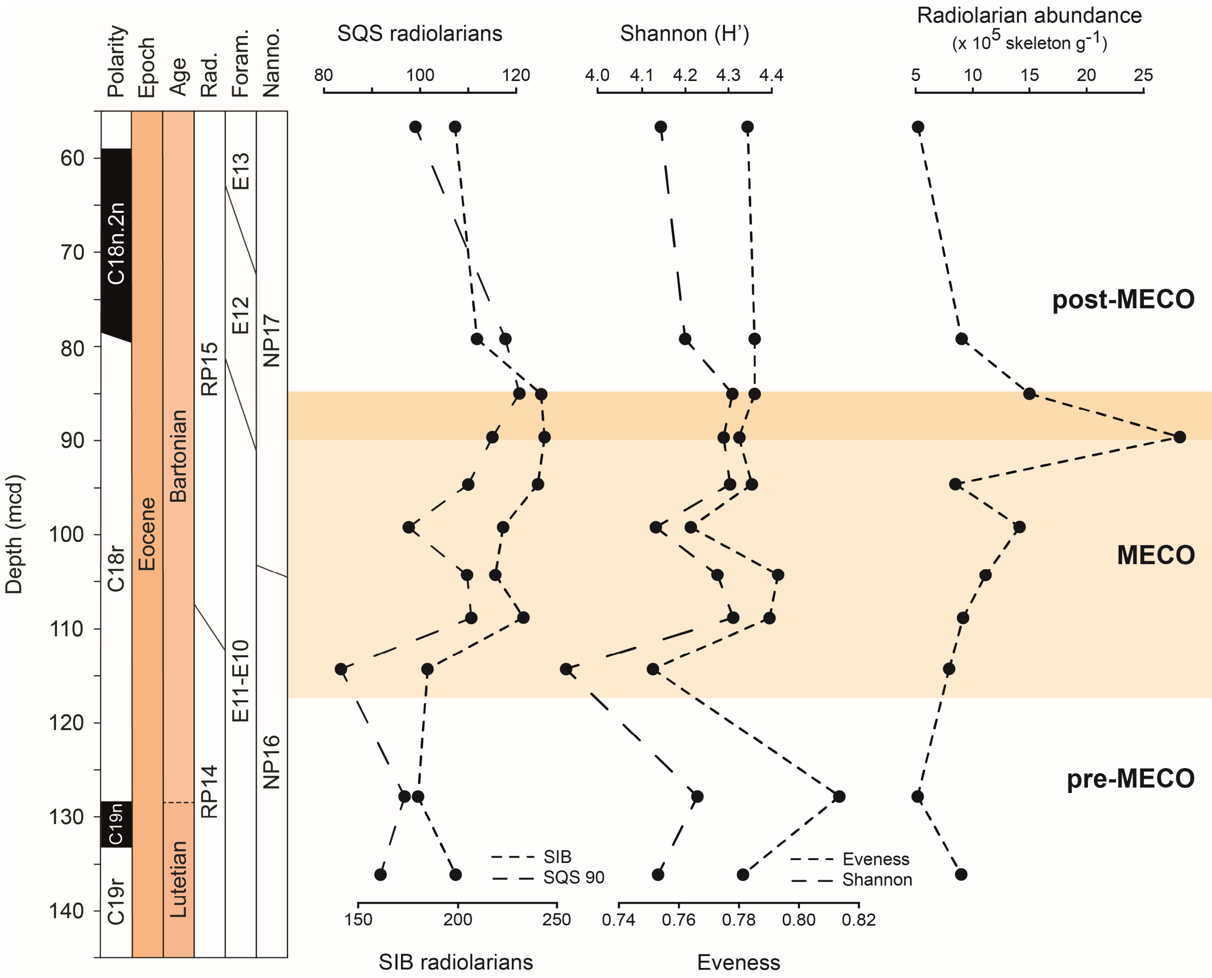

Figure IV.1.3. Radiolarian diversity patterns across the MECO interval of ODP Site 1051 (Blake Nose, western North Atlantic), plotted against magnetostratigraphy (Ogg and Bardot, 2001), radiolarian biostratigraphy (Sanfilippo and Blome, 2001), planktic foraminiferal biostratigraphy (Norris et al., 1998; Edgar et al., 2010), and calcareous nannofossil biostratigraphy (Mita, 2001). The darker orange zone highlights the peak-MECO interval, and black dots represent the samples examined (each one of which is 1 cm–thick). Abbreviations: Foram., planktic foraminifera; mcd, meters composite depth; Nanno., calcareous nannofossils; Rad., radiolarians; SQS, Shareholder Quorum Subsampling.

IV.1.4.2. Changes in faunal composition across the MECO

The clustering analysis performed on the 28 most abundant radiolarian species highlights the presence of three well-defined clusters (Figure IV.1.4). These species are shown in Plates IV.1.1 and IV.1.2, and their stratigraphic distribution and abundance fluctuations are given in Figure IV.1.5. Cluster A consists of seven species, including notably *Carpocanopsis ornata* (Ehrenberg) and *Rhopalosyringium* ? *biauritum* (Ehrenberg). This cluster accounts for 2% to 18% of the total assemblage, with the highest values recorded in the pre-MECO and showing a decline during the MECO (Figure IV.1.6).

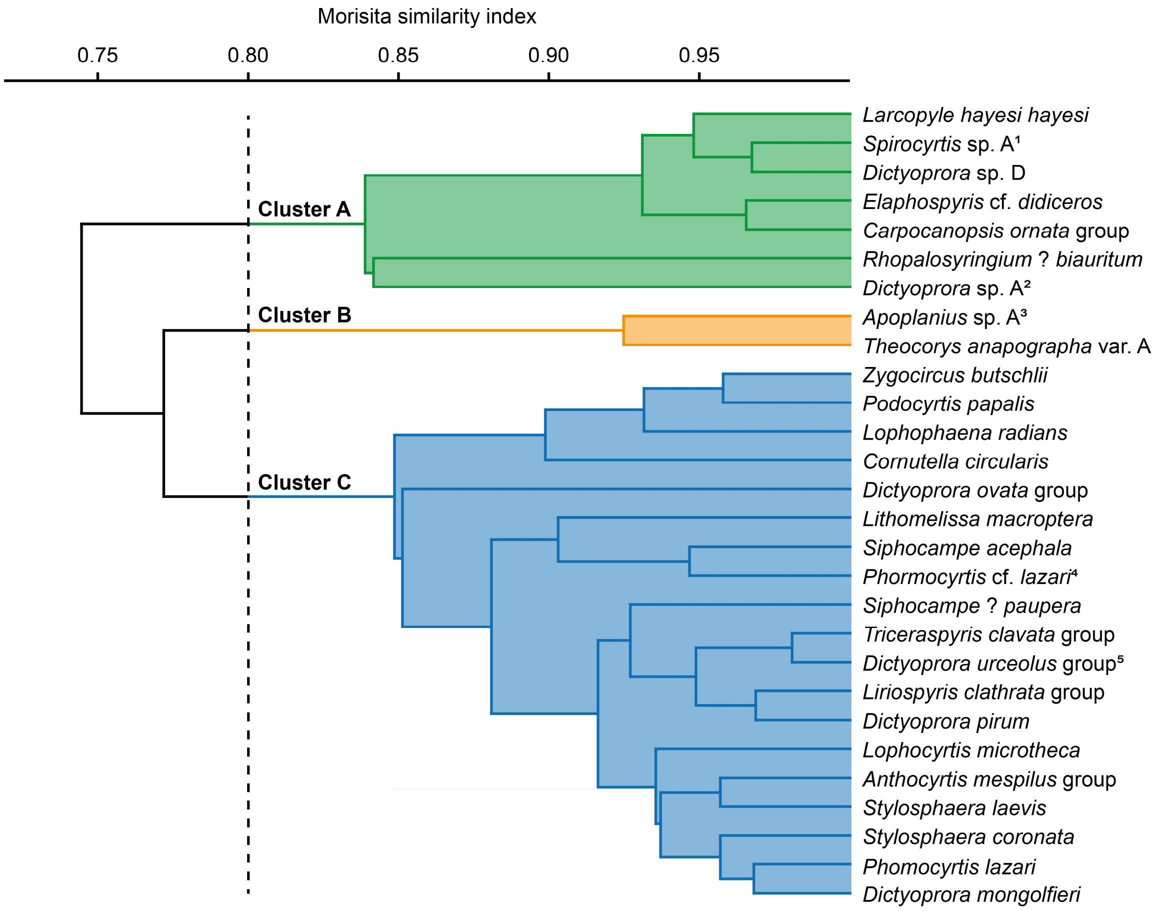

Figure IV.1.4. Hierarchical cluster analysis (UPGMA linkage and Morisita similarity index) of the 28 most abundant radiolarian species from ODP Site 1051 (Blake Nose, western North Atlantic). (1 – Described as *Spirocyrtis matsuokai* Meunier and Danelian n. sp. in Chapter II.3; 2 – Described as *Dictyoprora echidna* Meunier and Danelian n. sp. in Chapter II.3; 3 – Described as *Apoplanius hyalinus* Meunier and Danelian n. sp. in Chapter II.3; 4 – Described as *Phormocyrtis microtesta* Meunier and Danelian n. sp. in Chapter II.3; 5 – *Dictyoprora crassiceps* (Ehrenberg) group in Chapter II.2).

Cluster B consists of two species (*Apoplanius* sp. A[1] and *Theocorys anapographa* Sanfilippo and Riedel var. A) and shows a marked increase throughout the studied interval (Figure IV.1.6), although it represents only 0.2% to 4% of the total assemblage. Cluster C is the largest cluster with 19 taxa, including inter alia *Phormocyrtis lazari* Meunier and Danelian, *Siphocampe acephala* (Ehrenberg), *S.* ? *paupera* (Ehrenberg), and *Stylosphaera laevis* (Ehrenberg). This cluster is the major component of the radiolarian assemblages (33% to 49%) in the late middle Eocene interval of ODP Site 1051 (Figure IV.1.6).

The results of the one-way ANOSIM analysis indicated statistically significant differences in the taxonomic composition between the sample groups ($R = 0.75$, p-value = 0.001). Pairwise ANOSIM tests showed significant differences between the MECO interval and the pre-MECO and post-MECO intervals (p-values = 0.025 and 0.027, respectively), but not between the pre-MECO and post-MECO intervals (p-value = 0.331). SIMPER analysis allows the examination of the species that contribute the most to the dissimilarity between groups (Table IV.1). SIMPER analyses show that the radiolarian assemblage of the pre-MECO interval differs from those of the MECO interval in being characterized by a higher abundance of *Larcopyle hayesi hayesi* (Chen), *Rhopalosyringium* ? *biauritum* (Ehrenberg), and *Stylosphaera laevis* Ehrenberg, whereas the MECO interval is mostly defined by the predominance of *Apoplanius* sp. A[2], *Siphocampe acephala* (Ehrenberg), *S.* ? *paupera* (Ehrenberg), and *Theocorys anapographa* Riedel and Sanfilippo var. A. According to SIMPER analyses, the most significant differences between the post-MECO and the MECO intervals are the high abundance of *Carpocanopsis ornata* (Ehrenberg), *Cornutella circularis* Ehrenberg, *Dictyoprora* sp. D, *Elaphospyris* cf. *didiceros*, *Spirocyrtis* sp. A[3] and *R.* ? *biauritum* throughout the MECO interval.

1 Described as *Apoplanius hyalinus* Meunier and Danelian in Chapter II.3.
2 Described as *Apoplanius hyalinus* Meunier and Danelian n. sp. in Chapter II.3.
3 Described as *Spirocyrtis matsuokai* Meunier and Danelian n. sp. in Chapter II.3.

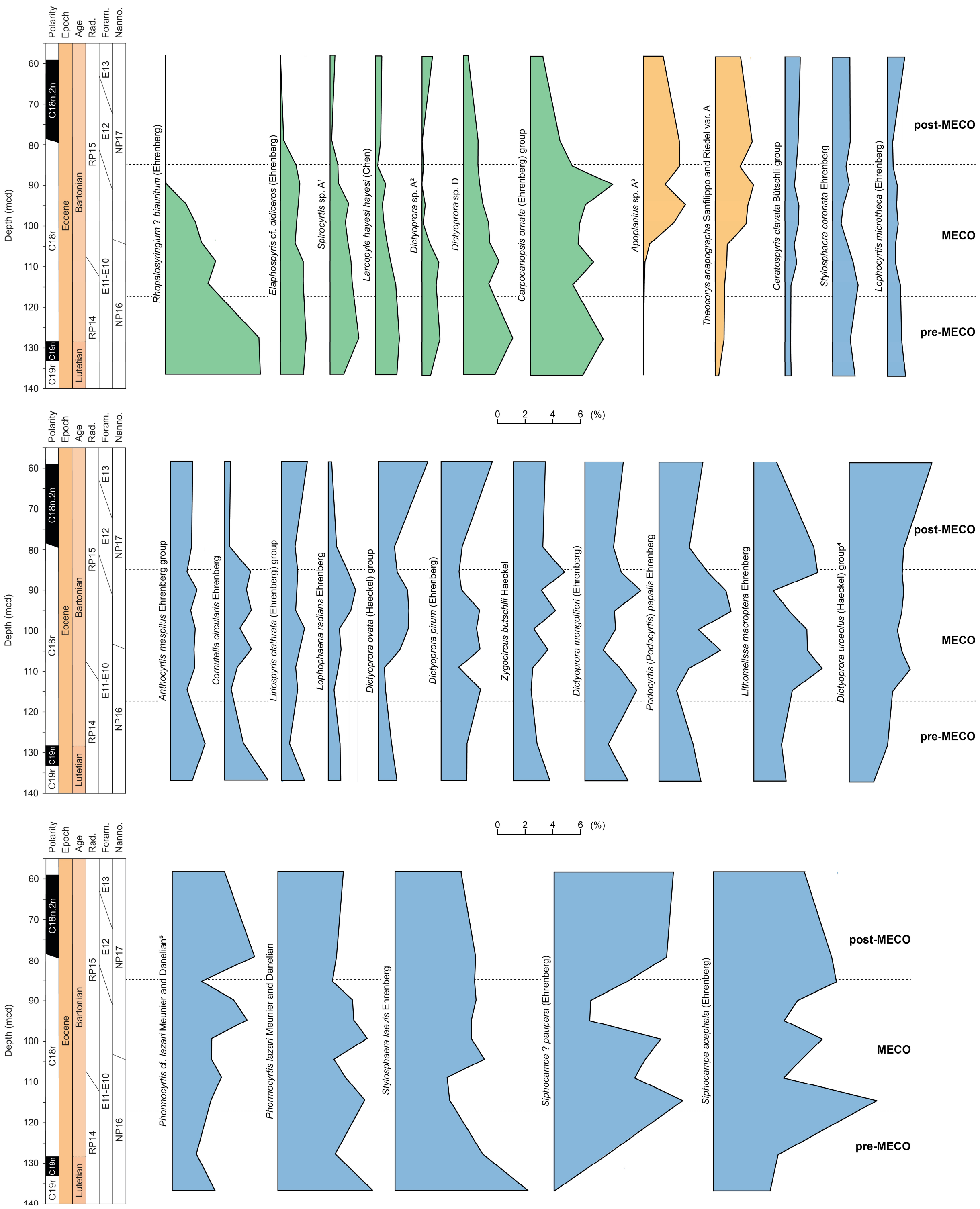

Figure IV.1.5. Relative abundance (%) variations of the 28 most abundant radiolarian species recognized for the MECO interval of ODP Site 1051 (Blake Nose, western North Atlantic) plotted against magnetostratigraphy (Ogg and Bardot, 2001), radiolarian biostratigraphy (Sanfilippo and Blome, 2001), planktic foraminiferal biostratigraphy (Norris et al., 1998; Edgar et al., 2010) and calcareous nannofossil biostratigraphy (Mita, 2001). Abbreviations: Foram., planktic foraminifera; mcd, meters composite depth; Nanno., calcareous nannofossils; Rad., radiolarians. The colors refer to the three clusters found by the hierarchical cluster analysis.

(1 – Described as *Spirocyrtis matsuokai* Meunier and Danelian n. sp. in Chapter II.3; 2 – Described as *Dictyoprora echidna* Meunier and Danelian n. sp. in Chapter II.3; 3 – Described as *Apoplanius hyalinus* Meunier and Danelian n. sp. in Chapter II.3; 4 –*Dictyoprora crassiceps* (Ehrenberg) group in Chapter II.2; 5 – Described as *Phormocyrtis microtesta* Meunier and Danelian n. sp. in Chapter II.3).

IV.1.5. Discussion

The radiolarian skeletons observed in our material exhibit an excellent quality of preservation, suggesting that the diagenetic influence on radiolarian biogenic silica, abundance, and assemblage structure is negligible. However, Witkowski et al. (2014) found that middle Eocene diatoms from ODP Site 1051 showed a rather moderate degree of dissolution (i.e., absence of delicate parts on valves). This difference of preservation may be due to the delicate and finely perforated diatom frustule as compared to the largely more robust radiolarian skeleton, which was particularly silica-rich for Paleogene radiolarians (Lazarus et al., 2009). Radiolarian abundance appears to be higher within the MECO, which is consistent with the planktic foraminiferal and diatom record from the same site, supporting increased eutrophication during the MECO warming interval (Edgar et al., 2013; Witkowski et al., 2014).

In addition to siliceous plankton, spicules from epibenthic siliceous sponges are also a major component of middle Eocene siliceous microfossils from ODP Site 1051 (Norris et al., 1998). However, their abundance could not be precisely quantified due to the difficulty of counting broken monaxons. It is likely that the pinakid-type sponge spicules observed in our material from ODP Site 1051 (Plate IV.1.2, Figure 15) belong to shallow-water demosponges of the order Astrophorida, and that they were probably redeposited from shallower shelf environments (Bąk et al., 2015).

As discussed above, the middle Eocene sedimentary sequences recovered at ODP Site 1051 are characterized by diverse radiolarian fauna. A total of 321 radiolarian species were identified in this study (with an average of 216 species per sample), while only 41 species were

Table IV.1. Summary of the SIMPER (similarity percentage) analysis. The first column shows taxa contributing the most to the average dissimilarities between groups, ranked in order of importance. A cut-off of a cumulative percentage of dissimilarity of 50% was applied. The second and third columns represent the individual and cumulative contributions of each taxon to the average dissimilarities between groups. The last columns show the mean relative abundance of taxa per group. (1 – Described as *Phormocyrtis microtesta* Meunier and Danelian n. sp. in Chapter II.3; 2 – *Dictyoprora crassiceps* (Ehrenberg) group in Chapter II.2; 3 – Described as *Apoplanius hyalinus* Meunier and Danelian n. sp. in Chapter II.3; 4 – Described as *Spirocyrtis matsuokai* Meunier and Danelian n. sp. in Chapter II.3).

Taxon	Average dissimilarity	Contribution (%)	Cumulative (%)	Frequency		
				post-MECO	MECO	pre-MECO
Siphocampe ? *paupera*	2.06	6.36	6.36	8.82	5.99	2.02
Rhopalosyringium ? *biauritum*	1.92	5.94	12.29	0.01	1.87	6.84
Siphocampe acephala	1.32	4.09	16.38	7.79	7.53	4.52
Carpocanopsis ornata	1.08	3.33	19.71	1.68	4.39	5.03
Stylosphaera laevis	0.98	3.04	22.76	5.46	5.41	8.20
Phormocyrtis cf. *lazari*[1]	0.81	2.52	25.28	4.87	3.43	2.42
Dictyoprora urceolus group[2]	0.77	2.37	27.65	4.93	3.75	2.25
Lithomelissa macroptera	0.71	2.21	29.86	2.90	3.32	2.10
Apoplanius sp. A[3]	0.67	2.08	31.93	1.95	1.39	0.02
Phormocyrtis lazari	0.62	1.91	33.84	4.53	5.27	5.56
Dictyoprora sp. D	0.62	1.91	35.75	0.67	1.62	2.83
Dictyoprora ovata group	0.54	1.66	37.41	2.32	1.44	1.12
Dictyoprora pirum	0.48	1.50	38.90	3.62	3.15	2.86
Cornutella circularis	0.43	1.33	40.23	0.29	1.04	1.66
Dictyoprora mongolfieri	0.43	1.32	41.55	2.40	2.64	2.38
Theocorys anapographa var. A	0.42	1.30	42.85	1.66	1.22	0.33
Spirocyrtis sp. A[4]	0.41	1.28	44.13	0.23	1.11	1.49
Zygocircus butschlii	0.37	1.14	45.27	2.22	2.19	2.17
Elaphospyris cf. *didiceros*	0.36	1.11	46.38	0.09	1.03	1.37
Stylodictya inaequalispina group	0.35	1.09	47.47	1.25	0.06	0.05
Larcopyle hayesi hayesi	0.35	1.07	48.54	0.41	0.75	1.58
Apoplanius kerasperus	0.34	1.05	49.58	0.37	0.84	0.61
Podocyrtis papalis	0.33	1.01	50.59	1.38	1.80	1.43

previously reported by Sanfilippo and Blome (2001) from the same stratigraphic interval. Radiolarians are more diverse than diatoms at ODP Site 1051, where a total of 137 diatom species were recorded in the MECO interval, with an average of 28 diatom species per sample (Witkowski et al., 2014). The most abundant radiolarian taxa rarely account for >5% of the total assemblage; numerous species are rather rare and represented by only a few specimens in our material, as this is also the case in some other recent detailed radiolarian studies (Renaudie and Lazarus, 2013b; Trubovitz et al., 2020).

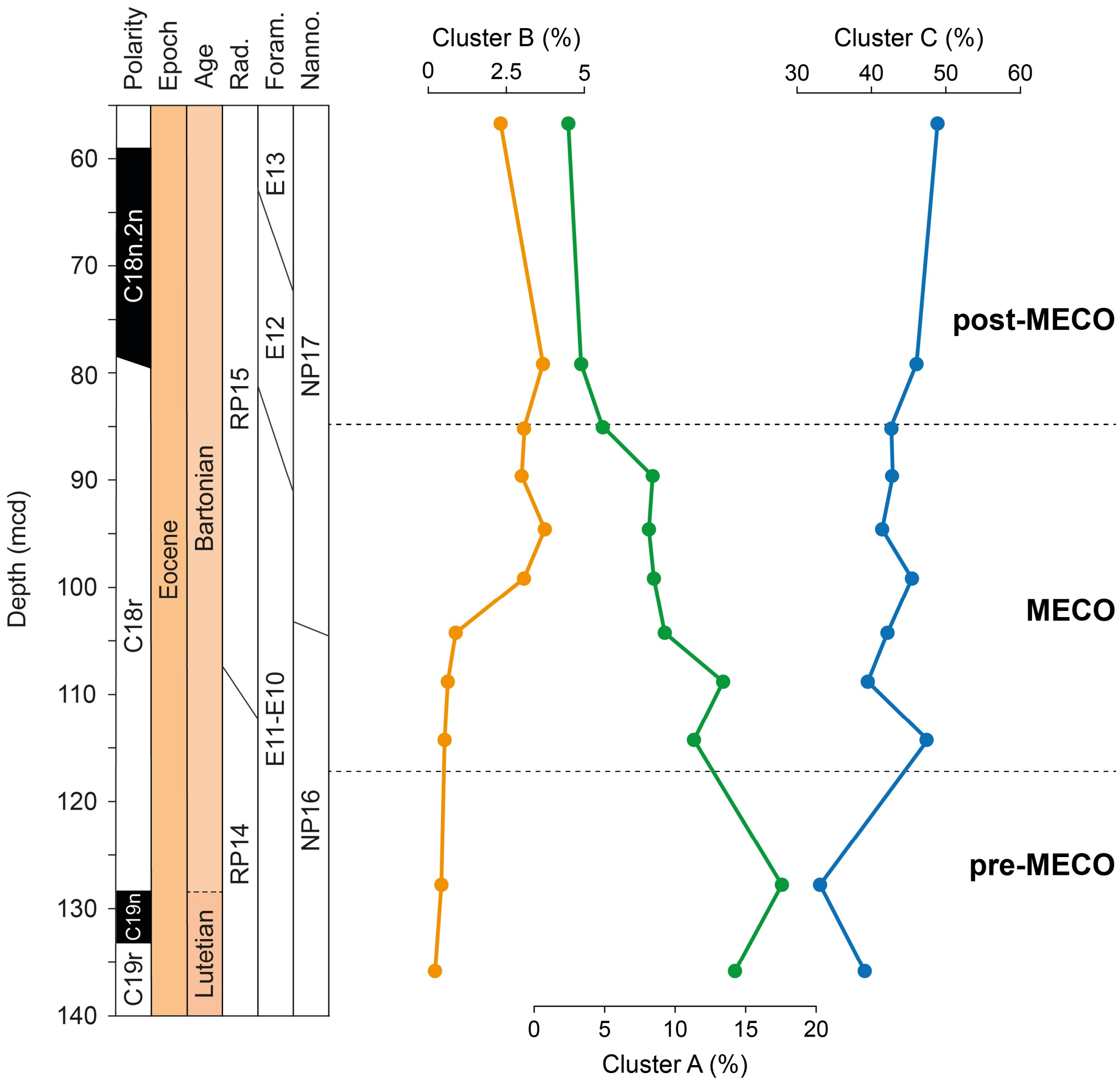

Figure IV.1.6. Relative abundance (%) variations of the three radiolarian clusters recognized across the MECO interval of ODP Site 1051 (Blake Nose, western North Atlantic) plotted against magnetostratigraphy (Ogg and Bardot, 2001), radiolarian biostratigraphy (Sanfilippo and Blome, 2001), planktic foraminiferal biostratigraphy (Norris et al., 1998; Edgar et al., 2010) and calcareous nannofossil biostratigraphy (Mita, 2001). The MECO interval is indicated by two dotted horizontal lines. Abbreviations: Foram., planktic foraminifera; mcd, meters composite depth; Nanno., calcareous nannofossils; Rad., radiolarians. Colors refer to the three clusters found by the hierarchical cluster analysis.

At ODP Site 1051, the total number of species per sample is relatively constant across the studied interval, although a ~30% increase in taxonomic richness was observed in samples coming from the warmest interval of the MECO. This increased richness is probably due to an influx of warm, low-latitude taxa that temporarily expanded their geographic range to higher latitudes, such as *Podocyrtis chalara* Riedel and Sanfilippo, whose occurrence coincides with the peak warming phase of the MECO. These migration events appear to be triggered by climate warming, and it is likely that they were facilitated by changes in surface ocean circulation that altered water mass boundaries during the Eocene (Vahlenkamp et al., 2018; Cramwinckel et al., 2020). Similarly, the acme of several emblematic tropical middle Eocene species lies in the warmest interval of the MECO, including *P. mitra* Ehrenberg, *P. papalis* Ehrenberg, *Thyrsocyrtis triacantha* Ehrenberg[4], and *T. rhizodon* Ehrenberg[5]. With the exception of these few well-known species, it is difficult to specify the latitudinal affinity of most of the taxa encountered, as nearly half of them are new to science, and most of the others are known only from their type locality. Nevertheless, the radiolarian fauna of ODP Site 1051 can be compared to the equatorial record of ODP Site 1260 (Demerara Rise, ~3500 km southeast of the Blake Plateau), which has recently been the subject of a detailed biostratigraphic study (Meunier and Danelian, 2022). Several species commonly found in upper middle Eocene sediments of the equatorial Atlantic ODP Site 1260 are missing from ODP Site 1051, including notably *Apoplanius klydus* (Sanfilippo and Caulet), *Dorcadospyris ombros* Sanfilippo *in* Nigrini et al., *Lithochytris vespertilio* Ehrenberg[6], *P. trachodes* Sanfilippo and Riedel, and *Theocorys* ? *scolopax* (Ehrenberg). Although the boundaries of the geographic range of radiolarian species are roughly explained by sea-surface temperature (e.g., Boltovskoy et al., 2010), their latitudinal

4 *Thyrsocyrtis* (*Pentalacorys*) *schomburgkii* (Ehrenberg, 1847) in Chapter II.2.
5 *Thyrsocyrtis* (*Thyrsocyrtis*) *argulus* (Ehrenberg, 1874) in Chapter II.2.
6 *Lithochytris pyramidalis* Ehrenberg, 1874 in Chapter II.2.

distribution is also controlled by other abiotic and biotic factors, including salinity, dissolved oxygen, nutrient availability, and interspecific interactions (Lazarus et al., 2021). The lack of poleward migration for some other tropical radiolarian species may be related to the difference in sampling effort between the two sites, or the result of a combination of some unknown environmental parameters. Similarly, some abundant species at ODP Site 1260 are found to be rare at ODP Site 1051, including the biostratigraphically important species *Sethochytris triconiscus* Haeckel and *Lychnocanium babylonis* (Clark and Campbell) group[7], and *Rhopalosyringium* ? *auriculaleporis* (Clark and Campbell), which is replaced at this subtropical site by *R*. ? *biauritum* (Ehrenberg).

It is noteworthy that Pascher et al. (2015), who studied the southern high-latitude radiolarian fauna of DSDP Site 277 (southwest Pacific, paleolatitude ~55°S), also found an increased taxonomic richness during the MECO, and a shift to higher latitudes of several tropical taxa, including the spumellarian species *Amphicraspedula murrayana* (Haeckel) and *A*. *prolixa* (Sanfilippo and Riedel) group. However, important middle Eocene tropical species of the genera *Podocyrtis* and *Thyrsocyrtis* appear to be absent from the southwest Pacific (Pascher et al., 2015; Hollis et al., 2020), suggesting that their ability to track their preferred thermal habitat is either limited to mid-latitudes or that temperatures were not sufficiently elevated in this part of the ocean during the MECO. Poleward migrations of tropical radiolarian species have also been observed in the Southern Hemisphere during the Paleocene-Eocene Thermal Maximum (Hollis et al., 2005a, 2005b; Hollis, 2006), as well as in other planktic groups such as the planktic foraminifera (Thomas and Shackleton, 1996; Arenillas et al., 1999; Lu and Keller, 1995; Berggren and Ouda, 2003) and the dinoflagellates (Bujak and Brinkhuis, 1998; Crouch et al., 2001, 2003; Sluijs et al., 2005, 2006).

7 *Lychnocanium tribulus* (Ehrenberg, 1874) group in Chapter II.2.

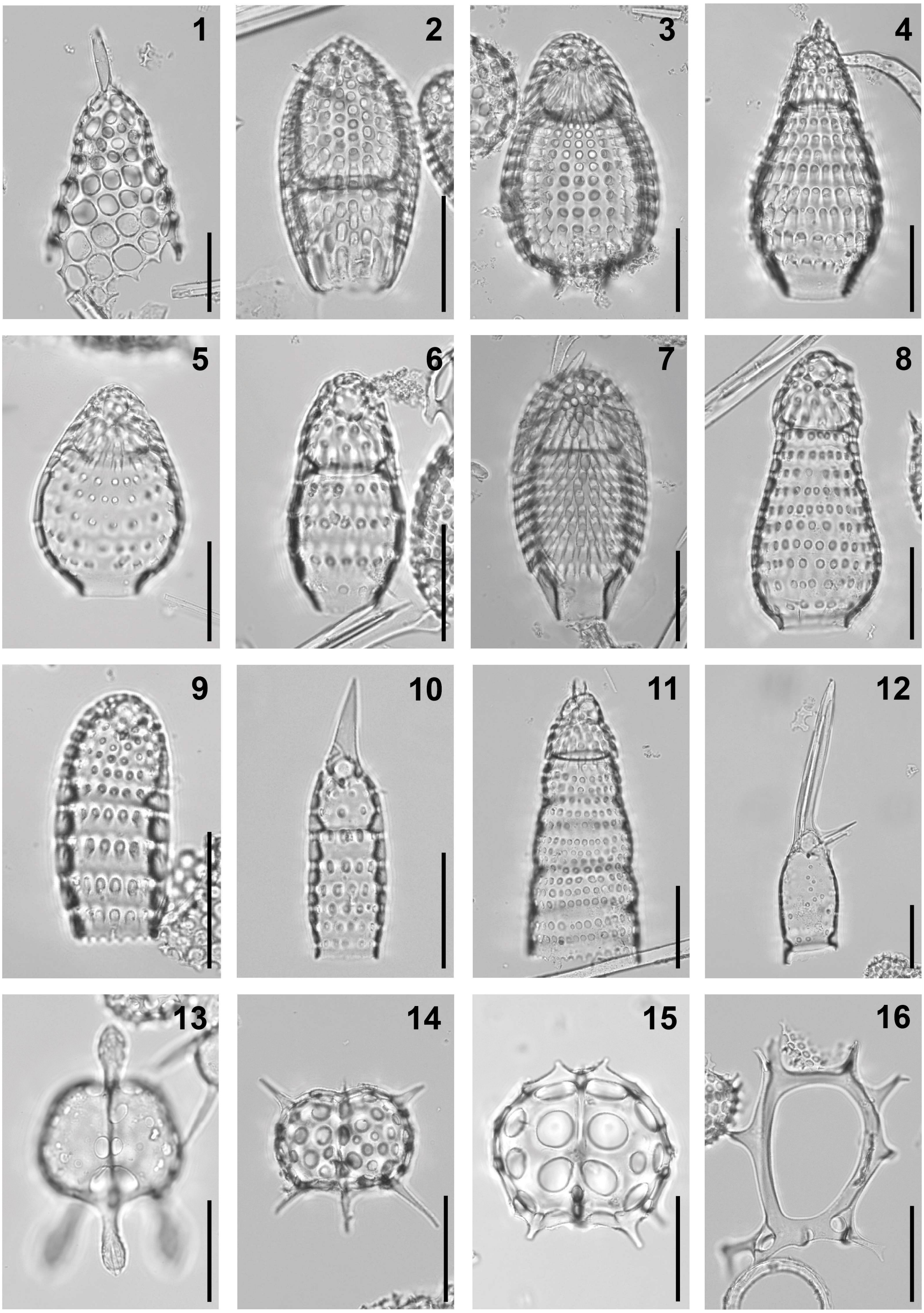
1
2
3
4
5
6
7
8
9
10
11
12
13
14
15
16

Plate IV.1.1. Composite light micrographs of selected radiolarians from ODP Site 1051. All scale bars equal 50 µm. (1) *Cornutella circularis* Ehrenberg, 171B-1051A-14H-5W, 52–54 cm, L1, USTL 4554; (2) *Carpocanopsis ornata* (Ehrenberg) group, 171B-1051A-9H-5W, 53–55 cm, L2, USTL 4528; (3) *Dictyoprora mongolfieri* (Ehrenberg), 171B-1051A-8H-5W, 61–63 cm, L1, USTL 4521; (4) *Dictyoprora ovata* (Haeckel) group, 171B-1051A-9H-5W, 53–55 cm, L3, USTL 4529; (5) *Dictyoprora pirum* (Ehrenberg), 171B-1051A-9H-5W, 53–55 cm, L3, USTL 4529; (6) *Dictyoprora urceolus* (Haeckel) group (= *Dictyoprora crassiceps* (Ehrenberg) group in Chapter II.2), 171B-1051A-9H-5W, 53–55 cm, L2, USTL 4528; (7) *Dictyoprora* sp. A (described as *Dictyoprora echidna* Meunier and Danelian n. sp. in Chapter II.3), 171B-1051A-6H-5W, 53–55 cm, L1, USTL 4518; (8) *Dictyoprora* sp. D, 171B-1051A-9H-5W, 53–55 cm, L2, USTL 4528; (9) *Siphocampe acephala* (Ehrenberg), 171B-1051A-9H-5W, 53–55 cm, L2, USTL 4528; (10) *Siphocampe* ? *paupera* (Ehrenberg), 171B-1051A-14H-5W, 52–54 cm, L1, USTL 4554; (11) *Spirocyrtis* sp. A (described as *Spirocyrtis matsuokai* Meunier and Danelian n. sp. in Chapter II.3), 171B 1051A-14H-5W, 52–54 cm, L1, USTL 4554; (12) *Rhopalosyringium* ? *biauritum* (Ehrenberg), 171B-1051A-14H-5W, 52–54 cm, L1, USTL 4554; (13) *Ceratospyris clavata* Bütschli group, 171B-1051A-14H-5W, 52–54 cm, L1, USTL 4554; (14) *Elaphospyris* cf. *didiceros* (Ehrenberg), 171B-1051A-14H-5W, 52–54 cm, L1, USTL 4554; (15) *Liriospyris clathrata* (Ehrenberg) group, 171B-1051A-9H-2W, 53–55 cm, L1, USTL 4524; (16) *Zygocircus butschlii* Haeckel, 171B-1051A-14H-5W, 52–54 cm, L1, USTL 4554.

In addition to this influx of tropical species, quantitative analysis of microfossil assemblages revealed only minor changes in the radiolarian faunal composition throughout the studied interval. Similarly, few changes in radiolarian assemblages have been documented at ODP Site 1051 during the PETM event (Sanfilippo and Blome, 2001), suggesting that subtropical radiolarians are relatively resilient to transient warming events.

The radiolarian fauna of the pre-MECO interval is characterized by a high abundance of cluster A species, especially *Larcopyle hayesi hayesi* (Chen) and *R*. ? *biauritum* (Ehrenberg). Since the relative abundance of Cluster A species tends to decrease over the study interval, they may represent species associated with colder water masses. A similar decline in cool-water taxa has also been observed in the eastern equatorial Pacific Ocean during the MECO (Kamikuri et al., 2013).

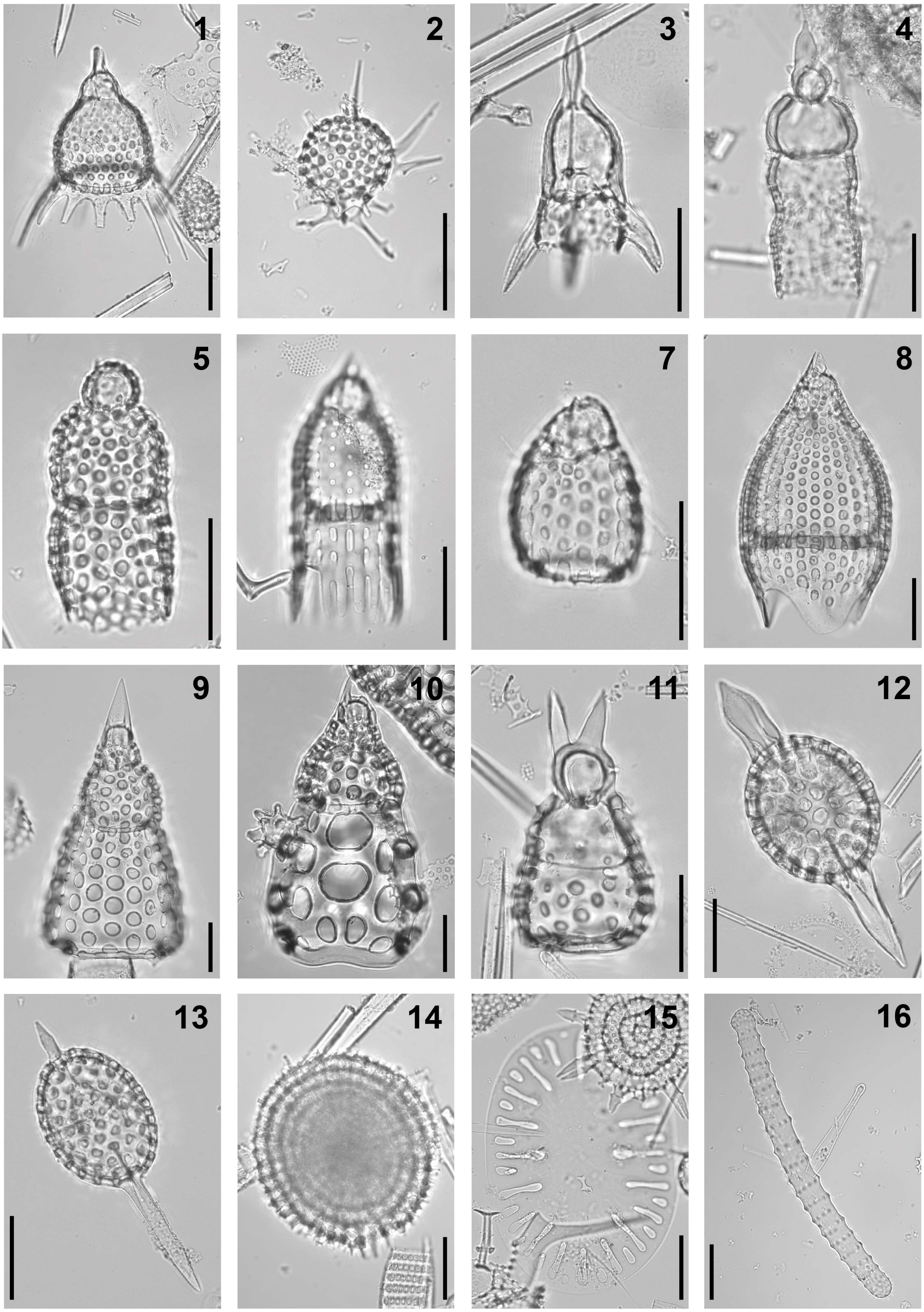
1
2
3
4
5
7
8
9
10
11
12
13
14
15
16

Plate IV.1.2. Composite light micrographs of selected radiolarians from ODP Site 1051. All scale bars equal 50 µm. (1) *Anthocyrtis* mespilus Ehrenberg group, 171B-1051A-9H-5W, 53–55 cm, L2, USTL 4528; (2) *Lophophaena radians* Ehrenberg, 171B-1051A-9H-2W, 53–55 cm, L1, USTL 4524; (3) *Lithomelissa macroptera* Ehrenberg, 171B-1051A-9H-5W, 53–55 cm, L3, USTL 4529; (4) *Apoplanius* sp. A (described as *Apoplanius hyalinus* Meunier and Danelian n. sp. in Chapter II.3), 171B-1051A-8H-5W, 61–63 cm, L1, USTL 4521; (5) *Lophocyrtis microtheca* (Ehrenberg), 171B-1051A-9H-5W, 53–55 cm, L2, USTL 4528; (6) *Phormocyrtis lazari* Meunier and Danelian, 171B-1051A-9H-2W, 53–55 cm, L1, USTL 4524; (7) *Phormocyrtis* cf. *lazari* Meunier and Danelian (described as *Phormocyrtis microtesta* Meunier and Danelian n. sp. in Chapter II.3), 171B-1051A-9H-2W, 53–55 cm, L3, USTL 4526; (8) *Podocyrtis* (*Podocyrtis*) *papalis* Ehrenberg, 171B-1051A-9H-5W, 53–55 cm, L3, USTL 4529; (9) *Podocyrtis* (*Lampterium*) *mitra* Ehrenberg, 171B-1051A-9H-5W, 53–55 cm, L3, USTL 4529; (10) *Podocyrtis* (*Lampterium*) *chalara* Riedel and Sanfilippo, 171B-1051A-9H-5W, 53–55 cm, L3, USTL 4529; (11) *Theocorys anapographa* Riedel and Sanfilippo var. A, 171B-1051A-9H-2W, 53–55 cm, L3, USTL 4526; (12) *Stylosphaera coronata* Ehrenberg, 171B-1051A-9H-2W, 53–55 cm, L3, USTL 4526; (13) *Stylosphaera laevis* Ehrenberg, 171B-1051A-9H-5W, 53–55 cm, L2, USTL 4528; (14) *Larcopyle hayesi hayesi* (Chen), 171B-1051A-9H-2W, 53–55 cm, L1, USTL 4524; (15) Pinakid (demosponge spicule), 171B-1051A-9H-2W, 53–55 cm, L3, USTL 4526; (16) Verticillated acanthostrongyle (demosponge spicule), 171B-1051A-9H-2W, 53–55 cm, L2, USTL 4525.

On the other hand, the MECO interval is mainly characterized by the dominance of cluster B species (*Apoplanius* sp. A[8] and *Theocorys anapographa* Riedel and Sanfilippo var. A), as well as two very abundant artostrobiid species: *Siphocampe acephala* (Ehrenberg) and *S.* ? *paupera* (Ehrenberg). Since the genus *Apoplanius* is considered to have originated in the tropics (Sanfilippo and Caulet, 1998), and *Theocorys anapographa* var. A is known only from tropical and subtropical localities (Ling, 1975; Sanfilippo and Blome, 2001; Hollis et al., 2020; Meunier and Danelian, 2022), cluster B is interpreted as a group of warm-water tropical species. The stratigraphic and geographic distributions of *S. acephala* and *S.* ? *paupera* are not well known, probably because these two species are relatively small for Eocene radiolarians (total length: ~80–100 µm) and can be therefore easily lost during sample preparation. This

8 Described as *Apoplanius hyalinus* Meunier and Danelian n. sp. in Chapter II.3.

emphasizes the need to use narrow mesh sieves (45 µm or less) in order to obtain reliable data for analyses of the entire radiolarian fauna. At ODP Site 1051, *S. acephala* and *S.* ? *paupera* are the most abundant species, representing on average 10% (up to 18%) of the total radiolarian assemblage. They may thus represent nutrient opportunists (r-strategists). In addition, these two species have a relatively simple morphology (see Plate 1, Plate 1.9 1.0), which is known to be a characteristic feature of opportunistic planktic species (e.g., Bé, 1982; Hemleben et al., 1989).

Finally, the major differences between the MECO and the post-MECO intervals are the abundance of *Carpocanopsis ornata* (Ehrenberg) group, *Cornutella circularis* Ehrenberg, *Dictyoprora* sp. D, *Elaphospyris* cf. *didiceros*, *Spirocyrtis* sp. A[9], and *R.* ? *biauritum* throughout the MECO interval. Interestingly, these cluster C species continue to decline in relative abundance during the post-MECO cooling phase, when recovery of cool-water species is expected. However, a better sampling of the post-MECO interval is needed to be conclusive.

IV.1.6. Conclusions

Our results on mid-latitude radiolarian assemblages from ODP Site 1051 are in good agreement with previous studies conducted on diatoms and planktic foraminifera from the same site, suggesting increased eutrophication during the MECO. Although radiolarians have apparently benefited from an increase in oceanic fertility induced by the MECO, this global warming event does not appear to have profoundly altered subtropical radiolarian fauna. Indeed, a detailed quantitative study of the entire radiolarian fauna preserved at Blake Nose did not reveal any significant faunal turnover during the MECO. On the contrary, we find here establish that radiolarian taxonomic richness increased during the warmest interval, a likely result of the northward incursion of several tropical radiolarian species. The biogeographic expansion of

9 Described as *Spirocyrtis matsuokai* Meunier and Danelian n. sp. in Chapter II.3.

low-latitude radiolarian species appears to have been initiated by the MECO global warming and is likely associated with changes in oceanic current circulation. Similarly, our quantitative analyses of the composition of the entire radiolarian assemblage indicate that ocean warming induced only a weak ecological response in radiolarian plankton. Indeed, the radiolarian fauna observed during MECO differs only slightly from the radiolarian fauna observed before and after the MECO, and this difference is mainly due to variations in the relative abundance of a small number of species. We have also identified two very abundant artostrobiid species (*Siphocampe acephala* and *S.* ? *paupera*) that may represent nutrient opportunists (r-strategists).

Finally, the MECO appears to be a minor event in the history of Paleogene radiolarians. It may be best considered as a poleward migration event of tropical radiolarians, as this is also the case for planktic foraminifera. However, the faunal changes reported here may have only a regional significance (i.e., the western subtropical Atlantic), and may not be representative of the effects of the MECO on radiolarian faunas at higher latitudes.

Author contributions

Mathias Meunier: Methodology, Investigation, Data curation, Software, Visualization, Writing – original draft, Writing – review and editing. **Taniel Danelian**: Conceptualization, Supervision, Resources, Writing – original draft, Writing – review and editing.

Acknowledgments

We thank the Ocean Drilling Program (ODP) for providing the samples used in this study. Claude Monnet is thanked for fruitful discussions on the quantitative analyses, and thanks are due to Sylvie Regnier and Jessie Cuvelier for technical assistance. The original manuscript was greatly improved thanks to the constructive comments of the two anonymous reviewers and of the editor, Xavier Crosta.

I.V.2. Morphological responses of the plankton to the Middle Eocene Climatic Optimum (MECO): The case of the radiolarian species *Podocyrtis papalis* from the western equatorial Atlantic (ODP Site 1260)

Mathias Meunier*, Claude Monnet, Rémi Habert, José Francisco Pínto Cabrera, Marie Cueille, Taniel Danelian

Univ. Lille, CNRS, UMR 8198 – Evo-Eco-Paleo, F-59000 Lille, France

<mathias.meunier@univ-lille.fr>

*Corresponding author

Abstract

The Middle Climatic Optimum (MECO) was a major event and carbon cycle perturbation that occurred at ca. 40 Ma and reversed the long-term Cenozoic cooling trend. Previous studies have highlighted changes in microfossil assemblages during the MECO interval, mainly affecting the relative abundance and biogeographic distribution of species, but very little is known about the morphological response of plankton species to this warming event. In this study, we apply a geometric morphometric approach to document and quantify, for the first time, variations in radiolarian disparity and morphological space occupancy in response to oceanographic perturbations induced by the MECO. Investigations were conducted on the nassellarian species *Podocyrtis papalis*, and a closely related morphotype (*P.* cf. *papalis*) that is particularly abundant during the MECO interval, as preserved at ODP Site 1260 (western equatorial Atlantic). Comparison of the quantified morphological variations with geochemical proxies recorded throughout the MECO establishes a differential response of the two studied taxa: *P. papalis* locally disappeared during the climatic interval, while *P.* cf. *papalis* became dominant and showed a wide range of morphological variability. The morphological diversification of *P.* cf. *papalis* expanded on pre-existing morphologies of *P. papalis* and culminated with the appearance of extreme shapes during the warmest interval of the MECO. Interestingly, the upheavals induced by the MECO event appear to be reversible; indeed, after the reappearance of *P. papalis* during the post-MECO cooling phase, the morphospace occupation returned to the original pre-MECO conditions. Our study highlights the great potential of geometric morphometrics to decipher subtle changes in radiolarian morphology in relation to climate change.

IV.2.1. Introduction

The Middle Eocene Climatic Optimum (MECO; Bohaty and Zachos, 2003; Bohaty et al., 2009) is one of the most significant global warming events of the Cenozoic. It occurred during the Bartonian (ca. 40 Ma) and temporarily interrupted the long-term cooling trend initiated at the end of the early Eocene climate optimum (Westerhold and Röhl, 2013; Westerhold et al., 2020). The MECO has been recognized in the marine and continental record by a negative oxygen isotope excursion, which is interpreted as a ~4–6°C rise in seawater temperature (Bohaty and Zachos, 2003; Bohaty et al., 2009; Bijl et al., 2010; Edgar et al., 2010). However, in contrast to what is usually observed for other Paleogene hyperthermal events, the MECO corresponds to only a weak shift in carbon isotope values (Bohaty and Zachos, 2003; Bohaty et al., 2009; Bijl et al., 2010; Giorgioni et al., 2019). Although the actual triggering mechanisms of the MECO are still poorly understood, modeling of the carbon cycle suggests an imbalance in long-term carbon fluxes, resulting in elevated carbon dioxide levels in the ocean-atmosphere system and a shoaling of the carbonate saturation profile (Edgar et al., 2007; Bohaty et al., 2009; Sluijs et al., 2013; Cornaggia et al., 2020; Henehan et al., 2020). Previous studies investigating changes in plankton biodiversity during the MECO have found different types of changes in assemblages, mainly affecting the taxonomic richness, relative abundance, and biogeographic distribution of species (Villa et al., 2008; Bijl et al., 2010; Luciani et al., 2010; Renaudie et al., 2010; Toffanin et al., 2011; Witkowski et al., 2012, 2014; Edgar et al., 2013; Kamikuri et al., 2013; Pascher et al., 2015; Cramwinckel et al., 2019; D'Onofrio et al., 2021; Meunier and Danelian, 2023a). However, no major extinction event and/or prominent taxonomic turnover was observed in any of the plankton microfossil groups during the MECO warming event. In contrast, relatively little is known about the impact of this event on plankton morphology. As species richness and morphological disparity are known to be two distinct components of biodiversity that are often decoupled from each other (Foote, 1991, 1993; Hopkins, 2013), analysis of morphology may prove to be a valuable approach to the assessement of the impact of environmental perturbations that did not result in species extinctions. In addition, size changes and increased morphological disparity in planktic organisms have been reported in association with older Paleogene environmental perturbations, such as the Paleocene-Eocene Thermal Maximum (PETM) (Clay Kelly et al., 1996; Kaiho et al., 2006; Luciani et al., 2007; Yamaguchi et al., 2012; Gibbs et al., 2018; Westacott et al., 2023). These morphological changes induced by environmental forcing may have a significant impact on marine plankton because body size and shape are closely linked to many physiological, ecological, and life history traits.

Therefore, the main objective of this study is to evaluate radiolarian shape variation during environmental perturbations associated with the MECO. To date, the morphology of radiolarian shells has been quantified by biometric analyses, typically based on linear measurements mainly to differentiate closely related species (e.g. Kellogg, 1975, 1983; Lazarus, 1986; Granlund, 1990; Cortese and Bjørklund, 1997, 1998). In recent decades, advances in geometric morphometric methods have driven forward paleobiology by revealing previously unexplored aspects of the fossil record. In particular, quantitative approaches have benne used to extract evolutionary, ecological, and phylogenetic signals from fossils (e.g. Smith and Hendricks, 2013; Parins-Fukuchi, 2018; Bault et al., 2022, 2023; De Mendoza and Gómez, 2022) or to separate cryptic taxa (e.g. Danelian and MacLeod, 2019; Viertler et al., 2022). However, the more recent and powerful methods of geometric morphometrics have been used only occasionally (Sanfilippo and Riedel, 1990; Danelian and MacLeod, 2019).

As a case study, investigations were conducted here on the nassellarian species *Podocyrtis papalis* which is a prominent component of Eocene tropical radiolarian assemblages, from which the biostratigraphically important evolutionary lineages *Podocyrtoges* and *Lampterium* arose (Sanfilippo and Riedel, 1992). Although *P. papalis* is considered as a long-lived species that has experienced morphological stasis, it exhibits highly variable shell morphology throughout the MECO. This interval is marked by the proliferation of specimens with an atypical morphology, classified here as *P*. cf. *papalis*, which are characterized by a less spindle-shaped shell with a well-defined lumbar constriction (see Appendix 1. for a more detailed taxonomic description of the two studied taxa). In this study, we aim to 1) quantify the morphological variability of *P. papalis* and its related morphotypes by using geometric morphometrics on their shell outline, and 2) compare the evolution of the morphological disparity with stable isotope data to assess the effect of environmental perturbations on shape variation of *P. papalis* and its related morphotypes.

IV.2.2. Material and methods

IV.2.2.1. Stratigraphic and paleoclimatic framework

This study is based on Eocene sediment cores drilled at Ocean Drilling Program (ODP) Site 1260 (9°15′N, 54°32′W) on the northern slope of Demerara Rise, a submarine plateau off the coast of South America, on the French Guiana-Suriname margin (Figure IV.2.1). Two holes (1260A and 1260B) situated 50 m apart were drilled at a modern water depth of 2,549 m below sea level (mbsl) (Shipboard Scientific Party, 2004). A 325 m thick Paleogene sequence was recovered from ODP Site 1260, including a ~180 m thick middle Eocene interval dominated by nannofossil chalk rich in siliceous microfossils (Danelian et al., 2005, 2007; Renaudie et al., 2010; Meunier and Danelian, 2022, 2023a, 2023b). During the middle Eocene this site was situated even closer to the equator than it is today, at a paleolatitude of ∼1°N (Suganuma and Ogg, 2006).

At ODP Site 1260, significant shifts were recorded in both oxygen ($\delta^{18}O$) and carbon ($\delta^{13}C$) stable isotope records were recorded (Bohaty et al., 2009; Edgar et al., 2007) and

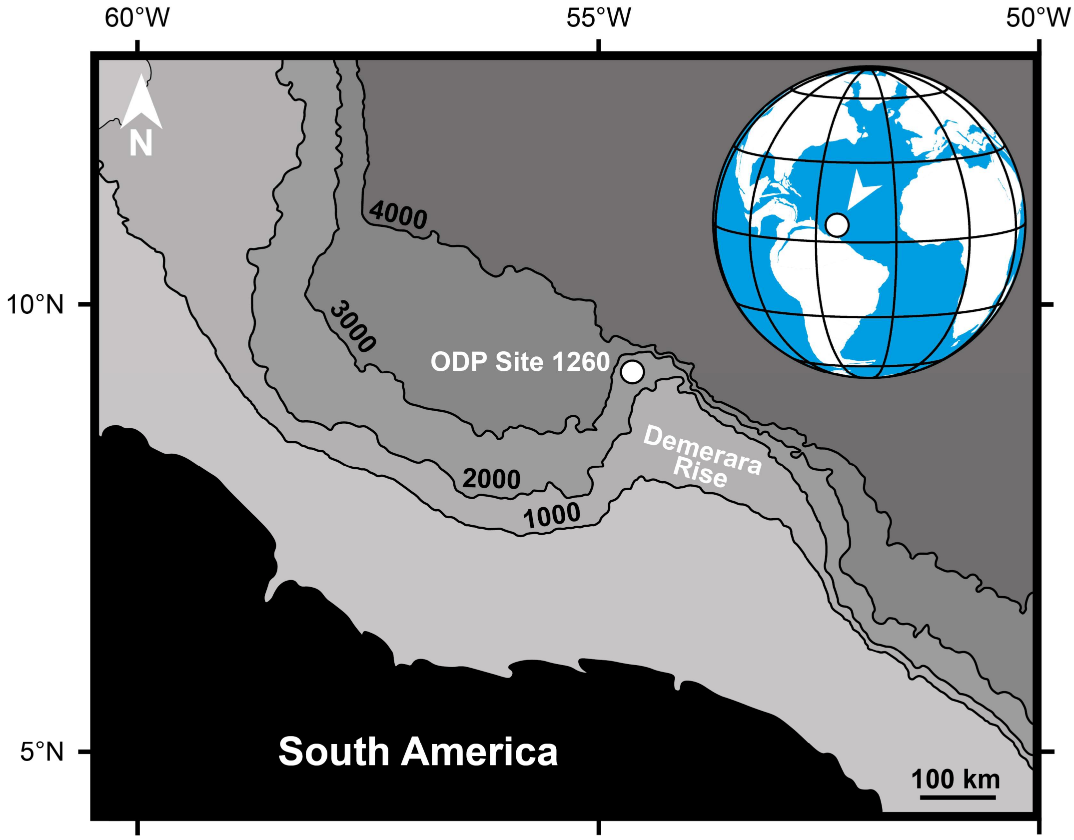

Figure IV.2.1. Geographic location of Demerara Rise and location of studied ODP Site 1260. Bathymetric map modified fromShipboard Scientific Party (2004) and the paleogeographic reconstruction form ODSN Plate Tectonic Reconstruction Service (http://www.odsn.de/odsn/services/paleomap/paleomap.html, last accessed: 14 May, 2023).

correlated with the MECO event (Figure IV.2.2). The onset of the MECO is located at about 52 rmcd, in the upper part of the magnetochron C18r (Edgar et al., 2007); benthic foraminiferal $\delta^{18}O$ values subsequently decreased (~1.0 ‰) toward the peak warming interval of the MECO at 44 rmcd (Figure IV.2.2). The warmer interval is also marked at this site by a negative excursion (~0.5‰) in benthic foraminiferal $\delta^{13}C$ values (Edgar et al., 2007). The peak warming phase was followed by a rapid return to the conditions that prevailed prior to the MECO (Bohaty et al., 2009; Edgar et al., 2010; Westerhold and Röhl, 2013). A high-resolution cyclostratigraphic framework also been developed for ODP Site 1260 (Westerhold and Röhl, 2013). Astrochronological calibration allowed us to date the onset of the MECO at ~40.50 ±

0.02 Ma, the peak warming at ~40.07 ± 0.02 Ma, and the end of the MECO at ~40.05 ± 0.02 Ma (Westerhold and Röhl, 2013).

The studied sequence has a thickness of 15.22 m and is estimated to have been accumulated between 40.66 Ma and 39.84 Ma, during the late middle Eocene (Bartonian). A total of 15 samples covering the MECO interval were selected from hole 1260A (Figure IV.2.2). Mean sample spacing is approximately 1.67 m and the mean age difference between two consecutive samples is ~58 kyr.

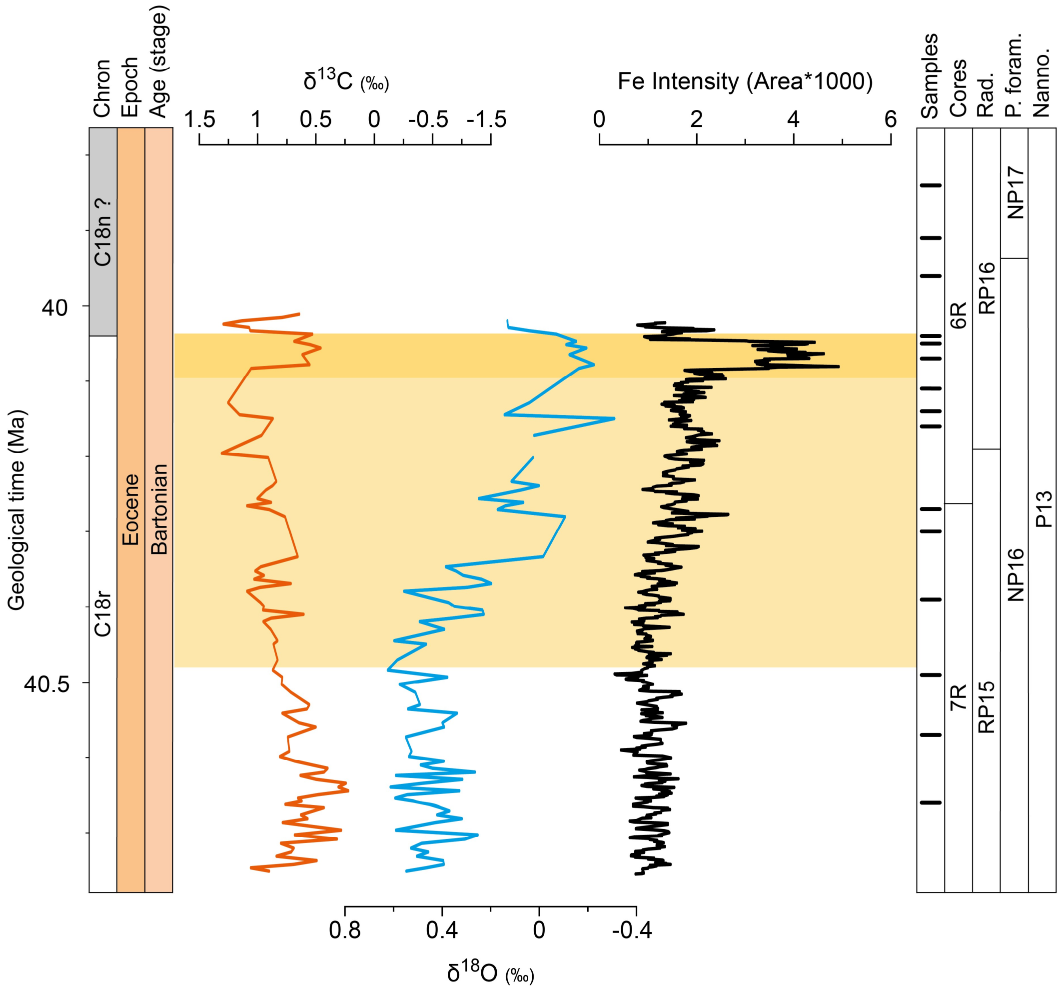

Figure IV.2.2. Variation of geochemical proxies through the MECO interval of ODP Site 1260 (Demerara Rise, equatorial Atlantic Ocean). The darker orange zone highlights the peak warming MECO interval. Stable isotope data are from Edgar et al. (2007), magnetostratigraphy from Suganuma and Ogg (2006), calcareous nannofossil and planktc foraminiferal biostratigraphy from the Shipboard Scientific Party (2004), and radiolarian biozonation is from Meunier and Danelian (2022).

IV.2.2.2. Sample preparation

Samples were processed according to the procedures described in Sanfilippo et al. (1985) and Tetard et al. (2020). Approximately 2 cm² of unprocessed sediment was first soaked for 2 hours in a polypropylene beaker containing 30 mL of 30% hydrochloric acid (HCl) to dissolve the carbonate content and to concentrate siliceous microfossils. The residues were then washed with distilled water. After decantation, the excess water was slowly removed with a pipette, and the residues were soaked in 30 mL of 10% hydrogen peroxide (H_2O_2) for two hours to remove organic matter. The resulting residues were finally washed through a 63 µm sieve to remove clay and small radiolarian fragments and transferred to a storage vial.

IV.2.2.3. Morphometric data and analyses

To describe the morphological response of *Podocyrtis papalis* to the paleoenvironmental changes that occurred during the MECO, we applied a landmark-based geometric morphometric approach to study shell shape variation (Bookstein, 1991; Rohlf and Marcus, 1993; Rohlf, 1999; Mitteroecker and Gunz, 2009; Zelditch et al., 2012; Adams et al., 2013). A total of 491 complete specimens of *P. papalis* were manually collected under a Zeiss SteREO Discovery V20 binocular microscope. The shells were positioned in lateral view using the trilobate pterocorythid cephalis (see Petrushevskaya, 1971, pl. 9, figs. I, II), with the longitudinal axis oriented parallel to the glass slide. The right side of the shell was selected for this study, and the left-sided shells were mirrored for analysis. Each specimen was photographed in the sagittal plane of the shell, allowing the entire shell contour to be seen in a single image. Based on these photos, two-dimensional landmark coordinates were extracted using TpsDig, version 2.31 (Rohlf, 2010, 2015). The shape of the shell was described by a set of six anatomical landmarks placed at the collar and lumbar strictures, and at the intersection of the abdomen and the feet, as well as by four curves of 10 equidistant semilandmarks describing the thoracic and abdominal outlines (Figure IV.2.3). The cephalis was not included in this analysis because previous studies suggest its low taxonomic value for species discrimination within the genus *Podocyrtis* (Sanfilippo and Riedel, 1992; Danelian and MacLeod, 2019).

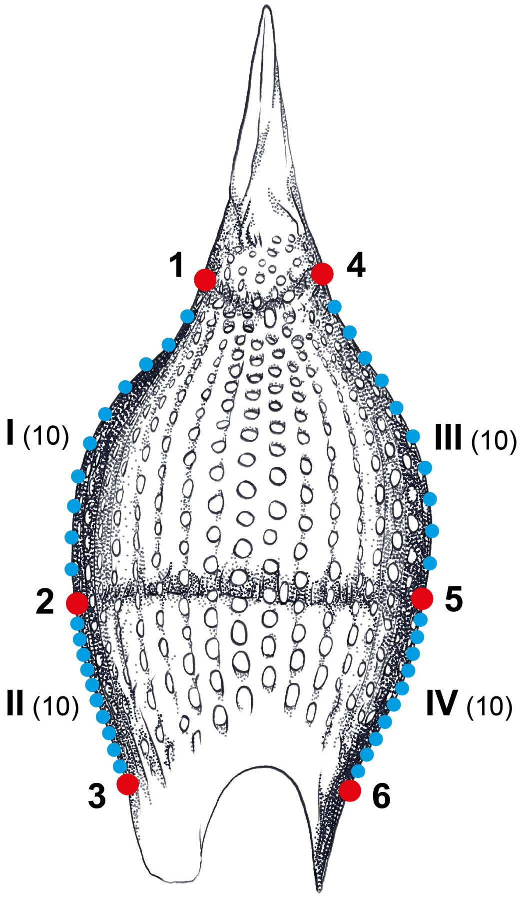

Figure IV.2.3. Diagrammatic representation of a *Podocyrtis* shell in lateral view, including the location of the six selected landmarks (Arabic numerals) and the four semi-landmark curves (Roman numerals, with the number of points per curve indicated in parentheses).

The acquired 2D landmark coordinates of the studied specimens were then superimposed using a generalized Procrustes analysis (GPA; Rohlf and Slice, 1990). Next, a morphological space (Dryden and Mardia, 1998; Kendall et al., 1999; Klingenberg, 2020) was constructed by means of a principal component analysis (PCA; Ringnér, 2008; Abdi and Williams, 2010). This morphospace allows the description and quantification of the morphological disparity of the two studied taxa through time (Ciampaglio et al., 2001; Wills, 2001; Guillerme et al., 2020). Here, morphospace occupancy is estimated by the sum of ranges (SoR), which refers to the total range of morphospace occupancy (Foote, 1991), as well as the sum of variances (SoV), which measures the variance in distance between examined specimens in the morphospace (Van Valen, 1974; Foote, 1991, 1993; Wills, 2001). In order to assess the effect of sample size variation overtime, confidence intervals for the computed disparity values were calculated using a bootstrap approach by iteratively calculating SoR and SoV (1000 times) from random resampling with replacement of the individual points in the morphospace (Foote, 1993). Finally, the measurement error associated with the precision of landmark digitization was evaluated by comparing the distribution of the Procrustes distances among all specimens with those of 10 specimens digitized each by two different observers. Here, a permutational ANOVA test indicated that this replicability error accounted for ~12% of the total variance and, therefore, had a reduced impact (Appendix IV.2.2).

All shape analyses were performed in the scientific environment R (v. 4.1.3; R Core Team 2022), using the packages geomorph (v. 4.0.3; Adams and Otárola-Castillo, 2013), MASS (v. 7.3-60; Ripley et al., 2013), vegan (v. 2.5-6; Oksanen et al., 2019), and epaleo (v. 1.0.0; Monnet, unpub.).

IV.2.3. Results

IV.2.3.1. Global morphological space

Thefirst two principal components (PCs) of the morphospace explain 78.8% of the total variance in shell shape variation for the radiolarians *Podocyrtis papalis* and *P*. cf. *papalis* (PC1 = 63.3%; PC2 = 15.5%; Figure IV.2.4). The morphological interpretation of the shape changes associated with each axis of the morphospace can be investigated by plotting reconstructed virtual shapes at different locations along the principal components. The first axis of the PCA, which accounts for more than half of the total variation in intraspecific shell morphology of the two studied taxa, clearly shows a gradient in the transversal asymmetry and lateral thickness of the abdominal segment (Figure IV.2.4). On the one hand, high PC1 values show typical *P. papalis* morphotypes with a relatively short abdomen, giving the shell a spindle-shaped to pyriform overall shape. In addition, the shell is widest just above the lumbar stricture, which is not usually expressed externally, and the thorax/abdomen ratio is greater than 1. On the other hand, low PC1 scores indicate a longer abdomen, giving the shell a more elongated appearance, sometimes with a slight lumbar constriction and a thorax/abdomen ratio closer to 1 (Figure IV.2.4). The second axis of the PCA shows variations in thorax elongation. Morphotypes situated on the positive side of the axis show a relatively short and swollen thoracic segment, whereas negative PC2 values reflect a much more slender thorax (Figure IV.2.4).

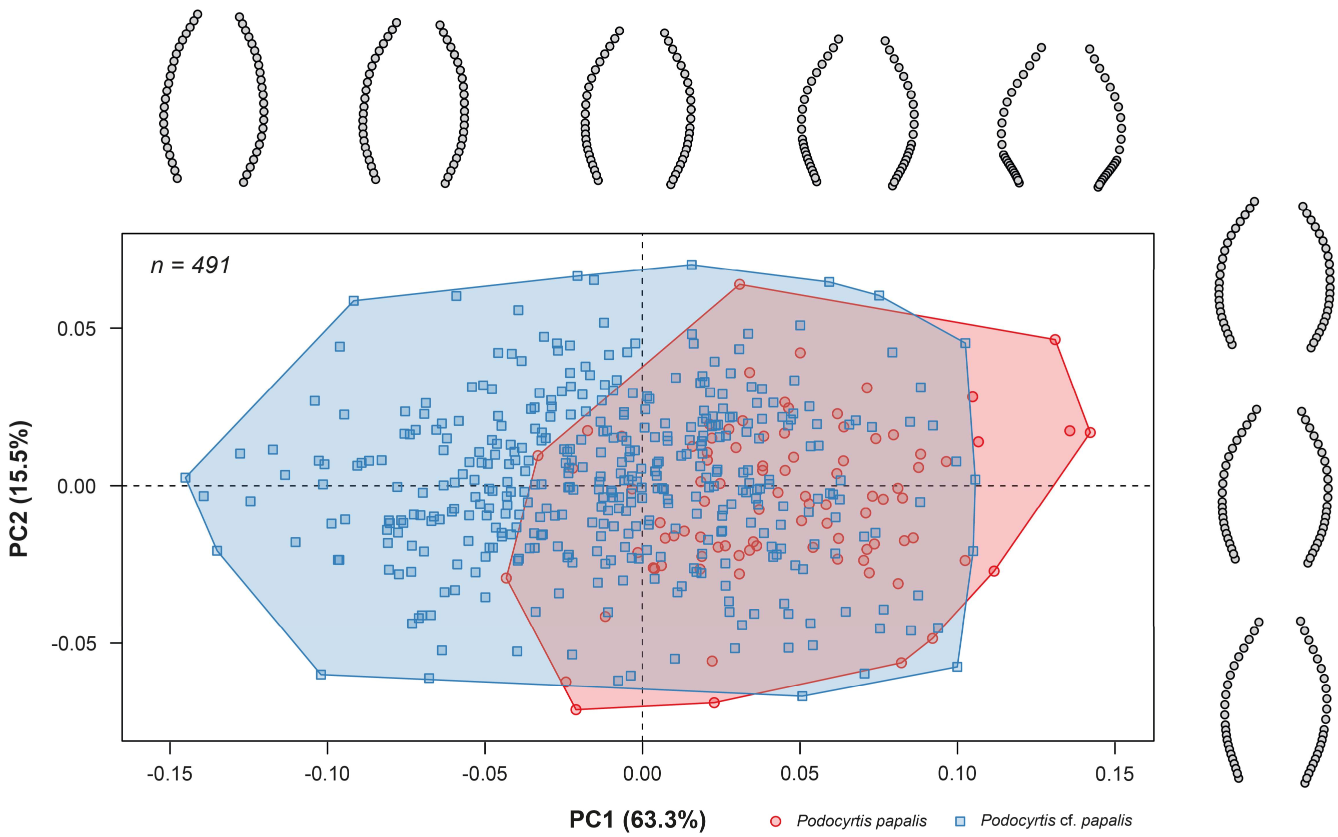

Figure IV.2.4. Results of the first two axes of the Principal Component Analysis (PCA) performed on the superimposed landmark coordinates. Above the PC plot are illustrated the reconstructed virtual shapes obtained after a back-transformatng of the PC scores of the first axis.

The morphospace overlaid with the two studied taxa (Figure IV.2.4) shows that they both cover the major shape changes discussed above. Also, the significant overlap between *P. papalis* and *P.* cf. *papalis* shows that these major shape changes (transversal asymmetry, lateral thickness, and thoracic elongation) are at the intraspecific level and are not discriminatory at the species level. However, *P.* cf. *papalis* shows the greatest disparity, occupying almost the entire morphospace, while *P. papalis* is more restricted to the 'right' half of the morphospace,lacking the most elongate and symmetrical shapes.

IV.2.3.2. Morphospace occupancy and morphological disparity through time

Changes in morphospace occupancy and morphological disparity through time for the two studied taxa are shown in FigureS IV.2.5 and IV.2.6, respectively. During the pre-MECO interval (Figures IV.2.5A–5C), the morphospace was characterized by a reduced occupancy, with low SoR and SoV values (Figures IV.2.6A–6B). The oldest sample examined (Figures IV.2.5A) contains only stypical *Podocyrtis papalis* specimens packed into a relatively compact point cloud whose center is in the positive part of PC1. The first appearance of *P.* cf. *papalis* around 40.57 Ma (~110 kyr before the onset of the MECO) marks the first changes in the morphospace occupancy. The point cloud corresponding to *P.* cf. *papalis* extends around the origin, occupying part of the morphological space previously occupied by *P. papalis* (Figures IV.2.5B), while the specimens corresponding to *P. papalis* are completely relegated to the positive part of PC1 (Figures IV.2.5B, 5C). It is noteworthy that *P.* cf. *papalis* was abundantsince its emergence, representing up to ~50% of the specimens examinedprior the onset of the MECO.

The MECO interval coincided with a protracted increase in morphological disparity indices (Figures IV.2.6A, 6B), corresponding to the spread of *P.* cf. *papalis*, which completely invaded the 'left' half of the morphospace (Figures IV.2.5D–5I). The maximal spread of *P.* cf.

papalis is observed during the warmest interval of the MECO (Figures IV.2.5J–5L). This increase in the occupancy of the morphospace is illustrated by the SoR values that begin to increase slowly at 40.2 Ma and peak at 40.05 Ma (Figures IV.2.6A). The SoV also showed a

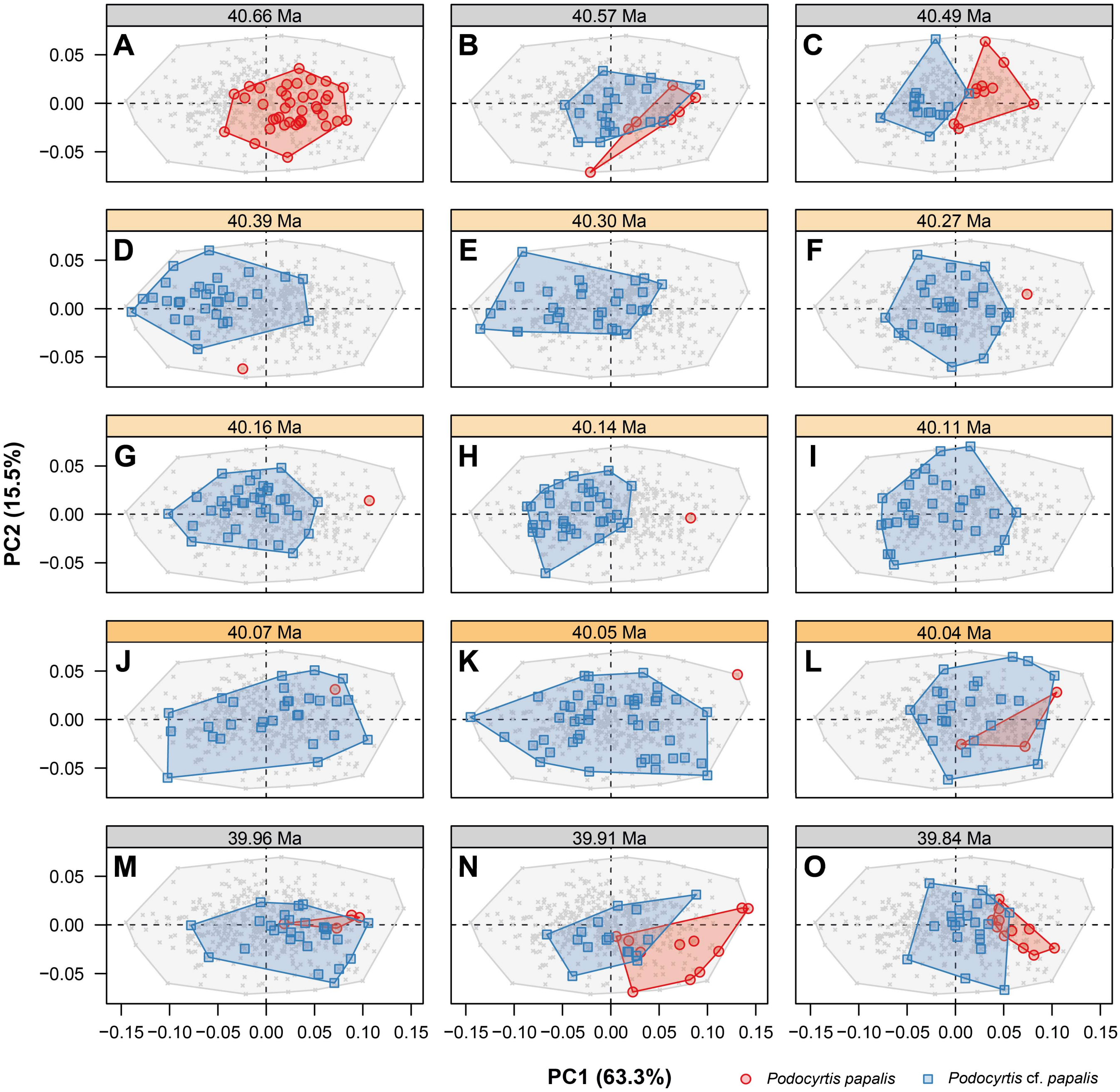

Figure IV.2.5. Changes in morphospace occupancy through time, with the typical morphotype of *Podocyrtis papalis* represented by red dots, and *P.* cf. *papalis* represented by blue squares. Estimated tuned ages are taken from Westerhold and Röhl (2013). The darker orange rectangles, highlight the peak warming MECO interval.

global increase peaking during the warmest interval of the MECO but, unlike the SoR, this global increase was interrupted by low values between ~40.3 and 40.1 Ma (Figures IV.2.6B).

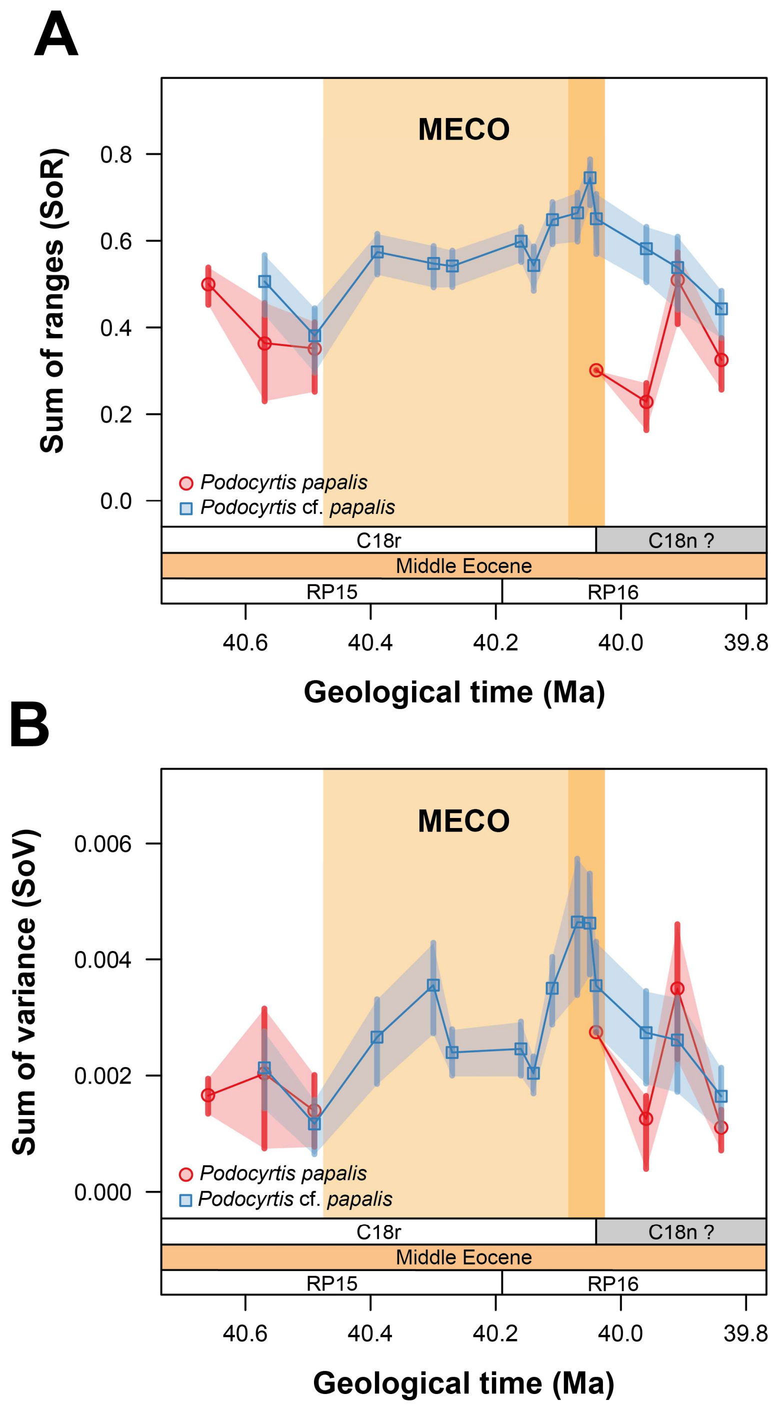

Figure IV.2.6. Evolution of *Podocyrtis* shell morphological disparity through the Middle Eocene Climate Optimum (MECO). The magnetostratigraphy follows Suganuma and Ogg (2006) and the radiolarian biozonation is from Meunier and Danelian (2022). Estimated tuned ages are taken from Westerhold and Röhl (2013). The darker orange zone highlights the peak warming MECO interval.

The post-MECO interval is marked by the recovery of typical *P. papalis* (ca. 39.9 Ma) and a striking concomitant decrease in the morphological disparity of *P.* cf. *papalis* , reflected in both SoR and SoV values (Figures IV.2.6A, 6B). Furthermore, this post-MECO pattern is clearly a return to the initial pre-MECO state of coexistence of the two taxa (compare Figures IV.2.5B–5C and 5M–5O), with the point cloud of *P.* cf. *papalis* extending around the morphospace origin and the specimens of *P. papalis* remaining confined to the positive part of PC1.

IV.2.4. Discussion

The major pattern revealed by the geometric analysis of the *Podocyrtis* shell outline is a profound, differential ecological response of *Podocyrtis papalis* and *P.* cf. *papalis* to environmental perturbations that did not cross the extinction threshold. Figure IV.2.7 shows an adaptive model derived from the temporal sequence of morphological space occupancy. First, the incidence of *P.* cf. *papalis* increased dramatically during the MECO interval (> 90% of the sampled specimens), while the typical *P. papalis* became increasingly rare until the end of the climatic event. Since *P. papalis* was found to be more abundant at mid-latitude ODP Site 1051 (North Atlantic) during the MECO interval (Meunier and Danelian, 2023a), its disappearance from equatorial ODP Site 1260 can be explained by a poleward migration that was triggered by the warming event. *P. papalis* would then have found refuge in the mid-latitudes by tracking its preferred temperature conditions. Interestingly, the migration of tropical radiolarian species to higher latitudes has also been documented in the Southern Hemisphere during the Paleocene-Eocene Thermal Maximum (Hollis et al., 2005a, b; Hollis 2006), as well as in paleoceanographic studies based on planktic foraminifera (Thomas and Shackleton, 1996; Arenillas et al., 1999; Lu and Keller, 1995; Berggren and Ouda, 2003) and dinoflagellates (Bujak and Brinkhuis, 1998; Crouch et al., 2001, 2003; Sluijs et al., 2005, 2006). The observed pattern of migration in response to environmental change appears to be a common biotic response of tropical/subtropical planktic species to Paleogene global warming events.

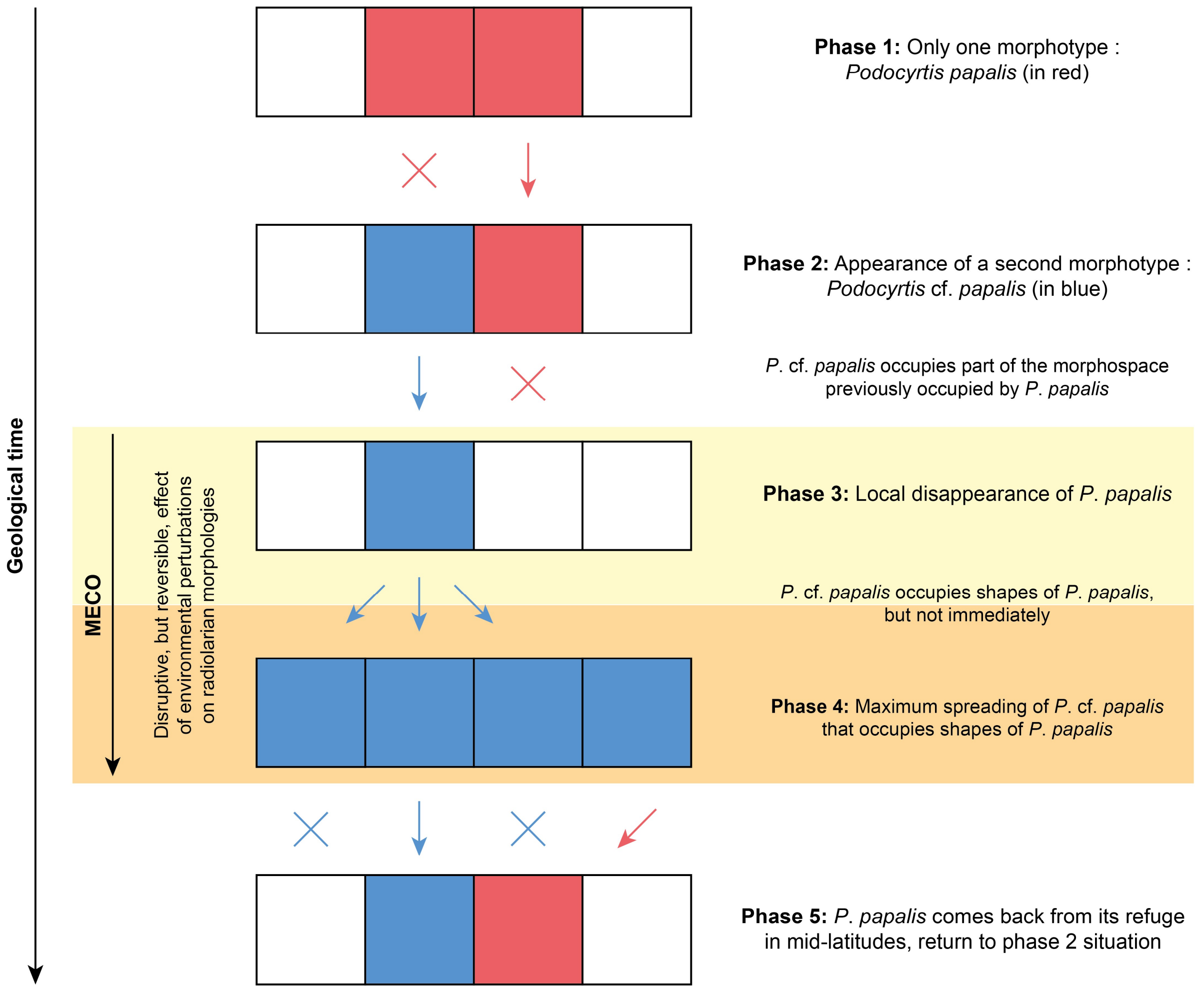

Figure IV.2.7. Adaptive model derived from the temporal sequence of morphological space occupancy by *Podocyrtis papalis* and *P.* cf. *papalis* through the Middle Eocene Climate Optimum (MECO). The darker orange zone highlights the peak warming MECO interval.

On the contrary, *P.* cf. *papalis* remains abundant at ODP Site 1260 throughout the MECO interval and appears to behave as an opportunistic species, taking advantage of the local disappearance of *P. papalis* to occupy the entire morphospace. A combination of range- and variance-based disparity metrics shows that the morphological diversification of *P.* cf. *papalis* culminated during the warmest interval of the MECO with the appearance of extreme shapes (see Appendix IV.2.1, Plate IV.2.2, Figures 13–16). Morphological instability has long been hypothesized to be indicative of environmental stress on the physiology of an organism during its development (Klingenberg et al., 2003), so it is likely that this increase in *P.* cf. *papalis* shell disparity is indicative of ecological stress induced by the warming event. In addition, it has been shown in several taxa that populations under environmental stress can respond by increasing trait variation, allowing species to persist under global change (e.g. Charmantier et al., 2008; Polechova and Storch, 2008; Nicotra et al., 2010). Thus, we can thus hypothesize that the specimens assigned to *P.* cf. *papalis* may have developed a diverse shell morphology to overcome transient MECO-associated environmental perturbations. Such events of morphological diversification in response to Paleogene environmental forcing have also been documented in the fossil record of planktonic foraminifera. For example, the genera *Morozovella* and *Acarinina* show increasing test variation during the PETM (Luciani et al., 2007). This transient diversification gave rise to several short-lived morphospecies, the so-called 'excursion taxa', whose stratigraphic range is limited to the climatic interval (Clay Kelly et al., 1996; Luciani et al., 2007, 2010; Ouda, 2018). Since the total range of *P.* cf. *papalis* exceeds the limits of the MECO, this morphotype cannot be considered as a, strictly speaking, excursion taxon, although the most extreme forms occurred only during the peak warming interval.

Although the disparity peak coincides with the temperature peak, the exact mechanism leading to the diversification of shell morphologies remains elusive. The isotopic data used to identify the MECO interval and to construct the temperature curve are a simplification of the perturbations that actually occurred during this climatic event, and reflect only one aspect of this complex phenomenon generated by the interactions of numerous abiotic parameters (Henehan et al., 2020). In previous studies, foraminiferal test deformations associated with the MECO warming have been tentatively linked to increased productivity and/or low oxygen levels in surface waters, although changes in temperature, pH, or salinity cannot be discarded

(Luciani et al., 2007, 2010). Similarly, in silicoflagellates, which are close to radiolarians in terms of morphology and skeletal composition, high morphological variability has been attributed to fluctuations in salinity (Dumitrică, 1972; McCartney and Wise, 1990) or to heavy metal contamination (Thomas et al., 1980). Variations in the composition of siliceous plankton assemblages at ODP Site 1260 indicate higher productivity in surface waters throughout the MECO interval (Renaudie et al., 2010; Meunier and Danelian, 2023a), which may have favored the morphological diversification of *P.* cf. *papalis*. However, the hypothetical effects of environmental parameters on the skeletogenesis of polycystine radiolarians are intricate and not well-documented because these pelagic organisms are too sensitive to be cultured under laboratory conditions (Anderson et al., 1986, 1989a, b). This technical problem, combined with an incomplete knowledge of the ecology of modern radiolarians, remains a serious obstacle to our understanding of radiolarian paleoecology.

Geometric morphometric shape analyses illustrate two possible responses of planktic organisms to global warming: either migrate to follow their preferred temperature conditions, or adapt by producing additional morphologies. This allows us to gain a deeper understanding of the impact of climate change on oceanic plankton, especially in the case of low-magnitude climatic events that did not result in taxonomic extinctions. In a world threatened by global changes induced by human activities, this information may be of significant importance for characterizing how biological systems respond to environmental perturbations, in order to better model and anticipate future upheavals. It is also interesting to note that the perturbations in the morphological space occupancy observed at ODP Site 1260 during the MECO warming ended with the recovery of *P. papalis* around 40 Ma. The two taxa returned to a balanced occupation of the morphological space, similar to pre-MECO conditions, highlighting the resilience of radiolarians to global change.

IV.2.5. Conclusions

The morphological response of radiolarians to the Middle Eocene Climatic Optimum (ca. 40 Ma) is examined for the first time in this study. Using geometric morphometric methods, we document variation in morphological disparity of the nassellarian species *Podocyrtis papalis* and a closely related taxon classified as *P*. cf. *papalis*, which is particularly abundant during the MECO interval.

Changes in morphospace occupancy through the MECO showed that the two studied taxa reacted differently to the environmental forcing. On the one hand, *P*. *papalis* almost completely disappeared from low latitudes during the climatic interval. The concurrent increase in the relative abundance of this species at mid-latitude ODP Site 1051 suggests that it has sought refuge at higher latitudes by tracking its optimal habitat. On the other hand, *P*. cf. *papalis* remains abundant at ODP Site 1260 during the MECO and exihits a wide range of morphological variability, culminating in the appearance of extreme shapes during the warmest interval of the MECO. The high morphological variability expressed by *P*. cf. *papalis* is interpreted as an indicator of the biological stress induced by the MECO. These results illustrate two possible responses of planktic organisms to global warming, either migration or adaptation through the production of additional morphologies. Despite the profound changes induced by the warming event, a return to pre-event conditions is observed at ODP Site 1260 following the recovery of *P*. *papalis* during the post-MECO cooling phase, highlighting the resilience of radiolarian species to climate change.

Finally, this study demonstrates that the application of modern geometric morphometrics to quantify variation in radiolarian shell morphology can be used as a reliable baseline for further paleontological research on radiolarians. This approach appears to be more sensitive than the traditional taxonomic richness to the study of low-magnitude climatic events that have not crossed the threshold to drive extinction in planktic species.

Acknowledgments

We acknowledge the Ocean Drilling Program (ODP) for supplying the samples used in this study. Bert Van Bocxlaer is thanked for fruitful discussions on geometric morphometric analyses. Maxime Lepot and Veronica Carlsson are thanked for their help in collecting material in the early stages of this project. Thanks are also due to Jessie Cuvelier and Sylvie Regnier for technical assistance.

Author contributions

Mathias Meunier: Conceptualization, Methodology, Investigation, Visualization, Writing-Original draft, Writing-Reviewing and Editing. **Claude Monnet**: Conceptualization, Methodology, Software, Data Analysis, Writing-Reviewing and Editing. **Rémi Habert**: Data collection, Data curation. **José Francisco Pínto Cabrera**: Methodology, Investigation, Data Curation. **Marie Cueille:** Visualization. **Taniel Danelian:** Conceptualization, Supervision, Resources, Writing-Original draft, Writing-Reviewing and Editing.

Appendix IV.2.1. Taxonomic framework

The text follows the morphological terminology of Sanfilippo and Riedel (1992) to designate the various parts of the Podocyrtis shell.

Class Polycystinea Ehrenberg, 1839

Order Nassellaria Ehrenberg, 1876

Superfamily Pterocorythoidea Haeckel, 1882 emend. Suzuki et al., 2021

Family Pterocorythidae Haeckel, 1882

Genus *Podocyrtis* Ehrenberg, 1846

Type species.— *Podocyrtis papalis* Ehrenberg, 1847, p. 55, fig. 2.

Podocyrtis (*Podocyrtis*) *papalis* Ehrenberg, 1847

Plate IV.2.1, Figures 1–6

1847 *Podocyrtis papalis* Ehrenberg, p. 55, fig. 2.
1854a *Podocyrtis papalis* Ehrenberg – Ehrenberg, pl. 36, fig. 23.
1874 *Podocyrtis papalis* Ehrenberg – Ehrenberg, p. 251.
1973 *Podocyrtis* (*Podocyrtis*) *papalis* Ehrenberg – Sanfilippo and Riedel, p. 531, pl. 20, figs. 11–14, pl. 36, figs. 2, 3.
1974 *Podocyrtis* (*Podocyrtis*) *papalis* Ehrenberg – Nigrini, p. 1069, pl. 1K, figs. 7–10.
2009 *Podocyrtis papalis* Ehrenberg – Ogane et al., pl. 58, figs. 1a–1f.

Description.— The shell is spindle-shaped, thick-walled, and trisegmented. The cephalis is trilobate, with a large eucephalic lobe that can be sub-hemispherical or longitudinally elongated, and two smaller subspherical lateral lobes. The apical spine protrudes as a moderately to well-developed apical horn, which is usually three-bladed, sometimes conical. The collar stricture is marked by a slight change in shell contour and underlined by a thin V-shaped dark line. Well-preserved specimens usually have a short axobate. The thorax is truncate-conical to inflated and perforated by circular, longitudinally arranged pores, which are separated by weak longitudinal costae. The shell is widest just above the lumbar stricture, which is not expressed externally but marked by a relatively thick internal ridge. The abdomen is inverted truncate-conical, short, and noticeably less voluminous than the thorax (with a thorax/abdomen ratio of approximately 2:1 for the typical morphotype of *Podocyrtis papalis*). The proximal part of the abdomen is perforated by pores that are similar in shape and size to those found on the thorax. The distal part, on the other hand, lacks pores and terminates in three broad, shovel-shaped feet.

Remarks.— *Podocyrtis papalis* is the earliest pterocorythid species found in the fossil record. Its first occurrence is near the Paleocene-Eocene boundary (Sanfilippo and Riedel, 1992), and its stratigraphic range extends from the late *Bekoma bidartensis* Zone (early Eocene) to the *Calocyclas bandyca* Zone (middle-late Eocene).

P. aphorma Riedel and Sanfilippo, 1970 can be distinguished from *P. papalis* by its less regular abdominal pores and the presence of a slight lumbar constriction. Similarly, *P. acalles* Sanfilippo and Riedel, 1992 is distinguished from *P. papalis* by the presence of a slight external lumbar constriction. Additionally, while the shell of *P. papalis* is widest above the lumbar stricture, *P. acalles* is widest at or slightly below the lumbar stricture (Sanfilippo and Riedel, 1992). In *P. acalles*, the size of abdominal pores is irregular and not always strictly aligned longitudinally. This results in more discrete and discontinuous longitudinal ridges between pore rows. Additionally, the thorax/abdomen ratio in both *P. aphorma* and *P. acalles* tends towards 1. Unfortunately, no differential diagnosis was provided to differentiate *P. acalles* from *P. aphorma*, which appears to be morphologically indistinguishable based on the photographs published along with their original descriptions.

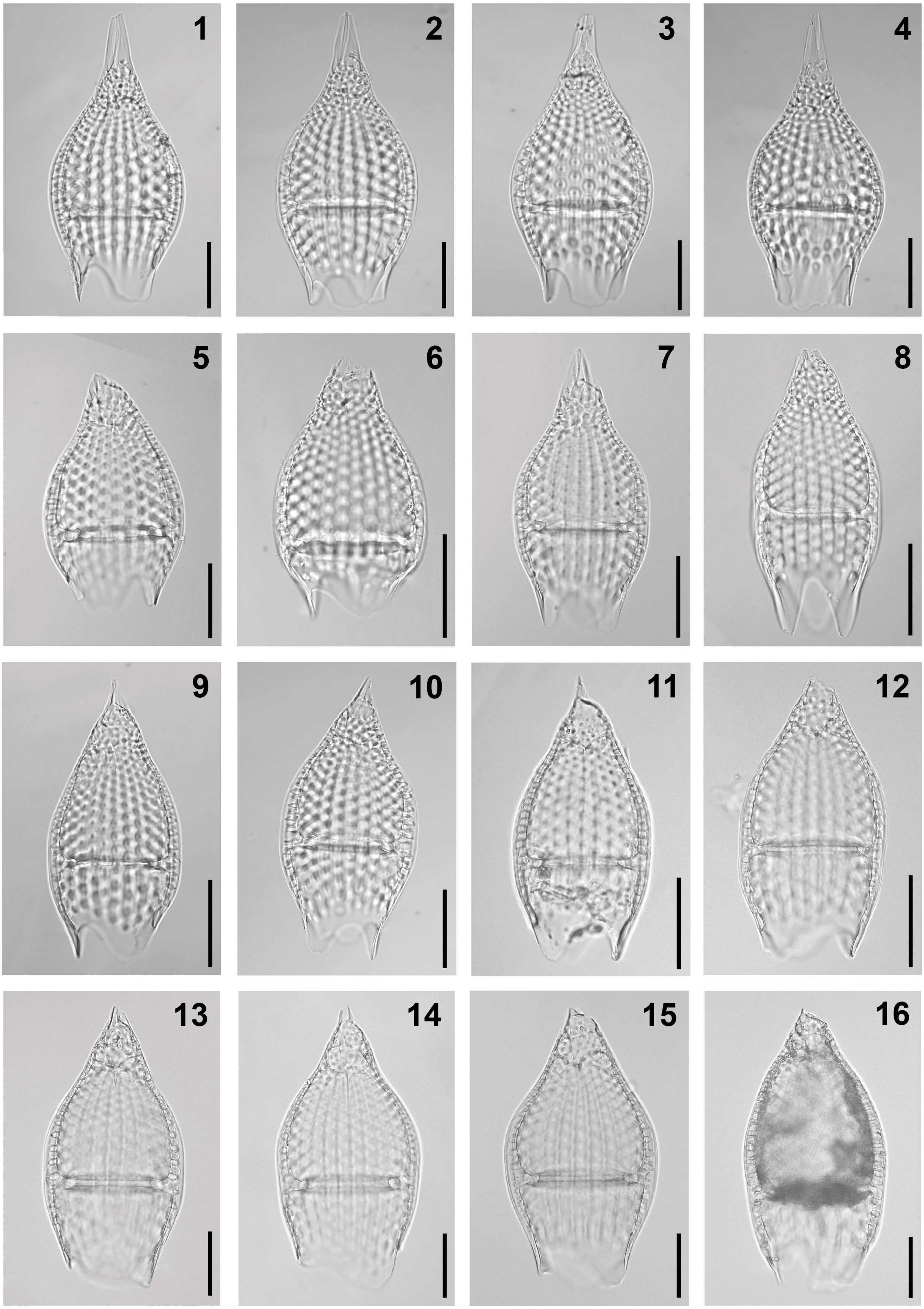
1
2
3
4
5
6
7
8
9
10
11
12
13
14
15
16

Plate IV.2.1. Composite light micrographs of analyzed radiolarian specimens from ODP Site 1260 (Demerara Rise, western equatorial Atlantic). (**1-6**) Typical *Podocyrtis papalis* Ehrenberg, 1847: (**1**) ODP 1260A-7H-5W, 70–72 cm; (**2**) ODP 1260A-7H-5W, 70–72 cm; (**3**) ODP 1260A-7H-5W, 70–72 cm; (**4**) ODP 1260A-7H-3W, 69–71 cm; (**5**) ODP 1260A-7H-1W, 22–24 cm; (**6**) specimen showing a reduced abdomen, ODP 1260A-6H-6W, 57–59 cm. (**7-12**) *Podocyrtis* cf. *papalis* Ehrenberg, 1847: (**7**) ODP 1260A-7H-2W, 19–21 cm; (**8**) ODP 1260A-6H-6W, 20–22 cm; (**9**) ODP 1260A-6H-6W, 57–59 cm; (**10**) ODP 1260A-6H-6W, 57–59 cm; (**11**) ODP 1260A-6H-4W, 119–121 cm; (**12**) ODP 1260A-6H-4W, 119–121 cm; (**13**) ODP 1260A-6H-3W, 18–20 cm; (**14**) ODP 1260A-6H-3W, 18–20 cm; (**15**) ODP 1260A-6H-3W, 18–20 cm; (**16**) ODP 1260A-6H-4W, 68–70 cm. All scale bars equal 50 µm.

Podocyrtis (*Podocyrtis*) cf. *papalis* Ehrenberg, 1847

Plate IV.2.1, Figures 7–16, Plate IV.2.2, Figures 1–16

1993 *Podocyrtis* (*Podocyrtis*) sp. aff. *P.* (*P.*) *papalis* Ehrenberg – Hull, pl. 8, fig. 3.
? 1999 *Podocyrtis mitrella* Ehrenberg – Kozlova, p. 174, pl. 18, fig. 24.
2006 *Podocyrtis* (*Podocyrtis*) *papalis* Ehrenberg – Funakawa et al., p. 29, pl. P9, figs. 13a, 13b.
2012 *Podocyrtis* (*Podocyrtoges*) *diamesa* Sanfilippo and Riedel – Kamikuri and Wade, pl. 1, figs. 7a, 7b.
2015 *Podocyrtis* (*Podocyrtis*) *papalis* Ehrenberg – Kamikuri, pl. 9, figs. 1a, 1b (part).

Remarks.— This morphotype is similar to *Podocyrtis papalis*, but it has a more elongated shape and a less pronounced lumbar constriction. It also has a thinner shell wall and a reduced tribladed apical horn, which is usually the same height as the cephalis. The attachment area of the horn on the cephalis appears to be relatively fragile, as the apical horn was broken in most of the observed specimens. The specimen illustrated by Kamikuri and Wade (2012) from ODP Site 1051 cannot be assigned to *P. diamesa* due to its small size. Additionally, its stratigraphic position in the upper part of the *P. goetheana* Zone (RP16) does not correspond to the known stratigraphic range of *P. diamesa*, whose last occurrence lies in the *P. ampla* Zone (Nigrini et al., 2005; Kamikuri et al., 2012a; Meunier and Danelian, 2022).

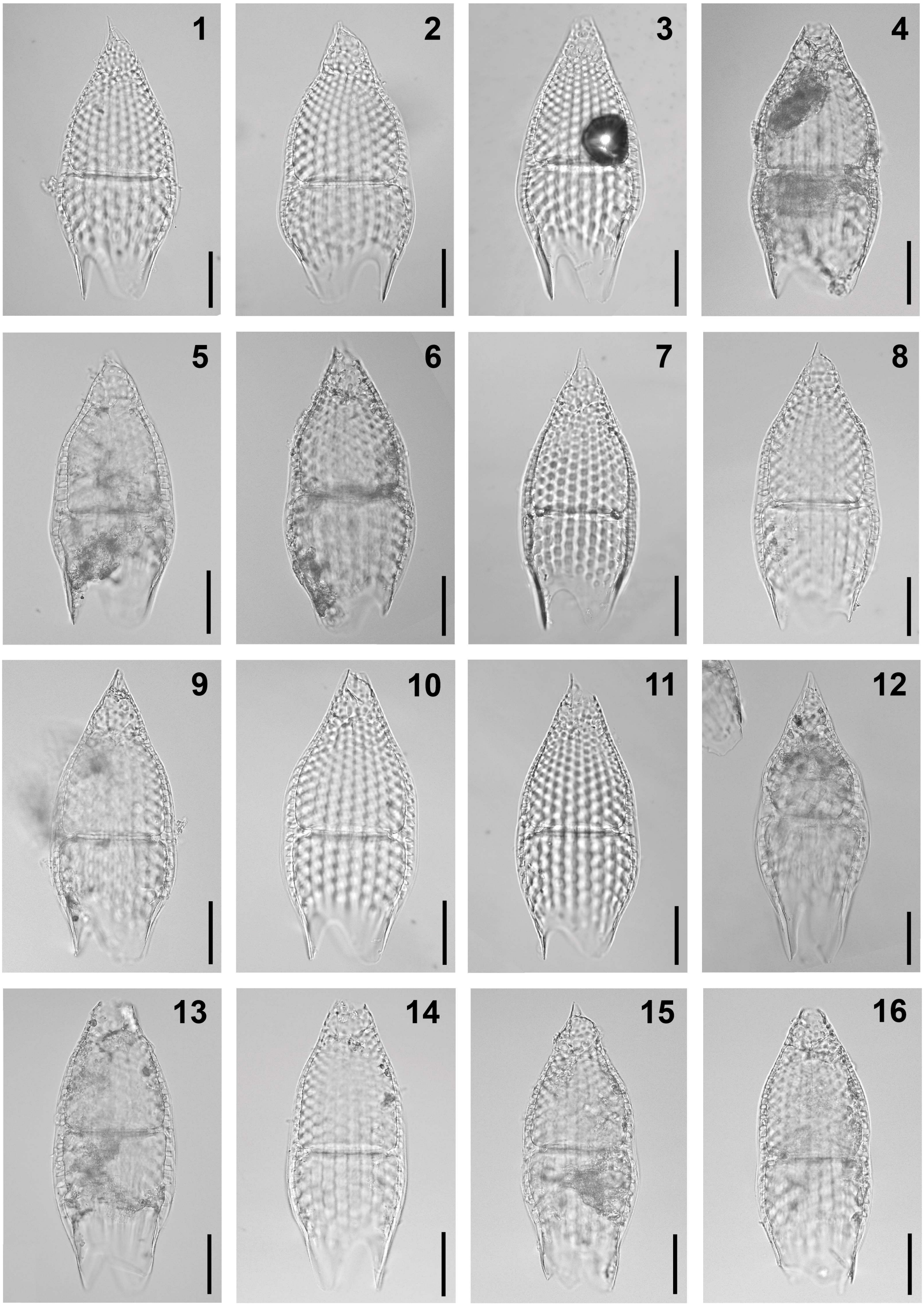
1
2
3
4
5
6
7
8
9
10
11
12
13
14
15
16

Plate IV.2.2. Composite light micrographs of analyzed radiolarian specimens from ODP Site 1260 (Demerara Rise, western equatorial Atlantic). (**1-16**) *Podocyrtis* cf. *papalis* Ehrenberg, 1847: (**1**) ODP 1260A-6H-6W, 20–22 cm; (**2**) ODP 1260A-6H-6W, 20–22 cm; (**3**) ODP 1260A-6H-6W, 57–59 cm; (**4**) ODP 1260A-6H-4W, 119–121 cm; (**5**) ODP 1260A-6H-4W, 68–70 cm; (**6**) ODP 1260A-6H-4W, 119–121 cm; (**7**) ODP 1260A-6H-6W, 57–59 cm; (**8**) ODP 1260A-6H-5W, 63–65 cm; (**9**) ODP 1260A-6H-4W, 119–121 cm; (**10**) ODP 1260A-6H-6W, 20–22 cm; (**11**) ODP 1260A-6H-6W, 57–59 cm; (**12**) ODP 1260A-6H-3W, 18–20 cm; (**13**) ODP 1260A-6H-4W, 68–70 cm; (**14**) ODP 1260A-6H-5W, 63–65 cm; (**15**) ODP 1260A-6H-4W, 119–121 cm; (**16**) ODP 1260A-6H-4W, 119–121 cm. All scale bars equal 50 µm.

Appendix IV.2.2. Evaluation of the measurement process bias (measurement error).

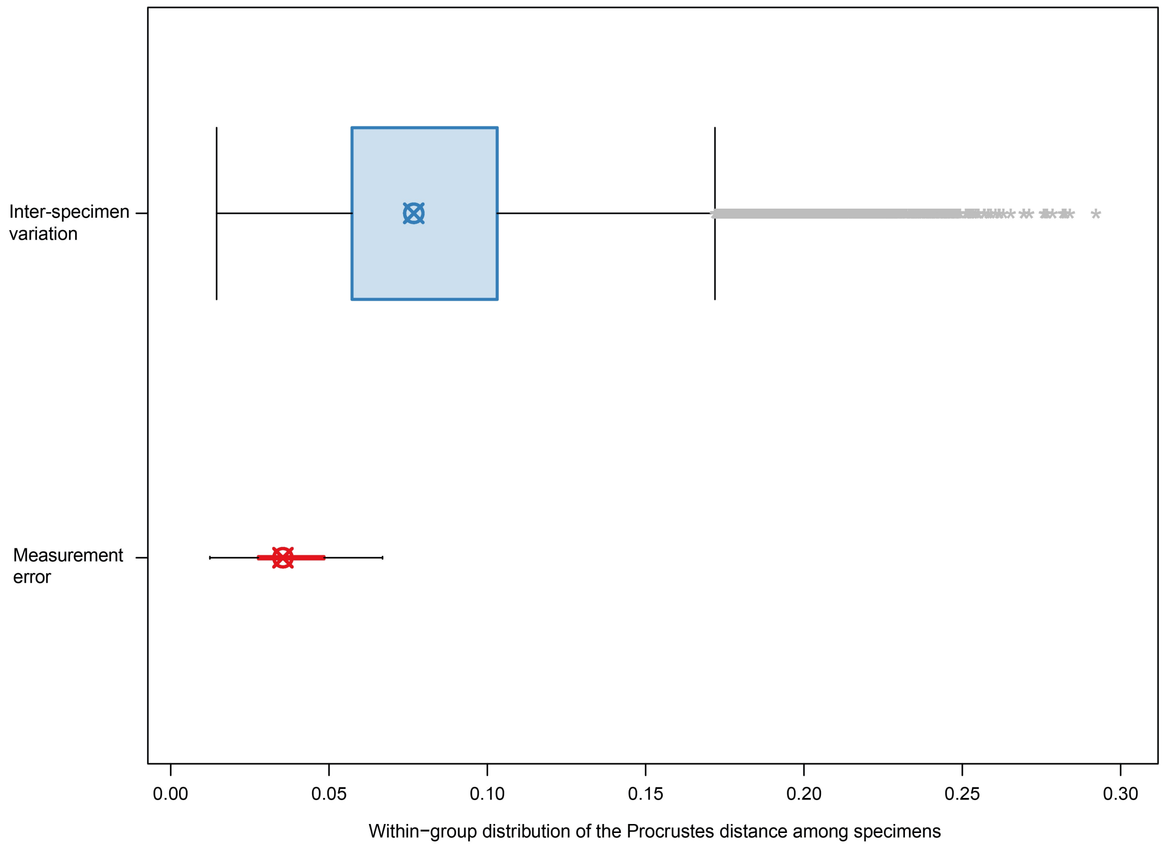

Chapter V – General conclusions and perspectives

Polycystine radiolarians represent one of the most diverse groups of marine plankton during the Eocene. A total of 245 morphospecies were identified in this study in a ~5.4 Ma stratigraphic interval spanning the late middle Eocene (early Lutetian to middle Bartonian). However, this astonishing diversity is far from being fully documented. Indeed, although radiolarians have attracted the attention of micropaleontologists since the nineteenth century, numerous rare morphotypes of no biostratigraphic value, or those belonging to morphologically complex taxa, remained undescribed. At ODP Site 1051, where we achieved the catalog of the whole radiolarian assemblage, unknown morphotypes account for 48% of the total diversity. This knowledge gap at the most basic level of species description is probably one of the main obstacles to the development of radiolarian research. To address this issue, 36 new radiolarian species have been formally described, including 32 nassellarians and four spumellarians. This represents an increase of ~14% to the total diversity inventoried during our taxonomic survey. Some of these new species are major components of radiolarian assemblages (e.g., *Apoplanius hyalinus* Meunier and Danelian and *Dictyoprora echidna* Meunier and Danelian at ODP Site 1051) and could prove to be good stratigraphic markers, or display interesting combinations of character states that improve our understanding of the evolution of some genera (e.g., *Aphetocyrtis zamenhofi* Meunier and Danelian and *Spirocyrtis* ? *renaudiei* Meunier and Danelian). Biostratigraphic information was also provided for each new taxon, and stratophenetic relationships to previously described species were proposed, leading to the establishment of four new evolutionary lineages.

Alpha-taxonomic studies are a prerequisite for developing radiolarian research, but a robust taxonomic framework at higher levels should also support the description of biodiversity. In Cenozoic radiolarians, the superfamily and family levels are relatively consistent, notably through the latest synthesis by Suzuki et al. (2021), who achieved an integrated classification of Cenozoic radiolarians based on morphological and molecular data. In the current state of Cenozoic radiolarian taxonomy, the main hurdle is at the genus level, which is poorly defined in most cases. Consequently, genus assignment is highly subjective and proceeds almost entirely based on the opinion of the author. A thorough revision of the descriptions and diagnoses of Cenozoic radiolarian genera is therefore urgently needed. This work was initiated by O'Dogherty et al. (2021), but unfortunately, the diagnoses they provide are often vague and too general for accurate identification and are unusable in the daily practice of taxonomy.

Our detailed inventory of late middle Eocene radiolarian species served as a starting point for a high-resolution biostratigraphic study at ODP Site 1260 (western equatorial Atlantic). Taking advantage of the precise cyclostratigraphic framework developed at this site, we calibrated astronomically the absolute ages of 71 radiolarian bioevents, including bioevents related to abundant species that are usually neglected in biostratigraphic studies. By comparison of our results with the equatorial Pacific record, we subsequently demonstrated the synchroneity of primary radiolarian bioevents that underpin the middle Eocene zonal scheme. This demonstration was achieved by means of two independent dating methods (magnetostratigraphy and astronomical calibration), reinforcing the robustness of the tropical radiolarian biozonation, and demonstrating that radiolarians are amongst the most accurate middle Eocene biostratigraphic microfossils.

After adjusting the taxonomic and biostratigraphic framework, the main aim of this thesis was to study the effects of global warming on polycystine radiolarians. Two categories of metrics were used to achieve this goal. On the one hand, diversity metrics were calculated to unravel the impact of the MECO at a large, macroevolutionary scale. This quantitative analysis of the entire radiolarian assemblage was conducted at subtropical ODP Site 1051. On the other hand, geometric morphometrics approaches were applied for the first time to quantify the morphological disparity of radiolarian shells. This latter study was focused on a single biostratigraphically important nassellarian species from tropical ODP Site 1260.

Firstly, the detailed examination of the radiolarian fauna at ODP Site 1051 did not reveal any significant turnover during the MECO. These results show that a rapid rise of ~4–6°C in sea surface temperature did not exceed the threshold to drive extinction in radiolarians. On the contrary, we documented an increase of ~30 % in radiolarian richness, coinciding with the warmest interval of the MECO (around 40 Ma). This increase is due to the poleward migration of several warm tropical radiolarian species that expanded their geographical ranges to higher latitudes during the warming event. Similarly, several typical middle Eocene tropical species, such as *Podocyrtis* (*L.*) *chalara* Riedel and Sanfilippo and *Podocyrtis* (*L.*) *mitra* Ehrenberg, have peak abundances during the warmest interval. Apart from these observations, quantitative analyses showed that ocean warming elicited only a weak response in radiolarians, with assemblages observed during the MECO interval differing sightly from those of the pre- and post-MECO intervals.

In terms of total radiolarian diversity, the MECO warming only represents a minor event that did not profoundly alter radiolarian assemblages. Since poleward migrations of planktic tropical species appear to be the most striking ecological feature of this event, we stated that the MECO is probably best classified as a migration event. It is should be noted, however, that the faunal changes documented in our study only have a local relevance (i.e., the western subtropical Atlantic) and may not be representative of the effects of the MECO on radiolarian assemblages in all oceanic regions. Given the climate sensitivity of polar planktic faunas (Trubovitz et al., 2020; Penn and Deutsch, 2022), different responses can be expected at higher latitudes. These aspects have already been studied in the Southern Ocean (DSDP Site 277, Campbell Plateau) by Pascher et al. (2015). However, this study examined too few stratigraphic levels to be conclusive, and more importantly, counts were only limited to a subset of abundant or biostratigraphically important species. An exhaustive study of high-latitude radiolarian assemblages is needed to obtain an accurate depiction of the biotic changes induced by the MECO warming.

The study of morphological disparity seems to be a valuable complement to traditional taxonomic richness analyses, especially for assessing the impact of low-magnitude environmental perturbations that did not result in extinctions. In the case of the MECO, geometric morphometric shape analyses have revealed two possible responses of planktic organisms to global warming: either migrate to track their preferred temperature conditions, or adapt by producing additional morphologies. Our results have also shown that fluctuations in the morphological disparity of radiolarian shells coincide with a shift in the stable isotope record. The peak of morphological disparity falls in the warmest interval of the MECO and is interpreted as an indicator of biological stress induced by the climatic event. However, further ecological interpretation is difficult, because the link between shell morphological variation and ecological function is intricate and not well-established in radiolarians. Finally, this pilot morphometric study can be seen as a first step in the investigation of previously unexplored aspects of the radiolarian fossil record. An interesting development would be to apply this method to a larger panel of species, in order to gain a better understanding of the general rules that shape plankton morphological diversity.

References

Abdi, H., and Williams, L.J., 2010. Principal component analysis. Wiley Interdisciplinary Reviews: Computational Statistics 2, 433–459.

Abelmann, A., 1990. Oligocene to Middle Miocene radiolarian stratigraphy of southern high latitudes from Leg 113, sites 689 and 690, Maud Rise, *in* Barker, P.F., Kennett, J.P., O'Connell, S., Berkowitz, S., Bryant, W.R., Burckle, L.H., Egeberg, P.K., Fiitterer, D.K., Qersonde, R.E., Qolovchenko, X., Hamilton, N., Lawver, L., Lazarus, D.B., Lonsdale, M., Mohr, B., Nagao, T., Pereira, C.P.Q., Pudsey, C.J., Robert, C.M., Schandl, E., Spieß, V., Stott, L.D., Thomas, E., Thompson, K.F.M., and Wise, S.W., Jr. (eds.), Proc. ODP, Sci. Results 113. Ocean Drill. Program, College Station, TX, USA, 675–708.

Adams, D.C., and Otárola-Castillo, E., 2013. Geomorph: an R package for the collection and analysis of geometric morphometric shape data. Methods in Ecology & Evolution 4, 393–399. https://cran.r-project.org/web/packages/geomorph/index.html.

Adams, D.C., Rohlf, F.J., and Slice, D.E., 2013. A field comes of age: geometric morphometrics in the 21st century. Hystrix 24, 7–14.

Agnini, C., Fornaciari, E., Raffi, I., Catanzariti, R., Pälike, H., Backman, J., and Rio, D., 2014. Biozonation and biochronology of Paleogene calcareous nannofossils from low and middle latitudes. Newsletters on Stratigraphy 47, 131–181.

Aitchison, J.C., Suzuki, N., Caridroit, M., Danelian, T., and Noble, P., 2017. Paleozoic radiolarian biostratigraphy. Geodiversitas 39, 503–531.

Alroy, J., 2010a. Fair sampling of taxonomic richness and unbiased estimation of origination and extinction rates. The Paleontological Society Papers 16, 55–80.

Alroy, J., 2010b. The shifting balance of diversity among major marine animal groups. Science 329, 1191–1194.

Alroy, J., 2010c. Geographic, environmental and intrinsic biotic controls on Phanerozoic marine diversification. Palaeontology 53, 1211–1235.

Anderson, O.R., 1978. Light and electron microscopic observation sof feeding behavior, nutrition and reproduction in laboratory cultures of *Thalassicolla nucleata*. Tissue & Cell 10, 401–412.

Anderson, O.R., 1983. Radiolaria. Springer-Verlag, New York, United States, 365 p.

Anderson, O.R., 1993. The trophic role of planktonic foraminifera and radiolaria. Marine Microbial Food Webs 7, 31–51.3

Anderson, O.R., Hemleben, C., Spindler, M., and Lindsey, J.L., 1986. A comparative analysis of the morphogenesis and morphometric diversity of mature skeletons of living *Didymocyrtis tetrathalamus* and *Hexalonche amphisiphon*. Marine Micropaleontology 11, 203–215.

Anderson, O.R., Bennett, P., and Bryan, M., 1989a. Experimental and observational studies of radiolarian physiological ecology: 1. Growth, abundance and opal productivity of the spongiose radiolarian *Spongaster tetras tetras*. Marine Micropaleontology 14, 257–265.

Anderson, O.R., Bennett, P., and Bryan, M., 1989b. Experimental and observational studies of radiolarian physiological ecology: 3. Effects of temperature, salinity and light intensity on the growth and survival of *Spongaster tetras tetras* maintained in laboratory culture. Marine Micropaleontology 14, 275–282.

Apel, M., Kiessling, W., Böhm, F., and Lazarus, D.B, 2002. Radiolarian faunal characteristics in Oligocene of the Kerguelen Plateau, Leg 183, Site 1138, *in* Frey, F.A., Coffin, M.F., Wallace, P.J., Antretter, M.J., Arndt, N.T., Barling, J., Boehm, F., Borre, M.K., Coxall, H.K., Damuth, J.E., Delius, H., Duncan, R.A., Inokuchi, H., Keszthelyi, L., Mahoney, J.J., Moore, C.L., Müller, R.D., Neal, C.R., Nicolaysen, K.E., Pringle, M.S., Reusch, D.N., Saccocia, P.J., Teagle, D.A.H., Wähnert, V., Weis, D.A.M., Wise, S.W., Jr., and Zhao X. (eds.), Proc. ODP, Sci. Results 183. Ocean Drill. Program, College Station, TX, USA, 1–48.

Arenillas, I., Molina, E., and Schmitz, B., 1999. Planktic foraminiferal and $\delta^{13}C$ isotopic changes across the Paleocene/Eocene boundary at Possagno (Italy). International Journal of Earth Sciences 88, 352–364.

Bailey, J.W., 1856. Notice of microscopic forms found in the soundings of the Sea of Kamtschatka-with a plate. American Journal of Science And Arts, Second Series 22, 1–6.

Bąk, M., Górny, Z., and Bąk, K., 2015. Sponge growth on the Cenomanian carbonate shelves of the Carpathian Basin: a record from spicule-rich turbidites. Bulletin of Geosciences 90, 651–666.

Bault, V., Crônier, C., and Monnet, C., 2022. Morphological disparity trends in Devonian trilobites from North Africa. Palaeontology 65, e12623.

Bault, V., Crônier, C., Monnet, C., Balseiro, D., Serra, F., Waisfeld, B., Bignon, A., and Rustán, J.J., 2023. Rise and fall of the phacopids: the morphological history of a successful trilobite family. Palaeontology 65, 12673.

Bé, A.W.H., 1982. Biology of planktonic foraminifera, *in* Broadhead, T.W. (ed.), Foraminifera: notes for a short course. Series in Geology 6, 51–89.

Benson, R.N., 1972. Radiolaria, Leg 12, Deep Sea Drilling Project, *in* Laughton, A.S., Berggren, W.A., Benson, R.N., Davies, T.A., Franz, U., Musich, L.F., Perch-Nielsen, K., Ruffman, A.S., van Hinte, J.E., and Whitmarsh, R.B. (eds.), Init. Repts. DSDP 12. U.S. Govt. Print. Office, Washington DC, USA, 1085–1113.

Berggren, W.A., and Ouda, K., 2003. Upper Paleocene-lower Eocene planktonic foraminiferal biostratigraphy of the Dababiya section, Upper Nile valley (Egypt). Micropaleontology 49, 61–92.

Bijl, P.K., Houben, A.J., Schouten, S., Bohaty, S.M., Sluijs, A., Reichart, G.J., Sinninghe Damsté, J.S., and Brinkhuis, H., 2010. Transient Middle Eocene atmospheric CO_2 and temperature variations. Science 330, 819–821.

Bjørklund, K.R., 1976. Radiolaria from the Norwegian Sea, Leg 38 of the Deep Sea Drilling Project, *in* Talwani, M., Udintsev, G., Bjørklund, K., Caston, V.N.D., Faas, R.W., Kharin, G.N., Morris, D.A., Muller, C., Nilsen, T.H., van Hinte, J., Warnke, D.A., and White S.M. (eds.), Init. Repts. DSDP 38. U.S. Govt. Print. Office, Washington DC, USA, 1101–1168.

Blome, C.D., 1992. Radiolarians from Leg 122, Exmouth and Wombat Plateaus, Indian Ocean, *in* von Rad, U., Haq, B.U., O'Connell, S., Bent, A., Blome, C.D., Borella, P.E., Boyd, R., Bralower, T.J., Brenner, W.W., De Carlo, E.H., Dumont, T., Exon, N., Qalbrun, B., Qolovchenko, X., Qörür, N., Ito, M., Lorenzo, J.M., Meyers, P.A., Moxon, I., O'Brien, D.K., Oda, M., Sarti, M., Siesser, W.Q., Snowdon, L.R., Tang, C., Wilkens, R.H., Williamson, P., and Wonder, A.A.H. (eds.), Proc. ODP, Sci. Results 122. Ocean Drill. Program, College Station, TX, USA, 633–652.

Blueford, J., 1988. Radiolarian biostratigraphy of siliceous Eocene deposits in central California. Micropaleontology 34, 236–258.

Blueford, J.R., and Amon, E.O., 1993. Comparing elongated Spongodiscoidea (Radiolaria) from early Eocene deposits of northwest Turgay, Russia with present world-wide distribution. Micropaleontology, Special Publication 6, 72–89.

Bohaty, S.M., and Zachos, J.C., 2003. Significant Southern Ocean warming event in the late middle Eocene. Geology 31, 1017–1020.

Bohaty, S.M., Zachos, J.C., Florindo, F., and Delaney, M.L., 2009. Coupled greenhouse warming and deep-sea acidification in the middle Eocene. Paleoceanography 24, PA2207.

Boltovskoy, D., 2017a. Vertical distribution patterns of Radiolaria Polycystina (Protista) in the World Ocean: Living ranges, isothermal submersion and settling shells. Journal of Plankton Research 39, 330–349.

Boltovskoy, D., 2017b. Seasonality in the vertical flux and species composition of Radiolaria Polycystina (Protista): Patterns and drivers. Marine Ecology Progress Series 578, 51–72.

Boltovskoy, D., and Correa, N., 2016. Biogeography of Radiolaria Polycystina (Protista) in the world ocean. Progress in oceanography 149, 82–105.

Boltovskoy, D., Kling, S.A., Takahashi, K., and Bjørklund, K., 2010. World atlas of distribution of recent Polycystina (Radiolaria). Palaeontologia Electronica 13.3.18A, 1–230.

Boltovskoy, D., Anderson, O.R., and Correa, N., 2017. Radiolaria and phaeodaria, *in* Archibald, J.M., Simpson, A.G.B., and Slamovits, C.H. (eds.), Handbook of the protists, Second Edition. Cham, Switzerland, Springer, 731–763.

Bookstein, F.L., 1991. Morphometric Tools for Landmark Data. Cambridge University Press, New York, 456 p.

Borisenko, N.N., 1960. Radiolyarii nizhnego i srednego eotsena Zapadnoyi Kubani Geologicheskiy sbornik, Krasnodarskiy Filial, Vcesoyuznogo Neftegazovogo Nauchno-Issledovatel'skogo Instituta (Gosgortekhizdat), Moscow, 4, 219–232.

Boscolo Galazzo, F., Giusberti, L., Luciani, V., and Thomas, E., 2013. Paleoenvironmental changes during the Middle Eocene Climatic Optimum (MECO) and its aftermath: The benthic foraminiferal record from the Alano section (NE Italy). Palaeogeography, Palaeoclimatology, Palaeoecology 378, 22–35.

Boscolo Galazzo, F., Thomas, E., and Giusberti, L., 2015. Benthic foraminiferal response to the Middle Eocene climatic optimum (MECO) in the south-eastern Atlantic (ODP Site 1263). Palaeogeography, Palaeoclimatology, Palaeoecology 417, 432–444.

Boulila, S., Vahlenkamp, M., De Vleeschouwer, D., Laskar, J., Yamamoto, Y., Pälike, H., Kirtland Turner, S., Sexton, P.F., Westerhold, T., and Röhl, U., 2018. Towards a robust and consistent middle Eocene astronomical timescale. Earth and Planetary Science Letters 486, 94–107.

Brandt, R., 1935. Radiolaria, *in* Wetzel, O. (ed.), Die Mikropalaontologie des Heiligengener Kieseotones (Ober-Eozän). Siebenundzwanzigster Jahresbericht des Niedersächsischen geologischen Vereins. Geologische Abteilung der Naturhistorischen Gesellschaft zu Hannover 27, 41–81.

Bujak, J.P., and Brinkhuis, H., 1998. Global warming and dinocyst changes across the Paleocene/Eocene Epoch boundary, *in* Aubry, M.-P., Lucas, S.G., and Berggren, W.A. (eds.), Late Paleocene–Early Eocene Biotic and Climatic Events in the Marine and Terrestrial Records. Columbia University Press, New York, United States, 277–295.

Bunge, J., and Fitzpatrick, M., 1993. Estimating the number of species: a review. Journal of the American Statistical Association 88, 364–373.

Burke, K.D., Williams, J.W., Chandler, M.A., Haywood, A.M., Lunt, D.J., and Otto-Bliesner, B.L., 2018. Pliocene and Eocene provide best analogs for near-future climates. Proceedings of the National Academy of Sciences 115, 13288–13293.

Bury, P.S., 1862. Polycystins, Figures of Remarkable Forms & c., in the Barbados Chalk Deposit, (Chiefly Collected by Dr. Davy, and Notice in a Lecture to the Agricultural Society of Barbados, in July, 1846). W. Weldon, London, UK, 8 p.

Bütschli, O., 1882a. Erste Band, Protozoa, *in* Bronn, H.G. (ed.), Klassen und Ordnungen des Thier-Reiches, wissenschaftlich dargestlet. Leipzig und Heidelberg, C.F. Winter, Leipzig, Germany, 482 p.

Bütschli, O., 1882b. Beiträge zur Kenntnis der Radiolarienskelette, insbesondere der Cyrtida. Zeitschrift für Wissenschaftliche Zoologie, 36, 485–540.

Campbell, A.S., 1951. New genera and subgenera of Radiolarida. Journal of Paleontology 25, 527–530.

Campbell, A.S., 1953. A new radiolarian genus. Journal of Paleontology 27, 296.

Campbell, A.S., 1954. Radiolaria, *in* Moore, R.C. (ed.), Treatise on Invertebrate Paleontology, Part. D, Protista 3. Geological Society of America and University of Kansas Press, Lawrence, Kansas, USA, 11–195.

Campbell, A.S., and Clark, B.L., 1944. Radiolaria from Upper Cretaceous of Middle California. Geological Society of America, Special Papers 57, 61 p.

Carter, F.B., 1893. Classification of the Radiolaria: Key to the species of Barbados. The American monthly microscopical journal 14, 6–213.

Carter, F.B., 1895. Classification of the Radiolaria: Key to the species of Barbados. The American monthly microscopical journal 16, 81–85.

Carter, F.B., 1896a. Classification of the Radiolaria: Key to the species of Barbados. The American monthly microscopical journal 17, 19–25.

Carter, F.B., 1896b. Radiolaria: A new species from Barbados. The American monthly microscopical journal 17, 25–26.

Carter, F.B., 1896c. Radiolaria: A new species from Barbados. The American monthly microscopical journal 17, 57–58.

Carter, F.B., 1896d. Radiolaria: A new genus from Barbados. The American monthly microscopical journal 17, 96–97.

Carter, F.B., 1896e. Radiolaria, a new species. The American monthly microscopical journal, 18, 241–242.

Caulet, J.-P., 1985. Radiolarians from the southwest Pacific, in Kennett, J.P., von der Borch, C.C., Baker, P.A., Barton, C.E., Boersma, A., Caulet, J.-P., Dudley, W.C., Jr., Gardner, J.V., Graham Jenkins, D., Lohman, W.H., Martini, E., Merrill, R.B., Morin, R., Nelson, C.S., Robert, C., Srinivasan, M.S., Stein, R., and Takeuchi, A. (eds.), Init. Repts. DSDP 90. U.S. Govt. Print. Office, Washington DC, USA, 835–861.

Caulet, J.-P., 1991. Radiolarian from the Kerguelen Plateau, Leg 119, *in* Barron, J., Larsen, B., Baldauf, J., Alibert, C., Berkowitz, S., Caulet, J.-P., Chambers, S., Cooper, A., Cranston, R., Dorn, W., Ehrmann, W., Fox, R., Fryxell, G., Hambrey, M., Huber, B., Jenkins, C., Kang, S.-H., Keating, B., Mehl, K., Noh, I., Ollier, G., Pittenger, A., Sakai, H., Schroder, C., Solheim, A., Stockwell, D., Thierstein, H., Tocher, B., Turner, B., and Wei, W. (eds.), Proc. ODP, Sci. Results 119. Ocean Drill. Program, College Station, TX, USA, 513–546.

Cavalier-Smith, T., 1999. Principles of protein and lipid targeting in secondary symbiogenesis: euglenoid, dinoflagellate, and sporozoan plastid origins and the eukaryote family tree. Journal of Eukaryotic Microbiology 46, 347–366.

Cavalier-Smith, T., 2002. The phagotrophic origin of eukaryotes and phylogenetic classification of Protozoa. International journal of systematic and evolutionary microbiology 52, p. 297–354.

Cavalier-Smith, T., 2003. Protist phylogeny and the high-level classification of Protozoa. European Journal of Protistology 39, 338–348.

Cavalier-Smith, T., Chao, E.E., and Lewis, R., 2018. Multigene phylogeny and cell evolution of chromist infrakingdom Rhizaria: contrasting cell organisation of sister phyla Cercozoa and Retaria. Protoplasma 255, 1517–1574.

Chao, A., Gotelli, N.J., Hsieh, T.C., Sander, E.L., Ma, K.H., Colwell, R.K., and Ellison, A.M., 2014. Rarefaction and extrapolation with Hill numbers: a framework for sampling and estimation in species diversity studies. Ecological Monographs 84, 45–67.

Chao, A., Kubota, Y., Zelený, D., Chiu, C.-H., Li, C.-F., Kusumoto, B., Yasuhara, M., Thorn, S., Wei, C.-L., Costello, M.J., and Colwell, R.K., 2020. Quantifying sample completeness and comparing diversities among assemblages. Ecological Research 35, 292–314.

Charmantier, A., McCleery, R.H., Cole, L.R., Perrins, C., Kruuk, L.E., and Sheldon, B.C., 2008. Adaptive phenotypic plasticity in response to climate change in a wild bird population. Science 320, 800–803.

Chediya, D.M., 1959. Obzor Sistematiki Radiolyarii: Tadzhikskii Gosudarstvennyi Universitet, Stalingrad, USSR, 330 p.

Chen, P.-H., 1974. Some new Tertiary Radiolaria from Antarctic deep-sea sediments. Micropaleontology 20, 480–492.

Chen, P.-H., 1975. Antarctic Radiolaria, *in* Hayes, D.E., Frakes, L.A., Barrett, P.J., Burns, D.A., Chen, P.-H., Ford, A.B., Kaneps, A.G., Kemp, E.M., McCollum, D.W., Piper, D.J.W., Wall, R.E., and Webb, P.N. (eds.), Init. Repts. DSDP 28. U.S. Govt. Print. Office, Washington DC, USA, 437–513.

Ciampaglio, C.N., Kemp, M., and McShea, D.W., 2001. Detecting changes in morphospace occupation patterns in the fossil record: characterization and analysis of measures of disparity. Paleobiology 27, 695–715.

Cita, M.B., Nigrini, C., and Gartner, S., Jr., 1970. Biostratigraphy, *in* Peterson, M.N.A., Edgar, N.T., Cita, M.B., Gartner, S., Jr., Goll, R., Nigrini, C., and von der Borch, C. (eds.), Init. Repts. DSDP 2. U.S. Govt. Print. Office, Washington DC, USA, 391–411.

Clark, B.L., and Campbell, A.S., 1942. Eocene radiolarian faunas from the Monte Diablo area, California. Geological Society of America, Special Papers 39, Waverly Press, Baltimore, MD, USA, 112 p.

Clark, B.L., and Campbell, A.S., 1945. Radiolaria from the Kreyenhagen Formation near Los Banos, California. Geological Society of America, Memoir. 10, Waverly Press, Baltimore, MD, USA, 66 p.

Clarke, K.R., 1993. Non-parametric multivariate analysis of changes in community structure. Austral Ecology 18, 117–143.

Clay Kelly, D., Bralower, T.J., Zachos, J.C., Silva, I.P., and Thomas, E., 1996. Rapid diversification of planktonic foraminifera in the tropical Pacific (ODP Site 865) during the late Paleocene thermal maximum. Geology 24, 423–426.

Cornaggia, F., Bernardini, S., Giorgioni, M., Silva, G.L., Nagy, A.I.M., and Jovane, L., 2020. Abyssal oceanic circulation and acidification during the Middle Eocene Climatic Optimum (MECO). Scientific Reports 10, 1–9.

Cortese, G., and Bjørklund, K.R., 1997. The morphometric variation of *Actinomma boreale* (Radiolaria) in Atlantic boreal waters. Marine Micropaleontology 29, 271–282.

Cortese, G., and Bjørklund, K.R., 1998. The taxonomy of boreal Atlantic Ocean Actinommida (Radiolaria). Micropaleontology 44, 149–160.

Coxall, H.K., Wilson, P.A., Pälike, H., Lear, C.H., and Backman, J., 2005. Rapid stepwise onset of Antarctic glaciation and deeper calcite compensation in the Pacific Ocean. Nature 433, 53–57.

Cramwinckel, M.J., van der Ploeg, R., Bijl, P.K., Peterse, F., Bohaty, S.M., Röhl, U., Schouten, S., Middelburg, J.J., and Sluijs, A., 2019. Harmful algae and export production collapse in the equatorial Atlantic during the zenith of Middle Eocene Climatic Optimum warmth. Geology 47, 247–250.

Cramwinckel, M.J., Woelders, L., Huurdeman, E.P., Peterse, F., Gallagher, S.J., Pross, J., Burgess, C.E., Reichart, G.-J., Sluijs, A., and Bijl, P.K., 2020. Surface-circulation change in the southwest Pacific Ocean across the Middle Eocene Climatic Optimum: inferences from dinoflagellate cysts and biomarker paleothermometry. Climate of the Past 16, 1667–1689.

Crouch, E.M., Heilmann-Clausen, C., Brinkhuis, H., Morgans, H.E.G., Rogers, K.M., Egger, H., and Schmitz, B. 2001. Global dinoflagellate event associated with the late Paleocene thermal maximum. Geology 29, 315–318.

Crouch, E.M., Brinkhuis, H., Visscher, H., Adatte, T., and Bolle, M.-P., 2003. Late Paleocene–early Eocene dinoflagellate cyst records from the Tethys: Further observations on the global distribution of *Apectodinium*, *in* Wing, S.L., Gingerich, P.D., Schmitz, B., and Thomas, E. (eds.), Causes and Consequences of Globally Warm Climates in the Early Paleogene. Geological Society of America Special Paper 369, 113–131.

D'Onofrio, R., Zaky, A.S., Frontalini, F., Luciani, V., Catanzariti, R., Francescangeli, F., Giorgioni, M., Coccioni, R., Özcan, E., and Jovane, L., 2021. Impact of the Middle Eocene Climatic Optimum (MECO) on foraminiferal and calcareous nannofossil assemblages in the Neo-Tethyan Baskil Section (Eastern Turkey): Paleoenvironmental and paleoclimatic reconstructions. Applied Sciences 11, 11339.

Danelian, T., and Macleod, N., 2019. Morphometric analysis of two Eocene related radiolarian species of the *Podocyrtis* (*Lampterium*) lineage. Paleontological Research 23, 314–330.

Danelian, T., Le Callonec, L., Erbacher, J., Mosher, D.C., Malone, M.J., Berti, D., Bice, K., Bostock, H., Brumsack, H.-J, Forster, A., Heidersdorf, F., Henderiks, J., Janecek, T., Junium, C., Macleod, K., Meyers, P., Mutterlose J., Nishi, H., Norris, R., Ogg, J., O'Regan, M., Rea, B., Sexton, P., Sturt, H., Suganuma, Y., Thurow, J., Wilson, P., Wise, S.W., Jr., and Glatz, C., 2005. Preliminary results on Cretaceous-Tertiary tropical Atlantic pelagic sedimentation (Demerara Rise, ODP Leg 207): Comptes Rendus Geoscience 337, 609–616.

Danelian, T., Saint Martin, S., and Blanc-Valleron, M.-M., 2007. Middle Eocene radiolarian and diatom accumulation in the equatorial Atlantic (Demerara Rise, ODP Leg 207): Possible links with climatic and palaeoceanographic changes. Comptes Rendus Palevol 6, 103–114.

Danelian, T., Aitchison, J.C., Noble, P., Caridroit, M., Suzuki, N., and O'Dogherty, L., 2017. Historical insights on nearly 130 years of research on Paleozoic radiolarians. Geodiversitas 39, 351–361.

De Mendoza, R.S., and Gómez, R.O., 2022. Ecomorphology of the tarsometatarsus of waterfowl (Anseriformes) based on geometric morphometrics and its application to fossils. The Anatomical Record 305, 3243–3253.

de Souza, A.L., Eilert, V.M.P., de Souza Lima Fidalgo, T., and Mendonça Filho, J.G., 2017. Early to middle Eocene radiolarian biostratigraphy for the mid-latitude South Atlantic Ocean, Site 356, DSDP LEG 39. Marine Micropaleontology 136, 66–89.

de Souza, A.L., Eilert, V.M.P., de Souza Lima Fidalgo, T., dos Reis, I.P., Vilela, C.G., and Mendonça Filho, J.G., 2021. Late middle Eocene to early Oligocene radiolarian biostratigraphy in the Southern Ocean (Agulhas Ridge, ODP Leg 117, Site 1090). Marine Micropaleontology 169, 102038.

De Wever, P., 1981. Spyrids, Artostrobiids, and Cretaceous Radiolarians from the Western Pacific, Deep Sea Drilling Project Leg 61, *in* Larson, R.L., Schlanger, S.O., Batiza, R., Boyce, R.E., Cepek, P., De Wever, P., Fujii, N., Jenkyns, H.C., Koporulin, V., Moberly, R., Premoli Suva, I., Rea, D., Riech, V., Sayer, W.O., Seifert, K., Shcheka, S., Sliter, W.V., Steiner, M., Thiede, J., Thierstein, H., Tokuyama, H., Valuer, T., and Windom, K. (eds.), Init. Repts. DSDP 61. U.S. Govt. Print. Office, Washington DC, USA, 507–520.

De Wever, P., Dumitrică, P., Caulet, J.-P., Nigrini, C.A., and Caridroit, M., 2001. Radiolarians in the sedimentary record. Gordon and Breach Science Publishers, Amsterdam, Netherlands, 533 p.

Decelle, J., and Not, F., 2015. Acantharia. Encyclopedia of Life Sciences, 1–10.

Dinkelman, M.G., 1973. Radiolarian stratigraphy: Leg 16, Deep Sea Drilling Project, *in* Van Andel, T.H., Heath, G.R., Bennett, R.H., Bukry, J.D., Charleston, S., Cronan, D.S., Dinkelman, M.G., Kaneps, A.G., Rodolfo, K.S., and Yeats, R.S. (eds.), Init. Repts. DSDP 16. U.S. Govt. Print. Office, Washington DC, USA, 747–813.

Dreyer, F., 1889. Die Pylombildungen in der vergleichend-anatomischer und entwicklungsgeschichtlicher Beziehung bei Radiolarien und bei Protisten überhaupt, nebst System ünd Beschreibung neuer ünd der bis jetzt bekannten pylomatischen Spumellarien. Jenaische Zeitschrift fur Naturwissenschaft 23, 77–214.

Dryden, I.L., and Mardia, K.V., 1998. Statistical shape analysis. Wiley, Chichester, UK, 347 p.

Dumitrică, P., 1972. Miocene and Quaternary Silicoflagellates in sediments from the Mediterranean Sea, *in* Ryan, W.B.F., Hsü, K.J., Cita, M.B., Dumitrică, P., Lort, J.M., Mayne, W., Nesteroff, W.D., Pautot, G., Stradner, H., and Wezel, F.C. (eds.), Init. Repts. DSDP 13. U.S. Govt. Print. Office, Washington DC, USA, 902–933.

Dumitrică, P., 1973. Cretaceous and Quaternary Radiolaria in deep sea sediments from the northeast Atlantic Ocean and Mediterranean Sea, *in* Ryan, W.B.F., Hsü, K.J., Cita, M.B., Dumitrică, P., Lort, J.M., Maync, W., Nesteroff, W.D., Pautot, G., Stradner, H., and Wezel, F.C. (eds.), Init. Repts. DSDP 13. U.S. Govt. Print. Office, Washington DC, USA, 829–901.

Dumitrică, P., 1978. Badenian Radiolaria from central Paratethys, *in* Brestenska, E. (ed.), Chronostratigraphie und Neostratotypen, Miozaen der Zentralen Paratethys, vol. 6. VEDA, Verlag der Slowakischen Akademie der Wissenschaften, Bratislava, Czechoslovakia, 231–261

Dumitrică, P., 1983. Systematics and evolution of the genus *Suttonium* Schaff (Radiolaria). Revue de Micropaléontologie 26, 36–47.

Dumitrică, P., 1984. Systematics of Sphaerellarian radiolarian, *in* Petrushevskaya M.G. and Stepanjants, S.D. (eds.), Morphology, ecology and evolution of radiolarians. Material from the IV symposium of European radiolarists EURORAD IV. Akademiya Nauk SSSR, Zoological Institute, Leningrad, USSR, 91–102. [in Russian].

Dumitrică, P., 1985. Internal morphology of the Saturnalidae (Radiolaria): systematic and phylogenetic consequences. Revue de Micropaléontologie 28, 181–196.

Dumitrică, P., 1989. Internal skeletal structures of the superfamily Pyloniacea (Radiolaria), a basis of a new systematics. Revista española de Micropaleontología 21, 207–264.

Dumitrică, P., 2004. New Mesozoic and early Cenozoic spicular Nassellaria and Nassellaria-like Radiolaria. Revue de Micropaléontologie 47, 193–224.

Dumitrică, P., 2019. Cenozoic spumellarian Radiolaria with eccentric microsphere. Acta palaeontologica romaniae 15, 39–60.

Dumitrică, P., 2020. Some new or newly interpreted Cenozoic larnacillid radiolarian taxa. Revue de Micropaléontologie 66, 100405.

Dumitrică, P., and Hungerbühler, A., 2017. Asymmetry of the ring of the Saturnalidae (entactinarian Radiolaria): Causes and morphological and evolutionary consequences. Revue de micropaléontologie 60, 87–135.

Dzinoridze, R.N., Jousé, A.P., Koroleva-Golikova, G.S., Kozlova, G.E., Nagaeva, G.S., Petrushevskaya, M.G., and Strelnikova, N.I., 1976. Diatom and radiolarian Cenozoic stratigraphy, Norwegian Basin; DSDP Leg 38, *in* Talwani, M., Udintsev, G., Bjørklund, K., Caston, V.N.D., Faas, R.W., Kharin, G.N., Morris, D.A., Muller, C., Nilsen, T.H., van Hinte, J., Warnke, D.A., and White, S.M. (eds.), Init. Repts. DSDP 38. U.S. Govt. Print. Office, Washington DC, USA, 289–427.

Edgar, K.M., Wilson, P.A., Sexton, P.F., and Suganuma, Y., 2007. No extreme bipolar glaciation during the main Eocene calcite compensation shift. Nature 448, 908–911.

Edgar, K.M., Wilson, P.A., Sexton, P.F., Gibbs, S.J., Roberts, A.P., and Norris, R.D., 2010. New biostratigraphic, magnetostratigraphic and isotopic insights into the Middle Eocene Climatic Optimum in low latitudes. Palaeogeography, Palaeoclimatology, Palaeoecology 297, 670–682.

Edgar, K.M., Bohaty, S.M., Gibbs, S.J., Sexton, P.F., Norris, R.D., and Wilson, P.A., 2013. Symbiont 'bleaching' in planktic foraminifera during the Middle Eocene Climatic Optimum. Geology 41, 15–18.

Ehrenberg, C.G., 1839. Über die Bildung der Kreidefelsen und des Kreidemergels durch unsichtbare Organismen. Abhandlungen der Königlich Preussischen Akademie der Wissenschaften zu Berlin, Jahre 1838, 59–147.

Ehrenberg C.G., 1844. Über 2 neue Lager von Gebirgsmassen aus Infusorien als Meeres-Absatz in Nord-Amerika und eine Vergleichung derselben mit den organischen Kreide-Gebilden in Europa und Afrika. Bericht über die zur Bekanntmachung geeigneten Verhandlungen der Königlich Preussischen Akademie der Wissenschaften zu Berlin, Jahre 1844, 57–97.

Ehrenberg, C.G., 1846. Über eine halibiolithische, von Herrn R. Schomburgk entdeckte, vorherrschend aus mikroskopischen Polycystinen gebildete, Gebirgsmasse von Barbados. Bericht über die zur Bekanntmachung geeigneten Verhandlungen der Königlich Preussischen Akademie der Wissenschaften zu Berlin, Jahre 1846, 382–385.

Ehrenberg, C.G., 1847. Über die mikroskopischen kieselschaligen Polycystinen als mächtige Gebirgsmasse von Barbados und über das Verhältniss deraus mehr als 300 neuen Arten bestehenden ganz eigenthumlichen Formengruppe jener Felsmasse zu den jetzt lebenden Thieren und zur Kreidebildung Eine neue Anregung zur Erforschung des Erdlebens. Bericht über die zur Bekanntmachung geeigneten Verhandlungen der Königlich Preussischen Akademie der Wissenschaften zu Berlin, Jahre 1847, 40–60.

Ehrenberg, C.G., 1854a. Mikrogeologie. Das Erden und Felsen schaffende Wirken des unsichtbar kleinen selbststandigen Lebens auf der Erde. Verlag von Leopold Voss, Leipzig, xxviii + 374 p., Atlas, 31 p.

Ehrenberg, C.G., 1854b. Über das organischen Leben des Meeresgrundes in bis 10800 und 12000 Fuss Tiefe. Bericht über die zur Bekanntmachung geeigneten Verhandlungen der Königlich Preussischen Akademie der Wissenschaften zu Berlin, 54–75.

Ehrenberg, C.G., 1854c. Die systematische Charakteristik der neuen mikroskopischen Organismen des tiefen atlantischen Oceans. Bericht über die zur Bekanntmachung geeigneten Verhandlungen der Königlich Preussischen Akademie der Wissenschaften zu Berlin, 236–250.

Ehrenberg, C.G., 1861a. Über die organischen und unorganischen Mischungsverhältnisse des Meeresgrundes in 19,800 Fuss Tiefe nach Lieut. Brookes Messung. Monatsberichte der Königlich Preussischen Akademie der Wissenschaften zu Berlin, Jahre 1860, 765–774.

Ehrenberg, C.G., 1861b. Über den Tiefgrund des stillen Oceans zwischen Californien und den Sandwich-Inseln aus bis 15600' Tiefe nach Lieutenant Brooke. Monatsberichte der Königlich Preussischen Akademie der Wissenschaften zu Berlin, Jahre 1860, 819–833.

Ehrenberg, C.G., 1862. Übersicht die Tiefgrund-Verhältnisse des Oceans am Eingange der Davisstrasse und bei Island: Monatsberichte der Koniglichen Preussische Akademie der Wissenschaften zu Berlin, Jahre 1861, 275–315.

Ehrenberg, C.G., 1873a. Mikrogeologische Studien als Zusammenfassung seiner Beobachtungen des kleinsten Lebens der Meeres-Tiefgrunde aller Zonen und dessen geologischen Einfluss. Monatsberichte der Königlich Preussischen Akademie der Wissenschaften zu Berlin, Jahre 1872, 265–322.

Ehrenberg, C.G., 1873b. Mikrogeologische Studien über das kleinste Leben der Meeres-Tiefgrunde aller Zonen und dessen geologischen Einfluss. Abhandlungen der Königlich Preussischen Akademie der Wissenschaften zu Berlin, Jahre 1872, 131–399.

Ehrenberg, C.G., 1874. Grössere Felsproben des Polycystinen-Mergels von Barbados mit weiteren Erläuterungen. Abhandlungen der Königlich Preussischen Akademie der Wissenschaften zu Berlin, Jahre 1873, 213–263.

Ehrenberg, C.G., 1876. Fortsetzung der mikrogeologischen Studien als Gesammt–Uebersichtder mikroskopischen Paläontologie gleichartig analysirter Gebirgsarten der Erde, mit specieller Rücksicht auf den Polycystinen-Mergel von Barbados. Abhandlungen der Königlich Preussischen Akademie der Wissenschaften zu Berlin, Jahre 1875, 225 p.

Empson-Morin, K.M., 1981. Campanian Radiolaria from DSDP Site 313, Mid-Pacific Mountains. Micropaleontology 27, 249–292.

Foote, M. 1991. Morphological and taxonomic diversity in a clade's history: the blastoid record and stochastic simulations. Contributions from the Museum of Paleontology, University of Michigan 28, 101–140.

Foote, M., 1993. Discordance and concordance between morphological and taxonomic diversity. Paleobiology 19, 185–204.

Foreman, H.P., 1973, Radiolaria of Leg 10 with systematics and ranges for the families Amphipyndacidae, Artostrobiidae and Theoperidae, *in* Worzel, J.L., Bryant, W., Beall, A.O., Jr., Capo, R., Dickinson, K., Foreman, H.P., Laury, R., McNeely, B.W., and Smith, L.A. (eds.), Init. Repts. DSDP 10. U.S. Govt. Print. Office, Washington DC, USA, p. 407–474.

Foreman, H.P., 1975. Radiolaria from the North Pacific, Deep Sea Drilling Project, Leg 32, *in* Larson, R.L., Moberly, R., Bukry, D., Foreman, H.P., Gardner, J.V., Keene, J.B., Lancelot, Y., Luterbacher, H., Marshall, M.C., and Matter, A. (eds.), Init. Repts. DSDP 32. U.S. Govt. Print. Office, Washington DC, USA, 579–676.

Foreman, H.P., 1978. Mesozoic Radiolaria in the Atlantic Ocean off the northwest coast of Africa, Deep Sea Drilling Project, Leg 41, *in* Lancelot, Y., Seibold, E., Dean, W.E., Jansa, L.F., Eremeev, V., Gardner, J., Cepek, P., Krasheninnikov, V.A., Pflaumann, U., Johnson, D., Rankin, J.G., and Traban, P. (eds.), Init. Repts. DSDP 41. U.S. Govt. Print. Office, Washington DC, USA, 739–761.

Frizzell, D.L., and Middour, E.S., 1951. Paleocene Radiolaria from southeastern Missouri. Bulletin of Missouri School of Mines and Metallurgy 77, 1–41.

Funakawa, S., 1994. Plagiacanthidae (Radiolaria) from the upper Miocene of eastern Hokkaido, Japan. Transactions and Proceedings of the Palaeontological Society of Japan, New Series 174, 458–483.

Funakawa, S., 1995a. Intrageneric variation and temporal change in the internal skeletal structure of plagiacanthids (Radiolaria) from Hokkaido, Japan. Transactions and proceedings of the Palaeontological Society of Japan, New series 180, 208–225.

Funakawa, S., 1995b. Lophophaeninae (Radiolaria) from the upper Oligocene to lower Miocene and intrageneric variation in their internal skeletal structures. Journal of Geosciences, Osaka City University 38, 13–59.

Funakawa, S., and Nishi, H., 2005. Late middle Eocene to late Oligocene radiolarian biostratigraphy in the Southern Ocean (Maud Rise, ODP Leg 113, site 689). Marine Micropaleontology 54, 213–247.

Funakawa, S., Nishi, H., Moore, T.C., and Nigrini, C.A., 2006. Data report: Late Eocene-early Oligocene radiolarians, ODP Leg 199 Holes 1218A, 1219A, and 1220A, central Pacific, *in* Wilson, P.A., Lyle, M., and Firth, J.V. (eds.), Proc. ODP, Sci. Results 199. Ocean Drill. Program, College Station, TX, USA, 74 p.

Gibbs, S.J., Sheward, R.M., Bown, P.R., Poulton, A.J., and Alvarez, S.A., 2018. Warm plankton soup and red herrings: calcareous nannoplankton cellular communities and the Palaeocene–Eocene Thermal Maximum. Philosophical Transactions of the Royal Society A: Mathematical, Physical and Engineering Sciences 376, 20170075.

Giorgioni, M., Jovane, L., Rego, E.S., Rodelli, D., Frontalini, F., Coccioni, R., Catanzariti, R., and Özcan, E., 2019. Carbon cycle instability and orbital forcing during the Middle Eocene Climatic Optimum. Scientific Reports 9, 1–10.

Göke, G., 1958. Formenzauber der Radiolarien. Mikrokosmos 47, 271–276.

Göke, G., 1986. 150 Jahre Radiolarienforschung. Mikrokosmos 75, 33–46.

Goll, R.M., 1968. Classification and phylogeny of Cenozoic Trissocyclidae (Radiolaria) in the Pacific and Caribbean basins, Part I. Journal of Paleontology 42, 1409–1432.

Goll, R.M., 1969. Classification and phylogeny of Cenozoic Trissocyclidae (Radiolaria) in the Pacific and Caribbean basins, Part II. Journal of Paleontology 43, 322–339.

Goll, R.M., 1979. The Neogene evolution of *Zygocircus*, *Neosemantis* and *Callimitra*: their bearing on nassellarian classification. A revision of the Plagiacanthoidea. Micropaleontology 25, 365–396.

Good, I.J., 1953. The population frequencies of species and the estimation of population parameters. Biometrika 40, 1–237.

Gotelli, N.J., and Colwell, R.K., 2001. Quantifying biodiversity: procedures and pitfalls in the measurement and comparison of species richness. Ecology Letters 4, 379–391.

Gradstein, F.M., Ogg, J.G., Schmitz, M.D., and Ogg, G.M., 2012. The geologic time scale 2012. Elsevier, Amsterdam, Netherlands, 1176 p.

Granlund, A., 1990. Evolutionary trends of *Antarctissa* in the Quaternary using morphometric analysis. Marine Micropaleontology 15, 265–286.

Guillerme, T., Puttick, M.N., Marcy, A.E., and Weisbecker, V., 2020. Shifting spaces: which disparity or dissimilarity measurement best summarize occupancy in multidimensional spaces? Ecology & Evolution 10, 7261–7275.

Haeckel, E., 1861. Über neue, lebende Radiolarien des Mittelmeeres und die dazu gehörigen Abbildungen. Monatsberichte der Königlich Preussischen Akademie der Wissenschaften zu Berlin, Jahre 1860, 794–817.

Haeckel, E., 1862. Die Radiolarien (Rhizopoda Radiaria). Eine Monographie. Reimer, Berlin, Germany, 572 p.

Haeckel, E., 1879. Naturliche Schopfungs-Geschichte. Reimer, Berlin, Germany, 718 p.

Haeckel, E., 1882. Entwurf eines Radiolarien–Systems auf Grund von Studien der Challenger–Radiolarien. Jenaische Zeitschrift für Naturwissenschaft 15, 418–472.

Haeckel, E., 1887. Report on the Radiolaria collected by H.M.S. Challenger during the years 1873–1876. Report on the Scientific Results of the Voyage of the H.M.S. Challenger, Zoology, 18, 1803 p.

Haecker, V., 1908. Tiefsee-Radiolarien. Spezieller Teil. Die Tripyleen, Collodarienund Mikroradiolarien der Tiefsee, *in* Chun, C. (ed.), Wissenschaftliche Ergebnisse der Deutschen Tief-see-Expedition auf dem Dampfer "Valdivia", 1898-1899, Volume 14, Jena, Germany, 336–476.

Hammer, Ø., Harper, D.A., and Ryan, P.D., 2001. PAST: Paleontological statistics software package for education and data analysis. Palaeontologia Electronica 4, 1–9.

Hemleben, C., Spindler, M., and Anderson, O.R., 1989. Taxonomy and Species Features, *in* Hemleben, C., Spindler, M., and Anderson, O.R. (eds.), Modern Planktonic Foraminifera. Springer, New York, United States, 8–32.

Henehan, M.J., Edgar, K.M., Foster, G.L., Penman, D.E., Hull, P.M., Greenop, R., Anagnostou, E., and Pearson, P.N., 2020. Revisiting the Middle Eocene Climatic Optimum "Carbon Cycle Conundrum" with new estimates of atmospheric pCO2 from boron isotopes. Paleoceanography and Paleoclimatology 35, e2019PA003713.

Hertwig, R., 1879. Der Organismus der Radiolarien. G. Fischer, Jena, Germany, iv + 149 p.

Holdsworth, B.K., 1975. Cenozoic Radiolaria biostratigraphy: Leg 30: tropical and equatorial Pacific, *in* Andrews, J.E., Packham, G., Eade, J.V., Holdsworth, B.K., Jones, D.L., deVries Klein, G., Kroenke, L.W., Saito, T., Shafik, S., Stoeser, D.B., and van der Lingen, G.J. (eds.), Init. Repts. DSDP 30. U.S. Govt. Print. Office, Washington DC, USA, 499–537.

Hollande, A., and Enjumet, M., 1960. Cytologie, évolution et systématique des Sphaeroïdés (Radiolaires). Archives du Muséum national d'Histoire naturelle, Paris 7, 134 p.

Hollis, C.J., 1993. Latest Cretaceous to Late Paleocene radiolarian biostratigraphy: A new zonation from the New Zealand region. Marine Micropaleontology 21, 295–327.

Hollis, C.J., 2002. Biostratigraphy and paleoceanographic significance of Paleocene radiolarians from offshore eastern New Zealand. Marine Micropaleontology 46, 265–316.

Hollis, C.J., 2006. Radiolarian faunal turnover through the Paleocene–Eocene transition, Mead Stream, New Zealand. Eclogae Geologicae Helvetiae 99, 579–599.

Hollis, C.J., Waghorn, D.B., Strong, C.P., and Crouch, E.M., 1997. Integrated Paleogene biostratigraphy of DSDP site 277 (Leg 29): foraminifera, calcareous nannofossils, radiolaria, and palynomorphs. Institute of Geological and Nuclear Sciences, Science report 97/07, 1–73.

Hollis, C.J., Dickens, G.R., Field, B.D., Jones, C.M., and Strong, C.P., 2005a. The Paleocene–Eocene transition at Mead Stream, New Zealand: a southern Pacific record of early Cenozoic global change. Palaeogeography, Palaeoclimatology, Palaeoecology 215, 313–343.

Hollis, C.J., Field, B.D., Jones, C.M., Strong, C.P., Wilson, G.J., and Dickens, G.R., 2005b. Biostratigraphy and carbon isotope stratigraphy of upper-most Cretaceous–lower Cenozoic Muzzle Group in middle Clarence valley. Journal of the Royal Society of New Zealand 35, 345–383.

Hollis, C.J., Pascher, K.M., Sanfilippo, A., Nishimura, A., Kamikuri, S.-i., and Shepherd, C.L., 2020. An Austral radiolarian biozonation for the Paleogene. Stratigraphy 17, 213–278.

Hopkins, M.J., 2013. Decoupling of taxonomic diversity and morphological disparity during decline of the Cambrian trilobite family Pterocephaliidae. Journal of Evolutionary Biology, 26, 1665–1676.

Hsieh, T.C., Ma, K.H., and Chao, A., 2016. iNEXT: an R package for rarefaction and extrapolation of species diversity (Hill numbers). Methods in Ecology and Evolution 7, 1451–1456. https://cran.r-project.org/web/packages/iNEXT/index.html.

Hull, D.M., 1993. Quaternary, Eocene, and Cretaceous radiolarians from the Hawaiian Arch, northern equatorial Pacific Ocean, *in* Wilkens, R.H., Dziewonski, A., Firth, J.V., Baker, D.J., Jr., Briden, J.C., Carson, B., Collins, J.A., De Carlo, E.H., Duennebier, F.K., Dürbaum, H.-J., Francis, T.J.Q., Garcia, M.O., Goldberg, D., Gross, G., He, W., Helsley, C.E., Hull, D., Jacobson, R., Janecek, T.R., Kanazawa, T., Kappel, E., Karczewski, J.-F., Mello, U., Moss, M., Naka, J., Tribble, J.S., and Waggoner, G. (eds.), Proc. ODP, Sci. Results 136. Ocean Drill. Program, College Station, TX, USA, 3–25.

Hull, D.M., 1996. Paleoceanography and biostratigraphy of Paleogene radiolarians from the Norwegian-Greenland Sea, *in* Thiede, J., Myhre, A. M., Firth, J. V., Ahagon, N., Black, K.S., Bloemendal, J., Brass, Q.W., Bristow, J.F., Chow, N., Cremer, M., Davis, L., Flower, B., Fronval, T., Hood, J., Hull, D., Koç, N., Larsen, B., Lyle, M.W., McManus, J., O'Connell, S., Osterman, L.E., Rack, F.R., Sato, T., Scherer, R.P., Spiegler, D., Stein, R., Tadross, M., Wells, S., Williamson, D., Witte, B., and Wolf-Welling, T. (eds.), Proc. ODP, Sci. Results 151. Ocean Drill. Program, College Station, TX, USA, 125–152.

Hutchinson, D.K., Coxall, H.K., Lunt, D.J., Steinthorsdottir, M., De Boer, A.M., Baatsen, M., von der Heydt, A., Huber, M., Kennedy-Asser, A.T., Kunzmann, L., Ladant, J.-B., Lear, C.H., Moraweck, K., Pearson, P.N., Piga, E., Pound, M.J., Salzmann, U., Scher, H.D., Sijp, W.P., Śliwińska, K.K., Wilson, P.A., and Zhang, Z., 2021. The Eocene-Oligocene transition: a review of marine and terrestrial proxy data, models and model-data comparisons. Climate of the Past 17, 269–315.

Jackett, S.J., Baumgartner, P.O., and Bandini, A.N., 2008. A new low-latitude late Paleocene-early Eocene radiolarian biozonation based on unitary associations: applications for accreted terranes. Stratigraphy 5, 39–62.

Johnson, D.A., 1974. Radiolaria from the Eastern Indian Ocean, DSDP Leg 22, *in* Von der Borch, C.C., Sclater, J.G., Gartner, J., Jr., Hekinian, R., Johnson, D.A., McGowran, B., Pimm, A.C., Thompson, R.W., Veevers, J.J., and Waterman, L.S. (eds.), Init. Repts. DSDP 22. U.S. Govt. Print. Office, Washington DC, USA, 521–575.

Johnson, D.A., 1978. Cenozoic Radiolaria from the eastern tropical Atlantic, DSDP Leg 41, *in* Lancelot, Y., Seibold, E., Dean, W.E., Jansa, L.F., Eremeev, V., Gardner, J., Cepek, P., Krasheninnikov, V.A., Pflaumann, U., Johnson, D., Rankin, J.G., and Trabant, P. (eds.), Init. Repts. DSDP 41. U.S. Govt. Print. Office, Washington DC, USA, 763–789.

Johnson, D.A., 1983. Cenozoic radiolarians from the Brazil Basin and Rio Grande Rise, *in* Barker, P.F., Johnson, D.A., Carlson, R.L., Cepek, P., Coulbourn, W.T., Gamboa, L.A., Hamilton, N., de Melo, U., Pujol, C., Shor, A.N., Suzyumov, A.E., Tjalsma, L.R.C., and Walton, W.H. (eds.), Init. Repts. DSDP 72. U.S. Govt. Print. Office, Washington DC, USA, 783–791.

Johnson, D.A., and Nigrini, C.A., 1985a. Time-transgressive late Cenozoic radiolarian events of the equatorial Indo-Pacific. Science 20, 538–540.

Johnson, D.A., and Nigrini, C.A., 1985b. Synchronous and time-transgressive Neogene radiolarian datum levels in the equatorial Indian and Pacific Oceans. Marine Micropaleontology 9, 489–524.

Kaiho, K., Takeda, K., Petrizzo, M.R., and Zachos, J.C., 2006. Anomalous shifts in tropical Pacific planktonic and benthic foraminiferal test size during the Paleocene–Eocene thermal maximum. Palaeogeography, Palaeoclimatology, Palaeoecology 237, 456–464.

Kamikuri, S.-i., 2015. Radiolarian assemblages during the middle-late Eocene transition at Site 1052, ODP Leg 171B, Blake Nose, western North Atlantic Ocean. News of Osaka Micropaleontologists, Special Volume 15, 139–167.

Kamikuri, S.-I., and Wade, B.S., 2012. Radiolarian magnetobiochronology and faunal turnover across the middle/late Eocene boundary at Ocean Drilling Program Site 1052 in the western North Atlantic Ocean. Marine Micropaleontology 88, 41–53.

Kamikuri, S.-i., Moore, T.C., Jr., Ogane, K., Suzuki, N., Pälike, H., and Nishi, H., 2012a. Early Eocene to early Miocene radiolarian biostratigraphy for the low-latitude Pacific Ocean. Stratigraphy 9, 77–108.

Kamikuri, S.-i., Moore, T.C., Jr., Ogane, K., Suzuki, N., Pälike, H., and Nishi, H., 2012b. Data report: early to middle Eocene radiolarian biostratigraphy, IODP Expedition 320 Site U1331, eastern equatorial Pacific, *in* Pälike, H., Lyle, M., Nishi, H., Raffi, I., Gamage, K., Klaus, A., and the Expedition 320/321 Scientists (eds.), Proc. IODP 320/321. Int. Ocean Drill. Program, Management International, Tokyo, Japan, 1–11.

Kamikuri, S.-I., Moore, T.C., Jr., Lyle, M., Ogane, K., and Suzuki, N., 2013. Early and Middle Eocene radiolarian assemblages in the eastern equatorial Pacific Ocean (IODP Leg 320 Site U1331): Faunal changes and implications for paleoceanography. Marine Micropaleontology 98, 1–13.

Kellogg, D.E., 1975. The role of phyletic change in the evolution of *Pseudocubus vema* (Radiolaria). Paleobiology 1, 359–370.

Kellogg, D.E., 1983. Phenology of morphologic change in radiolarian lineages from deep-sea cores: implications for macroevolution. Paleobiology 9, 355–362.

Kendall, D.G., Barden, D., Carne, T.K., and Le, H., 1999. Shape and shape theory. Wiley, Chichester, UK, 306 p.

Kennett, J.P., and Stott, L.D., 1991. Abrupt deep-sea warming, palaeoceanographic changes and benthic extinctions at the end of the Palaeocene. Nature 353, 225–229.

Kim, K.H., 1992. Paleogene radiolarian biostratigraphy from high-latitude south Atlantic. Journal of the Paleontological Society of Korea 8, 24–51.

Kling, S.A., 1971. Radiolaria: Leg 6 of the Deep Sea Drilling Project. Fischer, A.G., Heezen, B.C., Boyce, R.E., Bukry, D., Douglas, R.G., Garrison, R.E., Kling, S.A., Krasheninnikov, V., Lisitzin, A.P., and Pimm, A.C. (eds.), Init. Repts. DSDP 6. U.S. Govt. Print. Office, Washington DC, USA, 1069–1117.

Klingenberg, C.P., 2003. A developmental perspective on developmental instability: theory, models and mechanisms. Developmental instability: causes and consequences 1, 14–34.

Klingenberg, C.P., 2020. Walking on Kendall's shape space: understanding shape spaces and their coordinate systems. Evolutionary Biology 47, 334–352.

Kochhann, K.G.D., Baecker-Fauth, S., and Fauth, G., 2013. Systematic paleontology and biostratigraphy of Paleocene to late Oligocene Radiolaria from DSDP Site 329, Falkland Plateau, South Atlantic Ocean. Micropaleontology 59, 529–554.

Kozlova, G.E., 1983. Radiolarian associations of boreal regions in the lower Paleocene, *in* Lyubinova P.C., and Myatlyuk E.V. (eds.), The Use of Microfauna in the Study of Sediments from the Continents and Oceans (Miscellaneous Scientific Reports). Transactions of the All Union Petroleum Scientific Research Institute for Geological Survey (VNIGRI), Leningrad, 84–112 [in Russian].

Kozlova, G.E., 1999. Paleogene boreal radiolarians from the Russia. Ministry of Natural resources of Russian Federation, All-Russian Petroleum research Exploration Institute (VNIGRI), Practical manual of microfauna 9, 323 p. [in Russian].

Kozur, H., and Mostler, H., 1972. Beiträge zur Erforschung der mesozoischen Radiolarien. Teil I: Revision der Oberfamilie Coccodiscacea HAECKEL 1862 emend. und Beschreibung ihrer triassischen Vertreter. Geologisch Paläontologische Mitteilungen Innsbruck 2, 1–60.

Kozur, H., and Mostler, H., 1982. Entactinaria subordo nov., a new radiolarian suborder. Geologisch Paläontologische Mitteilungen Innsbruck 11, 399–414.

Krasheninnikov, V.A., 1960. Some radiolarians of the Lower and Middle Eocene of the Western Pre-Caucasus, *in* Sazonov, N.T., and Shchutskaya, E.K. (eds.), Paleontological collection 3. Transactions of the All Union Petroleum Scientific Research Institute for Geological Survey (VNIGRI), Leningrad, USSR, 16, 271–308. [in Russian].

Kruglikova, S.B., 1969. Radiolarians in the core of station 4066 (northern part of the Pacific Ocean), *in* Jouse, A.P. (ed.), Basic problems of Micropaleontology and the accumulation of organogenic sediments in oceans and seas. Izdatelstvo Nauka, Akademiya Nauk SSSR, Okeanografitcheskaya Komissiya, Moscow, USSR, 115-126. [in Russian].

Kruglikova, S.B., 1974. The characteristic species of Radiolaria in bottom sediments of the Pacific boreal zone, *in* Zhuze, A.P. (ed.), Micropaleontology of Oceans and Seas: Academy of Sciences of the USSR, Oceanographic Commission, Moscow, USSR, 187-196. [in Russian].

Land, L.A., Paull, C.K., and Spiess, F.N., 1999. Abyssal erosion and scarp retreat: Deep Tow observations of the Blake Escarpment and Blake Spur. Marine Geology 160, 63–83.

Lazarus, D.B., 1986. Tempo and mode of morphologic evolution near the origin of the radiolarian lineage *Pterocanium prismatium*. Paleobiology 12, 175–189.

Lazarus, D.B., 2005. A brief review of radiolarian research. Paläontologische Zeitschrift 79, 183–200.

Lazarus, D.B., Kotrc, B., Wulf, G., and Schmidt, D.N., 2009. Radiolarians decreased silicification as an evolutionary response to reduced Cenozoic ocean silica availability. Proceedings of the National Academy of Sciences 106, 9333–9338.

Lazarus, D.B., and Pallant, A., 1989. Oligocene and Neogene radiolarians from the Labrador Sea, ODP LEG 105, *in* Srivastava, S.P., Arthur, M.A., Clement, B., Aksu, A., Baldauf, J., Bohrmann, G., Busch, W., Cederberg, T., Cremer, M., Dadey, K., De Vernal, A., Firth, J., Hall, F., Head, M., Hiscott, R., Jarrard, R., Kaminski, M., Lazarus, D.B., Monjanel, A.-L., Bjorslev Nielsen, O. Stein, R., Thiebault, F., Zachos, J., and Zimmerman, H. (eds.), Proc. ODP, Sci. Results 105. Ocean Drill. Program, College Station, TX, USA, 349–380.

Lazarus, D.B, Faust, K., and Popova-Goll, I., 2005. New species of prunoid radiolarians from the Antarctic Neogene. Journal of Micropalaeontology 24, 97–121.

Lazarus, D.B., Suzuki, N., Ishitani, Y., and Takahashi, K., 2021. Paleobiology of the Polycystines Radiolaria. Wiley-Blackwell, Hoboken, 481 p.

Levinton, J., 1988. Genetics, paleontology and macroevolution. Cambridge University Press, New York, United States, 516 p.

Ling, H.Y., 1975. Radiolaria, *in* Karig, D.E., Ingle, J.C., Jr., Bouma, A.H., Ellis, C.H., Haile, N., Koizumi, I., Ling, H.Y., MacGregor, I., Moore, J.C., Ujiie, H., Watanabe, T., White, S.M., and Yasui, M. (eds.), Init. Repts. DSDP 31. U.S. Govt. Print. Office, Washington DC, USA, 703–761.

Llopis Monferrer, N., Boltovskoy, D., Tréguer, P., Sandin, M.M., Not, F., and Leynaert, A., 2020. Estimating biogenic silica production of Rhizaria in the global ocean. Global Biogeochemical Cycles 34, e2019GB006286.

Lourens, L.J., Hilgen, F.J., Shackleton, N.J., Laskar, J., and Wilson, D.S., 2004. Chapter 21: The Neogene Period, *in* Gradstein, F.M., Ogg, J.G., and Smith, A.G. (eds.), The Geologic Time Scale 2004. Cambridge University Press, Cambridge, UK, 409–440.

Lourens, L.J., Sluijs, A., Kroon, D., Zachos, J.C., Thomas, E., Röhl, U., Bowles, J., and Raffi, I., 2005. Astronomical pacing of late Palaeocene to early Eocene global warming events. Nature 435, 1083–1087.

Lowery, C.M., Bown, P.R., Fraass, A.J., and Hull, P.M., 2020. Ecological response of plankton to environmental change: thresholds for extinction. Annual Review of Earth and Planetary Sciences 48, 403–429.

Lu, G., and Keller, G., 1995. Ecological stasis and saltation: species richness change in planktic foraminifera during the late Paleocene to early Eocene, DSDP Site 577. Palaeogeography, Palaeoclimatology, Palaeoecology 117, 211–227.

Luciani, V., Giusberti, L., Agnini, C., Backman, J., Fornaciari, E., and Rio, D., 2007. The Paleocene–Eocene Thermal Maximum as recorded by Tethyan planktonic foraminifera in the Forada section (northern Italy). Marine Micropaleontology 64, 189–214.

Luciani, V., Giusberti, L., Agnini, C., Fornaciari, E., Rio, D., Spofforth, D.J., and Pälike, H., 2010. Ecological and evolutionary response of Tethyan planktonic foraminifera to the middle Eocene climatic optimum (MECO) from the Alano section (NE Italy). Palaeogeography, Palaeoclimatology, Palaeoecology 292, 82–95.

Lyle, M., Lyle, A.O., Backman, J., and Tripati, A., 2005. Biogenic sedimentation in the Eocene equatorial Pacific – The stuttering greenhouse and Eocene carbonate compensation depth, *in* Wilson, P.A., Lyle, M., and Firth, J.V. (eds.), Proc. ODP, Sci. Results 199. Ocean Drill. Program, College Station, TX, USA, 35 p.

Lyle, M., Barron, J., Bralower, T.J., Huber, M., Olivarez Lyle, A., Ravelo, A.C., Rea, D.K., and Wilson, P.A., 2008. Pacific Ocean and Cenozoic evolution of climate. Reviews of Geophysics 46, RG2002.

Mamedov, N.A., 1969a. New representatives of Eocene radiolarians in Azerbaidzhan, *in* Vyalov, O.S. (ed.), Fossil and Recent Radiolarians: Materials of the Second All Union Seminar on Radiolaria. Izdatelstvo Lvovskogo Universiteta (Lvov University), Lvov, USSR, 94–101. [in Russian].

Mamedov, N.A., 1969b. Nekotoryie nobyie predstabiteli eostenovyikh radiolyariy Azerbaydzhana. Izvestiya Akademii Nauk Azerbaidzhanskoy USSR, 6, 32–40.

Mamedov, N.A., 1969c. Novyie vidyi radiolyariy iz eotsenovyikh otlozheniy azerbaydzhana. Izvestiya Akademii Nauk Azerbaidzhanskoy USSR, 4, 21–29.

Matsuoka, A., 2007. Living radiolarian feeding mechanisms: new light on past marine ecosystems. Swiss Journal of Geosciences 100, 273–279.

Matsuoka, A., and Anderson, O.R., 1992. Experimental and observational studies of radiolarian physiological ecology: Temperature and salinity tolerance of *Dictyocoryne truncatum*. Marine Micropaleontology 19, 299–313.

Matsuzaki, K.M., Suzuki, N., and Nishi, H., 2015. Middle to Upper Pleistocene Polycystine Radiolarians from Hole 902-C9001C, Northwestern Pacific. Paleontological Research 19, 1–77.

McCartney, K., and Wise, S.W., Jr., 1990. Cenozoic silicoflagellates and ebridians from ODP Leg 113: biostratigraphy and notes on morphologic variability, *in* Barker, P.F., Kennett, J.P., O'Connell, S., Berkowitz, S., Bryant, W.R., Burckle, L.H., Egeberg, P.K., Fiitterer, D.K., Qersonde, R.E., Qolovchenko, X., Hamilton, N., Lawver, L., Lazarus, D.B., Lonsdale, M., Mohr, B., Nagao, T., Pereira, C.P.Q., Pudsey, C.J., Robert, C.M., Schandl, E., Spieß, V., Stott, L.D., Thomas, E., Thompson, K.F.M., and Wise, S.W., Jr. (eds.), Proc. ODP, Sci. Results 113. Ocean Drill. Program, College Station, TX, USA, 729–760.

Meunier, M., and Danelian, T., 2022. Astronomical calibration of late middle Eocene radiolarian bioevents from ODP Site 1260 (equatorial Atlantic, Leg 207) and refinement of the global tropical radiolarian biozonation. Journal of Micropalaeontology 41, 1–27.

Meunier, M., and Danelian, T., 2023a. Progress in understanding middle Eocene nassellarian (Radiolaria, Polycystinea) diversity; new insights from the western equatorial Atlantic Ocean. Journal of Paleontology 97, 1–25.

Meunier, M., and Danelian, T., 2023b. No dramatic changes observed in subtropical radiolarian plankton assemblages during the Middle Eocene Climatic Optimum (MECO); evidence from the North Atlantic ODP Site 1051. Marine Micropaleontology 184, 102272.

Miller, K.G., Fairbanks, R.G., and Mountain, G.S., 1987. Tertiary oxygen isotope synthesis, sea level history, and continental margin erosion. Paleoceanography 2, 1–19.

Mita, I., 2001. Data report: Early to late Eocene calcareous nannofossil assemblages of Sites 1051 and 1052, Blake Nose, northwestern Atlantic Ocean, *in* Kroon, D., Norris, R.D., and Klaus, A. (eds.), Proc. ODP, Sci. Results 171B. Ocean Drill. Program, College Station, TX, USA, 1–28.

Mitteroecker, P., and Gunz, P., 2009. Advances in geometric morphometrics. Evolutionary Biology 36, 235–247.

Moebius, I., Friedrich, O., and Scher, H.D., 2014. Changes in Southern Ocean bottom water environments associated with the Middle Eocene Climatic Optimum (MECO). Palaeogeography, Palaeoclimatology, Palaeoecology 405, 16–27.

Moebius, I., Friedrich, O., Edgar, K.M., and Sexton, P.F., 2015. Episodes of intensified biological productivity in the subtropical Atlantic Ocean during the termination of the Middle Eocene Climatic Optimum (MECO). Paleoceanography 30, 1041–1058.

Moore, T.C., Jr., 1971. Radiolaria, *in* Tracey, J.I., Jr., Sutton, G.H., Nesteroff, W.D., Galehouse, J., Von der Borch, C.C., Moore, T.C., Jr., Lipps, J., Ul Haq, U.Z.B., and Beckmann, J.P. (eds.), Init. Repts. DSDP 8. U.S. Govt. Print. Office, Washington DC, USA, 727–775.

Moore, T.C., Jr., 1972. Mid-Tertiary evolution of the radiolarian genus *Calocycletta*. Micropaleontology 18, 144–152.

Moore, T.C., Jr., and Kamikuri, S.-i., 2012. Data report: radiolarian stratigraphy across the Eocene/Oligocene boundary in the equatorial Pacific, Sites 1218, U1333, and U1334, *in* Pälike, H., Lyle, M., Nishi, H., Raffi, I., Gamage, K., Klaus, A., and the Expedition 320/321 Scientists (eds.), Proc. IODP 320/321. Int. Ocean Drill. Program, Management International, Tokyo, Japan, 1–37.

Moore, T.C., Jr., Skackleton, N.J., and Pisias, N.G., 1993. Paleoceanography and the diachrony of radiolarian events in the eastern equatorial Pacific. Paleoceanography 8, 567–586.

Morisita, M., 1959. Measuring of the dispersion of individuals and analysis of the distributional patterns. Memoirs of the Faculty of Science, Kyushu University, Series E, 2, 215–235.

Nicotra, A.B., Atkin, O.K., Bonser, S.P., Davidson, A.M., Finnegan, E.J., Mathesius, U., P. Poot, P., Purugganan, M.D., Richards, C.L., Valladares, F., and van Kleunen, M., 2010. Plant phenotypic plasticity in a changing climate. Trends in plant science 15, 684–692.

Nigrini, C., 1967. Radiolaria in pelagic sediments from the Indian and Atlantic Oceans. Bulletin of the Scripps Institution of Oceanography, University of California, San Diego La Jolla, California, USA, 2, 125 p.

Nigrini, C., 1974. Cenozoic Radiolaria from the Arabian Sea, DSDP Leg 23, *in* Whitmarsh, R.B., Weser, O.E., Ali, S., Boudreaux, J.E., Fleisher, R.L., Jipa, D., Kidd, R.B., Mallik, T.K., Matter, A., Nigrini, C., Siddiquie, H.N., and Stoffers, P. (eds.), Init. Repts. DSDP 23. U.S. Govt. Print. Office, Washington DC, USA, 1051–1121.

Nigrini, C., 1977. Equatorial Cenozoic Artostrobiidae (Radiolaria). Micropaleontology 23, 241–269.

Nigrini, C., and Caulet, J.-P., 1992. Late Neogene radiolarian assemblages characteristic of Indo-Pacific areas of upwelling. Micropaleontology 38, 139–164.

Nigrini, C., and Sanfilippo, A., 2000. Paleogene radiolarians from Sites 998, 999, and 1001 in the Caribbean, *in* Leckie, R.M., Sigurdsson, H., Acton, G.D., Abrams, L.J., Bralower, T.J., Carey, S.N., Chaisson, W.P., Cotillon, P., Cunningham, A.D., D'Hondt, S.L., Droxler, A.W., Galbrun, B., Gonzalez, J., Haug, G., Kameo, K., King, J., Lind, I.L., Louvel, V., Lyons, T.W., Murray, R.W., Mutti, M., Myers, G., Pearce, R.B., Pearson, D.G., Peterson, L.C., and Röhl, U. (eds.), Proc. ODP, Sci. Results 165. Ocean Drill. Program, College Station, TX, USA, 57–81.

Nigrini, C., Sanfilippo, A., and Moore, T.J., Jr., 2005. Cenozoic radiolarian biostratigraphy: a magnetobiostratigraphic chronology of Cenozoic sequences from ODP Sites 1218, 1219, and 1220, equatorial Pacific, *in* Wilson, P.A., Lyle, M., and Firth, J.V. (eds)., Proc. ODP, Init. Repts 199. Ocean Drill. Program, College Station, TX, USA, 1–76.

Nishimura, A., 1987. Cenozoic Radiolaria in the western North Atlantic, Site 603, Leg 93 of the Deep Sea Drilling Project, *in* van Hinte, J.E., Wise, S.W., Jr., Biart, B.N.M., Mitchener Covington, J., Dunn, D.A., Haggerty, J.A., Johns, M.W., Meyers, P.A., Moullade, M.R., Muza, J.P., Ogg, J.G., Okamura, M., Sarti, M., and von Rad, U. (eds.), Init. Repts. DSDP 93. U.S. Govt. Print. Office, Washington DC, USA, 713–737.

Nishimura, A., 1992. Paleocene radiolarian biostratigraphy in the northwest Atlantic at Site 384, Leg 43, of the Deep Sea Drilling Project. Micropaleontology 38, 317–362.

Norris, R.D., Kroon, D., and Klaus, A., 1998. Shipboard scientific party, *in* Kroon, D., Norris, R.D., and Klaus, A. (eds.), Proc. ODP, Init. Repts 171B. Ocean Drill. Program, College Station, TX, USA, 351–360.

Obut, O.T., and Iwata, K., 2000. Lower Cambrian Radiolaria from the Gorny Altai (southern West Siberia). News of paleontology and stratigraphy 2, 33–38.

O'Connor, B., 1994. Seven new radiolarian species from the Oligocene of New Zealand. Micropaleontology 40, p. 337–350.

O'Connor, B., 1997a. New radiolaria from the Oligocene and early Miocene of Northland, New zealand. Micropaleontology 43, 63–100.

O'Connor, B., 1997b. Lower Miocene Radiolaria from Te Kopua Point, Kaipara Harbour, New Zealand. Micropaleontology 43, 101–128.

O'Connor, B., 1999a. Radiolaria from the Late Eocene Oamaru Diatomite, South Island, New Zealand. Micropaleontology 45, 1–55.

O’Connor, B., 1999b. Distribution and biostratigraphy of latest Eocene to latest Oligocene Radiolaria from the Mahurangi Limestone, Northland, New zealand. New Zealand Journal of Geology and Geophysics 42, 489–511.

O'Connor, B., 2000. Stratigraphic and geographic distribution of Eocene-Miocene Radiolaria from the Southwest Pacific. Micropaleontology 46, 189–228.

O'Dogherty, L., Caulet, J.-P., Dumitrică, P., and Suzuki, N., 2021, Catalogue of Cenozoic radiolarian genera (Class Polycystinea). Geodiversitas 43, 709–1185.

Ogane, K., Suzuki, N., Aita, Y., Sakai, T., Lazarus, D.B., and Tanimura, Y., 2009. Ehrenberg’s radiolarian collections from Barbados, *in* Tanimura, Y., and Aita, Y. (eds.), Joint Haeckel and Ehrenberg Project: Reexamination of the Haeckel and Ehrenberg Microfossil Collection as a historical and scientific legacy. National Museum of Nature and Science Monographs 40, Tokyo, Japan, 97–106.

Ogg, J.G., and Bardot, L., 2001. Aptian through Eocene magnetostratigraphic correlation of the Blake Nose Transect (Leg 171B), Florida continental margin, *in* Kroon, D., Norris, R.D., and Klaus, A. (eds.), Proc. ODP, Sci. Results 171B. Ocean Drill. Program, College Station, TX, USA, 1–58.

Oksanen, J., Blanchet, F.G., Friendly, M., Kindt, R., Legendre, P., McGlinn, D., Minchin, P.R., O’Hara, R., Simpson, G.L., Solymos, P., Stevens, M.H.H., Szoecs, E., and Wagner, H., 2019. vegan: Community Ecology Package. R, package version 2.5-6, https://CRAN.R-project.org/package=vegan.

Ouda, K.A.K., 2018. Morphologic change and evolution of *Acarinina sibaiyaensis* and its descendants during the earliest Eocene CIE/PETM interval in southern Egypt. Journal of African Earth Sciences 147, 78–125.

Pälike, H., Lyle, M.W., Nishi, H., Raffi, I., Ridgwell, A., Gamage, K., Klaus, A., Acton, G., Anderson, L., Backman, J., Baldauf, J., Beltran, C., Bohaty, S.M., Bown, P., Busch, W., Channell, J.E.T., Chun, C.O.J., Delaney, M., Dewangan, P., Dunkley Jones, P., Edgar, K.M., Evans, H., Fitch, P., Foster, G.L., Gussone, N., Hasegawa, H., Hathorne, E.C., Hayashi, H., Herrle, J.O., Holbourn, A., Hovan, S., Hyeong, K., Iijima, K., Ito, T., Kamikuri, S.-i., Kimoto, K., Kuroda, J., Leon-Rodriguez, L., Malinverno, A., Moore, T.C., Murphy, B.H., Murphy, D.P., Nakamura, H., Ogane, K., Ohneiser, C., Richter, C., Robinson, R., Rohling, E.J., Romero, O., Sawada, K., Scher, H., Schneider, L., Sluijs, A., Takata, H., Tian, J., Tsujimoto, A., Wade, B.S., Westerhold, T., Wilkens, R., Williams, T., Wilson, P.A., Yamamoto, Y., Yamamoto, S., Yamazaki, T., and Zeebe, R., 2012. A Cenozoic record of the equatorial Pacific carbonate compensation depth. Nature 488, 609–614.

Parins-Fukuchi, C., 2018. Bayesian placement of fossils on phylogenies using quantitative morphometric data. Evolution 72, 1801–1814.

Pascher, K.M., Hollis, C.J., Bohaty, S.M., Cortese, G., McKay, R.M., Seebeck, H., Suzuki, N., and Chiba, K., 2015. Expansion and diversification of high-latitude radiolarian assemblages in the late Eocene linked to a cooling event in the southwest Pacific. Climate of the Past 11, 1599–1620.

Penn, J.L., and Deutsch, C., 2022. Avoiding ocean mass extinction from climate warming. Science 376, 524–526.

Pessagno, E.A., 1976. Radiolarian zonation and stratigraphy of the Upper Cretaceous portion of the Great Valley Sequence, California Coast Ranges. Micropaleontology, Special Publication 2, 1–95.

Petrushevskaya, M.G., 1967. Antarctic Spumelline and Nasselline radiolarians, Issledovaniya Fauny Morei, Resultaty Biologicheskikh Issledovanii Sovetskoi Antarkticheskoi Ekspeditsii 1955-1958, Volume 4. Zoologicheskii Institut Academiya Nauk SSSR, 5–186. [in Russian].

Petrushevskaya, M.G., 1971. Nassellarian radiolarians in the plankton of the World Ocean, in Bykhovskij, B.E. (ed.), Radiolarians of the World Ocean according to the data of Soviet Expeditions. Akademiya nauk SSSR, Zoologicheskii Institut, Issledovaniya Fauny Morei 9, 1–294. [in Russian].

Petrushevskaya, M.G., 1975. Cenozoic radiolarians of the Antarctic, Leg 29, DSDP, *in* Kennet, J.P., Houtz, R.E., Andrews, P.B., Edwards, A.R., Gostin, V.A., Hajós, M., Hampton, M.A., Jenkins, D.G., Margolis, S.V., Ovenshine, A.T., and Perch-Nielsen, K. (eds.), Init. Repts. DSDP 29. U.S. Govt. Print. Office, Washington DC, USA, 541–675.

Petrushevskaya, M.G., 1981. Nassellarian radiolarians from the world oceans. Nauka, Leningradskoe Otdelenie, Leningrad, USSR, Publications of the Zoological Institute, Academy of Sciences of the USSR, 405 p. [in Russian].

Petrushevskaya, M.G., 1984. On the classification of Polycystine radiolarians, *in* Petrushevskaya M.G., and Stepanjants, S.D. (eds.), Morphology, ecology and evolution of radiolarians. Material from the IV symposium of European radiolarists EURORAD IV. Akademiya Nauk SSSR, Zoological Institute, Leningrad, USSR, 124–149. [in Russian].

Petrushevskaya, M.G., and Kozlova, G.E., 1972. Radiolaria: Leg 14, Deep Sea Drilling Project, *in* Hayes, D.E., Pimm, A.C., Beckmann, J.P., Benson, W.E., Berger, W.H., Roth, P.H., Supko, P.R., and von Rad, U. (eds.), Init. Repts. DSDP 14. U.S. Govt. Print. Office, Washington DC, USA, 495–648.

Petrushevskaya, M.G., and Kozlova, G.E., 1979. Opisanie rodov i vidov radiolyariy in Sterlkov, A.A., and Petrushevskaya, M.G. (eds.), Istoriya mikroplanktona Norvezhskogo, Volume 23. Akademii Nauk SSSR, Issledovanie Faunyi Morey, Leningrad, SSSR, 86–157.

Pielou, E.C., 1966. The measurement of diversity in different types of biological collections. Journal of Theoretical Biology 13, 131–144.

Pínto, F., Carlsson, V., Meunier, M., Van Bocxlaer, B., Elbez, H., Cueille, M., Boulet, P., and Danelian, T., 2023. Morphometrics and machine learning discrimination of the middle Eocene radiolarian species *Podocyrtis chalara*, *Podocyrtis goetheana* and their morphological intermediates. Marine Micropaleontology, 102293.

Polechová, J., and Storch, D., 2008. Ecological niche, *in* Jorgensen, S.E., and Fath, B.D. (eds.), Encyclopedia of ecology, Volume 2. Elsevier Science, 1088–1097.

Popofsky, A., 1913. Die Nassellarien des Warmwassergebietes, *in* Drygalski, E. (ed.), Deutsche Sudpolar-Expedition, 1901-1903, Volume 14. Georg Reimer, Berlin, Germany, 217–416.

Popova, I.M., Baumgartner, P.O., Guex, J., Tochilina, S.V., and Glezer, Z.I., 2002. Radiolarian biostratigraphy of Palaeogene deposits of the Russian Platform (Voronesh Anticline). Geodiversitas 24, 7–59.

Pouille, L., Obut, O., Danelian, T., and Sennikov, N., 2011. Lower Cambrian (Botomian) polycystine Radiolaria from the Altai Mountains (southern Siberia, Russia). Comptes Rendus Palevol 10, 627–633.

R Core Team 2022. R: a language and environment for statistical computing. R Foundation for Statistical Computing. https://www.R-project.org.

Raup, D.M., 1972. Taxonomic diversity during the Phanerozoic. Science 177, 1065–1071.

Renaudie, J., and Lazarus, D.B., 2012. New species of Neogene radiolarians from the Southern Ocean. Journal of Micropalaeontology 31, 29–52.

Renaudie, J., and Lazarus, D.B., 2013a. New species of Neogene radiolarians from the Southern Ocean–Part II. Journal of Micropalaeontology 32, 59–86.

Renaudie, J., and Lazarus, D.B., 2013b. On the accuracy of paleodiversity reconstructions: a case study in Antarctic Neogene radiolarians. Paleobiology 39, 491–509.

Renaudie, J., and Lazarus, D.B., 2015. New species of Neogene radiolarians from the Southern Ocean–part III. Journal of Micropalaeontology 34, 181–209.

Renaudie, J., Danelian, T., Saint Martin, S., Le Callonnec, L., and Tribovillard, N., 2010. Siliceous phytoplankton response to a Middle Eocene warming event recorded in the tropical Atlantic (Demerara Rise, ODP Site 1260A). Palaeogeography, Palaeoclimatology, Palaeoecology 286, 121–134.

Renz, G.W., 1984. Cenozoic radiolarians from the Barbados Ridge, Lesser Antilles subduction complex, Deep Sea Drilling Project Leg 78A, *in* Biju-Duval, B., Moore, J.C., Bergen, J.A., Blackinton, G., Claypool, G.E., Cowan, D.S., Davis, D., Guerra, R.T., Hemleben, C.H.J., Marlow, M.S., Pudsey, C., Renz, G.W., Tardy, M., Wilson, D.S., and Wright, A.W. (eds.), Init. Repts. DSDP 78A. U.S. Govt. Print. Office, Washington DC, USA, 447–462.

Reyment, R.A., and Jöreskog, K., 1993. Applied factor analysis in the natural sciences. Cambridge University Press, Second Edition, UK, 371 p.

Riedel, W.R., 1957a. Eocene Radiolaria, *in* Johnson, J.H., Bramlette, M.N., Riedel, W.R., Todd, R., Cole, W.S., and Cooke, C.W. (eds.), Geology of Saipan, Mariana Islands; Part. 3, Paleontology. Geological Survey, Professional Paper 280-E-J, 257–263.

Riedel, W.R., 1957b. Radiolaria: a preliminary stratigraphy, *in* Petterson, H. (ed.), Reports of the Swedish Deep-Sea Expedition, 1947–1948. Elanders Boktryckeri Aktiebolag, Göteborg, Sweden, 6, 59–96.

Riedel, W.R., 1967a. Some new families of Radiolaria. Proceedings of the geological Society of London 1640, 148–149.

Riedel, W.R., 1967b. Subclass Radiolaria, *in* Harland, W.B. (ed.), The Fossil Record. Geological Society of London, London, 291–298.

Riedel W.R., and Campbell, A.S., 1952. A new Eocene radiolarian genus. Journal of Paleontology 26, 667–669.

Riedel, W.R., and Hays, J.D., 1969. Cenozoic Radiolaria from Leg 1, *in* Ewing, M., Worzel, J.L., Beall, A.O., Berggren, W.A., Bukry, D., Burk, C.A., Fischer, A.G., and Pessagno, E.A., Jr. (eds.), Init. Repts. DSDP 1. U.S. Govt. Print. Office, Washington DC, USA, 400–402.

Riedel, W.R., and Sanfilippo, A., 1970. Radiolaria, Leg 4, Deep Sea Drilling Project, *in* Bader, R.G., Gerard, R.D., Benson, W.E., Bolli, H.M., Hay, W.W., Rothwell, Jr., T., Ruef, M.H., Riedel, W.R., and Sayles, F.L. (eds.), Init. Repts. DSDP 4. U.S. Govt. Print. Office, Washington DC, USA, 503–575.

Riedel, W.R., and Sanfilippo, A., 1971. Cenozoic Radiolaria from the western equatorial Pacific, Leg 7, *in* Winterer, E.L., Riedel, W.R., Brönnimann, P., Gealy, E.L., Heath, G.R., Kroenke, L., Martini, E., Moberly, R., Jr., Resig, J., and Worsley, T. (eds.), Init. Repts. DSDP 7. U.S. Govt. Print. Office, Washington DC, USA, 1529–1672.

Riedel, W.R., and Sanfilippo, A., 1973. Cenozoic Radiolaria from the Caribbean, Deep Sea Drilling Project, Leg 15, *in* Edgar, N.T., Saunders, J.B., Bolli, H.M., Boyce, R.E., Broecker, W.S., Donnelly, T.W., Gieskes, J.M., Hay, W.W., Horowitz, R.M., Maurrasse, F., Perez Nieto, H., Prell, W., Silva, I.P., Riedel, W.R., Schneidermann, N., and Waterman, L.S. (eds.), Init. Repts. DSDP 15. U.S. Govt. Print. Office, Washington DC, USA, 705–751.

Riedel, W.R., and Sanfilippo, A., 1977. Cainozoic Radiolaria, *in* Ramsay, A.T.S. (ed.), Oceanic Micropalaeontology, Volume 2. Academic Press, London, UK, 847–912.

Riedel, W.R., and Sanfilippo, A., 1978. Stratigraphy and evolution of equatorial Cenozoic radiolarians. Micropaleontology 24, 61–96.

Riedel, W.R., and Sanfilippo, A., 1986. Morphological characters for a natural classification of Cenozoic Radiolaria, reflecting phylogenies. Marine Micropaleontology 11, 151–170.

Ringnér, M., 2008. What is principal component analysis? Nature Biotechnology 26, 303–304.

Ripley, B., Venables, B., Bates, D.M., Hornik, K., Gebhardt, A., Firth, D., and Ripley, M.B., 2013. Package 'mass'. Cran R 538, 113–120. https://cran.rproject.org/web/packages /MASS/index.html.

Rohlf, F.J., 1999. Shape statistics: Procrustes superimpositions and tangent spaces. Journal of Classification 16, 197–223.

Rohlf, F.J., 2010. TpsDig, version 2.31. Department of ecology and evolution. State University of New York, Stony Brook, New York, USA.

Rohlf, F.J., 2015. The tps series of software. Hystrix 26, 9–12.

Rohlf, F.J., and Marcus, L.F., 1993. A revolution morphometrics. Trends in ecology & evolution 8, 129–132.

Rohlf, F.J., and Slice, D., 1990. Extensions of the Procrustes method for the optimal superimposition of landmarks. Systematic Biology 39, 40–59.

Roy, K., and Foote, M., 1997. Morphological approaches to measuring biodiversity. Trends in Ecology & Evolution 12, 277–281.

Rüst, D., 1885. Beiträge zur Kenntniss der fossilen Radiolarien aus Gesteinen des Jura. Palaeontographica 31, 269–321.

Sandin, M.M., Pillet, L., Biard, T., Poirier, C., Bigeard, E., Romac, S., Suzuki, N., and Not, F., 2019. Time calibrated morpho-molecular classification of Nassellaria (Radiolaria). Protist 170, 187–208.

Sanfilippo, A., 1990. Origin of the subgenera *Cyclampterium*, *Paralampterium* and *Sciadiopeplus* from *Lophocyrtis* (*Lophocyrtis*) (Radiolaria, Theoperidae). Marine Micropaleontology 15, 287–312.

Sanfilippo, A., and Blome, C.D., 2001. Biostratigraphic implications of mid-latitude Palaeocene-Eocene radiolarian faunas from Hole 1051A, ODP Leg 171B, Blake Nose, western North Atlantic, *in* Kroon, D., Norris, R.D., and Klaus, A. (eds.), Western North Atlantic Palaeogene And Cretaceous Palaeoceanography. Geological Society, London, Special Publications 183, l85–224.

Sanfilippo, A., and Caulet, J.-P., 1998. Taxonomy and evolution of Paleogene Antarctic and tropical Lophocyrtid radiolarians. Micropaleontology 44, 1–43.

Sanfilippo, A., and Fourtanier, E., 2003. Oligocene radiolarians, diatoms, and ebridians from the Great Australian Bight (ODP Leg 182, Site 1128), *in* Hine, A.C., Feary, D.A., Malone, M.J., Andres, M., Betzler, C., Brooks, G.R., Brunner, C.A., Fuller, M., Molina Garza, R.S., Holbourn, A.E., Huuse, M., Isern, A.R., James, N.P., Ladner, B.C., Li, Q., Machiyama, H., Mallinson, D.J., Matsuda, H., Mitterer, R.M., Robin, C., Russell, J.L., Shafik, S., Simo, J.A.T., Smart, P.L., Spence, G.H., Surlyk, F.C., Swart, P.K., and Wortmann, U.G. (eds.), Proc. ODP, Sci. Results 182. Ocean Drill. Program, College Station, TX, USA, 1–24.

Sanfilippo, A., and Nigrini, C., 1998a. Upper Paleocene–Lower Eocene Deep-Sea Radiolarian Stratigraphy and the Paleocene/Eocene Series Boundary, *in* Aubry, M.-P., Lucas, S.G., and Berggren, W.A. (eds.), Late Paleocene-Early Eocene climatic and biotic events in the marine and terrestrial records. Columbia University Press, USA, 244–274.

Sanfilippo, A., and Nigrini, C., 1998b. Code numbers for Cenozoic low latitude radiolarian biostratigraphic zones and GPTS conversion tables. Marine Micropaleontology 33, 109–156.

Sanfilippo, A., and Riedel, W.R., 1970. Post-Eocene "closed" theoperid radiolarians. Micropaleontology 16, 446–462.

Sanfilippo, A., and Riedel, W.R., 1973. Cenozoic Radiolaria (exclusive of theoperids, artostrobiids and amphipyndacids) from the Gulf of Mexico, DSDP Leg 10, *in* Worzel, J.L., Bryant, W., Beall, A.O., Jr., Capo, R., Dickinson, K., Foreman, H.P., Laury, R., McNeely, B.W., and Smith, L.A. (eds.), Init. Repts. DSDP 10. U.S. Govt. Print. Office, Washington DC, USA, 475–611.

Sanfilippo, A., and Riedel, W.R., 1982. Revision of the radiolarian genera *Theocotyle*, *Theocotylissa* and *Thyrsocyrtis*. Micropaleontology 28, 170–188.

Sanfilippo, A., and Riedel, W.R., 1990. Chapter 19: Morphometric analysis of evolving Eocene *Podocyrtis* (Radiolaria) morphotypes using shape coordinates, *in* Rolph, F.J., and Bookstein, F.L. (eds.), Proceedings of the Michigan Morphometrics Workshop. University of Michigan, Michigan, USA, 345–362.

Sanfilippo, A., and Riedel, W.R., 1992. The origin and evolution of Pterocorythidae (Radiolaria); a Cenozoic phylogenetic study. Micropaleontology 38, 1–36.

Sanfilippo, A., Westberg-Smith, M.J., and Riedel, W.R., 1985. Cenozoic Radiolaria, *in* Bolli, H.M., Saunders, J.B., and Perch-Nielsen, K. (eds.), Plankton Stratigraphy. Cambridge University Press, Cambridge, UK, 631–712.

Saunders, J.B., Bernoulli, D., Mueller-Merz, E., Oberhaensli, H., Perch-Nielsen, K., Riedel, W.R., Sanfilippo, A., and Torrini, R., Jr., 1984. Stratigraphy of the late middle Eocene to early Oligocene in the Bath Cliff section, Barbados, West Indies. Micropaleontology 30, 390–425.

Schaaf, A., 1976. *Suttonium praedicator* nov. gen., nov. sp. (Radiolaria, Nassellaria) et la famille des Suttonidae nov. fam. Geobios 9, 789–793.

Scher, H.D., Bohaty, S.M., Smith, B.W., and Munn, G.H., 2014. Isotopic interrogation of a suspected late Eocene glaciation. Paleoceanography 29, 628–644.

Scherer, R.P., 1991. Radiolarians of the Celebes Sea, Leg 124, Sites 767 and 770, *in* Silver, E.A., Rangin, C., von Breymann, M.T., Berner, U., Bertrand, P., Betzler, C., Brass, G.W., Hsu, V., Huang, Z., Jarrard, R.D., Lewis, S., Linsley, B.K., Merrill, D.L., Muller, C., Nederbragt, A., Nichols, G., Pubellier, M., Sajona, F.G., Scherer, R.P., Sheu, D.D., Shibua, H., Shyu, J.-P., Smith, R.B., Smith, T., Solidum, R.U., Spadea, P., and Tannant, D.D. (eds.), Proc. ODP, Sci. Results 124. Ocean Drill. Program, College Station, TX, USA, 345–357.

Schneider, C.A., Rasband, W.S., and Eliceiri, K.W., 2012. NIH Image to ImageJ: 25 years of image analysis. Nature Methods 9, 671–675.

Sexton, P.F., Norris, R.D., Wilson, P.A., Pälike, H., Westerhold, T., Röhl, U., Bolton, C.T., and Gibbs, S., 2011. Eocene global warming events driven by ventilation of oceanic dissolved organic carbon. Nature 471, 349–352.

Shannon, C.E., and Weaver, W., 1949. The Mathematical Theory of Communication. University of Illinois Press, Urbana, USA.

Shilov, V.V., 1995. Eocene-Oligocene Radiolarians from Leg 145, North Pacific, *in* Rea, D.K., Basov, I.A., Scholl, D.W., and Allan, J.F. (eds.), Proc. ODP, Sci. Results 145. Ocean Drill. Program, College Station, TX, 117–132.

Shipboard Scientific Party, 2004, Site 1260, *in* Erbacher, J., Mosher, D.C., Malone, M.J, Berti, D., Bice, K.L., Bostock, H., Brumsack, H.-J., Danelian, T., Forster, A., Glatz, C., Heidersdorf, F., Henderiks, J., Janecek, T.R., Junium, C., Le Callonnec, L., MacLeod, K., Meyers, P.A., Mutterlose, H.J., Nishi, H., Norris, R.D., Ogg, J.G., O'Regan, A.M., Rea, B., Sexton, P., Sturt, H., Suganuma, Y., Thurow, J.W., Wilson, P.A., and Wise, S.W., Jr. (eds.), Proc. ODP, Init. Repts. 207. Ocean Drill. Program, College Station, TX, USA, 113 p.

Simpson, E.H., 1949. Measurement of Diversity. Nature 163, 688.

Sluijs, A., Pross, J., and Brinkhuis, H., 2005. From greenhouse to icehouse; organic-walled dinoflagellate cysts as paleoenvironmental indicators in the Paleogene. Earth-Science Reviews 68, 281–315.

Sluijs, A., Schouten, S., Pagani, M., Woltering, M., Brinkhuis, H., Damsté, J.S.S., Dickens, G.R., Huber, M., Reichart, G.-J., Stein, R., Matthiessen, J., Lourens, L.J., Pedentchouk, N., Backman, J., Moran, K., and Expedition 302 Scientists, 2006. Subtropical Arctic Ocean temperatures during the Palaeocene/Eocene thermal maximum. Nature 441, 610–613.

Sluijs, A., Zeebe, R.E., Bijl, P.K., and Bohaty, S.M., 2013. A middle Eocene carbon cycle conundrum. Nature Geoscience 6, 429–434.

Smith, U.E., and Hendricks, J.R., 2013. Geometric morphometric character suites as phylogenetic data: extracting phylogenetic signal from gastropod shells. Systematic biology 62, 366–385.

Sokal, R.R., and Michener, C.D., 1958. A statistical method for evaluating systematic relationships. The University of Kansas science bulletin 38, 1409–1438.

Speijer, R.P., Pälike, H., Hollis, C.J., Hooker, J.J., and Ogg, J.G., 2020. Chapter 28: The Paleogene Period, *in* Gradstein, F.M., Ogg, J.G., Schmitz, M.D., and Ogg, G.M. (eds.), Geologic time scale 2020. Elsevier, Amsterdam, Netherlands, 1087–1140.

Spencer-Cervato, C., Lazarus, D.B., Beckmann, J.P., von Salis Perch-Nielsen, K., and Biolzi, M., 1993. New calibration of Neogene radiolarian events in the North Pacific. Marine Micropaleontology 21, 261–293.

Spencer-Cervato, C., Thierstein, H.R., Lazarus, D.B., and Beckmann, J.P., 1994. How synchronous are Neogene marine plankton events? Paleoceanography 9, 739–763.

Squinabol, S., 1904. Radiolarie cretacee degli Euganei. Atti e Memorie della reale Accademia di Scienze, Lettere ed Arti in Padova, Nuova Serie 20, 171–240 + 10 figures.

Stap, L., Lourens, L.J., van Dijk, A., Schouten, S., and Thomas, E., 2010. Coherent pattern and timing of the carbon isotope excursion and warming during Eocene Thermal Maximum 2 as recorded in planktic and benthic foraminifera. Geochemistry, Geophysics, Geosystems 11, Q11011.

Stöhr, E., 1880. Die Radiolarienfauna der Tripoli von Grotte, Provinz Girgenti in Sicilien. Palaeontographica 26, 71–124.

Strelkov, A.A., and Lipman, R.K., 1959. Subclass of Radiolaria. Systematical Part in Orlov, Y.A. (ed.), Fundamentals of Paleontology. USSR Academy of Sciences Publishing House, Moscow, USSR, 426–461. [in Russian].

Strong, C.P., Hollis, C.J., and Wilson, G.J., 1995. Foraminiferal, radiolarian, and dinoflagellate biostratigraphy of Late Cretaceous to middle Eocene pelagic sediments (Muzzle group), Mead Stream, Marlborough, New Zealand. New Zealand Journal of Geology and Geophysics 38, 171–209.

Suganuma, Y., and Ogg, J.G., 2006. Campanian through Eocene magnetostratigraphy of sites 1257–1261, ODP leg 207, Demerara rise (Western Equatorial Atlantic), *in* Mosher, D.C., Erbacher, J., Malone, M.J., Berti, D., Bice, K.L., Bostock, H., Brumsack, H.-J., Danelian, T., Forster, A., Glatz, C., Heidersdorf, F., Henderiks, J., Janecek, T.R., Junium, C., Le Callonnec, L., MacLeod, K., Meyers, P.A., Mutterlose, H.J., Nishi, H., Norris, R.D., Ogg, J.G., O'Regan, A.M., Rea, B., Sexton, P., Sturt, H., Suganuma, Y., Thurow, J.W., Wilson, P.A., and Wise, S.W., Jr. (eds.), Proc. ODP, Sci. Results 207. Ocean Drill. Program, College Station, TX, USA, 1–48.

Sugiyama, K., 1993. Skeletal structures of lower and middle Miocene Lophophaenids (Radiolaria) from central Japan. Transactions and Proceedings of the Palaeontological Society of Japan, New Series, 169, 44–72.

Sugiyama, K., 1998. Nassellarian fauna from the Middle Miocene Oidawara Formation, Mizunami Group, central Japan. News of Osaka Micropaleontologists, Special Volume 11, 227–250. [in Japanese].

Sutton, H.J., 1896a. Radiolaria; a new genus from Barbados. The American monthly microscopical journal 17, 61–62.

Sutton, H.J., 1896b. Radiolaria; a new species from Barbados. The American monthly microscopical journal 17, 58–60.

Sutton, H.J., 1896c. Radiolaria; a new genus from Barbados: The American monthly microscopical journal 17, 138–139.

Sutton, H.J., 1896d. Radiolaria; two new species from Barbados: The American monthly microscopical journal 17, 161–163.

Suzuki, N., and Aita, Y., 2011. Radiolaria: achievements and unresolved issues: taxonomy and cytology. Plankton & Benthos Research 6, 69–91.

Suzuki, N., and Not, F., 2015. Biology and ecology of radiolaria, *in* Ohtsuka, S., Suzaki, T., Horiguchi, T., Suzuki, N., and Not, F. (eds.), Marine protists: Diversity and dynamics. Springer, New York, USA, 179–222.

Suzuki, N., Ogane, K., Aita, Y., Sakai, T., and Lazarus, D.B, 2009a. Reexamination of Ehrenberg's Neogene Radiolarian Collections and its Impact on Taxonomic Stability, *in* Tanimura, Y., and Aita, Y. (eds.), Joint Haeckel and Ehrenberg Project: Reexamination of the Haeckel and Ehrenberg Microfossil Collections as a Historical and Scientific Legacy. National Museum of Nature and Science Monographs 40, 87–96.

Suzuki, N., Ogane, K., and Chiba, K., 2009b. Middle to Late Eocene polycystine radiolarians from the Site 1172, Leg 189, Southwest Pacific. News of Osaka Micropaleontologists, Special Volume 14, 239–296.

Suzuki, N., O'Dogherty, L., Caulet, J.-P., and Dumitrică, P., 2021. A new integrated morpho- and molecular systematic classification of Cenozoic radiolarians (Class Polycystinea), suprageneric taxonomy and logical nomenclatorial acts. Geodiversitas 43, 405–573.

Takemura, A., 1992. Radiolarian Paleogene biostratigraphy in the southern Indian Ocean, Leg 120, *in* Wise, S.W., Jr., Schlich, R., Jr., Palmer Julson, A.A., Aubry, M.-P., Berggren, W.A., Bitschene, P.R., Blackburn, N.A., Breza, J., Coffin, M.F., Harwood, D.M., Heider, F., Holmes, M.A., Howard, W.R., Inokuchi, H., Kelts, K., Lazarus, D.B., Mackensen, A., Maruyama, T., Munschy, M., Pratson, E., Quilty, P.Q., Rack, F., Salters, V.J.M., Sevigny, J.H., Storey, M., Takemura, A., Watkins, D.K., Whitechurch, H., and Zachos, J. (eds.), Proc. ODP, Sci. Results 120. Ocean Drill. Program, College Station, TX, USA, 735–756.

Takemura, A., and Ling, H.Y., 1997. Eocene and Oligocene radiolarian biostratigraphy from the Southern Ocean: correlation of ODP Legs 114 (Atlantic Ocean) and 120 (Indian Ocean). Marine Micropaleontology 30, 97–116.

Takemura, A., and Ling, H.Y., 1998. Taxonomy and phylogeny of the genus *Theocorys* (Nassellaria, Radiolaria) from the Eocene and Oligocene sequences in the Antarctic region. Paleontological Research 2, 155–169.

Tetard, M., Marchant, R., Cortese, G., Gally, Y., de Garidel-Thoron, T., and Beaufort, L., 2020. A new automated radiolarian image acquisition, stacking, processing, segmentation and identification workflow. Climate of the Past 16, 2415–2429.

Tetard, M., Carlsson, V., Meunier, M., and Danelian, T., 2023. Merging databases for CNN image recognition, increasing bias or improving results? Marine Micropaleontology 102296, 1–12.

Thomas, E., and Shackleton, N.J., 1996. The Paleocene-Eocene benthic foraminiferal extinction and stable isotope anomalies. Geological Society, London, Special Publications 101, 401–441.

Thomas, W.H., Hollibaugh, J.T., and Seibert, D.L., 1980. Effects of heavy metals on the morphology of some marine phytoplankton. Phycologia 19, 202–209.

Toffanin, F., Agnini, C., Fornaciari, E., Rio, D., Giusberti, L., Luciani, V., Spofforth, D.J.A., and Pälike, H., 2011. Changes in calcareous nannofossil assemblages during the Middle Eocene Climatic Optimum: Clues from the central-western Tethys (Alano section, NE Italy). Marine Micropaleontology 81, 22–31.

Trubovitz, S., Lazarus, D.B., Renaudie, J., and Noble, P.J., 2020. Marine plankton show threshold extinction response to Neogene climate change. Nature Communications 11, 5069.

Trubovitz, S., Renaudie, J., Lazarus, D.B, and Noble, P., 2022. Late Neogene Lophophaenidae (Nassellaria, Radiolaria) from the eastern equatorial Pacific. Zootaxa 5160, 158 p.

Vahlenkamp, M., Niezgodzki, I., De Vleeschouwer, D., Lohmann, G., Bickert, T., and Pälike, H., 2018. Ocean and climate response to North Atlantic seaway changes at the onset of long-term Eocene cooling. Earth and Planetary Science Letters 498, 185–195.

Van Valen, L., 1974. Multivariate structural statistics in natural history. Journal of Theoretical Biology 45, 235–247.

Vasilenko, L.N., 2019. New Radiolaria Species from the Cenozoic Deposits on the Island Slope of the Kuril-Kamchatka Trench. Paleontological Journal 53, 325–333.

Viertler, A., Baur, H., Spasojevic, T., Mennecart, B., and Klopfstein, S., 2022. Classifying fossil Darwin wasps (Hymenoptera: Ichneumonidae) with geometric morphometrics of fore wings. PLOS One 17, e0275570.

Villa, G., Fioroni, C., Pea, L., Bohaty, S., and Persico, D., 2008. Middle Eocene–late Oligocene climate variability: calcareous nannofossil response at Kerguelen Plateau, Site 748. Marine Micropaleontology 69, 173–192.

Vitukhin, D.I., 1993. Subdivision of the Russian far east Cenozoic sediments based on Radiolaria. Geologicheskii Institut, Rossiskaya Akademiya Nauk, Trudy, 485, 1–104.

Wade, B.S., Pearson, P.N., Berggren, W.A., and Pälike, H., 2011. Review and revision of Cenozoic tropical planktonic foraminiferal biostratigraphy and calibration to the geomagnetic polarity and astronomical time scale. Earth-Science Reviews 104, 111–142.

Wang, X., Reinhard, C.T., Planavsky, N.J., Owens, J.D., Lyons, T.W., and Johnson, T.M., 2016. Sedimentary chromium isotopic compositions across the Cretaceous OAE2 at Demerara Rise Site 1258. Chemical Geology 429, 85–92.

Weaver, F.M., and Dinkelman, M.G., 1978. Cenozoic radiolarians from the Blake Plateau and the Blake-Bahama Basin, DSDP Leg 44, *in* Benson, W.E., Sheridan, R.E., Pastouret, L., Enos, P., Freeman, T., Murdmaa, I.O., Worstell, P., Gradstein, F., Schmidt, R.R., Weaver, F.M., and Stuermer, D.H. (eds.), Init. Repts. DSDP 44. U.S. Govt. Print. Office, Washington DC, USA, 865–885.

Weinheimer, A.L., Sanfilippo, A., and Riedel, W.R., 1994. Radiolarians from Leg 134, Vanuatu region, southwestern tropical Pacific, *in* Greene, H.G., Collot, J.-Y., Stokking, L.B., Akimoto, K., Ask, M.V.S., Baker, P.E., Briqueu, L., Chabernaud, T.J., Coltorti, M., Fisher, M.A., Goud Collins, M.R., Hasenaka, T., Hobart, M.A., Krammer, A., Leonard, J.N., Martin, J.B., Martinez Rodriguez, J.I., Menger, S., Meschede, M., Pelletier, B., Perembo, R.C.B., Quinn, T.M., Reid, R.P., Riedel, W.R., Roperch, P., Staerker, T.S., Taylor, F.W., and Zhao, X. (eds.), Proc. ODP, Sci. Results 134. Ocean Drill. Program, College Station, TX, USA, 309–317.

Westacott, S., Hollis, C.J., Pascher, K.M., Dickens, G.R., and Hull, P.M., 2023. Radiolarian size and silicification across the Paleocene-Eocene boundary and into the early Eocene. Palaeogeography, Palaeoclimatology, Palaeoecology 609, 111287.

Westberg, J.M., Sanfilippo, A., and Riedel, W.R., 1980. Radiolarians from the Moroccan Basin, Deep Sea Drilling Project Leg 50, *in* Lancelot, Y., Winterer, E.L., Bosellini, A., Boutefeu, A.G., Boyce, R.E., Cepek, P., Fritz, D., Galimov, E.M., Melguen, M., Price, I., Schlager, W., Sliter, W., Taguchi, K., Vincent, E., and Westberg, J.M. (eds.), Init. Repts. DSDP 50. U.S. Govt. Print. Office, Washington DC, USA, 429–437.

Westberg-Smith, M.J., and Riedel, W.R., 1984. Radiolarians, *in* Barker, P.F., Johnson, D.A., Carlson, R.L., Cepek, P., Coulbourn, W.T., Gamboa, L.A., Hamilton, N., de Melo, U., Pujol, C., Shor, A.N., Suzyumov, A.E., Tjalsma, L.R.C., and Walton, W.H. (eds.), Init. Repts. DSDP 81. U.S. Govt. Print. Office, Washington DC, USA, 783–791.

Westerhold, T., Röhl, U., and Laskar, J., 2012. Time scale controversy: Accurate orbital calibration of the early Paleogene. Geochemistry, Geophysics, Geosystems 13, Q06015.

Westerhold, T., and Röhl, U., 2013. Orbital pacing of Eocene climate during the Middle Eocene Climate Optimum and the chron C19r event: Missing link found in the tropical western Atlantic. Geochemistry, Geophysics, Geosystems 14, 4811–4825.

Westerhold, T., Röhl, U., Pälike, H., Wilkens, R., Wilson, P.A., and Acton, G., 2014. Orbitally tuned timescale and astronomical forcing in the middle Eocene to early Oligocene. Climate of the Past 10, 955–973.

Westerhold, T., Röhl, U., Frederichs, T., Bohaty, S.M., and Zachos, J.C., 2015. Astronomical calibration of the geological timescale: closing the middle Eocene gap. Climate of the Past 11, 1181–1195.

Westerhold, T., Marwan, N., Drury, A.J., Liebrand, D., Agnini, C., Anagnostou, E., Barnet, J.S.K., Bohaty, S.M., De Vleeschouwer, D., Florindo, F., Frederichs, T., Hodell, D.A., Holbourn, A.E., Kroon, D., Lauretano, V., Littler, K., Lourens, L.J., Lyle, M., Pälike, H., Röhl, U., Tian, J., Wilkens, R.H., Wilson, P.A., and Zachos, J.C., 2020. An astronomically dated record of Earth's climate and its predictability over the last 66 million years. Science 369, 1383–1387.

Wills, M.A., 2001. Morphological disparity: a primer, *in* Adrain, J.M., Edgecombe, G.D., and Lieberman, B.S. (eds.), Fossils, phylogeny, and form: an analytical approach. Kluwer Academic/Plenum Publishers, New York, USA, 55–144.

Witkowski, J., Bohaty, S.M., McCartney, K., and Harwood, D.M., 2012. Enhanced siliceous plankton productivity in response to middle Eocene warming at Southern Ocean ODP Sites 748 and 749. Palaeogeography, Palaeoclimatology, Palaeoecology 326, 78–94.

Witkowski, J., Bohaty, S.M., Edgar, K.M., and Harwood, D.M., 2014. Rapid fluctuations in mid-latitude siliceous plankton production during the Middle Eocene Climatic Optimum (ODP Site 1051, western North Atlantic). Marine Micropaleontology 106, 110–129.

Witkowski, J., Harwood, D.M., Wade, B.S., and Bryłka, K., 2020. Rethinking the chronology of early Paleogene sediments in the western North Atlantic using diatom biostratigraphy. Marine Geology 424, 106168.

Yamaguchi, T., Norris, R.D., and Bornemann, A., 2012. Dwarfing of ostracodes during the Paleocene–Eocene Thermal Maximum at DSDP Site 401 (Bay of Biscay, North Atlantic) and its implication for changes in organic carbon cycle in deep-sea benthic ecosystem. Palaeogeography, Palaeoclimatology, Palaeoecology 346, 130–144.

Zachos, J.C., Quinn, T.M., and Salamy, K.A., 1996. High resolution (104 years) deep sea foraminiferal stable isotope records of the Eocene–Oligocene climate transition. Paleoceanography 11, 251–266.

Zachos, J.C., Dickens, G.R., and Zeebe, R.E., 2008. An early Cenozoic perspective on greenhouse warming and carbon-cycle dynamics. Nature 451, 279–283.

Zelditch, M.L., Swiderski, D.L., and Sheets, H.D., 2012. Geometric morphometrics for biologists: A primer, Second Edition. Elsevier Academic Press, New York, USA, 488 p.

Zittel, K.A., 1876. Über einige fossile Radiolarien aus der norddeutschen Kreiden. Zeitschrift der deutschen geologischen Gesellschaft 28, 75–87.

Abstract

The Middle Eocene Climatic Optimum (MECO) is a global warming event that occurred ca. 40 Ma and temporarily interrupted the long-term Eocene cooling trend. Although the MECO represents one of the major climatic perturbations of the Paleogene, its impact on the biosphere is still poorly understood. Based on a wide range of quantitative methods, this thesis aims to study the radiolarian paleodiversity dynamics and morphological disparity through the MECO, to better understand the biotic perturbations associated with this climatic event. The taxonomic framework of the middle Eocene radiolarian was first clarified by documenting at the species level two well-preserved radiolarian faunas recovered from two distinct geographic regions: the equatorial Atlantic (ODP site 1260) and the North Atlantic (ODP site 1051). A total of 281 species were identified, including 36 new to science. Taking advantage of the cyclostratigraphic framework developed at Site 1260, we refined the global tropical radiolarian biozonation. The absolute ages of 71 radiolarian bioevents were calibrated and, by comparison with the equatorial Pacific record, the synchroneity of primary bioevents was demonstrated. Once the taxonomic and biostratigraphic frameworks were clarified, the main aim of this thesis was to assess the biotic sensitivity of radiolarians to climate change. Two categories of metrics were used to achieve this objective. First, we performed a quantitative analysis of the entire assemblage at ODP Site 1051. This detailed investigation of the radiolarian fauna did not reveal any prominent turnover during the MECO but only a slight increase in radiolarian taxic richness due to the poleward migration of several tropical radiolarian species. Then, we applied geometric morphometric approaches to quantify the morphological disparity of radiolarian shells through the MECO interval. This study was focused on a single species (*Podocyrtis papalis*) from Site 1260 and showed that fluctuations in morphological disparity coincide with the warmest interval of the MECO. This signal is interpreted as an indicator of biological stress induced by the warming event.

Keywords – Radiolarians, middle Eocene, biostratigraphy, diversity, disparity, ODP, Atlantic Ocean

Résumé

L’Optimum Climatique de l’Éocène Moyen (MECO) est un évènement de réchauffement climatique qui s’est produit il y a 40 Ma, interrompant temporairement la tendance générale au refroidissement observée durant l’Éocène. Bien que le MECO soit l’une des perturbations climatiques les plus importantes du Paléogène, son impact sur la biosphère demeure encore mal connu. Via un large éventail de méthodes quantitatives, cette thèse vise à étudier la dynamique de la paléodiversité et la disparité morphologique des radiolaires au cours du MECO, afin de mieux comprendre les bouleversements biotiques qui lui sont associés. La première étape de ce travail a consisté à dresser la liste taxinomique exhaustive des espèces de radiolaires éocènes rencontrés dans deux domaines géographiques distincts : l’Atlantique équatorial (ODP Site 1260) et l’Atlantique septentrional (ODP Site 1051). Au total, 281 taxons ont été identifiés, dont 36 nouvelles espèces. S’appuyant sur le cadre cyclostratigraphique développé au Site 1260, nous avons également affiné la biozonation des radiolaires tropicaux. Les âges absolus de 71 bioévènements ont été calibrés et, par comparaison avec l’enregistrement fossilifère du Pacifique équatorial, nous avons démontré la synchronicité des bioévènements qui définissent les limites des biozones de l’Éocène moyen. Une fois les cadres taxonomique et biostratigraphique clarifiés, l’objectif de cette thèse était d’évaluer l’impact du réchauffement climatique sur les radiolaires. Pour ce faire, deux grandes catégories de mesures ont été utilisées. D’une part, nous avons effectué une analyse quantitative de l’assemblage fossile du site 1051. Cette étude détaillée n’a révélé aucun changement de faune important au cours du MECO. Seule une légère augmentation de la richesse taxinomique a été documentée, due à la migration de certaines espèces tropicales vers les hautes latitudes durant le MECO. D’autre part, nous avons employé des méthodes de géométrie morphométrique pour quantifier la disparité morphologique du squelette des radiolaires. Cette étude s’est concentrée sur une espèce de nassellaire (*Podocyrtis papalis*) du Site 1260. Nous avons montré que les fluctuations de la disparité morphologique du contour du squelette coïncidaient avec le pic de température du MECO. Ce signal est interprété comme un indicateur de stress biologique induit par le réchauffement climatique.

Mots-clefs – Radiolaires, Éocène moyen, biostratigraphie, diversité, disparité, ODP, Océan Atlantique